ISSN: 1309 - 2251

KAFKAS ÜNİVERSİTESİ VETERİNER FAKÜLTESİ DERGİSİ

Journal of the Faculty of Veterinary Medicine, Kafkas University

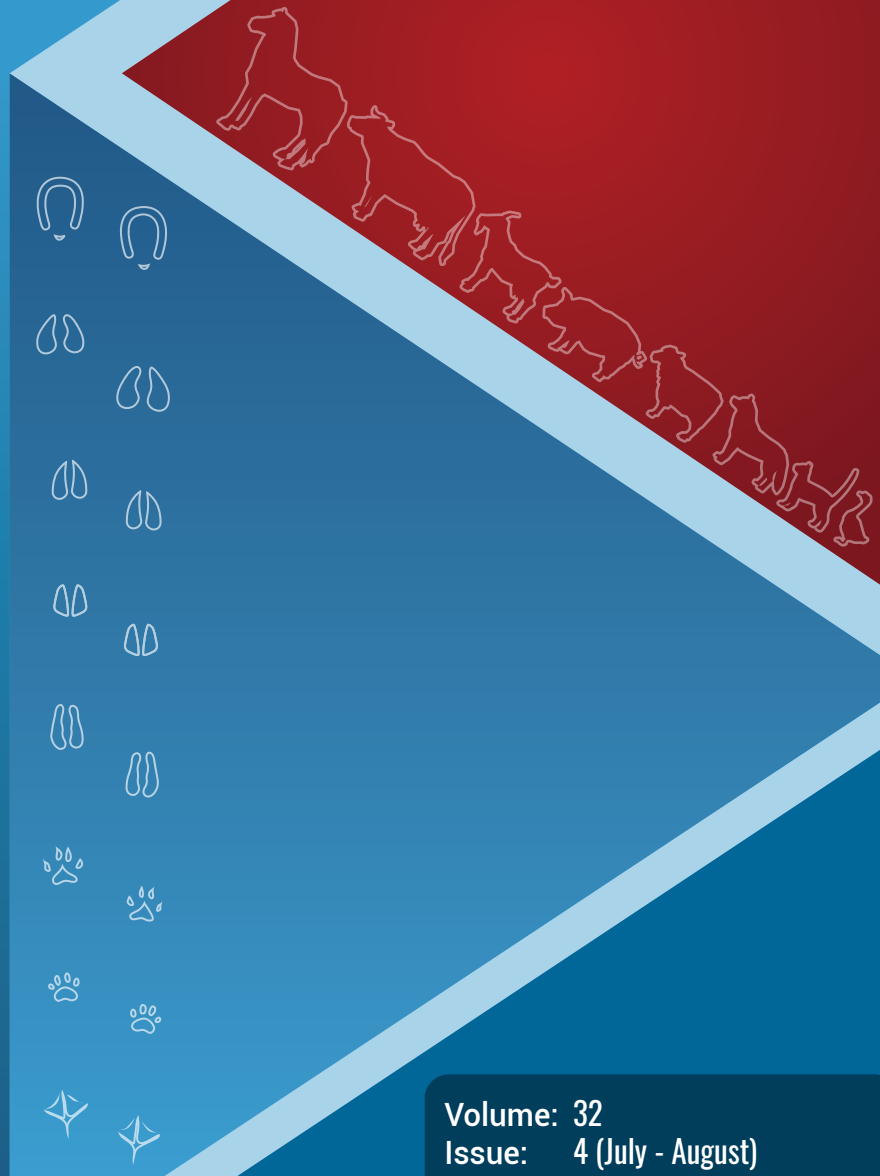

http://vetdergi.kafkas.edu.tr

Online Submission
http://vedergikafkas.org

Volume: 32
Issue: 4 (July - August)
Year: 2026

E-ISSN: 1309-2251

This journal is published bi-monthly, by the Faculty of Veterinary Medicine, University of Kafkas, Kars - Turkey

This journal is indexed and abstracted in:

- Web of Science Core Collection: Science Citation Index Expanded (since 2007)
- Additional Web of Science Indexes: Essential Science Indicators - Zoological Record
- CABI - Veterinary Science Database
- China Knowledge Resource Integrated (CNKI)
- DOAJ
- EBSCO - Academic Search Premier
- Elsevier - SCOPUS
- Elsevier - EMBASE
- SOBİAD Atıf Dizini
- TÜBİTAK/ULAKBİM TR-Dizin
- Türkiye Atıf Dizini

Address for Correspondence
Kafkas Üniversitesi Veteriner Fakültesi Dergisi Editörlüğü 36040, Kars - TÜRKİYE
Phone: +90 474 2426807-2426836/5228 Fax: +90 474 2426853 E-mail: vetdergi@kafkas.edu.tr
Electronic Edition http://vetdergikafkas.org
Online Submission http://submit.vetdergikafkas.org

Kafkas Universitesi Veteriner Fakultesi Dergisi
Journal Home-Page: http://vetdergikafkas.org
E-ISSN: 1309-2251

Kafkas Univ Vet Fak Derg
Volume: 32, Issue: 4, Year: 2026

Kafkas Universitesi Veteriner Fakultesi Dergisi
Journal Home-Page: http://vetdergikafkas.org
E-ISSN: 1309-2251

Kafkas Univ Vet Fak Derg
Volume: 32, Issue: 4, Year: 2026

EDITORIAL BOARD

Kafkas Universitesi Veteriner Fakultesi Dergisi
Journal Home-Page: http://vetdergikafkas.org
E-ISSN: 1309-2251

Kafkas Univ Vet Fak Derg
Volume: 32, Issue: 4, Year: 2026

EDITORIAL BOARD

Kafkas Universitesi Veteriner Fakultesi Dergisi
Journal Home-Page: http://vetdergikafkas.org
E-ISSN: 1309-2251

Kafkas Univ Vet Fak Derg
Volume: 32, Issue: 4, Year: 2026

CONTENTS

Kafkas Universitesi Veteriner Fakultesi Dergisi
Journal Home-Page: http://vetdergikafkas.org
E-ISSN: 1309-2251

Kafkas Univ Vet Fak Derg
Volume: 32, Issue: 4, Year: 2026

CONTENTS

Kafkas Universitesi Veteriner Fakultesi Dergisi
Journal Home-Page: http://vetdergikafkas.org
E-ISSN: 1309-2251

Kafkas Univ Vet Fak Derg
32 (4): 459-473, 2026
DOI: 10.9775/kvfd.2026.36365

Review Article

Perioperative Nociception and Pain in Dogs and Cats - Part II: Nociception Assessment, Therapeutic Strategies and Multimodal Analgesia

Ubedullah KAKA [1 (*)], Muhammad Waseem ASLAM [1,2], Ali SAJID [1], Hui Cheng CHEN [1], Yong Meng GOH [3], Kirk A. MUNOZ [4]

[1] Universiti Putra Malaysia, Faculty of Veterinary Medicine, Department of Companion Animal Medicine & Surgery, 43400, Serdang, MALAYSIA

[2] The Veterinary Referral Centre, Al Murooj Complex, Trade-Centre 2, DIFC, Dubai, UNITED ARAB EMIRATES

[3] Universiti Putra Malaysia, Faculty of Veterinary Medicine, Department of Veterinary Preclinical Sciences, 43400, Serdang, MALAYSIA

[4] The Ohio State University, College of Veterinary Medicine, Department of Veterinary Clinical Sciences, 43210, Columbus, UNITED STATE OF AMERICA

(*) Corresponding author:
Ubedullah Kaka
Phone: +60 3 9769 4284
Cellular phone: +60172037281
Fax: +60 3 8947 1971/1972
E-mail: dr_ubedkaka@upm.edu.my

How to cite this article?

Kaka U, Aslam MW, Sajid A, Chen HC, Goh YM, Munoz KA: Perioperative Nociception and Pain in Dogs and Cats - Part II: Nociception Assessment, Therapeutic Strategies and Multimodal Analgesia. *Kafkas Univ Vet Fak Derg*, 32 (4): 459-473, 2026.
DOI: 10.9775/kvfd.2026.36365

Article ID: KVFD-2026-36365
Received: 06.02.2026
Accepted: 11.05.2026
Published Online: 24.05.2026

Abstract

Optimal perioperative analgesia in dogs and cats depends on the appropriate selection and combination of analgesic agents based on pain mechanisms and accurate pain assessment. Building on the physiological and assessment principles discussed in Part I, this review focuses on therapeutic strategies for perioperative pain management in small animals. Commonly used pharmacological agents, including opioids, non-steroidal anti-inflammatory drugs, local anesthetics, and adjunctive analgesics, are reviewed with respect to their mechanisms of action, clinical applications, and roles in perioperative care. This review is presented in two complementary parts. Part I focuses on pain pathophysiology and assessment, forming the foundation for Part II, which focuses on pharmacological analgesic modalities and the clinical application of pain management strategies ranging from unimodal techniques to pre-emptive and multimodal analgesia, with emphasis on achieving balanced intraoperative and postoperative pain control. The integration of multimodal approaches targeting different components of the nociceptive pathway is highlighted as a cornerstone of modern veterinary anesthesia, aiming to enhance analgesic efficacy while minimizing adverse effects.

Keywords: Cat, Dog, Nociceptive pathways, Pain assessment, Perioperative pain, Sensitization

Introduction

Based on the foundational understanding of pain mechanisms and assessment outlined in Part I, effective perioperative pain management in dogs and cats requires timely, targeted, and multimodal therapeutic interventions. Appropriate analgesic strategies not only mitigate nociceptive input but also attenuate neuroendocrine stress responses, support physiological stability, and promote recovery and patient welfare. This second part of the review focuses on contemporary pharmacological and non-pharmacological approaches to perioperative analgesia, emphasizing multimodal protocols, species-specific considerations, and patient-centered decision-making. By integrating accurate pain assessment with tailored therapeutic strategies, this review aims to provide clinicians with practical guidance to optimize analgesic efficacy, minimize adverse effects, and reduce the risk of pain chronicity and perioperative complications.

Assessment of Nociception

Parasympathetic Tone Activity Index

Parasympathetic tone activity (PTA) has been used as an

objective method to assess nociception intraoperatively [1,2] and postoperatively [3] in dogs. Parasympathetic tone activity (PTA) is an index to assess the nociception/analgesia balance in anaesthetised animals. This is an objective method and is similar to the analgesia nociception index in humans, a validated method for the detection of intraoperative nociception [4]. This index has been derived based on the heart rate variability (HRV) and reflects parasympathetic tone and sympathovagal balance of the patient [1].

A monitor displaying PTA index (PhysioDoloris®; Mdoloris Medical Systems, Lille, France) has been developed and used to assess nociception intraoperatively. This monitor displays an index score from 0 to 100. The lower index values reflect low parasympathetic tone indicating any potential nociception as a result of increased sympathetic tone. While a higher value indicates high parasympathetic tone, reflecting the absence of nociception due to adequate analgesia. This monitor uses ECG signals to assess HRV with low and high frequency variations. Low frequency (LF) ranges from 0.004 to 0.15 Hz, whereas high frequency (HF) range from 0.15 to 0.5 Hz. High frequency reflects predominance of the parasympathetic activity, mainly influenced by respiratory sinus arrhythmia. Low frequency is associated activation of both the sympathetic and parasympathetic systems. Surface ECG is recorded using a 3-lead system. The monitor detects R wave and calculates RR interval from 250 Hz digitized EEG signal. The RR series are filtered in real time using a non-linear artefact removal algorithm preventing artefact-induced inaccurate measurement of these series. After mean centering, RR series are resampled at 8 Hz and normalised using the vectorial norm of the RR series over 64 s for inter subject comparability. The mean centered and normalised RR series are then band pass filtered from 0.15 Hz to 0.5 Hz using a 4 coefficient Daubeuchies wavelet-based filter. This provides RRhf in order to keep only HF variations and display the influence of respiratory sinus arrhythmia in the RR series, which corresponds to the parasympathetic tone of the patient. The amplitude of the normalised and filtered RR series is comprised between 0 and 0.2 (normalised unit). Parasympathetic tone is assessed from the high-frequency component of the RR interval (RRhf). Local maxima and minima of the RRhf signal are identified to construct upper and lower envelopes. The area between these envelopes is calculated within four consecutive 16-second subwindows, yielding areas A1, A2, A3, and A4. The minimum area under the curve (AUCmin) is then determined as the smallest of these four values (AUCmin = min[A1, A2, A3, A4]). This parameter reflects the lowest level of parasympathetic activity observed during the analyzed recording period. [1,2].

The PTA index is then calculated in order to express a fraction of the total window surface, based on formula, PTA = (100 ∗ [α ∗ AUCmin + β]/12.8) ∗ 100/161, where α = 5.1 and β = 1.2 have been determined in order to keep the coherence between the visual effect of respiratory influence on RR series and the quantitative measurement of ANI; 100/12.8 and 100/161 are coefficients determined to obtain PTA values between 0 and 100, with 100/161 being specific for the dog. The PhysioDoloris® monitor continuously displays an average measurement of PTA made over the previous 4 min. Like ANI, PTA values are scored between 0 and 100 [1].

Parasympathetic tone activity index has been reported to be very useful to monitor nociception intraoperatively [2] as well as postoperatively [3] in dogs. Although very few studies have been reported on PTA index for nociception/analgesia balance in dogs, these studies have demonstrated its usefulness in monitoring for analgesia. Future studies are warranted in other species to prove its effectiveness in clinical setup.

Plethysmography Index

Plethysmography or surgical pleth Index (SPI) has been used in humans to detect and anticipate perioperative nociception and antinociception. It is an objective nociception-monitoring device that assesses nociception using photo-plethysmographic signals [5]. Surgical pleth Index detects the degree of nociception during surgery under general anaesthesia with great accuracy, consequently, provides better guidance for administration of various opioids, faster recovery and lower pain scores [5].

The Surgical Pleth Index monitor uses photo-plethysmographic signals of finger arterioles and balances the nociception and antinociception during general anaesthesia. This monitor uses the equation, SPI = 100 – (0.33 × HBI + 0.67 × PPGA), where HBI is the heartbeat interval and PPGA is the photo-plethysmographic waveform amplitude. This monitor requires only a pulse oximeter attached to a finger. The values for the SPI range from 0-100; the lower the values the less nociception there is there is and vice versa. For adequate intraoperative analgesia, recommended values are 20-50 [5].

The additional advantage of SPI is to help predict the intensity of postoperative pain and analgesic requirement, immediately before patient arousal. The values before consciousness toward the end of surgery had close association with pain in the post anaesthesia care unit [6-8]. Lower incidence of delirium was observed in post anaesthesia care unit, after SPI guided analgesia, in elderly patients [9]. However, in children SPI might not be useful due to higher blood vessel distensibility and baseline heart rates than adults, making SPI values less valid in children than in adults [10]. Age is a factor that confounds

the SPI monitoring, since the HBI and PPGA, the main determinants of SPI are directly related to age. Thus, the reference values for heart rate variability for paediatric, young and older age groups vary, for example <20 years vs >60 years. Since vascular elasticity and arterial stiffness vary with age, PPGA depends on vascular wall distensibility and intravascular pulse pressure. Leading to more variation in the values among age groups. In children SP value of <40 has been recommended as a target for adequate intraoperative analgesia [5]. Besides age, a few other factors such as, underlying diseases, different anesthetic and analgesics, may have an impact on SPI results. This warrants further research.

In veterinary medicine, the use of PSI has been reported recently in one study in dogs [11]. These dogs were of ASA class I and II, with testicular tumours, 3 months to 12 years of age and 6 to 50 kg. Acepromazine and methadone were used as premedication. The baseline SPI values were 63-65 in the absence of nociception, higher than SPI values for humans [5]. The authors concluded that analgesics and nociceptive perioperative events caused variation in SPI values. Its ability to predict a hemodynamic reaction was limited by high specificity but low sensitivity. They suggested modification of the algorithm to specifically accommodate for the canine species. The results of this one study in dogs warrant further research for the search of perfect method to assess nociception-antinociception in veterinary species.

Subjective Methods of Pain Scoring

Behaviour

Behavioural response has been recognised as a good indicator of pain in dogs and cats. In general, the behavioural changes to be considered in dogs and cats include response to call, posture (arched back, cornering at one side), vocalisation, aggression, attention to wound, reaction to touch near incision, self-mutilation, interaction with people and ability to walk. It is very important for a clinician to observe the particular animal´s normal behaviour (when not in pain) after admission of the patient at the clinic or hospital and before surgery and use this as a baseline (authors practice) in order to differentiate between the normal and abnormal behaviour (due to pain) of that animal postoperatively to properly treat pain. In addition to general behavioural characteristics, each species exhibits distinct behaviours that are not necessarily applicable to other species, for example cats have been reported to reduce activity, tend to hide and avoid interaction, may perform excessive licking, interfering with their normal grooming, rigid posture and loss of appetite [12,13], especially when cats are alone; however, they mask these behaviours when interacting with other individuals [14]. Dogs show refusal to move, vocalisation, excessive tears, licking and guarding the affected site and, more commonly depression; however, aggression has been reported as well [15,16].

Unidimensional Pain Scales

Assessment of pain and evaluation of the efficacy of analgesics is the major purpose of the pain scoring scales [17]. Various pain scales have been developed and used for pain measurement in veterinary practices, such as, simple descriptive scale, numerical rating scale, and visual analogue scale [17-23]. The principle of all these scales is based on subjective assessment of behaviour, as a consequence, significant interobserver variations in pain scores have been reported [21]. One of the factors for the variation among these scales is lack of clarity of definition for the particular descriptor used. For instance, the same "term" may be interpreted differently by two observers, such as "uncomfortable" [24], "frequent" [23], "responds to calm voice" [23,25]. Similarly, lack of linearity in scores (unequal difference in pain with each increment), inter-observer variability and requirement of more knowledge and skills are the disadvantages of these systems *(https://doi.org/10.5281/zenodo.20612885)*.

Visual Analogue Scale (VAS)

This numerical scale has been described extensively in human practice [26]. However, this is also used in veterinary medicine for postoperative pain measurement [18,19,22,23,25,27]. The VAS consists of a straight 100 mm line starting with 0 as no pain to 100 as worst possible pain. The researcher or observer draws a line intersecting the 100 mm straight line at various intervals, which best describes the estimated level of animal pain. The VAS pain score is then calculated by measuring the distance (in millimeters) between the left end of the line and the intersection. Similarly, VAS can also be used for the sedation score [18,22]. The advantage of VAS is that it is more sensitive and is not labelled to categories. However, lack of linearity in scores (unequal difference in pain with each increment), inter-observer variability and requirement of more knowledge and skills are the disadvantages of the VAS system.

Simple Descriptive Scale

This scale describes different levels of pain intensity with the help of four or five expressions. These expressions are given a number that describes the pain score for that animal. For example, 0 = no pain, 1= mild pain, 2 = moderate pain, and 3 = severe pain [21]. The advantage of this scale is that it is very simple to use. The disadvantages are interobserver variability, which may result in over- or underestimation of pain due to a lack of more pain descriptors [21].

Numerical Rating Scale

This scale works with the same simple descriptive scale principle except that it comprises multiple categories of descriptive definitions for pain behaviours in each category. The observer decides a number which represents the pain score of the animals. Its advantages are easy score tabulation and detailed assessment of the patient due to more categories. Disadvantages include lack of specificity with descriptive pain behaviours. The distribution of the results is not normal, leading to inappropriate statistical analysis [21].

These unidimensional pain scales, despite their limitations, are useful for subjective pain assessment in animals post-operatively and clinical settings. These can be used with other pain scales to improve accuracy.

Multidimensional Pain Scales

The multidimensional pain scales are more advance in a way that, they assess pain more comprehensively than unidimensional pain scales. Unlike unidimensional scales, multidimensional scales assess behavioural and physiological parameters, such as, vocalisation, posture, response to palpation, heart and respiratory rates *(https://doi.org/10.5281/zenodo.20612885)*.

Glasgow Composite Measure Pain Scale

The Glasgow composite measure pain scale has been described as the most validated scale [28], consisting of six behavioural categories with 30 pain descriptors. Based on the intensity of pain, descriptors are ranked numerically. Observer assigns the pain score after selecting the appropriate descriptor in response to the patients' discomfort in each category; sum up of the scores in each category gives the total score. The maximum possible pain score is 24 or 20 if the patient is immobile. It has been shown that the total score of the CMPS-SF is a useful indicator of analgesic requirements. An analgesic intervention has been recommended at 6/24 or 5/20 [29]. The advantage of this scale is that it evaluates multiple aspects for signs of pain in the animal, and does not require any specialized skill or experience to use because the pain descriptors were taken from practicing veterinary surgeons, frequently assessing dogs and cats for acute pain behavior [29]. Each descriptor is well defined to avoid misinterpretation and takes a few minutes to perform. This scale is considered a reliable tool for assessing pain and provides an objective means to quantify pain scores, guiding clinical decision-making during postoperative pain management.

University of Melbourne Pain Scale (UMPS)

The UMPS is a categorized ordinal scale developed by Firth and Haldane [19] in 1999. This system consists of behavioural and physiological parameters, which are divided into six categories: physiological data (heart and respiratory rate), response to palpation, activity, mental status, posture, and vocalization. Each of the categories has been assigned a score for pain. The advantage of this system is that multiple parameters result in better sensibility and accuracy, whereas the disadvantage is the requirement of extensive knowledge of pain demonstration in animals. It can only be used postoperatively and is unable to detect subtle behavioural changes [30].

Colorado Canine and Feline Acute Pain Scale

The Colorado State University Canine and Feline Acute Pain Scales (CSU-CAP and CSU-FAP) are composite pain scales developed at Colorado State University. They incorporate behavioral and psychological indicators, along with responses to wound palpation and body tension, and are influenced by earlier multidimensional pain scales developed at institutions such as the University of Glasgow and the University of Melbourne [32]. The overall numeric pain score is 0 - 4. Patients are scored a quarter per ticked box. A minimum score of 2 or more requires analgesic intervention [31]. The advantages of the CSU pain scale are easy to use, and minimal interpretation is required. The major disadvantage of this scale is the lack of validation by clinical studies [33-36]. In a recent feline study, this scale showed moderate to good inter-rater reliability to assess pain in an ovariohysterectomy model. Although its validity still fell short of current guidelines for correlation coefficients, further refinement is warranted to improve its performance [34].

The UNESP - Botucatu Multidimensional Composite Pain Scale (UNESP - Botucatu MCPS)

This scale encompasses behavioural observations, physiological measurements and intervention levels [36]. This is the first scale that has been validated for post-operative pain in cats [37,38]. Ten items are divided into three subscales. Each scale item is ranked numerically and is assigned a score from 0 to 3. A score of ≥7/30 requires intervention [39]. Drugs such as ketamine and gabapentin, demeanours such as shy, fearful and aggressive behaviours can influence the actual score of the UNESP - Botucatu MCPS and Glasgow composite measure pain scale-feline [40].

Feline Grimace Scale

The Feline Grimace Scale (FGS) was developed and validated as a tool for assessing acute pain in cats. Ear position, head position, muzzle tension, orbital tightening, and whisker change are five action units (AU) identified to record (0-2 for each AU) for this scale. Overall, excellent intra-rater reliability with excellent internal consistency and very strong correlation with another validated instrument for pain assessment have been observed in

cats [41]. Furthermore, a trend is increasing to validate this scale in different pain models. Recently, this scale has been validated reliably in a feline dental extraction model [42].

Since these scoring scales rely on observable behavioral responses and interaction with animals, they are suitable for pain assessment during the postoperative period to evaluate the animal's level of comfort and guide decisions regarding analgesic intervention.

Frontline Drugs Used to Manage Surgical and Non-Surgical Pain

The most effective way of properly addressing postoperative pain would be pre-emptive multimodal analgesia [43-45]. This method involves using different classes of drugs acting on various pain pathways involved in nociception and subsequent central sensitization, thus preventing or blocking changes in the central nervous system. Opioids are often considered a cornerstone in acute analgesia. In addition to that, NSAIDs inhibit cyclooxygenase enzymes *(Fig. 1)*, and have the ability to relieve mild to moderate and even severe pain with relatively longer duration of action and offer a great synergistic action with opioids. As research into the multimodal aspects of pain management in veterinary medicine has evolved, various additional drug classes such as alpha-2 adrenergic agonists [46,47], local anesthetics *(Table 1)* [48–52], and NMDA receptor antagonists *(Table 2)* [53–55] have been reported to be effective. *Table 3* serves as a concise reference summarizing commonly used analgesics, anti-inflammatory drugs, anesthetics, and their reversal agents in dogs and cats, particularly from the perspective of pain management and analgesia [56-58].

Perioperative Pain Management Strategies

Why and How to Control Perioperative Nociception?

Surgery instigates a cascade of inflammatory events in the immune system and subsequent changes in the central nervous system (CNS), leading to peripheral and central sensitization. This sensitization of the CNS leads to the development of a condition known as allodynia (pain due to a stimulus that would not normally provoke pain) and hyperalgesia (increased pain from a stimulus that normally provokes pain) (IASP, 2020) [59]. This is the stage that needs to be addressed properly. If this stage is untreated or improperly managed and the pain is maintained, the changes in the CNS may lead to abnormal processing of nociceptive stimuli, and acute pain may lead to chronic pain [60]. Severe acute pain is strongly associated with the development of chronic pain. Therefore, efforts should be made to adequately manage acute pain [61].

Impact of Postoperative Pain on the Health of Animal: Animal Welfare

Perioperative Nociception and Postoperative Pain: Impact of Perioperative Nociception on Postoperative Pain

It is worthwhile to mention, that a clinician must have knowledge of the events which are taking place during the surgical procedure. As discussed above, it is understood from the established knowledge of the nociception, peripheral and central sensitization (see section 1.6) that these phenomena occur as a result of surgical insult and subsequent continuous surgical manipulation as well as duration of the procedure. This intense surgical injury stimulates the C fibers to fire at a very high frequency and speed [62] resulting in the expression of all the receptors and channels involved in nociception, and if not addressed properly, this can lead to the development of central sensitisation. This also includes recruiting silent nociceptors [62,63], which are normally not involved in the process of pain; this is responsible for the enhanced pain during the postoperative period. Therefore, it is of utmost importance that analgesia be provided continuously throughout the procedure, starting before the surgical incision, continuing during the surgery, and extending into the postoperative period to prevent the development of severe acute pain. This could be done with continuous monitoring of HR, BP and RR intraoperatively, and monitoring of behavioural indicators along with HR, BP and RR postoperatively. The selection of antinociceptive agents and their dosages is based on clinical experience, professional judgment, and the individual patient's physiological status and response at a given time.

Effective management of nociception during the perioperative period can prevent the development of central

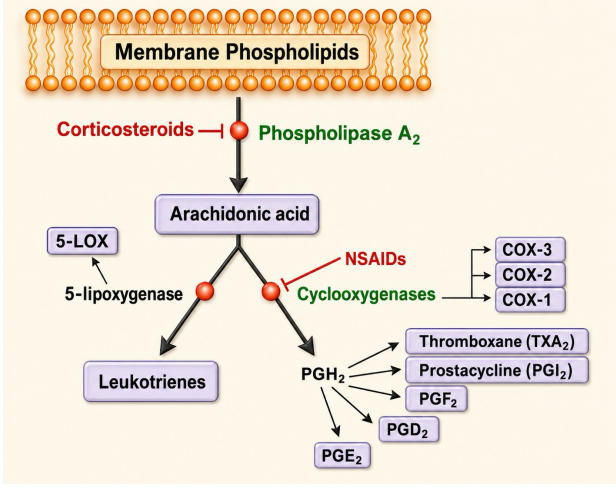

Fig 1. Schematic illustration of NSAIDs' mode of action

Table1. *Summary of various studies on the antinociceptive effects of IV lidocaine in dogs*

Pain Models	Pain Scoring Methods	Dose	Timing	Conclusion	Reference
Intraocular surgery (*)	Categorized Numerical behavioural scale	1) Morphine 0.15 mg/kg IV + 0.1 mg/kg/h CRI, 2) Lidocaine 1 mg/kg IV + 0.025 mg/kg/min CRI, 3) Saline 0.3 ml/kg IV + 0.2 mL/kg/h CRI	15 min pre-surgery until end of anaesthesia	Analgesic effect similar to that of morphine	[49]
Electric Stimulus in conscious dogs	Behavioral reactions	1) Lidocaine 2 mg/kg IV + 10, 25, 50, 75 and 100 µg/kg/min CRI 2) Saline equal volume	CRI for 12 h	No antinociceptive effect of lidocaine compared to saline	[50]
Soft tissue and orthopedic surgery (**)	20% increase in intra-operative HR & BP than previous readings taken as indicators of nociceptive responses due to surgery	1) Lidocaine 2 mg/kg IV + 50 µg/kg/min CRI 2) Saline equal volume	15 min pre-surgery	Inclusion of lidocaine as part of balanced anaesthesia reduced the intraoperative use of opioid compared to saline group	[51]
Ovariectomy (*#)	Categorized numerical behavioral scale	1) Lidocaine 2 mg/kg IV + 50 µg/kg/min CRI + Buprenorphine 0.02 mg/kg IV 2) Lidocaine 2 mg/kg IV + 50 µg/kg/min CRI + Fentanyl 4 µg/kg IV + 8 µg/kg/h CRI 3)Saline + Buprenorphine equal volume/dose 4) Saline + Fentanyl equal volume/dose	Pre-surgery up to skin closure	Systemic lidocaine infusion did not improve the quality of anesthesia. No effect on hemodynamic and respiratory function, peri-operative and post-operative pain relief	[52]
Ovariohysterectomy surgery (*)	Categorized numerical behavioral Scale and plasma cortisol level	1) Lidocaine 1 mg/kg IV + 0.025 mg/kg/min CRI 2) Meloxicam 0.2 mg/kg IV + LRS 10 mL/kg/h CRI 3) Lidocaine + Meloxicam (same dose as above)	5 min pre-surgery until end of anaesthesia	Lidocaine infusion provided similar analgesic effects to meloxicam up to 12 h	[48]

CRI: Continuous rate infusion; IV: Intravenous route; HR: Heart rate; BP: Blood pressure; LRS: Lactated ringer solution; (*): Acepromazine used as premedication, induced with propofol and maintained on isoflurane; (**): Premedication (acepromazine + buprenorphine), induction (propofol + midazolam) and maintenance with isoflurane; (#): premedication (Ketoprofen + diazepam), induction (Diazepam + Ketamine), maintenance with sevoflurane*

Table 2. *Summary of various studies on the antinociceptive effects of IV ketamine in dogs*

Pain Model	Pain Scoring Method	Dose	Timing	Conclusion	Ref.
Electric stimulus	Withdrawal reflexes, electromyography	Ketamine 0.5 mg/kg IV + 10 µg/kg/min CRI	Infused pre-stimulus for 1 h	No effects on withdrawal reflexes	[53]
Mastectomy (*)	French multiparametric scoring scale	1) Morphine 0.1 mg/kg IM + Ketamine 150 µg/kg IV + 2 µg/kg/min LCRI, 2) Morphine 0.1 mg/kg IM + Ketamine 700 µg/kg IV + 10 µg/kg/min HCRI 3) Morphine 0.1 mg/kg IM + Saline 0.09 ml/kg IV followed by 0.5 mL/kg/h CRI	Post-operative for 6 h	No effect of ketamine on postoperative morphine requirement. HCRI improved feed intake at 20th h postextubation	[54]
Forelimb amputation (**)	UMPS	1) Ketamine 0.5 mg/kg IV + 10 µg/kg/min CRI during surgery and 2 µg/kg/min CRI for 18 h after surgery 2) Saline same volume Note: Both groups received fentanyl 1-5 µg/kg/min CRI for the first 18 h post-surgery	Starting from pre-surgery, CRI during and 18 h after surgery	Dogs administered ketamine had lower pain scores at 12 h and 18 h and were more comfortable than control group	[55]

LCRI: Low continuous rate infusion; HCRI: High continuous rate infusion; CRI: Continuous rate infusion; UMPS: University of Melbourne pain scale; IV intravenous route; IM: Intramuscular route; (*): Premedicated with acepromazine and morphine; (**): Premedicated with glycopyrrolate and morphine, induction with propofol and maintained on isoflurane

sensitization; consequently, animals experience improved comfort in the postoperative period compared with those in which intraoperative nociception is inadequately controlled. As a consequence, less frequent dosing would be required during subsequent days of postoperative pain management, ultimately resulting in lower costs and reduced hospital stay.

Table 3. *Commonly used analgesics, anti-inflammatory drugs, and anaesthetics especially from the perspective of pain and analgesia and their reversal agents in dogs and cats*

Drugs	Class	Dose in Dogs	Dose in Cats	Duration of Effect	Reference
Opioids					
Morphine	μ-agonist	0.1-1.0 mg/kg IM, SC 0.1-0.34 mg/kg/h CRI 0.1 mg/kg **Epidural	0.1-0.25 mg/kg IM, SC 0.05-0.1 mg/kg/h CRI	3-4 h	[56-58]
Meperidine (Pethidine)	μ & κ-agonist	2-10 mg/kg IM, SC	2-5 mg/kg IM, SC	1-2 h	[56-58]
Hydromorphone	μ-agonist	0.05 to 0.2 mg/kg IV, IM, SC 0.02-0.04 mg/kg/h CRI	0.1 mg/kg IV, IM, SC 0.02-0.03 mg/kg/h CRI	3-4 h	[56-58]
Oxymorphone	μ-agonist	0.1 mg/kg IV, IM, SC 5-12 μg/kg/h CRI	25-50 μg/kg IV, IM, SC 2.5-5 μg/kg/h CRI	2-4 h	[56-58]
Methadone	μ, κ- and σ-agonist	0.1-0.5mg/kg IV, SC, IM	0.1-0.3 mg/kg IV, SC, IM	3-4 h	[56-58]
Fentanyl	μ-agonist	5-20 μg/kg bolus followed by 3-20 μg/kg/h IV Transdermal: 2.5-5 μg/kg/h DD with selected patch size (25-100 μg/h) according to total body weight, q72h	5-10 μg/kg bolus followed by 2-5 μg/kg/h IV Transdermal: 5.8-10.9 μg/kg/h DD with 25 μg/h patch size for cats ≥2 kg, q120h	0.5-2 h CRI dosing builds up in circulation	[56-58]
Remifentanil	μ-agonist	0.15-0.6 μg/kg/min CRI	0.2-0.4 μg/kg/min CRI	~10 min CRI dosing does NOT build up in circulation	[56-58]
Sufentanil	μ-agonist	3-5 μg/kg bolus followed by 2.6-3.4 μg/kg/h CRI	2-5 μg/kg IV titrated to effect	10-20 min	[56-58]
Alfentanil	μ-agonist	1-5 μg/kg IV followed by 0.5-2.5 μg/kg/min CRI	1 μg/kg IV to effect followed by 1 μg/kg/min CRI	10-20 min	[56-58]
Butorphanol	μ-anatgonist & κ-agonist	0.2-0.4 mg/kg IV, SC, IM	0.2-0.4 mg/kg IV, SC, IM	1-2 h	[56-58]
Buprenorphine	Partial μ-agonist	10-20 μg/kg IV, IM, SC	10-20 μg/kg IV, IM, SC, *OTM	6-8 h	[56-58]
Tramadol	μ-agonist (atypical)	2-4 mg/kg IV, IM, PO	2-4 mg/kg IV, IM, PO	6-12 h	[56-58]
Naloxone	Non-selective, competitive neutral opioid antagonist	0.004-0.04 mg/kg IV, IM, SC	0.005-0.02 mg/kg IV, IM, SC	40 min	[56-58]
Nalmefene	Non-selective, competitive neutral opioid antagonist	0.03 mg/kg IV	0.03 mg/kg IV	8-12 h	[56-58]
Naltrexone	Non-selective, competitive neutral opioid antagonist	0.003-0.1 mg/kg IV, use lowest dose for opioid antagonism and higher dose for reversal of overdose	0.003-0.1 mg/kg IV, q60sec, to effect	12-24 h	[56-58]
Non-steroidal Anti-inflammatory Drugs (NSAIDs)					
Acetaminophen (Paracetamol)	Non-selective COX inhibitor	10-15 mg/kg PO	Contraindicated in cats	8-12 h	[56-58]
Aspirin	Non-selective COX inhibitor	10-25 mg/kg PO q12h 0.5 mg/kg PO q24h for IMHA	10-25 mg/kg PO q48h 81 mg/cat PO q48-72h for TED	12-24 h (dogs) 48-72 h (cats)	[56-58]
Carprofen	Moderately selective COX-2 inhibitor	4 mg/kg PO q24h for 7 days followed by 2 mg/kg PO q24h if needed 4-4.4 mg/kg IV, SC q24h for 3 days followed by 2-2.2 mg/kg q12h if needed	4 mg/kg IV, SC q24h once only	24 h	[56-58]
Deracoxib	Selective COX-2 inhibitor	1-2 mg/kg PO for chronic pain 3-4 mg/kg PO for 7 days followed by 1-2 mg/kg PO for acute pain	1 mg/kg PO	24 h	[56-58]

Table 3. *Continue*

Drugs	Class	Dose in Dogs	Dose in Cats	Duration of Effect	Reference
Etodolac	Selective COX-2 inhibitor	5-15 mg/kg PO	Not used in cats	24 h	[56-58]
Firocoxib	Highly selective COX-2 inhibitor	5 mg/kg PO (Puppies <7 months age is very sensitive to >5 mg/kg dose)	1.5 mg/kg PO	24 h	[56-58]
Ketoprofen	Non-selective COX inhibitor	1-2 mg/kg IV, SC, IM for 3 days 1 mg/kg PO for 5 days 0.25 mg/kg PO for 30 days	1-2 mg/kg IV, IM, SC for 3 days 1 mg/kg PO up to 5 days	24 h	[56-58]
Mavacoxib	Selective COX-2 inhibitor	2 mg/kg PO q14d for first 2 doses then q1month for a total of maximum 7 doses	Not used in cats	2-4 weeks For dogs 12 month of age or older	[56-58]
Meloxicam	Preferential COX-2 inhibitor in dogs and cats	0.2 mg/kg IV, SC, PO once followed by 0.1 mg/kg IV, SC, PO	0.1-0.2 mg/kg IV, SC, PO once followed by 0.05 mg/kg PO up to 5 days	24 h	[56-58]
Nimesulide	Selective COX-2 inhibitor	5 mg/kg PO up to 5 days	Not used in cats	24 h	[56-58]
Piroxicam	Non-selective COX inhibitor	0.3 mg/kg PO q24h first 2 doses then q48h	1 mg/cat PO q24h for maximum 7 days	24-48 h	[56-58]
Robenacoxib	Highly selective COX-2 inhibitor	1-2 mg/kg PO 2 mg/kg SC maximum 2 doses	1 mg/kg PO maximum 3-6 days 2 mg/kg SC maximum 2 doses	24 h	[56-58]
Tepoxalin	Non-selective COX and LOX inhibitor	10-20 mg/kg PO on day one followed by 10mg/kg PO	Not used in cats	24 h	[56-58]
Tolfenamic acid	Non-selective COX inhibitor	4 mg/kg IM, SC q24h x two treatments 4 mg/kg PO q24h for 4 days a week and 3 days off (can be repeated on weekly basis)	4 mg/kg SC q24h x two treatments 4 mg/kg PO q24h for 3 days (cannot be repeated on weekly basis)	24 h	[56-58]
Alpha-2 adrenergic agonists and their reversal agents					
#Medetomidine	α_2 adrenergic agonist	10-30 µg/kg IM, IV, SC (light sedation) 30-80 µg/kg IM, IV, SC (moderate to deep sedation and analgesia) 2-4 µg/kg CRI (perioperative analgesia particularly as an adjunct to opioid)	100-150 µg/kg IM, SC (deep sedation) 50-100 µg/kg IM, SC (Moderate sedation) 40-80 µg/kg IM (sedation and analgesia) 10-40 µg/kg IV (sedation and analgesia) CRI same as dog for perioperative analgesia 10 µg/kg epidurally (epidural analgesic)	Duration of analgesia is almost 1 h at the dose rate of 10 µg/kg. Better analgesia achieved when combined with opioids	[56-58]
Dexmedetomidine	α_2 adrenergic agonist	2-20 µg/kg IM, IV for sedation and analgesia Perioperative analgesia and rousable sedation 1-2 µg/kg/h CRI	20-40 µg/kg IM, IV for sedation and analgesia Perioperative analgesia and rousable sedation 1-2 µg/kg/h CRI	Duration of analgesia is almost 1 h at the dose rate of 5 µg/kg. Better analgesia achieved when combined with opioids	[56-58]
Xylazine	α_2 adrenergic agonist	1.1 mg/kg IV (Sedation, analgesia, preanesthetic) 2.2 mg/kg IM (Sedation, analgesia, preanesthetic)	1.1 mg/kg IV (Sedation, analgesia, preanesthetic) 2.2 mg/kg IM (Sedation, analgesia, preanesthetic)	~30 min (analgesia) 1-2 h sedative effect	[56-58]
Atipamezole	Selective α_2 adrenergic antagonist	0.1-0.3 mg/kg IM	Same as dogs	Rapid effect: onset of arousal occurs within 5-10 min of IM injection	[56-58]

Table 3. Continue

Drugs	Class	Dose in Dogs	Dose in Cats	Duration of Effect	Reference
Yohimbine	Selective α_2 adrenergic antagonist	0.1-0.2 mg/kg IV, IM (start at low dose, titrate up if needed)	Same as dogs	Reversal of xylazine within 1-3 min of IV injection	[56-58]
Naloxone	Non-selective, competitive neutral opioid antagonist	0.02 mg/kg IM, IV (in severely hypotensive or comatose patients if specific alpha-2 antagonist is not available)	Same as dogs	40 min; Onset of action is within 1-2 min of IV and 2-5 min of IM or SC administration	[56-58]
Miscellaneous					
Gabapentin	Alpha-2- delta subunit of voltage gated calcium channels blocker	10-20 mg/kg PO q8h Cancer pain: 10-20 mg/kg PO q12-24h	5 mg/kg PO q24h Ramp up or taper to effect (range 5-20 mg/kg) Cancer pain: 2-10 mg/kg PO q12-24h	8-24 h in dogs 12-24 h in cats	[56-58]
Amantadine	NMDA-antagonist	3-5 mg/kg PO q12-24h	2-5 mg/kg PO q24h	24 h	[56-58]
Ketamine	NMDA-antagonist	0.25-0.5 mg/kg loading dose followed by 0.01 mg/kg/min CRI intraoperative or 0.002-0.005 mg/kg/min CRI postoperatively	Doses are same as dogs	Dogs: 15±8 min Cats: 20-40 min	[56-58]
Lidocaine	Sodium channel blocker	1 mg/kg loading dose (very slow IV) followed by 0.02-0.04 mg/kg/min CRI intraoperative and postoperatively if needed. Beware of drug accumulation	Avoid lidocaine for analgesia in cats due to the risk of drug accumulation	Systemic lidocaine is best used in combination with other analgesics drugs to achieve balanced analgesia	[56-58]

*Note: Use of some drugs may be considered "off label". Approval of use varies country to country. IV: Intravenous route; IM: Intramuscular route; SC: subcutaneous route; CRI: Continuous rate infusion; OTM: Oral transmucosal route; PO: per os or by mouth; DD: Delivered dose; ¨Preparation should be preservative free; IMHA: Immune-mediated haemolytic anaemia; TED: Thromboembolic disease; *indicates maximal effect obtained in 15 to 20 minutes; COX: Cyclooxygenase; LOX: lipoxygenase*

Pre-Emptive and Preventive Analgesia

The idea to prevent or "pre-empt" pain was introduced by Crile [64]; he blocked the regional nerves along with general anaesthesia. With increasing knowledge of the subject of pain, it can be considered that there are several factors that play a role in the development of central sensitization during the pre-, intra- and post-operative (peri-operative) periods. However, the extent to which each period contributes to central sensitization is not yet clear [60]. Pre-emptive analgesia has been defined as "administration of antinociceptive agent that inhibit setting up central sensitisation of the CNS" [45]. Although the terms "preventive" and "pre-emptive" are frequently used interchangeably, they represent distinct concepts. Pre-emptive analgesia refers to the administration of analgesic interventions prior to the onset of the surgical stimulus [41,65,66]. In contrast, preventive analgesia is not limited by timing relative to surgical incision and instead involves the use of analgesic interventions throughout the perioperative period, including preoperative, intra-operative, and postoperative phases [66].

Timing of Administration of Analgesics

A thorough understanding of drug pharmacokinetics is crucial for achieving effective analgesia. Factors including the onset of action, duration of effect, plasma concentration, and their relationship to the duration of the surgical procedure must be carefully considered. For example,

1. An intravenous fentanyl bolus administered 30 min prior to the start of surgery is generally inadequate for preoperative antinociceptive management, given its relatively short duration of action of about 20 min [67]. Consequently, its effects may dissipate before the onset of surgical stimulation. Furthermore, administration of a single fentanyl bolus during an orthopaedic procedure of 2-3 h duration is insufficient to provide continuous nociceptive control for optimal pain management.
2. The peak plasma concentration of commonly used NSAIDs following subcutaneous administration occurs within 0.5 to 2.4 h [68,69]. Likewise, buprenorphine has an onset of action of approximately 30-45 min [61]. Consequently, if surgical stimulation occurs during this interval, pre-emptive analgesia may not be achieved. This supports Woolf's assertion [70] that the timing of analgesic administration is a critical determinant of effective postoperative pain management.

The concept of pre-emptive analgesia was taken from

the strategy that post-operative abnormal sensibility could be prevented by reducing the stimulation of central neurons by the bombardment of afferent activity during surgery by pre- or intra-operative analgesic(s) administration [43]. Therefore, once central sensitization has developed, it cannot be reduced immediately [71]; hence, the traditional method of post-operative analgesic administration may not be sufficient to control pain, and high doses of the drugs would be required to counteract this phenomenon [72]. Thus, the evidence suggests that the timing of the administration of analgesia is the crucial factor for successful postoperative pain control [73].

Multimodal Analgesia

In multimodal analgesia, two or more analgesic agents that act on different pain pathways and neurotransmitter systems are used in combination to prevent nociception and reduce hyperalgesia *(Table 4, Table 5)* [74-77,79]. Since postoperative pain is the result of five major steps of nociception, transduction, transmission, modulation, projection and perception [83], it would not be possible to obtain the optimum analgesia with a single drug or method without potential side effects [73,83]. The rationale of multimodal analgesia should therefore be to prevent transduction and transmission at the periphery by agents acting on sodium channels, preventing nociceptive activity at the level of the dorsal horn of the spinal cord, such as opioids, and preventing central sensitization by inhibition of NMDA receptors through the use of NMDA antagonists. Thus, optimizing analgesic management during the acute phase is essential for improving patient comfort and reducing the risk of chronic pain development *(Fig. 2)* [49].

Pre-Emptive Multimodal Analgesia

"Pre-emptive multimodal analgesia" is the administration of multimodal analgesic therapy before surgical stimulation. An effective pre-emptive multimodal analgesia may raise the nociceptive threshold and decrease or block stimulation of nociceptors [45]. Pre-emptive multimodal analgesia is thought to be more efficient in treating post-operative pain than traditional unimodal (single drug) analgesia because of its enhanced efficacy, potential for drug synergism, decreased drug-related side effects [43], and decreased amount of inhalant anaesthetic required for maintaining general anaesthesia, thus minimizing cardiorespiratory depression [43,78]. The synergism between alpha-2-agonists and opioids [84] and NSAIDs and opioids has been reported in dogs [22,85]. Dose and the side effects (e.g., nausea, vomiting, sedation, respiratory depression, urinary retention, constipation and pruritus) can be minimized by using a non-opioid adjunct [44,86].

Although there are positive results of multimodal analgesia from the available literature, some studies have failed to observe the beneficial effects of multimodal analgesia compared with conventional unimodal analgesia [44,87]. This may be due to the small sample size and insensitive pain assessment tools.

The benefits of pre-emptive multimodal analgesia have been well established in human medicine. The trend in veterinary medicine has also increased recently and research has been carried out. However, there is an increase in the trend of investigation of various combinations for the purpose of optimum pain management. So far, an ideal, free of side effects protocol for postoperative pain management is not available. The availability of various analgesic agents

Table 4. *Summary of the studies conducted in dogs using various pre-emptive analgesic agents*

Model of Pain	Drug/Dose	Timing	Conclusion	Reference
Ovariohysterectomy surgery	Pethidine 5 mg/kg IM; Saline control	Pre versus post-operative	Preoperative pethidine group showed significantly lower pain scores than other two groups.	[74]
Ovariohysterectomy surgery	Carprofen 4mg/kg SC; Saline control	Pre versus post-operative	Greater analgesic effect was shown by carprofen given preoperatively than given postoperatively.	[75]
Tibial fracture surgery	Epidural 2% lidocaine 4 mg/kg, ketamine 3 mg/kg and saline (for control group)	Pre-operative	Higher wound swelling and hyperalgesia in saline group compared with lidocaine and ketamine group. Ketamine group had less wound hyperalgesia and swelling than lidocaine group	[79]
Ovariohysterectomy surgery	Pre ketamine 2.5 mg/kg IM; Post ketamine 2.5 mg/kg IM; Saline 0.025ml/kg	Pre versus post-operative	Saline group had significant hyperalgesia and required more rescue analgesia, while pre-surgery ketamine treatment was more beneficial than post-surgery treatment	[76]
Tibial fracture surgery	Epidural pethidine 2 mg/kg, ketamine 3 mg/kg and saline (for control group)	Pre-operative	Less wound swelling, hyperalgesia, pain and early weight bearing in ketamine compared with pethidine group	[77]

IM: Intramuscular route; SC: subcutaneous route

Table 5. *Summary of the studies using multimodal analgesic therapy for pain management*

Model of Pain	Drug/Dose	Conclusion	Reference
Ovariohysterectomy surgery	Pethidine alone; Carprofen alone; Pethidine + Carprofen	Combination of carprofen and pethidine provided good postoperative analgesia than pethidine alone	[18]
Toe pinching response	Medetomidine 20 µg/kg IV; Medetomidine + Hydromorphone 20 µg/kg + 0.1 mg/kg IV; Medetomidine + Butorphanol 20 µg/kg + 0.2 mg/kg IV	Combination of medetomidine with hydromorphone and butorphanol resulted in better analgesia but longer sedation and had cardiopulmonary effects compared with medetomidine alone	[46]
Ovariohysterectomy surgery	Epidural ketamine 1 mg/kg; Ketamine + Morphine 0.5 mg/kg + 0.05 mg/kg; Ketamine + Morphine 1 mg/kg + 0.025 mg/kg	All 3 groups provided adequate analgesia up to 8h. Combining morphine with ketamine did not improve the analgesic effects of ketamine	[87]
Elective orthopedic surgery of pelvic limb	Epidural morphine + bupivacaine 0.2 mg/kg + 1 mg/kg; Morphine 0.2 mg/kg alone; Saline 0.21 mL/kg	Morphine-bupivacaine combination induced better analgesia than morphine alone	[88]
Ovariohysterectomy surgery	Buprenorphine 0.02 mg/kg IM; Carprofen 4 mg/kg SC; Buprenorphine + Carprofen	Wound swelling and pain scores in buprenorphine + carprofen group were lower to buprenorphine alone at 6 h	[22]
Ovariohysterectomy surgery	Epidural morphine 0.1 mg/kg alone; Neostigmine 10 µg/kg alone; Morphine + Neostigmine 0.l mg + 10 µg/kg; Saline control	Adding neostigmine to epidurally administered morphine did not potentiate opioid-induced analgesia	[89]
Orchiectomy	Epidural lidocaine + tramadol 6 mg/kg + 1 mg/kg; Lidocaine + Morphine 6 mg/kg + 0.1 mg/kg; Lidocaine + Saline 6mg/kg + 0.01 mL/kg	Both combinations provided better analgesia for initial 12h compared to lidocaine alone	[80]
Deep pin prick into skin and muscles of thorax and forelimbs	Epidural lidocaine 3.8 mg/kg alone; Ketamine 3 mg/kg alone; Lidocaine + Ketamine	Ketamine provided analgesia for 30 min, lidocaine for 40 min and combination of Ketamine and lidocaine up to 90 min	[81]
Ovariohysterectomy surgery	IV bolus followed by CRI throughout anesthesia, then a CRI at a decreased dose for a further 4 h for all groups. Control group was butorphanol 0.4 mg/kg and infusion rate of 0.9% saline was 2 mL/kg/h. Test groups were: Fentanyl 5 µg/kg, 10 µg/kg/h, then 2.5 µg/kg/h; Ketamine 1 mg/kg, 40 µg/kg/min, then 10 µg/kg/min; Lidocaine 2 mg/kg, 100 µg/kg/min, then 25 µg/kg/min; Dexmedetomidine 1 µg/kg, 3 µg/kg/h, then 1 µg/kg/h; Combination of LKD at the afore mentioned doses	Fentanyl and combination of LKD resulted in adequate postoperative analgesia. Lidocaine, butorphanol, ketamine and dexmedetomidine alone were not effective for treatment of postoperative pain	[47]
Ovariohysterectomy surgery	Both groups received intravenous tramadol 4 mg/kg body weight as premedication. Immediately after induction, the KLT group received ketamine and lidocaine at 0.5 and 2 mg/kg loading dose, followed by continuous rate infusion of 50 and 100 µg/kg/min, respectively, for 2 h. Dogs in T group received saline bolus and continuous rate infusion at equi-volume	Addition of pre-emptive ketamine-lidocaine infusion to single intravenous dose of tramadol enhanced attenuation of central sensitization and improved intra- and postoperative analgesia	[82]

IV: Intravenous route; IM: Intramuscular route; SC: subcutaneous route; CRI: Continuous rate infusion; LKD: Lidocaine + Ketamine + Dexmedetomidine;KLT: Ketamine + Lidocaine + Tramadol

provides an opportunity to evaluate their use within pre-emptive multimodal analgesia approaches to identify the most suitable protocols with minimal side effects.

On the other hand, there are some factors that can be considered when comparing the results of multimodal analgesia with unimodal analgesia:

a) Use of opioids as pre-medication or as part of general anaesthesia in the control groups may mask pain scores and affect the results [88,89].

b) Testing pre- and post-operative analgesia during various trials, when comparing the tested drug with saline as a control, does not consider that

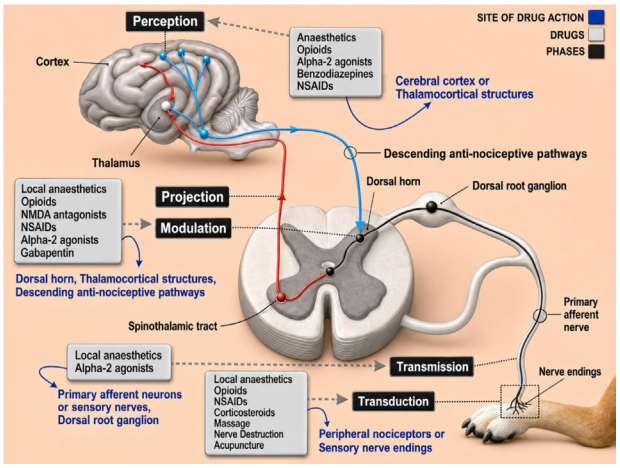

Fig 2. Illustrative summary of the drugs according to their anatomical site of action and phases of pain pathway

the comparison results are not positive. However, comparing the same drug in the pre- and post-injury or stimulus groups is ideal [45,46].

c) Selection of the analgesic agent should depend on the type and severity of the surgery, and it should cover the time from starting before surgery until the last suture is placed [89].

d) The choice of the dose, route and type of analgesic agent are also important factors to be considered to achieve successful analgesia without side effects [89].

The selection of drugs for pre-emptive multimodal analgesia should be based on their efficacy, ease of administration, cost-effectiveness, and additional benefits associated with clinical outcomes [90]. The choice of drug, dosage, and route of administration should be tailored to the type of surgery to achieve maximum benefit.

Successful Pre-Emptive Multimodal Analgesia

Irrespective of the outcomes of the clinical and experimental studies discussed above, a comprehensive understanding of the molecular mechanisms of nociceptive pathways is fundamental to the effective application of pre-emptive multimodal analgesia. This strategy targets multiple stages of nociception, including transduction, transmission, modulation, projection, and perception.

Agents such as lidocaine (sodium channel blockade), opioids (opioid receptor agonism), and ketamine (NMDA receptor antagonism), along with NSAIDs and alpha-2 adrenergic agonists, act at different sites within the nociceptive pathway and constitute effective components of multimodal pain management *(Table 3, Table 4, Table 5)* [18,22,46,47,56-58,74-77,79-82,87-91]. Moreover, continuous administration of antinociceptive agents during the postoperative period is essential and should be maintained until adequate pain control is achieved [47]. Agents with a short duration of action may be administered as a CRI to maintain therapeutic plasma concentrations and ensure consistent antinociceptive effects, such as ketamine, lidocaine, and fentanyl CRIs [47].

Conclusion

Since animals can not communicate verbally, objective evaluation of pain is a major challenge in the assessment of pain for both clinicians and researchers. Pain assessing scales such as feline grimace scale, Glasgow pan scale, UNESP - Botucatu MCPS, and VAS along with algometer offer a useful option and can be successfully used for post operative pain measurement and pain management.

Pre-emptive multimodal analgesia works on the principles of using more than one drug, with various modes of action, acting on different pathways. Thus, the rationale of pre-emptive multimodal analgesia should be targeting transduction, transmission, modulation, projection and perception. To date, there is no single ideal protocol, free of side effects; therefore, drugs acting on sodium channels, NMDA, COX and opioid receptors can be good options to be used to provide multimodal analgesia. In recent years, gabapentin and pregabalin have emerged as agents which may open new avenues for research into their role in pain management protocols. However, further studies are warranted to fully evaluate their efficacy and safety in veterinary medicine.

Declarations

Availability of Data and Materials: All the data generated are included in the manuscript

Acknowledgements: The authors are grateful to Universiti Putra Malaysia for funding this project (GP-IPM/2020/9684 100).

Competing of Interest: The authors declared that there is no competing of interests.

Declaration of Generative Artificial Intelligence (AI): The article and/or tables and figures were not written/created by AI and AI assisted technologies.

Author Contributions: YMG and UK contributed to the conceptualisation and methodology of the study .UK, MWA and AS were responsible for data extraction and editing. The original draft of manuscript was written by UK. YMG and CHC validated the extracted data and tables. KAM provided academic advice and critical revision UK, MWA and AS revised and finalised the manuscript. All authors read and approved the final version.

References

1. **Mansour C, Merlin T, Bonnet-Garin JM, Chaaya R, Mocci R, Ruiz CC, Junot S:** Evaluation of the Parasympathetic Tone Activity (PTA) index to assess the analgesia/nociception balance in anaesthetised dogs. *Res Vet Sci,* 115, 271-277, 2017. DOI: 10.1016/j.rvsc.2017.06.022

2. **Mansour C, El Hachem N, Jamous P, Saade G, Boselli E, Allaouchiche B, Bonnet JM, Junot S, Chaaya R:** Performance of the Parasympathetic Tone Activity (PTA) index to assess the intraoperative nociception

using different premedication drugs in anaesthetised dogs. *Int J Vet Sci Med,* 8 (1): 49-55, 2020. DOI: 10.1080/23144599.2020.1783090

3. **Hernández-Avalos I, Valverde A, Ibancovichi-Camarillo JA, Sánchez-Aparicio P, Recillas-Morales S, Rodríguez-Velázquez D, Acevedo-Arcique CM:** Clinical use of the parasympathetic tone activity index as a measurement of postoperative analgesia in dogs undergoing ovariohysterectomy. *J Vet Res,* 65 (1): 117-123, 2021. DOI: 10.2478/jvetres-2021-0020
4. **Boselli E, Bouvet L, Bégou G, Torkmani S, Allaouchiche B:** Prediction of hemodynamic reactivity during total intravenous anesthesia for suspension laryngoscopy using Analgesia/Nociception Index (ANI): A prospective observational study. *Minerva Anestesiol,* 81, 288-297, 2015.
5. **Oh SK, Won YJ, Lim BG:** Surgical pleth index monitoring in perioperative pain management: Usefulness and limitations. *Korean J Anesthesiol,* 77 (1): 31-45, 2024. DOI: 10.4097/kja.23158
6. **Ledowski T, Sommerfield D, Slevin L, Conrad J, von Ungern-Sternberg BS:** Surgical pleth index: Prediction of postoperative pain in children? *Br J Anaesth,* 119, 979-983, 2017. DOI: 10.1093/bja/aex300
7. **Park M, Kim BJ, Kim GS:** Prediction of postoperative pain and analgesic requirements using surgical pleth index: An observational study. *J Clin Monit Comput,* 34, 583-587, 2020. DOI: 10.1007/s10877-019-00338-4
8. **Hung KC, Huang YT, Kuo JR, Hsu CW, Yew M, Chen JY, Sun CK:** Elevated surgical pleth index at the end of surgery is associated with postoperative moderate-to-severe pain: A systematic review and meta-analysis. *Diagnostics,* 12 (9):2167, 2022. DOI: 10.3390/diagnostics12092167
9. **Won YJ, Oh SK, Lim BG, Kim YS, Lee DY, Lee JH:** Effect of surgical pleth index-guided remifentanil administration on perioperative outcomes in elderly patients: A prospective randomized controlled trial. *BMC Anesthesiol,* 23:57, 2023. DOI: 10.1186/s12871-023-02011-5
10. **Lim BG:** Nociception monitoring tools using autonomic tone changes for intraoperative analgesic guidance in pediatric patients. *Anesth Pain Med,* 14 (4): 380-392, 2019. DOI: 10.17085/apm.2019.14.4.380
11. **Gavet M, Cardinali M, Bernady A, Ruiz CC, Allaouchiche B, Junot S:** Evaluation of the Surgical Pleth Index (SPI) for the monitoring of the nociception-antinociception balance in dogs undergoing castration: A prospective clinical trial. *Res Vet Sci,* 171:105320, 2024. DOI: 10.1016/j.rvsc.2024.105320
12. **Reid J, Nolan AM, Scott EM:** Measuring pain in dogs and cats using structured behavioural observation. *Vet J,* 236:72-79, 2018. DOI: 10.1016/j.tvjl.2018.04.013
13. **Brondani JT, Luna SP, Padovani CR:** Refinement and initial validation of a multidimensional composite scale for use in assessing acute postoperative pain in cats. *Am J Vet Res,* 72, 174-183, 2011. DOI: 10.2460/ajvr.72.2.174
14. **Brondani JT, Mama KR, Luna SP, Wright BD, Niyom S, Ambrosio J, Vogel PR, Padovani CR:** Validation of the English version of the UNESP-Botucatu multidimensional composite pain scale for assessing postoperative pain in cats. *BMC Vet Res,* 9:143, 2013. DOI: 10.1186/1746-6148-9-143
15. **Franzini de Souza CC, Dias DPM, Souza RN, Salgado BS, Carreira L, Molento CFM:** Use of behavioural and physiological responses for scoring sound sensitivity in dogs. *PLoS One,* 13:e0200618, 2018. DOI: 10.1371/journal.pone.0200618
16. **Landa L:** Pain in domestic animals and how to assess it: A review. *Vet Med (Praha),* 57, 185-192, 2012. DOI: 10.17221/5915-VETMED
17. **Mathews KA:** Pain assessment and general approach to management. *Vet Clin North Am Small Anim Pract,* 30, 729-755, 2000. DOI: 10.1016/S0195-5616(08)70004-4
18. **Lascelles BD, Butterworth S, Waterman AE:** Postoperative analgesic and sedative effects of carprofen and pethidine in dogs. *Vet Rec,* 134, 187-191, 1994.
19. **Firth AM, Haldane SL:** Development of a scale to evaluate postoperative pain in dogs. *J Am Vet Med Assoc,* 214, 651-659, 1999. DOI: 10.2460/javma.1999.214.05.651
20. **Slingsby LS, Taylor PM, Waterman-Pearson AE:** Effects of two doses of buprenorphine four or six hours apart on nociceptive thresholds, pain and sedation in dogs after castration. *Vet Rec,* 159, 705-711, 2006. DOI: 10.1136/vr.159.21.705
21. **Holton LL, Scott EM, Nolan AM, Reid J, Welsh E, Flaherty D:** Comparison of three methods used for assessment of pain in dogs. *J Am Vet Med Assoc,* 212, 61-66, 1998.DOI: 10.2460/javma.1998.212.01.61
22. **Shih AC, Robertson S, Isaza N, Pablo L, Davies W:** Comparison between analgesic effects of buprenorphine, carprofen, and buprenorphine with carprofen for canine ovariohysterectomy. *Vet Anaesth Analg,* 35, 69-79, 2008. DOI: 10.1111/j.1467-2995.2007.00352.x
23. **Conzemius MG, Hill CM, Sammarco JL, Perkowski SZ:** Correlation between subjective and objective measures used to determine severity of postoperative pain in dogs. *J Am Vet Med Assoc,* 210, 1619-1622, 1997. DOI: 10.2460/javma.1997.210.11.1619
24. **Vesal N, Cribb PH, Frketic M:** Postoperative analgesic and cardiopulmonary effects in dogs of oxymorphone administered epidurally and intramuscularly, and medetomidine administered epidurally: A comparative clinical study. *Vet Surg,* 25, 361-369, 1996. DOI: 10.1111/j.1532-950X.1996.tb01428.x
25. **Grisneaux E, Pibarot P, Dupuis J, Blais D:** Comparison of ketoprofen and carprofen administered prior to orthopedic surgery for control of postoperative pain in dogs. *J Am Vet Med Assoc,* 215, 1105-1110, 1999.
26. **McQuay HJ, Moore RA:** Methods of therapeutic trials. **In,** Wall PD, Melzack R (Eds): Textbook of Pain. 4th ed., 1125-1138, Churchill Livingstone, Edinburgh, 1999.
27. **Budsberg SC, Cross AR, Quandt JE, Pablo LS, Runk AR:** Evaluation of intravenous administration of meloxicam for perioperative pain management following stifle joint surgery in dogs. *Am J Vet Res,* 63, 1557-1563, 2002. DOI: 10.2460/ajvr.2002.63.1557
28. **Holton L, Pawson P, Nolan A, Reid J, Scott EM:** Development of a behaviour-based scale to measure acute pain in dogs. *Vet Rec,* 148, 525-531, 2001. DOI: 10.1136/vr.148.17.525
29. **Reid J, Nolan A, Hughes JML, Lascelles D, Pawson P, Scott EM:** Development of the short-form Glasgow Composite Measure Pain Scale (CMPS-SF) and derivation of an analgesic intervention score. *Anim Welf,* 16 (S): 97-104, 2007. DOI: 10.1017/s096272860003178x
30. **Mich PM, Hellyer P:** Objective, categoric methods for assessing pain and analgesia. **In,** Gaynor JS, Muir WW (Eds): Handbook of Veterinary Pain Management. 2nd ed., 78-109, Mosby, St. Louis, 2008.
31. **Hellyer PW, Uhrig SR, Robinson NG:** Canine acute pain scale and feline acute pain scale. Colorado State University-CSU Veterinary Medical Center, 2006.
32. **Beilin B, Bessler H, Mayburd E, Smirnov G, Dekel A, Yardeni I, Shavit Y:** Effects of preemptive analgesia on pain and cytokine production in the postoperative period. *Anesthesiology,* 98, 151-155, 2003. DOI: 10.1097/00000542-200301000-00024
33. **Han ZA, Song DH, Oh HM, Chung ME:** Botulinum toxin type A for neuropathic pain in patients with spinal cord injury. *Ann Neurol,* 79, 569-578, 2016. DOI: 10.1002/ana.24609
34. **Shipley H, Guedes A, Graham L, Goudie-DeAngelis E, Wendt-Hornickle E:** Preliminary appraisal of the reliability and validity of the Colorado State University Feline Acute Pain Scale. *J Feline Med Surg,* 21, 335-339, 2019. DOI: 10.1177/1098612X18777506
35. **Mich PM, Hellyer PW, Kogan L, Schoenfeld-Tacher R:** Effects of a pilot training program on veterinary students' pain knowledge, attitude, and assessment skills. *J Vet Med Educ,* 37, 358-368, 2010. DOI: 10.3138/jvme.37.4.358
36. **Reid J, Nolan AM, Scott EM:** Measuring pain in dogs and cats using structured behavioural observation. *Vet J,* 236, 72-79, 2018. DOI: 10.1016/j.tvjl.2018.04.013
37. **Brondani JT, Luna SPL, Padovani CR:** Refinement and initial validation of a multidimensional composite scale for use in assessing acute postoperative pain in cats. *Am J Vet Res,* 72, 174-183, 2011. DOI: 10.2460/ajvr.72.2.174

38. **Brondani JT, Mama KR, Luna SPL, Wright BD, Niyom S, Ambrosio J, Vogel PR, Padovani CR:** Validation of the English version of the UNESP-Botucatu multidimensional composite pain scale for assessing postoperative pain in cats. *BMC Vet Res,* 9:143, 2013. DOI: 10.1186/1746-6148-9-143

39. **Della Rocca G, Catanzaro A, Conti MB, Bufalari A, De Monte V, Di Salvo A, Minicucci L, Lacava G, Vignoli M:** Validation of the Italian version of the UNESP-Botucatu multidimensional composite pain scale for the assessment of postoperative pain in cats. *Vet Ital,* 54, 49-61, 2018. DOI: 10.12834/VetIt.567.2704.2

40. **Steagall PV, Monteiro BP:** Acute pain in cats: Recent advances in clinical assessment. *J Feline Med Surg,* 21, 25-34, 2019. DOI: 10.1177/1098612X18808103

41. **Evangelista MC, Watanabe R, Leung VSY, Monteiro BP, O'Toole E, Pang DSJ, Steagall PV:** Facial expressions of pain in cats: The development and validation of a Feline Grimace Scale. *Sci Rep,* 9:19128, 2019. DOI: 10.1038/s41598-019-55693-8

42. **Watanabe R, Doodnaught GM, Evangelista MC, Monteiro BP, Ruel HLM, Steagall PV:** Inter-rater reliability of the Feline Grimace Scale in cats undergoing dental extractions. *Front Vet Sci,* 7:302, 2020. DOI: 10.3389/fvets.2020.00302

43. **Woolf CJ, Chong MS:** Preemptive analgesia-treating postoperative pain by preventing the establishment of central sensitization. *Anesth Analg,* 77, 362-379, 1993. DOI: 10.1213/00000539-199377020-00026

44. **Guignard B, Bossard AE, Coste C, Sessler DI, Lebrault C, Alfonsi P, Fletcher D:** Acute opioid tolerance: Intraoperative remifentanil increases postoperative pain and morphine requirement. *Anesthesiology,* 93, 409-417, 2000. DOI: 10.1097/00000542-200008000-00019

45. **Kelly DJ, Ahmad M, Brull SJ:** Preemptive analgesia II: Recent advances and current trends. *Can J Anesth,* 48, 1091-1101, 2001. DOI: 10.1007/BF03020375

46. **Kuo WC, Keegan RD:** Comparative cardiovascular, analgesic, and sedative effects of medetomidine, medetomidine-hydromorphone, and medetomidine-butorphanol in dogs. *Am J Vet Res,* 65, 931-937, 2004. DOI: 10.2460/ajvr.2004.65.931

47. **Gutierrez-Blanco E, Victoria-Mora JM, Ibancovichi-Camarillo JA, Sauri-Arceo CH, Bolio-González ME, Acevedo-Arcique CM, Moles-Mora M, Rodríguez-Vivas RI:** Postoperative analgesic effects of either a constant rate infusion of fentanyl, lidocaine, ketamine, dexmedetomidine, or the combination lidocaine-ketamine-dexmedetomidine after ovariohysterectomy in dogs. *Vet Anaesth Analg,* 42, 309-318, 2015. DOI: 10.1111/vaa.12215

48. **Tsai TY, Chang SK, Chou PY, Yeh LS:** Comparison of postoperative effects between lidocaine infusion, meloxicam, and their combination in dogs undergoing ovariohysterectomy. *Vet Anaesth Analg,* 40, 615-622, 2013. DOI: 10.1111/vaa.12064

49. **Smith LJ, Bentley E, Shih A, Miller PE:** Systemic lidocaine infusion as an analgesic for intraocular surgery in dogs: A pilot study. *Vet Anaesth Analg,* 31, 53-63, 2004. DOI: 10.1111/j.1467-2995.2004.00142.x

50. **MacDougall LM, Hethey JA, Livingston A, Clark C, Shmon CL, Duke-Novakovski T:** Antinociceptive, cardiopulmonary, and sedative effects of five intravenous infusion rates of lidocaine in conscious dogs. *Vet Anaesth Analg,* 36, 512-522, 2009. DOI: 10.1111/j.1467-2995.2009.00480.x

51. **Ortega M, Cruz I:** Evaluation of a constant rate infusion of lidocaine for balanced anesthesia in dogs undergoing surgery. *Can Vet J,* 52, 856-860, 2011.

52. **Columbano N, Secci F, Careddu GM, Sotgiu G, Rossi G, Driessen B:** Effects of lidocaine constant rate infusion on sevoflurane requirement, autonomic responses, and postoperative analgesia in dogs undergoing ovariectomy under opioid-based balanced anesthesia. *Vet J,* 193, 448-455, 2012. DOI: 10.1016/j.tvjl.2011.12.005

53. **Bergadano A, Andersen OK, Arendt-Nielsen L, Theurillat R, Thormann W, Spadavecchia C:** Plasma levels of a low-dose constant-rate infusion of ketamine and its effect on single and repeated nociceptive stimuli in conscious dogs. *Vet J,* 182, 252-260, 2009. DOI: 10.1016/j.tvjl.2008.06.003

54. **Sarrau S, Jourdan J, Dupuis-Soyris F, Verwaerde P:** Effects of postoperative ketamine infusion on pain control and feeding behaviour in bitches undergoing mastectomy. *J Small Anim Pract,* 48, 670-676, 2007. DOI: 10.1111/j.1748-5827.2007.00362.x

55. **Wagner AE, Walton JA, Hellyer PW, Gaynor JS, Mama KR:** Use of low doses of ketamine administered by constant rate infusion as an adjunct for postoperative analgesia in dogs. *J Am Vet Med Assoc,* 221, 72-75, 2002. DOI: 10.2460/javma.2002.221.72

56. **Plumb DC:** Plumb's Veterinary Drug Handbook. 7th ed., 1-1208, Wiley-Blackwell, Ames, 2011.

57. **Ramsey I:** BSAVA Small Animal Formulary. 8th ed., 1-480, British Small Animal Veterinary Association, Gloucester England, 2014.

58. **Kuehn NF:** North American Companion Animal Formulary. 12th ed., North American Compendiums, Inc., Port Huron, 2018.

59. **International Association for the Study of Pain:** IASP terminology. https://www.iasp-pain.org/resources/terminology/; *Accessed:* 08.01.2026.

60. **Gurney MA:** Pharmacological options for intra-operative and early postoperative analgesia: An update. *J Small Anim Pract,* 53, 377-386, 2012. DOI: 10.1111/j.1748-5827.2012.01243.x

61. **Schug SA, Palmer GM, Scott DA, Halliwell R, Trinca J:** Acute Pain Management: Scientific Evidence. 4th ed., 1-647, Australian and New Zealand College of Anaesthetists and Faculty of Pain Medicine, Melbourne, 2015.

62. **Muir WW, III, Woolf CJ:** Mechanisms of pain and their therapeutic implications. *J Am Vet Med Assoc,* 219 (10): 1346-1356, 2001. DOI: 10.2460/javma.2001.219.1346

63. **Willis WD, Westlund KN:** Neuroanatomy of the pain system and of the pathways that modulate pain. *J Clin Neurophysiol,* 14 (1): 2-31, 1997. DOI: 10.1097/00004691-199701000-00002

64. **Crile G:** The kinetic theory of shock and its prevention through anoci-association (shockless operation). *Lancet,* 182, 7-16, 1913. DOI: 10.1016/s0140-6736(01)65552-1

65. **Grape S, Tramèr MR:** Do we need preemptive analgesia for the treatment of postoperative pain? *Best Pract Res Clin Anaesthesiol,* 21, 51-63, 2007. DOI: 10.1016/j.bpa.2006.11.004

66. **Monteiro BP, Lascelles BDX, Murrell J, Robertson S, Steagall PVM, Wright B:** 2022 WSAVA guidelines for the recognition, assessment and treatment of pain. *J Small Anim Pract,* 64 (4): 177-254, 2023. DOI: 10.1111/jsap.13566

67. **Ramsey I (Ed):** Small Animal Formulary. 7th ed., 1-600, BSAVA, Gloucester, 2011.

68. **Busch U, Schmid J, Heinzel G, Schmaus H, Baierl J, Huber C, Roth W:** Pharmacokinetics of meloxicam in animals and the relevance to humans. *Drug Metab Dispos,* 26, 576-584, 1998.

69. **Jung M, Lees P, Seewald W, King JN:** Analytical determination and pharmacokinetics of robenacoxib in the dog. *J Vet Pharmacol Ther,* 32, 41-48, 2009. DOI: 10.1111/j.1365-2885.2008.01035.x

70. **Woolf CJ (Ed):** Central mechanisms of acute pain. **In,** *Proceedings of the 6th World Congress on Pain.* Elsevier, Amsterdam, 1991.

71. **Woolf CJ:** Evidence for a central component of post-injury pain hypersensitivity. *Nature,* 306, 686-688, 1983. DOI: 10.1038/306686a0

72. **Woolf CJ, Wall PD:** Morphine-sensitive and morphine-insensitive actions of C-fibre input on the rat spinal cord. *Neurosci Lett,* 64, 221-225, 1986. DOI: 10.1016/0304-3940(86)90104-7

73. **Dobromylskyj P, Flecknell PA, Lascelles BD, Pascoe PJ, Taylor P, Waterman-Pearson A:** Management of postoperative pain and other acute pain. **In,** Flecknell P, Waterman-Pearson A (Eds): Pain Management in Animals. 81-145, WB Saunders, London, 2000.

74. **Lascelles BDX, Cripps PJ, Jones A, Waterman-Pearson AE:** Post-operative central hypersensitivity and pain: The pre-emptive value of pethidine for ovariohysterectomy. *Pain,* 73, 461-471, 1997. DOI: 10.1016/S0304-3959(97)00141-3

75. **Lascelles BD, Cripps PJ, Jones A, Waterman-Pearson AE:** Efficacy and kinetics of carprofen, administered preoperatively or postoperatively, for the prevention of pain in dogs undergoing

ovariohysterectomy. *Vet Surg,* 27, 568-582, 1998. DOI: 10.1111/j.1532-950X.1998.tb00533.x

76. **Slingsby LS, Waterman-Pearson AE:** The post-operative analgesic effects of ketamine after canine ovariohysterectomy: A comparison between pre- or post-operative administration. *Res Vet Sci,* 69, 147-152, 2000. DOI: 10.1053/rvsc.2000.0406
77. **Raj H, Amarpal, Singh GR, Aithal HP:** Comparison of preemptive analgesia with epidural pethidine and ketamine for the management of postoperative pain in dogs. *Indian Vet J,* 79, 1059-1062, 2002.
78. **Kehlet H, Dahl JB:** The value of "multimodal" or "balanced analgesia" in postoperative pain treatment. *Anesth Analg,* 77, 1048-1056, 1993. DOI: 10.1213/00000539-199311000-00030
79. **Raj H, Amarpal, Singh GR, Aithal HP:** Postoperative pain management in dogs: Efficacy of pre-emptive analgesia with lignocaine and ketamine. *Indian J Anim Sci,* 70, 362-365, 2000.
80. **Almeida RM, Escobar A, Maguilnik S:** Comparison of analgesia provided by lidocaine, lidocaine-morphine or lidocaine-tramadol delivered epidurally in dogs following orchiectomy. *Vet Anaesth Analg,* 37, 542-549, 2010. DOI: 10.1111/j.1467-2995.2010.00563.x
81. **DeRossi R, Frazílio FO, Jardim PHA, Martins ARC, Schmidt R, Negrini-Neto JM:** Evaluation of thoracic epidural analgesia induced by lidocaine, ketamine, or both administered via a lumbosacral approach in dogs. *Am J Vet Res,* 72, 1580-1585, 2011. DOI: 10.2460/ajvr.72.12.1580
82. **Kaka U, Rahman NA, Abubakar AA, Goh YM, Fakurazi S, Omar MA, Chen HC, Ebrahimi M:** Pre-emptive multimodal analgesia with tramadol and ketamine-lidocaine infusion for suppression of central sensitization in a dog model of ovariohysterectomy. *J Pain Res,* 11, 743-752, 2018. DOI: 10.2147/JPR.S152475
83. **Kehlet H:** Surgical stress: The role of pain and analgesia. *Br J Anaesth,* 63, 189-195, 1989. DOI: 10.1093/bja/63.2.189
84. **Grimm KA, Tranquilli WJ, Thurmon JC, Benson GJ:** Duration of nonresponse to noxious stimulation after intramuscular administration of butorphanol, medetomidine, or a butorphanol-medetomidine combination during isoflurane administration in dogs. *Am J Vet Res,* 61, 42-47, 2000. DOI: 10.2460/ajvr.2000.61.42
85. **Slingsby LS, Waterman-Pearson AE:** Analgesic effects in dogs of carprofen and pethidine together compared with the effects of either drug alone. *Vet Rec,* 148, 441-444, 2001. DOI: 10.1136/vr.148.14.441
86. **Mao J:** Opioid-induced abnormal pain sensitivity: Implications in clinical opioid therapy. *Pain,* 100, 213-217, 2002. DOI: 10.1016/S0304-3959(02)00422-0
87. **Acosta AD-P, Gomar C, Correa-Natalini C, Bopp S, Polydoro A, Sala-Blanch X:** Analgesic effects of epidurally administered levogyral ketamine alone or in combination with morphine on intraoperative and postoperative pain in dogs undergoing ovariohysterectomy. *Am J Vet Res,* 66, 54-61, 2005. DOI: 10.2460/ajvr.2005.66.54
88. **Kona-Boun JJ, Cuvelliez S, Troncy E:** Evaluation of epidural administration of morphine or morphine and bupivacaine for postoperative analgesia after premedication with an opioid analgesic and orthopedic surgery in dogs. *J Am Vet Med Assoc,* 229, 1103-1112, 2006. DOI: 10.2460/javma.229.7.1103
89. **Marucio RL, Luna SPL, Neto FJT, Minto BW, Hatschbach E:** Postoperative analgesic effects of epidural administration of neostigmine alone or in combination with morphine in ovario-hysterectomized dogs. *Am J Vet Res,* 69, 854-860, 2008. DOI: 10.2460/ajvr.69.7.854
90. **Kehlet H:** Postoperative pain relief - What is the issue? *Br J Anaesth,* 72, 375-378, 1994. DOI: 10.1093/bja/72.4.375
91. **Gassel AD, Tobias KM, Egger CM, Rohrbach BW:** Comparison of oral and subcutaneous administration of buprenorphine and meloxicam for preemptive analgesia in cats undergoing ovariohysterectomy. *J Am Vet Med Assoc,* 227, 1937-1944, 2005. DOI: 10.2460/javma.2005.227.1937

Kafkas Universitesi Veteriner Fakultesi Dergisi
Journal Home-Page: http://vetdergikafkas.org
E-ISSN: 1309-2251

Kafkas Univ Vet Fak Derg
32 (4): 475-492, 2026
DOI: 10.9775/kvfd.2026.36578

Review Article

Efficacy of Essential Oil-based Interventions Against Avian Coccidiosis: A Meta-analysis

Ayed ALSHAMMARI [1(*)]

[1] University of Hafr Al Batin, College of Science, Department of Biology, 31991, Hafr Al Batin, SAUDI ARABIA

[(*)] **Corresponding author:**
Ayed Alshammari
Phone: +966 536199551
Cellular phone: +966 536199551
E-mail: aealrmali@uhb.edu.sa

How to cite this article?

Alshammari A: Efficacy of Essential Oil-based Interventions Against Avian Coccidiosis: A Meta-analysis. *Kafkas Univ Vet Fak Derg*, 32 (4): 475-492, 2026.
DOI: 10.9775/kvfd.2026.36578

Article ID: KVFD-2026-36578
Received: 12.03.2026
Accepted: 19.07.2026
Published Online: 28.07.2026

Abstract

Avian coccidiosis remains one of the most important parasitic diseases of poultry worldwide. Resistance to conventional anticoccidials and limitations of vaccination programs have stimulated the search for natural alternatives. Essential oils (EOs) are complex mixtures of bioactive terpenoids and phenolics. They possess antimicrobial, anti-inflammatory, and immunomodulatory activities that may disrupt *Eimeria* infection and enhance host resilience. This study aimed to quantify the efficacy of essential oil-based interventions, including individual oils, essential oil blends, and essential oil-containing multicomponent formulations, in poultry experimentally challenged with *Eimeria* spp. through a meta-analysis conducted according to PRISMA 2020 guidelines. For this, literature searches across major databases identified experimental trials. Eighteen eligible studies were included, reporting outcomes on BWG, feed intake, FCR, mortality, fecal oocyst counts, and serum total protein. EO supplementation was associated with a small, statistically non-significant increase in body weight gain (MD +8.08 g, 95% CI −0.08 to 16.24) and a modest improvement in feed conversion ratio (MD −0.13, 95% CI −0.24 to −0.01). Mortality was reduced (RR 0.49, 95% CI 0.27-0.89), and oocyst shedding decreased (MD −18.99, 95% CI −37.91 to −0.08). No consistent effects were observed for feed intake or serum total protein. Overall, essential oils may offer anticoccidial benefits, particularly for feed efficiency, mortality, and oocyst shedding, although their effect on body weight gain remains uncertain.

Keywords: *Eimeria*, Essential oils, Meta-analysis, Natural anticoccidials, Oocyst shedding, Poultry

Introduction

Avian coccidiosis is an intestinal disease caused by protozoan parasites of the genus *Eimeria*. It remains one of the most pervasive and costly challenges in global poultry production [1,2]. Infected birds suffer mucosal damage leading to diarrhea, poor nutrient absorption, reduced growth and egg production, and, in severe outbreaks, high morbidity and mortality [3]. The disease also predisposes chickens to secondary bacterial infections (e.g., *Clostridium perfringens*, *Salmonella*, *Campylobacter)* [1]. Coccidiosis is widely recognized as the parasitic disease with the highest economic impact on the poultry industry. Coccidiosis causes multibillion-dollar economic losses to the global poultry industry annually [4]. These losses arise from reduced feed efficiency, slower weight gain, increased feed and medication costs, and carcass condemnation [5].

Current control of coccidiosis relies heavily on prophylactic use of anticoccidial drugs (ionophores such as monensin, salinomycin, and synthetic chemicals like diclazuril) and live vaccines. These strategies can reduce disease severity, but each has significant drawbacks [6]. The extensive use of ionophores and chemical coccidiostats over decades has led to widespread development of drug-resistant *Eimeria* strains [1,7]. In practice, many flocks now harbor parasites with reduced sensitivity to one or more anticoccidials [8]. Moreover, drug residues in meat raise consumer safety and regulatory concerns [9]. In the European Union, for example, routine in-feed anticoccidials are banned except by veterinary prescription, reflecting public health and welfare pressures [7]. Anticoccidial vaccines (live oocyst vaccines) offer a drug-free option but also have limitations: they typically protect against only specific *Eimeria* species, require high cost and repeated administration, and can fail if production parameters or strain variations intervene [10]. Importantly, both therapeutic and vaccination programs are expensive, and public sentiment increasingly favors “chemical-free” poultry products. Even where vaccines are used, their high-cost limits use mainly to breeder or parent stock rather than large commercial broiler operations [7]. In short, traditional control measures are valuable but imperfect, and producers and consumers alike are seeking safer, sustainable alternatives [11].

Against this background, plant-derived essential oils (EOs) have attracted growing interest as natural anticoccidials. EOs are complex mixtures of terpenoids, phenolics, and other phytochemicals (for example, thymol and carvacrol in *Lamiaceae* oils, allicin and ajoene in garlic oil, eugenol in clove oil, cinnamaldehyde in cinnamon oil) that have antimicrobial, anti-inflammatory, and immunomodulatory properties. EOs are generally recognized as safe for food; they are viewed as consumer-friendly alternatives [5,12,13]. EO supplementation can exert anticoccidial effects *in vivo*. They can result in improvements in body weight gain and feed conversion, coupled with reductions in oocyst shedding and lesion scores [14]. Experimental work has also demonstrated that phenolic EO components such as thymol, carvacrol, and eugenol can disrupt parasite sporulation and compromise oocyst wall integrity, supporting a direct anticoccidial mechanism [15,16]. In addition to their antiparasitic properties, EOs can enhance gut health through improved villus morphology, stabilization of intestinal barrier function, and modulation of gut microbiota. These effects may improve nutrient utilization and increase resilience to infection. The dietary supplementation with essential oils also holds promise as a natural strategy for mitigating the effects of coccidiosis in poultry [17]. Nevertheless, the variability in outcomes highlights the need for quantitative synthesis and critical evaluation. A meta-analytical approach can integrate the data from many studies to estimate overall effect sizes of EO supplementation on key outcomes and to identify moderators of efficacy. Such analysis is timely and necessary because the inconsistent literature makes it hard to draw general conclusions about whether and how much EOs can replace or supplement anticoccidials in practice.

Previous reviews have primarily provided narrative summaries of the anticoccidial properties, potential mechanisms, and practical applications of essential oils and other phytogenic compounds in poultry [5-7,14]. Although these reviews have highlighted promising findings, they have not quantitatively estimated the overall magnitude and consistency of essential oil effects across controlled *Eimeria*-challenge studies. Consequently, uncertainty remains regarding whether the reported benefits are reproducible across different essential oil preparations, challenge models, and measured outcomes. The present meta-analysis addresses this gap by pooling comparative data for growth performance, feed efficiency, mortality, oocyst shedding, and serum total protein, while also evaluating heterogeneity, publication bias, and the influence of individual studies.

In this study, we conducted a comprehensive meta-analysis of controlled experiments in which poultry were challenged with *Eimeria* spp. and fed essential oils or EO-containing botanicals. We examined the impact of EO interventions on parameters relevant to coccidiosis: body weight gain, feed intake, feed conversion ratio, mortality, fecal oocyst counts (OPG), and serum total protein levels. By pooling data globally, we aimed to overcome the inconsistencies of individual trials and derive robust estimates of EO efficacy. The outcomes are of high practical importance. The weight gain, feed efficiency and mortality determine production performance and profitability, while OPG and blood protein reflect parasite burden and bird health. This meta-analysis provides a systematic synthesis of available evidence on the effects of essential oil supplementation in *Eimeria*-challenged poultry, addressing variability across individual studies and offering a more integrated assessment of their efficacy.

Material and Methods

Protocol and Reporting Standards

The meta-analysis was conducted in accordance with the PRISMA (Preferred Reporting Items for Systematic reviews and Meta-Analyses) 2020 statement [18]. The review protocol was not prospectively registered in PROSPERO or another systematic review registry. The eligibility criteria, literature search strategy, data extraction procedures, and statistical methods used in the review are described in the following sections to support transparency and reproducibility.

Literature Search Strategy

A comprehensive literature search was performed in PubMed, Web of Science Core Collection, Scopus, CAB Abstracts, and Google Scholar from database inception through June 2025. The complete PubMed search strategy was: ((“essential oil”[Title/Abstract] OR “essential oils”[Title/Abstract] OR thymol[Title/Abstract] OR carvacrol[Title/Abstract] OR eugenol[Title/Abstract] OR cinnamaldehyde[Title/Abstract] OR oregano[Title/Abstract] OR thyme[Title/Abstract] OR garlic[Title/Abstract] OR clove[Title/Abstract]) AND *(Eimeria* [Title/Abstract] OR coccidia[Title/Abstract] OR coccidiosis[Title/Abstract]) AND (poultry[Title/Abstract] OR chicken*[Title/Abstract] OR broiler*[Title/Abstract] OR hen*[Title/Abstract] OR turkey*[Title/Abstract] OR quail*[Title/Abstract])). This strategy was adapted to the indexing systems, field tags, and Boolean syntax of the other databases. No language restrictions were applied. Reference lists of the included studies and relevant review articles were also screened to identify additional eligible records.

All records were merged, and duplicate citations were identified and removed manually to yield a unique set of references. The unique records were screened by title and abstract, excluding clearly irrelevant studies. Full texts

were retrieved for the remaining candidates and assessed for eligibility. All search activities and screening decisions were documented to permit reproduction.

Eligibility Criteria

Studies were eligible if they were original controlled *in vivo* trials conducted in domestic poultry experimentally challenged with *Eimeria* spp. Eligible interventions included individual essential oils, blends composed of multiple essential oils or their defined bioactive constituents, and multicomponent formulations in which one or more essential oils were explicitly identified as active ingredients. Multicomponent formulations containing essential oils together with organic acids, vitamins, minerals, tannins, or other phytogenic substances were retained because such formulations are commonly evaluated as integrated feed-based interventions in poultry production. The effects of these interventions were interpreted as those of the complete essential oil-based formulation rather than as effects attributable exclusively to the essential oil component.

Eligible studies were required to include an *Eimeria*-challenged control group that did not receive the tested intervention and to report numerical data for at least one of the following outcomes: body weight gain or final body weight, feed intake, feed conversion ratio, mortality, fecal oocyst count, or serum total protein. Reviews, observational studies, uncontrolled field surveys, *in vitro*-only studies, conference abstracts without sufficient data, and studies without an experimentally described *Eimeria* challenge were excluded. Studies were also excluded when the essential oil component was not identified, its administration or dose was not adequately described, no appropriate challenged control group was available, or relevant quantitative data could not be extracted.

Data Extraction and Variables Collected

Data from each included study were extracted manually by using a standardized form. Interventions were classified during data extraction as: (i) individual essential oils, (ii) blends containing only essential oils or their defined constituents, or (iii) essential oil-containing multicomponent formulations that also included other active substances. This classification was used to distinguish effects attributable to essential oil-only interventions from formulation-level effects that could also reflect the contribution of accompanying active components. For each trial, the following variables were recorded: first author, year of publication, country of origin, poultry type and breed/strain, *Eimeria* species used for challenge, type and source of essential oil (including plant name and chemical composition if reported), and dietary dose of EO (e.g. mg/kg feed). The primary outcomes and any additional reported endpoints were also captured. In particular, for each reported outcome, we collected the treatment and control group means (or proportions, for mortality) along with measures of variability (standard deviation [SD] or standard error [SE]) and the sample size (n) for each group. The six target outcomes (body weight gain, feed intake, feed conversion ratio, mortality, oocyst count, total protein) were extracted along with any other performance or health variables reported. Records of each study's data were checked for completeness and correctness by cross-referencing tables, text, and supplementary materials. Studies for which key quantitative data could not be obtained were not included in the meta-analysis.

Statistical Analysis

Meta-analyses were performed using R software version 4.4.1 with the meta and metafor packages. A random-effects model was fitted for each outcome because clinical and methodological variability was expected across studies. Between-study variance (τ^2) was estimated using the restricted maximum-likelihood (REML) method for all analyses. Continuous outcomes were summarized as mean differences (MDs) with 95% confidence intervals when measurements were reported in comparable units. Dichotomous mortality data were summarized as risk ratios (RRs) with 95% confidence intervals. Study-specific estimates were weighted using inverse-variance weighting.

Heterogeneity was assessed using Cochran's Q test and quantified using the I^2 statistic. Because I^2 estimates may be imprecise when few studies are available, they were interpreted together with τ^2, prediction intervals, and the clinical and methodological diversity among studies. The primary analyses included all eligible essential oil-based interventions. A separate quantitative subgroup analysis according to intervention composition was considered; however, it was not performed because only a small number of multicomponent formulations contributed to each outcome and their accompanying active ingredients differed substantially. Under these conditions, separate pooled estimates would have been statistically unstable and potentially misleading. Therefore, multicomponent formulations were additionally examined through a separate descriptive comparison, and their effects were interpreted at the formulation level rather than as isolated essential oil effects. Statistical significance of pooled effects was taken at $\alpha=0.05$ (two-sided). To evaluate the potential influence of small-study effects and publication bias, we applied visual and statistical methods. Funnel plots were generated for each outcome to inspect symmetry. Egger's regression test and Begg's rank-correlation test were used as exploratory assessments of funnel-plot asymmetry. Because these tests may have low power and produce unstable results when based on a small number of studies, their findings were interpreted cautiously and were not

considered definitive evidence of publication bias. In addition, the trim-and-fill method was applied to estimate the number of potentially missing studies and to adjust the pooled effect sizes if necessary.

Additional analyses were conducted to probe the robustness of results. Influence diagnostics were computed using metafor functions: externally standardized residuals, DFFITS, Cook's distance, covariance ratios, and hat values were examined for outlying or influential studies [19]. A leave-one-out sensitivity analysis was performed by iteratively removing each study and recomputing the pooled effect [20]. Baujat plots were generated to identify studies that contributed disproportionately to overall variability. In a Baujat plot, each study's contribution to Cochran's Q is plotted against its influence on the pooled estimate, facilitating identification of outliers [21]. Finally, cumulative meta-analyses (adding studies in chronological order of publication) were performed to illustrate how the overall effect estimate evolved as evidence accumulated. For cumulative analyses, trials were ordered by publication year, and pooled effects were recomputed after each study addition [22].

All statistical analyses were conducted in R using functions from the metafor package, including rma() for random-effects model fitting and forest(), funnel(), influence(), baujat(), and cumul() for graphical and sensitivity analyses. The REML estimator was used consistently to estimate between-study variance for all continuous and dichotomous outcomes.

Data Presentation

Results of the meta-analyses were summarized in tables and figures. A summary table was prepared showing the pooled effect size (MD, SMD, or RR) and 95% confidence interval for each outcome. Graphical displays included forest plots *(Fig. 2, Fig. 3)* and funnel plots *(Fig. 4)*. Forest plots displayed the study-specific effect estimates and 95% confidence intervals together with the pooled random-effects estimate obtained using the REML estimator. Key outcomes with sufficient studies were also depicted with funnel plots to visualize publication bias. Additional plots were generated to aid interpretation: Baujat plots *(Fig. 6)*, influence plots *(Fig. 7, Fig. 8, Fig. 9, Fig. 10, Fig. 11, Fig. 12)* for outliers, and cumulative forest plots *(Fig. 5)* for evidence accumulation. The PRISMA flow diagram was included as *Fig. 1* (based on the recorded screening data).

Results

Literature Search and Study Selection

The systematic search across five databases (PubMed, Web of Science, Scopus, CAB Abstracts, and Google Scholar) yielded a total of 1,123 records. Following the removal of duplicates, 917 unique studies remained for screening. Title and abstract screening excluded 851 records as they did not meet the inclusion criteria (e.g., non-experimental design, absence of *Eimeria* challenge, use of non-poultry species, or interventions not involving essential oils). The remaining 76 full-text articles were assessed for eligibility. Of these, 58 studies were excluded after detailed review, most commonly due to incomplete or missing quantitative outcome data, combined interventions in which the effect of essential oils could not be isolated, or a lack of relevant outcomes. Ultimately, 18 experimental trials fulfilled all eligibility criteria and were included in the meta-analysis. These trials provided extractable data on at least one of the six pre-specified outcomes: body weight gain (BWG), feed intake (FI), feed conversion ratio (FCR), mortality, oocysts per gram (OPG), and serum total protein. The process of study identification, screening, exclusion, and inclusion is illustrated in the PRISMA flow diagram *(Fig. 1)*, which provides a transparent overview of study selection and reasons for exclusion.

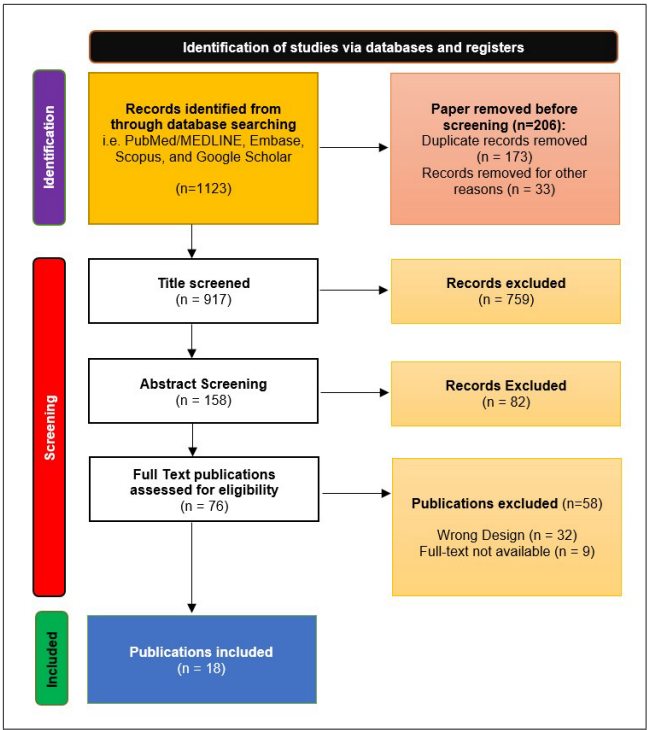

Fig 1. PRISMA Flow Chart in accordance with PRISMA 2020 statement

Study Characteristics

A total of 18 experimental trials fulfilled the eligibility criteria and were included in the meta-analysis *(Table 1)*. All studies were conducted in poultry under controlled *Eimeria*-challenge conditions and reported at least one of the six prespecified outcomes: body weight gain, feed intake, feed conversion ratio, mortality, oocysts per gram of feces, or serum total protein. The interventions were classified as individual essential oils, essential oil-

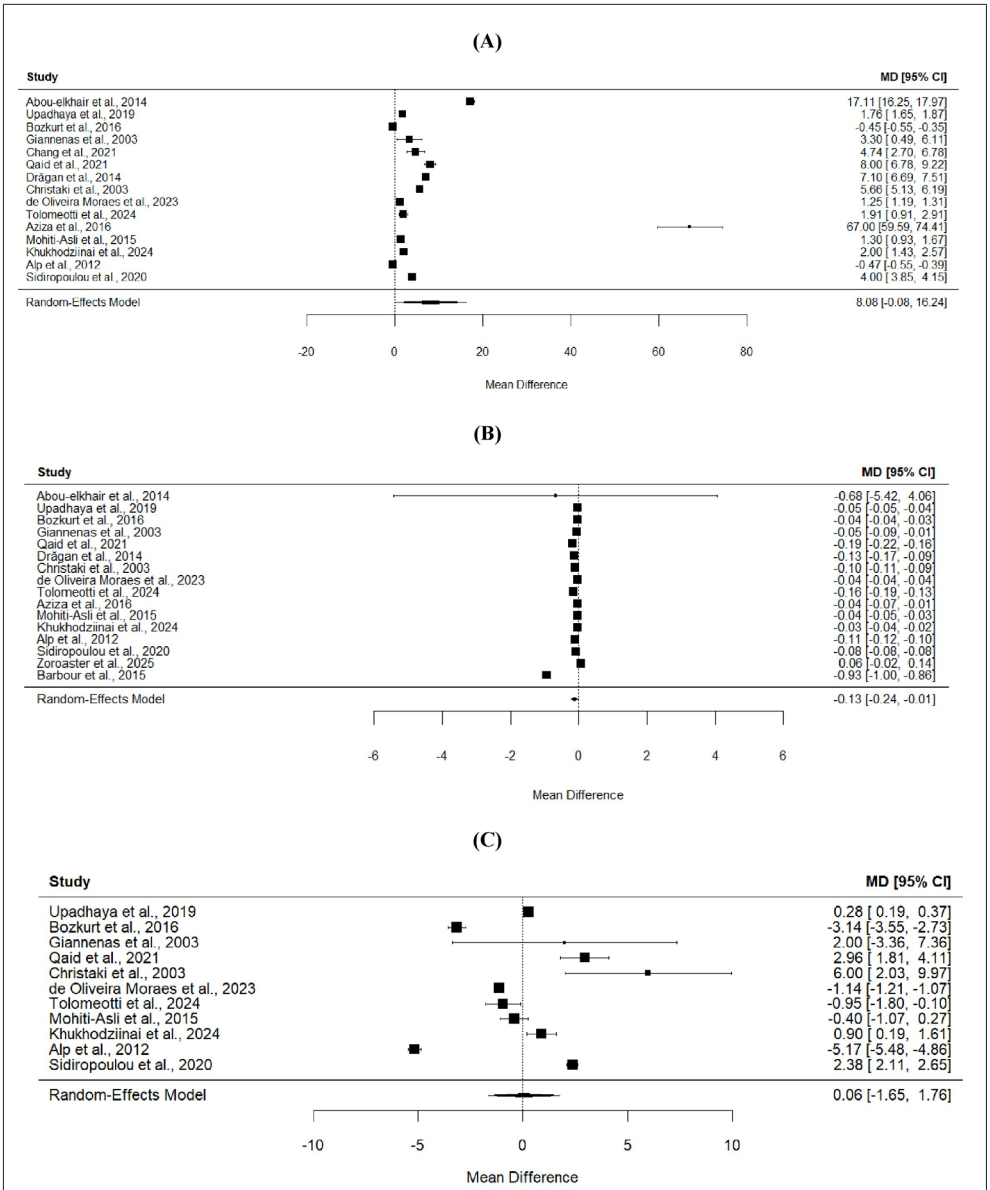

Fig 2. Forest plots for outcomes. Panels: **(A)** Body weight gain (BWG, g), **(B)** Feed conversion ratio (FCR), **(C)** Feed intake (FI). Squares represent study-specific effect estimates with 95% confidence intervals, and square size is proportional to inverse-variance weight. Diamonds represent the pooled random-effects estimate obtained using the restricted maximum-likelihood estimator; horizontal bars extending from the pooled estimate indicate the 95% prediction interval

only blends, or essential oil-containing multicomponent formulations. The latter included formulations in which essential oils were administered with components such as organic acids, benzoic acid, tannins, vitamins, or minerals. These studies were retained as evaluations of practically applied essential oil-based formulations, but their observed effects were not attributed exclusively to the essential oil component. Considerable variation was observed in poultry type, essential oil source, dose, formulation, administration route, supplementation period, and *Eimeria* challenge model.

The essential oil-containing multicomponent formulations were also considered separately in a descriptive assessment. Their findings were not uniform. Some formulations containing essential oils together with benzoic acid, organic acids, or vitamin D3 were associated with improvements in growth, feed efficiency, intestinal health, immune responses, or oocyst reduction. In contrast, the formulation containing essential oils, organic acids, tannins, vitamin E, and zinc showed limited effects under challenge conditions. Because these formulations differed considerably in composition and were represented by few studies within individual outcomes, their results do not permit conclusions regarding the independent contribution of essential oils or any specific accompanying component.

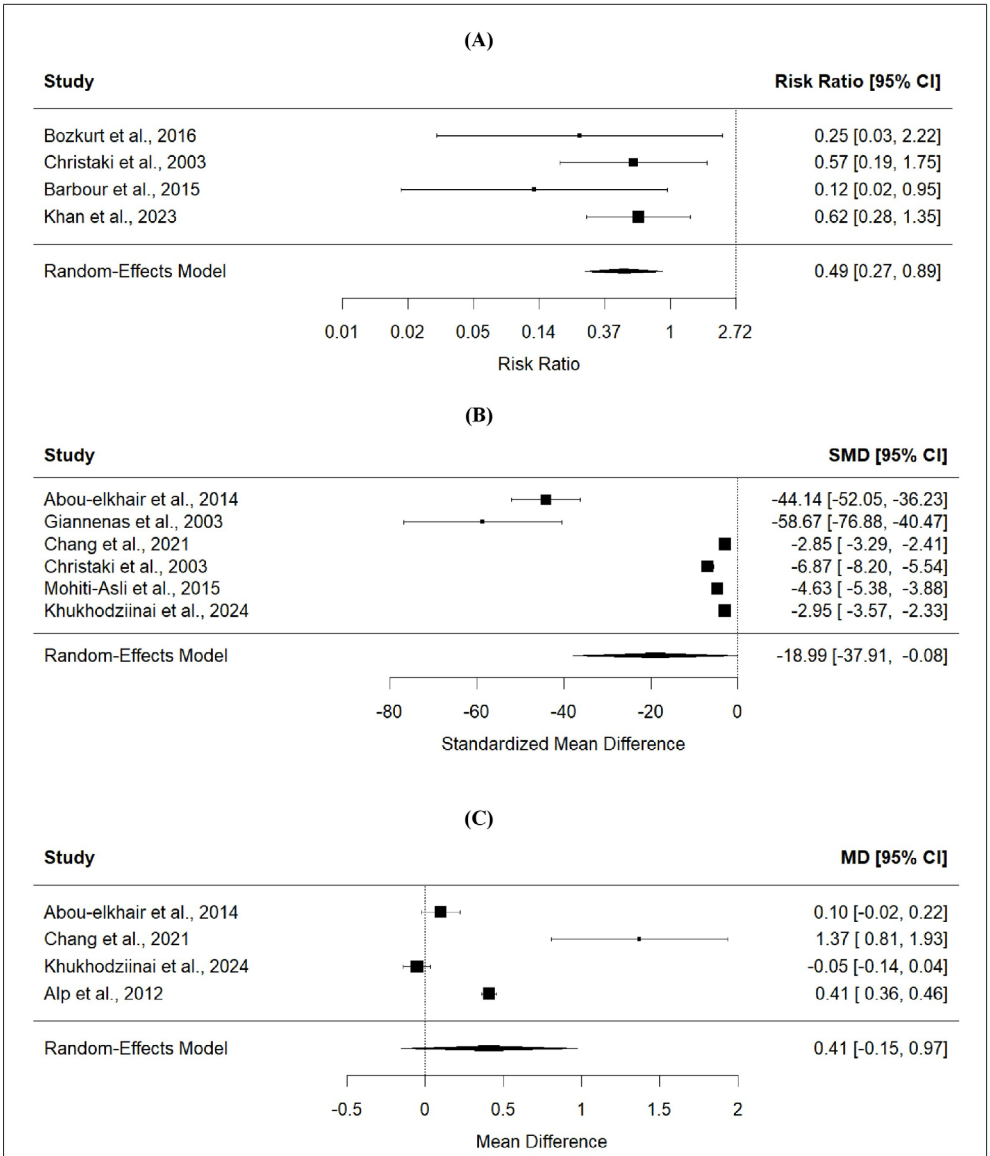

Fig 3. Forest plots for all outcomes. Panels: **(A)** Mortality (%), **(B)** OPG, **(C)** Total protein (g/dL). Squares represent study-specific effect estimates with 95% confidence intervals, and square size is proportional to inverse-variance weight. Diamonds represent the pooled random-effects estimate obtained using the restricted maximum-likelihood estimator; horizontal bars extending from the pooled estimate indicate the 95% prediction interval

Meta-analytical Results

All pooled estimates reported below were obtained using random-effects models with between-study variance estimated by REML. The meta-analytical results obtained for each outcome are summarized in *Table 2*.

Body Weight Gain (BWG)

Fifteen trials (total $N \approx 2384$ birds) contributed data on BWG. The pooled mean difference was +8.08 g (95% CI −0.08 to 16.24), indicating a trend toward improved body weight gain with essential oil supplementation. In the forest plot *(Fig. 2-A)*, most trials favored higher BWG with essential oils, but effect sizes varied (study-level MDs ranged from slightly negative to strongly positive). Notably, one study [38] reported an unusually large positive effect (≈+67 g), and a few reported small negative differences.

For body weight gain, Egger's regression suggested possible funnel-plot asymmetry (P=0.053), while Begg's test was statistically significant (P=0.0048). These findings may indicate small-study effects; however, they should not be interpreted as definitive evidence of publication bias because the analysis included only 15 studies and the two tests yielded different levels of evidence. The trim-and-fill procedure did not impute any missing studies, and the pooled estimate remained unchanged. Cumulative meta-analysis *(Fig. 5-A)* showed the pooled effect stabilizing around +8 g as studies were added chronologically, with confidence intervals gradually narrowing but still

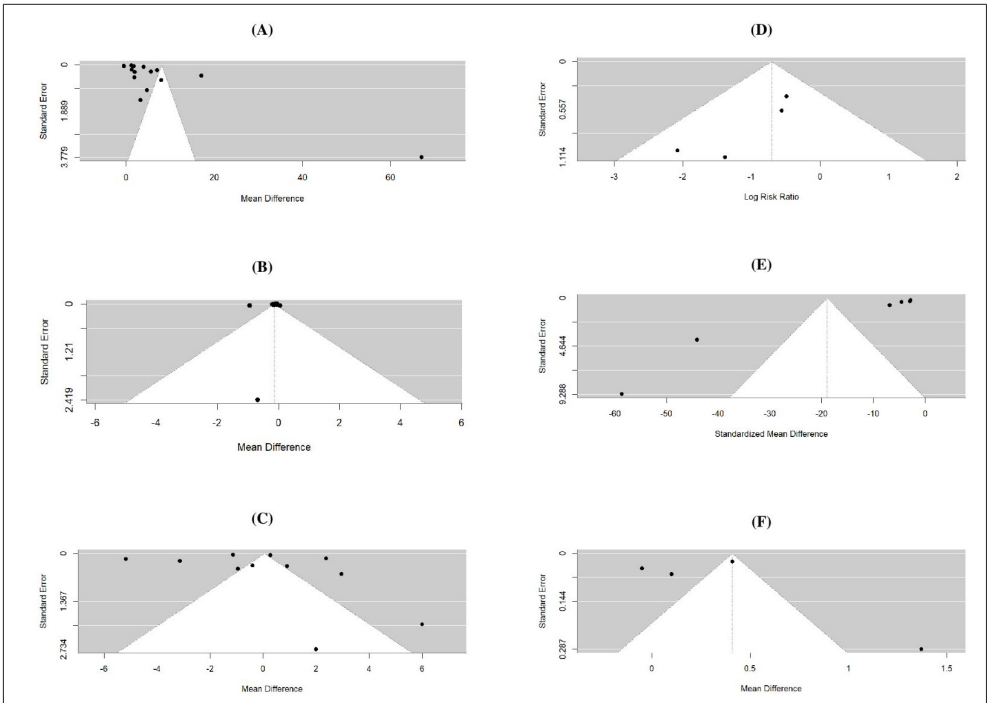

Fig 4. Funnel plots for all outcomes. Panels: **(A)** Body weight gain (BWG, g), **(B)** Feed conversion ratio (FCR), **(C)** Feed intake (FI), **(D)** Mortality (%), **(E)** OPG, **(F)** Total protein (g/dL)

overlapping zero. Influence analysis (leave-one-out) *(Fig. 7)* identified Aziza et al.[38] as an outlier: omitting this trial reduced the pooled estimate by about 4 g. Similarly, Baujat plot *(Fig. 6-A)* inspection indicated that the study by Aziza et al.[38] and a few others [35,36] contributed disproportionately to variability in results.

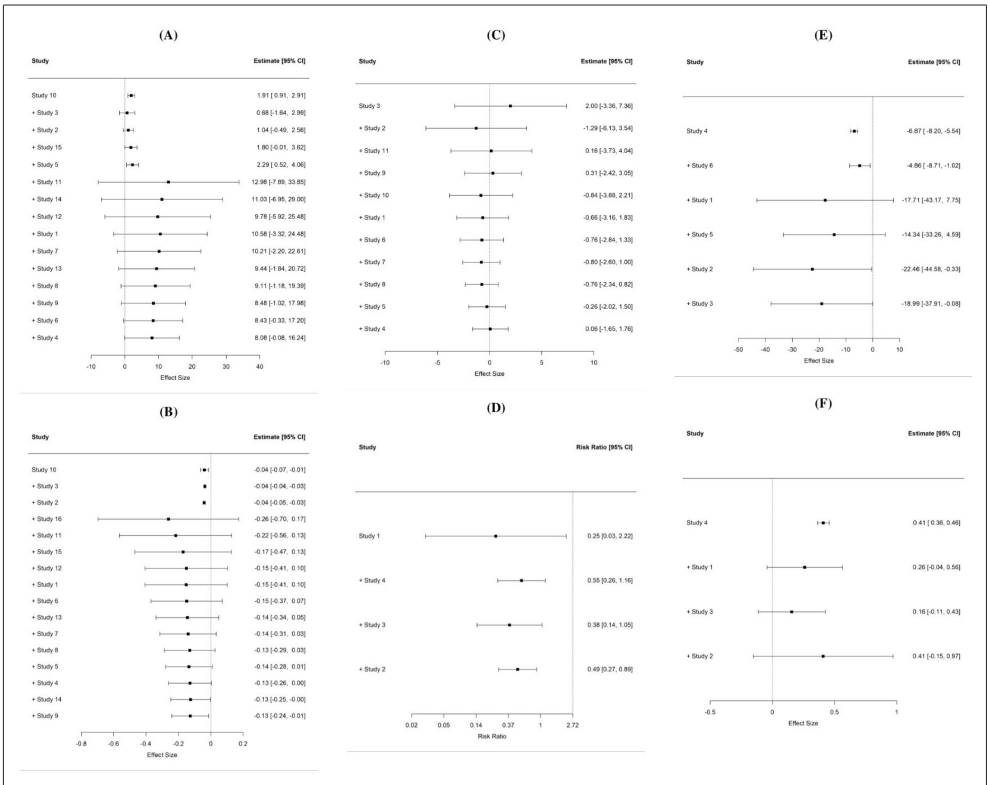

Fig 5. Cumulative meta-analysis across outcomes. Panels: **(A)** Body weight gain (BWG, g), **(B)** Feed conversion ratio (FCR), **(C)** Feed intake (FI), **(D)** Mortality (%), **(E)** OPG, **(F)** Total protein (g/dL)

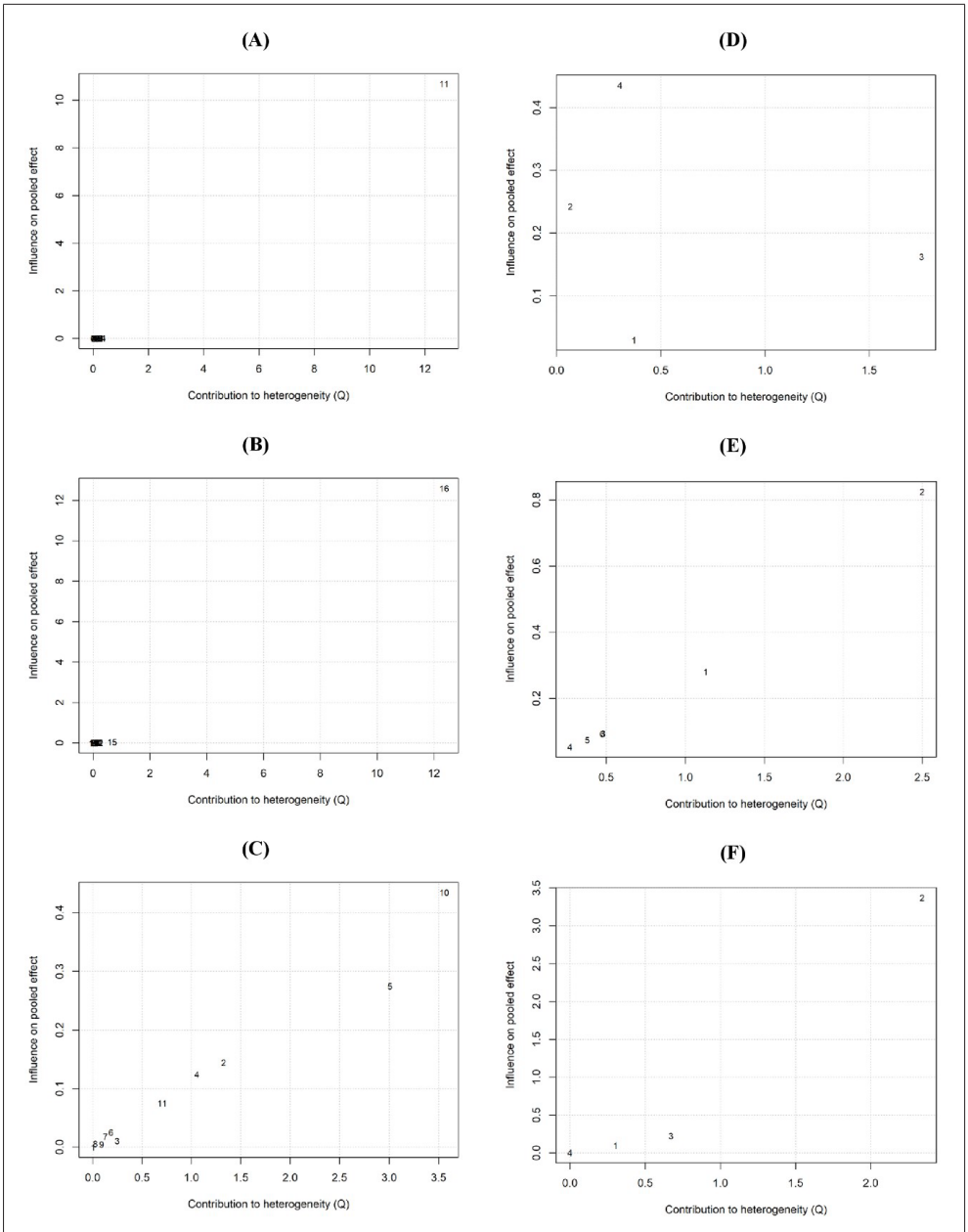

Fig 6. Baujat plots for all outcomes. Panels: **(A)** Body weight gain (BWG, g), **(B)** Feed conversion ratio (FCR), **(C)** Feed intake (FI), **(D)** Mortality (%), **(E)** OPG, **(F)** Total protein (g/dL)

Feed Conversion Ratio (FCR)

Sixteen studies (total $N \approx 2359$) reported FCR. The pooled mean difference was −0.13 (95% CI −0.24 to −0.01), indicating that essential oil supplementation was associated with a modest but statistically significant improvement in FCR (P≈0.032). The forest plot *(Fig. 2-B)* showed that most studies clustered near the null, with several reporting moderate improvements and a few showing slight adverse effects, reflecting variability across trials.

For feed conversion ratio, Egger's regression indicated possible funnel-plot asymmetry (P=0.020), whereas Begg's test was not statistically significant (P=0.079). The disagreement between these tests does not provide conclusive evidence of publication bias and may reflect differences in their statistical properties or the influence of between-study heterogeneity. The trim-and-fill procedure did not impute missing studies, and the adjusted pooled estimate remained unchanged. These findings were therefore interpreted as suggestive of possible small-study effects rather than confirmation of publication bias. Cumulative meta-analysis *(Fig. 5-B)* showed that the direction of effect (favoring essential oils) remained consistent over time, although confidence intervals narrowed only slightly as additional studies were added.

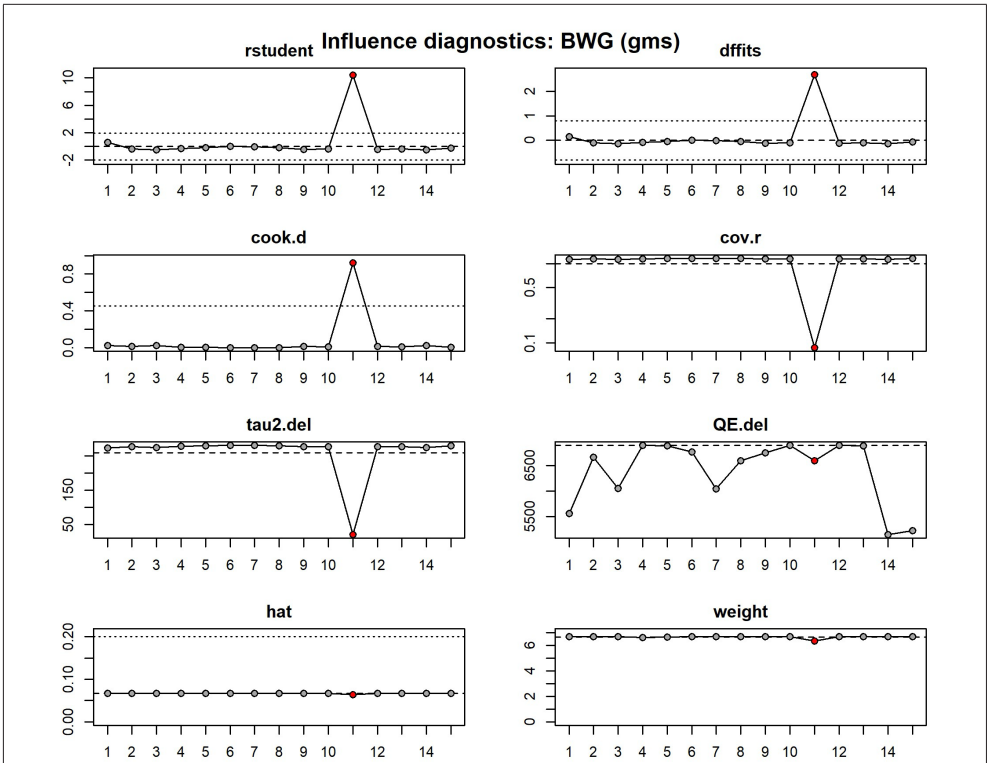

Fig 7. Influence diagnostics for Body weight Gain (BWG, g). Each panel shows the metafor influence diagnostics for the fitted random-effects model, including Cook's distance, hat (leverage), DFFITS, studentized residuals, covariance ratios, and related leave-one-out metrics

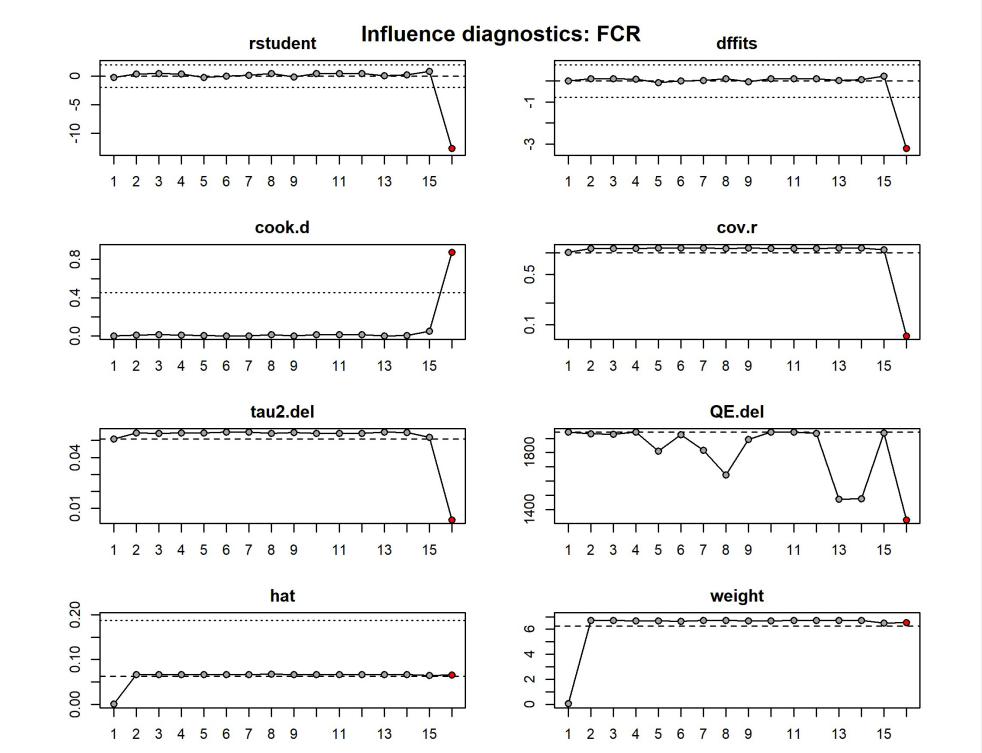

Fig 8. Influence diagnostics for Feed conversion ratio (FCR). Each panel shows the metafor influence diagnostics for the fitted random-effects model, including Cook's distance, hat (leverage), DFFITS, studentized residuals, covariance ratios, and related leave-one-out metrics

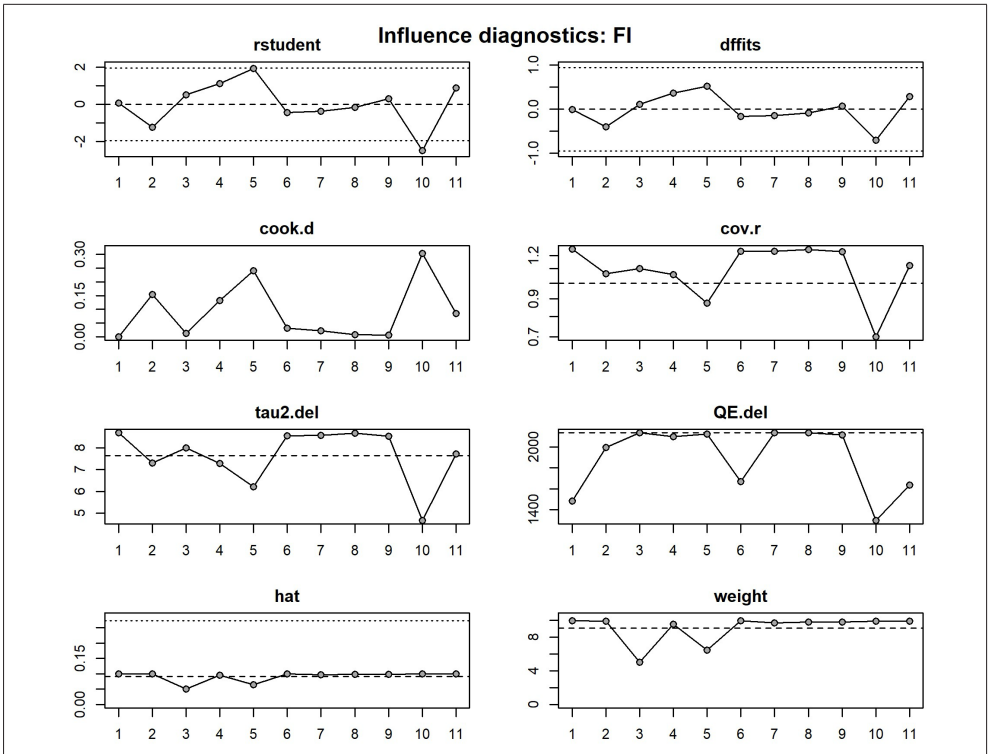

Fig 9. Influence diagnostics for Feed Intake (FI). Each panel shows the metafor influence diagnostics for the fitted random-effects model, including Cook's distance, hat (leverage), DFFITS, studentized residuals, covariance ratios, and related leave-one-out metrics

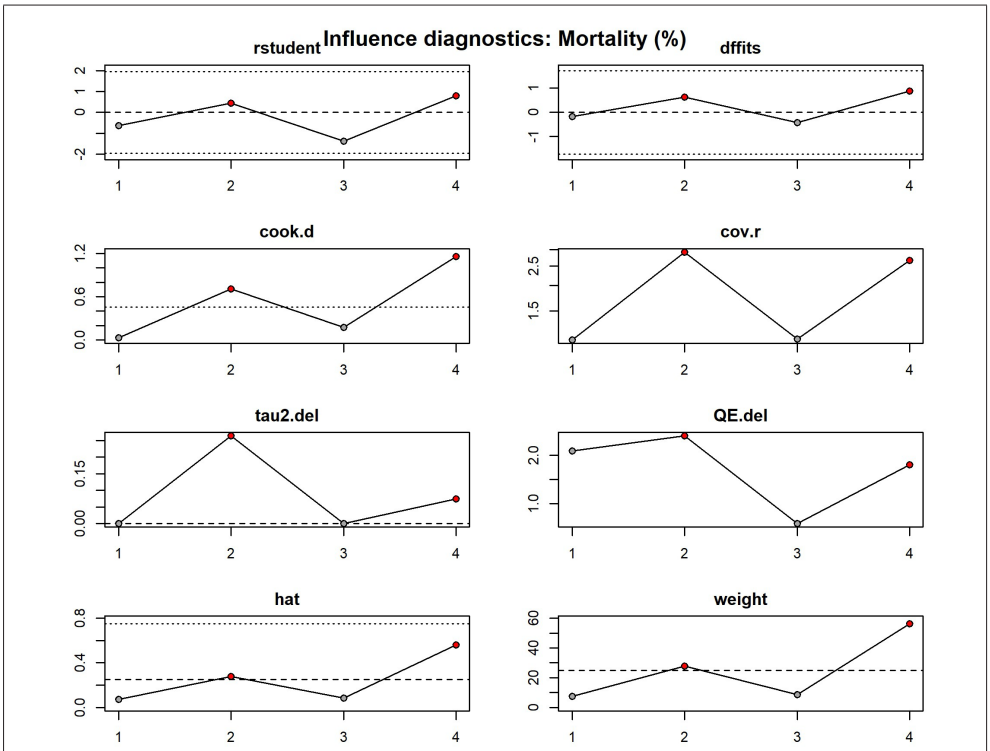

Fig 10. Influence diagnostics for Mortality (%). Each panel shows the metafor influence diagnostics for the fitted random-effects model, including Cook's distance, hat (leverage), DFFITS, studentized residuals, covariance ratios, and related leave-one-out metrics

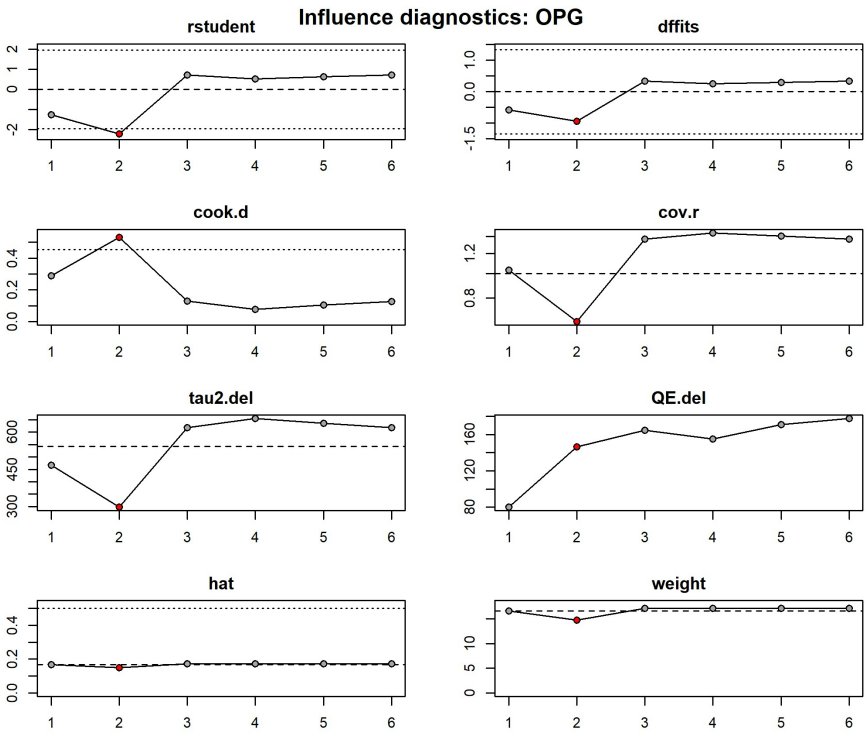

Fig 11. Influence diagnostics for OPG. Each panel shows the metafor influence diagnostics for the fitted random-effects model, including Cook's distance, hat (leverage), DFFITS, studentized residuals, covariance ratios, and related leave-one-out metrics

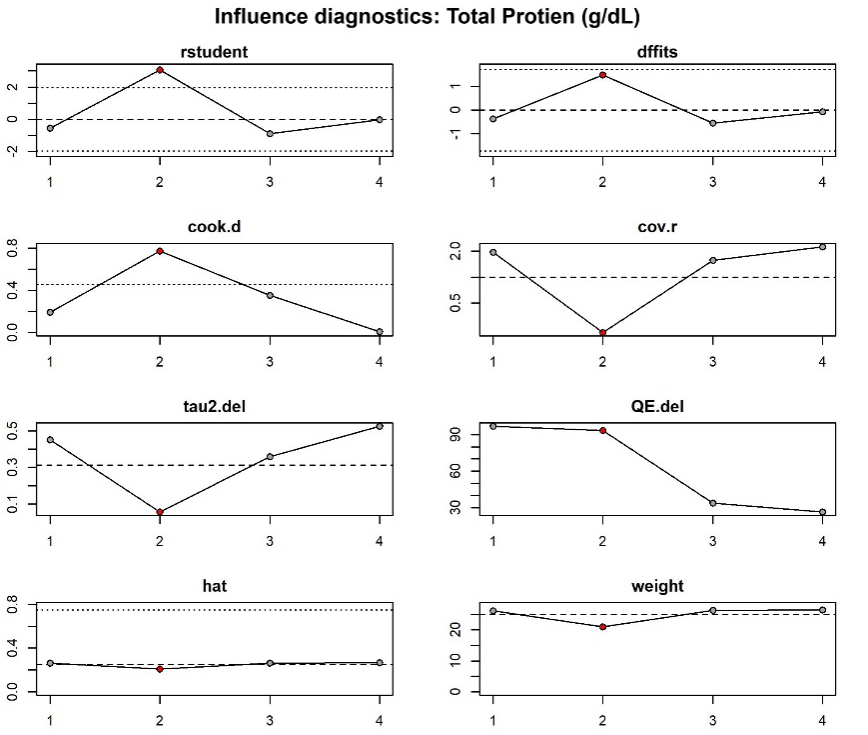

Fig 12. Influence diagnostics for Total Protein (g/dL). Each panel shows the metafor influence diagnostics for the fitted random-effects model, including Cook's distance, hat (leverage), DFFITS, studentized residuals, covariance ratios, and related leave-one-out metrics

Table 1. *Characteristics of the 18 included studies evaluating essential oil-based interventions in poultry, including country, poultry strain, Eimeria challenge, intervention composition and classification, duration, sample size, outcomes, and main findings*

Author (Year)	Country	Poultry Type & Strain	Challenge (Species, Dose)	Intervention Composition, Dose, and Classification	Duration	Outcomes Included in the Meta-analysis	Main Findings
Abou-Elkhair et al. (2014) [23]	Egypt	Broilers	Mixed *Eimeria* spp., 20,000 oocysts	Oregano + Thyme + Garlic EO blend (10-20 mg/kg oregano+thyme, 5-10 mg/kg garlic)	35 d	BWG, FCR, Total Protein, OPG	Improved growth, reduced oocyst shedding, comparable to amprolium
Alp et al. (2012) [24]	Türkiye	Broilers	*Eimeria* spp. (dose not specified)	Oregano essential oil (300 mg/kg feed); individual essential oil intervention	42 d	BWG, FCR, Total Protein, FI	Improved FCR, partial anticoccidial effect, higher IgG
Barbour et al. (2015) [25]	Lebanon	Broilers	8 *Eimeria* spp., 1.76×10^5 oocysts	Eucalyptus + Peppermint oils (0.69 mL/kg BW in water)	Trial period	BWG, FCR, Mortality	Reduced lesions, mortality, oocyst counts, better BWG
Bozkurt et al. (2016) [26]	Türkiye	Broilers (Ross 308)	Mixed *Eimeria* spp., challenge d12	Oregano EO (12–24 mg/kg), Monensin comparison	42 d	BWG, FCR, FI, Mortality	Improved gut health, antioxidant defenses; weaker than monensin
Chang et al. (2021) [27]	China	Laying hens	*E. tenella*, 50.000 oocysts	Garlic EO (0.04–0.08 mL/L in water)	Trial period	BWG, Total Protein, OPG	Reduced lesions, oocyst output, improved IgA/IgM, similar to diclazuril
Christaki et al. (2004) [28]	Greece	Broilers (Cobb-500)	*E. tenella*, 60.000 oocysts	Apacox herbal blend (0.5–1.0 g/kg diet)	35 d	BWG, FCR, OPG, FI, Mortality	Reduced diarrhea, mortality, moderate efficacy vs. lasalocid
de Oliveira Moraes et al. (2023) [29]	Brazil	Broilers (Cobb)	Mixed *Eimeria* spp.	Oregano EO (500 mg/kg), Clove EO (500 mg/kg), combo (250+250 mg/kg)	42 d	BWG, FCR, FI	Improved BWG, FCR, villus/crypt, higher IgA & IgG
Giannenas et al. (2003) [30]	Greece	Broilers	*E. acervulina* & *E. tenella*	Oregano EO (300–600 mg/kg)	Trial period	BWG, FCR, OPG, FI	600 mg/kg improved growth, reduced lesions; similar to salinomycin
Khan et al. (2023) [12]	Pakistan	Japanese quails	*Eimeria tenella*	Oregano EO (200–600 mg/kg)	Trial period	Mortality	Reduced oocysts, lesions, improved growth; weaker than amprolium
Khukhodziinai et al. (2024) [31]	Ukraine	Broilers (Cobb-500)	*E. acervulina, E. maxima, E. tenella, E. necatrix*	Benzoic acid (500 mg/kg), oregano essential oil (500 mg/kg), and their combination; individual EO and EO-containing multicomponent intervention arms	35 d	BWG, FCR, Total Protein, OPG, FI	Combo had best immunity, gut health, reduced oocysts; > salinomycin
Mohiti-Asli et al. (2015) [32]	Iran	Broilers	*E. acervulina, E. maxima, E. tenella* (Livacox overdose)	Oregano EO (300–500 ppm)	Trial period	BWG, FCR, OPG, FI	500 ppm reduced lesions & oocysts, similar to diclazuril
Qaid et al. (2021) [33]	Saudi Arabia	Broilers	Mixed *Eimeria*	EO + organic acid blend	Trial period	FCR, FI	Reduced lesions, improved villi, growth performance
Sidiropoulou et al. (2020) [34]	Greece	Broilers	Mixed *Eimeria*	Oregano and garlic essential oils; essential oil-only blend	Trial period	BWG, FCR, FI	Improved meat quality, antioxidant & immunity
Tolomeotti et al. (2024) [35]	Italy	Broilers	*Eimeria* spp.	EO blend + organic acids + tannins + vitamin E + zinc; EO-containing multicomponent formulation	Trial period	BWG, FCR, FI	Better FCR in starter, breast yield, villi in unchallenged; little effect when challenged
Upadhaya et al. (2019) [36]	South Korea	Broilers	*E. tenella* & *E. maxima* (300–500 oocysts)	EO blend containing eugenol, thymol, and piperine + vitamin D3; EO-containing multicomponent formulation	Trial period	BWG, FCR, FI	Improved BWG, FCR, Lactobacillus counts, lower lesions
Zoroaster et al. (2025) [37]	Italy	Black Livorno chickens	*E. necatrix, E. praecox, E. tenella*	Thymol (5 mg/kg), EO blend EP (50 mg/kg)	Trial period	FCR	*In vitro:* strong inhibition; *In vivo:* reduced OPG after d78, no growth effect
Aziza et al. (2016) [38]	USA	Broilers (Ross 708)	*E. acervulina* & *E. maxima*	*Artemisia annua* leaves (in feed)	Trial period	BWG, FCR	Reduced lesions & oocysts, better growth, immune response
Drăgan et al. (2014) [39]	Romania	Broilers (Ross 308)	*E. tenella*, 10,000 oocysts	*Artemisia annua* leaf powder (1.5% feed), *A. annua* + F. vulgare EO mix (7.5% water)	Trial period	BWG, FCR	Leaf powder: strong reduction in oocysts & lesions; EO mix: moderate effect

Table 2. Summary of pooled effect estimates obtained from random-effects models using the restricted maximum-likelihood estimator, heterogeneity tests, prediction intervals, and publication-bias assessments across outcomes

Outcome	Studies (k)	Egger p	Begg p	Pooled Effect	95% CI (LB-UB)	Q-test p	I^2 (%)	95% Prediction Interval
BWG (gms)	15	0.053	0.0048	8.08	-0.08 - 16.24	<0.001	69.8	-24.51 - 40.66
FCR	16	0.020	0.079	-0.13	-0.24 - -0.01	<0.001	99.0	-0.58 - 0.33
Total Protein (g/dL)	4	0.820	0.497	0.41	-0.15 - 0.97	<0.001	67.0	-0.82 - 1.64
OPG	6	0.0029	0.0048	-18.99	-37.91 - -0.08	<0.001	97.2	-68.44 - 30.45
FI	11	0.938	0.073	0.06	-1.65 - 1.76	<0.001	69.5	-5.63 - 5.74
Mortality (%) (RR)	4	0.092	0.174	0.49	0.27 - 0.89	0.476	0.0	0.27 - 0.89

Influence analysis (leave-one-out) *(Fig. 8)* demonstrated that the pooled result was not driven by any single trial. Baujat plot inspection *(Fig. 6-B)* suggested that a handful of studies contributed disproportionately to the variability in results, particularly those reporting unusually large effects in either direction.

Feed Intake (FI)

Eleven studies (total $N \approx 2064$) contributed FI data. The pooled mean difference was +0.055 (95% CI −1.655 to 1.765), effectively zero. No statistical significance was observed (CI includes zero). Forest plots *(Fig. 2-C)* showed mixed small effects: studies reported differences ranging from about −5.17 to +6.00 in FI, with most estimates near zero.

Tests for publication bias did not suggest strong asymmetry. Egger's P=0.938 and Begg's P=0.073 indicate no clear bias, though Begg's test was borderline. Trim-and-fill analysis imputed two small studies ($K_0=2$), which modestly adjusted the pooled MD to −0.723 (95% CI −2.559 to 1.113); this adjustment did not reveal a significant effect. The cumulative meta-analysis *(Fig. 5-C)* showed the pooled estimate remaining near zero as studies accrued, with consistently overlapping CIs. Influence analysis *(Fig. 9)* did not identify any single dominant study (the largest leave-one-out change was <0.5), suggesting no outsized influence. By the Baujat plot *(Fig. 6-C)*, no study stood out dramatically and variability in results appeared to reflect random small differences across trials.

Mortality

Four trials (total N≈672) reported mortality, analyzed as a risk ratio (RR). Essential oil supplementation significantly reduced mortality risk. The pooled RR was 0.493 (95% CI 0.273–0.891), indicating about a 51% relative reduction. This result reached statistical significance, as the 95% CI excludes 1.0. Notably, heterogeneity was negligible ($I^2=0\%$, $\tau^2=0$) and the Q-test P=0.476, suggesting consistent effects across studies. The 95% prediction interval (0.273-0.891) was the same as the confidence interval in this case. The forest plot *(Fig. 3-A)* showed that all studies had RR<1 (favoring essential oils), although two had wide confidence intervals crossing 1.0.

Assessment of funnel-plot asymmetry for mortality was highly uncertain because only four studies contributed data. Egger's test (P=0.092) and Begg's test (P=0.174) were not statistically significant, but the small number of studies provided insufficient power to exclude small-study effects or publication bias. The trim-and-fill procedure imputed one hypothetical study and produced a slightly attenuated pooled risk ratio; however, this adjustment should also be interpreted cautiously because trim-and-fill estimates are unstable when few studies are available. Cumulative meta-analysis *(Fig. 5-D)* showed that early results were variable: adding the final study [28] stabilized the pooled RR around 0.49. Leave-one-out analysis indicated that no single trial was overly influential (the largest change was $\Delta RR \approx -0.14$ when omitting Khan et al. [12] *(Fig. 10)*. In the Baujat plot *(Fig. 6-D)*, the modest heterogeneity arose mainly when an outlying study [25] was added, but overall heterogeneity stayed at zero after all studies were included. In summary, essential oils were associated with significantly lower mortality in coccidiosis-challenged birds.

Oocysts Per Gram (OPG)

Six studies (N≈484) provided oocyst count outcomes. The pooled mean difference was −18.99 (95% CI −37.91 to −0.08), indicating significantly lower oocyst shedding with essential oil treatment (negative MD favors essential oil). In the forest plot *(Fig. 3-B)*, all individual study MDs were negative (ranging roughly from −2.85 to −58.67), consistently favoring essential oils, but with one or two studies showing much larger reductions.

For oocyst counts, Egger's regression (P=0.0029) and Begg's test (P=0.0048) indicated funnel-plot asymmetry. These findings raise the possibility of small-study effects or selective publication; however, only six studies were available, limiting the reliability of both tests. Funnel asymmetry may also arise from substantial heterogeneity, differences in outcome measurement, or other methodological variation

rather than publication bias alone. The trim-and-fill procedure did not impute missing studies, but this result should not be considered sufficient to exclude reporting bias. Cumulative analysis *(Fig. 5-E)* showed a gradually strengthening negative effect, reaching significance only after the last study [30] was included. Influence analysis *(Fig. 11)* identified Giannenas et al.[30] as highly influential: removing it shifted the pooled MD by +7.04 (toward zero). In sum, the data suggested the potential benefit of essential oils in lowering coccidia shedding.

Total Protein

Four studies (N≈464) reported serum total protein (g/dL). The pooled difference was +0.409 (95% CI –0.155 to 0.972), favoring essential oils but not statistically significant. In the forest plot *(Fig. 3-C)*, one study [27] showed a large positive effect (+1.37), while others were closer to zero.

Egger's test (P=0.820) and Begg's test (P=0.497) did not indicate funnel-plot asymmetry. Nevertheless, only four studies contributed to this outcome, and the absence of statistical significance should not be interpreted as evidence that publication bias was absent. The trim-and-fill procedure did not impute missing studies, and the pooled estimate remained unchanged. Cumulative meta-analysis *(Fig. 5-F)* showed the pooled effect declining from +1.37 (from the first trial) to +0.409 as more studies were added, with confidence intervals tightening but always overlapping zero. Leave-one-out analysis *(Fig. 12)* identified Chang et al.[27] as influential (omitting it increased the pooled estimate by 0.253). Overall, there was no obvious evidence that essential oils significantly altered total protein levels.

General Synthesis

Across the evaluated outcomes, essential oil-based interventions showed variable effects in poultry challenged with *Eimeria* spp. The most consistent finding was a reduction in mortality, while oocyst shedding and feed conversion ratio also showed statistically significant pooled improvements. In contrast, the pooled increase in body weight gain was small and its confidence interval included the null value. Feed intake and serum total protein were not significantly affected. Wide prediction intervals for several outcomes further indicated that the magnitude and direction of effects may differ across intervention formulations and experimental conditions. Overall, the evidence suggests potential benefits for selected coccidiosis-related outcomes but does not support consistent improvement across all measures of growth performance and health.

Discussion

This meta-analysis evaluated the effects of essential oil-based interventions in poultry experimentally challenged with *Eimeria* spp. The pooled findings indicated a modest improvement in feed conversion ratio and reductions in mortality and fecal oocyst shedding. However, the estimated increase in body weight gain was small and statistically uncertain, while feed intake and serum total protein were not significantly affected. These results suggest that essential oil-based interventions may alleviate selected consequences of coccidial infection, particularly mortality, feed inefficiency, and parasite shedding, but they do not demonstrate consistent benefits across all growth and health outcomes.

These findings echo the results of many primary trials. For growth performance, multiple studies have reported that EOs improve weight gain and feed efficiency in coccidiosis-challenged chickens. Mohiti-Asli et al.[32] found that dietary oregano oil *(Origanum vulgare)* significantly increased BW gain and improved FCR in *Eimeria*-infected broilers. Similarly, Lee et al.[40] reported that an encapsulated blend of thymol and carvacrol (major oregano oil constituents) raised BW gain to levels comparable to a non-challenged control in vaccine-challenged broilers. Niknia et al.[41] likewise observed that broilers fed a thymol-carvacrol blend during *Eimeria* challenge had significantly greater BW gain and lower FCR than untreated infected birds. A blend of oregano and garlic oils also produced weight gains and feed efficiency similar to uninfected controls [34]. These improvements in BWG and FCR with EOs are consistent with our meta-pattern: in each case EO-supplemented birds "caught up" to healthy performance. In contrast, sham-challenged positive controls lagged behind. Notably, Chang et al.[27] showed that garlic oil alone prevented the weight loss normally caused by *Eimeria tenella*. They showed garlic EO-treated chickens had body weights significantly higher than untreated infected birds (and similar to those given the anticoccidial drug diclazuril). Taken together, individual trials frequently reported improvements in growth performance, but the pooled evidence was less definitive. Feed conversion ratio improved significantly, whereas the pooled effect on body weight gain remained statistically uncertain because the confidence interval included the null value. Differences in dose, formulation, challenge severity, and study duration may partly explain the variable responses. The findings therefore support a possible performance benefit but do not establish that essential oil-based interventions consistently improve growth under all challenge conditions [32,40,41].

Essential oil treatment also consistently reduced oocyst shedding and gut pathology. In our meta-analysis, EO supplementation was associated with a reduction in fecal oocyst counts. This aligns with reports by Chang et al.[27], who found that garlic EO significantly lowered cecal lesions and oocyst counts in *E. tenella*-infected birds.

Mohiti-Asli et al.[32] similarly showed that broilers fed 500 ppm oregano oil had much lower lesion scores and fecal OPG than infected controls, with values comparable to birds on diclazuril. In study by Sidiropoulou et al.[34], broilers given a premix of oregano + garlic oils excreted significantly fewer oocysts (~0.3-0.5 log unit reductions on days 28 and 37) than untreated birds. Thus, across many trials, EO supplementation reduced parasite load. Mortality was generally low across trials, but pooled results indicated a protective effect of EO treatment.

Beyond these primary outcomes, EOs appear to boost health indices. Coccidiosis typically depresses serum proteins and alters biochemical markers, and there is limited evidence that EOs can counteract this. For example, Chang et al.[27] reported that garlic EO treatment yielded higher levels of IgM, IgG and IgA (immunoglobulins) than controls. It indicated improved immune function and possibly reflecting better serum protein profiles (globulins). However, Lee et al.[40] saw no significant change in total protein with thymol/carvacrol dosing. In our meta, the paucity of serum protein data means we cannot conclusively quantify EO effects on this outcome. Overall, the consensus is that EOs likely mitigate the protein-depleting effect of coccidiosis by improving gut integrity and reducing inflammation.

The ability of EOs to alleviate coccidial effects is biologically plausible given their well-established antimicrobial, anti-inflammatory, and immunomodulatory properties. Many EOs contain phenolic compounds (e.g. thymol, carvacrol, eugenol, cinnamaldehyde, allicin) that are known to be lethal to pathogens. *In vitro* experiments confirm that these compounds directly damage *Eimeria* parasites: for instance, thymol and carvacrol at ≥2% concentration destroyed 90-96% of *E. tenella* oocysts and inhibited sporulation [5]. Piper betle leaf oil (rich in eugenol and terpenes) similarly caused dose-dependent inhibition of oocyst sporulation and wall disintegration *in vitro. In vivo,* such actions would translate to fewer infective oocysts and reduced cecal invasion. These antimicrobial effects are complemented by the broader activity of EOs against gut pathogens and microbiota: many studies (including the BA+OEO trial) noted that EOs suppressed harmful bacteria *(Salmonella, E. coli, Clostridium)* while boosting beneficial Lactobacilli. This shift in the microbiome can enhance gut health and indirectly reduce the severity of coccidiosis [31].

EOs also exert strong immunomodulatory and anti-inflammatory effects that support resistance to *Eimeria*. Several studies highlight that EO components stimulate host immunity: for example, cinnamaldehyde supplementation increased intestinal cytokine gene expression (IL-1β, IL-6, IL-15, IFN-γ) and reduced weight loss and oocyst shedding in infected birds [42]. In the BA+OEO study, oregano oil upregulated interferon-γ (IFN-γ) mRNA and suppressed interleukin-10 and TLR-4 expression, while enhancing *Eimeria*-specific IgY antibody titer [31]. These immunostimulatory effects can fortify the host's defenses, helping control the parasite. At the same time, EOs' anti-inflammatory action protects intestinal tissues: by quenching oxidative stress and moderating pro-inflammatory signaling, EOs reduce tissue damage that would otherwise impair digestion and absorption [43] .

The results of our meta-analysis carry significant implications for commercial poultry production, particularly under conditions where the use of conventional drugs is restricted (e.g., organic or antibiotic-free systems). Resistance to traditional coccidiostats (ionophores and chemicals) is increasing, while consumer demand for antibiotic-free poultry products continues to rise [44]. Essential oil-based interventions may have potential as complementary components of anticoccidial-control programs, although the present evidence is insufficient to establish them as direct replacements for conventional anticoccidial agents. The BA+OEO trial explicitly concluded that oregano oil plus benzoic acid "can substitute for a commercial anti-coccidial agent (salinomycin)" by controlling coccidiosis and enhancing growth and immunity. Similarly, the encapsulated thymol/carvacrol blend was as effective as salinomycin in a vaccine-challenge model [40]. Thus, selected essential oil-based formulations may be considered for integration into feed as part of broader coccidiosis-management strategies, but their effectiveness should be confirmed through standardized comparative and field-based trials. They may also pair well with vaccines; for example, encapsulated oils offset the temporary growth depression often seen after coccidiosis vaccination. Moreover, because EOs can improve general gut health and microbiota balance, they could provide broad performance benefits in intensive systems [41,42].

However, practical adoption requires addressing challenges. The cost and consistency of EOs vary widely; high-quality, food-grade oils can be expensive. Regulatory approval for the use of plant extracts in organic systems is another hurdle. Also, effects may differ by species and environment [7]. Nevertheless, the literature suggests that EOs can fit into antibiotic- and anticoccidial-free programs: for example, synbiotic blends of probiotics and EO extracts have been shown to ameliorate coccidiosis impacts in broilers, improving intestinal health [42]. In summary, EOs represent a promising tool for sustainable poultry production, but they should be viewed as part of an integrated management strategy (along with vaccination, biosecurity, nutrition) rather than a standalone cure.

The main challenge in interpreting these findings is the variability among studies. Differences in EO source, dose,

formulation, delivery method, bird strain, age, housing, and infection model contributed to between-study heterogeneity. Some trials used mild vaccine challenges, while others employed high-dose *Eimeria* inoculations of mixed species, leading to differences in disease severity and response to EOs. Moreover, many trials were small (few pens) and measured outcomes only over a short window (often 1-2 weeks post-infection). Another limitation is the diversity in reported outcomes. Although subgroup analysis and meta-regression could potentially identify sources of heterogeneity, the limited number of studies per outcome and the inconsistent reporting of essential oil composition, dose, administration route, and challenge characteristics precluded meaningful moderator analyses. While most trials assessed growth and oocyst counts, relatively few included immunological, microbiological, or detailed histological parameters, restricting deeper understanding of mechanisms.

Possible publication bias should also be considered when interpreting the pooled findings. Funnel-plot asymmetry and statistical tests suggested potential small-study effects for body weight gain and, more clearly, for oocyst counts. Therefore, the pooled estimates for these outcomes may partly overestimate the true effects of essential oils, particularly if small studies reporting null or unfavorable results remain unpublished. Nevertheless, publication-bias tests have limited reliability when few studies are available, and the trim-and-fill analysis did not identify missing studies for either outcome. Accordingly, the observed effects, especially the reduction in oocyst shedding, should be interpreted cautiously rather than regarded as definitive. Some studies did find minimal effects of EOs on growth - for example, Zoroaster et al.[37] reported no significant improvement in ADG or FCR with low-dose thymol/carvacrol *in vivo*, despite potent *in vitro* effects. A specific limitation is the lack of standardization in challenge protocols. Some used live commercial vaccines (attenuated *Eimeria),* others used purified sporulated oocysts of one or more species. The intensity of infection and timing relative to measurements varied. For instance, Mohiti-Asli & Ghanaatparast-Rashti [32] challenged with a vaccine and measured on day 28, whereas Chang et al.[27] infected with *E. tenella* oocysts and measured over 7 days. These differences influence the apparent efficacy of EOs. A formal risk-of-bias assessment of the included studies was not performed, which represents an important limitation of this meta-analysis. Several primary studies provided insufficient information regarding random sequence generation, allocation concealment, blinding of investigators or outcome assessors, and selective outcome reporting. Consequently, the methodological quality and internal validity of the included evidence could not be systematically quantified, and the pooled estimates should therefore be interpreted with appropriate caution.

Future research should prioritize adequately powered, standardized, and long-term trials. Experimental protocols should clearly define poultry species, strain, age, housing conditions, *Eimeria* species, inoculation or vaccine dose, challenge timing, and outcome-assessment periods. Essential oil source, chemical composition, formulation, dose, and administration route should also be reported consistently. Trials should evaluate essential oil-only interventions separately from multicomponent formulations to allow the independent effects of essential oils to be determined. In addition to growth performance and oocyst shedding, future studies should assess lesion scores, intestinal histology, microbiota composition, inflammatory and immune markers, product quality, safety, and economic feasibility. Field-based studies conducted under commercial production conditions are particularly needed to determine whether the observed experimental effects translate into practical benefits.

Conclusion

This meta-analysis indicates that essential oil-based interventions were associated with a modest improvement in feed conversion ratio and reductions in mortality and oocyst shedding in poultry challenged with *Eimeria* spp. The pooled effect on body weight gain was statistically uncertain, while feed intake and serum total protein were not significantly affected. The findings therefore do not demonstrate consistent benefits across all evaluated outcomes. In addition, because some interventions contained other active components, their effects cannot be attributed exclusively to essential oils. Essential oil-based interventions may have potential as components of integrated coccidiosis-management programs, but further standardized, adequately powered, and field-based studies are required before firm conclusions regarding their practical efficacy can be made.

Declaration

Availability of Data and Materials: All data analyzed in this study were obtained from the published articles cited in the manuscript. The extracted dataset used in the meta-analysis is available from the corresponding author upon reasonable request.

Acknowledgements: The author has no acknowledgements to declare.

Competing Interests: The author declares that there are no commercial, financial, or personal relationships that could be construed as potential competing interests.

Declaration of Generative Artificial Intelligence: No GenAI was used in preparation of the manuscript.

Authors' Contributions: Ayed Alshammari: Conceptualization, data curation, formal analysis, project administration, supervision, writing-original draft, and writing-review and editing. The author read and approved the final version of the manuscript.

References

1. **Felici M, Tugnoli B, De Hoest-Thompson C, Piva A, Grilli E, Marugan-Hernandez V:** Thyme, oregano, and garlic essential oils and their main active compounds influence *Eimeria tenella* intracellular development. *Animals,* 14:77, 2023. DOI: 10.3390/ani14010077
2. **Badri M, Olfatifar M, Hayati A, Bijani B, Samimi R, Abdoli A, Nowak O, Diaz D, Eslahi AV:** The global prevalence and associated risk factors of *Eimeria* infection in domestic chickens: A systematic review and meta-analysis. *Vet Med Sci,* 10:e1469, 2024. DOI: 10.1002/vms3.1469
3. **Mousa MR, Attia MM, Salem HM, Al-Hoshani N, Thabit H, Ibrahim MA, Albohiri HH, Khan SA, El-Saadony MT, El-Tarabily KA, El-Saied MA:** Coinfection of the gut with protozoal and metazoal parasites in broiler and laying chickens. *Poult Sci,* 103:103227, 2024. DOI: 10.1016/j.psj.2023.103227
4. **Mathis GF, Lumpkins B, Cervantes HM, Fitz-Coy SH, Jenkins MC, Jones MK, Price KR, Dalloul RA:** Coccidiosis in poultry: Disease mechanisms, control strategies, and future directions. *Poult Sci,* 104:104663, 2025. DOI: 10.1016/j.psj.2024.104663
5. **Zoroaster A, Singh Y, Simonato G, Raffaelli M, Frangipane di Regalbono A:** Essential oils effectiveness against the most impactful parasites in poultry farming: A review. *Worlds Poult Sci J,* 81, 917-945, 2025. DOI: 10.1080/00439339.2025.2510425
6. **Bharti P, Tanveer S, Wani ZA, Rather SA, Parray ZA:** Insight into poultry coccidiosis: a dual focus on anticoccidial drugs and herbal plants for pharmacological and prevention strategies. *J Parasit Dis,* 49, 565-582, 2025. DOI: 10.1007/s12639-025-01805-3
7. **Saeed Z, Alkheraije KA:** Botanicals: A promising approach for controlling cecal coccidiosis in poultry. *Front Vet Sci,* 10:1157633, 2023. DOI: 10.3389/fvets.2023.1157633
8. **Snyder R:** Coccidiosis in commercial broiler chickens: Improving management of *Eimeria* species using live-vaccination or anticoccidial medication and developing and applying quantitative species-specific molecular assays. 2021. https://atrium.lib.uoguelph.ca/server/api/core/bitstreams/dde4b4d6-77a7-4a68-af30-7ad3f363704a/content; *Accessed:* 08 September 2025
9. **Mesfin YM, Mitiku BA, Tamrat Admasu H:** Veterinary drug residues in food products of animal origin and their public health consequences: A review. *Vet Med Sci,* 10:e70049, 2024. DOI: 10.1002/vms3.70049
10. **Hauck R, Macklin KS:** Vaccination against poultry parasites. *Avian Dis,* 67, 441-449, 2023. DOI: 10.1637/aviandiseases-D-23-99989
11. **Zhao D, Suo J, Liang L, Liang R, Zhou R, Ding J, Liu X, Suo X, Zhang S, Tang X:** Innovative prevention and control of coccidiosis: Targeting sporogony for new control agent development. *Poult Sci,* 103:104246, 2024. DOI: 10.1016/j.psj.2024.104246
12. **Khan M, Chand N, Naz S, Khan RU:** Dietary tea tree *(Melaleuca alternifolia)* essential oil as alternative to antibiotics alleviates experimentally induced *Eimeria tenella* challenge in Japanese quails. *J Anim Physiol Anim Nutr (Berl),* 107, 643-649, 2023. DOI: 10.1111/jpn.13719
13. **Geng T, Ruan X, Xie Y, Shen B, Fang R, Zhao J, Zhou Y:** Anticoccidial activity of a botanical natural product based on eucalyptus, apigenin and eugenol against *Eimeria tenella* in broiler chickens. *Parasit Vectors,* 17:327, 2024. DOI: 10.1186/s13071-024-06409-z
14. **Rusli RK, Santi MA, Nuraini, Hilmi M, Mirzah, Hidayat C, Darmawan A, Khairani, Mutia R, Mirnawati, Jayanegara A, Irawan A:** Essential oils alleviate coccidiosis impact in broiler chickens: A meta-analysis. *Anim Biosci,* 38, 2726-2740, 2025. DOI: 10.5713/ab.25.0267
15. **Zuhair D, Mounia A, Ayman D, Samia B:** The anti-parasitic activity of *Thymus vulgaris* (Thyme): A literature review. *Intl J Sci Res Arch,* 11, 2243-2258, 2024. DOI: 10.30574/ijsra.2024.11.1.0302
16. **Gattan HS, Wakid MH, Qahwaji RM, Altwaim S, Mahjoub HA, Alfaifi MS, Elshazly H, Al-Megrin WAI, Alshehri EA, Elshabrawy HA:** *In silico* and *in vivo* evaluation of the anti-cryptosporidial activity of eugenol. *Front Vet Sci,* 11:1374116, 2024. DOI: 10.3389/fvets.2024.1374116
17. **Galamatis D, Stylianaki I, Mantzios T, Makri V, Papadopoulos E, Caldwell J, Harrington D, Blake D, Tsiouris V, Giannenas I:** The effectiveness of phytobiotic additives on performance and intestinal health of broilers after challenging with *Eimeria* spp. *Discover Animals,* 2:32, 2025. DOI: 10.1007/s44338-025-00074-x
18. **Page MJ, McKenzie JE, Bossuyt PM, Boutron I, Hoffmann TC, Mulrow CD, Shamseer L, Tetzlaff JM, Akl EA, Brennan SE:** The PRISMA 2020 statement: An updated guideline for reporting systematic reviews. *BMJ,* 372:n71, 2021. DOI: 10.1136/bmj.n71
19. **Viechtbauer W, Cheung MWL:** Outlier and influence diagnostics for meta-analysis. *Res Synth Methods,* 1, 112-125, 2010. DOI: 10.1002/jrsm.11
20. **Mao Y, Shen Y, Yang Q, Shi Q, Li S:** A leave-one-out algorithm for contribution analysis in component network meta-analysis. *BMC Med Res Methodol,* 25:191, 2025. DOI: 10.1186/s12874-025-02619-w
21. **Baujat B, Mahé C, Pignon J, Hill C:** A graphical method for exploring heterogeneity in meta-analyses: Application to a meta-analysis of 65 trials. *Stat Med,* 21, 2641-2652, 2002. DOI: 10.1002/sim.1221
22. **Kulinskaya E, Mah EY:** Cumulative meta-analysis: What works. *Res Synth Methods,* 13, 48-67, 2022. DOI: 10.1002/jrsm.1522
23. **Abou-Elkhair R, Gaafar KM, Elbahy NM, Helal MA, Mahboub HD, Sameh G:** Bioactive effect of dietary supplementation with essential oils blend of oregano, thyme and garlic oils on performance of broilers infected with *Eimeria* species. *Glob Vet,* 13, 977-985, 2014.
24. **Alp M, Midilli M, Kocabağlı N, Yılmaz H, Turan N, Gargılı A, Acar N:** The effects of dietary oregano essential oil on live performance, carcass yield, serum immunoglobulin G level, and oocyst count in broilers. *J Appl Poult Res,* 21, 630-636, 2012. DOI: 10.3382/japr.2012-00551
25. **Barbour EK, Bragg RR, Karrouf G, Iyer A, Azhar E, Harakeh S, Kumosani T:** Control of eight predominant *Eimeria* spp. involved in economic coccidiosis of broiler chicken by a chemically characterized essential oil. *J Appl Microbiol,* 118, 583-591, 2015. DOI: 10.1111/jam.12731
26. **Bozkurt M, Ege G, Aysul N, Akşit H, Tüzün AE, Küçükyılmaz K, Borum AE, Uygun M, Akşit D, Aypak S, Şimşek E, Seyrek K, Koçer B, Bintaş E, Orojpour A:** Effect of anticoccidial monensin with oregano essential oil on broilers experimentally challenged with mixed *Eimeria* spp. *Poult Sci,* 95, 1858-1868, 2016. DOI: 10.3382/ps/pew077
27. **Chang L, Di K, Xu J, Chen Y, Xi J, Wang DH, Hao E, Xu L, Chen H, Zhou R:** Effect of natural garlic essential oil on chickens with artificially infected *Eimeria* tenella. *Vet Parasitol,* 300:109614, 2021. DOI: 10.1016/j.vetpar.2021.109614
28. **Christaki E, Florou-Paneri P, Giannenas I, Papazahariadou M, Botsoglou NA, Spais AB:** Effect of a mixture of herbal extracts on broiler chickens infected with *Eimeria tenella*. *Anim Res,* 53, 137-144, 2004. DOI: 10.1051/animres:2004006
29. **de Oliveira Moraes P, da Silva Pires PG, Benetti Filho V, Lima ALF, Kindlein L, Taschetto D, Favero A, Wagner G:** Intestinal health of broilers challenged with *Eimeria* spp. using functional oil blends in two physical forms with or without anticoccidials. *Sci Rep,* 13:14612, 2023. DOI: 10.1038/s41598-023-41743-9
30. **Giannenas I, Florou-Paneri P, Papazahariadou M, Christaki E, Botsoglou NA, Spais AB:** Effect of dietary supplementation with oregano essential oil on performance of broilers after experimental infection with *Eimeria tenella*. *Arch Anim Nutr,* 57, 99-106, 2003. DOI: 10.1080/0003942031000107299
31. **Khukhodziinai JS, Das PK, Mukherjee J, Banerjee D, Ghosh PR, Das AK, Samanta I, Jas R, Mondal S, Patra AK:** Effect of dietary benzoic acid and oregano essential oil as a substitute for an anti-coccidial agent on growth performance and physiological and immunological responses in broiler chickens challenged with *Eimeria* species. *Animals,* 14:3008, 2024. DOI: 10.3390/ani14203008
32. **Mohiti-Asli M, Ghanaatparast-Rashti M:** Dietary oregano essential oil alleviates experimentally induced coccidiosis in broilers. *Prev Vet Med,* 120, 195-202, 2015. DOI: 10.1016/j.prevetmed.2015.03.014

33. **Qaid MM, Al-Mufarrej SI, Azzam MM, Al-Garadi MA:** Anticoccidial effectivity of a traditional medicinal plant, *Cinnamomum verum,* in broiler chickens infected with *Eimeria tenella*. *Poult Sci,* 100:100902, 2021. DOI: 10.1016/j.psj.2020.11.071

34. **Sidiropoulou E, Skoufos I, Marugan-Hernandez V, Giannenas I, Bonos E, Aguiar-Martins K, Lazari D, Blake DP, Tzora A:** *In vitro* anticoccidial study of oregano and garlic essential oils and effects on growth performance, fecal oocyst output, and intestinal microbiota *in vivo*. *Front Vet Sci,* 7:420, 2020. DOI: 10.3389/fvets.2020.00420

35. **Tolomeotti LS, Goes RHTB, Cangianelli GH, Khatlab AS, Pontes KM, Matos EB, Vesco AP Del, Miglioranza S, Gasparino E:** Effect of a blend of essential oils, organic acids, tannins, vitamin E and zinc on the intestinal health of broiler chickens challenged with *Eimeria* spp., *Salmonella Minnesota*, *Escherichia coli* and *Clostridium perfringens*. *Pesqui Vet Bras,* 44:e07404, 2024. DOI: 10.1590/1678-5150-pvb-7404

36. **Upadhaya SD, Cho SH, Chung TK, Kim IH:** Anti-coccidial effect of essential oil blends and vitamin D on broiler chickens vaccinated with purified mixture of coccidian oocyst from *Eimeria tenella* and *Eimeria maxima*. *Poult Sci,* 98, 2919-2926, 2019. DOI: 10.3382/ps/pez040

37. **Zoroaster A, Raffaelli M, Diaferia M, Veronesi F, Marzoni Fecia di Cossato M, Contiero B, Marani R, Frangipane di Regalbono A, Perrucci S:** *In vitro* and *in vivo* effectiveness of essential oils against coccidia in Black Livorno chickens. *BMC Vet Res,* 21:465, 2025. DOI: 10.1186/s12917-025-04916-4

38. **Aziza AE, Orma OA, Awadin WF, Seady YE:** Effects of supplementation of broiler diets with fish oil and linseed oil on growth performance, cytokines, and cecal histopathological changes in broiler chickens infected by *Eimeria*. *Intl J Agri Sci Vet Med,* 4, 12-27, 2016.

39. **Drăgan L, Györke A, Ferreira JFS, Pop IA, Dunca I, Drăgan M, Mircean V, Dan I, Cozma V:** Effects of *Artemisia annua* and *Foeniculum vulgare* on chickens highly infected with *Eimeria tenella* (Phylum Apicomplexa). *Acta Vet Scand,* 56:22, 2014. DOI: 10.1186/1751-0147-56-22

40. **Lee JW, Kim DH, Kim YB, Jeong SB, Oh ST, Cho SY, Lee KW:** Dietary encapsulated essential oils improve production performance of coccidiosis-vaccine-challenged broiler chickens. *Animals,* 10:481, 2020. DOI: 10.3390/ani10030481

41. **Niknia A, Vakili R, Palangi V:** Feeding a blend of thymol and carvacrol to coccidiosis challenged broilers: Effect on performance and gut health. *J Hellenic Vet Med Soc,* 75, 8335-8342, 2025. DOI: 10.12681/jhvms.36991

42. **Khater HF:** Avian coccidiosis: Recent advances in alternative control strategies and vaccine development. *Agrobiol Rec,* 1, 11-25, 2020. DOI: 10.47278/journal.abr/2020.003

43. **Spisni E, Petrocelli G, Imbesi V, Spigarelli R, Azzinnari D, Donati Sarti M, Campieri M, Valerii MC:** Antioxidant, anti-inflammatory, and microbial-modulating activities of essential oils: implications in colonic pathophysiology. *Int J Mol Sci,* 21:4152, 2020. DOI: 10.3390/ijms21114152

44. **Pokludová L:** Poultry. Antimicrobials in Livestock 2: Choices of Prevention and Treatment, 135-214, Cham: Springer Nature Switzerland, 2024.

Kafkas Universitesi Veteriner Fakultesi Dergisi
Journal Home-Page: http://vetdergikafkas.org
E-ISSN: 1309-2251

Kafkas Univ Vet Fak Derg
32 (4): 493-500, 2026
DOI: 10.9775/kvfd.2026.36538

RESEARCH ARTICLE

Antibacterial Activity of Chlorocresol Nanoemulsion Disinfectant Against *E. coli* and Its Application Evaluation

Xuefeng YANG [1,2 (#)], Yawei SUN [1,2 (#)], Dongyang LIU [1,2], Zhixing AN [1,2], Changzhong LIU [1,2 (*)]

[#] *These authors contributed equally to this work*

[1] Henan Institute of Science and Technology, College of Animal Science and Veterinary Medicine, Veterinary Medicine Department, 453003, Xinxiang City, CHINA

[2] Henan International Joint Laboratory of Animal Health Breeding and Disease Prevention and Control, Henan Institute of Science and Technology, College of Animal Science and Veterinary Medicine, Veterinary Medicine Department, 453003, Xinxiang City, CHINA

[(*)] **Corresponding author:**
Changzhong Liu
Phone: +86 373 3040718
Cellular phone: +86 15103733474
Fax: +86 373 3040718
E-mail: 693361358@qq.com

How to cite this article?

Yang X, Sun Y, Liu D, An Z, Liu C: Antibacterial Activity of Chlorocresol Nanoemulsion Disinfectant Against *E. coli* and Its Application Evaluation. *Kafkas Univ Vet Fak Derg*, 32 (4): 493-500, 2026.
DOI: 10.9775/kvfd.2026.36538

Article ID: KVFD-2026-36538
Received: 08.03.2026
Accepted: 01.07.2026
Published Online: 03.07.2026

Abstract

This study investigated the antibacterial activity and disinfection efficacy of chlorocresol nanoemulsion disinfectant (CND) against *Escherichia coli*. The minimum inhibitory concentration (MIC) and minimum bactericidal concentration (MBC) were determined, and alterations in bacterial ultrastructure were examined using scanning and transmission electron microscopy (SEM and TEM). The disinfection performance was further evaluated through simulated and field surface disinfection trials. The results showed that the MIC and MBC of CND against *E. coli* were 100 μg/mL and 200 μg/mL, respectively. After 0.06% CND treatment for 10 min, SEM revealed disrupted surface architecture with flagella loss and cell wall damage, while TEM showed compromised internal integrity including periplasmic narrowing and cytoplasmic aggregation. The disinfectant efficacy of CND increased with increasing contact time and concentration. In simulated surface trials, effective disinfection was achieved with 0.1% CND applied for ≥15 min or with CND concentrations ≥0.2%. In field trials, effective disinfection was achieved with 0.05% CND applied for ≥10 min or with CND concentrations ≥0.1%. These findings indicate that CND exhibits strong antibacterial activity against E. coli, causes significant ultrastructural alterations, and demonstrates effective disinfection performance.

Keywords: Antibacterial activity, Chlorocresol nanoemulsion disinfectant, Disinfection efficacy, *E. coli*, Ultrastructure

INTRODUCTION

The global transition of animal husbandry toward intensification and large-scale operations has led to high-density farming models. These models significantly enhance pathogen transmission and accelerate the spread of drug-resistant microorganisms, posing severe challenges to animal disease prevention and control [1,2]. To block the transmission of pathogenic microorganisms, environmental disinfection has become one of the most fundamental and critical measures for establishing a biosecurity system on farms [3,4]. Extensive evidence indicates that disinfection is an essential measure for the effective prevention and control of infectious diseases [5-7]. Disinfectants play a leading role in reducing the spread of pathogens among animals and their transfer from animals to humans as well as limiting the infections in animals and humans [6]. Currently, the thorough and standardized application of disinfectants in livestock housing and the environment is a key preventive strategy. It interrupts transmission routes, eliminates sources of infection, and inactivates pathogens. This approach represents one of the most efficient and practical methods for implementing a preventive disease control strategy. However, some disinfectants exhibit limitations, including unstable efficacy, a propensity to induce pathogen resistance, and the generation of substantial by-products, which restrict their widespread application [8,9]. Therefore, the development and practical implementation of novel disinfectants with high efficacy, environmental safety, and low cost is a key task in veterinary sanitation [5].

Chlorocresol is a chemical disinfectant composed of chlorine and phenols [10,11]. It is primarily used for

disinfecting livestock housing, vehicles, equipment, and the environment [12-14]. However, its development and clinical application are limited by several drawbacks, notably poor water solubility and a characteristic phenolic odor [12]. According to the Veterinary Drug Quality Standards (2017 ed., Chemical Drugs Volume), the existing formulation is Chlorocresol Solution [15]. Chlorocresol nanoemulsion disinfectant (CND) is a novel environmental disinfectant developed by our research group, with chlorocresol as the active ingredient. It offers several advantages, including good water solubility, reduced phenolic odor, strong disinfection efficacy, and a simple production process [16,17]. Additionally, our group has previously investigated its bactericidal effects and mechanism of action against common microorganisms found in livestock and poultry environments, such as *Staphylococcus aureus* [18] and *Candida albicans* [19]. While the efficacy of CND against these microorganisms has been established, its activity against Gram-negative bacteria, particularly *Escherichia coli,* a key indicator organism in environmental hygiene, remains unexplored. *E. coli* is a Gram-negative bacterium widely present in the natural environment. Given its impact on animal and human health, developing effective management strategies is essential [20]. The purpose of this study was to evaluate the antibacterial activity of CND against *E. coli*, its effects on bacterial ultrastructure, and its field disinfection efficacy. The findings are intended to support its future clinical application.

Material and Methods

Ethical Statement

This study did not require ethical approval.

Bacterial Strain

E. coli 8099 was used in accordance with the guidelines of China's Technical Standard for Disinfection (Ministry of Health of the People's Republic of China, 2002) [21]. This bacterial strain was maintained and supplied by the Animal Pharmacology Laboratory at Henan Institute of Science and Technology, in Xinxiang, China.

Disinfectant Preparation

CND was prepared as previously described by Yang et al.[17]. CND was an O/W nanoemulsion and its mean droplet size was 27.43 nm with normal distribution. The conductivity, viscosity and pH values were 479.67 μs/cm, 204.33 cp and 2.52, respectively. CND has good stability and could be stored for 2 years. Before use, CND was diluted to the required concentration with distilled water.

Neutralizer Selection

Selecting an appropriate neutralizer is essential for accurately evaluating disinfectant efficacy [22]. To ensure precise quantification of surviving microorganisms, a suitable neutralizer must be applied immediately after the contact period to rapidly inactivate any residual disinfectant, thereby preventing its continued antimicrobial action. To ensure accurate efficacy assessment, a neutralizer validation test was conducted following the Technical Standard for Disinfection (2002) [21]. The results confirmed that a solution of 3% Tween 80 in phosphate-buffered saline (PBS) effectively neutralized CND without affecting *E. coli* viability, and was therefore used as the appropriate neutralizer for all subsequent antimicrobial evaluations [17].

Determination of *In Vitro* Antibacterial Activity

The minimum inhibitory concentration (MIC) of CND against *E. coli* was determined using the broth dilution method, following the Technical Standard for Disinfection (2002) [21]. First, CND was diluted with distilled water to obtain a series of test solutions at concentrations of 10, 30, 50, 100, 200, 300, 400, and 500 μg/mL. Then, 2.5 mL of each test solution was added to tubes containing 2.5 mL of Mueller-Hinton broth (MHB) and mixed thoroughly. Subsequently, 100 μL of an *E. coli* suspension (10^8 CFU/mL) was inoculated into each tube to form the test groups. For the positive control, the bacterial suspension was inoculated into tubes containing MHB without disinfectant, following the same procedure. The tube served as the positive control group. Another tube containing only MHB medium was used as the negative control. All tubes from the test, positive control, and negative control groups were incubated at 37°C for 24 h, after which the results were observed and recorded. The MIC was considered as the lowest concentration capable of inhibiting 100% of microbial growth [23]. Furthermore, 1 mL of broth from each tube showing no visible growth was subcultured onto disinfectant-free agar medium. After incubation at 37°C for 24 h, the minimum concentration at which no bacterial growth was observed on the subculture was defined as the minimum bactericidal concentration (MBC). The experiment was repeated five times, and the mode values were taken as the final MIC and MBC [24].

Effects of CND on the Ultrastructure of *E. coli*

Sample Preparation

A 5 mL aliquot of an *E. coli* suspension (1×10^8 to 5×10^8 CFU/mL) was added to 45 mL of 0.06% CND and mixed thoroughly. After 10 min of exposure, the mixture was rapidly neutralized by adding 450 mL of a neutralizer solution (3% Tween 80) and mixed for an additional 10 min. The sample was then centrifuged at 6000 rpm for 3 min at 4°C. The supernatant was discarded, and the resulting bacterial pellet was washed three times with PBS by centrifugation. The final pellet was retained for

subsequent analysis. For the control group, PBS was used in place of CND, while all other steps remained identical. Both the test and control samples were each divided into two portions: one for observation by scanning electron microscopy (SEM) and the other for transmission electron microscopy (TEM).

Preparation and Observation of SEM Samples

The bacterial pellet was resuspended and fixed in 2.5% glutaraldehyde, then stored overnight at 4°C. It was subsequently centrifuged at 6000 rpm for 3 min at 4°C. After discarding the supernatant, the pellet was dehydrated in a graded ethanol series (30%, 50%, 70%, 80%, 90%, and 100%), with each step lasting 8 min. The sample was then resuspended in 100% ethanol for an additional 8 min. A drop of the suspension was evenly spread on a glass slide and air-dried. Finally, the sample was sputter-coated with gold. Morphological changes in *E. coli* before and after disinfectant treatment were observed and photographed using a scanning electron microscope (SEM, Quanta 200, FEI Company, USA). Control group samples were processed identically.

Preparation and Observation of TEM Samples

The bacterial pellet was fixed with 2.5% glutaraldehyde and then post-fixed with 1% osmium tetroxide. Dehydration was performed sequentially in 50% ethanol for 20 min, 70% ethanol overnight, 90% ethanol for 20 min, followed by another overnight incubation in 90% ethanol. The sample was further dehydrated in a 1:1 (v/v) mixture of 90% acetone and the bacterial suspension for 20 min, followed by 90% acetone for an additional 20 min. It was then infiltrated with 100% acetone three times (15 min each) at room temperature. Subsequently, the sample was embedded in resin and sectioned into ultrathin slices. The sections were stained with uranyl acetate and lead citrate, then observed and photographed using a transmission electron microscope (TEM, H-7500, digital CCD camera system, Hitachi Company, Japan). Control group samples were processed identically.

Simulated Field Trial for Surface Disinfection

A simulated field trial was conducted following a standard method for evaluating disinfection efficacy on general surfaces [21]. A wooden desktop was used as the representative test surface. The test microbial suspension was *E. coli* at a concentration of 2.5×10^7 to 1.25×10^8 CFU per sample, which was used to evaluate the disinfectant efficacy of CND.

The trial included a negative control group, a positive control group, and CND test groups. For the test groups, CND was applied at concentrations of 0.1%, 0.2%, 0.5%, and 1.0%. The contact times tested for each concentration were 5, 10, and 15 min.

The experimental procedure was conducted as follows:

Wooden desktop surfaces were disinfected by applying different concentrations of CND. After 5, 10, and 15 min of contact, a sterile cotton swab was moistened in a tube containing 10 mL of neutralizer solution, pressed against the tube wall to remove excess liquid, and then used to swab the disinfected area. The swab tip was aseptically cut into the original neutralizer tube, mixed thoroughly, and subjected to bacterial culture and counting as the test group sample. For the positive control group, a sterile cotton swab was moistened in a tube containing 10 mL of PBS dilution solution, pressed against the tube wall, and then used to swab the control area. The swab tip was aseptically cut into the original dilution tube, mixed thoroughly, appropriately diluted, and then cultured for bacterial counting. Samples of the neutralizer solution, dilution solution, swabs, and culture media from the same batch were cultured and counted as the negative control.

The test was repeated three times. Killing log (KL) value was calculated as follows: KL value = l g (viable bacterial concentration in the positive control) - l g (viable bacterial concentration in the test group). According to the Chinese Technical Standard for Disinfection (2002), effective disinfection was defined as achieving a mean KL value ≥3 for the simulated field trial.

Field Trial for Surface Disinfection

A field trial was conducted on the concrete floor of the Animal Physiology Laboratory at Henan University of Science and Technology to evaluate the disinfection efficacy of CND. The procedure followed the standard method for field evaluation of disinfection efficacy on general surfaces [21], as described in reference [17]. The experimental groups and contact times were identical to those used in the simulated field trial. However, the disinfectant concentrations tested for the CND groups were 0.05%, 0.1%, 0.2%, and 0.5%. The test was repeated three times. According to the Chinese Technical Standard for Disinfection (2002), effective disinfection was defined as achieving a mean KL value ≥1 for the field trial, whereas a mean KL value ≥3 was required for the simulated field trial.

Results

In Vitro Antibacterial Activity

After incubation, no visible bacterial growth was observed in the negative control tube or in tubes containing CND at concentrations ranging from 100 to 250 μg/mL. In contrast, visible growth was observed in the positive control tube and in tubes with CND concentrations between 5 and 50 μg/mL. These results indicated that the MIC of CND against *E. coli* was 100 μg/mL. Subsequently, broth from tubes containing CND at concentrations of

100 to 250 µg/mL was subcultured onto agar medium. Bacterial growth was observed from subcultures of tubes with CND concentrations between 100 and 150 µg/mL, while no growth occurred from those with concentrations between 200 and 250 µg/mL. These findings demonstrate that the MBC of CND against *E. coli* was 200 µg/mL.

Effects of CND on the Ultrastructure of *E. coli* Cells

SEM Observations

SEM observations of *E. coli* were shown in *Fig. 1*. Untreated *E. coli* cells exhibited a short, rod-shaped morphology with peritrichous flagella and rounded ends. The cell surfaces were smooth, without folds, protrusions, or depressions *(Fig. 1-A)*. After treatment with CND for 10 min, significant alterations in surface structure were observed. The peritrichous flagella were absent, and the cell surfaces became rough and uneven. Some bacteria exhibited distinct depressions or protrusions *(Fig. 1-B)*. In other cells, damage to the cell wall structure was observed, characterized by spiky projections *(Fig. 1-C)* or severe surface disruption leading to fragmentation, accompanied by wrinkling and spiky protrusions *(Fig. 1-D)*.

TEM Observations

TEM observations of *E. coli* were shown in *Fig. 2*. Untreated cells displayed a short, rod-shaped morphology with intact structure. A clear periplasmic space was observed between the thick, electron-dense outer cell wall and the inner cell membrane. The cytoplasm was uniformly distributed, and no gaps were observed between the cytoplasmic boundary and the cell membrane *(Fig. 2-A)*. After treatment with CND for 10 min *(Fig.2-B,C)*, the cellular architecture was altered. The periplasmic space appeared markedly narrower than that of untreated cells. In most bacteria, the cell wall appeared thinned, ruptured, or entirely absent. Gaps of varying sizes formed between the cytoplasmic boundary and the cell membrane. Furthermore, the intracellular contents exhibited an uneven distribution with aggregation.

Results of Simulated Field Trial for Surface Disinfection

The results of the simulated field trial evaluating the efficacy of CND in disinfecting general surfaces were presented in *Table 1*. The disinfectant efficacy of CND increased with longer contact time and higher concentrations. When surfaces were treated with 0.1% CND for 5 or 10 min, mean KL values were below 3, and thus did not meet the disinfection criterion. However, when the contact time was extended to ≥15 min, mean KL values exceeded 3, indicating effective disinfection. For CND concentrations

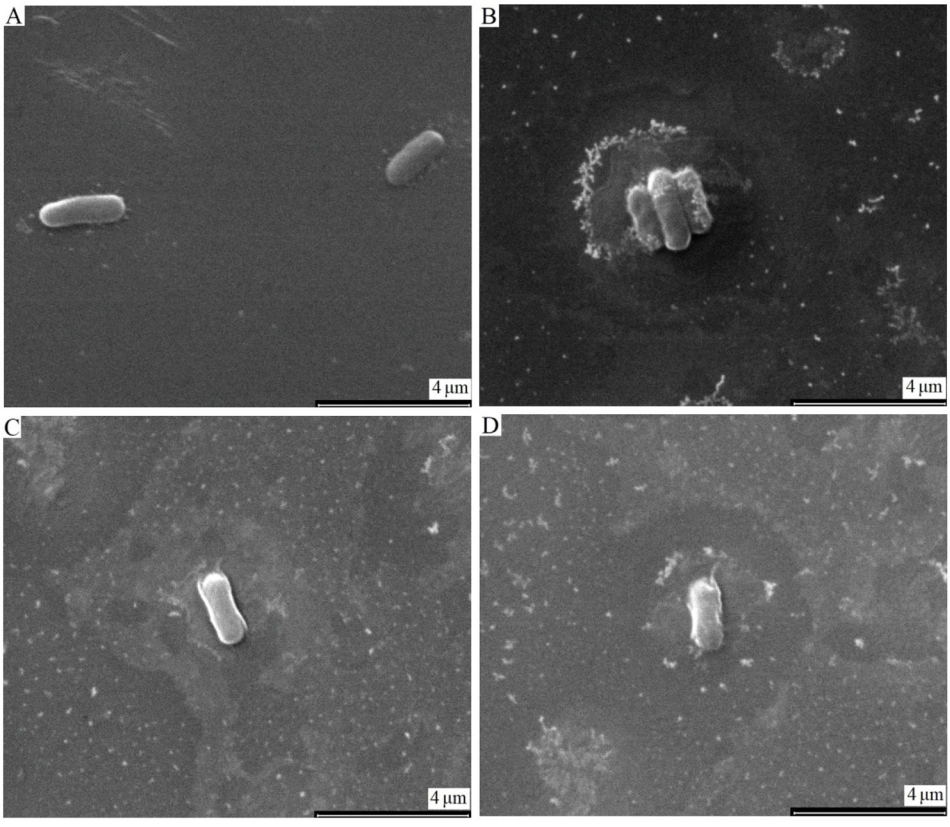

Fig 1. Scanning electron microscope observation about the effect of CND on the ultrastructure of *E. coli*. **A-** *E. coli* of the control group (×12 000); **B, C** and **D-** *E. coli* disinfected with CND for 10 min (× 12 000)

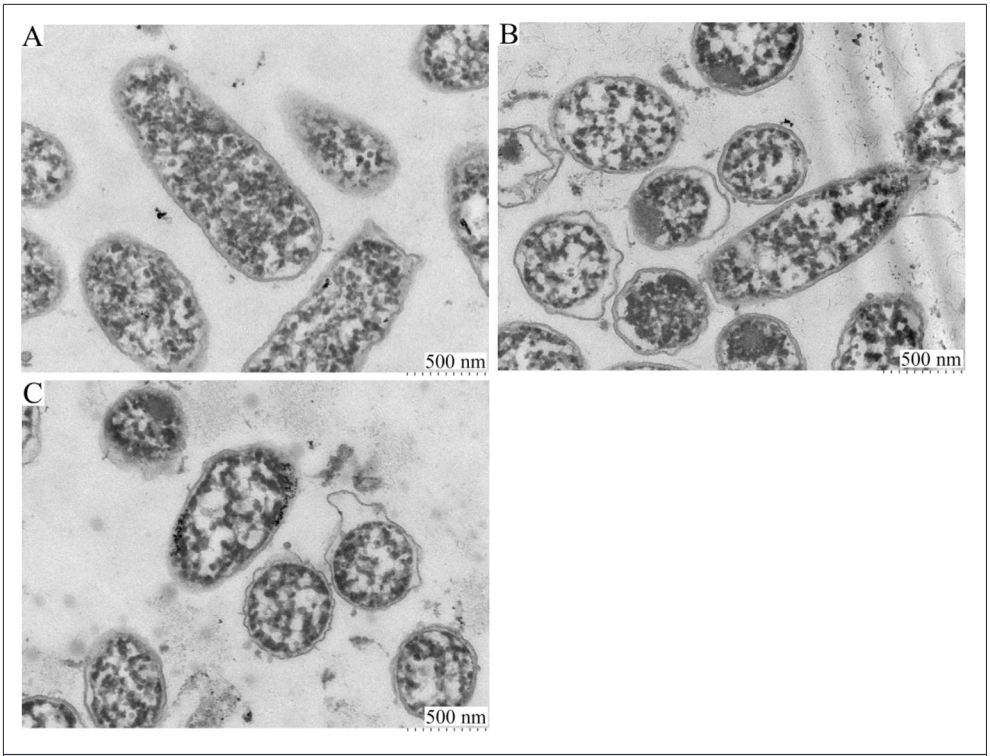

Fig 2. Transmission electron microscope observation about the effect of CND on the ultrastructure of *E. coli*. **A**- *E. coli* in the control group (×12 000); **B** and **C**- *E. coli* disinfected with CND for 10 min (×12 000)

≥0.2%, mean KL values consistently exceeded 3 under all tested contact times, demonstrating effective disinfection. These results indicated that CND exhibited effective disinfection performance under simulated field conditions.

Results of Field Trial for Surface Disinfection

The results of the field trial evaluating the surface disinfection efficacy of CND were presented in *Table 2*. The disinfectant efficacy increased gradually with

Table 1. *Results of simulated field trial for surface disinfection*

Group	Log Values of Viable Bacteria Concentration After Disinfecting for Different Time			Mean KL Values After Disinfecting for Different Time		
	5 min	10 min	15 min	5 min	10 min	15 min
0.1% CND	4.78	5.05	4.46	2.97	2.70	3.29
0.2% CND	4.62	4.54	4.39	3.13	3.21	3.36
0.5% CND	4.58	4.30	3.07	3.17	3.45	4.68
1.0% CND	4.44	3.92	2.62	3.31	3.83	5.13

Log value of viable bacteria concentration was 7.75 in the positive control group, and no bacterial growth occurred in the negative control groups

Table 2. *Results of field trial for surface disinfection*

Group	Log Values of Viable Bacteria Concentration After Disinfecting for Different Time			Mean KL Values After Disinfecting for Different Time		
	5 min	10 min	15 min	5 min	10 min	15 min
0.05% CND	2.79	2.60	2.50	0.87	1.06	1.16
0.1% CND	2.62	2.18	1.60	1.04	1.48	2.06
0.2% CND	1.95	1.43	1.11	1.71	2.23	2.55
0.5% CND	1.41	-	-	2.25	3.66	3.66

Log value of viable bacteria concentration was 3.66 in the positive control group, and no bacterial growth occurred in the negative control groups

longer contact time and higher concentrations. When 0.05% CND was applied for 5 min, the mean KL value was less than 1, and thus did not meet the disinfection standard. However, with contact time ≥10 min, mean KL values exceeded 1, indicating effective disinfection. For disinfectant concentrations ≥0.1%, all applications with contact time ≥5 min yielded mean KL values greater than 1, meeting the disinfection requirement. Notably, the 0.5% CND solution achieved complete inactivation of natural microorganisms on surfaces when applied for 10 min or longer. These results demonstrated that CND exhibited effective disinfection performance under field conditions.

Discussion

Disinfectants are effective in inhibiting or eliminating microorganisms on surfaces and within transmission media, and are extensively applied in various industries. Thorough and standardized disinfection of livestock housing and the environment serves as a crucial preventive measure to block transmission routes, eliminate sources of infection, and inactivate pathogens. It is also one of the most efficient and practical approaches for disease prevention. *E. coli* is an opportunistic pathogen widely present in nature. Although it can cause severe illnesses in humans and animals, it also plays a significant role in the commensal microbiota [20]. Therefore, *E. coli* serves as an ideal indicator organism for evaluating the efficacy of environmental disinfectants. Following the Technical Standard for Disinfection (2002) [21], this study used *E. coli* to evaluate the antibacterial activity of CND, a novel environmental disinfectant, as well as its effects on bacterial ultrastructure and its field disinfection efficacy.

Some nanomaterial-based disinfectants have been reported in recent years. Jamshidinia et al.[25] demonstrated that nanomaterial-augmented formulations enhanced the antiviral activity of disinfectants and antiseptics against respiratory viruses, particularly SARS-CoV-2. These formulations are thought to enhance disinfectant efficacy by inhibiting viral penetration into cells, disrupting the lipid bilayer envelope, and increasing reactive oxygen species production. Similarly, sandalwood nanoemulsion had shown strong antibacterial efficacy and could be used as a disinfectant for various applications, including hand hygiene, surface disinfection, and surgical instrument sterilization [26]. Risso et al.[23] demonstrated that chlorhexidine nanoemulsion could decrease chlorhexidine concentrations. Both *in vitro* and *in vivo* experiments indicated its potential as an antiseptic for cutaneous microbiota. In another study, nano-emulsified cresol disinfectant had been reported for environmental disinfection in biosafety cabinets (BSCs). It is considered an ideal alternative to formaldehyde and chlorine dioxide for BSCs disinfection [27]. Collectively, these findings highlight the potential of nanostructured formulations as effective disinfectants [23], supporting the development of CND as a novel nanoemulsion-based disinfectant for environmental applications.

To evaluate the antibacterial activity of CND, its in *vitro* efficacy against *E. coli* was first examined. The results showed that the MIC and MBC of CND against *E. coli* were 100 μg/mL and 200 μg/mL, respectively. Our previous findings demonstrated that the MIC and MBC of CND against *S. aureus* were 100 μg/mL and 200 μg/mL, respectively [18]. In contrast, both the MIC and MBC for *Candida albicans* were 3 mg/mL [19]. In the present study, CND showed strong inhibitory activity against *E. coli* (Gram-negative). Taken together with our previous findings showing its efficacy against *S. aureus* (Gram-positive) and *Candida albicans* (fungus), these results indicate that CND possesses broad-spectrum antimicrobial activity. Notably, its bactericidal potency against both Gram-negative and Gram-positive bacteria appears to be greater than its fungicidal activity.

Previous studies from our research group indicated that exposure to 0.06% CND for 10 min led to varied outcomes in quantitative suspension tests [17]. Some bacterial cells died, some survived, and others showed partial loss of structural integrity. To investigate the antibacterial mechanism of CND against *E. coli*, bacterial samples were treated with 0.06% CND for 10 min and then processed into ultrathin sections for electron microscopic observation of ultrastructural changes. SEM observations showed that CND exerts its antibacterial effect by damaging the surface structure of bacterial cells. TEM further revealed that CND disrupted the internal structural integrity of *E. coli*, contributing to its antibacterial activity. The bacterial cell wall is a specialized structure that serves not only as the primary barrier against external threats but also plays essential roles in maintaining cell morphology, providing protection against damage, and mediating adhesion to host cells. These observations underscore the critical role of cell wall integrity in bacterial survival. Once the cell wall or membrane is compromised, bacteria lose their normal shape; the exchange of materials across the membrane is hindered; and membrane-associated enzymes fail to function properly. This reduces nutrient uptake and ultimately inhibits bacterial growth. Other studies have shown that upon contact with microorganisms, nanoemulsions fuse with the microbial cell membrane via their lipid bilayers, releasing the energy stored in the oil and disinfectants. This process destabilizes the bacterial lipid membrane, ultimately leading to cell death [26]. The present results suggest that one likely mechanism of CND against *E. coli* involves inducing ultrastructural alterations in bacterial cells. However, as this conclusion is primarily based on morphological observations, it remains partly

hypothetical within the scope of the current study and requires further mechanistic validation.

Disinfection is a key measure for interrupting pathogen transmission, and evaluating its efficacy is a primary focus in environmental hygiene. To further evaluate the environmental disinfectant performance of CND and support its future practical application, simulated and field trials for surface disinfection were conducted. The results demonstrated that the disinfectant efficacy of CND improved with longer contact time and higher concentrations. In the simulated surface disinfection trial, effective disinfection was achieved with 0.1% CND applied for ≥15 min or with CND concentrations ≥0.2%. In the field trial, effective disinfection was achieved with 0.05% CND applied for ≥10 min or with CND concentrations ≥0.1%. Notably, 0.5% CND applied for ≥10 min completely inactivated natural microorganisms on surfaces, resulting in a 100% bactericidal rate. These findings indicate that CND performs effectively under field conditions. Previous studies from our group have also shown that CND exhibits stronger disinfectant efficacy than conventional chlorocresol formulations [17-19]. Therefore, CND has great potential for use as a new-generation disinfectant. Extensive literature indicates that nanoemulsions serve as an ideal drug delivery system with unique advantages over other carriers, such as enhancing the solubility of poorly soluble drugs, improving bioavailability, and promoting transdermal absorption [28-30]. Nanoemulsions can be exploited in the formulation of sanitizers or related products with antibacterial activity [26,31]. In this study, CND was developed as a novel formulation using a nanoemulsion as the drug carrier. Its superior field disinfection efficacy is likely attributable to the distinctive properties of this nanoemulsion-based delivery system. CND is an oil-in-water nanoemulsion [17], in which chlorocresol is encapsulated within the nanoemulsion droplets. The resulting nanoscale particle size facilitates penetration through the bacterial cell wall, increasing the intracellular drug concentration and enhancing antibacterial activity [18], thereby contributing to its potent bactericidal effect. It has also been reported that the reduced particle size may enhance passive cellular absorption, facilitating drug entry into microbial cells and thereby increasing antimicrobial activity and improving the therapeutic index [23,32]. Furthermore, the nanoemulsion structure itself has been reported to possess broad-spectrum antimicrobial properties [33].

Several limitations of this study should be acknowledged. This study focused only on *E. coli* under controlled conditions; the efficacy of CND against other Gram-negative bacteria, drug-resistant strains, viruses, and spores remains unknown. Furthermore, the precise molecular mechanism of action has not been fully elucidated. Although our research group has systematically evaluated CND against multiple microorganisms, future studies should focus on elucidating the molecular mechanism using biochemical and omics approaches, evaluating its antiviral and sporicidal activity, and conducting long-term safety and ecotoxicological assessments.

In conclusion, this study evaluated the antibacterial efficacy of CND against *E. coli* by determining the MIC and MBC. The effects of CND on bacterial ultrastructure were examined using SEM and TEM. Furthermore, its disinfection performance was assessed through simulated and field trials on general surfaces. The results demonstrate that CND exhibits strong antibacterial activity against *E. coli*, induces significant alterations in cellular ultrastructure, and demonstrates effective disinfection under field conditions. Therefore, CND represents a promising environmental disinfectant, although further toxicity and *in vivo* safety assessments are needed before clinical application.

Declarations

Availability of Data and Materials: Data and materials for this research are available upon request.

Acknowledgements: We appreciate the constructive comments from the editors and anonymous reviewers.

Funding Support: This study was supported by the grant of the Key Project of Henan Research and Development (Grant No. 251111111900) and Characteristic Innovation Project of the Henan Institute of Science and Technology (Grant No. 2015ZD09).

Ethical Statement: This study did not require ethical approval.

Competing Interests: The authors declare that there is no competing of interest.

Declaration of Generative Artificial Intelligence (AI): The authors declare that the article, tables and figures were not written/created by AI and AI-assisted technologies.

Author Contributions: Conceived of or designed study: XF Y, CZ L; Performed research: XF Y, YW S; Analyzed data: ZX A, DY L; Wrote the paper: XF Y. All authors critically reviewed and approved the final version of the manuscript.

References

1. **Ramesh A, Bailey ES, Ahyong V, Langelier C, Phelps M, Neff N, Sit R, Tato C, DeRisi JL, Greer AG, Gray GC:** Metagenomic characterization of swine slurry in a North American swine farm operation. *Sci Rep,* 11 (1): 16994, 2021. DOI: 10.1038/s41598-021-95804-y
2. **Wang T, Fan H, Chai M, He T, Li Y, Han X, Li Y, Bai H, Jiang S:** Study on the disinfection efficacy of common commercial disinfectants in China against mastitis-causing pathogens and bedding materials in large-scale dairy farms. *Vet Sci,* 12 (11):1072, 2025. DOI: 10.3390/vetsci12111072
3. **Kim YJ, Kim JB, Song CS, Nahm SS:** Disinfection of various materials with 3-(trimethoxysilyl)-propyldimethyloctadecyl ammonium chloride in hatchery facilities. *Anim Biosci,* 35 (4): 631-637, 2021. DOI: 10.5713/ab.21.0302

4. **Bai Y, Ding X, Zhao Q, Sun H, Li T, Li Z, Wang H, Zhang L, Zhang C, Xu S:** Development of anorganic acid compound disinfectant to control food-borne pathogens and its application in chicken slaughterhouses. *Poultry Sci,* 101 (6):101842, 2022. DOI: 10.1016/j.psj.2022.101842
5. **Shcherbakova GS, Popov NI, Shuteeva EN, Kuvshinchikov NN, Pirozhikhin VA, Gruznova OA, Gruznov DV:** Antimicrobial properties of a new bactericide for veterinary disinfection. *BIO Web Conf,* 161:1-5, 2025. DOI: 10.1051/bioconf/202516100036
6. **Tyski S, Bocian E, Laudy AE:** Animal health protection-assessing antimicrobial activity of veterinary disinfectants and antiseptics and their compliance with European standards: A narrative review. *Pol J Microbiol,* 73 (4): 413-431, 2024. DOI: 10.33073/pjm-2024-043
7. **Matsubara T, Maki S, Toshimori Y:** The effectiveness of a nonalcoholic disinfectant containing metal ions, with broad antimicrobial activity. *Sci Rep,* 11 (1):1072, 2021. DOI: 10.1038/s41598-020-80443-6
8. **Wang WZ, Li Y, Dai F, Wang JY, Gu WY, Zhang S, Zhao YH, Ren XX, Fan JH, Zuo YZ:** Bactericidal effect of three disinfectants on four common bacteria in pig farms. *Prog Vet Med,* 45 (8): 139-144, 2024. DOI: 10.3969/j.issn.1007-5038.2024.08.026
9. **Lin XD, Ma WJ, Xu XY, Huo MX, Fang MY, Kou ZY, Huang LL:** Research progress on the environmental safety of veterinary disinfectants. *Chin J Vet Med,* 60 (8): 97-104, 2024.
10. **Zhang S, Angel C, Gu X, Liu Y, Li Y, Wang L, Zhou X, He R, Peng X, Yang G, Xie Y:** Efficacy of a chlorocresol-based disinfectant product on *Toxocara canis* eggs. *Parasitol Res,* 119, 3369-3376, 2020. DOI: 10.1007/s00436-020-06769-2
11. **Phendinvay O, Thongseesuksai T, Boonmars T, Laummaunwai P:** Evaluation of the cysticidal activity of chlorocresol against *Acanthamoeba polyphaga*. *J Parasitol,* 110 (5): 423-427, 2024. DOI: 10.1645/24-15
12. **Hu GZ, Qiu YS:** Medicines commonly used in poultry and their rational use. 27, Henan Science and Technology Press, Zhengzhou, 2010.
13. **Hu GZ, Li RY:** New complete veterinary manual. 31, Henan Science and Technology Press, Zhengzhou, 2015.
14. **Li CY, He SZ:** Animal pharmacology. 101, China Agricultural University Press, Beijing, 2007.
15. **Chinese Veterinary Drug Code Committee:** Veterinary drug quality standards (2017 ed., Chemical drugs volume). 306-307, China Agricultural Press, Beijing, 2017.
16. **Yang XF, Li RF, Ren XJ, Liu DY, Sun YW, Wang ZL, Zhang HH, Hu JH, Mu SY, Bai YZ, Shi YL:** A kind of chlorocresol nanoemulsion disinfectant and its preparation method [P]. China: 201510074247.2, 2015.
17. **Yang XF, Sun YW, Mu SY, Liu DY, Hu JH, Xu YZ, Bai YZ, Shi YL:** Evaluation of characterization and disinfection efficacy of chlorocresol nanoemulsion disinfectant. *RSC Advances,* 6 (16): 12730-12736, 2016. DOI: 10.1039/c5ra18573d
18. **Zhang YF, Sun YW, Liu XH, An ZX. Yang XF:** The study on bactericidal effect and ultrastructural alterations of chlorocresol nanoemulsion disinfectant against *Staphylococcus aureus*. *Pol J Vet Sci,* 26 (1): 13-20, 2023. DOI: 10.24425/pjvs.2023.145002
19. **Yin M, Zhang DL, Sun YJ, Li XH, Li YY, Xu P, Xue MQ, Jin MY, Yang XF:** Fungicidal effect of chlorcresol nanoemulsion disinfectant. *J Northwest A&F Univ (Nat Sci Ed),* 48 (10): 18-23, 2020. DOI: 10.13207/j.cnki.jnwafu.2020.10.003
20. **Khallaf RM, Abd El-Hamied SS, Refaie AZ, Elewasy OA, Elmesalamy SM:** A study on the effect of rutin in the antibiotics enhancement controlling *E. coli* infection in broiler chicken. *Kafkas Univ Vet Fak Derg,* 31 (6): 791-800, 2025. DOI: 10.9775/kvfd.2025.35119
21. **Ministry of Health of the People's Republic of China:** Technical standard for disinfection. 20-86, Ministry of Health of the People's Republic of China, Beijing, 2002.
22. **Eissa M, Ashour ED, Mansy MS:** Neutralizer evaluation study of some microbial isolates against two strong disinfectants with and without the presence of synthetic detergent. *World Appl Sci J,* 20, 823-831, 2012.
23. **Risso NH, Stopiglia CDO, Oliveira MT, Haas SE, Maciel TR, Lazzari NR, Kelmer EL, Vilela JAP, Beckmann DV:** Chlorhexidine nanoemulsion: A new antiseptic formulation. *Int J Nanomedicine,* 15, 6935-6944, 2020. DOI: 10.2147/IJN.S228280
24. **Yang XF, Qi YH, Ning HM, Wang QH:** Preparation and quality evaluation of enrofloxacin nanoemulsion. *J Zhejiang Univy Agric Life Sci,* 38 (6): 693-699, 2012. DOI: 10.3785/j.issn.1008-9209.2012.01.051
25. **Jamshidinia N, Mohammadipanah F:** Nanomaterial-augmented formulation of disinfectants and antiseptics in controlling SARS CoV-27. *Food Environ Virol,* 14 (2): 105-119, 2022. DOI: 10.1007/s12560-022-09517-0
26. **Meghani N, Mansuri A, Chaudhari R, Kumar A:** Fabrication, assessment, and potential anti-bacterial activity of sandalwood oil nanoemulsion and its hand rub sanitizer. *Environ Sci Pollut Res Int,* 31 (34): 46546-46557, 2023. DOI: 10.1007/s11356-023-26945-y
27. **You NK, Wang S, Han H:** The efficacy of nano-emulsified disinfectant in disinfecting the workplace environment. *Nanosci Nanotechnol Lett,* 12 (9): 1114-1119, 2020. DOI: 10.1166/NNL.2020.3216
28. **Zeng T, Song F, Yang Z, Yan X, Jiang L, Li D, Huang Z:** Nanoemulsion encapsulation of fat-soluble vitamins: Advances in technology, bioaccessibility and applications. *Foods,* 15 (1):156, 2026. DOI: 10.3390/foods15010156
29. **Ashagrie YN, Tadesse MG, Bachheti RK, Nijhawan G, Tyagi S, Bachheti A:** Formulation and characterization of *Caesalpinia decapetala* seed oil nanoemulsion: physicochemical properties, stability, and antibacterial activity. *Sci Rep,* 15 (1): 14598, 2025. DOI: 10.1038/s41598-025-87732-y
30. **Saha M, Gupta A, Kunkalienkar S, Dhas N, Shetty S, Gupta A, Mutalik S, Krishnadas N, Chandrashekar R, Narasimhaswamy N, Moorkoth S:** Nanoemulsion as a promising drug delivery strategy for effective eradication of *Helicobacter pylori:* Current insights. *Drug Deliv Transl Res,* 16 (1): 17-44, 2025. DOI: 10.1007/s13346-025-01986-7
31. **Marchese E, D'onofrio N, Balestrieri ML, Castaldo D, Ferrari G, Donsì F:** Bergamot essential oil nanoemulsions: Antimicrobial and cytotoxic activity. *Zeitschrift Für Naturforschung C,* 75, 279-290, 2020. DOI: 10.1515/znc-2019-0229
32. **Donsì F, Annunziata M, Vincensi M, Ferrari G:** Design of nanoemulsion-based delivery systems of natural antimicrobials: effect of the emulsifier. *J Biotechnol,* 159 (4): 342-350, 2012. DOI: 10.1016/j.jbiotec.2011.07.001
33. **Hamouda T, Myc A, Donovan B, Shih AY, Reuter JD, Baker JR:** A novel surfactant nanoemulsion with a unique non-irritant topical antimicrobial activity against bacteria, enveloped viruses and fungi. *Microbiol Res,* 156, 1-7, 2001. DOI: 10.1078/0944-5013-00069

Kafkas Universitesi Veteriner Fakultesi Dergisi
Journal Home-Page: http://vetdergikafkas.org
E-ISSN: 1309-2251

Kafkas Univ Vet Fak Derg
32 (4): 501-509, 2026
DOI: 10.9775/kvfd.2026.36545

Research Article

Histopathological Evaluation and Computer-Aided Mechanistic Prediction of *Murraya koenigii* Extract on Excisional Wound Healing in Rats

Tarshan Sharma SURESH [1], Zahir THORIQ [2], Eko ALIF BIN ANTO [1], Sandraa Victor JEYARAJ [3], Yadjnes Iswaran KODISWARAN [4], Rini Kusumawar DHANY [5], Danti Nur INDIASTUTI [6], Moh Nurkholis ROUFI [7], Kuncoro Puguh SANTOSO [8], Eka Pramyrtha HESTIANAH [8], Rahmi SUGIHARTUTI [8], Ayesha MASOOD [9], Lita Rakhma YUSTINASARI [8 (*)]

[1] Master's Program in Reproductive Biology, Faculty of Veterinary Medicine, Universitas Airlangga, Surabaya, INDONESIA
[2] Master's Program in Vaccinology and Immunotherapeutics, Faculty of Veterinary Medicine, Universitas Airlangga, Surabaya, INDONESIA
[3] Faculty of Veterinary Medicine, Universitas Airlangga, Surabaya, INDONESIA
[4] Faculty of Dentistry, Universitas Airlangga, Surabaya, INDONESIA
[5] Department of Ophthalmology, Faculty of Medicine, Universitas Muhammadiyah Surabaya, Surabaya, INDONESIA
[6] Department of Anatomy, Histology, and Pharmacology, Faculty of Medicine, Universitas Airlangga, Surabaya, INDONESIA
[7] General Hospital Wahidin Sudiro Husodo, Mojokerto, INDONESIA
[8] Department of Veterinary Science, Faculty of Veterinary Medicine, Universitas Airlangga, Surabaya, INDONESIA
[9] Department of Anatomy and Histology, Faculty of Veterinary Science, The Islamia University Bahawalpur, PAKISTAN

[(*)] **Corresponding author:**
Lita Rakhma Yustinasari
Phone: +62 822-9779-1609
E-mail: lita-r-y@fkh.unair.ac.id

How to cite this article?

Suresh TS, Thoriq Z, Alif bin Anto E, Jeyaraj SV, Kodiswaran YI, Dhany RK, Indiastuti DN, Roufi MN, Santoso KP, Hestianah EP, Sugihartuti R, Masood A, Yustinasari LR: Histopathological Evaluation and Computer-Aided Mechanistic Prediction of *Murraya koenigii* Extract on Excisional Wound Healing in Rats. *Kafkas Univ Vet Fak Derg*, 32 (4): 501-509, 2026.
DOI: 10.9775/kvfd.2026.36545

Article ID: KVFD-2026-36545
Received: 07.03.2026
Accepted: 02.07.2026
Published Online: 14.07.2026

Abstract

Wound healing involves coordinated epithelial regeneration, extracellular matrix remodeling, and inflammatory regulation. This study evaluated the histopathological effects of topical *Murraya koenigii* leaf extract on excisional wound healing in rats and explored potential molecular mechanisms in silico. Fifty male Rattus norvegicus were divided into five groups (n=10 per group): unwounded control (CN), positive control (Bioplacenton®), and treatment groups 10%, 20%, and 40% *Murraya koenigii* ointment respectively. A standardized 1-cm full-thickness dorsal excisional wound was created, treatments were applied twice daily for 14 days, and tissues were collected on day 15. Sections were assessed using the SPOT scoring system (re-epithelialization, epithelial thickness index, keratinization, granulation thickness, remodeling, and scar elevation index). Kruskal-Wallis exhibited a significant difference in the composite SPOT score among groups ($H=40.838$, $P<0.001$) with a large effect ($\varepsilon^2=0.819$). Histopathologically, the 40% group showed the most promising repair, with more complete epithelial coverage, improved epidermal maturation, denser granulation tissue, and early dermal remodeling compared with lower concentrations. Molecular docking indicated favorable binding of major carbazole alkaloids (mahanine, mahanimbine, mahanimbicine) to FAAH and GSK3β, targets implicated in inflammation and regenerative signaling. These findings indicate that topical *Murraya koenigii* extract enhances structural wound repair and highlights its potential as a plant-based therapeutic candidate for wound management.

Keywords: Carbazole alkaloids, Endocannabinoid system, Wound repair, β-catenin signaling, Health, Phytotherapy

Introduction

Cutaneous wound healing is a highly regulated process with overlapping phases of hemostasis, inflammation, proliferation, and remodeling that restores tissue structure and function [1,2]. During proliferation, granulation tissue formation, angiogenesis, fibroblast proliferation, and re-epithelialization drive tissue restoration [3]. The rat excisional wound model provides standardized wound geometry and supports serial macro- and microscopic evaluation, including histopathological assessment of epithelial regeneration, inflammatory infiltration, and

collagen deposition [4-6]. In human studies, despite advances in wound care and topical therapeutics, delayed or impaired healing remains a clinical challenge, motivating continued exploration of bioactive compounds that modulate inflammation, oxidative stress, and extracellular matrix remodeling [7,8].

Natural products and plant-derived phytochemicals are increasingly studied for wound healing because of antioxidant, anti-inflammatory, and antimicrobial activities; among these, *Murraya koenigii* (curry leaf) is rich in carbazole alkaloids, flavonoids, and phenolic compounds with documented biological activities [9-12]. Formulations containing *Murraya koenigii* extract have been reported to enhance wound contraction, promote re-epithelialization, and support collagen synthesis *in vivo*, potentially via modulation of inflammatory mediators and oxidative-related pathways that influence tissue regeneration, matching trajectories observed in other therapeutic plant oil models [9,12-16].

However, although several studies have reported the wound-healing effects of *Murraya koenigii* based on macroscopic wound contraction and biochemical markers, systematic histopathological evaluation using standardized scoring systems remains limited [13,17]. Structured scoring approaches such as the SPOT system allow semi-quantitative assessment of epithelial regeneration, keratinization, granulation tissue maturation, and tissue remodeling. In addition to morphological assessment, *in silico* approaches such as molecular docking can provide mechanistic insights by predicting interactions between phytochemical compounds and proteins involved in inflammation, angiogenesis, and extracellular matrix regulation [18]. Integrating histopathological evaluation with computational analysis may therefore provide a more comprehensive understanding of the therapeutic potential of plant-derived compounds.

Therefore, the present study aimed to evaluate the effects of topical *Murraya koenigii* leaf extract on excisional wound healing in *Rattus norvegicus* using SPOT-based histopathological scoring and to explore potential molecular mechanisms through molecular docking analysis.

Material and Methods

Ethical Approval

All procedures were approved by the Institutional Animal Care and Use Committee (IACUC), Faculty of Veterinary Medicine, Universitas Airlangga, Indonesia (Approval No.: 1.KEH.043.03.2023), and conducted according to institutional animal care guidelines.

Study Design and Animals

A completely randomized design was used. Fifty male *Rattus norvegicus* (150-200 g; 3-4 months old) were acclimatized for one week and randomly assigned into five groups (n=10 per group): CN (truly unwounded and untreated control; these animals underwent no surgical procedures, anesthesia, or wound creation, and served as a histopathological benchmark for physiological normalcy), CP (Bioplacenton® ointment, Kalbe Farma, Indonesia serving as a widely used regional clinical standard for wound care that provides a benchmark for a successful healing trajectory), T1 (10% *Murraya koenigii),* T2 (20%), and T3 (40%). Each rat was considered one experimental unit. Group sizes (n=10 per group) and extract concentrations (10%, 20%, 40%) were selected based on established preclinical excisional wound-healing model parameters reported in the literature [4,5,19,20]. Treatments were applied topically twice daily for 14 consecutive days. Tissue samples were collected on day 15 for histopathological examination.

Animals were individually housed in polypropylene cages under controlled environmental conditions: ambient temperature 22±2°C, relative humidity 50-60%, and a 12-h light/dark cycle. All animals received a standard commercial pelleted rodent diet and had continuous access to clean water ad libitum throughout the study period. A mandatory one-week acclimatization period was observed prior to any experimental procedures, during which all animals were confirmed to be in good health before randomization.

Excisional Wound Model

The dorsal area of each rat was shaved and disinfected with 70% ethanol before surgery. Animals were anesthetized using ketamine (100 mg/kg) and xylazine (5 mg/kg) administered intraperitoneally. A circular full-thickness excisional wound with a diameter of 1 cm was created on the dorsal skin using a sterile biopsy punch. The wounds were left unsutured to allow secondary intentional healing. Postoperative assessment was monitored twice daily throughout the 14-day observation period using the Rat Grimace Scale (RGS), a validated objective tool for quantifying pain-related facial expressions in laboratory rodents [21]. Meloxicam (2 mg/kg, subcutaneous) was prepared as a rescue analgesic and designated for administration if any animal's RGS score exceeded the established clinical threshold for distress. Animals that exceeded the predetermined pain-score threshold received appropriate rescue analgesia to ensure animal welfare and alleviate pain-related distress. This reactive analgesic strategy was intentionally employed to balance ethical animal care with the need to minimize potential confounding effects of systemic non-steroidal anti-inflammatory drugs (NSAIDs) on the inflammatory and proliferative phases of wound healing, which were the primary histopathological outcomes assessed in the present study.

Preparation of *Murraya koenigii* Extract and Ointment

Cold dried curry leaves *(Murraya koenigii)* were macerated in 96% ethanol for 72 h at room temperature. The extract was filtered and concentrated under reduced pressure using a rotary evaporator at 40-45°C to obtain a viscous crude extract. The resulting extract was incorporated into a Vaselin flavum base to prepare ointments at concentrations of 10%, 20%, and 40% (total weight 50 g per formulation). All formulations were prepared under sterile conditions and stored in sealed containers until use *(Table 1)*.

Tissue Processing and Histopathology

Histopathological slides were independently evaluated by two blinded observers to minimize observer bias. Each SPOT parameter was assessed on a 0-2 ordinal scale (0 = absent/minimal; 1 = partial; 2 = complete/normal), following the criteria described by van de Vyver et al.[17]. Specifically: re-epithelialization scored the degree of continuous neo-epithelium coverage across the wound surface; the Epithelial Thickness Index (ETI) evaluated epidermal thickness relative to adjacent unwounded skin; keratinization assessed the organization of superficial keratin layers; granulation tissue maturation captured fibroblast density and early extracellular matrix deposition within the wound bed; remodeling evaluated collagen fibre organization and maturity; and the Scar Elevation Index (SEI) quantified epidermal architecture relative to the surrounding normal dermis. Interobserver agreement between the two blinded scorers was evaluated post hoc using Cohen's κ statistic. The analysis yielded a κ coefficient indicative of strong agreement across all six SPOT parameters, confirming the robustness of the semi-quantitative scoring. Any discrepancy between observers was resolved by consensus review.

In Silico Target Prediction and Molecular Docking

SMILES and three-dimensional structures of the ligands (mahanimbicine, mahanimbine, and mahanine) were obtained from PubChem. Potential protein targets were predicted using SwissTargetPrediction (species: *Rattus norvegicus)*. Protein sequences and structures were retrieved from the RCSB Protein Data Bank and UniProt databases. Sequence conservation between species was verified using Clustal Omega when necessary.

Table 1. *Composition of Murraya koenigii Ointment Formulations*

Group	Extract Concentration	*M. koenigii* Extract (g)	Vaselin Flavum (g)	Total Weight (g)
T1	10%	5	45	50
T2	20%	10	40	50
T3	40%	20	30	50

Ligand geometry optimization was performed using ORCA at the B3LYP/def2-SVP level with dispersion correction [22,23]. Protein and ligand preparation were carried out using BIOVIA Discovery Studio and ChimeraX. Docking validation was conducted by re-docking native inhibitors into the binding site to ensure reliability of the docking protocol, with acceptable root-mean-square deviation (RMSD ≤ 2 Å).

Molecular docking simulations were performed using AutoDock 4.2.6 with 100 genetic algorithm (GA) runs, a population size of 150, and 25×10^6 energy evaluations. Ligand-protein interactions were visualized using BIOVIA Discovery Studio [22].

Statistical Analysis

The data were analyzed using non-parametric statistical methods because the variables were ordinal. Differences among groups were evaluated using the Kruskal-Wallis test. When significant differences were detected, pairwise comparisons were further analyzed using the Mann-Whitney U test. To control the family-wise error rate, a Bonferroni correction was applied to all post-hoc pairwise comparisons. With ten possible pairwise comparisons among five experimental groups (C (5,2) = 10), the corrected significance threshold was adjusted to $\alpha = 0.005$ (0.05÷10). All pairwise differences reported as statistically significant met this corrected threshold.

Results

Histopathological Evaluation of Wound Healing

Histopathological examination performed on day 15 using the SPOT scoring system revealed significant differences among experimental groups across all evaluated parameters *(Table 2)*. Analysis using the Kruskal-Wallis test demonstrated statistically significant differences in scar elevation index (SEI), re-epithelialization, granulation tissue maturation, keratinization, epithelial thickness index (ETI), remodeling, and the total composite SPOT score ($P<0.05$ for all parameters).

Re-epithelialization differed significantly among groups ($H = 9.971$, $P=0.041$, $\varepsilon^2 = 0.133$). Pairwise comparisons using the Mann-Whitney U test revealed significant differences between CN and T1, CN and T2, as well as between T1 and T3 and T2 and T3. However, no significant difference was observed between T3 and the positive control group (CP) as well as T3 and the negative control group (CN). Histopathological sections demonstrated progressive epithelial bridging across the wound surface in the treated groups. The T3 group exhibited nearly complete epithelial coverage, indicating greater epidermal regeneration compared with the lower treatment concentrations *(Fig. 1)*.

Table 2. *Median and interquartile range (IQR) for each SPOT parameter across all experimental groups (CN, CP, T1, T2, T3), with overall Kruskal-Wallis H statistic presenting p-value, and ε^2 effect size*

Parameter	CN (n=10)	CP (n=10)	T1 10% (n=10)	T2 20% (n=10)	T3 40% (n=10)	H	p-value	ε^2
Re-epithelialization	2.0 [2.0-2.0]	2.0 [2.0-2.0]	2.0 [1.0-2.0]	2.0 [1.0-2.0]	2.0 [2.0-2.0]	9.971	0.041	0.133
Keratinization	2.0 [2.0-2.0]^a	2.0 [1.4-2.0]^a	1.2 [0.8-1.2]^b	2.0 [0.9-2.0]^a	2.0 [1.3-2.0]^a	20.966	0.000	0.377
ETI	2.0 [2.0-2.0]^a	2.0 [2.0-2.0]^a	1.0 [1.0-1.0]^b	2.0 [1.0-2.0]^a	2.0 [2.0-2.0]^a	27.601	0.000	0.524
Granulation	2.0 [2.0-2.0]^a	1.0 [1.0-2.0]^b	1.0 [1.0-1.0]^b	1.0 [0.3-1.0]^b	2.0 [2.0-2.0]^a	31.316	0.000	0.607
Remodeling	2.0 [2.0-2.0]^a	1.7 [1.2-2.0]^a	0.2 [0.1-0.4]^b	1.6 [1.1-2.0]^a	1.8 [1.5-2.0]^a	25.065	0.000	0.468
SEI	2.0 [2.0-2.0]^a	2.0 [2.0-2.0]^a	1.0 [0.25-2.0]^b	2.0 [1.0-2.0]^a	2.0 [2.0-2.0]^a	11.905	0.018	0.176
Total SPOT Score	12^a	10.7^a	6.4^b	10.6^a	11.8^a	40.838	0.000	0.819

CN = unwounded control; CP = positive control (Bioplacenton®); T1–T3 = 10%, 20%, 40% M. koenigii ointment; ETI = epithelial thickness index; SEI = scar elevation index.^{a,b} *values within a row with different superscript letters are significantly different (P<0.05) based on post-hoc pairwise comparisons*

Granulation tissue thickness demonstrated the most pronounced intergroup variation (H = 31.316, P<0.001, ε^2 = 0.607). The treated groups showed higher mean ranks compared with the control groups, indicating enhanced granulation tissue development. Histopathologically, this was characterized by greater fibroblast proliferation, increased vascularization, and early extracellular matrix deposition within the wound bed. These findings were most prominent in the T3 group, suggesting enhanced proliferative-phase activity.

Keratinization also differed significantly among groups (H = 20.966, P<0.001, ε^2 = 0.377). The T3 group demonstrated more organized keratin layers and improved epidermal maturation compared with T1 and T2. Similarly, the epithelial thickness index (ETI) showed significant variation (H = 27.601, P<0.001, ε^2 = 0.524). Groups treated with lower concentrations (T1 and T2) displayed increased epithelial thickness consistent with active epithelial proliferation, whereas the T3 group showed a more normalized epithelial architecture approaching that of the unwounded control.

Significant differences were also observed in the remodeling parameter (H = 25.065, P<0.001), reflecting variations in connective tissue organization and collagen maturation. Histopathological sections from the T3 group demonstrated early remodeling features, including more organized collagen fibers and reduced inflammatory infiltration compared with the lower-dose groups.

Importantly, the total composite SPOT score differed significantly among groups (H = 40.838, P<0.001, ε^2 = 0.819). The large effect size indicates that treatment with *Murraya koenigii* ointment accounted for a substantial proportion of the variation in overall histopathological healing outcomes. Mean rank comparisons further suggested a dose-dependent improvement in wound healing parameters, with the highest scores consistently observed in the T3 group. A comprehensive summary of the median and interquartile range (IQR) for each

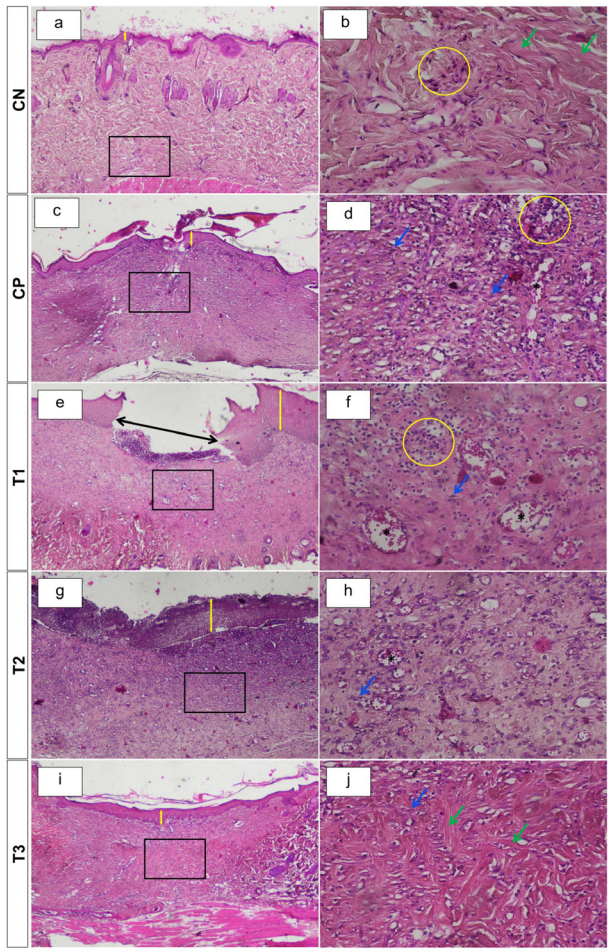

Fig 1. Histopathological features of experimental *Rattus norvegicus* skin tissue on day 15 of wound healing. Panels a, c, e, g, and i (H&E, 40×) show selected areas (*black boxes*), magnified in panels b, d, f, h, and j (H&E, 200×). Incomplete re-epithelialization (*black arrow*) was observed in T1. The CP and T3 groups showed thinner epithelial thickness (*yellow lines*) comparable to CN. Loose granulation tissue with angiogenesis, dilated blood vessels (*asterisks*), inflammatory infiltration (*yellow circles*), fibroblasts (*blue arrows*), and thin collagen fibers (*green arrows*) was evident in CP, T1, and T2. In contrast, T3 exhibited denser granulation tissue, fewer inflammatory cells, and thicker collagen fibers (*green arrows*), resembling CN

individual SPOT parameter across all experimental groups, together with the Kruskal–Wallis H statistic, p-value, and ε^2 effect size, is presented in *Table 2*.

In Silico Mechanism Prediction

In silico target prediction identified fatty acid amide hydrolase (FAAH) and glycogen synthase kinase-3 beta (GSK3β) as potential molecular targets associated with epithelial regeneration and tissue repair. Docking validation was performed through re-docking of the native FAAH inhibitor into the active site, yielding a root-mean-square deviation (RMSD) value of 0.81 Å, which confirmed the reliability of the docking protocol *(Fig. 2)*. Sequence alignment analysis further supported the use of the human GSK3β structure as a surrogate model due to the high conservation of the catalytic binding pocket.

Molecular docking simulations demonstrated stable binding conformations for the carbazole alkaloids mahanimbicine, mahanimbine, and mahanine toward both target proteins. For FAAH, binding energies ranged from -9.69 to -10.16 kcal/mol, with mahanine exhibiting the strongest binding affinity (-10.16 kcal/mol) *(Fig. 2)*. For GSK3β, binding energies ranged from -8.41 to -8.95 kcal/mol, again with mahanine demonstrating the most favorable interaction (-8.95 kcal/mol) *(Fig. 3)*. To provide an overview of the experimental outcomes, the pathways linking the administration of mahanine, mahanimbine, and mahanimbicine to the observed changes in inflammatory markers and tissue regeneration are summarized in *Fig. 4*.

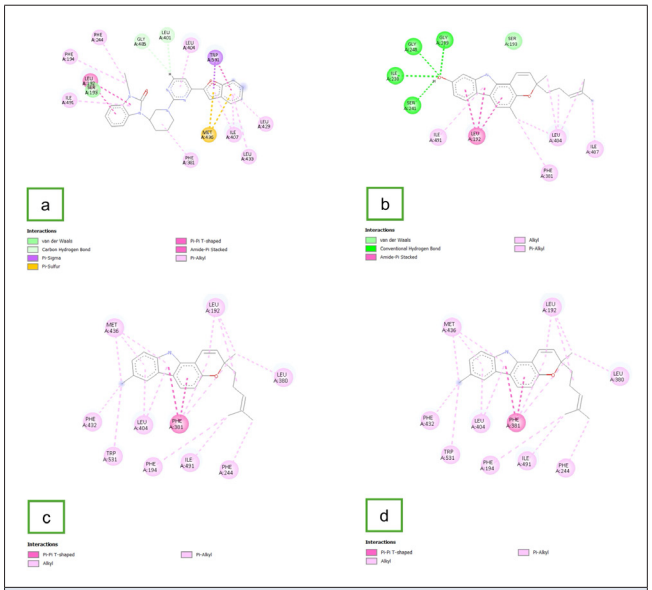

Fig 2. Molecular docking interaction diagrams illustrating the binding interactions of selected compounds from *Murraya koenigii* with the FAAH protein. Panels show the interaction profiles of **(a)** Native ligand QJ9, **(b)** mahanimbicine, **(c)** mahanimbine, and **(d)** mahanine within the FAAH active site, highlighting hydrogen bond and hydrophobic interactions with key amino acid residues

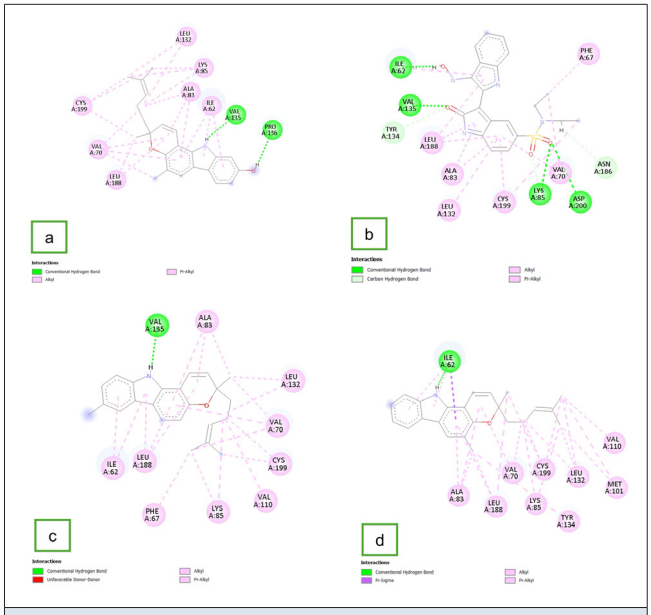

Fig 3. Molecular docking interaction diagrams of selected bioactive compounds from *Murraya koenigii* with the GSK3β protein. **(a)** Native ligand OFT, **(b)** mahanimbicine, **(c)** mahanimbine, and **(d)** mahanine docked within the GSK3β binding pocket, showing hydrogen bond and hydrophobic interactions with key amino acid residues

Visualization of ligand-protein interactions revealed several stabilizing contacts within the binding pocket, including hydrogen bonding, hydrophobic interactions,

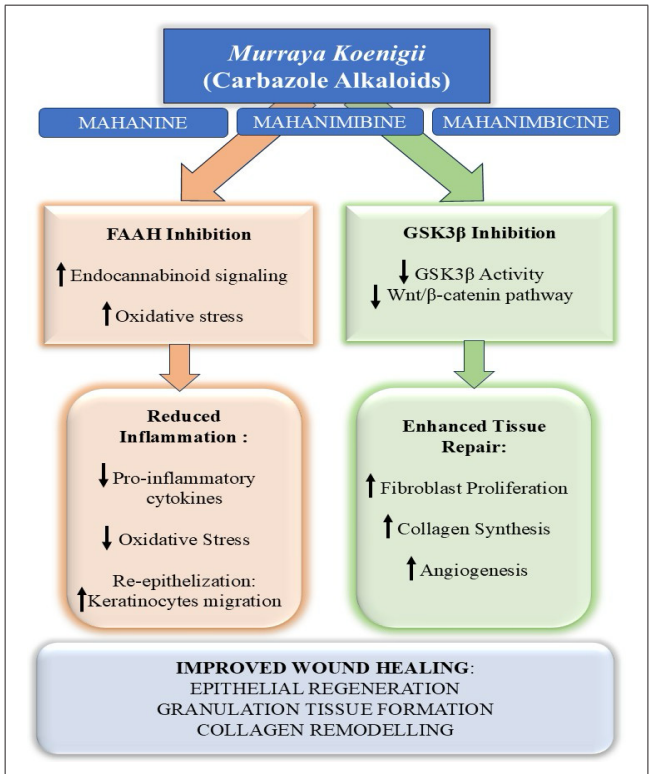

Fig 4. Schematic flowchart summarizing the mechanism of action of *Murraya koenigii* carbazole alkaloids in relation to inflammatory reduction and tissue repair markers

and van der Waals interactions. These interactions suggest potentially stable ligand-protein complexes that, if confirmed experimentally, may contribute to modulation of signaling pathways involved in inflammation and tissue regeneration.

Discussion

This study constitutes a foundational, exploratory investigation integrating standardized semi-quantitative histopathological scoring with *in silico* computational target prediction to characterize the wound-healing potential of topical *Murraya koenigii* extract in a rat excisional model. Cutaneous wound healing is a dynamic, multiphase process encompassing haemostasis, inflammation, proliferation, and remodeling, coordinated by keratinocytes, fibroblasts, endothelial cells, and immune effectors [1,3]. Successful repair requires re-epithelialization, angiogenesis-supported granulation tissue formation, progressive extracellular matrix remodeling, and epidermal maturation [24-26]. Plant-derived phytochemicals represent an actively investigated avenue for wound care, given their multi-target antioxidant, anti-inflammatory, and tissue-restorative activities [9,10,15]. Against this biological backdrop, the histopathological and computational findings of the present study are interpreted and contextualized below. It is important to emphasize that the *in silico* component of this work is intended as a hypothesis-generating tool to identify candidate molecular targets for future experimental investigation, and not as confirmation of pharmacological mechanism.

The overall histopathological evaluation demonstrated significant differences among experimental groups, with the Kruskal-Wallis test confirming that the total SPOT score differed across groups ($H = 40.838$, $P<0.001$), indicating that *Murraya koenigii* extract influenced wound healing [13,17,19,20]. The large effect size ($\varepsilon^2 = 0.819$) indicates that treatment explained a substantial proportion of variability in histopathological outcomes, suggesting a substantial treatment effect on histopathological wound-healing outcomes [1,3].

Consistent with SPOT-defined healing domains, group differences were expressed across re-epithelialization, granulation tissue formation, keratinization, fibroblast activity, and remodeling features [1,3,17,25,26]. Higher concentrations improved epidermal and dermal architecture. This was reflected by more complete epithelial coverage, increased fibroblast density, and denser collagen deposition. These findings are consistent with the proliferative and early remodeling phases of wound healing [25,26].

In addition, these findings align with previous studies highlighting the role of extracellular matrix components, particularly collagen and glycosaminoglycans such as hyaluronic acid (HA), in accelerating wound healing. HA is known to promote epithelial cell migration, proliferation, angiogenesis, and granulation tissue formation, especially during the early phases of repair. The observed increase in re-epithelialization, epidermal thickness, and collagen deposition in the treated groups may therefore reflect enhanced extracellular matrix dynamics and improved cellular activity, contributing to more efficient tissue regeneration [27,28].

Microscopically, treated groups demonstrated improved epithelial regeneration, as evidenced by partial to nearly complete epithelial coverage and increased epidermal thickness, indicating active keratinocyte-driven barrier restoration [29-32]. These findings indicate progression into the proliferative phase, characterized by re-epithelialization and tissue rebuilding, consistent with rat excisional wound models where topical agents such as resveratrol, ozonated olive oil, or insulin derivatives enhance epithelial regeneration and angiogenesis [33,34]. In parallel with these findings, the present study also showed more mature granulation tissue, reflected by increased fibroblast proliferation, neovascularization, and early collagen deposition, where these structural changes indicate active angiogenesis and extracellular matrix formation, both of which are essential for supporting tissue regeneration [17,25,27,35-37]. Similar histopathological improvements, including enhanced re-epithelialization, collagen deposition, and tissue organization, have been reported following topical treatment, likely mediated by moisture retention that preserves cellular viability, promotes angiogenesis, and enhances growth factor activity, thereby accelerating wound healing [35]. Taken together, these findings indicate that the enhanced histopathological features observed in the treated groups are not only consistent with previous experimental models but are also supported by underlying biological mechanisms that facilitate more efficient wound repair and tissue remodeling [24,26].

To explore plausible molecular mechanisms underlying these histopathological improvements, docking was performed against two repair-relevant targets associated with inflammation control and regenerative signaling: FAAH and GSK3β [22,23,29,36,37].

Regarding the specific interaction with FAAH, this enzyme degrades endocannabinoids (notably anandamide), and endocannabinoid system signaling has been linked with regulation of inflammation, nociception, and repair-associated cellular behavior; therefore, FAAH inhibition could potentially increase endocannabinoid signaling and contribute to a pro-healing wound microenvironment [29-31]. In the present docking results, *Murraya koenigii* carbazole alkaloids demonstrated favorable predicted binding affinity

toward FAAH, with mahanine exhibiting the lowest binding energy (-10.16 kcal/mol), followed by mahanimbine (-9.70 kcal/mol) and mahanimbicine (-9.69 kcal/mol), suggesting their potential as candidate FAAH inhibitors requiring further experimental confirmation [11,12,22,23,29]. If FAAH inhibition were experimentally confirmed, increased local endocannabinoid tone could plausibly attenuate excessive inflammation and support repair-associated cellular activities, including keratinocyte migration/proliferation and fibroblast-related extracellular matrix dynamics [29-31].

Parallel to the endocannabinoid pathway, the second computational target evaluated, GSK3β, serves as a key regulatory node in Wnt/β-catenin signalling, which can influence fibroblast activity, angiogenesis, and extracellular matrix dynamics during wound repair [36]. In addition, GSK3β-linked signalling has been implicated in keratinocyte migration and proliferation during re-epithelialization [37]. The carbazole alkaloids also exhibited favorable interactions with GSK3β (mahanine -8.95 kcal/mol; mahanimbine -8.85 kcal/mol; mahanimbicine -8.41 kcal/mol), suggesting potentially stable ligand-protein interactions [21,22]. Because GSK3β inhibition can stabilize β-catenin and activate Wnt signaling, such modulation may influence fibroblast activity, collagen deposition, and angiogenesis, aligning with the enhanced fibroblast density, granulation tissue organization, and extracellular matrix deposition in treated groups [36,37].

Overall, the observed wound-healing activity is consistent with evidence that plant-derived bioactive compounds and antioxidant-rich topical formulations can support repair through anti-inflammatory and tissue-restorative mechanisms, and prior work on *Murraya koenigii* also reports wound-healing relevant bioactivities, although many studies emphasize macroscopic contraction or general histopathological assessment rather than structured scoring [9-15,20,35]. By integrating SPOT-based histopathology with docking analysis, this study links structural repair outcomes to molecular targets involved in inflammation and regeneration [17,29,36,37].

Grounded in the integration of these histopathological observations and molecular docking predictions, a broader, integrated mechanistic model can be synthesized to describe the therapeutic activity of *Murraya koenigii*. It is critical to emphasize that the mechanistic narrative presented here is speculative and based exclusively on in silico computational predictions. No direct experimental confirmation of FAAH inhibition, GSK3β modulation, endocannabinoid elevation, or downstream Wnt/β-catenin pathway activation has been performed within the scope of this study. The proposed model should therefore be interpreted solely as a predictive roadmap to guide future wet-laboratory validation (e.g., Western blot, qPCR, immunohistochemistry, enzymatic activity assays) and not as evidence of confirmed pharmacological mechanism. Causal relationships between the carbazole alkaloids and the observed histopathological improvements cannot be established from the present data alone.

Based on the integration of histopathological observations and molecular docking predictions, a potential mechanistic model can be proposed to explain the wound-healing activity of *Murraya koenigii*. Although experimental validation is required, the carbazole alkaloids present in the extract may simultaneously modulate multiple molecular pathways involved in tissue repair.

First, inhibition of FAAH may increase endocannabinoid levels in the wound microenvironment, thereby reducing inflammatory responses and promoting keratinocyte migration, which accelerates re-epithelialization [26-30]. Second, modulation of GSK3β activity may enhance wound repair by promoting keratinocyte EMT, migration, and proliferation to accelerate re-epithelialization; rFGF4 treatment has also been associated with increased collagen deposition and vascular markers *in vivo* [14,33,35]. These processes facilitate granulation tissue formation, extracellular matrix deposition, and tissue remodelling during the proliferative phase of wound healing [20,24,25]. The combined modulation of these pathways may create a favourable microenvironment for tissue regeneration, resulting in improved histopathological outcomes such as enhanced epithelial coverage, increased granulation tissue organization, and early epidermal maturation [19,25,32,33].

Overall, these findings suggest that the carbazole alkaloids present in *Murraya koenigii* are predicted to exert complementary modulatory effects that promote wound healing through both anti-inflammatory mechanisms and stimulation of tissue regeneration *(Fig. 4)*. The integration of *in vivo* histopathological evaluation and *in silico* molecular docking analysis therefore provides complementary evidence supporting the therapeutic potential of *Murraya koenigii* as a candidate for wound-healing applications. Nevertheless, several important limitations temper these conclusions and are addressed comprehensively further.

First, histopathological assessment was conducted only at day 15; therefore, temporal changes during the early inflammatory and intermediate proliferative phases could not be characterized. Future studies should incorporate multiple sampling time points to capture the complete wound-healing trajectory. Second, the proposed involvement of FAAH and GSK3β was inferred from molecular docking analyses without experimental validation. Future investigations should employ molecular and biochemical approaches, such as gene and protein expression analyses, to confirm target engagement and elucidate underlying mechanisms. Third, a wounded

untreated control group was not included. Consequently, the therapeutic effect of the treatment could not be directly compared with the natural healing process. Inclusion of a spontaneous-healing control group would allow more accurate estimation of treatment efficacy. Fourth, the contribution of the vehicle could not be independently evaluated because a vehicle-only control group was not included. Future studies should incorporate a petrolatum-only treatment arm to distinguish vehicle-related effects from those of the plant extract. Fifth, phytochemical standardization of the extract was not performed, limiting reproducibility and precise dose–response interpretation. Quantitative characterization of major bioactive constituents using chromatographic techniques is therefore warranted. Finally, functional and biochemical wound-healing outcomes, including wound contraction, tensile strength, oxidative stress markers, and inflammatory mediators, were not assessed. Integrating these endpoints in future studies would provide a more comprehensive evaluation of therapeutic efficacy and mechanism of action.

Despite these limitations, the present study provides preliminary evidence supporting the wound-healing potential of *Murraya koenigii* and identifies FAAH and GSK3β as promising targets for future mechanistic investigation.

Declarations

Availability of Data and Materials: The datasets generated and analyzed during the current study are available from the corresponding author (LRY) upon reasonable request.

Acknowledgements: The authors would like to express their sincere gratitude to the Faculty of Veterinary Medicine, Universitas Airlangga, for providing facilities and technical support throughout the conduct of this research.

Funding Support: The authors declare that this research did not receive any specific grant or financial support from funding agencies in the public, commercial, or not-for-profit sectors.

Competing Interests: The authors declare that they have no competing financial or personal interests that could have influenced the work reported in this paper.

Declaration of Generative Artificial Intelligence (AI): The authors explicitly declare that the text, tables, and figures within this manuscript were not written, generated, or created by artificial intelligence (AI) or AI-assisted technologies. Generative AI tools were utilized strictly for language editing, grammar corrections, and readability improvements. The final scientific content, data interpretation, and integrity of the work remain entirely the responsibility of the human authors.

Author Contributions: T.S.S. and L.R.Y. conceived and designed the study. Z.T. conducted the molecular docking analysis. E.A.b.A., S.V.J., and Y.I.K. performed the experimental procedures and primary data collection. R.K.D. and R.S. contributed to extract preparation and formulation development. L.R.Y., A.M., and E.P.H. conducted the histopathological evaluation, microscopic imaging, and data interpretation. D.N.I., M.N.R., and K.P.S. performed the statistical analysis. T.S.S., Y.I.K., and L.R.Y. drafted and reviewed the manuscript. All authors critically revised the manuscript and approved the final version for publication.

References

1. **Rodrigues M, Kosaric N, Bonham CA, Gurtner GC:** Wound healing: A cellular perspective. *Physiol Rev,* 99 (1): 665-706, 2019. DOI: 10.1152/physrev.00067.2017
2. **Shedoeva A, Leavesley D, Upton Z, Fan C:** Wound healing and the use of medicinal plants. *Evid Based Complement Alternat Med,* 2019 (9): 1-30, 2019. DOI: 10.1155/2019/2684108
3. **Wilkinson HN, Hardman MJ:** Wound healing: Cellular mechanisms and pathological outcomes. *Open Biol,* 10 (9):200223, 2020. DOI: 10.1098/rsob.200223
4. **Masson-Meyers DS, Andrade TA, Caetano GF, Guimaraes FR, Leite MN, Leite SN, Frade MA:** Experimental models and methods for cutaneous wound healing assessment. *Int J Exp Pathol,* 101 (1-2): 21-37, 2020. DOI: 10.1111/iep.12346
5. **Staianov J, Struz JMR, Vieira RV, Luiz RM, Zarpelon-Schutz A, Teixeira KN, Bernardi-Wenzel J:** Histomorphometric analysis of excisional cutaneous wounds with different diameters in an animal model. *Int J Exp Pathol,* 105 (5): 207-219, 2024. DOI: 10.1111/iep.12520
6. **Özaydın İ, Aydın U:** Experimental skin-wound methods and healing-assessment in animal models: A review. *Pak Vet J,* 43 (3): 396-404, 2023. DOI: 10.29261/pakvetj/2023.090
7. **Falanga V, Isseroff R, Soulika A, Romanelli M, Margolis D, Kapp S, Granick M, Harding K:** Chronic wounds. *Nat Rev Dis Primers,* 8 (1):50, 2022. DOI: 10.1038/s41572-022-00377-3
8. **Schilrreff P, Alexiev U:** Chronic inflammation in non-healing skin wounds and promising natural bioactive compounds treatment. *Int J Mol Sci,* 23 (9):4928, 2022. DOI: 10.3390/ijms23094928
9. **Cedillo-Cortezano M, Martinez-Cuevas L, Márquez López JA, Barrera López IL, Escutia-Perez S, Petricevich V:** Use of medicinal plants in the process of wound healing: A literature review. *Pharmaceuticals,* 17 (3): 303, 2024. DOI: 10.3390/ph17030303
10. **Sobeh M, Mahmoud MF, Monti D, Criollo-Mendoza MS, Contreras-Angulo L, Leyva-López N, Gutiérrez-Grijalva EP, Jiménez-Ortega LA, Heredia JB:** Wound healing properties of natural products: Mechanisms of action. *Molecules,* 28 (2):598, 2023. DOI: 10.3390/molecules28020598
11. **Balakrishnan R, Vijayraja D, Jo SH, Ganesan P, Kim IS, Choi D:** Medicinal profile, phytochemistry, and pharmacological activities of *Murraya koenigii* and its primary bioactive compounds. *Antioxidants,* 9 (2):101, 2020. DOI: 10.3390/antiox9020101
12. **Franyoto Y, Nurrochmad A, Fakhrudin N:** *Murraya koenigii* L. Spreng: An updated review of chemical composition, pharmacological effects, and toxicity studies. *J Appl Pharm Sci,* 14 (6): 1-15, 2024. DOI: 10.7324/JAPS.2024.169254
13. **Andilala A, Sihombing JS:** Wound healing activity of ethanol extract-based ointment from curry leaves. *J Food Pharm Sci*, 13 (4): 480-489, 2025. DOI: 10.22146/jfps.25000
14. **Viteritti E, Oliva E, Eugelio F, Fanti F, Palmieri S, Bafile E, Compagnone D, Sergi M:** Analysis of carbazole alkaloids in *Murraya koenigii* by high performance liquid chromatography coupled to tandem mass spectrometry. *J Chromatogr Open,* 2:100055, 2022. DOI: 10.1016/j.jcoa.2022.100055
15. **Yazarlu O, Iranshahi M, Khayat Kashani HR, Reshadat S, Habtemariam S, Iranshahy M, Hasanpour M:** Perspective on the application of medicinal plants and natural products in wound healing: A mechanistic review. *Pharmacol Res,* 174:105841, 2021. DOI: 10.1016/j.phrs.2021.105841
16. **Balkan Bozlak ÇE, Yiğit S, Kağan Tolga C, Yılmaz A, Yıldız U, Çelik S, Bekis Bozkurt H, Çelebi Ö, Aksoy Ö, Özaydın İ, Halıcı Z, Çelebi D:** In rats effects of Thymus vulgaris oil extract and *Hypericum*

perforatum oil extract on wound healing in the second degree burn model infected with *Pseudomonas aeruginosa. Fresenius Environ Bull,* 31 (2): 1747-1755, 2022.

17. **van de Vyver M, Boodhoo K, Frazier T, Hamel K, Kopcewicz M, Levi B, Maartens M, Machcinska S, Nunez J, Pagani C, Rogers E, Walendzik K, Wisniewska J, Gawronska-Kozak B, Gimble JM:** Histology scoring system for murine cutaneous wounds. *Stem Cells Dev,* 30 (23): 1141-1152, 2021. DOI: 10.1089/scd.2021.0124
18. **Uma Maheswari K, Sankar S:** *In silico* molecular docking of phytochemicals of *Murraya koenigii* against *Streptococcus mutans*. *Cureus,* 16 (2):e53679, 2024. DOI: 10.7759/cureus.53679
19. **Nagappan T, Segaran TC, Wahid ME, Ramasamy P, Vairappan CS:** Efficacy of carbazole alkaloids, essential oil and extract of *Murraya koenigii* in enhancing subcutaneous wound healing in rats. *Molecules,* 17 (12): 14449-14463, 2012. DOI: 10.3390/molecules171214449
20. **Moni SS, Tripathi P, Sultan MH, Alshahrani S, Alqahtani SS, Madkhali OA, Bakkari MA, Pancholi SS, Elmobark ME, Jabeen A, Sanobar S, Ashafaq M, Siddiqui MAH:** Wound-healing and cytokine-modulating potential of medicinal oil formulation comprising leaf extract of *Murraya koenigii* and olive oil. *Braz J Biol,* 82:e256158, 2022. DOI: 10.1590/1519-6984.256158
21. **Sotocinal SG, Sorge RE, Zaloum A, Tuttle AH, Martin LJ, Wieskopf JS, Mapplebeck JCS, Wei P, Zhan S, Zhang S, McDougall JJ, King OD, Mogil JS:** The rat grimace scale: A partially automated method for quantifying pain in the laboratory rat via facial expressions. *Mol Pain,* 7:55, 2011. DOI: 10.1186/1744-8069-7-55
22. **Ivanova L, Karelson M:** The impact of software used and the type of target protein on molecular docking accuracy. *Molecules,* 27 (24):9041, 2022. DOI: 10.3390/molecules27249041
23. **Ramírez D, Caballero J:** Is it reliable to take the molecular docking top scoring position as the best solution without considering available structural data? *Molecules,* 23 (5):1038, 2018. DOI: 10.3390/molecules23051038
24. **Spielman AF, Griffin MF, Parker J, Cotterell AC, Wan DC, Longaker MT:** Beyond the scar: A basic science review of wound remodeling. *Adv Wound Care (New Rochelle),* 12 (2): 57-67, 2023. DOI: 10.1089/wound.2022.0049
25. **Cialdai F, Risaliti C, Monici M:** Role of fibroblasts in wound healing and tissue remodeling on Earth and in space. *Front Bioeng Biotechnol,* 10:958381, 2022. DOI: 10.3389/fbioe.2022.958381
26. **Mathew-Steiner SS, Roy S, Sen CK:** Collagen in wound healing. *Bioengineering (Basel),* 8 (5):63, 2021. DOI: 10.3390/bioengineering8050063
27. **Singer AJ:** Healing mechanisms in cutaneous wounds: Tipping the balance. *Tissue Eng Part B Rev,* 28 (5): 1151-1167, 2022. DOI: 10.1089/ten.TEB.2021.0114
28. **Ermutlu CŞ, Kılıç E, Aksoy Ö, Yayla S, Baran V, Dağ S, Ulkay MB, Aydın U, Demirtaş B:** Effect of bovine corpus vitreum on full-thickness dermal wound healing: An experimental study in rats. *Kafkas Univ Vet Fak Derg*, 24 (1): 33-38, 2018. DOI: 10.9775/kvfd.2017.18189
29. **Santoso AD, De Ridder D:** Fatty acid amide hydrolase: An integrative clinical perspective. *Cannabis Cannabinoid Res,* 8 (1): 56-76, 2023. DOI: 10.1089/can.2021.0237
30. **Healy CR, Gethin G, Pandit A, Finn DP:** Chronic wound-related pain, wound healing and the therapeutic potential of cannabinoids and endocannabinoid system modulation. *Biomed Pharmacother,* 168:115714, 2023. DOI: 10.1016/j.biopha.2023.115714
31. **Parikh AC, Jeffery CS, Sandhu Z, Brownlee BP, Queimado L, Mims MM:** The effect of cannabinoids on wound healing: A review. *Health Sci Rep,* 7 (2):e1908, 2024. DOI: 10.1002/hsr2.1908
32. **Al-Dhubaibi MS, Mohammed GF, Bahaj SS, AbdElneam AI, Al-Dhubaibi AM, Atef LM:** The role of keratinocytes in skin health and disease. *Dermatol Rev,* 6:e70028, 2025. DOI: 10.1002/der2.70028
33. **Şahin Öksüz C, Çakmakçı E, Kibar B, Belge A:** Comparison of the effects of resveratrol and ozonated olive oil on open wound healing: An experimental rat model. *Res Vet Sci,* 204:106149, 2026. DOI: 10.1016/j.rvsc.2026.106149
34. **Özaydin İ, Aksoy Ö, Yayla S, Kurt B, Kılıç E, Bingöl SA, Can İ, Deprem T:** Clinical, histopatological and immunohistochemical evaluation of the effects of topical NPH-insulin on full-thickness open wounds: An *in-vivo* study in diabetic and non-diabetic mice. *Ankara Univ Vet Fak Derg,* 65, 219-228, 2018. DOI: 10.1501/Vetfak_0000002850
35. **Irma J, Kartasasmita AS, Kartiwa A, Irfani I, Rizki SA, Onasis S:** From growth factors to structure: PDGF and TGF-β in granulation tissue formation. A literature review. *J Cell Mol Med,* 29 (11):e70374, 2025. DOI: 10.1111/jcmm.70374
36. **Gumede DB, Abrahamse H, Houreld NN:** Targeting Wnt/β-catenin signaling and its interplay with TGF-β and Notch signaling pathways for the treatment of chronic wounds. *Cell Commun Signal,* 22 (1):244, 2024. DOI: 10.1186/s12964-024-01623-9
37. **Sun J, Zhou J, Zhou J, Xu W, Du Y, Jia Z, Shen Y, Lin X, Wang X, Bao Y, Rao Z, Dong S, Luo Y, Cong W, Jin L, Li X:** FGF4 promotes skin wound repair through p38 MAPK and GSK3β-mediated stabilization of Slug. *J Invest Dermatol,* 143 (6): 1073-1084.e8, 2023. DOI: 10.1016/j.jid.2022.11.015

Kafkas Universitesi Veteriner Fakultesi Dergisi
Journal Home-Page: http://vetdergikafkas.org
E-ISSN: 1309-2251

Kafkas Univ Vet Fak Derg
32 (4): 511-519, 2026
DOI: 10.9775/kvfd.2026.36550

RESEARCH ARTICLE

Improvement of IBDV VP2 Protein Expression in *Escherichia coli* Through a Staged pH Control Strategy

Qiang FU [1], Xiubao ZHAO [1], Yu SUN [2], Weiqin MENG [1], Chuwen LIN [1], Lizhong MIAO [1], Wenxiu WANG [1], Likun CHENG [1 (*)]

[1] Binzhou Key Laboratory of Synthetic Biotechnology, Shandong Binzhou Animal Science and Veterinary Research Academy, Binzhou 256600, CHINA
[2] School of Life Science, NingXia University, Yinchuan, NingXia 750021, CHINA

[(*)] **Corresponding author:**
Likun Cheng
Phone: +86-543-3171209
Cellular phone: +86-13854359698
E-mail: clksd@126.com

How to cite this article?

Fu Q, Zhao X, Sun Y, Meng W, Lin C, Miao L, Wang W, Cheng L: Improvement of IBDV VP2 Protein Expression in *Escherichia coli* Through a Staged pH Control Strategy. *Kafkas Univ Vet Fak Derg*, 32 (4): 511-519, 2026. DOI: 10.9775/kvfd.2026.36550

Article ID: KVFD-2026-36550
Received: 13.03.2026
Accepted: 23.06.2026
Published Online: 08.07.2026

Abstract

Infectious bursal disease (IBD), caused by infectious bursal disease virus (IBDV), severely endangers the global poultry industry. The VP2 subunit vaccine represents a primary strategy for the prevention and control of IBD. *Escherichia coli* is widely used for recombinant VP2 production; however, acetate overflow during fermentation severely inhibits cell growth and target protein synthesis. Additionally, conventional constant-pH strategies and empirical pH regulation approaches fail to achieve a balance between high cell density, low by-product accumulation, and efficient expression of active VP2 protein. This study aimed to investigate the effects of various ions from pH regulators on the growth of the engineered strain *E. coli* 0125. Aqueous ammonia ($NH_3 \cdot H_2O$) was identified as the optimal regulator. Based on real-time monitoring of dissolved oxygen (DO) dynamics, the optimal pH for strain growth was determined to be 7.2. Subsequently, nine staged pH control strategies were established to optimize the fermentation process. The optimal protocol was to maintain the pH at 7.2 during the initial 0-6 h of fermentation, followed by adjustment to pH 6.8 during 6-12 h using $NH_3 \cdot H_2O$. Under these conditions, the wet cell concentration reached 28.37 g/L, the specific VP2 titer increased to 96 U/g, and acetate content was maintained at a low level of 2.19 g/L ($P<0.05$). Compared with the group maintained at pH 7.0 using sodium hydroxide, the total VP2 titer of the optimized group increased by 2.95 times. This refined staged pH control strategy effectively resolves the contradictions in *E. coli* fermentation and provides a practical technical approach for the large-scale industrial production of IBDV VP2 subunit vaccines.

Keywords: Acetate, *Escherichia coli*, IBDV, pH regulation, VP2 protein

INTRODUCTION

Infectious bursal disease (IBD) is a highly contagious and immunosuppressive disease in poultry caused by the infectious bursal disease virus (IBDV). It leads to increased mortality, growth retardation, and secondary infections in chickens, and even compromises the efficacy of other vaccinations, causing enormous economic losses to the global poultry industry [1,2]. Vaccination remains the primary strategy for the prevention and control of IBD. Compared with traditional live vaccines, VP2-based subunit vaccines exhibit superior biosafety and immunogenicity, and have emerged as a major focus in the research and development of IBDV vaccines [3]. The expression level and biological activity of the VP2 protein directly determine vaccine efficacy and industrialization potential. Therefore, achieving high-efficiency heterologous expression of VP2 is essential for promoting the industrial application of VP2 subunit vaccines.

As a classic heterologous expression host, *Escherichia coli* possesses several advantages, including a clear genetic background, low cultivation cost, and fast proliferation, and is commonly used for VP2 protein production. Nevertheless, the low yields and poor biological activity of recombinant VP2 remain major obstacles restricting its large-scale industrial production. Protein expression is jointly affected by intrinsic properties of the expression system and external fermentation parameters. Among various process factors, pH plays a decisive role in regulating bacterial metabolism and recombinant protein synthesis.

pH is a vital environmental factor in microbial fermentation. It modulates cell growth, membrane permeability, and gene expression profiles, reshapes intracellular metabolic

flux to control by-product formation, and ultimately affects the synthesis efficiency of heterologous proteins [4,5]. Acetate is a major inhibitory by-product generated during *E. coli* cultivation and has adverse impacts on both cell growth and recombinant protein expression [6]. At low concentrations, acetate can reduce respiratory activity and glucose consumption, and even trigger cell autolysis. When the acetate concentration exceeds 40 mmol/L, recombinant protein expression is significantly suppressed, with genetically engineered strains exhibiting high sensitivity to acetate stress [4,7]. The toxic mechanism of acetate is mainly attributed to protonated acetate penetrating cell membranes and decreasing intracellular pH. Cells consume large amounts of ATP to extrude hydrogen ions for pH homeostasis, forming futile energy cycles and disrupting normal metabolism, thereby drastically inhibiting the accumulation of target proteins [4,8].

In *E. coli*, acetate is mainly synthesized through two metabolic pathways. The AckA–Pta pathway is the major route of acetate production, in which excess carbon sources drive the conversion of acetyl-coenzyme A (acetyl-CoA) into acetate [9]. In addition, the PoxB pathway can be activated under conditions of low oxygen and high glucose, catalyzing the oxidation of pyruvate to generate additional acetate [10]. Previous studies have demonstrated that knockout of acetate-synthesizing genes, including *ackA*, *pta*, and *poxB*, induces impaired cell growth, suggesting that genetic modification is not a feasible approach for relieving acetate accumulation [9,11]. In contrast, precise pH regulation offers a promising approach to optimize carbon flux distribution and reduce by-product synthesis. By influencing membrane properties and enzyme activities, pH stabilizes intracellular acid–base homeostasis, improving plasmid stability and protein folding efficiency [12,13]. Furthermore, pH also modulates key glycolytic enzymes to optimize carbon distribution and reduce futile metabolism, ultimately creating a favorable intracellular environment for heterologous protein expression [5,9].

pH regulation and staged pH control are commonly used for optimizing *E. coli* fermentation. However, the selection of pH regulators has received little attention; improper pH regulators tend to accumulate inhibitory ions in the system and induce metabolic disorders, leading to reduced yield and unstable product quality. In addition, single-factor experiments cannot analyze interactive effects among variables and fail to achieve global process optimization, limiting their value for industrial-scale production [14]. Given the high toxicity and cost of isopropyl-β-D-thiogalactoside, lactose was selected as a safer and more economical alternative inducer in this study.

Dynamic feedback control integrated with metabolic flux analysis and intelligent algorithms has emerged as an advanced strategy for fermentation optimization [15]. Nevertheless, it demands sophisticated equipment and high operational costs. In this study, we optimized the staged pH process for VP2 protein expression, including selecting proper pH regulators through ionic effect evaluation, identifying the optimal growth pH using dissolved oxygen (DO) curves, and constructing multi-gradient staged pH control regimes. The resulting pH control strategy enabled high-level VP2 production in *E. coli* 0125, mitigating the limitations of constant-pH fermentation and achieving high cell density, low acetic acid content, and high yield of active VP2. The methodologies developed for pH regulator screening and pH parameter determination provide a practical approach for optimizing recombinant protein fermentation processes.

Material and Methods

Ethical Statement

Ethical approval was not required for this study.

Bacterial Strain

The engineered strain *E. coli* 0125 for VP2 protein expression was constructed by transforming competent *E. coli* BL21 (DE3) cells with the recombinant plasmid pET28a-rVP2 harboring the VP2-encoding gene. This strain is preserved in the Culture Collection Center of the Shandong Binzhou Animal Science and Veterinary Research Institute. The expression vector pET28a is a medium-to-low copy-number plasmid.

Culture Media

Seed Medium

The seed medium consisted of yeast extract (5.0 g/L), peptone (10.0 g/L), sodium chloride (NaCl; 10.0 g/L), and glucose (5.0 g/L).

Fermentation Medium

The fermentation medium contained glycerol (10 g/L), yeast extract (5 g/L), peptone (2 g/L), ammonium sulfate [$(NH_4)_2SO_4$; 4 g/L], potassium dihydrogen phosphate (KH_2PO_4; 3 g/L), potassium chloride (KCl; 1.5 g/L), magnesium sulfate ($MgSO_4$; 2 g/L), citric acid (2 g/L), betaine (1.5 g/L), ferrous sulfate ($FeSO_4$; 0.5 g/L), thiamine (0.05 g/L), biotin (0.02 g/L), and trimethylglycine (2.0 g/L). Additional inorganic salts were supplemented into the fermentation medium according to experimental designs.

Culture Conditions

Seed Culture

A single colony of *E. coli* 0125 was picked, inoculated into a 100-mL Erlenmeyer flask containing 50 mL of the seed medium, and cultured at 37°C with shaking at 180 r/min for 12 h.

Shake-flask Culture

The seed culture was inoculated into a 500-mL Erlenmeyer flask containing 100 mL of the fermentation medium at an inoculum size of 2%, followed by cultivation at 37°C and 180 r/min for 12 h.

10-L Fermenter Culture

The seed culture was inoculated into a 10-L fermenter (GRJ-10; Zhenjiang Green Bioengineering, China) containing 6 L of the fermentation medium at an inoculum size of 2%. The temperature was maintained at 37°C, and DO was maintained above >20% by adjusting the stirring speed and the aeration rate. The pH was kept at the preset value throughout fermentation as required. When the optical density at 600 nm reached 2.0, lactose was added to a final concentration of 10 g/L to induce recombinant VP2 production. Once the initial carbon source was depleted, glycerol was supplied through a DO-feedback-controlled feeding strategy.

Staged pH Regulation Strategy

Based on the effects of different pH conditions on VP2 protein expression observed in this study, and with reference to the design method reported by Zhao et al. [5], nine two-stage pH control strategies were designed and evaluated. Different pH values were applied during the early culture stage to determine the optimal conditions for strain growth, and a series of pH gradients were arranged for the late stage to evaluate their effects on acetic acid production and VP2 expression. The detailed parameters for each group are shown in *Table 1*.

Determination of Fermentation Parameters

Real-time monitoring of temperature, pH, and DO was performed using the built-in electrodes of the fermenter.

Fermentation broth samples were appropriately diluted, and the absorbance at 600 nm was measured to assess cell growth. The cells were harvested by centrifugation at 8000 g for 10 min at 4°C. The wet cell weight (g/L) was determined immediately.

Table 1. *Design of pH regulation strategy*

Strategy No.	First-stage pH and Time	Second-stage pH and Time
I	7.2 (0–8 h)	7.0 (8–12 h)
II	7.2 (0–8 h)	6.8 (8–12 h)
III	7.2 (0–8 h)	6.5 (8–12 h)
IV	7.2 (0–6 h)	7.0 (6–12 h)
V	7.2 (0–6 h)	6.8 (6–12 h)
VI	7.2 (0–6 h)	6.5 (6–12 h)
VII	7.2 (0–4 h)	7.0(4–12 h)
VIII	7.2 (0–4 h)	6.8 (4–12 h)
IX	7.2 (0–4 h)	6.5 (4–12 h)

Acetate concentration was determined by high-performance liquid chromatography (HPLC). The HPLC system consisted of an Agilent 1260 HPLC instrument (Agilent Technologies, CA, USA) equipped with an Aminex HPX-87H column (Bio-Rad, CA, USA) and a refractive index detector. Fermentation samples were centrifuged at 12.000 *g* for 3 min prior to detection. The supernatant was diluted 10 times and filtered through a microporous membrane. The mobile phase was 0.005 M sulfuric acid (H_2SO_4) at a constant flow rate of 0.5 mL/min.

Detection and Activity Definition of VP2 Protein

Preservation of the three-dimensional structure of the VP2 protein is critical for its immunogenicity. The agar gel precipitation (AGP) assay can preserve native protein conformation and ensure specific recognition of functional epitopes by antibodies. Accordingly, VP2 antigen titer was determined by AGP in accordance with the national standard GB/T 19167-2020 *Diagnostic Techniques for Infectious Bursal Disease* [16]. To improve the accuracy of endpoint judgment, continuous gradient dilution was adopted in addition to the conventional two-fold serial dilution. The highest dilution that produced clear, specific precipitation lines was recorded as the antigen titer of the sample.

The specific VP2 titer (U/g) was defined as the VP2 activity per gram of wet cells, which directly reflected the functional expression level of recombinant VP2. Compared with total protein quantification, this indicator provides a more objective evaluation of the effects of fermentation conditions on VP2 biological activity. The total VP2 titer was calculated as follows:

Total VP2 titer per unit volume (U/L) = Wet cell weight (g/L) × Specific VP2 titer (U/g)

Statistical Analysis

Data were expressed as mean ± standard deviation. All statistical analyses were performed using R software, version 4.5.1. Data normality and homogeneity of variance were assessed using the Shapiro-Wilk test and Levene's test, respectively. One-way analysis of variance was performed for data satisfying the assumptions of parametric tests. The Kruskal-Wallis *H* test was used for nonparametric analysis. Multiple comparisons were conducted using Duncan's new multiple range test using the agricolae package. Differences were considered statistically significant at $P<0.05$.

Results

Influence of Inorganic Salt Cations on the Growth of the *E. coli* 0125 Strain

The effects of different inorganic salt cations on the growth of *E. coli* 0125 are shown in *Fig. 1-A*. NaCl supplementation

at concentrations of 0-125 mmol/L did not significantly affect cell density (P>0.05), indicating that Na^+ had neither growth-promoting nor inhibitory effects on the strain. In contrast, ammonium chloride (NH_4Cl) and KCl supplementation significantly increased cell density (P<0.05) in a concentration-dependent manner *(Fig. 1-B, C)*. The maximum cell density was observed at 100 mmol/L for both NH_4Cl and KCl, indicating their strongest growth-promoting effect at this concentration. As Cl^- was present in all three salts, its contribution to the observed strain growth could be excluded. Collectively, these results confirmed that NH_4^+ and K^+ significantly promoted the growth of *E. coli* 0125, whereas Na^+ had no such effect.

Influence of Inorganic Salt Anions on the Growth of Strain *E. coli* 0125

The effects of different anions on the growth of *E. coli* 0125 were further evaluated. As shown in *Fig. 2*, supplementation with sodium nitrate ($NaNO_3$) and sodium sulfate (Na_2SO_4) significantly increased cell density in a concentration-dependent manner (P<0.05). For both salts, the maximum cell density was achieved at 100 mmol/L. Combined with the results obtained for NaCl (*Fig. 1-A*), the three treatments shared the same cation (Na^+), which had previously been shown to exert no significant effect on strain growth. Therefore, the contribution of the cation could be excluded, and the effects of the respective anions were evaluated. The results demonstrated that Cl^- had no significant influence on cell growth (P>0.05), whereas both NO_3^- and SO_4^{2-} significantly promoted cell proliferation of *E. coli* 0125 (P<0.05).

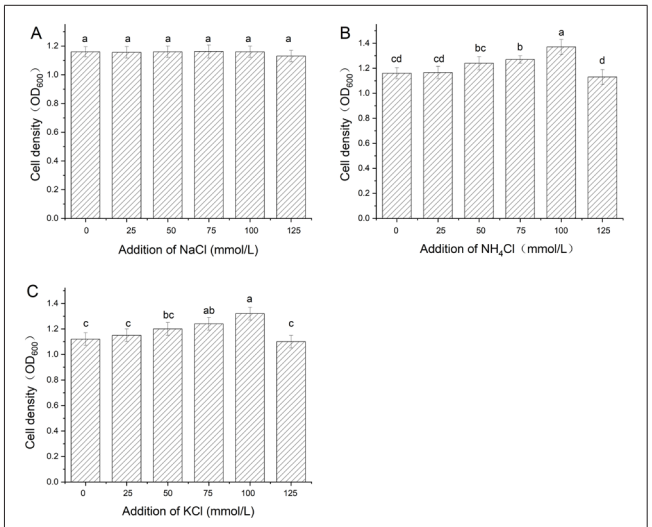

Fig 1. Effects of different concentrations of NaCl, NH_4Cl, and KCl on the growth of E. coli 0125. **(A)** NaCl addition; **(B)** NH_4Cl addition; and **(C)** KCl addition. Data are presented as mean ± standard deviation of three independent biological replicates (n = 3). Different lowercase letters above the bars denote significant differences (P<0.05)

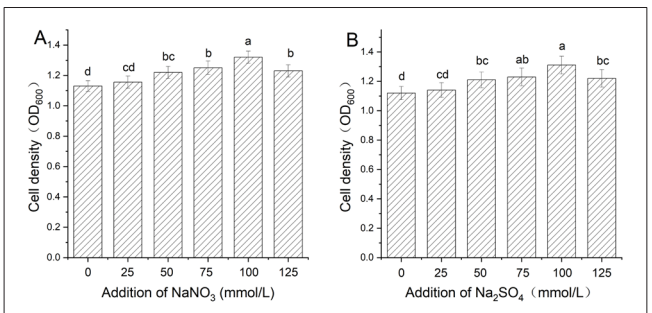

Fig 2. Effects of different concentrations of $NaNO_3$ and Na_2SO_4 on the growth of E. coli 0125. **(A)** $NaNO_3$ addition and **(B)** Na_2SO_4 addition. Data are presented as mean ± standard deviation of three independent biological replicates (n = 3). Different lowercase letters above the bars denote significant differences (P<0.05)

Screening of the Optimal pH Regulator for the *E. coli* 0125 Strain

Based on the cation screening results *(Fig. 1-B, C)*, NH_4^+ and K^+ were identified as growth-promoting ions. Therefore, aqueous ammonia ($NH_3{\cdot}H_2O$) and potassium hydroxide (KOH) were selected as candidate pH regulators, and sodium hydroxide (NaOH) served as the control. As shown in *Fig. 3-A*, the maximum cell density in the NaOH group was 19.23 g/L, whereas that in the $NH_3{\cdot}H_2O$ and KOH groups increased to 22.76 g/L (18.47% increase) and 21.85 g/L (13.62% increase), respectively. Moreover, the specific VP2 titer in both the $NH_3{\cdot}H_2O$ and KOH groups reached 64 U/g, which was significantly higher than that in the NaOH group (48 U/g; P<0.05; *Fig. 3-B)*. Notably, when $NH_3{\cdot}H_2O$ was used for pH control, the strain entered the stationary phase in approximately 8 h *(Fig. 3-A)*.

Identification of the Optimal Growth pH Using DO Profiles

The optimal growth pH of *E. coli* 0125 was determined by monitoring DO dynamics. Because hydrochloric acid (HCl) and NaOH exerted no obvious adverse effects on strain growth, pH adjustment was conducted after the strain entered the stationary phase. First, the pH was reduced to 6.0 using HCl within 10 min, and then

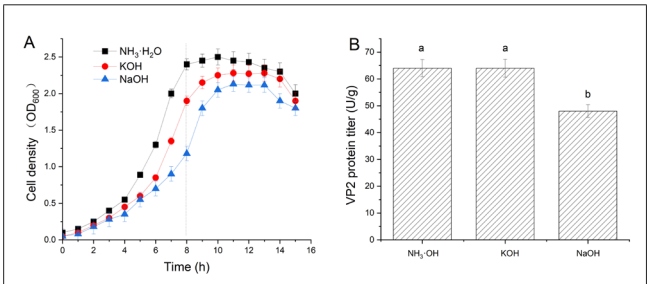

Fig 3. Validation of the optimal pH regulator and determination of the stationary phase for E. coli 0125. **(A)** Time course of cell density under different pH regulators. **(B)** Specific VP2 titer. Data are presented as mean ± standard deviation of three independent biological replicates (n = 3). Different lowercase letters denote significant differences (P<0.05)

gradually increased to 9.0 using NaOH over a period of 30 min. The corresponding DO profiles are presented in *Fig. 4*.

As the pH increased from 6.0 to 7.2, the DO content decreased continuously, suggesting an increase in the oxygen consumption rate and cellular metabolic activity. The minimum DO value was observed at pH 7.2, which corresponded to the highest oxygen consumption rate, vigorous respiratory metabolism, and strong physiological activity of the strain. When pH exceeded 7.2, the DO concentration rebounded, indicating a reduction in oxygen uptake and a decline in metabolic activity. Based on the principle that the DO trough corresponds to the maximum oxygen consumption rate, pH 7.2 was identified as the optimal growth pH for *E. coli* 0125.

Determination of the Optimal Growth pH Value for the *E. coli* 0125 Strain

The effects of constant-pH control on cell growth, VP2 expression, and acetate accumulation were further evaluated *(Fig. 5)*. As shown in *Fig. 5-A*, the highest wet cell weight (25.62 g/L) was achieved at pH 7.2, exceeding the values observed at pH 6.8, 7.0, and 7.4 by 26.08%, 12.57%, and 19.55%, respectively (P<0.05). The specific VP2 titer reached 80 U/g at both pH 7.0 and pH 7.2, which was significantly higher than the values observed at pH 6.8 and pH 7.4 (P<0.05; *Fig. 5-B)*. However, acetate accumulation was also the highest at pH 7.2, reaching 2.49 g/L, which was 1.20-, 1.11-, and 1.15-fold higher than that measured at pH 6.8, 7.0, and 7.4, respectively (P<0.05; *Fig. 5-C)*.

Collectively, the findings revealed that high cell density at pH 7.2 was accompanied by severe acetate overflow.

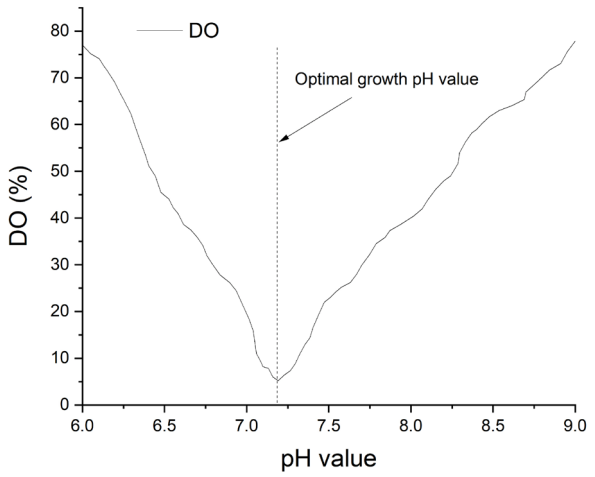

Fig 4. Changes in DO levels of E. coli 0125 during the stationary phase under varying pH conditions. The dashed line marks the optimal growth pH value (7.2). Note: The curve shows a schematic representation of the overall trend

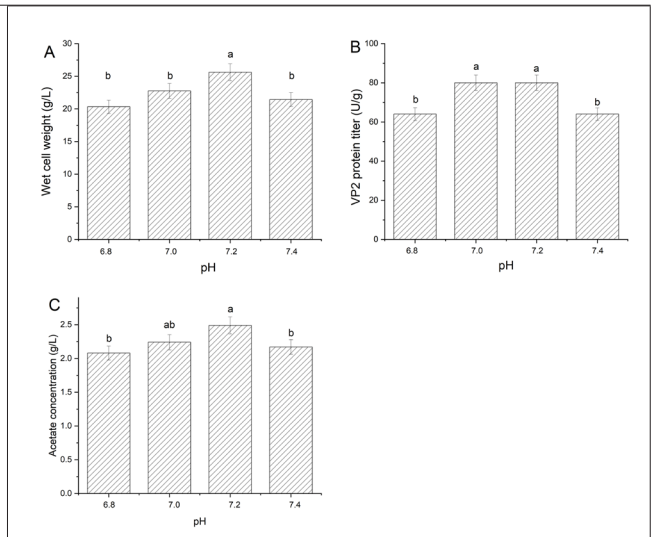

Fig 5. Effects of different constant-pH control levels on E. coli 0125 fermentation. **(A)** Wet cell weight, **(B)** specific VP2 titer, and **(C)** acetate concentration. Data are presented as mean ± standard deviation of three independent biological replicates (n = 3). Different lowercase letters denote significant differences (P<0.05)

Therefore, a single constant-pH strategy is insufficient to simultaneously balance cell growth, recombinant protein expression, and by-product control. These results further highlight the necessity of developing a staged pH regulation strategy for this process.

Influence of Various Staged pH Control Strategies on VP2 Protein Expression

The effects of nine staged pH regulation strategies on cell growth, VP2 expression, and acetate accumulation were evaluated *(Fig. 6)*. Significant differences in all three indicators were observed among the groups (P<0.05).

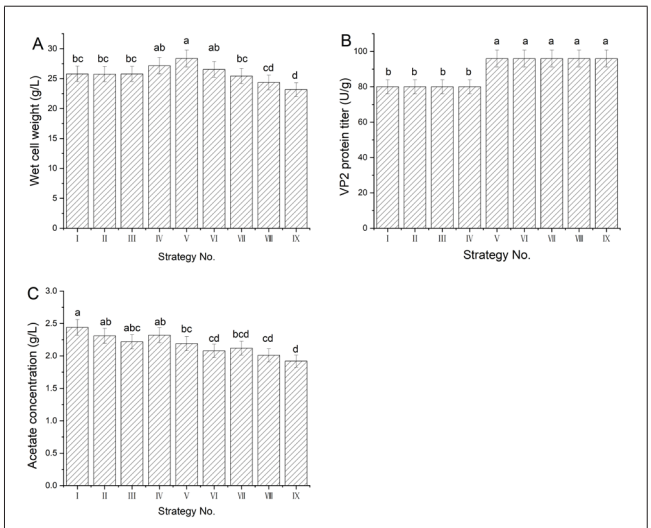

Fig 6. Effects of different staged pH control strategies on E. coli 0125 fermentation and VP2 protein expression. **(A)** Wet cell weight, **(B)** specific VP2 titer, and **(C)** acetate concentration. Data are presented as mean ± standard deviation of three independent biological replicates (n = 3). Different lowercase letters denote significant differences (P<0.05)

Group V exhibited the best comprehensive performance. It achieved the highest wet cell weight of 28.37 g/L, which was significantly higher than most constant-pH groups *(Fig. 6-A)*. The specific VP2 titer reached 96 U/g, whereas acetate concentration remained at a relatively low level of 2.19 g/L *(Fig. 6-B, C)*.

Further analysis showed that maintaining pH at 7.2 during the first 6 h resulted in significantly higher cell density compared with the 4 or 8 h initial periods ($P<0.05$). Moreover, the lowest acetate accumulation was observed in groups that shifted to a lower pH in the second stage, which effectively reduced overflow metabolism. Lower acetate levels contributed to improved VP2 activity, as the specific titer in Groups V-IX reached 96 U/g, significantly higher than that in Groups I-IV ($P<0.05$).

Discussion

As a critical environmental factor, pH modulates the growth, carbon metabolism distribution, and heterologous protein production of *E. coli*. Dynamic changes in pH can significantly affect intracellular metabolism, by-product formation, and protein folding, thereby playing a vital role in the optimization of recombinant protein fermentation. Focusing on the fermentation characteristics of recombinant IBDV VP2 protein, this study systematically carried out three sets of experiments: screening of ionic pH regulators, determination of baseline pH based on DO profiles, and multi-gradient optimization of staged pH control. Based on the findings, a tailored pH regulation system was established for the engineered strain *E. coli* 0125 and VP2 antigen production. This strategy successfully addresses the dilemma of conventional constant-pH fermentation, which often fails to simultaneously achieve robust cell growth, minimize acetate accumulation, and maintain high-activity protein synthesis. The findings provide valuable technical references for the industrial fermentation of VP2 subunit vaccines.

In fermentation systems, inorganic anions and cations introduced through pH regulators can modulate cellular metabolism by changing membrane permeability, intracellular enzyme activity, and environmental osmotic pressure. Such ionic effects are essential considerations when selecting acid-base regulators [17,18]. To eliminate interference from mixed ions, we adopted a single-variable design with paired fixed ions to separately evaluate the effects of different cations and anions on strain growth *(Fig. 1; Fig. 2)*. The results showed that Na^+ exerted no significant influence on cell proliferation, whereas NH_4^+, K^+, NO_3^-, and SO_4^{2-} significantly promoted cell growth. Based on these findings, $NH_3{\cdot}H_2O$ and KOH were selected as optimal pH regulators for subsequent tests. Compared with NaOH, $NH_3{\cdot}H_2O$ supplies an additional nitrogen source while regulating pH, making it more widely applicable in industrial fermentation [19]. Shen et al.[20] also reported that $NH_3{\cdot}H_2O$ stabilized pH and provided supplemental nitrogen during amylase production by *Bacillus*. The results of this study further validated this advantage: the cell density in the $NH_3{\cdot}H_2O$ group increased by 18.36% relative to the NaOH group, and the specific VP2 titer reached 80 U/g. These findings highlight the practical significance of rational regulator selection for industrial production and indicate that focusing merely on pH values while ignoring ionic effects will lead to mismatched process parameters in practical manufacturing.

Following the selection of appropriate pH regulators, online DO monitoring was employed to identify the favorable growth pH for the strain. Previous studies have shown that stable agitation and aeration conditions allow oxygen consumption rate to indicate cellular respiratory activity, and DO troughs usually coincide with high physiological performance [21,22]. In this study, aeration, stirring speed, and tank pressure were maintained at constant levels during the stationary phase of the VP2 expression strain to ensure a stable oxygen supply. Under these conditions, DO profiles were considered to indirectly reflect cell growth. Therefore, the pH corresponding to peak oxygen consumption was selected as the optimal growth pH, which was determined to be 7.2 *(Fig. 4)*. Regulators with little impact on cell growth were used in this study. Validation results revealed that biomass at pH 7.2 increased by 26.08% compared with that at pH 6.8 *(Fig. 5-A)*. This rapid screening technique has been patented [23]. Nevertheless, its applicability is limited, and it is primarily suitable for pH condition screening of aerobic microorganisms.

However, the pH conditions that favor optimal growth also present obvious disadvantages. A high growth rate accelerates glycolysis and triggers acetyl-CoA overflow, leading to massive acetate accumulation. The acetate concentration reached 2.49 g/L at pH 7.2, which was 1.2-fold higher than that at pH 6.8 *(Fig. 5-C)*. Excess acetate further inhibited heterologous protein expression [21,22], consistent with previous studies [24,25]. These results highlight an inherent contradiction between the optimal pH for cell growth and that for target protein synthesis. Consequently, a single constant-pH strategy is unable to simultaneously achieve high cell density, low by-product formation, and high-activity protein production, which is the core motivation for developing the staged pH strategy in this study.

Microorganisms usually require distinct pH conditions for cell growth and product synthesis. Staged dynamic pH regulation, in which pH is dynamically adjusted to meet the stage-specific physiological demands, has emerged as a classic strategy to balance cell proliferation and product

formation [26]. Mital et al.[27] reported that weakly alkaline conditions suppressed cell growth but improved soluble expression of intracellular alcohol dehydrogenase. Guo et al.[28] applied a two-stage differentiated pH strategy in mixed-strain fermentation and achieved a substantial increase in ethanol yield. Both studies demonstrated the superiority of staged pH control. For *E. coli*, the conventional optimal growth pH ranges from 7.0 to 7.5. However, this pH range induces excessive carbon flux and severe acetate overflow, and also increases plasmid loss and reduces recombinant protein stability [29]. Therefore, maintaining the optimal growth pH in the early phase to ensure cell proliferation, followed by a shift to weakly acidic pH in the middle and late phases to reduce acetate accumulation, is a feasible strategy for VP2 production.

Based on the effects of different pH values on VP2 fermentation, nine staged pH control modes were established in this study *(Table 1; Fig. 6)*. As pH 7.2 was identified as the optimal condition for strain growth, it was used throughout the early fermentation stage. Acetic acid content increased with rising pH during cultivation, while favorable fermentation performance was achieved at pH 6.5, 6.8, and 7.0. Therefore, these values were selected for pH regulation in the late stage. Rapid cell proliferation is known to accelerate acetic acid synthesis. Accordingly, three duration gradients (0-4 h, 0-6 h, and 0-8 h) were designed to represent different phases of exponential growth. Although the specific cell growth rate was not measured in this study, staged pH adjustment was employed to regulate cell growth status, so as to reduce acetic acid accumulation and improve VP2 production. The results demonstrated that the retention time of pH 7.2 in the early stage significantly affected the final biomass yield. Maintaining pH 7.2 for the first 6 h resulted in satisfactory biomass accumulation, whereas lowering pH at 4 h in advance caused acid stress and inhibited cell growth. Shortening the duration of initial high pH combined with low pH regulation in the later stage effectively reduced the total acetic acid production *(Fig. 6-C)*. Group IX exhibited the lowest acetic acid content, which was 22.89% lower than that at constant pH 7.2 conditions. A negative correlation was observed between acetic acid accumulation and VP2-specific potency, and Groups VI-IX achieved a specific potency of 96 U/g *(Fig. 6-B)*. Thus, a two-stage pH control strategy could simultaneously achieve high-density culture and efficient VP2 synthesis. Previous studies have demonstrated that mild acidic conditions can reshape carbon metabolism, alleviate glucose overflow metabolism in *E. coli*, and restrict acetic acid formation without severely interfering with primary metabolic pathways [30,31]. These observations were highly consistent with the findings of this study. Specifically, the results of this study demonstrated that pH 6.5 could inhibit acetic acid accumulation more effectively compared with neutral pH. Therefore, appropriately decreasing pH during the middle and late fermentation stages represents an efficient approach to relieve overflow metabolism and increase recombinant protein yield. This approach provides a valuable reference for by-product control in other fermentation processes of recombinant proteins expressed by *E. coli*.

Unlike conventional studies that focus solely on optimizing a single pH value or adopting fixed staged control regimes, this study combined the screening of pH regulators with the stage-dependent physiological characteristics of cells to develop a novel staged pH control process. This process does not require molecular modifications such as gene knockout, thereby avoiding growth defects caused by strain engineering. It has a lower technical threshold and is easier to popularize in practical production.

All fermentation experiments in this study were performed in triplicate. The experimental data showed minimal variation and consistent trends across replicates, indicating excellent batch-to-batch repeatability and stability of the established staged pH strategy. For industrial applications, this strategy relies solely on conventional acid-base feeding, ensuring compatibility with existing equipment while minimizing material costs, thereby meeting the requirements of large-scale vaccine production. In terms of scale-up potential, the core principle of "promoting cell growth at the early stage and restraining by-product formation at the late stage" is consistent with the general metabolic characteristics of high-density *E. coli* fermentation, thereby facilitating gradual process scale-up.

In conclusion, this study established a refined, physiology-driven staged pH control strategy for the high-yield production of active IBDV VP2. Unlike empirical and universal pH control methods, this study innovatively integrated ionic effect evaluation with real-time DO monitoring, achieving coordinated optimization of cell growth, reduction of acetic acid overflow, and synthesis of functional antigens. Owing to its favorable stability, ease of implementation, and potential for industrial scale-up, the proposed process provides a practical and reliable approach for industrial fermentation of IBDV VP2 subunit vaccines.

Declarations

Availability of Data and Materials: The data supporting the findings of this study are available from the corresponding author upon reasonable request.

Acknowledgments: We thank all authors for their significant contributions to this study.

Financial Support: This study was funded by the Young Science

and Technology Rising Star Program, Binzhou (QMX2023003), and the Natural Science Foundation of Shandong Province (ZR2023MC196).

Conflicts of Interest: The authors declare no conflicts of interest.

Declaration of Generative Artificial Intelligence (AI): The authors confirm that no generative AI created the manuscript text, tables or figures. AI tools were only used for linguistic revision.

Author Contributions: Q.F. and Y.S.: Data curation, data analysis, methodology, writing - original draft preparation. X.Z. and W.M.: Supervision, writing - review. L.M. and W.W.: Supervision, writing - review and editing. C.L. and L.C.: Conceptualization, experimental design, supervision, writing – review and editing.

References

1. **Beshah A, Ahmed A, Dandecha M:** Epidemiology and risk factors of infectious bursal disease: A review. *J Bacteriol Mycol,* 11 (2): 1219, 2024. DOI: 10.26420/jbacteriolmycol.2024.1219
2. **Muneeb JM, Pawaskar DK, Ullah-Rafiqui M, Siddiqui R, Shabir N, Pawaskar NK:** A comprehensive overview of infectious bursal disease, a major threat to poultry health and production. *Int J Adv Biochem Res,* 8, 154-63, 2024. DOI: 10.33545/26174693.2024.v8.i12sc.3092
3. **Ramon G, Legnardi M, Cecchinato M, Cazaban C, Tucciarone CM, Fiorentini L, Gambi L, Mato T, Berto G, Koutoulis K, Franzo G:** Efficacy of live attenuated, vector and immune complex infectious bursal disease virus (IBDV) vaccines in preventing field strain bursa colonization. *Front Vet Sci,* 9:978901, 2022. DOI: 10.3389/fvets.2022.978901
4. **Liu S, Xu J, Zhang W:** Advances and prospects in metabolic engineering of *Escherichia coli* for L-tryptophan production. *World J Microbiol Biotechnol,* 38:22, 2022. DOI: 10.1007/s11274-021-03212-1
5. **Zhao C, Fang H, Wang J, Zhang S, Zhao X, Li Z, Lin C, Shen Z, Cheng L:** Application of fermentation process control to increase l-tryptophan production in *Escherichia coli*. *Biotechnol Prog,* 36:e2944, 2020. DOI: 10.1002/btpr.2944
6. **Sangareddy V, Mallu MR, Matur RV, Shaik FB, Nettem B, Puladas S:** Enhancing *Escherichia coli* cell density and recombinant protein production through the control of acetate accumulation. *3 Biotech,* 15:316, 2025. DOI: 10.1007/s13205-025-04490-4
7. **Zhao C, Cheng L, Wang J, Shen Z, Chen N:** Impact of deletion of the genes encoding acetate kinase on production of L-tryptophan by *Escherichia coli*. *Ann Microbiol,* 66, 261-269, 2016. DOI: 10.1007/s13213-015-1103-4
8. **Zhao C, Cheng L, Xu Q, Wang J, Shen Z, Chen N:** Improvement of the production of L-tryptophan in *Escherichia coli* by application of a dissolved oxygen stage control strategy. *Ann Microbiol,* 66, 843-854, 2016. DOI: 10.1007/s13213-015-1172-4
9. **Schütze A, Benndorf D, Püttker S, Kohrs F, Bettenbrock K:** The impact of *ackA, pta,* and *ackA-pta* mutations on growth, gene expression and protein acetylation in *Escherichia coli* K-12. *Front Microbiol,* 11:233, 2020. DOI: 10.3389/fmicb.2020.00233
10. **Nahku R, Valgepea K, Lahtvee PJ, Erm S, Abner K, Adamberg K, Vilu R:** Specific growth rate dependent transcriptome profiling of *Escherichia coli* K12 MG1655 in accelerostat cultures. *J Biotechnol,* 145 (1): 60-65, 2010. DOI: 10.1016/j.jbiotec.2009.10.007
11. **Ping J, Wang L, Qin Z, Zhou Z, Zhou J:** Synergetic engineering of *Escherichia coli* for efficient production of l-tyrosine. *Synth Syst Biotechnol,* 8, 724-731, 2023. DOI: 10.1016/j.synbio.2023.10.005
12. **Poolman B:** Physicochemical homeostasis in bacteria. *FEMS Microbiol Rev,* 47 (4):fuad033, 2023. DOI: 10.1093/femsre/fuad033
13. **Monterroso B, Margolin W, Boersma AJ, Rivas G, Poolman B, Zorrilla S:** Macromolecular crowding, phase separation, and homeostasis in the orchestration of bacterial cellular functions. *Chem Rev,* 124 (4): 1899-1949, 2024. DOI: 10.1021/acs.chemrev.3c00622
14. **Gupta PK, Edula JR:** Strategies for enhancing product yield: Design of experiments (DOE) for *Escherichia coli* cultivation. **In,** Laranjo M (Ed): Fermentation - Processes, Benefits and Risks. *InTech Open,* 3:15, 2021. DOI: 10.5772/intechopen.99288
15. **Krausch N, Doff-Sotta M, Cannon M, Neubauer P, Bournazou MN:** Deep learning adaptive model predictive control of fed-batch cultivations. *Comp Chem Eng,* 203:109344, 2025. DOI: 10.1016/j.compchemeng.2025.109344
16. **Standardization Administration of the P.R.C. Diagnostic Techniques for Infectious Bursal Disease:** GB/T 19167-2020. Beijing: Standards Press of China, 2020.
17. **Csitári B, Bedics A, Felföldi T, Boros E, Nagy H, Máthé I, Székely AJ:** Anion-type modulates the effect of salt stress on saline lake bacteria. *Extremophiles,* 26 (1):12, 2022. DOI: 10.1007/s00792-022-01260-5
18. **Kim S, Jeong CH, Kim JC, Lee M, Jeong SG, Kim HM, Park HW:** Optimizing divalent cation supplementation to enhance the production of the kimchi starter strain *Latilactobacillus curvatus* WiKim0094. *J Microbiol Biotechnol,* 35:e2505011, 2025. DOI: 10.4014/jmb.2505.05011
19. **Abadli M, Dewasme L, Tebbani S, Dumur D, Wouwer AV:** Experimental validation of a nonlinear model predictive controller regulating the acetate concentration in fed-batch *Escherichia coli* BL21(DE3) cultures. *Adv Cont Appl,* 4:e95, 2022. DOI: 10.1002/adc2.95
20. **Shen P, Niu D, Permau K, Tian, K, Singh S, Wang Z:** Exploitation of ammonia-inducible promoters for enzyme overexpression in *Bacillus licheniformis. J Ind Microbiol Biotechnol,* 48 (5-6):kuab037, 2021. DOI: 10.1093/jimb/kuab037
21. **Wu C, Qu J, Zhang H, Gao M, Zhu L, Zhan X:** New two-stage pH combined with dissolved oxygen control strategy for cyclic β-1,2 glucans synthesis. *Appl Microbiol Biotechnol,* 107, 2235-2247, 2023. DOI: 10.1007/s00253-023-12463-x
22. **Liu E, Wilkins M:** Process optimization and scale-up production of fungal aryl alcohol oxidase from genetically modified *Aspergillus nidulans* in stirred-tank bioreactor. *Biores Technol,* 315:123792, 2020. DOI: 10.1016/j.biortech.2020.123792
23. **Shandong Binzhou Animal Husbandry and Veterinary Research Institute, Shandong Lvdu Biotechnology Co., Ltd:** Method for rapidly screening optimal pH regulator and determining optimal growth pH of aerobic microorganisms. Chinese Patent CN107129934B, 2020.
24. **Candry P, Radić L, Favere J, Carvajal-Arroyo J, Rabaey K, Ganigué R:** Mildly acidic pH selects for chain elongation to caproic acid over alternative pathways during lactic acid fermentation. *Water Res,* 186:116396, 2020. DOI: 10.1016/j.watres.2020.116396
25. **Li S, Meng X, Zhang S, Zhang Y, Yang R, Wang D, Yang Y, Liu P, Kang J:** A unified intracellular pH landscape with SITE-pHorin: A quantum-entanglement-enhanced pH probe. *Sci China Life Sci,* 69, 239-257, 2026. DOI: 10.1007/s11427-025-2971-5
26. **Bühlmann C, Mickan B, Tait S, Batstone D, Mercer G, Bahri P:** Lactic acid from mixed food waste fermentation using an adapted inoculum: Influence of pH and temperature regulation on yield and product spectrum. *J Clean Prod,* 373:133716, 2022. DOI: 10.1016/j.jclepro.2022.133716
27. **Mital S, Christie G, Alcasabas A, Mellor R, Dikicioglu D:** pH-modulated soluble expression of alcohol dehydrogenases in *Escherichia coli* using adaptive laboratory evolution. *Trend Biotechnol,* 43 (11): 2904-2925, 2025. DOI: 10.1016/j.tibtech.2025.07.013
28. **Guo X, Huang Y, Tang Y, Xia A, Zhu X, Zhu X, Liao Q:** Two-step pH regulating ethanol production through continuous CO/CO_2 gas fermentation by mixed bacteria from rabbit faeces. *Renewable Energy,* 228 (C), 2024. DOI: 10.1016/j.renene.2024.120564
29. **Manavalan T, Bi J, Naulchan K, Bich Van NT, Chua XY, Yow R, Lee SY, Ming Chew LJ, Ottenheim C, Sugii S, Lakshmanan M, Zhou W, Arumugam P, Wong FT, Weingarten M, Ang EL:** Hyper-expression of functional human basic fibroblast growth factor 2 in *Escherichia coli*. *Protein Expr Purif,* 240:106894. DOI: 10.1016/j.pep.2026.106894
30. **Nasrin F, Azad DAK, Hasan MR, Kader DMM, Rahman BGMS, Hasan CMM:** Adaptive responses in the metabolism of *Escherichia coli*

in view of gene expressions under aerobic and micro-aerobic condition. *Am J Microbiol Res,* 7 (3): 91-97, 2019. DOI: 10.12691/ajmr-7-3-4

31. **Orr J, Christensen D, Wolfe A, Rao C:** Extracellular acidic pH inhibits acetate consumption by decreasing gene transcription of the tricarboxylic acid cycle and the glyoxylate shunt. *J Bacteriol,* 201 (2):e00410-18, 2018. DOI: 10.1128/JB.00410-18

Kafkas Universitesi Veteriner Fakultesi Dergisi
Journal Home-Page: http://vetdergikafkas.org
E-ISSN: 1309-2251

Kafkas Univ Vet Fak Derg
32 (4): 521-528, 2026
DOI: 10.9775/kvfd.2026.36599

RESEARCH ARTICLE

Sequential Intravesical Instillation of Epirubicin and IL-15/IL-15Rα Enhances Antitumor Efficacy in Orthotopic Bladder Cancer Through Immunogenic Cell Death and CD8+ T Cell-Dependent Immune Activation

Jiawei MA[1], Shichao WEI[1], Feifei PAN[1(*)]

[1] Department of Urology, Nanjing Tongren Hospital, School of Medicine, Southeast University, Nanjing 210000, Jiangsu Province, CHINA

(*) **Corresponding author:**
Feifei PAN
Phone: +86-18952553162
E-mail: panffnth@shu-edu.cn

How to cite this article?

Ma J, Wei S, Pan F: Sequential Intravesical Instillation of Epirubicin and IL-15/IL-15Rα Enhances Antitumor Efficacy in Orthotopic Bladder Cancer Through Immunogenic Cell Death and CD8+ T Cell-Dependent Immune Activation. *Kafkas Univ Vet Fak Derg*, 32 (4): 521-528, 2026.
DOI: 10.9775/kvfd.2026.36599

Article ID: KVFD-2026-36599
Received: 16.03.2026
Accepted: 18.07.2026
Published Online: 28.07.2026

Abstract

This study aimed to investigate whether sequential intravesical instillation of epirubicin (EPI) followed by interleukin-15 (IL-15)/interleukin-15 receptor alpha (IL-15Rα) could integrate cytotoxic and immune-stimulatory effects for improved antitumor efficacy. EPI-induced immunogenic cell death (ICD) was assessed in MB49 cells by measuring calreticulin (CRT) exposure and adenosine triphosphate (ATP) release. Cytotoxic activity of splenocytes against MB49 cells was evaluated by co-culture apoptosis assays and IFN-γ quantification. In vivo efficacy was examined in C57BL/6 mice bearing orthotopic bladder tumors. Tumor volume survival, and immune infiltration were analyzed, and CD8+ T cell depletion was performed to assess the contribution of these cells to therapeutic efficacy. EPI treatment increased surface CRT and ATP release. In co-culture assays, EPI pretreatment enhanced splenocyte-mediated MB49 cell apoptosis and IFN-γ secretion, and these effects were further augmented by IL-15/IL-15Rα. *In vivo*, sequential therapy significantly reduced tumor volume, prolonged survival, and promoted a favorable immune microenvironment, characterized by increased $CD8^+$ T and $NK1.1^+$ cell infiltration, reduced Treg population, an elevated CD8/Treg ratio, and increased IFN-γ level. Importantly, $CD8^+$ T cell depletion attenuated these therapeutic benefits. Sequential intravesical administration of EPI and IL-15/IL-15Rα enhanced antitumor efficacy in an orthotopic bladder cancer model by promoting ICD-associated changes and cytotoxic immune responses. These findings provide preclinical evidence supporting further investigation of EPI-based chemo-immunotherapy for bladder cancer, including BCG-unresponsive or high-risk non-muscle-invasive bladder cancer (NMIBC).

Keywords: Chemo-immunotherapy, EPI, IL-15/IL-15Rα, NMIBC

INTRODUCTION

Bladder cancer (BC) is a common malignancy, with non-muscle invasive bladder cancer (NMIBC) accounting for approximately 75% of all cases [1,2]. Transurethral Resection of Bladder Tumor (TURBT) remains the gold-standard treatment strategy for NMIBC, whereas adjuvant intravesical therapy is selected according to the risk of recurrence and progression [3]. Bacillus Calmette-Guérin (BCG) therapy is widely used for high-risk NMIBC, while radical cystectomy may be considered for selected patients with very high-risk or treatment-refractory disease [4,5]. BCG binds to and is internalized by urothelial tumor cells, thereby triggering a broad immune response involving natural killer (NK) cells and $CD8^+$ T cells that contributes to tumor elimination [6]. Nevertheless, a substantial proportion of patients fails to respond to BCG therapy or experience disease recurrence, and BCG administration may also cause clinically significant adverse effects [7]. Therefore, novel strategies with improved efficacy and acceptable toxicity are urgently needed for NMIBC.

Interleukin-15 (IL-15), recognized as a promising target for cancer immunotherapy, has demonstrated antitumor potential in several malignancies, including ovarian, gastric, and bladder cancers [8-11]. As a common γ-chain cytokine, IL-15 plays an important role in the development, proliferation, and survival of NK cells and $CD8^+$ T cells [12]. Complex formation between IL-15 and IL-15Rα enhances IL-15-mediated stimulation of NK and T cells and has led to the development of IL-15 superagonists and IL-15/IL-15Rα complexes with improved biological

activity [13-15]. ALT-803 (N-803), an IL-15 superagonist, has demonstrated promising clinical activity NMIBC, and its combination with BCG has been developed for BCG-unresponsive carcinoma in situ [16,17]. These findings highlight the therapeutic potential of IL-15/IL-15Rα-based approaches in NMIBC.

Epirubicin (EPI) is a widely used anthracycline chemotherapeutic agent that exerts antitumor activity through DNA intercalation, topoisomerase II inhibition, and induction of apoptosis [18]. Intravesical EPI administered after TURBT effectively can reduce recurrence in NMIBC while limiting systemic exposure, making it suitable for local administration [19]. Beyond its direct cytotoxicity, EPI has also been reported to induce ICD, thereby potentially enhancing anti-tumor immune responses [20]. These properties provide a rationale for sequentially combining EPI with IL-15/IL-15Rα to integrate chemotherapy-induced tumor cell injury with immune stimulation.

In this study, we explored the antitumor effects and potential immune mechanisms of sequential intravesical administration of EPI followed by IL-15/IL-15Rα in an orthotopic bladder cancer model, with the aim of providing preclinical evidence for a novel chemo-immunotherapy strategy.

Material and Methods

Ethical Approval

All animal experimental procedures were conducted in accordance with the Guide for the Care and Use of Laboratory Animals issued by the Ministry of Science and Technology of China, and were approved by the Animal Ethics Committee of Nanjing Tongren Hospital, Southeast University (Approval No.: SHU2023/021).

Cell Culture and Treatment

The C57BL/6-derived murine BC cell line MB49 (cat. no. iCell-m030; iCell Bioscience Inc) were cultured in DMEM (cat. no. iCell-0001) supplemented with 10% FBS and 1% penicillin-streptomycin. Cells were maintained at 37°C in a humidified atmosphere containing 5% CO_2. For EPI treatment, cells were exposed to 0.2 or 1.2 μg/mL EPI for 24 h [21].

Assessment of ICD

To assess ICD-associated changes, MB49 cells were seeded in 6-well plates and stained with an Alexa Fluor 488-conjugated anti-CRT antibody. Surface CRT expression was subsequently quantified by flow cytometry. To evaluate extracellular ATP release, culture supernatants were collected and analyzed using the ENLITEN ATP Assay System Bioluminescence Detection Kits according to the manufacturer's instructions.

Animal and Model Establishment

The female C57BL/6 mice (aged 6-8 weeks) were obtained from Beijing Vital River Laboratory Animal Technology Co., Ltd. All mice were acclimatized for 1 week with free access to water and food. The orthotopic bladder cancer model was established as previously described [22]. In brief, mice were anesthetized with isoflurane and placed on a warming pad. Residual urine was expelled by gently pressing the bladder. A 24G x 0.75-inch catheter was then inserted transurethrally, and the bladder was conditioned with 50 μL of poly-L-lysine (Sigma, 1 μg/mL in PBS) for 10 min. The solution was subsequently removed by gently pressing the bladder, which was then rinsed with 50 μL PBS, and instilled with $1x10^5$ MB49 cells. After incubation, the catheter was withdrawn, and the mice were transferred to recovery cages for post-procedure monitoring.

Experimental Groups and Treatment Protocol

All mice were randomly assigned into four groups (n=8): PBS, EPI, EPI+IL-15/IL-15Rα and EPI+IL-15/IL-15Rα+anti-CD8 antibody. Four days after tumor cell instillation, mice in EPI group received an intravesical instillation of EPI at 5 mg/kg, which was retained in the bladder for approximately 1 h [23]. Mice in EPI+IL-15/IL-15Rα group additionally received an intravesical instillation of 2.5 μg IL-15/IL-15Rα complexes 24 h following EPI administration [24]. To deplete $CD8^+$ T cells, a CD8-specific monoclonal antibody (mAb) was used. Mice in EPI+IL-15/IL-15Rα + anti-CD8 antibody group received an initial intraperitoneal injection of 10 μg anti-CD8 antibody 1 day before intravesical treatment with EPI and IL-15/IL-15Rα [25]. Thereafter, the same dose of anti-CD8 antibody was administered intraperitoneally every four days until sacrifice [26]. Intravesical administration of EPI and/or IL-15/IL-15Rα complexes was performed twice weekly for three consecutive weeks. Mice in the PBS group received 50 μL PBS intravesically as a control. At the experimental endpoint, tumor-bearing bladders were excised and examined macroscopically. Tumor areas were identified as nodular lesions or focal irregular thickening clearly distinguishable from the adjacent normal-appearing bladder wall, with boundaries defined by the visible lesion-normal tissue interface. Identified tumor tissues were collected for subsequent analyses.

Splenocyte Isolation

Spleens were collected from tumor-free C57BL/6 mice. Splenic tissues were gently dissociated between two frosted microscope slides, and the resulting homogenates were washed with RPMI-1640. After centrifugation at 200 g for 10 min, the splenic homogenates cell pellets were resuspended in 360 μL distilled water for 10 s to induce hemolysis, followed immediately by neutralization with 40 μL of 10× PBS. Pooled splenocytes were cultured in

5 mL RPMI-1640 medium supplemented with 0.05 mM β-mercaptoethanol, 10% FBS, and 1% antibiotics [27]. After 2 h of incubation, the cell-containing supernatant was collected for subsequent co-culture assays.

Co-culture Assay of MB49 Cells and Splenocytes

Splenocytes were co-cultured with MB49 cells at an effector-to-target (E:T) ratio of 10:1 in complete RPMI-1640 medium for 24 h. Three experimental groups were established: (i) untreated MB49 cells co-cultured with splenocytes, (ii) EPI (1.2 μg/mL)-pretreated MB49 cells co-cultured with splenocytes, and (iii) EPI-pretreated MB49 cells co-cultured with splenocytes in the presence of IL-15/IL-15Rα complexes (7 ng/mL) [24].

Cell Apoptosis

Following indicated treatment, MB49 cells were washed with PBS and resuspended in 100 μL binding buffer. The cells were then incubated with 2 μL Annexin-V-FITC on ice in the dark, following by PI staining [28]. Cell apoptosis was analyzed using a CytoFLEX flow cytometer according to the manufacturer's protocol.

Flow Cytometry

Mice were sacrificed and bladder and tumor tissues were harvested. Tumor samples were digested with collagenase (300 U/mL) and hyaluronidase (100 U/mL) [29]. During digestion, the samples were gently pipetted every 15 min and incubated at 37°C for 3 h to generate single-cell suspensions. The suspensions were then filtered through a 200-μm cell strainer and washed with PBS. Cells were subsequently resuspended in FACS buffer and stained with antibodies against CD45, CD3, CD8, NK1.1 and Foxp3. Samples were analyzed using a BD FACSCanto II flow cytometry, and the data were processed using FlowJo software.

ELISA

Splenocytes were co-cultured with MB49 cells for 24 h, after which the culture supernatants were collected. IFN-γ concentrations in the supernatants were measured using commercially available ELISA kits according to the manufacturer's instructions. For *in vivo* sample collection, 0.5 mL of PBS was instilled into the bladder and subsequently aspirated. The recovered fluid was centrifuged at 2.000 x g to remove cells, and the supernatant was stored at -80°C until analysis. IFN-γ concentrations were measured using the same ELISA procedure and expressed as ng/mL.

Statistical Analysis

Data from three independent experiments were analyzed using GraphPad Prism 8.0 software. Normally distributed continuous variables are presented as mean ± SD. Comparisons among multiple groups were performed using one-way analysis of variance followed by Tukey's post-hoc test. For non-normally distributed data, the Kruskal-Wallis test was used. Survival analyses were conducted using the Kaplan-Meier method, and differences were evaluated with the log-rank test. P-values <0.05 was considered statistical significance.

Results

Compared with the Control group, EPI treatment elevated surface CRT level and ATP release in a concentration-dependent manner, suggesting that EPI induced ICD-associated changes in MB49 cells *in vitro* (*Fig. 1-A, B*).

Following the co-culture of MB49 cells with splenocyte, cell apoptosis was assessed by flow cytometry. Compared with the Control group, EPI pre-treatment significantly increased MB49 cell apoptosis, and this effect was further enhanced by the addition of IL-15/IL-15Rα complexes (*Fig. 2-A, B*). ELISA showed that EPI pretreatment significantly increased IFN-γ secretion during co-culture. Following the addition of IL-15/IL-15Rα complexes, IFN-γ levels were further increased (*Fig. 2-C*). These findings indicated that EPI pretreatment enhanced splenocyte-mediated cytotoxicity against MB49 cells and that IL-15/IL-15Rα further strengthened this immune response.

Given that EPI induced ICD-associated changes and IL-15/IL-15Rα enhanced effector immune cell activity, we next

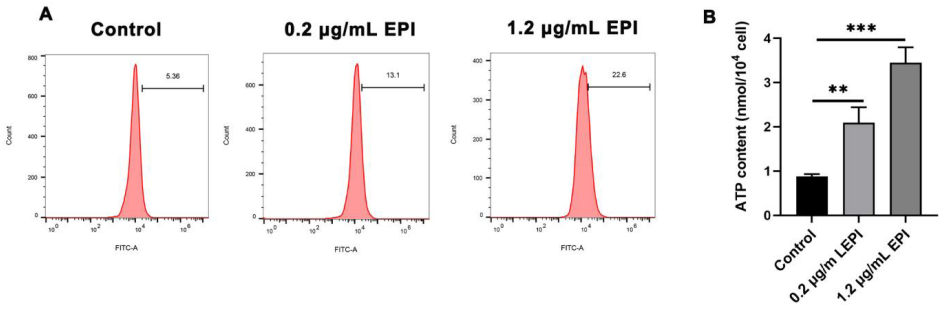

Fig 1. EPI contributed to ICD. **(A)** CRT level was detected using flow cytometry. **(B)** The ATP level was detected using ENLITEN ATP Assay System Bioluminescence Detection Kits. **P<0.01 and ***P<0.001

evaluated whether sequential administration of these agents could improve antitumor efficacy *in vivo*. EPI monotherapy significantly reduced tumor volume compared with PBS treatment, whereas sequential administration of EPI followed by IL-15/IL-15Rα resulted in a further reduction in tumor volume *(Fig. 3-A, B)*. Consistent with these findings, survival analysis demonstrated the longest survival in the EPI+IL-15/IL-15Rα group, followed by the EPI monotherapy group, with the PBS group displaying the shortest survival *(Fig. 3-C)*. Importantly, body weights remained generally stable across all groups, and no severe adverse events were observed, suggesting that the treatment regimen was well tolerated under the experimental conditions.

Because EPI-induced ICD may influence the tumor immune microenvironment, we next examined whether sequential combination therapy altered immune cell infiltration *in vivo*. Flow cytometric analysis showed that sequential EPI and IL-15/IL-15Rα therapy significantly increased the infiltration of $CD8^+$ T cells and $NK1.1^+$ cells compared with both the PBS and EPI groups. In contrast, the proportion of regulatory T cells (Tregs) was significantly lower in the EPI+IL-15/IL-15Rα group *(Fig. 4-A)*. The CD8/Treg ratio was increased in the EPI group compared with the PBS group, and was highest in the EPI+IL-15/IL-15Rα group *(Fig. 4-B)*. Consistently, IFN-γ levels were increased after EPI treatment and further elevated after sequential treatment with IL-15/IL-15Rα *(Fig. 4-C)*. Together, these findings indicated that sequential treatment enhanced cytotoxic immune responses while reducing immunosuppressive features of the tumor microenvironment.

Because sequential EPI and IL-15/IL-15Rα therapy was associated with increased $CD8^+$ T cell infiltration, we

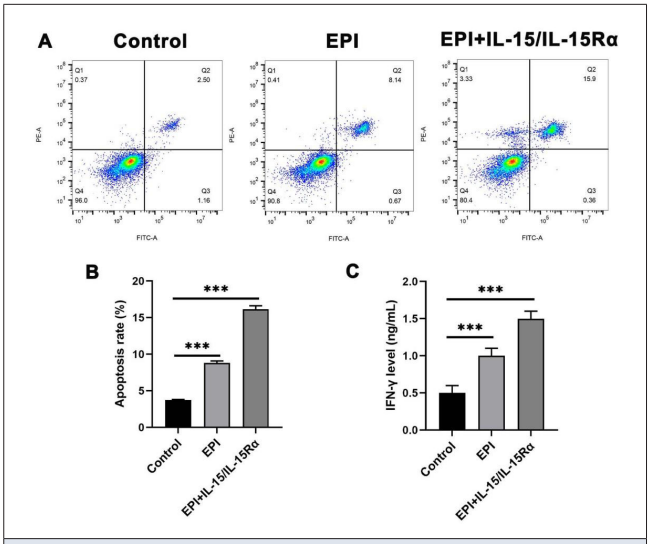

Fig 2. IL-15/IL-15Rα augmented splenocyte-mediated cytotoxicity against MB49 cells. **(A-B)** The cell apoptosis was detected using flow cytometry. (C) The level of IFN-γ was detected using ELISA-related IFN-γ assay kits. ***P<0.001

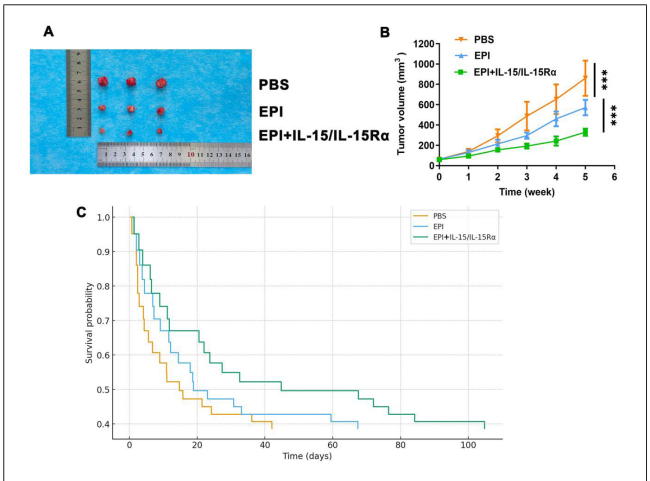

Fig 3. Sequential EPI and IL-15/IL-15Rα therapy exhibited superior antitumor efficacy. **(A)** The tumor appearance. **(B)** The tumor size. **(C)** The survival analysis. ***P<0.001

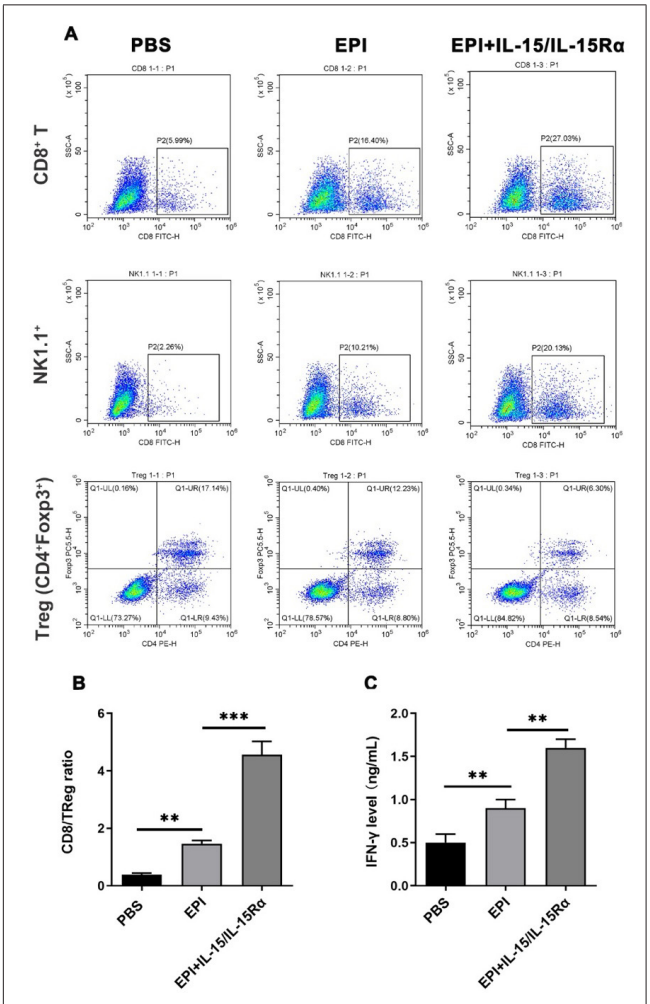

Fig 4. Sequential EPI and IL-15/IL-15Rα treatment augments antitumor immunity. **(A)** Flow cytometry was used for the detection of tumor-infiltrating immune cells. **(B)** The CD8/Treg ratio. **(C)** The level of IFN-γ was detected using ELISA-related IFN-γ assay kits. **P<0.01 and ***P<0.001

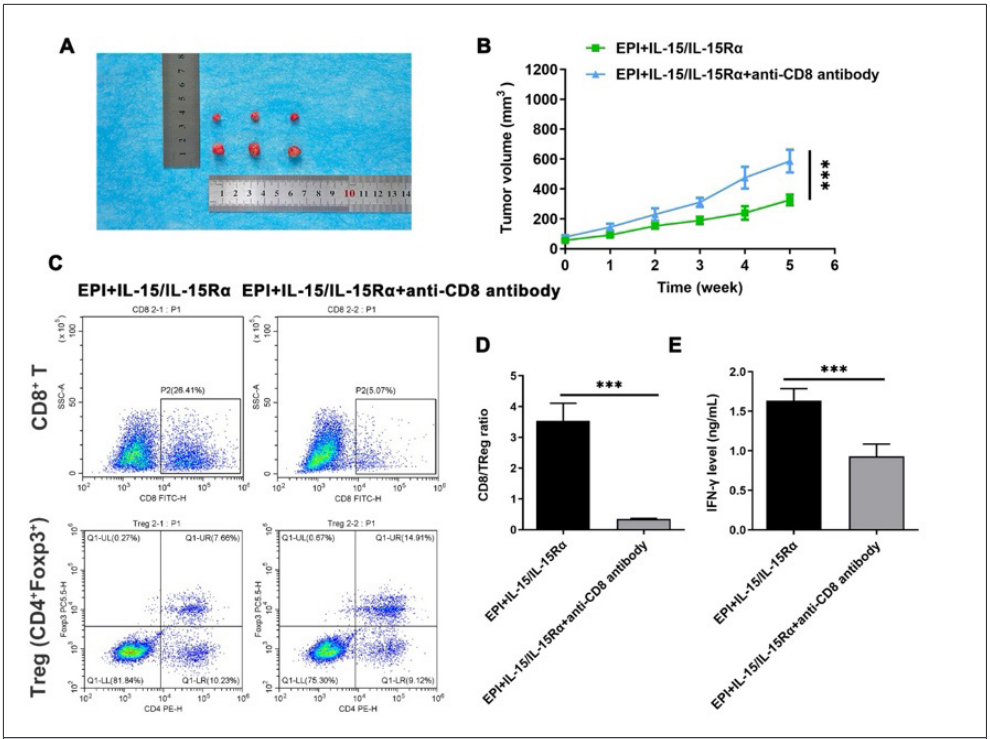

Fig 5. $CD8^+$ T cells are essential for the antitumor efficacy of sequential therapy. **(A)** The tumor appearance. **(B)** The tumor size. **(C)** Flow cytometry was used for the detection of tumor-infiltrating immune cells. **(D)** The CD8/Treg ratio. (E) IFN-γlevels measured by ELISA. ***P<0.001

next investigated whether $CD8^+$ T cells contributed to the antitumor effect. Compared with the EPI+IL-15/IL-15Rα group, tumor volume was increased following administration of anti-CD8 antibody *(Fig. 5-A, B)*. Consistent immunological changes were also observed: $CD8^+$ T cell infiltration and IFN-γ levels were reduced, and the CD8/Treg ratio was lower in the EPI+IL-15/IL-15Rα+anti-CD8 antibody group than in the EPI+IL-15/IL-15Rα group *(Fig. 5-C, D, E)*. These findings suggested that $CD8^+$ T cells make an important contribution to the therapeutic activity of sequential treatment.

Discussion

BC, particularly NMIBC, remains a therapeutic challenge due to high recurrence rates and the substantial proportion of patients who experience recurrence or inadequate responses following BCG therapy [30]. Although intravesical chemotherapy and immunotherapy are widely used, their benefits are often constrained by suboptimal responses or adverse effects [31]. These limitations highlight the need for novel strategies that combine direct cytotoxic effects with immune modulation. In this context, we explored sequential administration of EPI and IL-15/IL-15Rα as a potential approach to integrate chemotherapy-induced tumor cell death with immune activation. Our results showed that EPI induced ICD-associated changes, while IL-15/IL-15Rα further enhanced splenocyte-mediated cytotoxicity and IFN-γ production. *In vivo*, the sequential regimen reduced tumor burden, prolonged survival, and promoted a favorable immune microenvironment. Importantly, $CD8^+$ T cell depletion diminished these effects, indicating their central contribution to the therapeutic activity. Together, these findings support a model in which EPI-induced tumor immunogenicity provides an initial immune stimulus that is subsequently amplified by IL-15/IL-15Rα-mediated activation of antitumor effector cells.

Previous studies have shown that certain chemotherapeutic agents, including anthracyclines, can promote ICD in addition to exerting direct cytotoxic effects, thereby enhancing tumor antigen exposure and immune recognition [32]. Our data are consistent with these findings, as EPI treatment upregulated CRT exposure and ATP release in MB49 cells, both of which are widely recognized features associated with ICD [33]. Surface-exposed CRT can function as a pro-phagocytic signal, whereas extracellular ATP contributes to the recruitment and activation of immune cells, providing a potential link between chemotherapy-induced tumor injury and subsequent immune activation [34,35]. However, induction of ICD-associated signals alone does not necessarily guarantee a durable antitumor immune response.

IL-15 is essential for the proliferation, maintenance, and survival of $CD8^+$ T cells and NK cells [36]. Upon association with IL-15Rα, IL-15 has enhanced stability and biological activity, thereby promoting more sustained stimulation

of cytotoxic lymphocytes [37]. Previous preclinical studies have demonstrated the antitumor activity of IL-15/IL-15Rα-based complexes, although treatment efficacy may vary with the tumor model and delivery strategy [24]. In our study, the addition of IL-15/IL-15Rα complexes after EPI treatment further increased splenocyte-mediated cytotoxicity and IFN-γ secretion. IFN-γ is traditionally regarded as a key mediator of cellular immune responses [38], and its increased production may therefore reflect enhanced activation of antitumor effector cells. These findings suggest that EPI-induced tumor immunogenicity and IL-15/IL-15Rα-mediated effector-cell stimulation may act in a complementary manner, providing a possible explanation for the stronger antitumor effect of the sequential regimen.

The tumor immune microenvironment plays a decisive role in tumor progression and therapeutic response, where immunosuppressive components such as Tregs can facilitate immune evasion, while increased infiltration of effector cells like $CD8^+$ T cells and NK cells is generally linked to favorable prognosis [39,40]. In our study, sequential treatment with EPI and IL-15/IL-15Rα increased the infiltration of $CD8^+$ T cells and NK cells, decreased the Treg population, and increased the CD8/Treg ratio. These changes were accompanied by increased IFN-γ levels, indicating enhanced cytotoxic immune activity. Previous studies have also reported that intravesical chemotherapy can promote $CD8^+$ T cell activity and alter immunosuppressive cell populations in BC [41,42]. However, in our study, EPI alone produced less pronounced immune changes than the sequential regimen. This difference may be related to the chemotherapeutic agent, treatment schedule, tumor model, or timing of immune evaluation. It may also suggest that chemotherapy-induced immune priming can be further reinforced by IL-15/IL-15Rα-mediated activation of cytotoxic lymphocytes. Therefore, the therapeutic benefit of sequential treatment may involve both direct tumor cell injury and favorable modulation of the tumor immune microenvironment.

The functional importance of $CD8^+$ T cells was further supported by the depletion experiments. Administration of anti-CD8 antibody attenuated the tumor-suppressive effect of sequential treatment, accompanied by lower IFN-γ production and a decreased CD8/Treg ratio. These results highlighted $CD8^+$ T cells as indispensable effectors of the sequential therapy. This observation is consistent with prior reports showing that $CD8^+$ T cells are key mediators of response to immune checkpoint inhibitors and cytokine-based therapies [43,44]. Although IL-15 can also activate NK cells, our depletion experiments suggest a particularly important contribution of $CD8^+$ T cells in the present model. Differences in the relative contribution of $CD8^+$ T cells and NK cells across previous studies may reflect differences in tumor type, treatment regimen, and route of cytokine administration. Further studies using selective depletion of additional immune cell populations are needed to define their individual contributions.

The present findings also differ conceptually from previous IL-15-based strategies in NMIBC, which have mainly investigated IL-15 superagonists in combination with BCG [11,45]. In contrast, our strategy used EPI to induce tumor cell injury and immunogenic signals before administration of IL-15/IL-15Rα. This sequential approach may allow cytokine-mediated immune stimulation to build upon chemotherapy-induced tumor immunogenicity. Nevertheless, because simultaneous and sequential administration were not directly compared, further studies are required to determine whether the treatment sequence itself contributes to the improved efficacy.

Despite these promising results, several limitations should be acknowledged. First, our study was limited to a murine orthotopic BC model, and validation in additional models would strengthen the generalizability of our findings. Second, we did not evaluate potential long-term immune memory responses, which could provide important insights into recurrence prevention. Third, although $CD8^+$ T cell depletion supported the involvement of $CD8^+$ T cells, the specific contribution of NK cells and other immune populations was not directly examined. Fourth, CRT exposure and ATP release supported ICD-associated changes, but further studies assessing antigen presentation and tumor-specific T cell responses would provide stronger mechanistic evidence. Finally, while sequential EPI and IL-15/IL-15Rα therapy was well tolerated in mice, further investigation is warranted to assess potential toxicities and optimize dosing regimens for translational applications.

In conclusion, our study provides preclinical evidence that sequential intravesical administration of EPI and IL-15/IL-15Rα complexes enhances antitumor efficacy by inducing ICD-associated changes, strengthening cytotoxic immune responses, and alleviating immunosuppression in the tumor microenvironment. The reduced therapeutic efficacy following $CD8^+$ T cell depletion further supports an important contribution of $CD8^+$ T cell-mediated immunity. These findings provide a basis for further investigation of chemo-immunotherapy strategies combining anthracycline-based chemotherapy with IL-15-based immune stimulation in BC.

Declarations

Availability of Data and Materials: The datasets used and/or analyzed during the current study are available from the corresponding author (FP) on reasonable request.

Acknowledgements: None.

Funding Support: None.

Ethical Approval: All animal experimental procedures were conducted in accordance with the Guide for the Care and Use of Laboratory Animals issued by the Ministry of Science and Technology of China, and were approved by the Animal Ethics Committee of Nanjing Tongren Hospital, Southeast University (Approval No.: SHU2023/021).

Competing Interests: The authors declared that there is no conflict of interest.

Declaration of Generative Artificial Intelligence (AI): The article and/or tables and figures were not written/created by AI and AI-assisted technologies.

Authors' Contributions: JM and FP designed this study and drafted the manuscript; JM and SW performed this study and analyzed the data; JM designed this study and significantly revised the manuscript. All authors have approved the submission and publication of this manuscript.

References

1. **Babjuk M, Burger M, Capoun O, Cohen D, Compérat EM, Dominguez Escrig JL, Gontero P, Liedberg F, Masson-Lecomte A, Mostafid AH, Palou J, van Rhijn BWG, Rouprêt M, Shariat SF, Seisen T, Soukup V, Sylvester RJ:** European Association of Urology Guidelines on non-muscle-invasive bladder cancer (Ta, T1, and carcinoma *in situ). Eur Urol,* 81 (1): 75-94, 2022. DOI: 10.1016/j.eururo.2021.08.010
2. **Siegel RL, Miller KD, Wagle NS, Jemal A:** Cancer statistics, 2023. *CA Cancer J Clin,* 73 (1): 17-48, 2023. DOI: 10.3322/caac.21763
3. **Osman Y, Elawdy M, Taha DE, Zahran MH, Abouelkheir RT, Sharaf DE, Mosbah A, Ali-El Dein B:** Bladder perforation as a complication of transurethral resection of bladder tumors: the predictors, management, and its impact in a series of 1570 at a tertiary urology institute. *Int Urol Nephrol,* 55 (9): 2161-2167, 2023. DOI: 10.1007/s11255-023-03638-6
4. **Matulewicz RS, Steinberg GD:** Non-muscle-invasive bladder cancer: Overview and contemporary treatment landscape of neoadjuvant chemoablative therapies. *Rev Urol,* 22 (2): 43-51, 2020.
5. **Lamm DL, Thor DE, Stogdill VD, Radwin HM:** Bladder cancer immunotherapy. *J Urol,* 128 (5): 931-935, 1982. DOI: 10.1016/s0022-5347(17)53283-8
6. **Redelman-Sidi G, Glickman MS, Bochner BH:** The mechanism of action of BCG therapy for bladder cancer - A current perspective. *Nat Rev Urol,* 11 (3): 153-162, 2014. DOI: 10.1038/nrurol.2014.15
7. **Lidagoster S, Ben-David R, De Leon B, Sfakianos JP:** BCG and alternative therapies to BCG therapy for non-muscle-invasive bladder cancer. *Curr Oncol,* 31 (2): 1063-1078, 2024. DOI: 10.3390/curroncol31020079
8. **Robinson TO, Schluns KS:** The potential and promise of IL-15 in immuno-oncogenic therapies. *Immunol Lett,* 190, 159-168, 2017. DOI: 10.1016/j.imlet.2017.08.010
9. **Vidal-Manrique M, Nieuwenstein T, Hooijmaijers L, de Jonge PKJD, Djojoatmo M, Jansen J, van der Waart AB, Brock R, Dolstra H:** IL-15 transpresentation by ovarian cancer cells improves CD34(+) progenitor-derived NK cell's anti-tumor functionality. *Oncoimmunology,* 14 (1):2465010, 2025. DOI: 10.1080/2162402X.2025.2465010
10. **Hu Y, Liu D, Cui P, Zhang W, Chen H, Piao C, Lu Y, Liu X, Wang Y, Liu J, Lu X:** IL-15-induced lymphocytes as adjuvant cellular immunotherapy for gastric cancer. *Invest New Drugs,* 39 (6): 1538-1548, 2021. DOI: 10.1007/s10637-021-01160-z
11. **Chamie K, Chang SS, Kramolowsky E, Gonzalgo ML, Agarwal PK, Bassett JC, Bjurlin M, Cher ML, Clark W, Cowan BE, David R, Goldfischer E, Guru K, Jalkut MW, Kaffenberger SD, Kaminetsky J, Katz AE, Koo AS, Sexton WJ, Tikhonenkov SN, Trabulsi EJ, Trainer AF, Spilman P, Huang M, Bhar P, Taha SA, Sender L, Reddy S, Soon-Shiong P:** IL-15 superagonist NAI in BCG-unresponsive non-muscle-invasive bladder cancer. *NEJM Evid,* 2 (1):EVIDoa2200167, 2023. DOI: 10.1056/EVIDoa2200167
12. **Choi YH, Lim EJ, Kim SW, Moon YW, Park KS, An HJ:** IL-27 enhances IL-15/IL-18-mediated activation of human natural killer cells. *J Immunother Cancer,* 7 (1):211, 2019. DOI: 10.1186/s40425-019-0688-8
13. **Tamzalit F, Barbieux I, Plet A, Heim J, Nedellec S, Morisseau S, Jacques Y, Mortier E:** IL-15.IL-15Rα complex shedding following trans-presentation is essential for the survival of IL-15 responding NK and T cells. *Proc Natl Acad Sci U S A,* 111 (23): 8565-8570, 2014. DOI: 10.1073/pnas.1405514111
14. **Burkett PR, Koka R, Chien M, Chai S, Boone DL, Ma A:** Coordinate expression and transpresentation of interleukin-15Rα and IL-15 supports natural killer cell and memory CD8+ T cell homeostasis. *J Exp Med,* 200 (7): 825-834, 2004. DOI: 10.1084/jem.20041389
15. **Margolin K, Morishima C, Velcheti V, Miller JS, Lee SM, Silk AW, Holtan SG, Lacroix AM, Fling SP, Kaiser JC, Egan JO, Jones M, Rhode PR, Rock AD, Cheever MA, Wong HC, Ernstoff MS:** Phase I trial of ALT-803, a novel recombinant IL-15 complex, in patients with advanced solid tumors. *Clin Cancer Res,* 24 (22): 5552-5561, 2018. DOI: 10.1158/1078-0432.CCR-18-0945
16. **Chen W, Liu N, Yuan Y, Zhu M, Hu X, Hu W, Wang S, Wang C, Huang B, Xing D:** ALT-803 in the treatment of non-muscle-invasive bladder cancer: Preclinical and clinical evidence and translational potential. *Front Immunol,* 13:1040669, 2022. DOI: 10.3389/fimmu.2022.1040669
17. **Chamie K, Chang SS, Rosser CJ, Kramolowski E, Gonzalgo ML, Sexton WJ, Spilman P, Sender L, Reddy S, Soon-Shiong P:** N-803 plus BCG treatment for BCG-naïve or -unresponsive non-muscle invasive bladder cancer: A plain language review. *Future Oncol,* 20 (31): 2307-2317, 2024. DOI: 10.1080/14796694.2024.2363744
18. **Xu K, Zhang Y, Cheng H, Chen W, Chen C, Zhang M, Song H, Wang F:** Triple-negative breast cancer treatment with core-shell Magnetic@Platinium-metal organic framework/epirubicin nano-platforms for chemo-photodynamic combinational therapy: A review. *Medicine (Baltimore),* 103 (39):e39845, 2024. DOI: 10.1097/MD.0000000000039845
19. **Onrust SV, Wiseman LR, Goa KL:** Epirubicin: A review of its intravesical use in superficial bladder cancer. *Drugs Aging,* 15 (4): 307-333, 1999. DOI: 10.2165/00002512-199915040-00006
20. **Li Z, Zhang Q, Li Z, Ren L, Pan D, Gong Q, Gu Z, Cai H, Luo K:** Branched glycopolymer prodrug-derived nanoassembly combined with a STING agonist activates an immuno-supportive status to boost anti-PD-L1 antibody therapy. *Acta Pharm Sin B,* 14 (5): 2194-2209, 2024. DOI: 10.1016/j.apsb.2024.02.006
21. **Chen JF, Yu BX, Yu R, Ma L, Lv XY, Cheng Y, Ma Q:** Monoclonal antibody Zt/g4 targeting RON receptor tyrosine kinase enhances chemosensitivity of bladder cancer cells to epirubicin by promoting G1/S arrest and apoptosis. *Oncol Rep,* 37 (2): 721-728, 2017. DOI: 10.3892/or.2017.5356
22. **Bazargan S, Bunch B, Ojwang' AME, Blauvelt J, Landin A, Ali J, Abrahams D, Cox C, Hall AM, Beatty MS, Poch M, Rejniak KA, Pilon-Thomas S:** Targeting myeloid-derived suppressor cells with gemcitabine to enhance efficacy of adoptive cell therapy in bladder cancer. *Front Immunol,* 14:1275375, 2023. DOI: 10.3389/fimmu.2023.1275375
23. **Hong X, Chen X, Wang H, Xu Q, Xiao K, Zhang Y, Chi Z, Liu Y, Liu G, Li H, Fang J, Lin T, Zhang Y:** A HER2-targeted antibody-drug conjugate, RC48-ADC, exerted promising antitumor efficacy and safety with intravesical instillation in preclinical models of bladder cancer. *Adv Sci (Weinh),* 10 (32):e2302377, 2023. DOI: 10.1002/advs.202302377
24. **Guo S, Smeltz RB, Nanajian A, Heller R:** IL-15/IL-15Rα heterodimeric complex as cancer immunotherapy in murine breast cancer models. *Front Immunol,* 11:614667, 2020. DOI: 10.3389/fimmu.2020.614667
25. **Cross EW, Blain TJ, Mathew D, Kedl RM:** Anti-CD8 monoclonal antibody-mediated depletion alters the phenotype and behavior of surviving CD8+ T cells. *PLoS One,* 14 (2):e0211446, 2019. DOI: 10.1371/journal.pone.0211446

26. **Li J, Huang K, Yang B, Hu X, Mei B, Cheng X, Zhong X, Cao C, Chen Z, Wang H, Zhang J:** TRA upregulates OTUD6B to recruit CD8+ T cells to suppress colorectal liver metastasis by stabilizing DDX5/STAT3/CXCL11 axis. *Cell Death Dis,* 16 (1):521, 2025. DOI: 10.1038/s41419-025-07837-0

27. **Santana JPP, Marcato PD, Massaro TNC, Godoy NL, Anibal FF, Borra RC:** Efficacy of instillation of MB49 cells and thermoreversible polymeric gel in urothelial bladder carcinoma immunization. *Lab Anim Res,* 38 (1):11, 2022. DOI: 10.1186/s42826-022-00122-7

28. **Zhang LC, Wu XY, Yang RB, Chen F, Liu JH, Hu YY, Wu ZD, Wang LF, Sun X:** Recombinant protein *Schistosoma japonicum*-derived molecule attenuates dextran sulfate sodium-induced colitis by inhibiting miRNA-217-5p to alleviate apoptosis. *World J Gastroenterol,* 27(46): 7982-7994, 2021. DOI: 10.3748/wjg.v27.i46.7982

29. **Parikh A, Shin J, Faquin W, Lin DT, Tirosh I, Sunwoo JB, Puram SV:** Malignant cell-specific CXCL14 promotes tumor lymphocyte infiltration in oral cavity squamous cell carcinoma. *J Immunother Cancer,* 8 (2):e001048, 2020. DOI: 10.1136/jitc-2020-001048

30. **Campistol M, Lozano F, Carrion A, Raventós CX, Morote J, Trilla E:** Active surveillance in non-muscle invasive bladder cancer: A systematic review. *Cancers (Basel),* 17 (10):1714, 2025. DOI: 10.3390/cancers17101714

31. **Zhao X, Qi X, Liu D, Che X, Wu G:** A novel approach for bladder cancer treatment: Nanoparticles as a drug delivery system. *Int J Nanomedicine,* 19, 13461-13483, 2024. DOI: 10.2147/IJN.S498729

32. **Showalter A, Limaye A, Oyer JL, Igarashi R, Kittipatarin C, Copik AJ, Khaled AR:** Cytokines in immunogenic cell death: Applications for cancer immunotherapy. *Cytokine,* 97, 123-132, 2017. DOI: 10.1016/j.cyto.2017.05.024

33. **Li X, Zheng J, Chen S, Meng FD, Ning J, Sun SL:** Oleandrin induces immunogenic cell death via the PERK/eIF2α/ATF4/CHOP pathway in breast cancer. *Cell Death Dis,* 12 (4):314, 2021. DOI: 10.1038/s41419-021-03605-y

34. **Obeid M, Tesniere A, Ghiringhelli F, Fimia GM, Apetoh L, Perfettini JL, Castedo M, Mignot G, Panaretakis T, Casares N, Métivier D, Larochette N, van Endert P, Ciccosanti F, Piacentini M, Zitvogel L, Kroemer G:** Calreticulin exposure dictates the immunogenicity of cancer cell death. *Nat Med,* 213 (1): 54-61, 2007. DOI: 10.1038/nm1523

35. **Michaud M, Martins I, Sukkurwala AQ, Adjemian S, Ma Y, Pellegatti P, Shen S, Kepp O, Scoazec M, Mignot G, Rello-Varona S, Tailler M, Menger L, Vacchelli E, Galluzzi L, Ghiringhelli F, di Virgilio F, Zitvogel L, Kroemer G:** Autophagy-dependent anticancer immune responses induced by chemotherapeutic agents in mice. *Science,* 334 (6062): 1573-1577, 2011. DOI: 10.1126/science.1208347

36. **Hangasky JA, Chen W, Dubois SP, Daenthanasanmak A, Müller JR, Reid R, Waldmann TA, Santi DV:** A very long-acting IL-15: implications for the immunotherapy of cancer. *J Immunother Cancer,* 10 (1):e004104, 2022. DOI: 10.1136/jitc-2021-004104

37. **Stoklasek TA, Schluns KS, Lefrançois L:** Combined IL-15/IL-15Rα immunotherapy maximizes IL-15 activity *in vivo. J Immunol,* 177 (9): 6072-6080, 2006. DOI: 10.4049/jimmunol.177.9.6072

38. **Lu Y, Waller EK:** Dichotomous role of interferon-gamma in allogeneic bone marrow transplant. *Biol Blood Marrow Transplant,* 15 (11): 1347-1353, 2009. DOI: 10.1016/j.bbmt.2009.07.015

39. **Zheng Y, Chen Z, Han Y, Han L, Zou X, Zhou B, Hu R, Hao J, Bai S, Xiao H, Li WV, Bueker A, Ma Y, Xie G, Yang J, Chen S, Li H, Cao J, Shen L:** Immune suppressive landscape in the human esophageal squamous cell carcinoma microenvironment. *Nat Commun,* 11 (1):6268, 2020. DOI: 10.1038/s41467-020-20019-0

40. **Nicolini A, Ferrari P:** Involvement of tumor immune microenvironment metabolic reprogramming in colorectal cancer progression, immune escape, and response to immunotherapy. *Front Immunol,* 15:1353787, 2024. DOI: 10.3389/fimmu.2024.1353787

41. **Chen R, Ding S, Fu X, Liu G:** Intravesical chemotherapy enhances anti-tumor immunity in bladder cancer by modulating CD8(+) T cell activation and Treg populations. *Biochem Biophys Res Commun,* 764:151782, 2025. DOI: 10.1016/j.bbrc.2025.151782

42. **Hori S, Miyake M, Tatsumi Y, Onishi S, Morizawa Y, Nakai Y, Tanaka N, Fujimoto K:** Topical and systemic immunoreaction triggered by intravesical chemotherapy in an N-butyl-N-(4-hydroxybutyl) nitorosamine induced bladder cancer mouse model. *PLoS One,* 12 (4):e0175494, 2017. DOI: 10.1371/journal.pone.0175494

43. **Principe N, Kidman J, Goh S, Tilsed CM, Fisher SA, Fear VS, Forbes CA, Zemek RM, Chopra A, Watson M, Dick IM, Boon L, Holt RA, Lake RA, Nowak AK, Lesterhuis WJ, McDonnell AM, Chee J:** Tumor-infiltrating effector memory antigen-specific CD8(+) T cells predict response to immune checkpoint therapy. *Front Immunol,* 11:584423, 2020. DOI: 10.3389/fimmu.2020.584423

44. **Feng B, Bai Z, Zhou X, Zhao Y, Xie YQ, Huang X, Liu Y, Enbar T, Li R, Wang Y, Gao M, Bonati L, Peng MW, Li W, Tao B, Charmoy M, Held W, Melenhorst JJ, Fan R, Guo Y, Tang L:** The type 2 cytokine Fc-IL-4 revitalizes exhausted CD8(+) T cells against cancer. *Nature,* 634 (8034): 712-720, 2024. DOI: 10.1038/s41586-024-07962-4

45. **Gomes-Giacoia E, Miyake M, Goodison S, Sriharan A, Zhang G, You L, Egan JO, Rhode PR, Parker AS, Chai KX, Wong HC, Rosser CJ:** Intravesical ALT-803 and BCG treatment reduces tumor burden in a carcinogen induced bladder cancer rat model; a role for cytokine production and NK cell expansion. *PLoS One,* 9 (6):e96705, 2014. DOI: 10.1371/journal.pone.0096705

Kafkas Universitesi Veteriner Fakultesi Dergisi
Journal Home-Page: http://vetdergikafkas.org
E-ISSN: 1309-2251

Kafkas Univ Vet Fak Derg
32 (4): 529-538, 2026
DOI: 10.9775/kvfd.2026.36621

RESEARCH ARTICLE

DNA Barcoding and Genetic Characterization of *Haemaphysalis parva* (Acari: Ixodidae) from Central Anatolia, Türkiye Using Mitochondrial *cox1* Sequences

Maide Nur GÜNDOĞDU [1,2] Ömer ORKUN [1 (*)]

[1] Ticks and Tick-Borne Diseases Research Laboratory, Department of Parasitology, Faculty of Veterinary Medicine, Ankara University, TR-06070 Ankara - TÜRKİYE

[2] Graduate School of Health Sciences, Ankara University, TR-06070 Ankara - TÜRKİYE

[(*)] **Corresponding author:**
Ömer Orkun
Phone: +90 312 317 0315-24 4347
Fax: +90 312 316 4472
E-mail: omerorkun@yahoo.com.tr

How to cite this article?

Gündoğdu MN, Orkun Ö: DNA Barcoding and Genetic Characterization of *Haemaphysalis parva* (Acari: Ixodidae) from Central Anatolia, Türkiye Using Mitochondrial cox1 Sequences. *Kafkas Univ Vet Fak Derg*, 32 (4): 529-538, 2026.
DOI: 10.9775/kvfd.2026.36621

Article ID: KVFD-2026-36621
Received: 18.03.2026
Accepted: 16.06.2026
Published Online: 01.07.2026

Abstract

Ticks of the genus *Haemaphysalis* (Acari: Ixodidae) comprise a diverse group of species widely distributed across the Palearctic region and are known to harbor a variety of pathogens of medical and veterinary importance. Despite its relatively wide geographic distribution, the tick species *Haemaphysalis parva* remains relatively understudied from a molecular perspective, and reliable DNA barcode data for this species are largely lacking in global genetic databases. In the present study, we performed a mitochondrial *cox1*-based DNA barcoding and genetic characterization of *H. parva* specimens collected from active populations in Central Anatolia, Türkiye. A total of 16 adult ticks (eight females and eight males) collected from eight sampling sites were morphologically identified and subjected to molecular analyses. Sequencing of the mitochondrial *cox1* gene revealed seven distinct haplotypes among the analyzed specimens, with moderate haplotype diversity (h = 0.6917) and low nucleotide diversity (π = 0.00162). BLAST analyses demonstrated high sequence similarity with previously reported *H. parva* sequences from Türkiye, Iran, and Ghana. Bayesian phylogenetic reconstruction confirmed that all haplotypes identified in this study clustered within the main *H. parva* lineage and revealed two well-supported subclades within the species. The analysis also suggested possible inconsistencies among the taxonomic annotations of certain publicly available sequences in genetic databases. The generated sequences were deposited in GenBank and the Barcode of Life Data System (BOLD), establishing the first validated DNA barcode reference for *H. parva*. The findings of this study expand the currently available genetic data for this species and provide an important molecular reference for future taxonomic, ecological, and epidemiological investigations of *H. parva*.

Keywords: DNA barcoding, *cox1*, haplotype diversity, *Haemaphysalis*, phylogenetic analysis, tick genetics, Anatolia

INTRODUCTION

Ticks are among the most important arthropod vectors worldwide and represent a major threat to the health of both humans and domestic animals on a global scale [1]. Members of the genus *Haemaphysalis* (Acari: Ixodidae) have a wide geographic distribution and represent the second most species-rich genus among ticks, comprising approximately 174 recognized species worldwide [2]. Species of this genus typically exhibit a three-host life cycle and parasitize a broad range of vertebrate hosts, contributing to their wide geographic distribution and ecological diversity [3]. In the Western Palearctic region, including Türkiye, several species of this genus have been reported, such as *Haemaphysalis parva, Haemaphysalis punctata, Haemaphysalis sulcata, Haemaphysalis caucasica, Haemaphysalis concinna, Haemaphysalis hispanica, Haemaphysalis erinacei,* and *Haemaphysalis kopetdaghica*. In addition, *Alloceraea inermis* (formerly *Haemaphysalis inermis),* which has recently been transferred to the genus *Alloceraea* but remains phylogenetically closely related to *Haemaphysalis,* is also present in this region [4-6]. Species belonging to the genus *Haemaphysalis* are also of considerable importance due to their role as vectors of a wide range of pathogens of medical and veterinary significance, including protozoan, bacterial, and viral agents [7-9]. Despite the high species diversity within the genus, the vector competence and ecological roles of

many *Haemaphysalis* species have not yet been fully characterized [6].

Haemaphysalis parva is a widely distributed tick species that exhibits a three-host life cycle and is considered an exophilic species adapted to a variety of habitats. Adult ticks parasitize medium and large wild and domestic mammals, whereas immature stages feed on a broad range of small- and medium-sized wild mammals (including hedgehogs, hares, rodents, and carnivores), ground-feeding birds, and even reptiles. Adult ticks also commonly infest domestic mammals and humans [3,10-12]. Although some populations, particularly in Anatolia, have been reported to reach relatively high abundance compared with other ixodid ticks [10], knowledge regarding the ecology, biology, and vectorial competence of this species remains limited both locally and globally. In recent years, pathogen screening studies have revealed the presence of various protozoan, bacterial, and viral agents in *H. parva* collected from different hosts, drawing increasing attention to its potential epidemiological importance [13-21]. Among these are pathogens of significant medical and veterinary importance, including Crimean-Congo hemorrhagic fever virus, *Francisella tularensis*, *Coxiella burnetii*, *Babesia ovis,* and *Babesia rossi* [22-28]. However, relatively few studies have focused on host-seeking (questing) *H. parva* ticks. A study on pathogens in questing adult *H. parva* collected in Türkiye reported the presence of *Babesia crassa, B. rossi, Rickettsia hoogstraalii,* a novel *Babesia* species *(Babesia* sp. Ucbas), and an uncharacterized *Hepatozoon* species [13]. These findings highlight the potential epidemiological significance of *H. parva* and provide additional context for future studies focusing on questing tick populations.

From a genetic perspective, the available data on *H. parva* are derived from studies based on different genetic markers and specimen sets [29-33]. In addition, several cases of misidentification have been reported in previous molecular studies [34,35]. Validated DNA barcode records for *H. parva* in the Barcode of Life Data System (BOLD) remain underrepresented, underscoring the importance of expanding reference datasets for molecular identification. Therefore, the aim of the present study was to provide a validated genetic characterization and DNA barcode reference for *H. parva* based on mitochondrial *cox1* sequences obtained from active populations in Central Anatolia, Türkiye, to assess intraspecific haplotype diversity, and to investigate the phylogenetic relationships of this species within the genus *Haemaphysalis*.

Material and Methods

Ethical Statement

This study did not involve the use of live animals or human participants. All tick specimens were collected as host-seeking individuals from the environment without direct interaction with vertebrate hosts. Therefore, ethical approval was not required.

Study Area and Tick Collection

A total of 16 adult tick specimens (eight females and eight males) used in this study were collected from several localities within Ankara Province, Türkiye, including the districts of Kızılcahamam, Çubuk, Çamlıdere, Akyurt, Kalecik, and Sincan, during 2021-2022 *(Fig. 1)*. The specimens consisted of host-seeking (questing) adults collected from vegetation using the flagging method. After collection, the ticks were transported to the Ticks and Tick-Borne Diseases Research Laboratory (TTBDRL), Department of Parasitology, Faculty of Veterinary Medicine, Ankara University. The specimens were preserved in 70% ethanol and stored at +4°C under appropriate laboratory conditions until further analyses were performed. Detailed information on the collected specimens, including sampling localities and specimen codes, is provided in *Table 1*.

Morphological Identification

All collected tick specimens (eight females and eight males) were morphologically identified to species level using standard taxonomic keys [4,36]. Based on the diagnostic morphological characters, all specimens were confirmed as adult *H. parva*. Following identification, the specimens were examined and photographed under a Zeiss Stemi 2000-C stereomicroscope (Zeiss, Germany) equipped with an AxioCam digital camera and the ZEN imaging software. Dorsal and ventral images were obtained for each specimen, and representative dorsoventral microscopic images of all examined individuals are presented according to sex in *Fig. 2* (females) and *Fig. 3* (males).

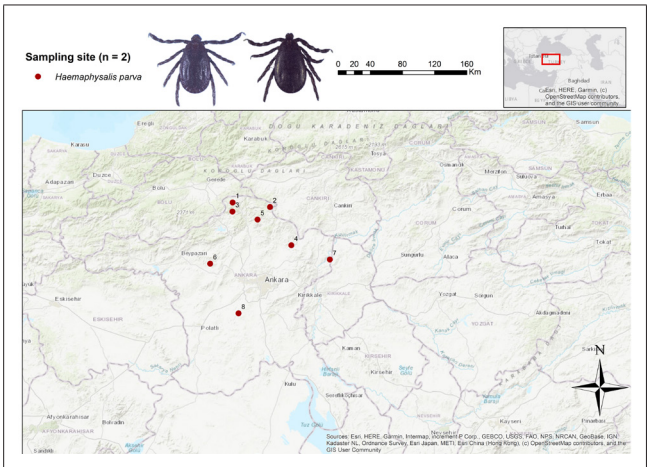

Fig 1. Geographic distribution of the sampling sites of *Haemaphysalis parva* in Ankara Province, Türkiye. Sixteen specimens (one female and one male from each locality) were collected from eight sampling sites. The inset map indicates the location of the study area within Türkiye

Table 1. Sampling details of Haemaphysalis parva specimens collected from eight localities in Ankara Province, Türkiye

Study Site	Sample Code	Species	Gender	Location (Village/District)	Coordinates (Lat./Long.)	Collection Date
1	Hpa-1785	*Haemaphysalis parva*	Female	Gebeler/Kızılcahamam	40.628955/32.49913833	24.09.2021
1	Hpa-1786	*Haemaphysalis parva*	Male	Gebeler/Kızılcahamam	40.628955/32.49913833	24.09.2021
2	Hpa-1787	*Haemaphysalis parva*	Female	Semer/Kızılcahamam	40.59123167/32.91630667	13.10.2022
2	Hpa-1788	*Haemaphysalis parva*	Male	Semer/Kızılcahamam	40.59123167/32.91630667	13.10.2022
3	Hpa-1789	*Haemaphysalis parva*	Female	Kuşcu/Çamlıdere	40.552806/32.497469	12.10.2021
3	Hpa-1790	*Haemaphysalis parva*	Male	Kuşcu/Çamlıdere	40.552806/32.497469	12.10.2021
4	Hpa-1791	*Haemaphysalis parva*	Female	Karadana/Çubuk	40.26625667/33.15500333	06.04.2022
4	Hpa-1792	*Haemaphysalis parva*	Male	Karadana/Çubuk	40.26625667/33.15500333	06.04.2022
5	Hpa-1793	*Haemaphysalis parva*	Female	Yıldırımören/Çubuk	40.48433333/32.77777667	18.04.2022
5	Hpa-1794	*Haemaphysalis parva*	Male	Yıldırımören/Çubuk	40.48433333/32.77777667	18.04.2022
6	Hpa-1795	*Haemaphysalis parva*	Female	Ahmetadil/Akyurt	40.10857167/33.24836333	15.04.2022
6	Hpa-1796	*Haemaphysalis parva*	Male	Ahmetadil/Akyurt	40.10857167/33.24836333	15.04.2022
7	Hpa-1797	*Haemaphysalis parva*	Female	Buğra/Kalecik	40.14484833/33.58530667	01.03.2022
7	Hpa-1798	*Haemaphysalis parva*	Male	Buğra/Kalecik	40.14484833/33.58530667	01.03.2022
8	Hpa-1799	*Haemaphysalis parva*	Female	Ücret/Sincan	39.68348/32.56499	24.09.2022
8	Hpa-1800	*Haemaphysalis parva*	Male	Ücret/Sincan	39.68348/32.56499	24.09.2022

DNA Extraction, PCR Amplification and Sequencing

Prior to molecular analyses, the tick specimens were rinsed again with 70% ethanol and air-dried on sterile filter paper. Each adult *H. parva* specimen was processed individually for nucleic acid extraction. Ticks were mechanically homogenized in bead-containing tubes using a SpeedMill PLUS cooling homogenizer (Analytik Jena, Jena, Germany) to ensure efficient tissue disruption. Genomic DNA was subsequently isolated from the homogenates using the BlackPREP Tick DNA/RNA Kit (IST Innuscreen GmbH, Berlin, Germany) according to the manufacturer's instructions. The extracted DNA samples were stored at –20°C until further analysis.

PCR amplification targeted a 710 bp fragment of the mitochondrial cytochrome C oxidase subunit I *(cox1)* gene using the universal primers LCO1490 and HCO2198 [37]. The thermal cycling conditions consisted of an initial denaturation at 95°C for 2 min, followed by 35 cycles of denaturation at 95°C for 30 s, annealing at 55°C for 30 s, and extension at 72°C for 1 min, with a final extension

Fig 2. Dorsal and ventral views of female *Haemaphysalis parva* specimens examined in this study. **(a-b)** Hpa-1785; **(c-d)** Hpa-1787; **(e-f)** Hpa-1789; **(g-h)** Hpa-1791; **(i-j)** Hpa-1793; **(k-l)** Hpa-1795; **(m-n)** Hpa-1797; **(o-p)** Hpa-1799. For each specimen, the left image shows the dorsal view and the right image shows the ventral view

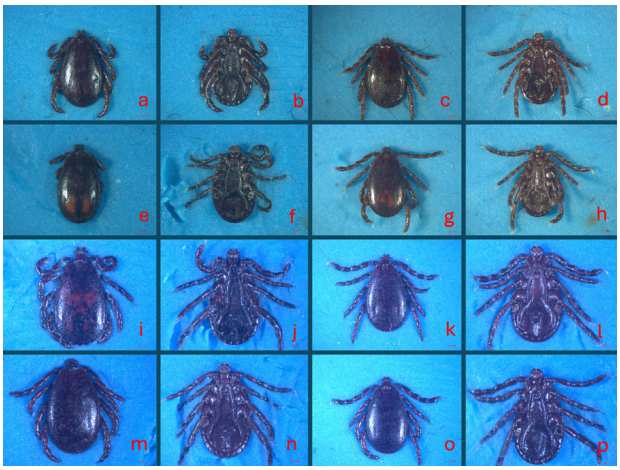

Fig 3. Dorsal and ventral views of male *Haemaphysalis parva* specimens examined in this study. **(a-b)** Hpa-1786; **(c-d)** Hpa-1788; **(e-f)** Hpa-1790; **(g-h)** Hpa-1792; **(i-j)** Hpa-1794; **(k-l)** Hpa-1796; **(m-n)** Hpa-1798; **(o-p)** Hpa-1800. For each specimen, the left image shows the dorsal view and the right image shows the ventral view

step at 72°C for 7 min. Positive amplicons were stored at –20°C until sequencing analyses. PCR products were purified using the PureLink™ Quick Gel Extraction Kit (Invitrogen, Löhne, Germany) following the manufacturer's protocol. The purified DNA samples were sequenced bidirectionally using the Sanger sequencing method on an Applied Biosystems™ 3130xl Genetic Analyzer (Applied Biosystems, Foster City, CA, USA) with the BigDye™ Terminator v3.1 Cycle Sequencing Kit (Applied Biosystems) according to the manufacturer's instructions.

Sequence Processing and Population Genetic Analyses

Chromatograms were visually inspected, edited, and assembled into consensus sequences using AliView v1.26 [38]. The obtained sequences were subsequently compared against the GenBank (National Center for Biotechnology Information, *https://www.ncbi.nlm.nih.gov/genbank)* and BOLD *(http://www.boldsystems.org)* databases using nucleotide similarity searches (BLAST) to confirm species identification. All sequences generated in this study were compiled into a single dataset for haplotype-based population genetic analyses.

Prior to downstream analyses, the sequences were translated into amino acid sequences in AliView v1.26 to check for potential stop codons and NUMTs (nuclear mitochondrial DNA segments). Because *cox1* is a protein-coding gene, sequence alignment was performed using the MUSCLE algorithm [39] while considering the translated amino acid sequences. The aligned dataset was then used for population genetic analyses, including calculation of nucleotide diversity (π), number of haplotypes *(k),* haplotype diversity *(h),* relationships among haplotypes, and the distribution of haplotypes among sampling sites using DnaSP v6.12.03 [40].

Phylogenetic Analyses

For phylogenetic analyses, the haplotypes identified in this study were combined with available *cox1* sequences of *H. parva* and other *Haemaphysalis* species (also *Alloceraea* spp.) retrieved from GenBank. In addition, two *Bothriocroton* species *(B. undatum* and *B. concolor)* were included as outgroup taxa. Prior to alignment, the reliability of the dataset was evaluated using GUIDANCE2 [41], and sequences or columns with low confidence scores were excluded if necessary. The remaining sequences were aligned again using the MUSCLE algorithm based on the translated amino acid sequences. The reliability of the final alignment was further assessed by calculating p-distances (mean genetic distances) in MEGA v11.0.13 [42].

The most appropriate nucleotide substitution model for phylogenetic reconstruction was determined using jModelTest v2.1.10 [43]. Bayesian phylogenetic inference was performed using the Markov chain Monte Carlo (MCMC) method implemented in the BEAST2 software package (BEAUti v2.7.6, BEAST v2.7.6, and TreeAnnotator v2.7.4) [44]. The MCMC chain was run for 100 million generations, and convergence as well as effective sample size (ESS) values were evaluated in Tracer v1.7.2 [45]. After discarding the first 20% of trees as burn-in, a maximum clade credibility tree was generated using TreeAnnotator v2.7.4. The resulting phylogenetic tree was visualized and edited using FigTree v1.4.4 *(http://tree.bio.ed.ac.uk/software/figtree).*

Data Availability

The genetic and barcode data generated in this study were deposited in the NCBI and BOLD databases. For this purpose, the *cox1* sequences of *H. parva* specimens together with detailed barcode metadata -including dorsoventral photographs of all examined specimens and their corresponding geographic coordinates- were submitted to BOLD, where the specimens were assigned to the barcode index number BIN:ADA9786. The same *cox1* sequence data were also deposited in the GenBank database of the NCBI and assigned accession numbers PQ725627-PQ725642. These records ensure public availability and traceability of the barcode data generated in this study.

Results

A total of 16 adult ticks were collected from eight different localities in Ankara Province, Türkiye, with one female and one male specimen obtained from each site *(Table 1).* The geographic distribution of the sampling sites is shown in *Fig. 1.* All specimens were morphologically identified as *H. parva* based on established diagnostic characters, and no morphological anomalies were observed. However, descriptive morphological variation was observed among the examined individuals. The most prominent differences included variation in the density and depth of punctations on the scutum and conscutum. In addition, some male specimens exhibited distinct light and dark areas on the scutum, and the pattern and extent of these color variations differed among individuals. No quantitative assessment of these traits was performed, and these observations were considered to represent normal intraspecific variation within the species. Representative dorsal and ventral views of the examined females and males are presented in *Fig. 2* and *Fig. 3,* respectively. Consequently, all specimens were included in subsequent genetic analyses.

Genomic DNA was successfully extracted from all 16 *H. parva* specimens, and PCR amplification of the mitochondrial *cox1* gene yielded amplicons of the expected size in all individuals. The PCR products were sequenced bidirectionally, and the resulting sequences were validated through BLAST homology searches against

the GenBank and BOLD databases. The characterized sequences were deposited in GenBank under accession numbers PQ725627-PQ725642 and in BOLD under the BIN:ADA9786 *(Table 2)*.

Haplotype-based population genetic analyses revealed that the 16 sequences were grouped into seven distinct haplotypes *(k*=7). The calculated haplotype diversity *(h)* was 0.6917, while the nucleotide diversity *(π)* was 0.00162. Among the detected haplotypes, Haplotype 6 represented the most common variant and included nine specimens (Hpa-1800, Hpa-1795, Hpa-1786, Hpa-1789, Hpa-1790, Hpa-1792, Hpa-1793, Hpa-1796, and Hpa-1798). Haplotype 7 comprised two specimens (Hpa-1785 and Hpa-1788), whereas the remaining haplotypes were each represented by a single specimen *(Table 2)*. Sequence polymorphism analysis indicated the presence of eight segregating sites *(S*=8), including seven singleton variable sites and one parsimony-informative site. Detailed haplotype information and sequence similarity values are presented in *Table 2*, while the geographical distribution of haplotypes across the sampling sites is illustrated in *Fig. 4*.

BLAST homology searches of the detected haplotypes revealed high similarity with previously reported *H. parva* sequences available in public databases. When considering matches with ≥90% query coverage, the highest similarity was observed with a sequence obtained from *H. parva* in Türkiye (GenBank accession PX122095), showing 99.42-99.71% identity at 100% coverage. In addition, the haplotypes showed 99.37-100% identity with 92-93% coverage to a sequence of *H. parva* reported from Ghana (PV125849). BLAST similarity values and corresponding reference sequences are summarized in *Table 2*. Furthermore, the haplotypes obtained in this study displayed 99.81-100% identity with approximately 75% coverage to two *H. parva* sequences previously reported from Iran (MH532296 and MH532297). BLAST searches also revealed high similarity with four sequences deposited under the name *"Hyalomma impeltatum"* from Israel (KT989628-KT989631), showing 98% coverage and 98.96-99.40% identity. In contrast, no barcode records of *H. parva* were available in the BOLD database, and therefore a direct sequence similarity comparison within the BOLD system could not be performed.

To infer the phylogenetic relationships of the detected haplotypes, a comprehensive dataset was constructed based on all available *H. parva cox1* sequences deposited in GenBank. A total of six *H. parva* records were available (accessed 11 March 2026) and included in the dataset, comprising three sequences from Türkiye, two from Iran, and one from Ghana. In addition, four sequences from Israel deposited under the name *"Hyalomma impeltatum"* and one sequence from Türkiye recorded as *"Haemaphysalis inermis"* were also incorporated into the dataset because BLAST analyses indicated close sequence similarity with *H. parva*. The final dataset consisted of 66 sequences, including the seven haplotypes identified

Table 2. *Mitochondrial cox1 haplotypes of Haemaphysalis parva identified in this study and their corresponding GenBank and BOLD accession numbers with BLAST similarity values*

Study Site	Sample Code	Haplotype Name	GenBank Accession No.	BOLD ID.*	BLAST Homology**
1	Hpa-1785	Haplotype7	PQ725627	HAPA001-24	99.56[a], 99.53[b]
1	Hpa-1786	Haplotype6	PQ725628	HAPA002-24	99.71[a], 99.69[b]
2	Hpa-1787	Haplotype3	PQ725629	HAPA003-24	99.56[a], 99.53[b]
2	Hpa-1788	Haplotype7	PQ725630	HAPA004-24	99.53[b], 99.42[a]
3	Hpa-1789	Haplotype6	PQ725631	HAPA005-24	99.69[b], 99.56[a]
3	Hpa-1790	Haplotype6	PQ725632	HAPA006-24	99.71[a], 99.69[b]
4	Hpa-1791	Haplotype1	PQ725633	HAPA007-24	99.42[a], 99.37[b]
4	Hpa-1792	Haplotype6	PQ725634	HAPA008-24	99.71[a], 99.69[b]
5	Hpa-1793	Haplotype6	PQ725635	HAPA009-24	99.71[a], 99.69[b]
5	Hpa-1794	Haplotype4	PQ725636	HAPA010-24	99.56[a], 99.53[b]
6	Hpa-1795	Haplotype6	PQ725637	HAPA011-24	99.71[a], 99.69[b]
6	Hpa-1796	Haplotype6	PQ725638	HAPA012-24	99.69[b], 99.57[a]
7	Hpa-1797	Haplotype5	PQ725639	HAPA013-24	99.69[b], 99.56[a]
7	Hpa-1798	Haplotype6	PQ725640	HAPA014-24	99.71[a], 99.69[b]
8	Hpa-1799	Haplotype2	PQ725641	HAPA015-24	100[b]
8	Hpa-1800	Haplotype6	PQ725642	HAPA016-24	99.71[a], 99.69[b]

** BOLD BIN:ADA9786; ** BLAST homology with over 90% coverage has been considered*
[a] PX122095 Haemaphysalis parva; [b] PV125849 Haemaphysalis parva voucher T5

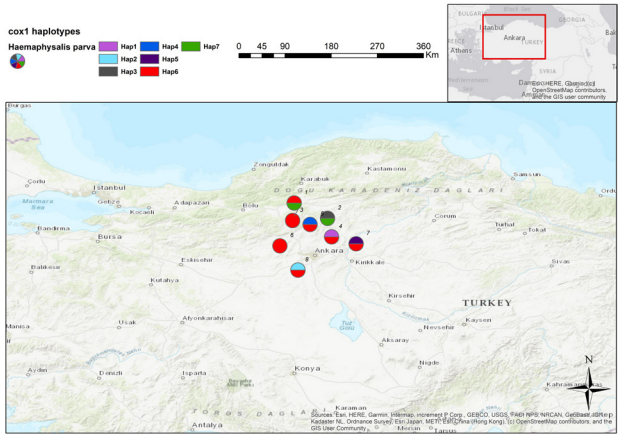

Fig 4. Geographic distribution of mitochondrial *cox1* haplotypes of *Haemaphysalis parva* detected in this study. Pie charts illustrate the haplotype composition and relative frequency at each sampling locality in Ankara Province, Türkiye. The inset map shows the position of the study area within Türkiye

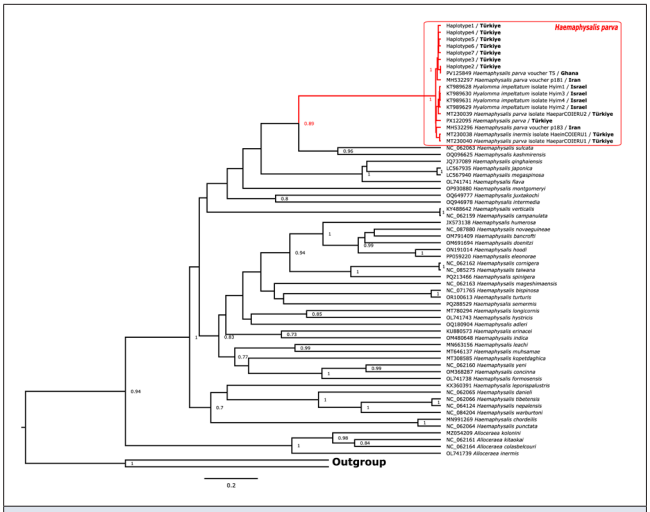

Fig 5. Bayesian phylogenetic tree inferred from mitochondrial *cox1* sequences of *Haemaphysalis* ticks. The analysis was performed using a dataset of 66 sequences and 686 aligned nucleotide positions under the TN93+I+G4 substitution model. *Bothriocroton undatum* (NC_017757) and *Bothriocroton concolor* (NC_017756) were used as outgroup taxa to root the tree. Node labels represent posterior probability values, with values < 0.7 omitted for clarity. Haplotypes identified in this study are highlighted in red, and the *Haemaphysalis parva* clade is indicated by a boxed frame. GenBank accession numbers are provided before species names, and the country of origin of sequences within the *Haemaphysalis parva* clade is indicated after the sequence names. The scale bar represents the number of nucleotide substitutions per site

in this study, while the remaining sequences represented various species of the genus *Haemaphysalis* retrieved from GenBank. Four sequences belonging to *Alloceraea* spp. were included as sister taxa, whereas *B. undatum* and *B. concolor* were used as outgroup taxa.

The Bayesian phylogenetic tree showed that all haplotypes identified in this study clustered within the main *H. parva* clade together with the previously reported sequences from Ghana and Iran. The *H. parva* lineage was strongly supported and split into two well-defined subclades with maximum posterior probability (posterior=1). One subclade contained the haplotypes identified in this study together with the sequences from Ghana and Iran, whereas the second subclade comprised three sequences from Türkiye together with one sequence recorded as *"Haemaphysalis inermis"* from Türkiye and four sequences from Israel deposited under the name *"Hyalomma impeltatum"*. Furthermore, *H. parva* formed a monophyletic lineage with *H. sulcata* and *Haemaphysalis kashmirensis,* supported by a high posterior probability value (posterior=0.89) *(Fig. 5)*. Overall, the phylogenetic reconstruction confirmed the taxonomic placement of the studied specimens within the *H. parva* lineage.

Discussion

The present study provides the first validated DNA barcode reference for *H. parva* based on mitochondrial *cox1* sequences obtained from active populations in Central Anatolia, Türkiye. Despite the relatively wide geographic distribution of this species across the Palearctic region [10,11,36,46], genetic information available for *H. parva* remains relatively limited and is based on a small number of studies and specimens [29-33]. In the present study, all examined specimens were morphologically confirmed as *H. parva* and subsequently characterized using *cox1*-based molecular analyses, revealing the presence of seven haplotypes among 16 morphologically confirmed specimens. In addition, the generated sequences were deposited in both GenBank and BOLD, thereby establishing the first barcode reference dataset for this species within the BOLD framework. The availability of such validated barcode records represents an important step toward improving the molecular identification and taxonomic reliability of *H. parva*, particularly given the previously reported cases of misidentification [34,35] and the limited representation of this species in global genetic databases.

The molecular characterization of *H. parva* has historically been based on relatively few specimens and genetic markers. The first partial genetic data for this species were generated from two specimens collected from sheep in Romania, in which the nuclear ITS1 and ITS2 regions were sequenced and reported to be identical between the samples [29]. Subsequently, Burger et al.[34] sequenced the mitochondrial genome together with partial nuclear 18S and 28S rRNA genes from a specimen preserved in the Queensland Museum and suggested that *H. parva*, together with *A. inermis*, was highly divergent from the remaining species of the genus *Haemaphysalis*. However, this interpretation was later questioned by Orkun [30], who performed a molecular characterization of ticks collected in Türkiye based on mitochondrial 16S rRNA sequences. In that study, a questing *H. parva* specimen collected in

Ankara showed the highest nucleotide similarity (92.2%) to *H. sulcata*, and the phylogenetic reconstruction did not support the placement of the previously published *H. parva* sequence reported by Burger et al.[34]. These findings suggested that the Romanian specimen might actually represent *A. inermis* rather than *H. parva*. This issue was subsequently clarified when the authors of the original study re-evaluated the specimen and acknowledged a morphological misidentification, correcting the record as *A. inermis* [35]. More recently, additional molecular data have been generated from a small number of specimens. For instance, Faghihi et al.[31] analyzed *H. parva* ticks collected from sheep and goats in Iran and sequenced the partial mitochondrial *cox1* gene from two specimens as well as the ITS2 region from four specimens. Very recently, a partial *cox1* sequence from a specimen collected from a dog in Ghana was reported [32], and the complete mitochondrial genome of a specimen collected from a human in Türkiye was also characterized [33]. Despite these contributions, the number of publicly available sequences for *H. parva* remains limited, and most studies rely on one or a few specimens. In comparison, the present study provides a substantially expanded molecular dataset based on 16 morphologically validated specimens, revealing seven distinct *cox1* haplotypes within a single regional population and establishing the first DNA barcode reference for this species within the BOLD system. These findings expand the currently available molecular data for *H. parva* and provide a valuable genetic reference for future taxonomic, ecological, and epidemiological studies.

Molecular genetic approaches have become increasingly important for the genetic characterization, DNA barcoding, population structure analysis, and phylogenetic reconstruction of vector ticks, thereby contributing to our understanding of tick evolution and tick-borne diseases [47,48]. Among the available genetic markers, the mitochondrial genome occupies a central role in arthropod molecular studies and has been widely used to investigate the phylogeny and genetic diversity of ticks [6,49,50]. Within the mitochondrial genome, the *cox1* gene is one of the most widely used evolutionary markers, representing a relatively conserved yet sufficiently informative region for investigating genetic variation among closely related taxa [47]. Consequently, *cox1* has been extensively applied in genetic characterization and population genetic studies of ticks [51-56]. In particular, Lv et al.[53] emphasized that the *cox1* region should be considered a primary marker for standard DNA barcoding studies of ticks. For these reasons, the mitochondrial *cox1* gene was selected as the barcode marker in the present study.

The haplotype-based analyses performed in the present study revealed the presence of seven distinct *cox1* haplotypes among 16 *H. parva* specimens, indicating a relatively moderate haplotype diversity within the examined population. Although the number of haplotypes was relatively high compared with the sample size, the overall nucleotide diversity was low, suggesting limited sequence divergence among haplotypes. Such a pattern, characterized by multiple closely related haplotypes with low nucleotide divergence, has been reported in geographically restricted populations of various organisms [57,58]. However, the underlying demographic processes cannot be inferred from the present dataset alone. The dominance of a single haplotype (Haplotype 6), which was represented by the majority of specimens, further supports the presence of a central haplotype surrounded by several less frequent variants. Similar patterns have been reported in mitochondrial studies of other ixodid ticks, where closely related haplotypes often differ by only a small number of mutational steps due to the relatively conserved nature of mitochondrial genes such as *cox1* [56,59,60]. In this context, the haplotype structure observed in the present study is consistent with intraspecific genetic variation within the local *H. parva* population rather than the presence of deeply divergent lineages. Nevertheless, it should be noted that the present analysis was based on a relatively limited number of specimens collected from a geographically restricted area. Therefore, broader sampling across the distribution range of *H. parva* would be necessary to better understand the overall genetic diversity and population structure of this species.

The BLAST similarity analyses and phylogenetic reconstruction conducted in the present study collectively support the taxonomic placement of the analyzed specimens within the *H. parva* lineage. The obtained *cox1* haplotypes showed the highest nucleotide similarity with previously reported *H. parva* sequences from Türkiye [33], Iran [31], and Ghana [32], indicating a clear genetic affinity among geographically distant populations of this species. Such high levels of sequence similarity across different regions may reflect the relatively conserved nature of the mitochondrial *cox1* gene and the wide geographic distribution of *H. parva* throughout the Palearctic and adjacent regions. The Bayesian phylogenetic tree further confirmed this relationship, as all haplotypes identified in the present study clustered within the main *H. parva* clade together with sequences originating from Ghana and Iran [31,32]. The phylogenetic reconstruction also revealed two well-supported subclades within the *H. parva* lineage. One of these subclades included the haplotypes identified in the present study together with sequences from Ghana and Iran, whereas the second subclade contained sequences reported from Türkiye as well as several sequences originally deposited under the

name "*Hyalomma impeltatum*" (KT989628-KT989631) from Israel and one sequence recorded as "*Haemaphysalis inermis*" from Türkiye (MT230038). The placement of these sequences within the *H. parva* clade may indicate possible inconsistencies in taxonomic annotation in public databases. However, additional morphological and multilocus molecular data would be required to clarify their taxonomic status. These findings also highlight potential inconsistencies in publicly available sequence annotations and emphasize the importance of generating well-validated reference datasets for reliable molecular identification of tick species. In this context, the present study also provides morphologically validated reference sequences that may facilitate future assessments of taxonomic annotation in public databases.

Although the present study provides the first validated DNA barcode reference for *H. parva*, several limitations should be acknowledged. First, the analyses were based on a relatively small number of specimens collected from a geographically restricted region of Central Anatolia, Türkiye, which may not fully represent the genetic diversity of the species across its distribution range. Second, the present study relied on a single mitochondrial marker *(cox1),* and additional nuclear or genomic markers may provide further insights into population structure and phylogenetic relationships. Therefore, future studies incorporating broader geographic sampling and multilocus approaches will be important for obtaining a more comprehensive understanding of the genetic diversity and evolutionary history of *H. parva*.

Overall, the present study expands the currently available molecular data for *H. parva* by providing a validated *cox1*-based DNA barcode reference from active populations in Central Anatolia, Türkiye. These findings contribute to improving the molecular identification of *H. parva* and provide a valuable genetic resource for future taxonomic studies of this species. Considering the increasing evidence that *H. parva* may harbor a variety of pathogens of medical and veterinary importance [11,13], a better understanding of its genetic diversity and phylogenetic relationships is also essential for future ecological and epidemiological investigations. The barcode data generated in this study therefore provide a valuable molecular resource that may facilitate future taxonomic, ecological, and epidemiological investigations of *H. parva*.

Declarations

Availability of Data and Materials: The datasets used and/or analyzed during the current study are available from the corresponding author (ÖO) on reasonable request.

Funding Support: This study was supported by the Scientific and Technological Research Council of Türkiye (TUBITAK) BIDEP 2209 Programme, Grant No. 1919B012319216. The funding agency had no role in the study design, data collection and analysis, decision to publish, or preparation of the manuscript.

Congress-Symposium Information: The results of this study were presented in an oral presentation at the 24. Parazitoloji Kongresi, held in Bursa, Türkiye, from 30 October to 02 November 2025, and were published in the congress proceedings as an abstract.

Competing interests: The authors declare no competing interests.

Ethical Statement: This study did not involve the use of live animals or human participants. All tick specimens were collected as host-seeking individuals from the environment without direct interaction with vertebrate hosts. Therefore, ethical approval was not required.

Declaration of Generative Artificial Intelligence (AI): Authors declare that the article, tables, and figures were not written or created by AI and AI-assisted technologies.

Authors' contributions: Conceptualization: ÖO, Data curation: ÖO, Formal analysis: MNG and Ö.O, Investigation: MNG and Ö.O, Methodology: ÖO, Project administration: MNG and ÖO, Resources: ÖO, Software: ÖO, Supervision: ÖO, Validation: ÖO, Writing - original draft: ÖO, Writing-review and editing: MNG and ÖO. All authors have read and agreed to the published version of the manuscript.

References

1. **Dortz LLL, Rouxel C, Polack B, Boulois HJ, Lagree AC, Deshuillers L, Haddal N:** Tick-borne diseases in Europe: Current prevention, control tools and the promise of aptamers. *Vet Parasitol*, 328:110190, 2024. DOI: 10.1016/j.vetpar.2024.110190
2. **Guglielmone AA, Petney TN, Robbins RG:** Ixodidae (Acari: Ixodea): Descriptions and redescriptions of all known species from 1758 to December 31, 2019. *Zootaxa,* 4871 (1): 1-322, 2020. DOI: 10.11646/zootaxa.4871.1.1
3. **Hoogstraal H, Kim KC:** Tick and mammal coevolution, with emphasis on *Haemaphysalis*. **In,** Coevolution of Parasitic Arthropods and Mammals. 505-568, Wiley, 1985.
4. **Estrada-Peña A, Pfäffle MP, Petney TN:** Genus *Haemaphysalis* Koch, 1844. **In,** Estrada-Pena A, Mihalca AD, Petney TN (Eds): Ticks of Europe and North Africa. 225-229, Springer International Publishing, 2017.
5. **Orkun Ö, Vatansever Z:** Rediscovery and first genetic description of some poorly known tick species: *Haemaphysalis kopetdaghica* Kerbabaev, 1962 and *Dermacentor raskemensis* Pomerantzev, 1946. *Ticks Tick Borne Dis,* 12:101726, 2021. DOI: 10.1016/j.ttbdis.2021.101726
6. **Kelava S, Apanaskevich DA., Shao R, Gofton AW, Mans BJ, Teo EJM, Norval G, Baker D, Nakao R, Barker SC:** Insights from entire mitochondrial genome sequences into the phylogeny of ticks of the genera *Haemaphysalis* and *Archaeocroton* with the elevation of the subgenus *Alloceraea* Schulze, 1919 back to the status of a genus. *Med Vet Entomol,* 38, 189-204, 2024. DOI: 10.1111/mve.12708
7. **Orkun Ö, Özdemir T, Gündoğdu MN, Yiğit M, Deniz A, Vatansever Z:** Molecular screening of tick-borne pathogens in host-seeking *Haemaphysalis punctata* Canestrini & Fanzago, 1878 (Ixodoidea: Ixodidae) in Anatolia with the first report of Burana virus. *Parasit Vector,* 19:201, 2026. DOI: 10.1186/s13071-026-07367-4
8. **Xu AL, XuH, Li Y, Wang X, Zheng JW, Shi FY, Cui QX, Lu Y, Cun DJ, Li LH:** Comprehensive meta-analysis of severe fever thrombocytopenia syndrome virus infections in humans, vertebrate hosts and questing ticks. *Parasit Vector,* 17:265, 2024. DOI: 10.1186/s13071-024-06341-2
9. **Lakew BT, Eastwood S, Walkden-Brown SW:** Epidemiology and transmission of *Theileria orientalis* in Australasia. *Pathogens,* 12:1187, 2023. DOI: 10.3390/pathogens12101187

10. **Orkun Ö:** Some ecological and epidemiological data belonging to tick species in Ankara and Around. *PhD thesis.* Graduate School of Health Sciences, Ankara University, Ankara, 2015.

11. **Vatansever Z:** *Haemaphysalis parva* (Neumann, 1897) (Figs. 100-102). **In,** Estrada-Pena A, Mihalca AD, Petney TN (Eds): Ticks of Europe and North Africa. 259-263, Springer International Publishing, 2017.

12. **Karaer Z, Guven E, Nalbantoglu S, Kar S, Orkun O, Ekdal K, Kocak A, Akcay A:** Ticks on humans in Ankara, Turkey. *Exp Appl Acarol,* 54, 85-91, 2011. DOI: 10.1007/s10493-010-9417-1

13. **Orkun Ö, Çakmak A, Nalbantoğlu S, Karaer Z:** Turkey tick news: A molecular investigation into the presence of tick-borne pathogens in host-seeking ticks in Anatolia; Initial evidence of putative vectors and pathogens, and footsteps of a secretly rising vector tick, *Haemaphysalis parva*. *Ticks Tick Borne Dis,* 11:101373, 2020. DOI: 10.1016/j.ttbdis.2020.101373

14. **Keysary A, Eremeeva ME, Leitner M, Din AB, Wikswo ME, Mumcupolu KY, Inbar M, Wallach AD, Shanas U, King R, Waner T:** Spotted fever group rickettsiae in ticks collected from wild animals in Israel. *Am J Trop Med Hyg,* 85 (5): 919-923, 2011. DOI: 10.4269/ajtmh.2011.10-0623

15. **Orkun Ö, Karaer Z:** Molecular characterization of *Babesia species* in wild animals and their ticks in Turkey. *Infect Genet Evol,* 55, 8-13, 2017. DOI: 10.1016/j.meegid.2017.08.026

16. **Dincer E, Timurkan MO, Akca S, Yuce FN:** Molecular characterisation of emerging tacheng tick virus 2 in ticks collected from livestock and dogs in Türkiye. *Exp Appl Acarol,* 97 (1):6, 2026. DOI: 10.1007/s10493-026-01149-4

17. **Papa A, Kontana A, Tsioka K, Saratsis A, Sotiraki S:** Novel phlebovirus detected in *Haemaphysalis parva* ticks in a Greek island. *Ticks Tick Borne Dis,* 8, 157-160, 2017. DOI: 10.1016/j.ttbdis.2016.10.012

18. **Orkun Ö, Nalbantoğlu S:** *Hepatozoon canis* in Turkish red foxes and their ticks. *Vet Parasitol Reg Stud Reports,* 13, 35-37, 2018. DOI: 10.1016/j.vprsr.2018.03.007

19. **Orkun Ö, Çakmak A:** Molecular identification of tick-borne bacteria in wild animals and their ticks in Central Anatolia, Turkey. *Comp Immunol Microbiol Infect Dis,* 63, 58-65, 2019. DOI: 10.1016/j.cimid.2018.12.007

20. **Orkun Ö, Emir H:** Identification of tick-borne pathogens in ticks collected from wild animals in Turkey. *Parasitol Res,* 119, 3083-3091, 2020. DOI: 10.1007/s00436-020-06812-2

21. **Orkun Ö:** Comprehensive screening of tick-borne microorganisms indicates that a great variety of pathogens are circulating between hard ticks (Ixodoidea: Ixodidae) and domestic ruminants in natural foci of Anatolia. *Ticks Tick Borne Dis,* 13:102027, 2022. DOI: 10.1016/j.ttbdis.2022.102027

22. **Shchelkanov ML, Kolobukhina LV, Moskvina TM, Aushev ID, Kartoev AA, Kelli EI, Merkulova LN, Grenkova EP, Samokhvalov EI, Petriaev VG, Serobian AG, Klimova EA, Galkina IV, Malyshev NA, Aristova VA, Slavskiĭ AA, Luk'ianova NA, Deriabin PG, Gromashevskiĭ VL, Efremenko VI, Onishchenko GG, L'vov DK:** Detection of the circulation of Crimean-Congo hemorrhagic fever virus in the piedmont steppes of the North Caucasus. *Vopr Virusol,* 50 (5): 9-15, 2005.

23. **Orkun Ö, Karaer Z, Çakmak A, Nalbantoğlu S:** Identification of tick-borne pathogens in ticks feeding on humans in Turkey. *PLoS Negl Trop Dis,* 8:e3076, 2014. DOI: 10.1371/journal.pntd.0003067

24. **Aydin MF, Aktas M, Dumanli N:** Molecular identification of *Theileria* and *Babesia* in ticks collected from sheep and goats in the Black Sea region of Turkey. *Parasitol Res,* 114, 65-69, 2015. DOI: 10.1007/s00436-014-4160-x

25. **Orkun Ö, Karaer Z, Çakmak A, Nalbantoğlu S:** Crimean-Congo hemorrhagic fever virus in ticks in Turkey: A broad range tick surveillance study. *Infect Genet Evol,* 52, 59-66, 2017. DOI: 10.1016/j.meegid.2017.04.017

26. **Chaligiannis I, Fernandez de Mera IG, Papa A, Sotiraki S, de la Fuente J:** Molecular identification of tick-borne pathogens in ticks collected from dogs and small ruminants from Greece. *Parasitol Res,* 74, 443-453, 2018. DOI: 10.1007/s10493-018-0237-z

27. **Mohammed RR, Enferadi A, Sidiq KR, Sarani S, Khademi P, Jaydari A, Ahmed AK:** Molecular Detection of *Francisella tularensis* isolated from ticks of livestock in Kurdistan Region, Iraq. *Vector Borne Zoonotic Dis,* 23 (10): 514-519, 2023. DOI: 10.1089/vbz.2023.0022

28. **Dinçer E, Timurkan MÖ, Oğuz B, Ozan E, Çoşkun N, Kızılteğe Ş, Dinçer PFP, Şahan A, Yalçınkaya D, Gölçecik ÖF, Nayir MB, Bayendur SH, Bourke BP, Linton YM, Ergunay K:** Striking tick-borne virus diversity and potential reservoirs documented during One-Health-based cross-sectional screening in Anatolia. *Parasit Vector,* 18:405, 2025. DOI: 10.1186/s13071-025-07046-w

29. **Chitimia L, Lin RQ, Cosoroaba I, Braila P, Song HQ, Zhu XQ:** Molecular characterization of hard and soft ticks from Romania by sequences of the internal transcribed spacers of ribosomal DNA. *Parasitol Res,* 105, 907-911, 2009. DOI: 10.1007/s00436-009-1474-1

30. **Orkun Ö:** Türkiye'de yayılış gösteren bazı ixodid kene türlerinin 16S rDNA filogenisi temelli moleküler karakterizasyonu. *Türkiye Parazitol Derg,* 42, 122-129, 2018. DOI: 10.5152/tpd.2018.5882

31. **Faghihi F, Hosseini-Chegeni A, Edalat H, Banafshi O, Telmadarraiy Z, Sedaghat MM:** Molecular identification of some *Haemaphysalis* species (Acari: Ixodidae) using mitochondrial and nuclear evidences in parts of Iran. *Syst App Acarol,* 25 (5): 809-820, 2020. DOI: 10.11158/saa.25.5.3

32. **Addo SO, Salley SN, Kofi MCAA, Tawaiah-Mensah CNL, Malm ROT, Obuam PK, Duker EO, Boakye JD, Agbotse GD, Ladzegpo D, Dadzie SK:** Molecular detection of tick-borne pathogens of zoonotic and veterinary importance in ticks from hunting dogs in Ghana. *Vet Res Com,* 50:101, 2026. DOI: 10.1007/s11259-025-11055-6

33. **Aydemir HB, Keskin A:** The complete mitogenome of *Haemaphysalis parva* (Arachnida: Ixodidae) and comparative mitogenomics of *Haemaphysalis* species. *Acta Parasitol,* 71:52, 2026. DOI: 10.1007/s11686-026-01243-y

34. **Burger TD, Shao R, Barker SC:** Phylogenetic analysis of the mitochondrial genomes and nuclear rRNA genes of ticks reveals a deep phylogenetic structure within the genus *Haemaphysalis* and further elucidates the polyphyly of the genus *Amblyomma* with respect to *Amblyomma sphenodonti* and *Amblyomma elaphense*. *Ticks Tick Borne Dis,* 4, 265-274, 2013. DOI: 10.1016/j.ttbdis.2013.02.002

35. **Kelava S, Mans BJ, Shao R, Barker D, Teo EJM, Chatanga E, Gofton AW, Moustafa MAM, Nakao R, Barker SC:** Seventy-eight entire mitochondrial genomes and nuclear rRNA genes provide insight into the phylogeny of the hard ticks, particularly the *Haemaphysalis* species, *Africaniella transversale* and *Robertsicus elaphensis*. *Ticks Tick Borne Dis,* 14:102070, 2023. DOI: 10.1016/j.ttbdis.2022.102070

36. **Filippova NA:** Fauna of Russia and neighboring countries, Arachnoidea. Vol. IV, Issue 5, Ixodid Ticks of Subfamily Amblyomminae. Nauka Publishing House, St. Petersburg. 1997.

37. **Folmer O, Black WH, Lutz R, Vrijenhok R:** DNA primers for amplification of mitochondrial cytochrome c oxidase subunit I from diverse metazoan invertebrates. *Mol Mar Biol Biotechnol,* 3 (5): 294-299, 1994.

38. **Larsson A:** AliView: A fast and lightweight alignment viewer and editor for large datasets. *Bioinformatics,* 30, 3276-3278, 2014. DOI: 10.1093/bioinformatics/btu531

39. **Edgar RC:** MUSCLE: A multiple sequence alignment method with reduced time and space complexity. *BMC Bioinformatics*, 5:113, 2004. DOI: 10.1186/1471-2105-5-113

40. **Rozas J, Ferrer-Mata A, Sanchez-DelBarrio JC, Guirao-Rico S, Librado P, Ramos-Onsins SE, Sanchez-Gracia A:** DnaSP 6: DNA sequence polymorphism analysis of large data sets. *Mol Biol Evol,* 34, 3299-3302, 2017. DOI: 10.1093/molbev/msx248

41. **Sela I, Ashkenazy H, Katoh K, Pupko T:** GUIDANCE2: Accurate detection of unreliable alignment regions accounting for the uncertainty of multiple parameters. *Nucleic Acids Res,* 43 (W1): W7-

W14, 2015. DOI: 10.1093/nar/gkv318

42. **Tamura K, Stecher G, Kumar S:** MEGA11: Molecular evolutionary genetics analysis version 11. *Mol Biol Evol,* 38, 3022-3027, 2021. DOI: 10.1093/molbev/msab120
43. **Darriba D, Taboada GL, Doallo R, Posada D:** jModelTest 2: More models, new heuristics and parallel computing. *Nature Methods,* 9, 772-772, 2012. DOI: 10.1038/nmeth.2109
44. **Bouckaert R, Vaughan TG, Barido-Sottani J, Duchêne S, Fourment M, Gavryushkina A, Heled J, Jones G, Kühnert D, De Maio N, Matschiner M, Mendes FK, Müller NF, Ogilvie HA, du Plessis L, Popinga A, Rambaut A, Rasmussen D, Siveroni I, Suchard MA, Wu CH, Xie D, Zhang C, Stadler T, Drummond AJ:** BEAST 2.5: An advanced software platform for Bayesian evolutionary analysis. *PLoS Comput Biol,* 15:e1006650, 2019. DOI: 10.1371/journal.pcbi.1006650
45. **Rambaut A, Drummond AJ, Xie D, Baele G, Suchard MA:** Posterior summarization in Bayesian phylogenetics using Tracer 1.7. *Syst Biol,* 67, 901-904, 2018. DOI: 10.1093/sysbio/syy032
46. **Guglielmone AA, Nava S, Robbins RG:** Geographic distribution of the hard ticks (Acari: Ixodida: Ixodidae) of the world by countries and territories. *Zootaxa,* 5251, 1-274, 2023. DOI: 10.11646/zootaxa.5251.1.1
47. **Araya-Anchetta A, Busch JD, Scoles GA, Wagner DM:** Thirty years of tick population genetics: A comprehensive review. *Infect Genet Evol,* 29, 164-179, 2015. DOI: 10.1016/j.meegid.2014.11.008
48. **McCoy KD, Leger E, Dietrich M:** Host specialization in ticks and transmission of tick-borne diseases: A review. *Front Cell Infect Microbiol,* 3:57, 2013. DOI: 10.3389/fcimb.2013.00057
49. **Burger TD, Shao R, Labruna MB, Barker SC:** Molecular phylogeny of soft ticks (Ixodida: Argasidae) inferred from mitochondrial genome and nuclear rRNA sequences. *Ticks Tick Borne Dis,* 5, 195-207, 2014. DOI: 10.1016/j.ttbdis.2013.10.009
50. **Uribe JE, Kelava S, Nava S, Cotes-Perdomo AP, Castro LR, Rivera-Paéz FA, Perea S, Mans BJ, Gofton A, Teo EJM, Zardoya R, Barker SC:** New insights into the molecular phylogeny, biogeographical history, and diversification of *Amblyomma* ticks (Acari: Ixodidae) based on mitogenomes and nuclear sequences. *Parasit Vectors,* 17 (1):139, 2024. DOI: 10.1186/s13071-024-06131-w
51. **Orkun Ö, Sarıkaya E, Yılmaz A, Yiğit M, Vatansever Z:** Population genetic structure and demographic history of *Dermacentor marginatus* Sulzer, 1776 in Anatolia. *Sci Rep,* 15:12570, 2025. DOI: 10.1038/s41598-025-97658-0
52. **Song S, Shao R, Atwell R, Barker S, Vankan D:** Phylogenetic and phylogeographic relationships in *Ixodes holocyclus* and *Ixodes cornuatus* (Acari: Ixodidae) inferred from COX1 and ITS2 sequences. *Int J Parasitol,* 41 (8): 871-80, 2011. DOI: 10.1016/j.ijpara.2011.03.008
53. **Lv J, Wu S, Zhang Y, Chen Y, Feng C, Yuan X, Jia G, Deng J, Wang C, Wang Q, Mei L, Lin X:** Assessment of four DNA fragments (COI, 16S rDNA, ITS2, 12S rDNA) for species identification of the Ixodida (Acari: Ixodida). *Parasit Vectors,* 7:93, 2014. DOI: 10.1186/1756-3305-7-93
54. **Zhang RL, Zhang B:** Prospects of using DNA barcoding for species identification and evaluation of the accuracy of sequence databases for ticks (Acari: Ixodida). *Ticks Tick Borne Dis,* 5 (3): 352-358, 2014. DOI: 10.1016/j.ttbdis.2014.01.001
55. **Kanduma EG, Mwacharo JM, Githaka NW, Kinyanjui PW, Njuguna JN, Kamau LM, Kariuki E, Mwaura S, Skilton RA, Bishop RP:** Analyses of mitochondrial genes reveal two sympatric but genetically divergent lineages of *Rhipicephalus appendiculatus* in Kenya. *Parasit Vectors,* 9 (1):353, 2016. DOI: 10.1186/s13071-016-1631-1
56. **Amzati GS, Pelle R, Muhigwa JB, Kanduma EG, Djikeng A, Madder M, Kirschvink N, Marcotty T:** Mitochondrial phylogeography and population structure of the cattle tick *Rhipicephalus appendiculatus* in the African Great Lakes region. *Parasit Vectors,* 11 (1):329, 2018. DOI: 10.1186/s13071-018-2904-7
57. **Fu YX:** Statistical tests of neutrality of mutations against population growth, hitchhiking and background selection. *Genetics,* 147 (2): 915-925, 1997. DOI: 10.1093/genetics/147.2.915
58. **Excoffier L, Lischer HE:** Arlequin suite ver 3.5: A new series of programs to perform population genetics analyses under Linux and Windows. *Mol Ecol Resour,* 10 (3): 564-567, 2010. DOI: 10.1111/j.1755-0998.2010.02847.x
59. **Krakowetz CN, Dergousoff SJ, Chilton NB:** Genetic variation in the mitochondrial 16S rRNA gene of the American dog tick, *Dermacentor variabilis* (Acari: Ixodidae). *J Vector Ecol,* 35 (1): 163-173, 2010. DOI: 10.1111/j.1948-7134.2010.00073.x
60. **King'ori EM, Obanda V, Nyamota R, Remesar S, Chiyo PI, Soriguer R, Morrondo P:** Population genetic structure of the elephant tick *Amblyomma tholloni* from different elephant populations in Kenya. *Ticks Tick Borne Dis,* 13 (3):101935, 2022. DOI: 10.1016/j.ttbdis.2022.101935

Kafkas Universitesi Veteriner Fakultesi Dergisi
Journal Home-Page: http://vetdergikafkas.org
E-ISSN: 1309-2251

Kafkas Univ Vet Fak Derg
32 (4): 539-547, 2026
DOI: 10.9775/kvfd.2026.36666

RESEARCH ARTICLE

Effects of *Saccharomyces cerevisiae* Pretreatment on Intestinal Immune Function in Mice with *Salmonella*-Induced Colitis

Yanling LI [1], Qingzhou ZENG [2], Xiaocong LI [2 (*)]

[1] School of Aeronautics and Astronautics, Southwest University of Science and Technology, Mianyang, Sichuan, 621010, CHINA
[2] College of Life Sciences and Agri-Forestry, Southwest University of Science and Technology, Mianyang, Sichuan, 621010 CHINA

[(*)] **Corresponding author:**
Xiaocong Li
Phone: +18728157786
E-mail: xclllyl19@swust.edu.cn

How to cite this article?

Li Y, Zeng Q, Li X: Effects of *Saccharomyces cerevisiae* Pretreatment on Intestinal Immune Function in Mice with *Salmonella*-Induced Colitis. *Kafkas Univ Vet Fak Derg*, 32 (4): 539-547, 2026.
DOI: 10.9775/kvfd.2026.36666

Article ID: KVFD-2026-36666
Received: 25.03.2026
Accepted: 19.06.2026
Published Online: 01.07.2026

Abstract

Salmonella is a major foodborne pathogen, and Saccharomycetes may offer preventive potential. This study evaluated the protective effect of *Saccharomyces cerevisiae* pre-gavage in mice infected with *Salmonella enteritidis*. Forty-eight ICR mice were randomly assigned to four groups: control group (Control), Saccharomycetes cerevisiae group (JM), *Salmonella* infection group (SM), and Saccharomycetes cerevisiae pre-gavage followed by *Salmonella* infection group (JM+SM). During a four-week prevention phase, JM and JM+SM mice received daily Saccharomycetes suspension (1×10^{10} CFU/mL), while Control and SM mice received saline. In the fifth week, SM and JM+SM mice were challenged with *Salmonella* suspension (5.19×10^{9} CFU/mL). Body weight was monitored throughout. At the end, spleen index, serum cytokines, colonic pathology, cytokine mRNA expression, and colonic immune factors were assessed. Compared with the Control group, SM mice showed significant weight loss, colonic damage, elevated spleen index, increased pro-inflammatory cytokines (IL-1β, IL-6, TNF-α) and their mRNA, and higher $CD3^{+}$ and $sIgA^{+}$ cells ($P<0.05$). JM mice showed no significant changes in any measured parameters compared with the Control group ($P>0.05$). Compared with SM mice, JM+SM mice had attenuated weight loss and significantly improved all measured parameters ($P<0.05$). In conclusion, *S. cerevisiae* pre-gavage effectively alleviates *Salmonella*-induced colitis in mice, likely by mitigating intestinal pathology, balancing pro-/anti-inflammatory factors, and modulating local immune responses.

Keywords: *Saccharomyces cerevisiae*, *Salmonella*, Colitis, Immunomodulation, Intestinal barrier

INTRODUCTION

Salmonella is one of the important foodborne pathogens worldwide, posing a particularly severe threat in the livestock and poultry breeding industry. Its infection can lead to a series of clinical symptoms in the host, such as acute gastroenteritis, bacteremia, subsequently causing impaired intestinal health, hindered animal growth, and decreased immune function [1]. Given the escalating challenge of antibiotic resistance, identifying safe and effective alternative control strategies has become a research priority. Probiotics, with their inherent advantage in regulating intestinal health, have emerged as a core focus in this field. As live microbial supplements, probiotics improve animal health and enhance production performance by modulating gut microbiota balance and strengthening the intestinal barrier, leading to their widespread application in livestock and poultry production [2-4]. Among numerous probiotics, Saccharomycetes (such as *Saccharomyces cerevisiae)* have become highly valuable strains due to their unique nutritional composition and immune-modulating potential. This strain's cells are rich in amino acids, vitamins, and various growth-promoting factors. These bioactive substances help improve the intestinal micro-environment, maintain microbial homeostasis, and enhance intestinal barrier function by regulating host immune responses [5,6]. Based on its dual regulatory effects on the intestinal microecology and immune function, Saccharomycetes are considered to have unique application value in preventing intestinal pathogenic microbial infections and alleviating intestinal damage, providing a new potential approach for the prevention and control of *Salmonella*-induced colitis.

The intestine, as the largest digestive organ and a core immune organ in the animal body, is the first line of

defense against *Salmonella* invasion. Its mucosal immune system concentrates over 70% of the body's immune cells, forming a triple defense system through physical barriers, chemical barriers, and immune barriers [7]. Among these, the intestinal immune barrier serves as the first line of defense against pathogenic microorganisms, with its integrity directly determining the host's resistance to *Salmonella* and overall health status [8]. Modulating the intestinal immune system not only maintains intestinal homeostasis and prevents pathogenic microbes from invading the internal environment but also synergizes with beneficial microorganisms in the gut. By participating in metabolic processes and immune regulation, this system collectively safeguards animal health [9]. However, *Salmonella* infection directly damages intestinal morphology, disrupts intestinal flora homeostasis, and consequently impairs intestinal immune barrier function. Research indicates that *Salmonella* can destroy tight junction proteins between intestinal epithelial cells by secreting toxins, degrade antimicrobial peptides in the mucus layer, and simultaneously induce excessive activation of Th17 cells leading to a cytokine storm, ultimately causing a systemic breakdown of barrier function [10]. Furthermore, *Salmonella* Typhimurium infection can lead to gastrointestinal dysfunction, intestinal mucosal damage, and systemic inflammatory responses [11]. Although the functional properties of Saccharomycetes in regulating immune responses and repairing the intestinal mucosal barrier have been preliminarily recognized, and their active components can specifically alleviate intestinal damage, the molecular mechanisms by which they regulate intestinal immune barrier repair through specific components in the context of *Salmonella* infection remain unclear. Moreover, key issues such as the effectiveness of pre-gavage intervention, long-term safety, and dosage optimization have not been resolved. Enhancing intestinal immune function and inhibiting *Salmonella* colonization and proliferation are precisely the core keys to preventing and controlling *Salmonella*-induced colitis, ensuring livestock and poultry health, and improving breeding efficiency.

In recent years, the positive role of Saccharomycetes in preventing and treating intestinal inflammation has been preliminarily confirmed, providing a theoretical basis for its application in preventing and controlling *Salmonella*-induced infectious colitis. Existing research indicates that Saccharomycetes, as probiotic biological agents, can effectively alleviate autoimmune inflammation (such as ulcerative colitis). The core mechanism lies in regulating immune responses and repairing the intestinal mucosal barrier, compensating for the limitations of traditional drugs, and offering advantages such as safety, high efficiency, and minimal side effects [12]. Concurrently, active Saccharomycetes can also improve the intestinal micro-ecological environment, promote intestinal development, and further enhance intestinal resistance to *Salmonella* by consuming intestinal oxygen, regulating the proportion of intestinal flora, and lowering intestinal pH [13]. In probiotic application research, *S. cerevisiae* has shown broad application prospects, and its value in alleviating intestinal inflammation has been experimentally confirmed. For instance, Marco Gentili et al.[14] found that a *S. cerevisiae* extract with prebiotic properties significantly improved tissue damage and diarrhea symptoms in colitis mice, a mechanism closely related to enhancing intestinal barrier function. This further supports the feasibility of Saccharomycetes alleviating intestinal inflammation by regulating the intestinal barrier. Currently, research on Saccharomycetes intervention mostly focuses on post-onset treatment of colitis, and the research system is relatively mature. However, there is still a lack of in-depth exploration regarding *Salmonella*-induced colitis, particularly the regulatory effect and mechanism of Saccharomycetes pre-gavage on intestinal immune function in this mice model [15]. As a commonly used experimental animal model, mice exhibit physiological and immune systems highly similar to other mammals [16].

Addressing this research gap, this study employs mice as an experimental model. By establishing a *Salmonella*-induced colitis model through *S. cerevisiae* pre-treatment, we systematically investigate the regulatory effects of Saccharomycetes on intestinal immune function in these mice and explore the underlying molecular mechanisms. The results of this study can not only enrich the immunomodulatory theory of Saccharomycetes in *Salmonella* infection prevention and control, clarify the application value of its pre-gavage method, but also provide practical experimental basis and new ideas for developing novel probiotic preparations based on Saccharomycetes and optimizing *Salmonella* prevention and control strategies in livestock and poultry, ultimately contributing to the healthy development of the livestock and poultry breeding industry.

Material and Methods

Ethical Statement

All experimental procedures were approved by the Animal Protection and Ethics Committee of the Southwest University of Science and Technology (Approval No. [L2024032]).

Experimental Materials

The primary materials used in this experiment included *Salmonella* Typhimurium (ATCC 14028, Haibo Bio), *S. cerevisiae* (a laboratory-owned strain, isolated and cultured from a local farm, and identified via sequencing as

S. cerevisiae), and 3-week-old SPF-grade healthy male ICR (Institute of Cancer Research) mice (Beijing Speifu Bio Co.). The yeast strain was identified by molecular methods as follows: genomic DNA was extracted from pure cultures, and the internal transcribed spacer (ITS) region of the ribosomal DNA was amplified using the universal fungal primers ITS1 (5'-TCCGTAGGTGAACCTGCGG-3') and ITS4 (5'-TCCTCCGCTTATTGATATGC-3'). The PCR products were sequenced via Sanger sequencing, and the obtained sequences were compared against the NCBI GenBank database using BLAST analysis. The sequence showed 99-100% identity with known *S. cerevisiae* sequences. The ITS sequence has been submitted to GenBank; the accession number will be provided upon manuscript acceptance. The full ITS sequence is also available as supplementary material.

Animal Husbandry and Management

A total of 48 three-week-old healthy male ICR mice were randomly divided into 4 groups: control group (Control), *S. cerevisiae*-only group (JM), *Salmonella* infection group (SM), and *Saccharomyces cerevisiae* pre-gavage followed by *Salmonella* infection group (JM+SM), with 12 mice per group. The mice were acclimated for one week with standard feeding. The formal experiment consisted of two phases: Weeks 1~4 served as the prevention phase, during which the Control and SM groups were daily gavaged with physiological saline (0.2 mL/mice/day), while the JM and JM+SM groups received an equal volume (0.2 mL/mice/day) of yeast suspension (1×10^{10} CFU/mL). The yeast concentration of 1×10^{10} CFU/mL and the gavage volume of 0.2 mL/mouse/day were selected based on previous studies demonstrating that daily oral administration of *S. cerevisiae* at concentrations of 10^9-10^{10} CFU/mL effectively modulates intestinal immunity and protects against pathogen infection in mouse models [17]. Specifically, Milani et al.[18] reported that daily gavage of *S. cerevisiae* at 10^9CFU/mL significantly reduced inflammation in a dose-dependent manner, while other studies have used similar volumes for yeast administration in mice. Based on these precedents, we selected 1×10^{10} CFU/mL to ensure sufficient yeast colonization and immunomodulatory effects during the four-week prevention phase. Week 5 was the colitis induction phase, during which the Control and JM groups were daily gavaged with physiological saline (0.2 mL/mice/day), while the SM and JM+SM groups received an equal volume (0.2 mLmice/day) of *Salmonella* Typhimurium suspension (5.19×10^9 CFU/mL). Bedding was changed, and cages and water bottles were cleaned every 3 days. The ambient temperature was maintained at 25±2°C.

Determination of Mice Growth Performance

During the experimental period, the body weight of mice in each group was measured and recorded weekly. Body weights were measured in grams (g) to assess growth dynamics throughout the study period. Data are presented as the mean±standard deviation, and trend charts of body weight changes over time for each group were plotted. Furthermore, the differences in body weight among groups at the end of the experiment were compared to analyze the impact of *Salmonella* infection on mice growth and the potential protective effect of yeast pre-treatment.

Determination of Organ Index and Histopathological Observation

After the experiment, mice were weighed, anesthetized with ether, and subjected to retro-orbital blood collection for serum separation. Mice were then euthanized by cervical dislocation. The spleens were collected, surface connective tissue was removed, and after washing, surface moisture was absorbed using filter paper. The spleen weight was measured, and the spleen index was calculated using the formula: Organ Index = (Organ Weight (mg)/Body Weight (g))×100%.

Subsequently, the mid-colon segments were collected and fixed in 4% paraformaldehyde. After thorough fixation, tissues were dehydrated through a graded alcohol series, embedded in paraffin, and sectioned at 5 μm thickness. Sections were rehydrated, sequentially stained with hematoxylin and eosin (H&E), dehydrated, cleared, and mounted with neutral resin. Colonic histological changes were observed under a microscope.

Detection of Serum Cytokine Concentrations

The serum collected and separated above was used to detect the concentrations of interleukins (IL-1β, IL-4, IL-6, IL-10) and tumor necrosis factor-α (TNF-α) using commercial ELISA kits, Specifically, the following kits were used: Mouse IL-1β ELISA Kit (Elabscience, E-EL-M0037), Mouse IL-4 ELISA Kit (Elabscience, E-EL-M0043), Mouse IL-6 ELISA Kit (Elabscience, E-EL-M0044), Mouse IL-10 ELISA Kit (Elabscience, E-EL-M0046), and Mouse TNF-α ELISA Kit (Elabscience, E-EL-M3063). All procedures were performed strictly according to the manufacturers' instructions.

Determination of Cytokine mRNA Expression Levels in Colonic Tissues

The middle 2 cm of the colon (approximately 1 cm from the cecum) was collected from mice under ether anesthesia, rinsed with physiological saline to remove intestinal contents, and then snap-frozen in liquid nitrogen. For analysis, the frozen tissue was removed from liquid nitrogen, ground into powder under liquid nitrogen, and an appropriate amount of tissue powder was taken. Total RNA was extracted using a Trizol reagent kit. RNA integrity was assessed by 1% agarose gel electrophoresis, and RNA concentration was measured using a UV spectrophotometer. RNA was reverse-transcribed into

cDNA using a reverse transcription kit, and then the mRNA expression levels of cytokines (IL-1β, IL-4, IL-6, IL-10, TNF-α) were analyzed using a real-time quantitative PCR instrument. The specific primer sequences for the corresponding genes are shown in *Table 1*. The relative mRNA expression levels of each target gene in the colonic tissue were calculated using the $2^{-}\Delta\Delta Ct$ method.

Fluorescence Staining of Paraffin Sections

Immunofluorescence staining for sIgA, CD3, and $FOXP_3$ was performed on colonic paraffin sections, with DAPI used for nuclear localization. The main steps were as follows: colonic samples were fixed, embedded, sectioned, deparaffinized, rehydrated, subjected to antigen retrieval, decolorized (if necessary), blocked, incubated with primary and secondary antibodies, developed with DAB, counterstained, dehydrated, and mounted. The slides were then scanned using a fluorescence microscope. Based on the scanned images, positive cell rates were quantified and calculated using the HALO platform (Indica Labs, USA).

Statistical Analyses

Differences between groups in the result data were analyzed using one-way analysis of variance (ANOVA). Normality of data distribution was assessed using the Shapiro-Wilk test, and homogeneity of variances was verified using Levene's test. All data met the assumptions for parametric analysis. When a significant overall difference was detected by ANOVA, Tukey's honest significant difference (HSD) test was performed as the post-hoc multiple comparison procedure to determine significant differences between specific groups (Control, JM, SM, and JM+SM). Visualization graphs were generated using GraphPad Prism 10 software. Data are presented as the mean ± standard deviation, with P=0.05 set as the threshold for statistical significance. The sample size of n=12 per group was determined based on a priori power analysis using G*Power software (version 3.1). Assuming a significance level of α=0.05, a statistical power of 80% (1-β=0.80), and an expected medium-to-large effect size (Cohen's f = 0.40) based on previous *Salmonella* colitis studies, the calculated minimum sample size was 8-10 mice per group. We therefore selected 12 mice per group to account for potential mortality, excluded outliers, and inter-individual variability, while ensuring adequate statistical power for all planned comparisons.

Results

Effect of *S. cerevisiae* on Body Weight Changes in *Salmonella*-Infected Mice

As shown in *Fig. 1*, during the 1-4 week prevention phase (0-28 days), the body weight of mice in all four groups showed a steady upward trend, with no significant differences observed among the groups (P>0.05). Upon entering the Week 5 enteritis induction phase (29-35 days), significant differences in body weight among the groups became apparent. Compared to the Control group, the body weight of the JM group was significantly higher, while that of the SM group was significantly lower. Simultaneously, the body weight of the JM+SM group showed no significant difference compared to the Control and JM groups, but was significantly higher than that of the SM group (P<0.05).

Effects of *S. cerevisiae* on Spleen and Colon Tissue in *Salmonella*-Infected Mice

As shown in *Fig. 2-A, B*, compared to the Control group, the spleens of the JM and JM + SM groups appeared larger in size; however, the spleens of the SM group were larger than those of the JM and JM + SM groups. The spleen index of SM mice was significantly higher than that of the Control, JM, and JM + SM groups (P<0.05). Meanwhile, the spleen index of JM + SM mice was significantly higher than that of the Control group (P<0.05).

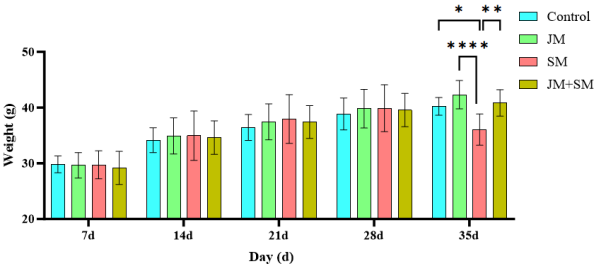

Fig 1. Mice body weight. At each time point, pairwise comparisons among the four groups show no significant differences (P>0.05) and are not labeled in the figure. Only those with significant differences (P<0.05) are annotated. * P<0.05, ** P<0.01, *** P<0.001, **** P<0.0001

Table 1. *Primer sequences of cytokines*

Target Gene	Forward (5'-3')	Reverse (3'-5')
IL-1β	TCGGCAAAGAAATCAAGATGGC	GTGCAAGTCTCATGAAGTGAGC
IL-6	ACAGAAGGAGTGGCTAAGGA	AGGCATAACGCACTAGGTTT
TNF-α	CGTCGTAGCAAACCACCAAG	TTGAAGAGAAACCTGGGAGTAGACA
IL-4	CTTCCAAGGTGCTTCGCATA	GATGAATCCAGGCATCGAAA
IL-10	AATTCCCTGGGTGAGAAAGCTGAAG	CTGCTCCACTGCCTTTGCTCTTAT

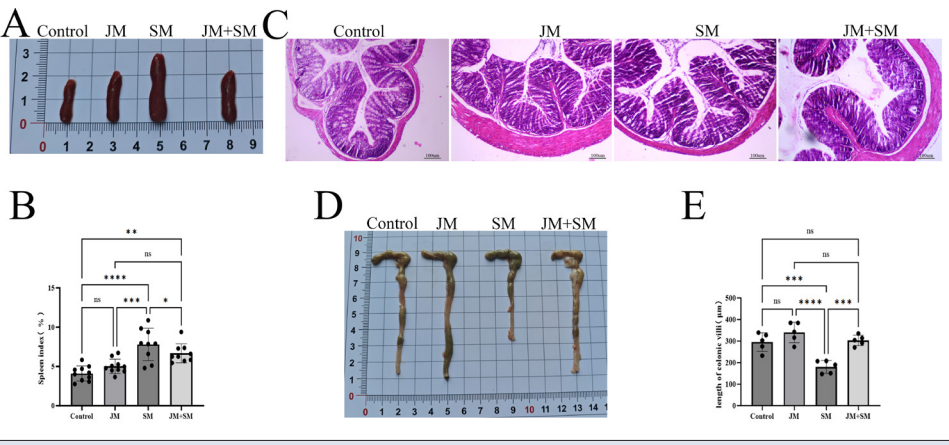

Fig 2. Histological morphology observation and quantitative analysis. **A.** Spleen appearance, **B.** Spleen organ index, **C.** Colon H&E staining (100×), **D.** Colon appearance, **E.** Colon villus length. * P<0.05, ** P<0.01, *** P<0.001, **** P<0.0001, ns P>0.05, The same notation applies subsequently

Morphological and histological alterations in mice colon are depicted in *Fig. 2-C,D,E*. The colons of SM mice showed a reduced number of goblet cells, obvious villus damage, and villus length was significantly shorter compared to the Control, JM, and JM + SM groups *(Fig. 2-C, E)*. The gross morphology also exhibited shortening in length. The degree of villus damage in the JM+SM group was lower than that in the SM group.

Effects of *S. cerevisiae* on Peripheral Blood Cytokine Levels in *Salmonella*-Infected Mice

The cytokine levels in the peripheral blood of mice are shown in *Fig. 3-A,B,C,D,E*. Compared to the Control group, the levels of IL-6, IL-10, IL-1β, and TNF-α were significantly increased in SM mice (P<0.05), while no significant difference was observed for IL-4 (P>0.05). No significant differences were found in the levels of IL-4, IL-6, IL-10, IL-1β, and TNF-α between the JM group and the Control group (P>0.05). The levels of IL-6, IL-10, IL-1β, and TNF-α in the JM+SM group were significantly higher than those in the Control group (P<0.05), but the level of IL-4 showed no significant difference compared to the Control (P>0.05). Compared to the SM group, the levels of IL-6, IL-1β, and TNF-α were significantly lower in the JM+SM group (P<0.05), while no significant differences were observed for IL-4 and IL-10 (P>0.05).

Effects of *S. cerevisiae* on Relative mRNA Expression Levels in Colon Tissue

Fig. 4-A,B,C,D,E present the relative mRNA expression levels of cytokines in mice colon. Compared to the Control group, the relative expression levels of IL-10, IL-6, IL-1β, and TNF-α were significantly increased in

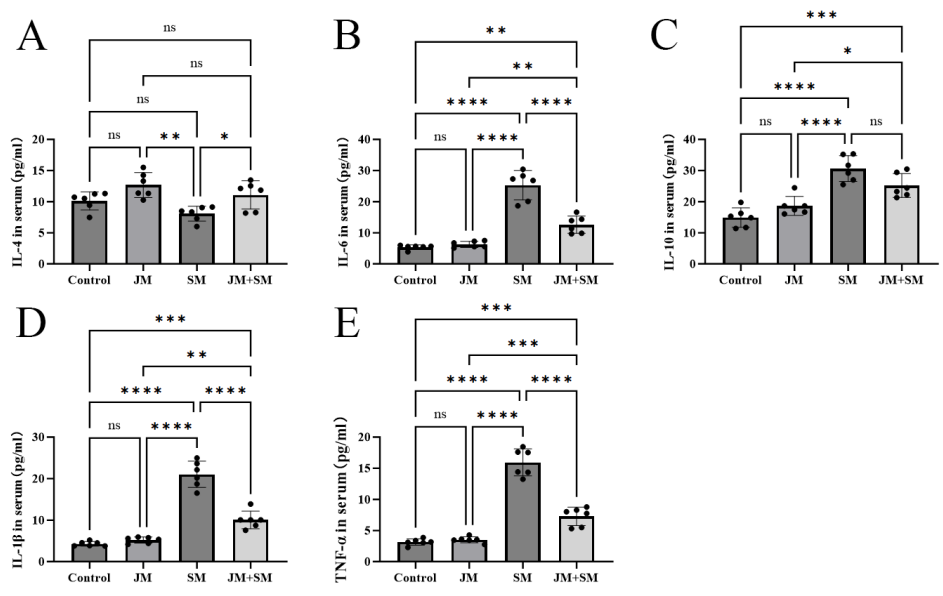

Fig 3. Cytokine levels in murine peripheral blood

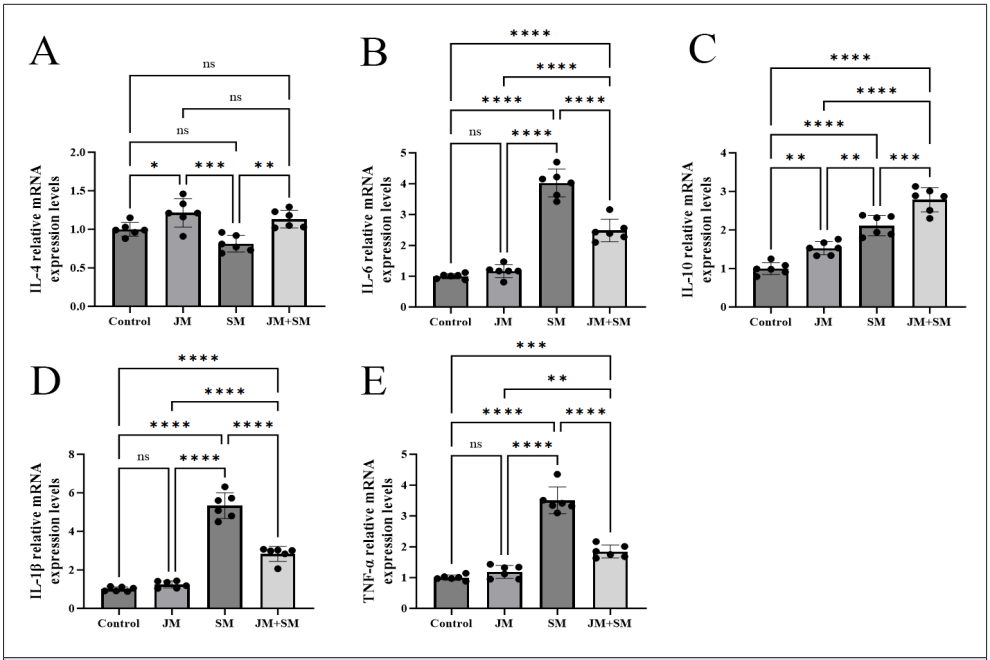

Fig 4. Relative mRNA expression levels of cytokines in murine colonic tissue

the colonic tissues of both the SM and JM+SM groups (P<0.05). In contrast, the relative expression of IL-4 in the SM and JM+SM groups showed no significant difference compared to the Control (P>0.05). No significant differences were observed in the expression of IL-4, IL-10, IL-6, IL-1β, and TNF-α between the JM group and the Control group (P>0.05). The expression levels of IL-4 and IL-10 in the JM+SM group were significantly higher than those in the SM group (P<0.05), while the levels of IL-6, IL-1β, and TNF-α were significantly lower than those in the SM group (P<0.05).

Effects of *S. cerevisiae* on Cytokines in the Colonic Tissue of *Salmonella*-Infected Mice

Fig. 5 shows the results of immunofluorescence staining and positive cell rate analysis for $FOXP_3$, sIgA, and CD3 in mice colonic tissue. The $FOXP_3$-positive cell rates showed no significant differences among the groups. The positive rates for sIgA and CD3 in the SM group were significantly higher than those in the Control, JM, and JM + SM groups (P<0.05); however, no significant differences in sIgA positive rates were observed among the remaining groups (P>0.05). Furthermore, the CD3-positive rate in the JM+SM group was significantly lower than that in the Control and JM groups (P<0.05).

Discussion

As a commonly used probiotic, *S. cerevisiae* possesses a robust survival capability within the intestinal tract, which forms the foundation for their immunomodulatory functions. Recent reviews have systematically summarized the immunomodulatory mechanisms of *S. cerevisiae*, highlighting its capacity to modulate both innate and adaptive immune responses through interactions with pattern recognition receptors on intestinal epithelial cells and immune cells. Studies have shown that Saccharomycetes are not easily inactivated after entering the intestine and can maintain high activity within 2-4 h [19]. Furthermore, their survival rate in simulated

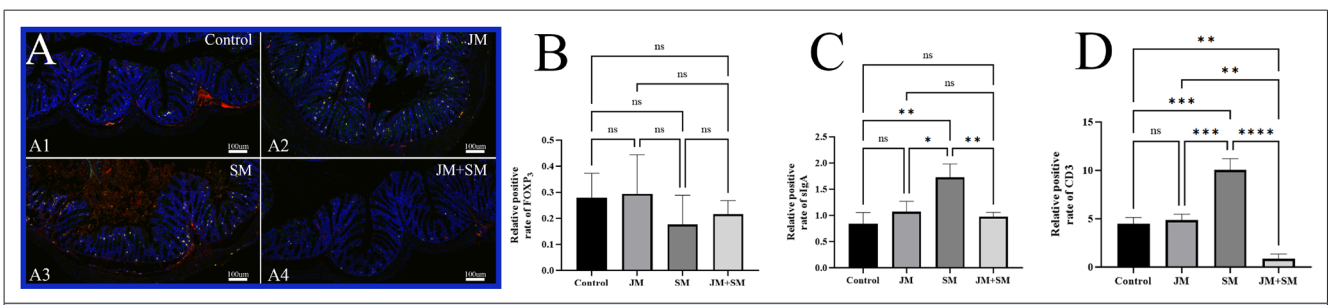

Fig 5. Immunofluorescence staining and quantitative analysis of murine colonic tissue. **A.** Immunofluorescence staining (400× magnification): FOXP3 (green), sIgA (red), CD3 (yellow), nuclear counterstain (blue), **B.** Quantification of FOXP3 cell frequency, **C.** Quantification of sIgA cell frequency, **D.** Quantification of CD3 cell frequency

gastrointestinal environments is significantly higher than that of other microecological agents such as lactobacilli and lactic acid bacteria [20], ensuring their sustained role in immunoregulation and antibacterial activities within the gut. In this study, a probiotic strain of Saccharomycetes was isolated and screened from a local farm. It was identified via 16S rDNA sequencing as *S. cerevisiae*. A suspension of this *S. cerevisiae* was administered via pre-gavage to mice to investigate its regulatory effects on *Salmonella*-induced colitis and intestinal immune function impairment. The results indicated that, compared to the Control group, the JM group showed no significant differences in intestinal immunity and barrier-related indicators. In contrast, the SM group exhibited typical intestinal immune dysfunction, characterized by increased expression of pro-inflammatory factors, decreased expression of anti-inflammatory factors, reduced expression of intestinal tight junction proteins, along with typical colitis symptoms, confirming the successful establishment of the *Salmonella*-induced colitis mouse model. Compared to the SM group, all the aforementioned indicators were significantly improved in the JM+SM group, suggesting that pre-treatment with this *S. cerevisiae* can effectively alleviate *Salmonella*-induced intestinal immune damage and colitis symptoms. This finding is consistent with previous research. Ju et al.[21] found that oral administration of *S. cerevisiae* CNCM I-3856 alleviated inflammatory responses in mice infected with *Salmonella* Typhimurium. Bum Ju Kil et al.[22] also reported that dietary supplementation with S. cerevisiae enhanced host immune responses and competitively inhibited pathogen colonization. Different from the aforementioned studies, the present research employed a pre-treatment intervention strategy, which offers greater preventive advantages compared to post-onset interventions, providing more practical experimental evidence for its application and promotion in livestock and poultry farming.

Intestinal morphology is one of the core indicators for evaluating intestinal health and integrity, playing a pivotal role in maintaining normal physiological functions of the organism. Studies have shown that probiotics can enhance intestinal barrier function by increasing the number of intestinal goblet cells and promoting mucus secretion [23]. In this study, compared to the Control group, SM group mice exhibited significantly shortened colonic villi, reduced goblet cells, and a thinner mucus layer, indicating that *Salmonella* severely disrupted intestinal structure, accompanied by weight loss. In contrast, JM+SM group mice showed alleviated damage to colonic villi, increased villus length, more orderly arrangement, partial restoration of goblet cells and the mucus layer, and a mitigated trend of weight loss. The results indicate that pre-gavage with the Saccharomycetes suspension significantly alleviated the damage caused by *Salmonella* to intestinal tissue morphology and markedly reduced the severity of colitis in mice.

Cytokines, as key signaling molecules that regulate immune function, play a crucial role in the body's defense against pathogenic microbial infections and in maintaining immune homeostasis [24]. The cytokines TNF-α, IL-1β, and IL-6 are key pro-inflammatory substances in colitis, while IL-10 and IL-4, as common anti-inflammatory cytokines, play pivotal roles in mediating humoral immune responses and in infectious diseases. Céline Nourrisson et al. found that intervention with *Saccharomyces boulardii* in rats infected with Blastocystis improved the levels of IL-4 and IL-10, thereby normalizing the intestinal microbial flora balance and immune regulatory functions, among other effects [25]. In this study, the expression levels of five cytokines -IL-4, IL-6, IL-10, IL-1β, and TNF-α- in murine peripheral blood and colonic tissue were measured to comprehensively evaluate the regulatory mechanism of Saccharomycetes on the intestinal immune response in *Salmonella*-infected mice. Compared to the Control, the SM group showed significantly elevated levels of IL-6, IL-1β, and TNF-α, reflecting the intense intestinal inflammatory response triggered by *Salmonella*. Simultaneously, IL-4 and IL-10, as core anti-inflammatory factors, increased following *Salmonella* infection, which caused intestinal damage and enhanced the body's compensatory anti-inflammatory response [26]. However, compared to the SM group, the JM+SM group exhibited decreased levels of IL-6, IL-1β, and TNF-α in peripheral blood cytokine content and mRNA expression in colonic tissue, suggesting that Saccharomycetes may alleviate the pro-inflammatory response by inhibiting the colonization of *Salmonella* [27]. This indicates that Saccharomycetes possess certain preventive and therapeutic effects against colitis induced by *Salmonella*.

The mucosa of the intestinal lining is an important immune tissue within the body. Its secretion and release of CD3, $FOXP_3$, and sIgA play crucial roles in maintaining intestinal homeostasis and immune responses [28]. CD3 is a key surface factor of T-cells, involved in T-cell activation and immunity; sIgA is the core antibody of intestinal mucosal immunity, responsible for neutralizing pathogens and preventing their adhesion to intestinal epithelial cells; $FOXP_3$ is the core transcription factor of regulatory T-cells, responsible for maintaining immune tolerance [29-31]. Previous studies indicate that *S. boulardii* can significantly increase sIgA content in the small intestine of mice and reduce intestinal colonization by pathogens such as *Salmonella* [32]. However, it is important to distinguish between therapeutic and preventive contexts: in the cited study, *S. boulardii* was administered as a treatment after infection

was established, where sIgA upregulation represents a protective compensatory response to an ongoing infection. In our preventive model, a different mechanism is at play. A characteristic of *Salmonella*-induced colitis is damage to the colonic epithelial barrier function and the intestinal lining mucosa. In this study, we further investigated the secretion of CD3, $FOXP_3$, and sIgA in the colons of *Salmonella*-infected mice treated with Saccharomycetes. The experiment revealed that $FOXP_3$ expression did not differ significantly among groups. However, the positive rates of CD3 and sIgA in the colonic tissue of the SM group were significantly higher than those in the Control group. This elevation likely represents a compensatory immune hyper-activation triggered by substantial *Salmonella* colonization and epithelial damage-a secondary reaction to an already breached intestinal barrier, rather than an effective protective response. In the JM+SM group, the positive rates of CD3 and sIgA were significantly lower than those in the SM group. Critically, this reduction does not indicate impaired immunity; rather, it suggests that *S. cerevisiae* pre-gavage effectively prevented or minimized initial *Salmonella* colonization, thereby reducing the need for a massive compensatory immune response [33]. Therefore, Saccharomycetes exert a certain protective effect on the mucosal tissue of the intestinal lining.

In summary, this study isolated a strain of *S. cerevisiae* from a local farm and investigated its effects on *Salmonella*-induced colitis and immune function impairment through pre-gavage with the yeast suspension. The results indicate that this yeast has a certain alleviating effect on *Salmonella*-induced colitis, demonstrates good safety, exerts antibacterial efficacy, and holds the potential to substitute for antibiotics.

Declarations

Availability of Data and Materials: The datasets generated and analyzed during the current study are available from the corresponding author (X.L.) upon reasonable request.

Acknowledgements: Not applicable.

Financial Support: Not Financial Support.

Conflict of Interest: The authors declared that there is no conflict of interest.

Declaration of Generative Artificial Intelligence (AI): The authors declare that the article, tables and figures were not written/created by AI and AI-assisted Technologies.

Author Contributions: Y.L.: Conceptualization, Investigation, Formal analysis, Writing-original draft, Visualization. Q.Z.: Methodology, Investigation, Data curation, Validation. X.L.: Conceptualization, Resources, Writing - review & editing, Supervision, Project administration, Funding acquisition. All authors have read and agreed to the published version of the manuscript.

References

1. **Viazis S, Lindsay M, Cripe J, Carran S, Greenlee T, Federman S S, Schwensohn C, Nguyen TA, Chen Parker C:** An overview of multistate outbreak investigations of *Salmonella* infections linked to fish and fishery products, United States, 2012-2021. *J Food Prot,* 8 (8):100566, 2025. DOI: 10.1016/j.jfp.2025.100566
2. **Alizadeh M, Fletcher C, Oladokun S, Mallick A I, Abdelaziz K, St-Denis M, Raj S, Blake K, Sharif S:** Treatment of chickens with probiotics under conditions conducive to necrotic enteritis development. *Res Vet Sci,* 192:105711, 2025. DOI: 10.1016/j.rvsc.2025.105711
3. **Zhang T, Zhang WQ, Feng CJ, Kwok LY, He QW, Sun ZH:** Stronger gut microbiome modulatory effects by postbiotics than probiotics in a mouse colitis model. *NPJ Sci Food,* 6 (1):53, 2022. DOI: 10.1038/s41538-022-00169-9
4. **Yue T, Lu Y, Ding W, Xu B, Zhang C, Li L, Jian F, Huang S:** The role of probiotics, prebiotics, synbiotics, and postbiotics in livestock and poultry gut health: A review. *Metabolites,* 15 (7): 478-478, 2025. DOI: 10.3390/METABO15070478
5. **Mekadim C, Mrazek J, Fliegerová KO, Sechovcová H, Mahayri TM, Jarošíková R, Husáková J, Wosková V, Tůma P, Polák J, Sojáková D, Němcová A, Dubský M, Fejfarová V:** The effect of the administration form of antibiotic therapy on the gut microbiome in patients with infected diabetic foot ulcers-DFIATIM trial. *BMC Microbiol,* 25 (1):339, 2025. DOI: 10.1186/s12866-025-04041-0
6. **Culpepper T, Senthil K, Vlcek J, Hazelton A, Heavey MK, Sellers RS, Nguyen J, Arthur JC:** Engineered probiotic *Saccharomyces boulardii* reduces colitis-associated colorectal cancer burden in mice. *Dig Dis Sci,* 70 (7): 2348-2367, 2025. DOI: 10.1007/s10620-025-09008-9
7. **Pannu A, Rundle CRA, Ulluwishewa D:** *In vitro* co-culture of bacterial and mammalian cells to investigate effects of potential probiotics on intestinal barrier function. *Bio Protoc,* 15 (12):e5361, 2025. DOI: 10.21769/BioProtoc.5361
8. **Zhang L, Gong X, Han R, Wang Y, Li J, Liu S, Chen H:** Early intervention with Si Ni Decoction enhances growth performance and immune status in broilers via modulation of gut microbiota and barrier function. *Poult Sci,* 104 (9):105464, 2025. DOI: 10.1016/j.psj.2025.105464
9. **Cornejo-Granados F, Gallardo-Becerra L, Romero-Hidalgo S, Lopez-Zavala AA, Cota-Huízar A, Cervantes-Echeverría M, Sotelo-Mundo RR, Ochoa-Leyva A:** Host genome drives the microbiota enrichment of beneficial microbes in shrimp: Exploring the hologenome perspective. *Anim Microbiome,* 7 (1):50, 2025. DOI: 10.1186/s42523-025-00414-y
10. **Lv Y, Zeng N, Feng Y, Li J, Zhang X, Wang Y, Liu Z:** Eugenol accelerates intestinal stem cell regeneration to protect the intestinal barrier integrity through inhibiting JAK2/STAT3 signaling pathway in *Salmonella enteritidis*-challenged broiler chicks. *J Animal Sci Biotechnol,* 16:40, 2025. DOI: 10.1186/s40104-025-01168-y
11. **Gaspari S, Akkermans S, Buysse I, Van Impe JF, Geeraerd AH:** Studying the defensive role of monoculture and polyculture gut microbiota against *Salmonella enterica:* An *in vitro* case study. *Food Microbiol,* 132:104798, 2025. DOI: 10.1016/j.fm.2025.104798
12. **Chai M, Zhu Y, Chen L, Zhang S, Huang Y, Zhang M, Jin W:** Yeast microcapsules encapsulating metal-phenolic nanozymes alleviate ulcerative colitis by mitigating oxidative stress and modulating the gut microbiota. *Mater Today Bio,* 32:101902, 2025. DOI: 10.1016/j.mtbio.2025.101902
13. **Mo X, Sun Y, Liang X, Li L, Hu S, Xu Z, Liu S, Zhang Y, Li X, Liu L:** Insoluble yeast β-glucan attenuates high-fat diet-induced obesity by regulating gut microbiota and its metabolites. *Carbohydr Polym,* 281:119046, 2022. DOI: 10.1016/j.carbpol.2021.119046
14. **Gentili M, Sabbatini S, Nunzi E, Lusenti E, Cari L, Mencacci A, Ballet N, Migliorati G, Riccardi C, Ronchetti S, Monari C:** Glucocorticoid-induced leucine zipper protein and yeast-extracted compound alleviate colitis and reduce fungal dysbiosis. *Biomolecules,* 14 (10):1321, 2024. DOI: 10.3390/biom14101321

15. **Yang CC, Zhang S, Zhang R, Zhao YN, Yang DW, Yang MY, Huang LJ:** Application of *Saccharomyces boulardii* in combination with sulfasalazine in ulcerative colitis patients demonstrates significant effectiveness. *World J Gastrointest Surg,* 17 (2):102342, 2025. DOI: 10.4240/wjgs.v17.i2.102342

16. **Czerucka D, Pontier-Bres R, Michel G, Rampal P, Peyron JF:** Effect of *Saccharomyces boulardii* strain CNCM I-745 on dendritic cells population in the lamina propria of mice following *Salmonella typhimurium* infection. *Gastroenterology,* 148 (4S1):S-724, 2015. DOI: 10.1016/S0016-5085(15)32472-0

17. **Milani TMS, Sandy CM, Calazans APCT, Fonseca VMB, Martins FS, Borges MC:** Dose-response effect of *Saccharomyces cerevisiae* UFMG A-905 on the prevention of asthma in an animal model. *Probiotics Antimicrob Proteins,* 16 (1): 53-61, 2024. DOI: 10.1007/s12602-022-10014-w

18. **Bonato M, Borges LL, Ingberman M, Fávaro Jr. C, Mesa D, Caron LF, Beirão BCB:** Effects of yeast cell wall on immunity, microbiota, and intestinal integrity of *Salmonella*-infected broilers. *J Appl Poultry Res,* 29 (3): 545-558, 2020. DOI: 10.1016/j.japr.2020.03.002

19. **Kathrani A, Theelen B, Bond R:** Isolation of *Malassezia* yeasts from dogs with gastrointestinal disease undergoing duodenal endoscopy. *J Small Anim Pract,* 64 (11): 661-668, 2023. DOI: 10.1111/jsap.13649

20. **Dong W, Zeng Y, Ma J, Cai K, Guo T, Tan G, Yu X, Hu Y, Peng N, Zhao S:** Characteristics and functions of dominant yeasts together with their applications during strong-flavor Baijiu brewing. *Foods,* 13 (15):2409, 2024. DOI: 10.3390/foods13152409

21. **Kil BJ, Pyung YJ, Park H, Kang JW, Yun CH, Huh CH:** Probiotic potential of Saccharomyces cerevisiae GILA with alleviating intestinal inflammation in a dextran sulfate sodium induced colitis mouse model. *Sci Rep,* 13 (1):6687, 2023. DOI: 10.1038/s41598-023-33958-7

22. **Lee J, Kil BJ, Choi Y, Chai HY, Lee DH, Jo HG, Lee DH:** Fermented Kamut wheat diet prevents DSS-induced colitis via modulating gut microbiota in mice. *Int J Mol Sci,* 26 (7): 3017, 2025. DOI: 10.3390/ijms26073017

23. **Zhang T, Zhang W, Feng C, Kwok LY, He Q, Sun Z:** Stronger gut microbiome modulatory effects by postbiotics than probiotics in a mouse colitis model. *NPJ Sci Food,* 6 (1): 53-53, 2022. DOI: 10.1038/s41538-022-00169-9

24. **Li B, Zhang H, Shi L, Li R, Luo Y, Deng Y, Li S, Li R, Liu Z:** *Saccharomyces boulardii* alleviates DSS-induced intestinal barrier dysfunction and inflammation in humanized mice. *Food Funct,* 13, 102-112, 2022. DOI: 10.1039/D1FO02752B

25. **Davoodi M, Karimooy FN, Budde T, Ortega-Martinez S, Moradi-Kor N:** Beneficial effects of Japanese sake yeast supplement on biochemical, antioxidant, and anti-inflammatory factors in streptozotocin-induced diabetic rats. *Diabetes Metab Syndr Obes,* 12, 1667-1673, 2019. DOI: 10.2147/DMSO.S220181

26. **Lu RL, Chen YR, Yang XF, Huang XY, Liu DZ, Hong XP:** Genetic liability to gut microbiota and inflammatory cytokines in relation to systemic lupus erythematosus risk: A multi-omics study. *Clin Rheumatol,* 44 (6): 2257-2268, 2025. DOI: 10.1007/s10067-025-07435-7

27. **Belousov DM, Golovko GN:** Dynamics of proinflammatory (IL-1, TNF), immunoregulatory (IL-4), and anti-inflammatory (IL-10) cytokines in the various outcomes of abdominal fever development. *J Infectol,* 12 (1): 85-90, 2020. DOI: 10.22625/2072-6732-2020-12-1-85-90

28. **Kim JH, Jeong M, Doo EH, Koo YT, Lee SJ, Jang JW, Park JHY, Huh CS, Byun S, Lee KW:** Glycine max fermented by a novel probiotic, *Bifidobacterium animalis* subsp. *lactis* LDTM 8102, increases immunomodulatory function. *J Microbiol Biotechnol,* 32 (9): 1146-1153, 2022. DOI: 10.4014/jmb.2206.06038

29. **Domoto H, Araki T, Ogai A, Inukai M, Chen CK, Tomita S, Mukai K, Nakamura N:** Surface CD3-negative monomorphic epitheliotropic intestinal T-cell lymphoma. *J Clin Exp Hematop,* 62 (3): 169-174, 2022. DOI: 10.3960/jslrt.22009

30. **Zheng Y:** Succinate undermines FOXP3 stability and disrupts T_{reg} cell function. *Nat Immunol,* 26 (6): 1-2, 2025. DOI: 10.1038/s41590-025-02167-x

31. **Jiang Q, Zhu X, Sun L, Xie C, Wang X, Ma L, Yan X:** Akkermansia muciniphila promotes SIgA production and alters the reactivity towards commensal bacteria in early-weaned piglets. *J Nutr,* 155 (1): 52-65, 2024. DOI: 10.1016/j.tjnut.2024.11.002

32. **Chai W, Yao W, Pan J, Huang Z, Wang B, Xu B, Fan X, He W, Wang W, Zhang W:** *Moniezia benedeni* drives CD3+ T cells residence in the sheep intestinal mucosal effector sites. *Front Vet Sci,* 11:1342169, 2024. DOI: 10.3389/fvets.2024.1342169

33. **Heavey MK, Hazelton A, Wang Y, Garner M, Anselmo AC, Arthur JC, Nguyen J:** Targeted delivery of the probiotic *Saccharomyces boulardii* to the extracellular matrix enhances gut residence time and recovery in murine colitis. *Nat Commun,* 15 (1): 3784, 2024. DOI: 10.1038/s41467-024-48128-0

Kafkas Universitesi Veteriner Fakultesi Dergisi
Journal Home-Page: http://vetdergikafkas.org
E-ISSN: 1309-2251

Kafkas Univ Vet Fak Derg
32 (4): 549-555, 2026
DOI: 10.9775/kvfd.2026.36738

Research Article

Ultrasonographic Assessment of Optic Nerve and Optic Nerve Sheath Diameters with Ocular Biometry in Brachycephalic versus Non-Brachycephalic Cats

Yusuf ŞEN [1], Burcu TOKGÖZ [2], İrem ERGİN [1 (*)]

[1] Ankara University, Faculty of Veterinary Medicine, Surgery Department, TR-06070 Ankara - TÜRKİYE
[2] Ankara University, Graduate School of Health Sciences, TR-06070 Ankara - TÜRKİYE

[(*)] **Corresponding author:**
İrem Ergin
Phone: +90 312 3170305
Fax: +90 312 3164472
E-mail: iremerg@gmail.com

How to cite this article?

Şen Y, Tokgöz B, Ergin İ: Ultrasonographic Assessment of Optic Nerve and Optic Nerve Sheath Diameters with Ocular Biometry in Brachycephalic versus Non-Brachycephalic Cats. *Kafkas Univ Vet Fak Derg*, 32 (4): 549-555, 2026. DOI: 10.9775/kvfd.2026.36738

Article ID: KVFD-2026-36738
Received: 03.04.2026
Accepted: 12.07.2026
Published Online: 13.07.2026

Abstract

Distinct craniofacial morphology in brachycephalic cats may alter ocular anatomy and predispose these breeds to specific ophthalmic conditions. This study evaluated the relationship between craniofacial conformation and optic nerve diameter (OND), optic nerve sheath diameter (ONSD), and ocular biometric parameters using high-resolution ultrasonography. Twenty-six clinically healthy cats were enrolled and categorized into brachycephalic and non-brachycephalic groups (n=13 per group). Comprehensive ophthalmic examinations, tonometry, and standardized ultrasonographic measurements -including axial globe length (AGL), lens thickness (LT), and vitreous chamber depth (VCD)- were performed. Although no statistically significant differences were detected between groups, several morphological tendencies emerged. Brachycephalic cats demonstrated shorter AGL and horizontal lens diameter, alongside increased anterior chamber depth and LT. Conversely, VCD appeared reduced in brachycephalic cats, potentially reflecting a more compact intraocular configuration associated with their craniofacial structure. By generating standardized ultrasonographic measurements, this study contributes to the establishment of morphology-specific reference intervals for OND and ONSD. Given the current scarcity of feline-specific normative data, these findings provide an essential preliminary framework to assist clinical diagnostics and neurological assessments in feline ophthalmology.

Keywords: Anatomic variations, Diagnostic imaging, Feline eye, Morphometry, Ocular ultrasound

Introduction

In brachycephalic cats, pronounced shortening of the skull, face, and craniofacial skeleton results in the characteristic rounded head conformation. This morphology is considered a breed-specific trait [1]. Beyond external appearance, craniofacial structure is associated with distinct anatomical alterations that may increase susceptibility to various breed-related diseases and disorders. In particular, brachycephalic breeds have been shown to be more predisposed to ocular diseases. With the growing popularity of brachycephalic cat breeds in recent years, these breed-associated ocular and respiratory conditions have gained increasing importance and warrant closer diagnostic evaluation [2-5].

Ocular ultrasonography is a fundamental, safe, and non-invasive imaging modality for the evaluation of intra-ocular and retrobulbar structures. This technique is indicated in a wide range of conditions, including ocular trauma, measurement of axial globe length, detection of intraocular foreign bodies, intraocular hemorrhage, lens luxation, and retinal detachment. In addition, ultrasonography provides substantial diagnostic value in cases where clinical examination of the anterior or posterior segment is limited due to opacification of the ocular media [6,7].

Another important application of ultrasonography in ophthalmology is ocular biometry. Ocular biometry is the measurement of the dimensions of the globe and its components, and measurement of axial globe length is of critical importance in the evaluation of conditions such as glaucoma, microphthalmia, macrophthalmia, phthisis bulbi, and persistent hyperplastic primary vitreous. However, information regarding normal ocular dimensions and interbreed variation in these measurements among different feline and canine breeds remains limited [8].

Among the structures of interest evaluated by ultrasonography are the optic nerve and its surrounding

sheath. Measurements of optic nerve diameter [9] and optic nerve sheath diameter (ONSD) [10] have gained increasing importance in the assessment of various clinical and physiological responses, particularly in the identification of pathological processes such as intracranial hypertension. In recent years, there has been a marked increase in studies focusing on the use of non-invasive ocular ultrasonography, especially ONSD measurements, for the diagnosis and monitoring of ocular diseases in veterinary medicine [6].

This study utilized high-resolution ultrasonography to investigate the relationship between craniofacial morphology and optic nerve and optic nerve sheath diameters, as well as key ocular biometric parameters, in brachycephalic and non-brachycephalic cats. The resulting data provide objective measurements that may contribute to the current literature and support future clinical evaluations.

Material and Methods

Ethical Statement

This study was reviewed by the Ankara University Local Ethics Committee for Animal Experiments (Decision date: 18.02.2026; Decision number: 2026-04-44). The Committee determined that the study did not require formal ethical approval. Informed consent for the clinical procedures had been obtained from the animal owners at the time of presentation.

Animals and Study Design

This retrospective cohort study included 26 cats of diverse breeds, ages, and sexes presented to the Ankara University Faculty of Veterinary Medicine Animal Hospital between April 2025 and March 2026. The study population was divided into two cohorts according to craniofacial morphology: brachycephalic (n=13) and non-brachycephalic (n=13). All brachycephalic cats meeting the inclusion criteria during the study period were enrolled. An equal number of eligible non-brachycephalic cats was selected to obtain comparable group sizes.

All cats underwent a comprehensive bilateral ophthalmic examination; however, only one eye per subject was included in the data analysis to avoid statistical bias related to inter-eye correlation. The standardized ophthalmic protocol integrated direct ophthalmoscopy, slit-lamp biomicroscopy, rebound tonometry, and transcorneal ultrasonography. To ensure procedural consistency and minimize inter-observer variability, all evaluations were performed by the same two veterinary clinicians.

The intraocular structures and fundus were assessed via direct ophthalmoscopy, while the cornea, anterior chamber, and limbal regions were evaluated using slit-lamp biomicroscopy. Intraocular pressure (IOP) was quantified using a rebound tonometer (iCare® TONOVET, Finland). To prevent iatrogenic elevations in IOP, particular emphasis was placed on minimizing patient stress and avoiding any jugular compression or excessive eyelid manipulation prior to and during measurements.

For tonometric assessment, the probe was positioned perpendicular to the central cornea at a distance of approximately 4-6 mm. The tonometer automatically calculated intraocular pressure based on the rebound velocity of a single-use probe following corneal contact. Three consecutive measurements were obtained, and the mean value was recorded. During measurements, care was taken to avoid manual pressure on the globe, and the eyelids were held open with minimal contact.

Ultrasonographic Assessment of Ocular Biometry

Ocular ultrasonography was performed using an ultrasound system equipped with a high-frequency hockey-stick transducer operating at 8-18 MHz (GE Logiq S8, GE Healthcare). A topical anesthetic eye drop containing proparacaine hydrochloride (Alcaine® 0.5%, Alcon, Türkiye) was instilled into the eye a few minutes prior to the procedure. The animals were gently restrained in sternal recumbency, and a sterile, water-based ultrasound gel was applied to the probe surface. The transducer was positioned transcorneally along the visual axis to obtain standardized sagittal images *(Fig. 1)*.

Following the acquisition of high-quality images, ocular

Fig 1. Ocular ultrasonographic examination of a cat. The animal was restrained in sternal recumbency, and the 18 MHz linear transducer was positioned transcorneally along the visual axis using sterile water-based coupling gel to obtain standardized sagittal images

biometric measurements were obtained based on predefined anatomical reference points. The parameters assessed included axial globe length (AGL), defined as the distance from the anterior corneal surface to the retinal layer, and horizontal lens diameter (HLD), measured as the maximal equatorial diameter of the lens along the horizontal plane. Anterior chamber depth (ACD) was determined as the distance between the posterior corneal surface and the anterior lens capsule, while lens thickness (LT) was defined as the distance between the anterior and posterior lens capsules along the visual axis. Furthermore, vitreous chamber depth (VCD) was measured as the distance from the posterior lens capsule to the retinal surface. All measurements were performed in a standardized and reproducible manner with reference to these established anatomical landmarks [11,12] *(Fig. 2)*.

Additionally, the optic nerve diameter (OND) and optic nerve sheath diameter (ONSD) were measured immediately posterior to the globe at the point where the nerve emerges from the sclera.

Ultrasonographic Assessment of Optic Nerve and Optic Nerve Sheath Diameters

Ultrasonographic evaluation of the optic nerve was performed using B-mode ultrasonography with a linear transducer operating at a frequency of 6-13 MHz. To clearly visualize the entry of the optic nerve into the globe, the transducer was rotated approximately 15° in a clockwise direction. The probe was then adjusted in dorsal and ventral directions until optimal visualization of the optic nerve was achieved. During image acquisition, the hyperechoic posterior lens capsule was used as an anatomical reference point. From the caudal aspect of the posterior lens capsule, imaging was extended over the retina toward the optic disc. Optic nerve diameter was determined by measuring the distance between the two hypoechoic outer borders of the nerve [12].

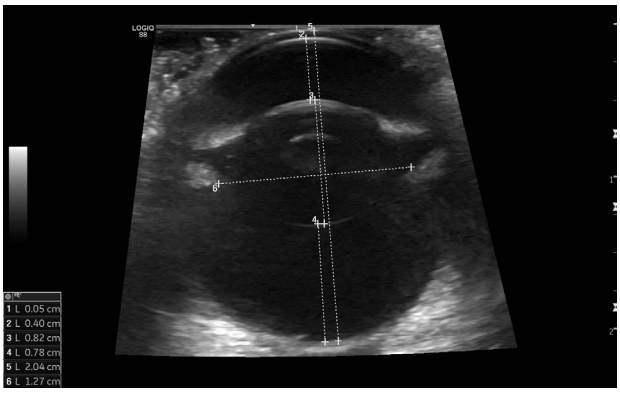

Fig 2. Ultrasonographic image of the feline eye illustrating ocular biometric measurements based on predefined anatomical landmarks. The numbered markers correspond to specific structures measured on the image as follows: 1, corneal thickness (CT); 2, anterior chamber depth (ACD); 3, lens thickness (LT); 4, vitreous chamber depth (VCD); 5, axial globe length (AGL); and 6, horizontal lens diameter (HLD). Axial globe length (AGL), anterior chamber depth (ACD), lens thickness (LT), horizontal lens diameter (HLD), and vitreous chamber depth (VCD) are indicated

Color Doppler ultrasonography was employed to differentiate the optic nerve from surrounding tissues and vascular structures. During ultrasonographic assessment, a transverse projection was used to identify the angle at which the optic nerve sheath was most clearly visualized. The images obtained at this optimal projection were recorded, and measurements were subsequently performed on the sections in which the nerve appeared at its maximum width.

All ultrasonographic recordings were standardized in the transverse plane at a gain setting of 60 dB. A generous amount of ultrasound gel was applied to the transducer, which was then gently placed on the superior aspect of the globe using a contact corneal technique. Transverse sections of the globe were sequentially scanned by fanning and sliding the transducer until the orbit and optic nerve were clearly visualized. The image in which the optic nerve appeared most clearly and at its maximum width was frozen, and diametric measurements were obtained. The same procedure was subsequently repeated for the contralateral eye. Video recordings of each examination were saved and archived for further evaluation.

All ocular ultrasonographic videos were independently reviewed by two investigators. The optic nerve was identified as a slightly curved hypoechoic band located caudal to the globe, whereas the optic nerve sheath (ONS) was defined as the hyperechoic bands flanking the optic nerve on either side. The outer boundaries of the hyperechoic bands farthest from the optic nerve were used as reference points for measuring the optic nerve sheath diameter (ONSD), which was assessed 3 mm caudal to the optic disc with the measurement line oriented perpendicular to the longitudinal axis of the optic nerve [13] *(Fig. 3)*. This 3-mm distance was determined by drawing a straight line parallel to the longitudinal axis of the optic nerve in the caudal direction from the optic disc. Upon completion of the ultrasonographic assessments, the eyes were gently irrigated with sterile saline solution.

Statistical Analysis

Descriptive statistics were calculated for all variables. Categorical variables were presented as frequencies (n) and percentages (%), while continuous variables were expressed as mean ± standard deviation (SD), median, and interquartile range (Q1-Q3), as appropriate. The normality of continuous variables was assessed using the Shapiro-Wilk test. Comparisons between brachycephalic and non-brachycephalic groups were performed using

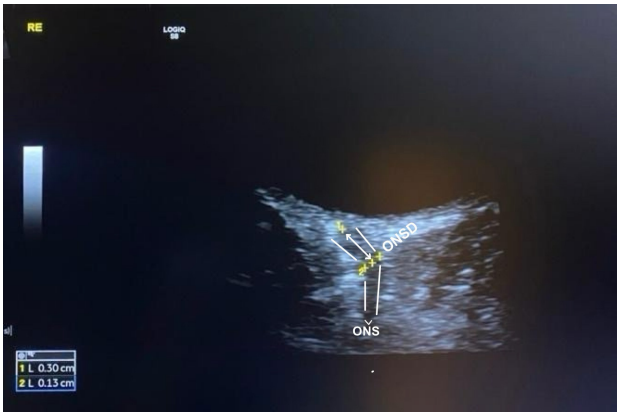

Fig 3. Ultrasonographic image of the feline optic nerve illustrating the measurement of optic nerve sheath diameter (ONSD). The optic nerve appears as a hypoechoic band, flanked by hyperechoic borders representing the optic nerve sheath (ONS). ONSD was measured 3 mm caudal to the optic disc, using the outer margins of the hyperechoic sheath as reference points, with the measurement line oriented perpendicular to the longitudinal axis of the optic nerve. Labels indicating ONS and ONSD are shown on the image

the independent samples t-test for normally distributed variables and the Mann-Whitney U test for non-normally distributed variables. A criterion of $P<0.05$ was used for all statistical comparisons. All statistical analyses were conducted using SPSS 30.0 software package.

Results

The cats were classified into two groups according to craniofacial morphology: brachycephalic (n=13) and non-brachycephalic (n=13). Overall, 13 cats (50.0%) were mixed-breed, while the remaining cats comprised British Shorthair (34.62%, n=9), Scottish Fold (11.54%, n=3), and Chinchilla (3.85%, n=1). The brachycephalic group consisted of British Shorthair, Scottish Fold, and Chinchilla cats, whereas the non-brachycephalic group comprised exclusively mixed-breed cats.

Regarding sex distribution, male cats were predominant in the overall study population 76.92% (n=20), while females represented 23.08% (n=6). Evaluation based on neutering status showed that 61.54% (n=16) of the cats were neutered, and 38.46% (n=10) were intact. This distribution was similar in both craniofacial morphology groups.

The mean age was 2.58±2.77 years in the brachycephalic group and 4.49±4.51 years in the non-brachycephalic group, with no significant difference between the groups (P=0.147). Statistical analysis revealed no significant correlations between age and any of the evaluated ocular biometric parameters (P>0.05). Specifically, neither the optic nerve diameter (OND) nor the optic nerve sheath diameter (ONSD) demonstrated age-dependent variations. A marginal positive trend was observed only between age and vitreous chamber depth (VCD) (P=0.061)

In terms of the eyes examined, the left eyes accounted for 53.85% (n=14) and the right eyes for 46.15% (n=12). The distribution of the eye side did not differ significantly between the brachycephalic and non-brachycephalic groups. The mean intraocular pressure (IOP) was 21.46±4.54 mmHg in brachycephalic cats and 23.23±3.19 mmHg in non-brachycephalic cats. Although the brachycephalic group exhibited numerically lower mean IOP values, no statistically significant difference was observed between the two craniofacial morphologies (P>0.05).

Ocular Biometric Findings

The ultrasonographic evaluation of ocular biometry revealed distinct morphological trends between skull types, although none of the measured parameters demonstrated statistically significant differences (P>0.05). Axial globe length (AGL) was numerically shorter in brachycephalic cats (18.89±2.33 mm) compared with non-brachycephalic cats (19.45±0.98 mm). Similarly, brachycephalic group showed slightly reduced vitreous chamber depth (VCD) (7.85±0.66 mm) and horizontal lens diameter (HLD) (11.13±1.21 mm) relative to the non-brachycephalic group (8.22±0.86 mm and 11.39±0.95 mm, respectively).

In contrast, the anterior chamber depth (ACD) and lens thickness (LT) were found to be marginally higher in the brachycephalic group. The mean ACD was 3.60±0.60 mm in brachycephalic cats versus 3.32±0.43 mm in non-brachycephalic cats, while the LT followed a similar trend with 7.95±0.75 mm and 7.75±0.83 mm, respectively. Detailed biometric results and statistical comparisons are summarized in *Table 1* and *Fig. 4*.

Optic Nerve and Optic Nerve Sheath Findings

Ultrasonographically, the optic nerve was identified as a slender, slightly curved hypoechoic structure posterior to the globe, surrounded by retrobulbar adipose tissue and musculature *(Fig. 5)*. The assessment of the optic nerve diameter (OND) revealed a notable trend toward higher values in brachycephalic cats (1.65±0.38 mm) compared to non-brachycephalic cats (1.43±0.12 mm), approaching but not reaching statistical significance (P=0.080).

The mean optic nerve sheath diameter (ONSD) was 2.99±0.51 mm (median: 3.00 mm; range: 2.60-3.30) in the brachycephalic group and 2.92±0.47 mm (median: 2.70 mm; range: 2.70-3.20) in the non-brachycephalic group. No statistically significant difference was detected in ONSD values between the two craniofacial morphologies (P=0.752).

Table 1. Comparison of ocular biometric parameters between brachycephalic and non-brachycephalic cats

Ocular Parameter (mm)	Brachycephalic Group		Non-brachycephalic Group		P
	Mean ± SD	Median (Q1-Q3)	Mean ± SD	Median (Q1-Q3)	
AGL	18.89±2.33	19.20 (19.00-19.90)	19.45±0.98	19.70 (19.50-20.00)	0.396
HLD	11.13±1.21	11.40 (10.50-11.70)	11.39±0.95	11.30 (10.70-12.00)	0.557
ACD	3.60±0.60	3.50 (3.20-4.10)	3.32±0.43	3.40 (2.90-3.60)	0.188
LT	7.95±0.75	8.10 (7.40-8.50)	7.75±0.83	7.70 (7.30-8.20)	0.526
VCD	7.85±0.66	7.80 (7.50-8.30)	8.22±0.86	8.10 (7.50-8.70)	0.222
ONSD	2.99±0.51	3.00 (2.60-3.30)	2.92±0.47	2.70 (2.70-3.20)	0.752
OND	1.65±0.38	1.60 (1.40-1.70)	1.43±0.12	1.50 (1.30-1.50)	0.080

OND, optic nerve diameter; ONSD, optic nerve sheath diameter; SD, standard deviation; AGL, axial globe length; HLD, horizontal lens diameter; ACD, anterior chamber depth; LT, lens thickness; VCD, vitreous chamber depth. A criterion of P<0.05 was used for all statistical comparisons. Data analysis was conducted using SPSS 30 software package

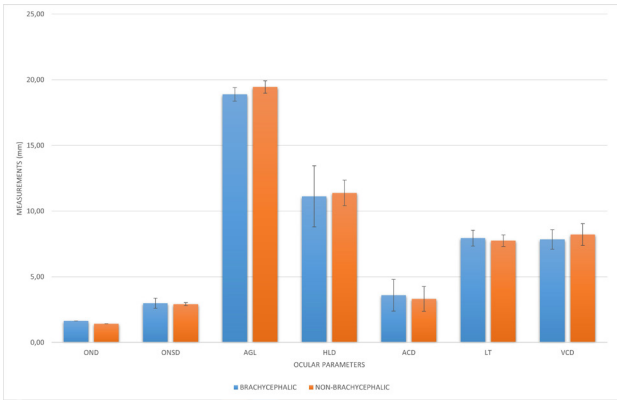

Fig 4. Comparison of ocular biometric parameters between brachycephalic and non-brachycephalic cats. Bars represent mean values, and error bars indicate the standard deviation (SD). OND, optic nerve diameter; ONSD, optic nerve sheath diameter; AGL, axial globe length; HLD, horizontal lens diameter; ACD, anterior chamber depth; LT, lens thickness; VCD, vitreous chamber depth. All measurements are expressed in millimeters. No statistically significant differences were observed between the two groups for any parameter (P>0.05)

Discussion

In feline medicine, biometric evaluation enables quantitative assessment of both anterior and posterior segment structures along the axial globe length. While both A-mode and B-mode ultrasonography are conventionally used to measure parameters such as corneal thickness, anterior chamber depth, lens thickness, equatorial lens diameter, vitreous chamber depth, and total axial length, B-mode remains the preferred modality for evaluating the posterior segment, including the retina-choroid-sclera complex [14].

Ultrasonographic studies have reported a positive association between eyeball length and age in cats, particularly during early developmental stages [11]. In the present study, no significant relationship was observed between age and the evaluated biometric parameters (P>0.05). This finding may be related to the predominance of adult cats in the study population, in which ocular

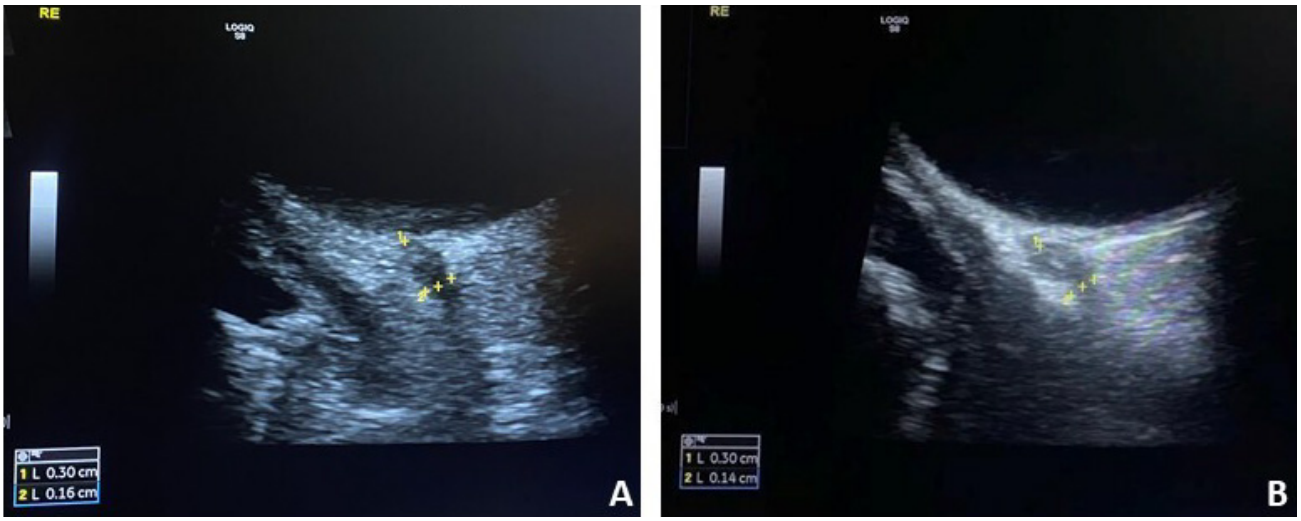

Fig 5. Representative B-mode ultrasonographic images of the optic nerve and optic nerve sheath in a brachycephalic **(A)** and a non-brachycephalic **(B)** cat. **(A)** A 3-year-old male British Shorthair, **(B)** a 4-year-old male mixed-breed cat. The optic nerve appears as a slender, slightly curved hypoechoic structure posterior to the globe, surrounded by retrobulbar adipose tissue and musculature. Calipers (+) indicate the site of optic nerve sheath diameter measurement

growth is likely already complete. Therefore, age-related biometric variation may have been less evident in this cohort. Overall, these results suggest that the observed differences in ocular biometry are more likely associated with craniofacial morphology rather than age-dependent physiological growth.

Ultrasonographic ocular biometric measurements play a crucial role in identifying anatomical differences across breeds. Previous studies have demonstrated a positive association between cranial dimensions and globe size, and have also highlighted the role of head type in shaping ocular morphology [7,11]. In particular, brachycephalic cats tend to exhibit wider globes than non-brachycephalic individuals [11]. Collectively, these findings suggest that variations in cranial morphology, body conformation, and ocular biometry may occur even within the same breed, underscoring the need for breed- and head-type–specific biometric evaluations and reference intervals to improve the early and accurate diagnosis of ocular diseases.

In the present study, although differences in ocular biometric parameters did not reach statistical significance, distinct morphological trends were observed between head types. Specifically, horizontal lens length tended to be lower in brachycephalic cats, whereas anterior chamber depth and lens thickness appeared higher, accompanied by a reduced vitreous chamber depth. These findings suggest that cranial conformation may be associated with globe morphology and the spatial arrangement of intraocular structures, although this interpretation should be considered in the context of the study's limitations. These findings suggest a relatively more compact orbital and intraocular configuration in brachycephalic cats.

Axial globe length and vitreous chamber depth were lower in brachycephalic cats than in non-brachycephalic cats, although these differences did not reach statistical significance. This trend may be related to the shallow orbital conformation characteristic of brachycephalic phenotypes, potentially affecting globe configuration along the sagittal axis. Previous studies across brachycephalic species have reported associations between craniofacial conformation, reduced orbital space, and alterations in posterior segment biometry, supporting the concept that head morphology plays a key role in shaping ocular dimensions [11,15,16]. These findings suggest that morphology-related anatomical variation may contribute to the biometric pattern observed in our cohort, although they should be interpreted within the context of the study's limitations.

Studies in dogs have demonstrated that head morphology, particularly in brachycephalic individuals, may affect the angle of the optic nerve within the orbit and the tension of the optic nerve sheath, with these anatomical variations representing important determinants of optic nerve sheath diameter (ONSD) measurements [10,13]. In contrast, data on the relationship between brachycephaly and optic nerve anatomy or ONSD in cats remain limited.

In the present study, optic nerve diameter (OND) tended to be higher in brachycephalic cats, whereas no statistically significant difference in ONSD was detected between the groups. Although brachycephalic cranial conformation could theoretically increase ONSD by reducing orbital volume and confining the optic nerve within a more restricted space, our findings do not support a clear effect in this regard. This may indicate that ONSD is maintained within relatively stable physiological limits despite variations in head morphology, or that ultrasonographic assessment may lack the sensitivity to detect subtle structural differences. Consequently, the extent to which ONSD reflects craniofacial conformation in brachycephalic cats warrants further investigation using larger cohorts and advanced imaging modalities.

The sigmoid structure of the optic nerve in dogs and cats, together with the plexiform arrangement of cilioretinal arteries, renders the optic nerve head anatomically heterogeneous [17]. In cats, retinal veins do not converge centrally within the optic nerve head but instead course parallel to the arteries and exit laterally, further complicating the clear delineation of optic disc boundaries. These species-specific anatomical features may affect ultrasonographic OND and ONSD measurements by limiting the identification of consistent anatomical landmarks [10]. Therefore, the absence of a measurable ONSD difference associated with head morphology in brachycephalic cats may reflect both true morphological similarity and the limited sensitivity of ultrasonographic assessment in detecting subtle structural variations.

As this was a retrospective study, the sample size was determined by the number of eligible cases identified during the study period, which limited the number of animals available for inclusion. As a result, an a priori power analysis could not be performed, and the study may have been underpowered to detect small differences between groups. In addition, the single-center design and the unequal distribution of breeds and sexes should be taken into account when interpreting the generalizability of the results. It is also worth noting that the brachycephalic group consisted mainly of British Shorthair and Scottish Fold cats. Although both breeds are generally classified as brachycephalic in the veterinary literature, their craniofacial conformation is less pronounced than that of some other brachycephalic breeds. Therefore, further studies including cats with more marked brachycephalic features would be useful to better assess the generalizability of the present findings.

In conclusion, the ocular biometric measurements obtained in this study addresses an existing gap in the literature regarding the ultrasonographic characterization of the optic nerve and nerve sheath diameter in cats. The concentration of existing research primarily on dogs and large animal species has left species-specific normative data for cats relatively limited. The data derived from our study contribute to a better understanding of optic nerve morphology in brachycephalic cats, aiming to enhance the accuracy of diagnostic interpretations in critical clinical evaluations such as intracranial hypertension. These standardized ultrasonographic measurements performed on healthy cats underscore the importance of developing head-type-specific reference intervals and provide a robust morphological foundation for future clinical and diagnostic research.

Declarations

Availability of Data and Materials: The data that support the findings of this study are available on request from the corresponding author (İE).

Acknowledgements: The authors would like to thank Ali Alparslan Sayım, Research Assistant at the Department of Biostatistics, Faculty of Veterinary Medicine, Ankara University, for his valuable assistance with the statistical analyses performed in this study.

Financial Support: This research received no specific grant from any funding agency in the public, commercial, or not-for-profit sectors.

Ethical Statement: This study was reviewed by the Ankara University Local Ethics Committee for Animal Experiments (Decision date: 18.02.2026; Decision number: 2026-04-44).

Competing Interest: The authors declare that there is no conflict of interest.

Declaration of Generative Artificial Intelligence (AI): **The authors** declare that the article, tables and figures were not written/created by AI and AI-assisted Technologies.

Authors' Contributions: YS: Conceptualization, data curation, methodology, writing-original draft. BT: Data curation, formal analysis, writing-review and editing. İE: Investigation, writing-review and editing, supervision.

References

1. **Schmidt MJ, Kampschulte M, Enderlein S, Gorgas D, Lang J, Ludewig E, Fischer A, Meyer-Lindenberg A, Schaubmar AR, Failing K, Ondreka N:** The relationship between brachycephalic head features in modern Persian cats and dysmorphologies of the skull and internal hydrocephalus. *J Vet Intern Med*, 31 (5): 1487-1501, 2017. DOI: 10.1111/jvim.14805
2. **Ergin I, Akçay A, Sainkaplan S, Şenel OO:** Risk factors associated with prolapsed nictitating membrane gland in cats with conjunctivitis: Analysis of 65 cases. *Kafkas Univ Vet Fak Derg*, 31 (4): 539-546, 2025. DOI: 10.9775/kvfd.2025.34201
3. **Ergin I, Sainkaplan S, Uygur A, Şenel OO:** The effects of breed, gender and environmental factors on feline entropion: A retrospective cohort study of 272 eyes. *Kafkas Univ Vet Fak Derg*, 31 (2): 189-196, 2025. DOI: 10.9775/kvfd.2024.31822
4. **Künzel W, Breit S, Oppel M:** Morphometric investigations of breed-specific features in feline skulls and considerations on their functional implications. *Anat Histol Embryol,* 32 (4): 218-225, 2003. DOI: 10.1046/j.1439-0264.2003.00448.x
5. **Schlueter C, Budras KD, Ludewig E, Mayrhofer E, Koenig HE, Walter A, Oechtering GU:** Brachycephalic feline noses: CT and anatomical study of the relationship between head conformation and the nasolacrimal drainage system. *J Feline Med Surg,* 11 (11): 891-900, 2009. DOI: 10.1016/j.jfms.2009.09.010
6. **Cho J:** Ocular ultrasound abnormalities and optic nerve sheath diameter in dogs and cats. *Vet Clin North Am Small Anim Pract,* 51 (6): 1295-1314, 2021. DOI: 10.1016/j.cvsm.2021.07.010
7. **Mirshahi A, Shafigh SH, Azizzadeh M:** Ultrasonographic biometry of the normal eye of the Persian cat. *Aust Vet J,* 92 (7): 246-249, 2014. DOI: 10.1111/avj.12189
8. **Chiwitt CLH, Baines SJ, Mahoney P, Tanner A, Heinrich CL, Rhodes M, Featherstone HJ:** Ocular biometry by computed tomography in different dog breeds. *Vet Ophthalmol,* 20 (5): 411-419, 2017. DOI: 10.1111/vop.12441
9. **Soldatos T, Karakitsos D, Chatzimichail K, Papathanasiou M, Gouliamos A, Karabinis A:** Optic nerve sonography in the diagnosis of increased intracranial pressure. *Crit Care,* 12 (3):R67, 2008. DOI: 10.1186/cc6922
10. **Evangelisti MA, Carta G, Burrai GP, Pinna Parpaglia ML, Cubeddu F, Ballocco I, Puggioni A, Manunta ML:** Repeatability of ultrasound examination of the optic nerve sheath diameter in the adult cat: Comparison between healthy cats and cats suffering from presumed intracranial hypertension. *J Feline Med Surg,* 22 (10): 959-965, 2020. DOI: 10.1177/1098612X19898006
11. **Yuwatanakorn K, Thanaboonnipat C, Tuntivanich N, Darawiroj D, Choisunirachon N:** Comparison of computed tomographic ocular biometry in brachycephalic and non-brachycephalic cats. *Vet World,* 14 (3): 727-733, 2021. DOI: 10.14202/vetworld.2021.727-733
12. **Hansen HC, Helmke K:** The subarachnoid space surrounding the optic nerve: An ultrasound study of the optic nerve sheath. *Neuroradiology,* 38 (6): 559-564, 1996. DOI: 10.1007/BF00626023
13. **Geeraerts T, Launey Y, Martin L, Pottecher J, Vigué B, Duranteau J, Benhamou D:** Ultrasonography of the optic nerve sheath diameter for detection of raised intracranial pressure: A systematic review and meta-analysis. *Intensive Care Med,* 33 (10): 1704-1711, 2007. DOI: 10.1007/s00134-011-2224-2
14. **Williams DL:** Ocular disease in cats. *J Feline Med Surg,* 6 (1): 1-13, 2004.
15. **Özkan E, Pazvant G, Kaya DA, Uğur S, Akçasız ZN, Yalın EE, Karabağlı M, Kurt T:** Computed tomography-based evaluation of skull measurements and eye biometrics in brachycephalic vs. non-brachycephalic cats. *Pak Vet J,* 44 (3): 910-916, 2024. DOI: 10.29261/pakvetj/2024.238
16. **Rujirekasuwan N, Sattasathuchana P, Theerapan W, Thengchaisri N:** Comparative analysis of ocular biometry, ocular protrusion, and palpebral fissure dimensions in brachycephalic and nonbrachycephalic dog breeds. *Vet Radiol Ultrasound,* 65: 437-446, 2024. DOI: 10.1111/vru.13351
17. **Samuelson DA:** Ophthalmic Anatomy. **In,** Gelatt KN (Ed): Veterinary Ophthalmology. 4th ed., 37-148, Blackwell Publishing, Iowa, 2007.

Kafkas Universitesi Veteriner Fakultesi Dergisi
Journal Home-Page: http://vetdergikafkas.org
E-ISSN: 1309-2251

Kafkas Univ Vet Fak Derg
32 (4): 557-567, 2026
DOI: 10.9775/kvfd.2026.36861

Research Article

Thiol-Disulfide Homeostasis and Selected Biomarkers in Neonatal Calves with Rotavirus-Coronavirus Coinfection-Associated Diarrhea and Sepsis: Association with Colostrum Intake Status

Mert SEZER [1] (*), Yusuf Umut BATI [1], Mustafa MAKAV [2], Enes AKYÜZ [1], Nazlıcan YERLİ [1], Kübra KAYA [2], Gürbüz GÖKCE [1], Mushap KURU [3]

[1] Kafkas University, Faculty of Veterinary Medicine, Department of Internal Medicine, TR-36100 Kars - TÜRKİYE
[2] Kafkas University, Faculty of Veterinary Medicine, Department of Physiology, TR-36100 Kars - TÜRKİYE
[3] Kafkas University, Faculty of Veterinary Medicine, Department of Obstetrics and Gynecology, TR-36100 Kars - TÜRKİYE

Abstract

This study included 20 Simmental calves (7-15 days old) presented with diarrhea and 10 healthy age- and breed-matched controls. Following clinical examination, mental status, dehydration score, respiratory rate, heart rate, and rectal temperature were recorded. Fecal samples were collected from diarrheic calves meeting sepsis criteria; calves positive for both rotavirus and coronavirus on a rapid immunochromatographic test were enrolled. The calves were hospitalized, treated, and monitored for 3 days. Blood samples were collected and clinical examinations were repeated before treatment (0 h) and during treatment (12, 24, 48, and 72 h). In septic calves, serum levels of reduced glutathione (GSH), total thiol (TT), native thiol (NT), endothelin-1 (ET-1), free triiodothyronine (fT3), free thyroxine (fT4), and insulin-like growth factor-1 (IGF-1), which were low before treatment, increased during therapy. Conversely, respiratory and heart rates and the levels of malondialdehyde (MDA), disulfide, and cortisol, which were high before treatment, decreased during therapy. Based on history, septic calves were further categorized as colostrum-fed or non-colostrum-fed, and group effects, time effects, and group x time interactions were evaluated. Among the evaluated parameters, MDA, IGF-1, and IgG showed the most pronounced group- and time-related differences. In conclusion, assessment of serum GSH, TT, NT, ET-1, fT3, fT4, IGF-1, MDA, disulfide, and cortisol (reflecting oxidative stress, endocrine response, and thiol-disulfide homeostasis) may contribute to the characterization and monitoring of systemic inflammatory, oxidative, endocrine, and immune alterations in neonatal calves with rotavirus-coronavirus coinfection-associated diarrhea and sepsis.

Keywords: Calf, Hormones, Immunoglobulin G (Ig-G), Neonatal period, Sepsis, Thiol-disulfide homeostasis

(*) **Corresponding author:**
Mert Sezer
Phone: +90 474 242 68 39-5201
Cellular phone: +90 538 605 91 70
Fax: +90 474 242 68 39
E-mail: sezermert100@gmail.com

How to cite this article?

Sezer M, Batı YU, Makav M, Akyüz E, Yerli N, Kaya K, Gökce G, Kuru M: Thiol-Disulfide Homeostasis and Selected Biomarkers in Neonatal Calves with Rotavirus-Coronavirus Coinfection-Associated Diarrhea and Sepsis: Association with Colostrum Intake Status. *Kafkas Univ Vet Fak Derg*, 32 (4): 557-567, 2026.
DOI: 10.9775/kvfd.2026.36861

Article ID: KVFD-2026-36861
Received: 18.04.2026
Accepted: 13.07.2026
Published Online: 14.07.2026

Introduction

Calves are considered a fundamental stage in the livestock industry. Since calf rearing is crucial for the sustainability of the meat and dairy industry, obtaining and preserving high-quality genetic material is essential. This, in turn, depends on good hygiene management and nutrition [1]. The neonatal period is defined as the first 28 days after birth. Diarrhea is among the most important health problems encountered during this time [2]. Diarrhea is a clinical sign characterized by an increased frequency of defecation accompanied by changes in fecal consistency and increased fecal volume, typically resulting from inflammation of the gastrointestinal tract [3]. Bovine rotavirus and coronavirus are among the major infectious agents implicated in the etiology of neonatal calf diarrhea [4,5]. In diarrheic neonatal calves, sepsis is one of the leading causes of mortality [6]. Sepsis is a life-threatening systemic response to infection characterized by dysregulated host responses and organ dysfunction [7].

Reactive oxygen species (ROS) generated as a consequence of metabolic activity are neutralized by antioxidant defenses [8]. When the balance between oxidants and antioxidants is disrupted, oxidative stress occurs. Oxidative stress is associated with lipid peroxidation, DNA damage, and disturbances in enzymatic reactions, which may ultimately lead to immunosuppression [9]. Malondialdehyde (MDA) and reduced glutathione (GSH) are commonly measured biomarkers for assessing oxidative stress [10,11]. MDA is a secondary end product of

lipid peroxidation of polyunsaturated fatty acids (including arachidonic acid) and reflects free radical-induced damage to cell membranes [12]. In contrast, GSH protects cells from oxidative injury by detoxifying peroxides and scavenging free radicals [13]. Thiol-containing compounds are also organic molecules that contribute to cellular protection against oxidative stress. Oxidative products generated during metabolic processes can oxidize thiol groups, leading to the formation of disulfide bonds. This reversible process is referred to as dynamic thiol-disulfide homeostasis. Inflammation and oxidative stress contribute to disruption of this balance [14].

Due to their placental structure, cows cannot transplacentally transfer macromolecular components such as IgG to their calves during the intrauterine period. Therefore, calves are born with almost completely underdeveloped immune systems. Immune components received through colostrum are of great importance in the survival of newborn calves. This form of immunity transferred from the mother to the newborn via colostrum is called passive immunity transfer [15]. The response of the host to pathogenic agents is referred to as the immune response. It comprises two major arms: innate and adaptive immunity. As part of adaptive immunity, antibodies (immunoglobulins) are produced. Immunoglobulin G (IgG) is one of the predominant immunoglobulin classes and accounts for approximately 70-80% of circulating immunoglobulins. It is produced by plasma cells in the spleen, lymph nodes, and bone marrow [16]. In calves, IgG constitutes approximately 90% of the immunoglobulins transferred to the neonate [17].

Thyroid hormones are synthesized in the follicles of the thyroid gland and play essential roles in multiple physiological processes. These include regulation of oxygen consumption, maintenance of basal metabolic rate, modulation of energy, protein, and lipid metabolism, and control of cellular differentiation and proliferation [18]. Thyroid hormone concentrations may change in disease states, and such alterations have been suggested to have prognostic value. Thyroid function is commonly assessed by measuring serum triiodothyronine and thyroxine concentrations [19,20].

Glucocorticoids play a key role in the physiological adaptation to stress and severe inflammatory conditions [21]. During stress and severe illness, activation of the hypothalamic-pituitary-adrenal (HPA) axis stimulates cortisol secretion [22,23]. Insulin-like growth factor-1 (IGF-1) is a 70-amino acid polypeptide hormone primarily synthesized in the liver. Circulating IGF-1 concentrations can vary in response to immune activation and inflammatory status [24].

Endothelin-1 (ET-1) is a 21-amino acid peptide produced and released by endothelial cells. It is a potent vasoconstrictor, and its circulating concentrations may change under inflammatory conditions [25].

Neonatal enteric sepsis is accompanied by coordinated disturbances in redox homeostasis, endothelial regulation, endocrine and metabolic adaptation, stress responses, and passive humoral immunity. Thiol-disulfide homeostasis, GSH, and MDA serve as complementary indicators of redox status; ET-1 reflects endothelial-vascular regulation; fT3, fT4, cortisol, and IGF-1 indicate endocrine, metabolic, and stress-related adaptation; and IgG reflects passive humoral immune status. Because colostrum provides immunoglobulins and bioactive constituents that support neonatal immune competence, intestinal maturation, and metabolic adaptation, colostrum intake status may be associated with the magnitude and temporal course of these systemic responses. We hypothesized that calves with rotavirus-coronavirus coinfection-associated diarrhea and sepsis would exhibit coordinated multisystem biomarker alterations relative to healthy calves, that these biomarkers would change during the 72 h treatment and monitoring period, and that their temporal trajectories would differ according to colostrum intake status. Accordingly, this study aimed to compare the selected biomarkers between septic and healthy neonatal calves, characterize their longitudinal changes over 72 h, and evaluate whether their temporal patterns were associated with colostrum intake status.

Material and Methods

Ethical Approval

The study was conducted after approval was obtained from the Kafkas University Animal Experiments Local Ethics Committee (KAÜ-HADYEK/2025-009).

Animal Material

The study population consisted of 20 Simmental calves aged 7-15 days with diarrhea. All 20 diarrheic calves tested concurrently positive for both rotavirus and coronavirus. The Control group consisted of 10 clinically healthy, age and breed-matched calves.

Clinical Examination and Pathogen Detection

Clinical examinations were performed to record mental status, dehydration score, respiratory rate, heart rate, and rectal temperature. Fecal samples were obtained from calves that met the sepsis criteria *(Table 1)* and were tested according to the manufacturer's instructions using a rapid antigen test kit (BoviD-5 Ag Test Kit®; Bionote Inc., Korea). Diarrheic calves positive for both rotavirus and coronavirus were included. Calves meeting the sepsis criteria were subsequently hospitalized and treated. Blood samples were collected and clinical examinations were repeated at predefined time points (0, 12, 24, 48, and 72 h).

Table 1. The presence of at least two of the following criteria was considered sufficient for the diagnosis of sepsis

Parameters	Criteria
Total leukocyte count (x10^3/μL)	<5x10^3/μL or >12x10^3/μL
Respiratory rate (/min)	>45
Heart rate (/min)	<90 or >120
Band neutrophils (%)	>10%
Body temperature (°C)	>39.0 or <36.6

Treatment Protocol

Calves meeting the sepsis criteria were hospitalized in individual stalls and monitored for 72 h. During hospitalization, routine nursing care and feeding were provided, and treatment was administered as follows. Based on the degree of dehydration, intravenous fluid therapy consisted of 0.9% sodium chloride (PVC®, 1000 mL; Eczacıbaşı Baxter, Istanbul, Türkiye), 1.3% sodium bicarbonate (Bikarvil®; Vilsan, Ankara, Türkiye), and 5% dextrose (Polifleks®; Polifarma, Tekirdağ, Türkiye). Because blood gas analysis was not available, the sodium bicarbonate requirement was estimated using a pragmatic base-deficit calculation described by Gökce [26]. For antimicrobial therapy, enrofloxacin was administered parenterally at 2.5-5 mg/kg (Baytril® 10%; Bayer, Germany). In addition, sulfadoxine-trimethoprim was administered intravenously at 5 mL/40 kg body weight for 3 days (Animar®; Ceva, France). An oral powder containing sulfadimidine and oxytetracycline was administered for 3 days at 2.5 g/40 kg body weight (Tetramezathine®; Ceva, France). Supportive therapy included a parenteral B-complex vitamin preparation for 3 days at 8-10 mL/calf (Berovit B_{12}®; Ceva, France), vitamin C at 4-6 mg/kg (Maxivit-C®; Bavet, Türkiye), vitamin AD_3E at 1 mL/50 kg (Ademin®; Ceva, France), and sodium selenite + vitamin E + vitamin B_1 at 2 mL/calf (Yeldif®; Ceva, France). To control inflammation, meloxicam was administered once at 0.5 mg/kg (Bavet Meloxicam®; Bavet, Türkiye). All sick calves recovered following treatment, and no deaths occurred during the 72 h monitoring period.

Collection of Blood Samples

Blood samples were obtained from diseased calves via jugular venipuncture before treatment (0 h) and during treatment (12, 24, 48, and 72 h); healthy calves were sampled once. Sampling was performed using a holder with compatible sterile needles (Vacuette®, Greiner Bio-One GmbH, Austria) and serum separator (gel) tubes (BD Vacutainer®, BD, UK). Samples were centrifuged at 3000 rpm for 10 min (Rotina 380R®; Hettich, Germany), and serum was aliquoted and stored at −20°C until analysis.

Analyses

Serum GSH, MDA, and thiol-disulfide homeostasis parameters were assessed. Total thiol (TT) and native thiol (NT) concentrations were measured spectrophotometrically according to Erel and Neselioglu [27]. Disulfide concentration and derived indices (disulfide/TT x 100, disulfide/NT × 100, and NT/TT x 100) were calculated from TT and NT values as previously described [28]. Reduced glutathione (GSH) was determined using the method of Beutler et al.[29], and malondialdehyde (MDA) was measured according to Yoshioka et al.[30].

Serum immunoglobulin G (IgG; mg/dL), free triiodothyronine (fT3; ng/L), free thyroxine (fT4; ng/dL), cortisol (μg/dL), and insulin-like growth factor-1 (IGF-1; ng/mL) concentrations were measured using a chemiluminescence method (Snibe Diagnostics®, China). Based on the medical history obtained, septic calves were classified according to colostrum intake status. Study parameters were compared between colostrum-fed and non-colostrum-fed calves, and the results are presented in *Table 2*, *Fig. 1* and *Fig. 2*.

Serum endothelin-1 concentrations were determined using a commercial bovine-specific ELISA kit (Bovine ET-1 ELISA Kit®; BT Lab, China) according to the manufacturer's instructions. Absorbance was read at 450 nm using a microplate reader (Thermo Scientific®, USA). ET-1 concentrations were calculated from the standard curve using regression analysis.

Statistical Analysis

The distributional properties of continuous variables were assessed using the Shapiro-Wilk test. The normality of data distribution was evaluated separately for each variable within each study group [healthy Control group (n = 10), overall Sepsis group (n = 20), colostrum-fed subgroup (n = 10), and non-colostrum-fed subgroup (n = 10)] and at each measurement time point (0, 12, 24, 48, and 72 h). All data are presented as mean ± standard deviation (SD). Statistical analyses were performed using GraphPad Prism (version 10; GraphPad Software, San Diego, CA, USA) and IBM SPSS Statistics (version 26.0; IBM Corp., Armonk, NY, USA). A two-sided P-value <0.05 was considered statistically significant for all analyses.

Blood samples from the healthy Control group were collected only once to provide baseline reference data. Therefore, this dataset was compared independently against each of the five sequential time points (0, 12, 24, 48, and 72 h) of the Sepsis group and its subgroups using independent comparisons. For normally distributed variables, an independent-samples t-test was used, and homogeneity of variances was assessed using Levene's

Table 2. *Main effects of colostrum intake (group), time, and the group × time interaction for the evaluated parameters within the Sepsis group (colostrum-fed vs. non-colostrum-fed calves)*

Parameters	Colostrum Status	Sepsis				
		0 h	12 h	24 h	48 h	72 h
GSH (mg/dL)	C (+)	4.86±0.65	5.02±0.67	4.98±0.61	5.57±1.48	5.97±1.58
	C (-)	3.33±0.27	3.94±0.98	4.58±0.86	4.12±0.70	4.70±1.38
MDA (µmol/L)	C (+)	2.06±0.52^{a**}	1.69±0.51^{ab***}	1.40±0.32^{ab***}	1.30±0.07^{b}	1.27±0.10^{b}
	C (-)	2.69±0.79^{a}	2.95±0.60^{a}	2.87±0.51^{a}	1.57±0.47^{b}	1.28±0.06^{b}
TT (µmol/L)	C (+)	624.59±47.50	668.02±62.78	683.44±61.85	692.37±46.17	765.42±69.97
	C (-)	504.08±25.33	561.50±60.71	572.36±60.79	603.43±29.18	602.51±47.67
NT (µmol/L)	C (+)	207.64±61.94	306.95±107.24	320.75±53.27	302.52±47.19	513.11±120.65
	C (-)	156.15±43.97	221.84±75.82	236.61±31.85	237.60±33.60	313.79±80.63
Disulfide (µmol/L)	C (+)	208.47±29.95	180.53±29.21	181.34±26.20	194.92±29.80	126.15±29.53
	C (-)	173.96±17.32	169.82±20.80	167.87±25.32	182.91±24.83	144.35±30.39
Disulfide/NT (%)	C (+)	111.21±43.14	72.23±50.76	58.29±13.90	66.70±17.53	26.91±11.68
	C (-)	123.96±55.25	91.16±51.35	71.86±13.21	79.27±20.65	50.73±22.71
Disulfide/TT (%)	C (+)	33.44±4.59	27.42±6.18	26.56±3.13	28.11±3.60	16.83±5.01
	C (-)	34.59±3.88	30.60±5.54	29.26±2.42	30.24±3.08	24.12±5.60
NT/TT (%)	C (+)	33.12±9.17	45.16±12.35	46.88±6.27	43.78±7.21	66.34±10.02
	C (-)	30.81±7.76	38.79±11.08	41.48±4.83	39.51±6.16	51.76±11.21
Endothelin-1 (pg/mL)	C (+)	54.42±6.04	54.91±10.45	59.04±7.39	64.28±5.72	67.20±12.91
	C (-)	40.64±9.90	44.25±8.11	46.07±3.73	53.05±6.66	54.34±1.54
fT_3 (ng/L)	C (+)	5.96±2.12	5.64±1.60	6.12±2.35	6.40±1.46	8.83±3.03
	C (-)	3.78±2.29	4.42±0.65	5.29±2.05	5.05±1.95	8.58±3.23
fT_4 (ng/dL)	C (+)	1.45±0.35	1.61±0.42	1.48±0.50	1.54±0.33	2.07±0.48
	C (-)	1.36±0.38	2.02±0.59	1.65±0.33	1.87±0.51	1.94±0.38
IGF-1 (ng/mL)	C (+)	296.50±14.41^{a**}	285.88±7.85^{ab**}	291.63±21.23^{ab***}	325.25±30.57^{c***}	335.75±42.84^{c*}
	C (-)	253.43±21.52^{a}	244.71±23.82^{a}	222.71±26.34^{b}	258.14±14.42^{a}	299.14±44.07^{c}
IgG (mg/dL)	C (+)	723±36.80^{a**}	711.75±23.41^{a**}	693±117.19^{a***}	722.63±77.54^{a***}	831.38±107.74^{b***}
	C (-)	609.14±73.10^{a}	581±72.48^{a}	513±16.15^{b}	516.57±81.67^{b}	634±86.49^{a}
Cortisol (µg/dL)	C (+)	4.25±1.53	4.16±1.77	4.02±2.07	4.71±2.15	2.01±0.58
	C (-)	7.53±4.67	7.84±4.52	6.53±2.69	5.14±2.49	3.68±1.62

GSH: *Reduced glutathione,* ***MDA:*** *Malondialdehyde,* ***TT:*** *Total thiol,* ***NT:*** *Native thiol,* ***fT3:*** *Free triiodothyronine,* ***fT4:*** *Free thyroxine,* ***IGF-1:*** *Insulin-like growth factor-1,* ***IgG:*** *Immunoglobulin G,* ***C (+):*** *Colostrum-fed,* ***C (–):*** *Non-colostrum-fed. Significance notation: *P<0.05, **P<0.01, ***P<0.001. Asterisks indicate significant differences between C (+) and C (–) at the same sampling time point (pairwise comparisons). Different lowercase letters* ***(a–c)*** *indicate significant differences among time points within the Sepsis group*

test (Welch's t-test was applied when the homogeneity assumption was violated). For variables that did not meet the normality assumption, between-group comparisons were performed using the Mann-Whitney U test.

To evaluate longitudinal (temporal) changes within the overall Sepsis group, repeated-measures analyses were performed on blood parameters measured sequentially in the same calves at 0, 12, 24, 48, and 72 h. For variables meeting parametric assumptions, a one-way repeated-measures ANOVA was performed, and the assumption of sphericity was evaluated using Mauchly's test; in cases of sphericity violation, degrees of freedom were corrected using the Greenhouse-Geisser correction. When a significant main effect of time was detected, Bonferroni-adjusted post-hoc multiple comparison tests were used to identify specific differences between time points. Temporal changes for parameters failing to meet normality assumptions were analyzed using the Friedman test, followed by post-hoc pairwise comparisons using Bonferroni-adjusted Wilcoxon signed-rank tests. Because all calves had complete repeated measurements at identical time points without missing observations, RM-ANOVA was considered an appropriate analytical approach for longitudinal analyses.

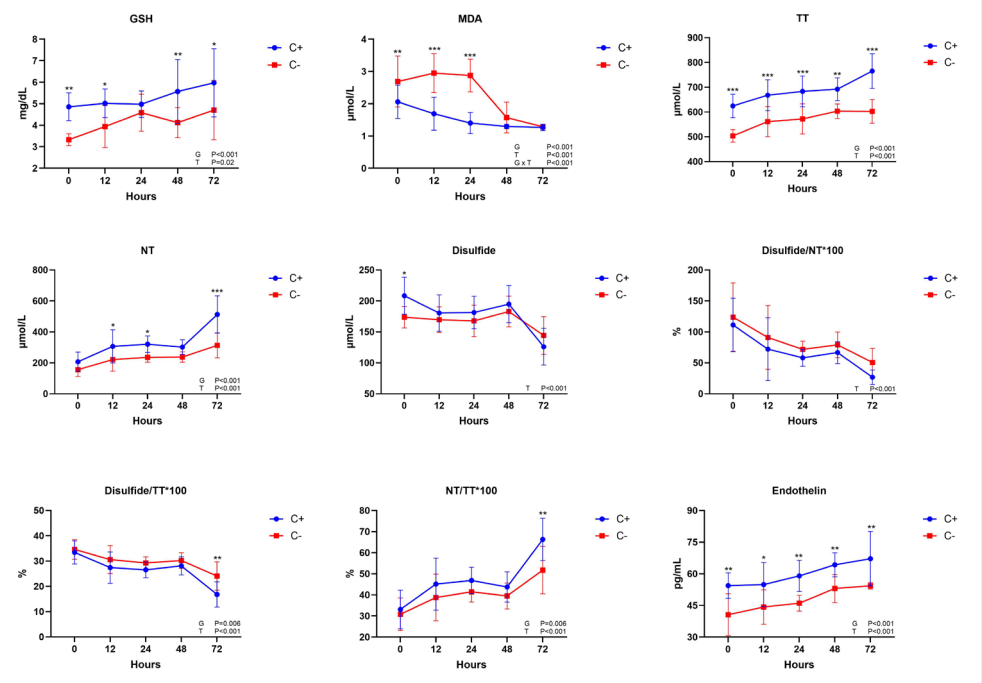

Fig 1. Longitudinal changes and time-course comparison of oxidative stress parameters, thiol-disulfide homeostasis variables, and endothelin-1 between colostrum-fed (C+) and non-colostrum-fed (C-) neonatal calves with sepsis secondary to rotavirus and coronavirus-associated diarrhea. The panels display reduced glutathione (GSH), malondialdehyde (MDA), total thiol (TT), native thiol (NT), disulfide, disulfide/NT ratio, disulfide/TT ratio, NT/TT ratio, and endothelin-1. Data are presented as mean ± standard deviation (SD). Asterisks (* P<0.05, ** P<0.01, *** P<0.001) indicate significant differences between the C+ and C- groups at the same sampling time point based on independent pairwise comparisons. G: Main effect of colostrum status (group); T: Main effect of time; G × T: Group × Time interaction effect determined by two-way mixed repeated-measures ANOVA

Additionally, a two-way mixed repeated-measures ANOVA was conducted to evaluate the longitudinal effects of colostrum-feeding status (colostrum-fed vs. non-colostrum-fed), time, and their interaction (group x time) on the measured parameters within the Sepsis group. In this model, colostrum-feeding status was designated as the between-subjects factor, while time was defined as the within-subjects repeated factor. When significant main effects or group x time

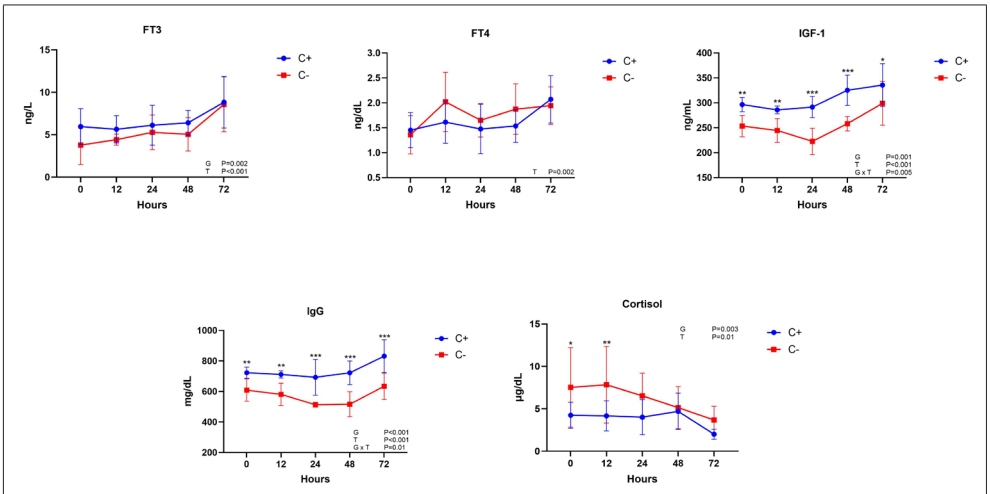

Fig 2. Longitudinal changes and time-course comparison of hormonal and immunological parameters between colostrum-fed (C+) and non-colostrum-fed (C-) neonatal calves with sepsis secondary to rotavirus and coronavirus-associated diarrhea. The panels display free triiodothyronine (FT3), free thyroxine (FT4), insulin-like growth factor-1 (IGF-1), immunoglobulin G (IgG), and cortisol. Data are presented as mean ± standard deviation (SD). Asterisks (*: P<0.05, **: P<0.01, ***: P<0.001) indicate significant differences between the C+ and C- groups at the same sampling time point based on independent pairwise comparisons. G: Main effect of colostrum-feeding status (group); T: Main effect of time; G × T: Group × Time interaction effect determined by two-way mixed repeated-measures ANOVA

interactions were detected, post-hoc multiple comparisons were completed using Bonferroni-adjusted tests.

Correlation analyses were conducted to evaluate associations among clinical, oxidative stress, hormonal, and immunological parameters. Pearson's correlation coefficient was used for normally distributed variables, whereas Spearman's rank correlation coefficient was used for non-normally distributed variables.

Results

Clinical Findings

Clinical examination of septic calves revealed severe enteritis and marked dehydration (10-12%), accompanied by enophthalmos, decreased skin turgor, weakness, severe depression, lateral recumbency, and absence of the suckling reflex.

Vital Findings

In the Sepsis group, respiratory rate at 0 h (pre-treatment) was higher than at subsequent time points. Between-group comparisons showed that respiratory rate at 0, 12, and 24 h was higher in the Sepsis group than in the Control group. Within the Sepsis group, heart rate at 0 h was higher than at 48 and 72 h; moreover, heart rate was higher in the Sepsis group than in the Control group at all assessed time points (0, 12, 24, 48, and 72 h). Rectal temperature at 0 h was lower in the Sepsis group than in the Control group *(Table 3)*.

Biochemical Findings

Effects of colostrum intake, time, and their interaction are summarized in *Table 2*. For GSH, TT, NT, ET-1, fT3, and cortisol, significant main effects of colostrum intake and time were observed, whereas the colostrum × time interaction was not significant. For fT4, disulfide, and disulfide/NT, only the main effect of time was significant. Similarly, for NT/TT, significant main effects of colostrum intake and time were detected, with no significant interaction.

For IGF-1 and IgG, significant main effects of colostrum intake and time were observed, and the colostrum × time interaction was also significant *(Table 2)*. Post hoc analyses indicated that IGF-1 differed between the Sepsis and Control groups at all assessed time points (0, 12, 24, 48, and 72 h). Within the sepsis subgroups, IGF-1 in colostrum-fed calves at 0 h differed from values at 48 and 72 h. In non-colostrum-fed calves, IGF-1 at 0, 12, and 48 h was higher than at 24 h and lower than at 72 h.

Table 3. *Within-group comparisons across time points in the Sepsis group and between-group pairwise comparisons of the Sepsis and Control groups at corresponding time points*

Parameters	Sepsis					Control
	0 h	12 h	24 h	48 h	72 h	
Respiratory rate (/min)	44.93±18.87^{Aa}	33.23±7.70^{Ab}	28.93±7.48^{Ab}	27.07±6.32^{Bb}	26.80±8.74^{Bb}	22.93±5.12^{B}
Heart rate (/min)	141.73±18.16^{Aa}	132.53±23.12^{Aab}	127.73±11.63^{Aab}	122.40±13.82^{Ab}	121.33±17.95^{Ab}	99.33±6.26^{B}
Rectal temperature (°C)	37.04±2.34^{A}	38±0.75^{B}	37.89±1.14^{B}	38.21±0.86^{B}	38.72±0.67^{B}	38.37±0.30^{B}
GSH (mg/dL)	4.15±0.93^{Ab}	4.51±0.97^{Aab}	4.79±0.74^{Aab}	4.89±1.37^{Aab}	5.38±1.58^{ABa}	6.28±1.30^{B}
MDA (µmol/L)	2.35±0.71^{Aa}	2.28±0.84^{Aa}	2.09±0.86^{Aa}	1.42±0.35^{ABb}	1.27±0.08^{ABb}	1.20±0.32^{B}
TT (µmol/L)	568.35±72.64^{Ab}	618.31±81.09^{Aab}	631.60±82.38^{Aab}	650.87±59.50^{Aab}	689.39±102.47^{Aa}	986.62±202.67^{B}
NT (µmol/L)	183.61±58.77^{Ac}	267.23±100.72^{Abc}	281.48±61.17^{Ab}	272.22±52.16^{Abc}	420.09±143.73^{Aa}	788.39±205.62^{B}
Disulfide (µmol/L)	192.37±29.91^{Aa}	175.54±25.36^{Aa}	175.06±25.82^{Aa}	189.32±27.33^{Aa}	134.65±30.34^{Ab}	99.12±26.64^{B}
Disulfide/NT (%)	117.16±47.77^{Aa}	81.06±50.14^{Ab}	64.62±14.85^{Abc}	72.57±19.46^{Abc}	38.02±20.99^{Ac}	13.52±5.6^{4B}
Disulfide/TT (%)	33.98±4.16^{Aa}	28.91±5.91^{Ab}	27.82±3.06^{Ab}	29.10±3.43A^{ab}	20.23±6.34^{Ac}	10.35±3.46^{B}
NT/TT (%)	32.04±8.32^{Ac}	42.19±11.82^{Ab}	44.36±6.12^{Ab}	41.79±6.86^{Abc}	59.54±12.68^{Aa}	79.29±6.92^{B}
Endothelin-1 (pg/mL)	46.16±10.26^{Ab}	51.77±10.20^{Aab}	52.98±8.84^{Aab}	59.04±8.31^{Aa}	61.19±11.34^{ABa}	72.04±20.25^{B}
fT_3 (ng/L)	4.94±2.40^{Ab}	5.07±1.37 ^{Ab}	5.73±2.18 ^{Ab}	5.77±1.78 ^{Ab}	8.71±3.02^{ABa}	11.17±3.9^{4B}
fT_4 (ng/dL)	1.41±0.36^{Ab}	1.80±0.53^{Aab}	1.56±0.42^{Ab}	1.69±0.44^{Aab}	2.01±0.42^{Aa}	2.66±0.74^{B}
IGF-1 (ng/mL)	276.40±28.23^{Ab}	266.67±26.94^{Ab}	259.47±42.30^{Ab}	293.93±41.92^{Aab}	318.67±45.90^{ABa}	325.80±35.47^{B}
IgG (mg/dL)	669.87±80.15^{Aab}	650.73±84.17^{Aab}	609±124.98^{Ab}	626.47±131.10^{Aab}	739.27±139.28^{ABa}	823.93±128.73^{B}
Cortisol (µg/dL)	5.78±3.66^{Aa}	5.88±3.73^{Aa}	5.19±2.63^{Aab}	4.91±2.24^{Aab}	2.79±1.43^{ABb}	2.02±0.77^{B}

GSH: *Reduced glutathione,* ***MDA:*** *Malondialdehyde,* ***TT:*** *Total thiol,* ***NT:*** *Native thiol,* ***fT3:*** *Free triiodothyronine,* ***fT4:*** *Free thyroxine,* ***IGF-1:*** *Insulin like growth factor-1,* ***IgG:*** *Immunoglobulin G. Different lowercase letters* ***(a–c)*** *indicate significant differences among time points within the Sepsis group. Different uppercase letters* ***(A–B)*** *indicate significant differences between each Sepsis time point and the Control group (pairwise comparisons)*

Table 4. Correlations among the parameters evaluated in the study

Parameters	GSH	MDA	TT	NT	Disulfide	ET-1	fT3	fT4	IGF-1	IgG
GSH										
MDA	-0.334**									
TT	0.283**	-0.352**								
NT	0.342**	-0.471**	0.866**							
Disulfide	-0.393**	0.424**	-0.387**	-0.735**						
ET-1	0.264*	-0.457**	0.251*	0.298**	-0.265*					
fT3	0.336**	-0.424**	0.419**	0.522**	-0.474**	0.199				
fT4	0.152	-0.250*	0.428**	0.498**	-0.425**	0.170	0.481**			
IGF-1	0.253*	-0.392**	0.217*	0.311**	-0.373**	0.191	0.459**	0.210*		
IgG	0.303**	-0.332**	0.276**	0.318**	-0.287**	0.238*	0.360**	0.191	0.314**	
Cortisol	-0.242*	0.376**	-0.490**	-0.502**	0.422**	-0.206	-0.296**	-0.239*	-0.194	-0.285**

***GSH:** Reduced glutathione, **MDA:** Malondialdehyde, **TT:** Total thiol, **NT:** Native thiol, **fT3:** Free triiodothyronine, **fT4:** Free thyroxine, **IGF-1:** Insulin-like growth factor-1, **IgG:** Immunoglobulin G; ** Correlation is significant at the 0.01 level (2-tailed); * Correlation is significant at the 0.05 level (2-tailed)*

For IgG, significant differences compared with the control group were observed at all sampling time points. Within the sepsis subgroups, IgG in colostrum-fed calves at 0 h differed from 72 h, whereas in non-colostrum-fed calves, IgG at 0, 12, and 72 h was higher than at 24 and 48 h.

Correlations among the evaluated parameters are summarized in *Table 4*. Overall, the analysis suggested that thiol-disulfide homeostasis was closely associated with the hormonal response. GSH, TT, and NT were positively correlated with fT3, fT4, and IGF-1 and negatively correlated with disulfide. Conversely, disulfide showed significant negative correlations with fT3, fT4, and IGF-1 and a positive correlation with cortisol. Notably, the positive association between NT and fT3 and the strong negative association between NT and disulfide suggest that, in sepsis, shifts in redox balance occur in parallel with hormonal regulation.

Discussion

Diarrheic neonatal calves commonly exhibit lethargy/mental depression, tachycardia associated with reduced arterial pressure (often with a weak pulse), tachypnea, loss of the suckling reflex, enophthalmos, and decreased skin turgor [31]. In the present study, clinical findings in the Sepsis group were consistent with these reports. These signs likely reflect circulatory compromise secondary to diarrhea-induced fluid losses. Following treatment including fluid therapy with supportive medications (anti-inflammatory agents, antimicrobials, and vitamins) clinical status improved, and the initially elevated respiratory and heart rates in the Sepsis group declined toward control values.

Rotavirus and coronavirus are among the principal viral pathogens responsible for neonatal calf diarrhea. Coronavirus can cause marked injury to the gastrointestinal tract, particularly the intestinal villi, where it may induce epithelial alterations (including a shift from cuboidal to squamous morphology) and reduce the villus-to-crypt ratio, thereby substantially compromising absorptive capacity. Moreover, coronavirus may exacerbate diarrhea by impairing fluid absorption in the large intestine [31,32]. In contrast, rotavirus primarily targets the brush border of small-intestinal villous epithelial cells, leading to villous atrophy and compensatory crypt hyperplasia [31,33]. As a consequence, severe dehydration and electrolyte disturbances in diarrheic calves may promote oxidative stress and are associated with an increased risk of mortality [34].

Fu et al.[35] reported increased serum MDA concentrations in diarrheic calves accompanied by reduced antioxidant capacity, and Sağıroğlu et al.[34] similarly observed increased MDA together with decreased GSH. These alterations were attributed to oxidative injury associated with fluid electrolyte imbalance and metabolic acidosis. In calves with SIRS, also found elevated MDA levels, consistent with previous reports [36,37], and this has been linked to infectious inflammation driven release of proinflammatory cytokines that promote oxidative stress and lipid peroxidation. In addition, Terzi et al.[38] with Koçak and Duru [39] reported reductions in total thiol and native thiol levels in diarrheic calves, and Terzi et al. [38] further reported increased disulfide concentrations, supporting disruption of thiol-disulfide homeostasis under oxidative stress. In the present study, serum MDA and disulfide were elevated, whereas GSH, total thiol, and native thiol were reduced before treatment, consistent

with oxidative stress accompanying gastrointestinal injury and fluid electrolyte derangements. Following treatment, MDA and disulfide decreased and GSH, total thiol, and native thiol increased, suggesting partial restoration of redox balance in parallel with clinical stabilization.

Thyroxine (T4) and triiodothyronine (T3) are synthesized in thyroid follicles and regulate a wide range of physiological processes, including oxygen consumption, basal metabolic rate, macronutrient metabolism, and cellular differentiation and maturation [18]. In clinical settings, thyroid status is commonly assessed by measuring circulating free T3 (fT3) and free T4 (fT4), which represent the biologically available (unbound) fractions. Alterations in thyroid hormone concentrations have been reported in systemic illness, supporting their potential prognostic relevance [19,20]. In severe inflammatory conditions, decreases in fT3 and fT4 may occur and are commonly described as nonthyroidal illness syndrome [40]. Proposed mechanisms include reduced thyroid-stimulating hormone (TSH) secretion, anorexia-associated fasting, and impaired thyroid hormone binding and metabolism during systemic disease [41]. In severely dehydrated diarrheic calves, Hajimohammadi et al.[20] and Çorapsız and Birdane [42] reported decreased fT3 and fT4, which they attributed to endotoxemia- and cytokine-mediated disruption of thyroid function [43]. Cytokines can reduce peripheral conversion of T4 to T3 by suppressing pituitary TSH release and by impairing thyroxine 5′-deiodinase activity in thyroid and hepatic tissues [44]. Moreover, in acute severe illness such as sepsis, reductions in thyroxine-binding globulin (TBG) have been implicated in lower circulating free hormone concentrations [43]. In the present study, serum fT3 and fT4 were decreased in diarrheic neonatal calves before treatment and increased during therapy. These findings may reflect combined effects of disease severity (including reduced TSH secretion), anorexia-associated fasting, endotoxemia/cytokine-mediated alterations in thyroid function and deiodination, and changes in thyroid hormone binding proteins such as TBG.

In severe inflammatory disease, activation of the hypothalamic pituitary adrenal (HPA) axis increases adrenal glucocorticoid output. Hypothalamic stimulation of the pituitary promotes adrenocorticotropic hormone (ACTH) release, which in turn stimulates the adrenal cortex to secrete cortisol [22,23]. Cortisol exerts pleiotropic effects that are particularly relevant during systemic inflammation, including modulation of the inflammatory response, support of cardiovascular homeostasis through permissive effects on vascular tone and fluid balance, and regulation of intestinal barrier function [45,46]. In circulation, cortisol is largely bound and transported by corticosteroid-binding globulin, a liver-derived plasma protein [47]. In sepsis, increased ACTH and cortisol concentrations have been reported and are commonly attributed to cytokine-driven inflammatory stress [48]. Accordingly, monitoring adrenal axis hormones has been suggested to provide prognostic information in septic patients and in conditions characterized by marked stress and inflammation [21,45,49]. In the present study, serum cortisol concentrations were elevated in diarrheic calves before treatment and decreased during therapy. These changes may reflect attenuation of systemic stress and inflammation as dehydration and circulatory compromise improved with treatment.

Insulin-like growth factor-1 (IGF-1) is produced primarily by the liver, acts in concert with growth hormone, and contributes to growth and tissue development, including the maturation of the small intestine and skeletal muscle. During the neonatal period, IGF-1 is abundant in the intestinal epithelium and supports enterocyte proliferation and maturation. It has also been suggested to enhance barrier integrity during gastroenteritis, thereby limiting the effects of enteric pathogens and their toxins [50,51]. Colostrum contains substantial amounts of IGF-1 and IGF-binding proteins, which may support neonatal growth and gastrointestinal development [50]. In neonatal ruminants, circulating IGF-1 concentrations can fluctuate, and previous studies have reported a tendency for initially higher concentrations early in life to decline over time. Malabsorption, maldigestion, and endotoxemia have been proposed as contributing factors to reduced IGF-1 concentrations [52,53]. Decreased IGF-1 has also been reported in sepsis, potentially reflecting intestinal barrier dysfunction and systemic inflammation. An increased intestinal bacterial load may promote epithelial apoptosis and facilitate bacterial translocation to mesenteric lymph nodes, the liver, and the bloodstream. In addition, mucosal permeability increases during systemic illness, and both inflammatory activation and hypoperfusion can further compromise barrier integrity, which has been associated with reductions in IGF-1 [54]. In the present study, serum IGF-1 concentrations were lower in diarrheic septic calves with rotavirus/coronavirus infection than in controls. This decrease may be attributable to multiple concurrent factors, including insufficient colostrum intake in a subset of calves,

impaired hepatic synthetic capacity during systemic illness, and inflammation-associated increases in intestinal permeability with secondary effects on gut bacterial burden. Furthermore, virus-induced gastrointestinal injury with malabsorption, together with dehydration-related circulatory compromise, may have contributed to the observed reduction in serum IGF-1.

Immunoglobulins (Ig), which are abundant in colostrum, are antibody proteins produced primarily by B lymphocytes. Their principal functions are to recognize and bind antigens such as bacteria, viruses, and other potentially harmful foreign substances and to facilitate their neutralization or clearance [55]. Immunoglobulin G (IgG) is a predominant immunoglobulin isotype and plays a pivotal role in host defense against invading pathogens. IgG mediates protection by engaging Fc receptor bearing innate immune effector cells and by activating the complement cascade [56,57]. In the present study, IgG concentrations were lower in diarrheic septic calves that did not receive colostrum than in those that received colostrum, most likely reflecting absent and/or inadequate colostrum intake.

During sepsis, reactive oxygen species (ROS) are generated by both the vascular endothelium and activated inflammatory cells, including neutrophils and macrophages. Excessive ROS in the setting of insufficient antioxidant defenses can disrupt endothelial homeostasis, alter vascular tone, promote platelet and leukocyte aggregation, increase vascular permeability, and shift the hemostatic balance toward a procoagulant state collectively contributing to endothelial dysfunction [58]. Endothelin-1 (ET-1), a potent vasoconstrictor peptide, is produced primarily by vascular endothelial cells [59]. In the present study, ET-1 concentrations were lower than controls at early time points, and the difference appeared to attenuate by 72 h. These results suggest impaired endothelial function associated with sepsis-related oxidative stress, which could attenuate ET-1 production and/or release.

In conclusion, thiol-disulfide homeostasis, endothelin-1, IgG, and the selected endocrine and oxidative biomarkers exhibited temporal alterations during the 72-h treatment and monitoring period in neonatal calves with rotavirus- and coronavirus-associated diarrhea and sepsis. The longitudinal profiles of several parameters also varied according to colostrum intake status. Collectively, these findings suggest that the simultaneous evaluation of redox, endothelial, humoral immune, endocrine, metabolic, and stress-related biomarkers may contribute to a more comprehensive characterization and monitoring of the systemic response associated with neonatal enteric sepsis. However, given the observational design, history-based classification of colostrum intake, limited sample size, and absence of different clinical outcome groups, the findings should be interpreted cautiously. Further prospective studies involving larger populations and clearly defined clinical outcomes are required to establish the clinical monitoring utility and potential prognostic relevance of these biomarkers.

Declarations

Availability of Data and Materials: The data that support the findings of this study are available from the corresponding author (M.S.) upon reasonable request.

Financial Support: This research did not receive any specific grant from funding agencies in the public, commercial, or not-for-profit sectors.

Ethical Approval: The study was conducted after approval was obtained from the Kafkas University Animal Experiments Local Ethics Committee (KAÜ-HADYEK/2025-009).

Competing Interests: The authors declare that they have no competing interests.

Generative Artificial Intelligence (AI): The authors declare that no generative artificial intelligence (AI) was used in the preparation of this manuscript

Authors Contribution: MK and MS conceived and designed the study. MS, YUB, KK, NY, MM, and EA executed the experiment and analyzed the sera samples. MM, MK analyzed the data. All authors interpreted the data, critically revised the manuscript for important intellectual contents and approved the final version.

References

1. **Yousif HM, El Mahdy AM, Hassan MF, Mansour MK:** Overview on antioxidant and oxidative stress markers after garlic oil supplement in suckling buffalo calves. *Kafkas Univ Vet Fak Derg,* 30 (1): 73-80, 2024. DOI: 10.9775/kvfd.2023.30499
2. **Sedky D, Ghazy AA, Abou-Zeina HAA:** Advances in diagnosis of diseases causing diarrhea in newborn calves. *Vet Res Commun,* 49 (5):293, 2025. DOI: 10.1007/s11259-025-10855-0
3. **Özkan C, Akgül Y:** Neonatal ishalli buzağılarda hematolojik, biyokimyasal ve elektrokardiyografik bulgular. *YYÜ Vet Fak Derg,* 15 (1-2): 123-129, 2004.
4. **Ates O, Yesilbag K:** Molecular epidemiology of group A rotavirus (RVA) and bovine coronavirus (BCoV) associated with neonatal calf diarrhea in Türkiye. *Trop Anim Health Prod,* 58 (3):188, 2026. DOI: 10.1007/s11250-026-04985-z
5. **Cui S, Guo S, Zhao Q, Li Y, Ma Y, Yu Y:** Alterations of microbiota and metabolites in the feces of calves with diarrhea associated with rotavirus and coronavirus infections. *Front Microbiol,* 14:1159637, 2023. DOI: 10.3389/fmicb.2023.1159637
6. **Ekinci G, Tüfekçi E, Cissé Y, Bekdik İK, Onmaz AC, Aslan Ö, Güneş V, Çitil M, Keleş İ:** Chloride and lactate as prognostic indicators of calf diarrhea from eighty-nine cases. *J Vet Sci,* 25 (3):e38, 2024. DOI: 10.4142/jvs.23155
7. **Silverstein D, Otto CM:** Sepsis. **In,** Greene CE (Ed): Infectious Diseases of the Dog and Cat. 4th ed., 359-369, Saunders Elsevier, St. Louis, Missouri, USA, 2012.
8. **Zhang Z, Kang S, Ni M, Guo X, Dong H, Wu Q, Chang Z:** Potential application of *Rhododendron* flavonoids anti-inflammatory and antioxidant activities in animal health support and protection. *Kafkas Univ Vet Fak Derg,* 32 (2): 173-187, 2026. DOI: 10.9775/kvfd.2025.35766

9. **Çenesiz S:** The role of oxidant and antioxidant parameters in the infectious diseases: A systematic literature review. *Kafkas Univ Vet Fak Derg,* 26 (6): 849-858, 2020. DOI: 10.9775/kvfd.2020.24618
10. **Sezer M, Gezer T, Merhan O, Akyuz E, Bozukluhan K, Gokce G:** Evaluation of iron, iron binding capacity, transferrin, some oxidative stress markers and hematological parameters in foot and mouth disease in cattle. *Medit Vet J,* 9 (1): 224-229, 2024. DOI: 10.24880/meditvetj.1517834
11. **Tesena P, Vinijkumthorn R, Preuksathaporn T, Piyakul P, Chotikaprakal T, Sirireugwipas R, Wongaree K, Prapaiwan N:** Evaluation of gastrointestinal tract lesions and serum malondialdehyde levels after repeated oral administration of phenylbutazone in horses. *Vet Res Commun,* 48 (4): 2343-2355, 2024. DOI: 10.1007/s11259-024-10415-y
12. **Hajimohammadi A, Ghane M, Ghari Tehrani M, Paravar B, Mirzaei A, Razavi SA, Nikzad M:** Association of the severity of colic in horses with oxidative stress biomarkers, acute-phase proteins, and certain trace elements. *J Equine Sci,* 34 (3): 73-81, 2023. DOI: 10.1294/jes.34.73
13. **Uzun N:** The Analysis of glutathione level and superoxide dismutase activity in normal and preeclampsia pregnant. *EAJS,* 5 (1): 23-29, 2019.
14. **Ayral M, Toprak SF, Dedeoğlu S, Sabancılar İ, Temiz H:** Kronik otitis media'da tiyol-disülfid homeostazının değişikliği. *Dicle Med J,* 48 (1): 197-204. 2021.
15. **Kara E, Öcal N, Duru Ö, Yasa Duru S, Şenel Y:** Evaluation of colostral passive immune transfer success in Turkish Kangal shepherd dogs. *Kafkas Univ Vet Fak Derg,* 30 (1): 47-52, 2024. DOI: 10.9775/kvfd.2023.30363
16. **Yang C, Du M, Ahmad AA, Cheng Y, Gebeyew K:** Passive immunity establishment through colostral Igg absorption in neonatal ruminants: Foundation for efficient ruminant production. *Animals,* 15 (21): 3093, 2025. DOI: 10.3390/ani15213093
17. **Marnila P, Korhonen H:** Encyclopedia of Dairy Sciences. 1950-1956, Elsevier Science Ltd., London, 2002.
18. **Squires EJ:** Applied Animal Endocrinology. CABI Publishing, Trowbridge, UK, 2003.
19. **Mebis L, Van den Berghe G:** Thyroid axis function and dysfunction in critical illness. *Best Pract Res Clin Endocrinol Metabol,* 25 (5): 745-757, 2011. DOI: 10.1016/j.beem.2011.03.002
20. **Hajimohammadi A, Roshan-Ghasrodashti A, Forouzesh SM, Saeb M:** A survey on relationships between thyroid hormone levels and clinical findings in dairy calf diarrhea. *Vet Sci Dev,* 5, 61-63, 2015.
21. **De Castro R, Ruiz D, Lavın BA, Lamsfus JA, Vazquez L, Montalban C, Marcano G, Sarabia R, Paz-Zulueta M, Blanco C, Santibanez M:** Cortisol and adrenal androgens as independent predictors of mortality in septic patients. *PLoS ONE,* 14 (4):e0214312, 2019. DOI: 10.1371/journal.pone.0214312
22. **Andanson S, Boissy A, Veissier I:** Conditions for assessing cortisol in sheep: The total form in blood v. the free form in saliva. *Animal,* 14 (9): 1916-1922, 2020. DOI: 10.1017/S1751731120000695
23. **Arfuso F, Minuti A, Liotta L, Giannetto C, Trevisi E, Piccione G, Lopreiato V:** Stress and inflammatory response of cows and their calves during peripartum and early neonatal period. *Theriogenology,* 196, 157-166, 2023. DOI: 10.1016/j.theriogenology.2022.11.019
24. **Le Roith D, Bondy C, Yakar S, Liu JL, Butler A:** The somatomedin hypothesis. *Endocr Rev,* 22 (1): 53-74, 2001. DOI: 10.1210/edrv.22.1.0419
25. **Erdoğan H, Fadıllıoğlu E, Emre M:** Endotelinler: Vazoaktif peptidler. *Int J Basic Clin Med,* 1 (2): 137-145, 2015.
26. **Gökce G:** Buzağı ishallerinde etiyoloji patogenezis ve tedavi seçenekleri. *Kafkas Univ Vet Fak Derg,* 1 (1-2): 98-102, 1995.
27. **Erel O, Neselioglu S:** A novel and automated assay for thiol/disulphide homeostasis. *Clin Biochem,* 47 (18): 326-332, 2014. DOI: 10.1016/j.clinbiochem.2014.09.026
28. **Boğa Kuru B, Makav M, Kuru M, Aras ŞY, Karadağ Sarı E, Bulut M, Alwazeer D, Bektaşoğlu F, Ölmez M, Kırmızıbayrak T, LeBaron TW:** Effects of hydrogen-rich water on growth, redox homeostasis and hormonal, histological and immune systems in rats exposed to high cage density stress. *Vet Med Sci,* 11 (2):e70305, 2025. DOI: 10.1002/vms3.70305
29. **Beutler E, Duron O, Kelly BM:** Improved method for the determination of blood glutathione. *J Lab Clin Med,* 61, 882-888, 1963.
30. **Yoshioka T, Kawada K, Shimada T, Mori M:** Lipid peroxidation in maternal and cord blood and protective mechanism against activated-oxygen toxicity in the blood. *Am J Obstet Gynecol,* 135 (3): 372-376. 1979 DOI: 10.1016/0002-9378(79)90708-7
31. **Sezer M, Gökce G:** sTREM-1, MR-Pro-Adrenomedullin, clinical biochemistry and hematology in calves with neonatal sepsis. *J Hellenic Vet Med Soc,* 74 (4): 6481-6490, 2024. DOI: 10.12681/jhvms.31046
32. **Atlı K, Yıldırım Y, Hasırcıoğlu S, Bulut O, Avcı O:** Buzağılarda ishale neden olan başlıca viral etkenler. *Ayrıntı Derg,* 5 (61): 70-74, 2018.
33. **Millemann Y:** Diagnosis of neonatal calf diarrhea. *Rev Med Vet,* 160 (8): 404-409, 2009.
34. **Sağıroğlu M, Çalışkan M, Geçmez Cahan K, Baykal A, Akça B:** Investigation of the relationship between blood gas and oxidative stress parameters in calves with diarrhea. *FU Vet J Health Sci,* 39 (2): 108-112, 2025.
35. **Fu ZL, Yang Y, Ma L, Malmuthuge N, Guan LL, Bu DP:** Dynamics of oxidative stress and immune responses in neonatal calves during diarrhea. *J Dairy Sci,* 107 (2): 1286-1298. 2024. DOI: 10.3168/jds.2023-23630
36. **Csontos C, Rezman B, Foldi V, Bogar L, Drenkovics L, Röth E, Weber G, Lantos J:** Effect of N-acetylcysteine treatment on oxidative stress and inflammation after severe burn. *Burns,* 38 (3): 428-437, 2012. DOI: 10.1016/j.burns.2011.09.011
37. **Chernigova SV, Chernigov YV, Vatnikov YA, Kulikov EV, Popova IA, Shirmanov VI, Molchanova MA, Likhacheva IF, Voronina YY, Lukina DM:** Special aspects of systemic inflammation course in animals. *Vet World,* 12 (7): 932-937. 2019, DOI: 10.14202/vetworld.2019.932-937
38. **Terzi OS, Kara E, Şenel Y, Ceylan E, Neselioglu S, Erel Ö:** Dynamic thiol-disulphide homeostasis and ischemia modified albumin levels in neonatal calf diarrhea. *Ankara Univ Vet Fak Derg,* 70 (1): 81-86, 2023. DOI: 10.33988/auvfd.928731
39. **Koçak E, Duru Ö:** İshal semptomu belirlenen buzağılardaki total tiyol/native tiyol düzeylerinin belirlenmesi. *1. Ulusal Sağlık Bilimleri Öğrenci Kongresi,* Kırıkkkale Univ, 69-75, 5-6 June, 2024.
40. **Cho YI and Yoon KJ:** An overview of calf diarrhea-infectious etiology, diagnosis, and intervention. *J Vet Sci,* 15 (1): 1-17, 2014. DOI: 10.4142/jvs.2014.15.1.1
41. **Melmed S, Polonsky KS, Larsen PR Kronenberg HM:** Williams Textbook of Endocrinology E-book. Elsevier Health Sciences, 2011.
42. **Çorapsız MF, Birdane FM:**. Neonatal dönem buzağı ishallerinde tiroid ve bazı kan-serum parametrelerinin değerlendirilmesi. *Master's Thesis,* Afyon Kocatepe Univ. Sağlık Bil. Enst., 2023.
43. **den Brinker M, Joosten KF, Visser TJ, Hop WC, de Rijke YB, Hazelzet JA, Boonstra VH, Hokken-Koelega AC:** Euthyroid sick syndrome in meningococcal sepsis: The impact of peripheral thyroid hormone metabolism and binding proteins. *J Clin Endocrinol Metabol,* 90 (10): 5613-5620, 2005. DOI: 10.1210/jc.2005-0888
44. **Kahl S, Elsasser T, Blum J:** Effect of endotoxin challenge on hepatic 5′-deiodinase activity in cattle. *Domest Anim Endocrinol,* 18 (1): 133-143, 2000. DOI: 10.1016/s0739-7240(99)00069-7
45. **Brückmann A, Höck C, Linke K, Hennies M, Schallenberger E:** Alterations of growth hormone, cortisol, luteinizing hormone, and insulin concentrations in early-postnatal calves affected with diarrhea. *Domest Anim Endocrinol,* 18 (2): 187-197, 2000. DOI: 10.1016/s0739-7240(99)00078-8
46. **Van den Berghe G, Teblick A, Langouche L, Gunst J:** The hypothalamus-pituitary-adrenal axis in sepsis- and hyperinflammation-induced critical illness: Gaps in current knowledge and future

translational research directions. *eBioMed,* 84:104284, 2022. DOI: 10.1016/j.ebiom.2022.104284

47. **Chadda K, Annane D:** The use of corticosteroids in severe sepsis and acute respiratory distress syndrome. *Ann Med,* 34 (7-8): 582-589, 2002. DOI: 10.1080/078538902321117805
48. **Gold JR, Divers TJ, Barton MH, Lamb SV, Place NJ, Mohammed HO, Bain FT:** Plasma adrenocorticotropin, cortisol, and adrenocorticotropin/cortisol ratios in septic and normal-term foals. *J Vet Intern Med,* 21 (4): 791-796, 2007. DOI: 10.1111/j.1939-1676.2007.tb03023.x
49. **Whittaker AC, Gallagher S:** Caregiving alters immunity and stress hormones: A review of recent research. *Curr Opin Behav Sci,* 28, 93-97, 2019. DOI: 10.1016/j.cobeha.2019.02.002
50. **Panzani S, Carluccio A, Faustini M, Prandi A, Probo M, Veronesi MC:** Comparative study on Insulin-Like Growth Factor I (IGF-I) plasma concentrations in new-born horse foals, donkey foals and calves. *Fetal, Neonat and Develop Med,* 1 (1): 1-6, 2017. DOI: 10.15761/FNDM.1000103
51. **Temizel EM, Karakuş AÖ, Kavukcu F, Küçükşen DU, Ercan İ:** IGF-1 and GH alterations in lambs with intestinal inflammation. *Turk J Vet Anim Sci,* 45 (2): 354-362, 2021. DOI: 10.3906/vet-2007-68
52. **DeBoer MD, Scharf RJ, Leite AM, Férrer A, Havt A, Pinkerton R, Lima AA, Guerrant RL:** Systemic inflammation, growth factors, and linear growth in the setting of infection and malnutrition. *Nutrition,* 33, 248-253, 2017. DOI: 10.1016/j.nut.2016.06.013
53. **Wang P, Li N, Li JS:** Mechanism of growth hormone insensitivity induced by endotoxin. *Acta Pharmacol Sin,* 23 (1): 16-22, 2016.
54. **Hunninghake GW, Doerschug KC, Nymon AB, Schmidt GA, Meyerholz DK, Ashare A:** Insulin-like growth factor-1 levels contribute to the development of bacterial translocation in sepsis. *Am J Respir Crit Care Med,* 182 (4): 517-25, 2010. DOI: 10.1164/rccm.200911-1757OC
55. **Phillips AC, Carroll D, Drayson MT, Batty GD:** Raised levels of immunoglobulin G, A and M are associated with an increased risk of total and causespecific mortality: The Vietnam experience study. *J Epidemiol Community Health,* 69 (2): 129-135, 2015. DOI: 10.1136/jech-2014-204345
56. **Bernth Jensen JM, Laursen NS, Jensen RK, Andersen GR, Jensenius JC, Sørensen UBS, Thiel S:** Complement activation by human IgG antibodies togalactose-α-1, 3-galactose. *Immunology,* 161 (1): 66-79, 2020. DOI: 10.1111/imm.13229
57. **Yanar KE, Gur C, Degirmencay S, Aydın Ö, Aktaş MS, Baysal S:** Insulin-like growth factor-1 expression levels in pro-inflammatory response in calves with neonatal systemic inflammatory response syndrome. *Vet Immunol Immunopathol,* 268:110706, 2024. DOI: 10.1016/j.vetimm.2023.110706
58. **Huet O, Dupic L, Harrois A, Duranteau J:** Oxidative stress and endothelial dysfunction during sepsis. *Front Biosci,* 16 (5): 1986-1995, 2011. DOI: 10.2741/3835
59. **Figueras-Aloy J, Gómez L, Rodríguez-Miguélez JM, Jordán Y, Salvia MD, Jiménez W, Carbonell-Estrany X:** Plasma nitrite/nitrate and endothelin-1 concentrations in neonatal sepsis. *Acta Paediatr,* 92 (5): 582-587, 2003. DOI: 10.1111/j.1651-2227.2003.tb02511.x

Kafkas Universitesi Veteriner Fakultesi Dergisi
Journal Home-Page: http://vetdergikafkas.org
E-ISSN: 1309-2251

Kafkas Univ Vet Fak Derg
32 (4): 569-583, 2026
DOI: 10.9775/kvfd.2026.36996

Research Article

Comparative Effect of Conventional and Green Silver Nanoparticles (AgNPs) on Physiological Properties, Immunity, and Oxidative Stress in N-methyl-N-nitrosourea-Induced Colon Cancer in Rat Model

Amirah S. ALAHMARI [1] (*), Sara Sabry MOHAMED [2], Alduwish Manal ABDUALLAH [3], Khalid M. ALSYAAD [4], Kamlah Ali MAJRASHI [5], Maha A. ALHASNANI [5], Amani Osman SHAKAK [5,6], Areej M. ALSOLAMI [7], Merfat O. ALJHDLI [8], Safia M.A. BAHSHWAN [5], Mada M. AL-QURASHI [5]

[1] Department of Biology, College of Science, Princess Nourah bint Abdulrahman University, P.O. Box 84428, Riyadh 11671, SAUDI ARABIA
[2] Department of Agricultural Microbiology, Faculty of Agriculture, Zagazig University, Zagazig 44511, EGYPT
[3] Department of Biology, College of Science and Humanities in Al-Kharj, Prince Sattam Bin Abdulaziz University, Alkarj 11942, SAUDI ARABIA
[4] Department of Biology, College of Science, King Khalid University, Abha, 61413, SAUDI ARABIA
[5] Biological Sciences Department, College of Science & Arts, King Abdulaziz University, Rabigh, 21911, SAUDI ARABIA
[6] Faculty of Medical Laboratory Sciences, University of Shendi, Shendi P.O. Box 142, SUDAN
[7] Department of Biology, College of Science, Jouf University, Sakaka, Al-Jouf, SAUDI ARABIA
[8] Department of Chemistry, College of Science and Arts, King Abdulaziz University, Rabigh 21911, SAUDI ARABIA

(*) **Corresponding author:**
Amirah S. Alahmari
Phone: +966 50 604460
Cellular phone: +966 50 604460
Fax: +966 50 604000
E-mail: amsalahmari@pnu.edu.sa

How to cite this article?

Alahmari AS, Mohamed SS, Abduallah AM, Alsyaad KM, Majrashi KA, Alhasnani MA, Shakak AO, Alsolami AM, Aljhdli MO, Bahshwan SMA, Al-Qurashi MM: Comparative Effect of Conventional and Green Silver Nanoparticles (AgNPs) on Physiological Properties, Immunity, and Oxidative Stress in N-methyl-N-nitrosourea-Induced Colon Cancer in Rat Model. *Kafkas Univ Vet Fak Derg*, 32 (4): 569-583, 2026.
DOI: 10.9775/kvfd.2026.36996

Article ID: KVFD-2026-36996
Received: 01.05.2026
Accepted: 19.07.2026
Published Online: 28.07.2026

Abstract

The rise of colorectal cancer and multidrug-resistant infections in immunocompromised patients demands eco-friendly therapies. This study compared conventional and green silver nanoparticles (AgNPs) synthesized via *Portulaca oleracea* leaf extract in terms of antibacterial, antioxidant, anticancer, and *in vivo* physiological activities against N-methyl-N-nitrosourea (MNU)-induced colon cancer in rats. AgNPs synthesized via *Portulaca oleracea* leaf extract exhibited an surface plasmon resonance (SPR) at 420 nm, a spherical morphology (7-22 nm), and protein capping. Against eight pathogens (including *S. aureus*, *E. coli*, and *P. aeruginosa*), green AgNPs (320 µg/mL) showed larger inhibition zones (26.3 vs. 20.1 mm for *S. aureus*) and MIC values ranging from 12.5-20 µg/mL, representing a two-fold decrease compared to chemical nanoparticles. In HCT-116 colon cancer cells, green AgNPs had a 2.3-fold lower IC_{50} (12.4 vs. 28.6 µg/mL), induced a 4.8-fold increase in Caspase-3 activity, and increased apoptotic cells to 42.6% (vs. 18.3%). In MNU-induced rat colon cancer, green AgNPs (320 mg/kg) restored physiological parameters i.e., body weight gain to 78.6% (vs. 15.4% in controls), reduced mortality to 0% (vs. 50%), lowered tumor incidence to 16.7% (vs. 100%), and normalized oxidative stress markers (MDA 2.5 vs. 8.4 nmol/mg). Preventive treatment completely abolished tumors. Green AgNPs consistently outperformed chemical counterparts, offering a potent, safe nanomedicine for dual antibacterial and anticancer applications against toxic carcinogens.

Keywords: Green silver nanoparticles, Purslane extract, Colon cancer, Antibacterial, Apoptosis, Oxidative stress, Antioxidant, Chemoprevention, Safety

Introduction

Silver nanoparticles (AgNPs) have emerged as one of the most extensively investigated nanomaterials in biomedicine due to their tunable physicochemical properties, broad-spectrum antimicrobial activity, and growing evidence of cytotoxic potential against various cancerous cells and carcinogen-induced tumor models [1]. Conventional synthesis relies predominantly on physical and chemical routes that require high energy inputs and reactive reducing agents (borohydride, hydrazine, and organic solvents). These approaches often suffer from complex purification, residual contaminants, and scalability issues, and can compromise biocompatibility and safety [2]. At the same time, the rapid expansion of AgNPs-based products for medical, pharmaceutical, and consumer applications has raised legitimate concerns about nanoparticle toxicity to cells, tissues, organs, and ecosystems, underscoring the need for safer design and rigorous toxicological assessment [3].

In response, green synthesis has gained substantial attention as an eco-friendly, cost-effective, and biocompatible alternative. Biological systems, including plants, microorganisms, and biowastes, can function as "bionanofactories," providing intrinsic reducing and capping agents that generate AgNPs under mild conditions and with lower environmental impact [4]. Plant-mediated AgNPs frequently display enhanced stability, narrow size distributions, and surface coronas rich in proteins, polysaccharides, and secondary metabolites, which can modulate their biological behavior [5].

Despite this progress, several critical gaps remain, where much of the green AgNP literature is *in vitro*, focusing on antimicrobial or cytotoxic assays, with relatively fewer systematic *in vivo* evaluations that integrate efficacy with comprehensive safety endpoints such as organ histopathology, hematology, and long-term toxicity [1]. Many green-synthesis studies emphasize plant extracts, whereas bacterial "bionanofactories" remain comparatively underexplored, even though bacteria offer fast growth, simple culture requirements, and the possibility of genetic engineering for precise control of nanoparticle properties [6]. Third, although reviews repeatedly highlight that surface chemistry, size, and shape critically influence biodistribution, toxicity, and therapeutic performance, there is still limited direct comparison between green and chemically synthesized AgNPs under identical experimental conditions, particularly in disease models such as cancer cachexia or chemoprevention [7].

Scientific evidence indicates that green AgNPs maintain a toxic profile, triggering oxidative stress, immunotoxicity, and organ injury, mediated by dose, size, functionalization, and route. Regulatory guidance for chronic or prophylactic use, especially in vulnerable populations such as cancer patients, remains fragmentary [1]. While some green-synthesized AgNPs show lower hemolysis and reduced toxicity to normal cells at therapeutic concentrations [5]. Robust *in vivo* data linking chemopreventive or anticancer efficacy to long-term safety margins remain scarce.

Within this context, the present study addresses several unmet needs. It employs a bacterial green-synthesis route, using plants as a bionanofactory and leveraging metabolites as natural reducing and capping agents. This approach is aligned with current efforts to harness microbial platforms for tunable, scalable AgNPs production, but remains less well characterized than plant-based methods [7]. The study undertakes a head-to-head comparison of green- and chemically synthesized AgNPs, examining their antimicrobial, antioxidant, and anticancer properties, as well as their *in vivo* chemopreventive efficacy in a cancer model [7]. Such parallel evaluation directly tests the common assumption, largely inferred but rarely demonstrated *in vivo*, that green AgNPs combine superior therapeutic performance with improved biosafety [8].

Beyond standard efficacy readouts, this work systematically evaluates growth performance, survival, and histological integrity of major organs, providing an integrated view of therapeutic index and subchronic toxicity that is often missing from AgNPs research. By linking restored appetite, feed efficiency, and body weight gain to tumor suppression and organ protection, the study examines whether green AgNPs can genuinely reverse cancer-associated wasting rather than merely alter weight through fluid shifts or organ hypertrophy. Finally, by defining a high-dose regimen that does not produce mortality or dose-limiting toxicity, the study contributes to the urgently needed dose-response and safety data required to guide potential chemopreventive or adjunctive use of green AgNPs in oncology [3,6]. Therefore, the main objectives of this study are to develop and characterize purslane extract-mediated green silver nanoparticles, compare them directly with conventional chemical AgNPs across multiple biological domains (antimicrobial, antioxidant, anticancer, and *in vivo* cytotoxicity activity), and rigorously assess their safety profile in terms of growth, survival, and tissue integrity.

Material and Methods

Ethical Approval

The animal study has been approved by the Unit of Biomedical Ethics, Research Ethics Committee (Ethical code number ZU-IACUC/2/F/313/2023).

Extraction and Physicochemical Properties of Purslane Extract

Aqueous extraction of dried *Portulaca oleracea* aerial parts in distilled water yielded polar bioactives. The

resulting extract was assessed for physicochemical and nutritional properties, minerals by AAS, total phenolics and flavonoids via colorimetry, and antioxidant capacity using DPPH and ABTS. Gallic acid and quercetin were further confirmed by HPLC-DAD.

Green Synthesis of Silver Nanoparticles

Silver nanoparticles were biosynthesized using aqueous purslane *(Portulaca oleracea)* leaf extract as a reducing and capping agent. The extract was heated at 45°C and filtered. Synthesis was optimized by varying $AgNO_3$:extract ratio (90:10-50:50), temperature (25-80°C), pH (3-10), and time (1-48 h). Optimal conditions (80:20, 60°C, pH 7.5, 24 h) in the dark facilitated Ag^+ reduction and capping, indicated by a reddish-brown color. Nanoparticles were harvested by centrifugation, washed with water and ethanol, then dried.

Characterization of Silver Nanoparticles

A UV-Visible spectrophotometer was used to detect surface plasmon resonance (SPR) band between 300-700 nm [9]. The morphology and shape of biosynthesized AgNPs were examined using TEM [10]. FTIR analysis was conducted to identify functional groups in the range of (4000-400 cm^{-1}) [10]. DLS and zeta potential were used to measure the size and charge of nanoparticles [10].

Antioxidant Activity

Antioxidant capacity of green and chemical AgNPs was evaluated using a freeradical scavenging assay (DPPH). Briefly, AgNPs at concentrations of 20, 40, 80, 160, and 320 µg/mL were incubated with 0.1 mM DPPH solution in methanol in the dark for a defined time, and absorbance was measured at ~517 nm. Percentage radical scavenging was calculated relative to a control without nanoparticles [11].

Antibacterial Activity

The antibacterial activity of green and chemically synthesized AgNPs was evaluated by agar well diffusion and broth microdilution methods against eight pathogenic bacterial isolates, including *Escherichia coli, Pseudomonas aeruginosa, Staphylococcus aureus, Klebsiella pneumoniae, Salmonella enterica Typhimurium, Enterococcus faecalis, Bacillus cereus*, and *Acinetobacter baumannii*. For the agar well diffusion assay, standardized inocula (0.5 McFarland) were spread on Mueller-Hinton agar plates, wells were filled with serial concentrations of AgNPs, and plates were incubated at 37°C for 18-24 h before measuring inhibition zones [10]. MICs determined by twofold serial dilution of AgNPs in Mueller-Hinton broth (96-well plates) with test bacteria; growth assessed at 660 nm [12].

In vitro Anticancer Assays

Cytotoxicity Activity: Cytotoxicity against HCT116 colon cancer cells was assessed using an MTT-type colorimetric assay [13]. Caspase-3 activation was quantified via colorimetric kit using DEVD-pNA; cleavage measured, fold change calculated. Green AgNPs gave ~4.8-fold increase vs ~2.1-fold for chemical AgNPs, indicating stronger intrinsic apoptosis, consistent with literature [14].

Expression of Bcl-2 and Bax in HCT 116 cells was evaluated post-AgNPs treatment. Proteins extracted, separated by SDS-PAGE, western-blotted, and densitometry-normalized to housekeeping for Bax/Bcl-2 ratios. Green AgNPs downregulated Bcl-2 and upregulated Bax versus chemical AgNPs, consistent with prior green AgNPs cancer studies.

Apoptosis quantified by flow cytometry (Annexin V/PI); early + late summed [14]. Green AgNPs induced ~42.6% apoptosis vs ~18.3% with the chemical.

Experimental Design for In vivo Colon Carcinogenesis: Male Albino rats (n=300; 8-10 weeks old; 180-220 g) were randomly allocated into ten experimental groups (30 rats/group) to establish an NmethylNnitrosourea (MNU)induced colon carcinogenesis model and to assess the preventive and therapeutic effects of biosynthesized (green) and chemically synthesized silver nanoparticles (AgNPs). Animals were housed under standard laboratory conditions (22±2°C, 50-60% relative humidity, 12 h light/dark cycle) with free access to standard pellet diet and water ad libitum, and were allowed one week of acclimatization before experimentation *(Fig. 1)*.

Colon carcinogenesis was induced by MNU (Sigma-Aldrich) administered either rectally or intraperitoneally at established carcinogenic doses and schedules, as previously described [15]. Following MNU exposure, rats received either green or chemical AgNPs by oral gavage at graded doses (80, 160, or 320 mg/kg body weight) once daily according to two protocols: (i) concomitant administration with MNU to evaluate chemopreventive efficacy, and (ii) delayed administration starting 4 weeks after the last MNU dose to assess therapeutic effects against established lesions. Control groups included a healthy negative control (vehicle only) and an MNUonly positive control. Throughout the experimental period, animals were monitored daily for clinical signs, and body weight and food intake were recorded weekly. At the end of the study, rats were fasted overnight, anesthetized, and euthanized; the entire colon was excised, opened longitudinally, rinsed with saline, and sampled for biochemical assays and histopathological examination.

Oxidative Stress and Antioxidant Markers in Colon Tissue

Colon segments were rapidly excised, rinsed in icecold saline, blotted, and homogenized in an appropriate buffer. The homogenates were centrifuged, and the supernatants were used to determine oxidative stress parameters. The

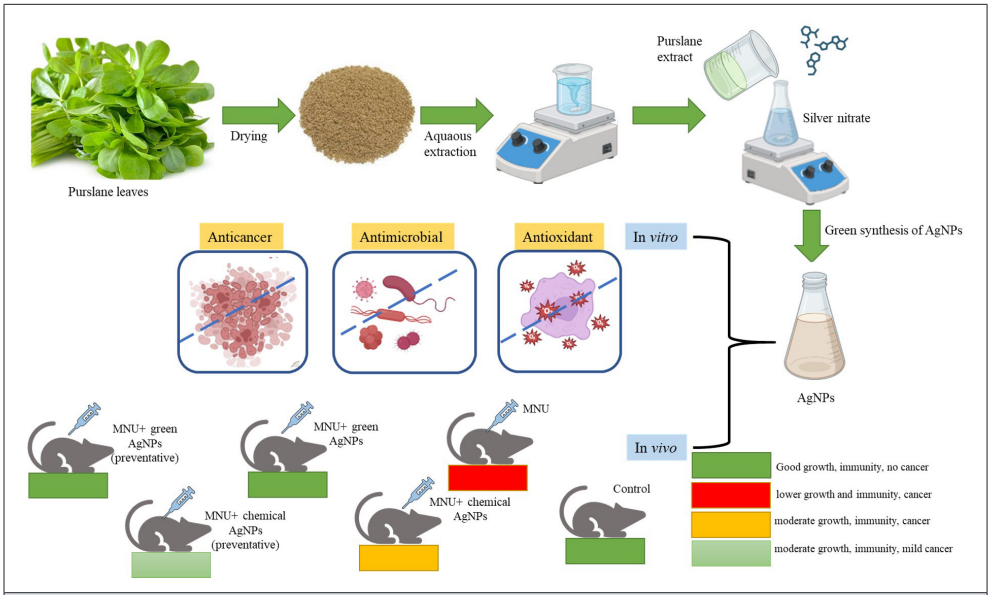

Fig 1. Experimental design of comparative effect of chemical and purslane extract silver nanoparticles with biological activities on N-methyl-N-nitrosourea rat model on growth, immunity, oxidative stress, and environmental pollution

following parameters were assessed following the methods in the study of Afrin et al.[16]. Malondialdehyde (MDA) levels were measured as an index of lipid peroxidation using the thiobarbituric acidreactive substances (TBARS) assay. Nitric oxide (NO) levels were estimated by measuring nitrite/nitrate using the Griess reaction. Antioxidant status was assessed by determining superoxide dismutase (SOD) and catalase (CAT) activities using standard spectrophotometric methods, and reduced glutathione (GSH) content using Ellman's reagent [17]. Total antioxidant capacity (TAC) was quantified using a commercial colorimetric kit following the manufacturer's instructions.

Histopathological Examination of Colon

Colon samples underwent FFPE processing (formalin fixation, graded alcohols, xylene, paraffin). Sections (4-5 µm) were cut, H&E-stained, and examined blindly by a pathologist. Crypt architecture, inflammation, dysplasia, and mucin were semi-quantitatively scored. Neoplastic lesions (adenoma, adenocarcinoma) were recorded for incidence and severity, following standard colorectal histopathology protocols [18].

Statistical Analysis

Data were expressed as mean ± standard error of the mean (SEM). All statistical analyses were executed using IBM SPSS Statistics for Windows, version 26.0 (IBM Corp., Armonk, NY, USA). Differences between groups were evaluated using one-way analysis of variance (ANOVA), followed by an appropriate post hoc multiple-comparison test (Tukey's test). A -values less than 0.05, 0.001, and 0.0001 were considered statistically significant.

Results

Physicochemical Properties of Purslane Extract

The aqueous extract of *Portulaca oleracea* L. demonstrates extraordinary nutritional density, with exceptionally high potassium (2652.00 mg/100g DW) and calcium (1005.20 mg/100g DW) *(Table 1)*, positioning it as a valuable functional food for electrolyte balance and skeletal integrity. HPLC profiling identifies gallic acid, quercetin, and ferulic acid as the dominant phenolic bioactives. Notably, total flavonoid content (133.23 mg RE/g) substantially surpasses total phenolic content (51.01 mg GAE/g), indicating that flavonoids are the principal drivers of the extract's biological efficacy. This compositional superiority translates into potent radical-scavenging capacity, with DPPH and ABTS IC_{50} values both below 60 µg/mL. Furthermore, the presence of photosynthetic pigments, including β-carotene and chlorophyll, adds synergistic photoprotective and anti-inflammatory value, broadening its therapeutic appeal.

Characterization of Silver Nanoparticles Synthesized by Purslane Extract

Biosynthesis was initially validated by UV-Vis spectroscopy, which revealed a characteristic surface plasmon resonance band centered at approximately 420 nm *(Fig. 2-A)*, confirming the successful reduction of Ag^{+} ions to metallic Ag^{0}. Transmission electron microscopy illustrated predominantly spherical nanoparticles *(Fig. 2-B)*, with a relatively narrow size distribution ranging from 7 to 22 nm *(Fig. 2-C)*. Zeta potential analysis yielded a strongly negative surface charge of -27.33 mV *(Fig. 2-D)*, ensuring

Table 1. *Chemical Composition, Antioxidant Activity, and IC50 Values of Purslane (Portulaca oleracea L.) Extracts*		
Component/Parameter	**Specific Compound/Measure**	**Specific Value (±SD)**
Macronutrients	Sodium (Na)	228.20±33.06 mg/100 g DW
	Potassium (K)	2652.00±432.1 mg/100 g DW
	Calcium (Ca)	1005.20±366.52 mg/100 g DW
	Potassium (K)	494 mg/100 g
	Magnesium (Mg)	68 mg/100 g
Phenolic Acids	Gallic acid	77.89 ppm/62.59 ppm
	Coumaric acid	19.25 ppm/16.25 ppm
	Ferulic acid	40.25 ppm/29.58 ppm
	Caffeic acid (suspected)	41.25 ppm
Flavonoids	Quercetin	58.78 ppm
	Kaempferol (Kemopferol)	24.15 ppm
Vitamins	Vitamin C	85.6 ppm
	Vitamin E	54.1 ppm
Pigments	Chlorophyll a	40.46 mg g^{-1} DW
	Chlorophyll b	9.94 mg g^{-1} DW
	β-Carotene	14.16 mg g^{-1} DW
Antioxidant Activity & IC50 Values		
Total Phenolic Content (TPC)	mg Gallic Acid Equivalent (GAE) g^{-1} DW	51.01 mg GAE g^{-1} DW
Total Flavonoid Content (TFC)	mg Rutin Equivalent (RE) g^{-1} DW	133.23 mg RE g^{-1} DW
DPPH Radical Scavenging Activity (IC_{50})	High Potency (Acetone)	57.23 µg mL^{-1}
ABTS Radical Scavenging Activity (IC_{50})	High Potency (Fresh)	52.86 µg mL^{-1}
FRAP (Ferric Reducing Antioxidant Power)	µmol Trolox Equivalent (TE) g^{-1} DW	43.5 ± 1.0 mg GAE g^{-1} DW
Ferrous Iron (Fe^{2+}) Chelating Activity	% Inhibition (Methanol extract)	12.78%
All values are presented as measurements (± standard deviation where available) on a Dry Weight (DW) basis		

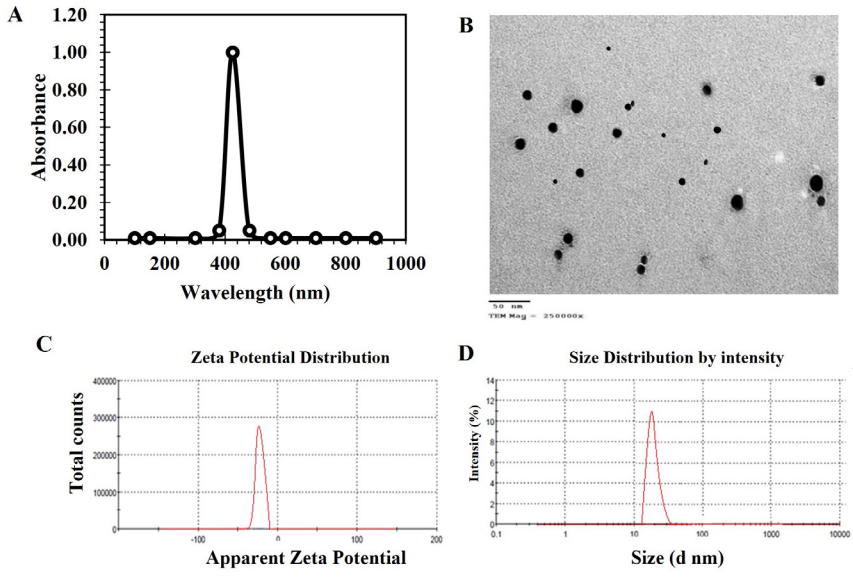

Fig 2. Characterization of green silver nanoparticles using purslane extract. **(A)** UV absorbance spectrum with peak near 420 nm indicating SPR. **(B)** TEM micrograph showing spherical AgNPs, well-dispersed, approximately 7-22 nm in size, at 250.000x magnification. **(C)** The zeta potential measures the net surface charge of AgNPs was -27.33 mV, and **(D)** the exact size of 20 nm detected by DLS zeta sizer

robust electrostatic repulsion that prevents aggregation and guarantees long-term colloidal stability in biological fluids. Dynamic light scattering corroborated these findings, placing the hydrodynamic diameter at approximately 20 nm, thus indicating a monodisperse population highly suitable for efficient cellular uptake and systemic administration.

Biological Activities

Antioxidant Activity: Both green and chemically synthesized AgNPs exhibited a clear, concentration-dependent radical-scavenging behavior. However, at every matched concentration across the tested range, green AgNPs consistently demonstrated substantially higher percentage inhibition, reaching 80-85% activity compared to the consistently lower values obtained for chemical AgNPs. This enhanced performance is synergistically augmented by the biomolecular corona comprising polyphenols, flavonoids, and organic acids that coats the green nanoparticles, providing an additional electron reservoir for efficient radical stabilization and sustained antioxidant activity *(Fig. 3)*.

Antibacterial Activity: The antimicrobial superiority of green AgNPs was systematically validated against eight clinically relevant, cancer-associated bacterial species using zone of inhibition (ZOI) and minimum inhibitory concentration (MIC) assays across 20-320 µg/mL *(Table 2)*.

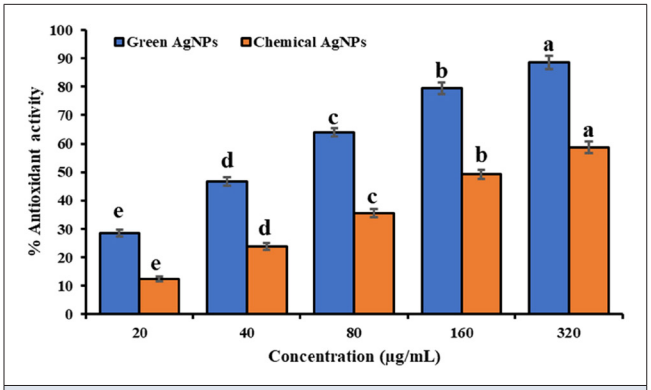

Fig 3. Antioxidant activity of green vs. chemical AgNPs against DPPH free radicals (% inhibition, mean ± SE). Values expressed as mean ± SE (n = 3). Data analyzed by two-way ANOVA (factors: nanoparticle type, concentration) followed by Tukey's post hoc test; P<0.05 considered significant. Different lowercase superscript letters within a row indicate significant differences between green and chemical AgNPs at the same concentration (P<0.05). Different uppercase superscript letters within a column indicate significant differences among concentrations for the same nanoparticle type (P<0.05)

A steep, dose-dependent increase in potency was observed; against MRSA, green AgNPs expanded the ZOI from 10.1 mm at 20 µg/mL to 26.3 mm at 320 µg/mL, whereas chemical AgNPs peaked at only 20.1 mm. The MIC data provided even stronger evidence: green AgNPs achieved an average two-fold reduction (range 1.8- to 2.5-fold) compared to chemical AgNPs, meaning equivalent bactericidal effects require substantially lower concentrations. *S. aureus* MRSA

Table 2. *Antimicrobial activity of green vs. chemical silver nanoparticles against pathogenic bacteria – Zone of Inhibition (mm ± SE) at 20-320 µg/mL and MIC (µg/mL ± SE)*

Bacterial Species	AgNPs Type	20 µg/mL	40 µg/mL	80 µg/mL	160 µg/mL	320 µg/mL	MIC (µg/mL)
Escherichia coli	Green	8.2±0.3	11.4±0.4	15.2±0.5	18.5±0.4	22.1±0.5	12.5±1.2
	Chemical	5.1±0.2	7.8±0.3	10.5±0.4	14.2±0.4	17.3±0.5	25.0±2.1
Pseudomonas aeruginosa	Green	9.4±0.4	12.8±0.5	16.7±0.5	20.3±0.5	24.5±0.6	10.0±0.9
	Chemical	5.8±0.3	8.5±0.4	11.9±0.4	15.8±0.5	19.2±0.5	20.0±1.8
Staphylococcus aureus	Green	10.1±0.4	13.9±0.5	18.0±0.5	22.1±0.5	26.3±0.6	8.0±0.7
	Chemical	6.2±0.3	9.1±0.4	12.5±0.4	16.5±0.5	20.1±0.5	16.0±1.5
Klebsiella pneumoniae	Green	8.9±0.3	12.1±0.4	15.8±0.5	19.7±0.4	23.5±0.5	12.5±1.1
	Chemical	4.9±0.2	7.5±0.3	10.2±0.4	13.9±0.4	17.0±0.5	25.0±2.0
Salmonella enterica Typhimurium	Green	7.8±0.3	10.5±0.4	14.0 0.4	17.9±0.4	21.4±0.5	15.0±1.3
	Chemical	4.5±0.2	6.8±0.3	9.3±0.3	12.6±0.4	15.8±0.4	30.0±2.5
Enterococcus faecalis	Green	7.2±0.3	9.8±0.4	13.1±0.4	16.8±0.4	20.2±0.5	18.0±1.5
	Chemical	4.1±0.2	6.2±0.3	8.5±0.3	11.5±0.4	14.7±0.4	35.0±2.8
Bacillus cereus	Green	6.5±0.3	8.9±0.4	11.9±0.4	15.4±0.5	18.9±0.5	20.0±1.7
	Chemical	3.7±0.2	5.6±0.3	7.8±0.3	10.3±0.4	13.4±0.4	40.0±3.0
Acinetobacter baumannii	Green	9.8±0.4	13.2±0.5	17.3±0.5	21.0±0.5	25.1±0.6	10.0±0.8
	Chemical	5.5±0.3	8.2±0.4	11.4±0.4	14.7±0.5	18.3±0.5	22.0±1.9

Values expressed as mean ± SE (n = 3). Data analyzed by two-way ANOVA (factors: nanoparticle type, concentration) followed by Tukey's post hoc test; P<0.05 considered significant

was the most susceptible (MIC 8.0 µg/mL), while *Bacillus cereus* showed relative tolerance (MIC 20.0 µg/mL). This broad-spectrum efficacy encompassed both Gram-positive strains *(E. faecalis* VRE) and notoriously resistant Gram-negative pathogens *(E. coli*, *K. pneumoniae*, *P. aeruginosa*, *A. baumannii)*. The mean ZOI difference between green and chemical AgNPs increased from 3.2 mm to 5.1 mm across the concentration gradient, unequivocally demonstrating that phytochemical capping agents enhance membrane disruption and intracellular ROS generation, yielding superior bactericidal outcomes.

Anticancer Activity: Against HCT-116 human colon adenocarcinoma cells, green-synthesized AgNPs exhibited an IC_{50} of 12.4 µg/mL, making them approximately 2.3-fold more potent than chemically synthesized AgNPs, which showed an IC_{50} of 28.6 µg/mL *(Table 3; Fig. 4)*. At 20 µg/mL, green AgNPs reduced viability to 58.3%, versus 82.5% for chemical; at 80 µg/mL, they nearly eradicated the population (14.2% viability), while chemical AgNPs left 41.8% intact. Mechanistically, this profound cytotoxicity is anchored in the intrinsic mitochondrial apoptotic pathway. Green AgNPs triggered a 4.8-fold surge in Caspase-3 activity, compared to a mere 2.1-fold increase induced by chemical AgNPs. Western blot analyses revealed that Bcl-2 was suppressed to 28.5% of control levels by green AgNPs, versus 61.3% by chemical, while Bax was upregulated to 312% of control, compared to 175% by chemical. This generated a massively elevated Bax/Bcl-2 ratio of 10.9, effectively lowering the apoptotic threshold, versus only 2.9 for chemical AgNPs. Flow cytometry quantified total apoptosis at 42.6% for green AgNPs-more than double the 18.3% observed for chemical confirming robust and selective engagement of the mitochondrial death cascade.

Growth Performance and Tumor-related Parameters: In the MNU-induced colon carcinogenesis rat model, the untreated cancer group developed severe cachexia, characterized by body weight gain of merely 15.4% (versus 95.6% in healthy controls), a 44% reduction in food intake, and 50% mortality by week 12 *(Table 4)*. Administration of green AgNPs at 80, 160, and 320 mg/kg effectuated a striking, dose-dependent reversal of this wasting syndrome. At 320 mg/kg, green AgNPs achieved weight gain (78.6%) and food intake statistically indistinguishable from healthy controls, with zero mortality. When directly compared at an equivalent dose (320 mg/kg), green AgNPs

Table 3. *Anticancer activity of green vs. chemical AgNPs against colon cancer cells*

Parameter	Green AgNPs (Mean ± SE)	Chemical AgNPs (Mean ± SE)
IC_{50} (µg/mL) - 48 h	12.4±1.1	28.6±2.3
Cell viability at 20 µg/mL (%)	58.3±2.1	82.5±2.8
Cell viability at 40 µg/mL (%)	31.7±1.9	64.2±2.5
Cell viability at 80 µg/mL (%)	14.2±1.2	41.8±2.1
Cell viability at 160 µg/mL (%)	6.8±0.7	26.5±1.9
Cell viability at 320 µg/mL (%)	2.1±0.3	14.3±1.2
Caspase-3 activity (fold change vs. control) - at IC_{50} conc.	4.8±0.4	2.1±0.2
Caspase-3 activity at 160 µg/mL	6.5±0.5	3.4±0.3
Caspase-3 activity at 320 µg/mL	7.9±0.6	4.2±0.4
Bcl-2 expression (% of control) - at IC_{50} conc.	28.5±2.2	61.3±3.1
Bcl-2 expression at 160 µg/mL (% of control)	15.2±1.5	42.6±2.8
Bcl-2 expression at 320 µg/mL (% of control)	7.8±0.9	28.4±2.1
Bax expression (% of control) - at IC_{50} conc.	312±18	175±12
Bax expression at 160 µg/mL (% of control)	415±22	238±15
Bax expression at 320 µg/mL (% of control)	487±25	291±18
Bax/Bcl-2 ratio - at IC_{50} conc.	10.9±0.9	2.9±0.3
Bax/Bcl-2 ratio at 160 µg/mL	27.3±2.1	5.6±0.5
Bax/Bcl-2 ratio at 320 µg/mL	62.4±4.5	10.2±0.9
Apoptotic cells (% by flow cytometry) - at IC_{50} conc.	42.6±2.5	18.3±1.7
Apoptotic cells at 160 µg/mL (%)	61.8±3.2	31.4±2.2
Apoptotic cells at 320 µg/mL (%)	78.5±3.8	45.2±2.9

Values expressed as mean ± SE (n=3). Data analyzed by two-way ANOVA (factors: nanoparticle type, concentration) followed by Tukey's post hoc test; P<0.05 considered significant

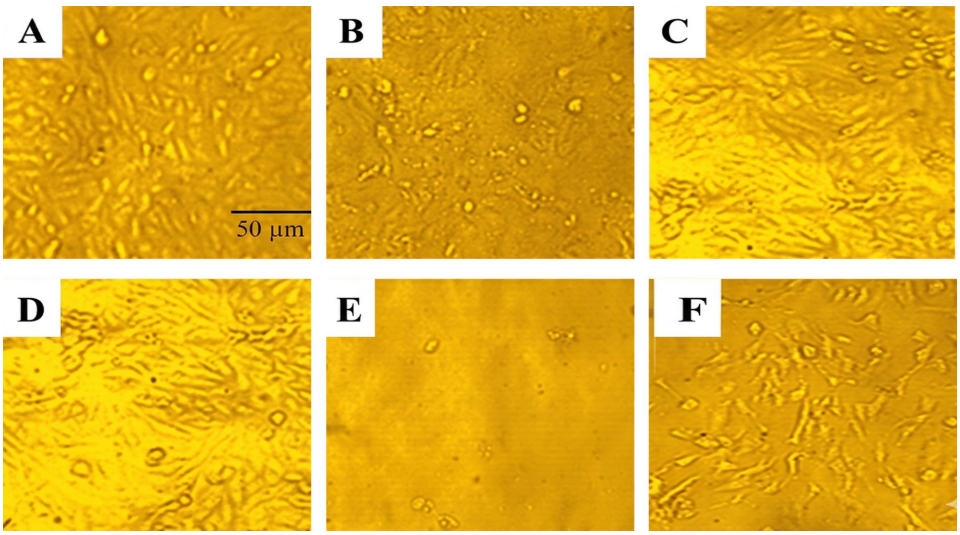

Fig 4. Comparative analysis of silver nanoparticle anti-cancer efficacy against HCT-116 colon cancer cells. Photomicrographs (A-F) show stained HCT-116 colon cancer cells under various treatment conditions. (**A**) Control cell line, exhibiting high cell viability and confluency with normal cellular structure. (**B**) Cells treated with 160 µg/mL Chemical AgNPs. **C:** Cells treated with 320 µg/mL Chemical AgNPs. Both B and C demonstrate dose-dependent effects on cell viability, with a clear reduction in cell number. (**D**) Cells treated with 160 µg/mL Green AgNPs. (**E**) Cells treated with 320 µg/mL Green AgNPs. D and E show significantly greater efficacy in reducing cell viability compared to equivalent chemical AgNP doses. (**F**) Cells treated with Doxorubicin (positive control), showing extensive cell death and characteristic changes in morphology consistent with effective anti-cancer therapy. The 50 µm scale bar is indicated in panel A

consistently outperformed chemical AgNPs, which were associated with 16.7% mortality and inferior weight gain (63.7%). Tumor-related parameters fully supported this: green AgNPs at 320 mg/kg reduced tumor incidence to 16.7% (vs. 50% for chemical), decreased average tumor size to 22 mm^3 (vs. 68 mm^3), lowered multiplicity to 0.5 tumors/rat (vs. 1.5), and improved histopathological scores to 0.9, indicating mild dysplasia (vs. 1.8 for chemical). Crucially, in a prophylactic setting where administration commenced concurrently with MNU, green AgNPs completely prevented tumor development (0% incidence, 0% mortality) and preserved near-normal histology (score 0.2), whereas chemical AgNPs still permitted 33.3% incidence and 16.7% mortality *(Table 5)*.

***Table 4**. The comparative effect of green and chemical silver nanoparticles at three concentrations (80, 160, and 320 mg/kg diet) on the growth parameters and mortality of MNU-induced colon cancer in rats*

Treatment	Description	Initial Body Weight (g)	Final Body Weight (g)	Body Weight Gain (%)	Food Intake (g/day)	Feed Efficiency Ratio (FCR)	Mortality (%)	Survival Rate (%)
T1	Healthy control (no MNU, no treatment)	180±5.2	352±8.1	95.6±3.2	22.4±0.8	0.32 ±0.02	0	100
T2	MNU-induced colon cancer, no treatment	182±4.8	210±6.5***	15.4±1.8***	12.6±0.6***	0.09±0.01***	50	50
T3	MNU + Green AgNPs (80 mg/kg)	181±5.0	248±7.2*	37.0±2.5*	15.8±0.7*	0.16±0.02*	33.3	66.7
T4	MNU + Green AgNPs (160 mg/kg)	183±4.9	288±7.8**	57.4±3.1**	18.5±0.8**	0.23±0.02**	16.7	83.3
T5	MNU + Green AgNPs (320 mg/kg)	182±5.1	325±8.2**	78.6±3.5**	21.2±0.9**	0.29±0.02**	0	100
T6	MNU + Chemical AgNPs (80 mg/kg)	181±4.7	228±6.9	26.0±2.2	14.1±0.6	0.12±0.01	41.7	58.3
T7	MNU + Chemical AgNPs (160 mg/kg)	184±5.0	258±7.4	40.2±2.8	16.5±0.7	0.18±0.02	33.3	66.7
T8	MNU + Chemical AgNPs (320 mg/kg)	182±4.9	298±7.9	63.7±3.2	19.3±0.8	0.25±0.02	16.7	83.3
T9	MNU + Green AgNPs (320 mg/kg) *- preventive*	183±5.2	341±8.5**	86.3±3.7**	21.8±0.9**	0.31±0.02**	0	100
T10	MNU + Chemical AgNPs (320 mg/kg) *- preventive*	182±5.0	312±8.0	71.4±3.4	20.1±0.8	0.27±0.02	16.7	83.3

*Values expressed as mean ± SE (n=3). Data analyzed by two-way ANOVA (factors: nanoparticle type, concentration) followed by Tukey's post hoc test; P<0.05; ** P<0.01; *** P<0.001 (one-way ANOVA with Tukey's post-hoc) considered significant*

***Table 5**. The effect of green and chemical AgNPs on Tumor-related parameters in MNU-induced colon cancer in rats (at study end, week 12)*

Treatment Group	Tumor Incidence (%)	Average Tumor Size (mm^3)	Tumor Multiplicity (n/rat)	Colon Histopathology Score (0-4)
T1 (Control)	0	0±0	0±0	0±0
T2 (MNU only)	100	285±32	4.8±0.6	3.8±0.2
T3 (Green 80)	83.3	156±21*	3.2±0.5*	2.9±0.3*
T4 (Green 160)	50.0	78±14**	1.8±0.4**	2.1±0.2**
T5 (Green 320)	16.7	22±6**	0.5±0.2**	0.9±0.2**
T6 (Chemical 80)	100	214±28	4.1±0.6	3.4±0.3
T7 (Chemical 160)	83.3	142±19	3.0±0.5	2.7±0.3
T8 (Chemical 320)	50.0	68±12*	1.5±0.3*	1.8±0.2*
T9 (Green preventive 320)	0	0±0**	0±0**	0.2±0.1**
T10 (Chemical preventive 320)	33.3	42±9	1.0±0.3	1.2±0.2

*Values expressed as mean ± SE (n=3). Data analyzed by two-way ANOVA (factors: nanoparticle type, concentration) followed by Tukey's post hoc test; P<0.05; ** P<0.01; *** P<0.001 (one-way ANOVA with Tukey's post-hoc) considered significant*

Oxidative Stress Markers: The oxidative stress data provide key mechanistic insights. The MNU-only group exhibited a profound imbalance, with malondialdehyde (MDA) and nitric oxide (NO) rising nearly 5-fold and 4.6-fold, respectively, indicating extensive lipid peroxidation and nitrosative stress *(Table 6)*. Concomitantly, endogenous antioxidant enzymes SOD, CAT, and GSH fell by approximately two-thirds, and total antioxidant capacity (TAC) declined by 66%. Administration of green AgNPs produced a clear dose-dependent restoration; at 320 mg/kg, all oxidative markers were restored to within 7-10% of normal values, and TAC reached 93% of the control level. At equivalent doses, green AgNPs consistently outperformed chemical AgNPs, yielding lower MDA/NO and higher SOD/CAT/GSH/TAC. This superiority is mechanistically attributed to the phytochemical coating, which facilitates direct radical scavenging, activates the Nrf2-driven transcriptional upregulation of endogenous antioxidant enzymes, inhibits pro-oxidant systems like NADPH oxidase, and chelates metal ions features absent in bare chemical AgNPs.

***Table 6.** Effect of green vs. chemical AgNPs on oxidative stress markers in MNU-induced colon cancer rats*

Treatment	Description	MDA (nmol/mg protein)	SOD (U/mg protein)	CAT (U/mg protein)	GSH (µmol/mg protein)	NO (µmol/mg protein)	TAC (mmol/L)
T1	Healthy control (no MNU, no treatment)	1.8±0.2	28.5±1.8	22.3±1.5	12.6±0.9	2.1±0.2	1.85±0.12
T2	MNU-induced colon cancer, no treatment	8.4±0.6***	9.2±0.8***	7.5±0.6***	3.8±0.3***	9.6±0.7***	0.62±0.05***
T3	MNU + Green AgNPs (80 mg/kg)	6.1±0.5*	14.8±1.2*	11.9±0.9*	5.9±0.5*	7.2±0.6*	0.94±0.07*
T4	MNU + Green AgNPs (160 mg/kg)	4.2±0.4**	20.1±1.5**	16.8±1.2**	8.7±0.7**	4.5±0.4**	1.35±0.09**
T5	MNU + Green AgNPs (320 mg/kg)	2.5±0.3**	26.4±1.9**	21.0±1.4**	11.5±0.9**	2.8±0.3**	1.72±0.11**
T6	MNU + Chemical AgNPs (80 mg/kg)	7.1±0.5	11.5±1.0	9.2±0.7	4.8±0.4	8.3±0.6	0.78±0.06
T7	MNU + Chemical AgNPs (160 mg/kg)	5.6±0.4	16.2±1.3	13.5±1.0	6.7±0.5	6.1±0.5	1.08±0.08
T8	MNU + Chemical AgNPs (320 mg/kg)	3.9±0.4*	22.3±1.6*	18.4±1.3*	9.5±0.7*	3.9±0.4*	1.48±0.10*
T9	MNU + Green AgNPs (320 mg/kg) – *preventive*	1.9±0.2**	27.9±2.0**	22.0±1.6**	12.3±0.9**	2.2±0.2**	1.82±0.12**
T10	MNU + Chemical AgNPs (320 mg/kg) – *preventive*	3.1±0.3	24.1±1.7	19.8±1.4	10.4±0.8	3.2±0.3	1.58±0.11

*P<0.05; ** P<0.01; *** P<0.001 (one-way ANOVA with Tukey's post-hoc) MDA = malondialdehyde (lipid peroxidation marker); SOD = superoxide dismutase; CAT = catalase; GSH = reduced glutathione; NO = nitric oxide; TAC = total antioxidant capacity. Tissue analyzed: Colon mucosa homogenate. Values: Mean ± SE (n = 6 rats per group). MNU induction: Single intrarectal dose (30 mg/kg) at week 0. Treatments: Daily oral gavage for 12 weeks*

Histology of Colon Tissues: H&E-stained sections provided a visual narrative aligned impeccably with the biochemical data. Healthy controls *(Fig. 5-A)* displayed well-organized crypts, intact epithelium, and abundant goblet cells. The MNU-only group *(Fig. 5-B)* exhibited severe disruption, fragmented crypts, extensive goblet cell loss, and robust inflammatory infiltration. Therapeutic chemical AgNPs *(Fig. 5-C)* offered only moderate restoration, with partially regenerated crypts but persistent residual inflammation. In stark contrast, therapeutic green AgNPs *(Fig. 5-D)* revealed near-normal crypt morphology with abundant goblet cells and only mild residual inflammatory foci. Preventive chemical AgNPs *(Fig. 5-E)* provided significant protection with well-aligned crypts and minimal inflammation, but it was the preventive green AgNPs group *(Fig. 5-F)* that exhibited the most profound histoprotection perfectly healthy crypts, abundant goblet cells, and a complete absence of inflammatory infiltrate. This histological progression unequivocally demonstrates that green-synthesized AgNPs are superior in both therapeutic and preventive settings, confirming that their anticancer mechanisms involve effective oxidative stress mitigation and mucosal integrity preservation.

Discussion

Green nanotechnology is gaining momentum as researchers seek safer, more biocompatible, and environmentally responsible alternatives to conventionally synthesized nanomaterials. Traditional chemical routes for AgNPs production often rely on harsh reducing agents and organic solvents, leaving residual contaminants on particle surfaces that can compromise biocompatibility and raise concerns about cytotoxicity and systemic toxicity in clinical use, especially for vulnerable groups such as cancer patients.

By contrast, green or bioinspired synthesis employs biological systems-plants, bacteria, fungi, algae, or purified biomolecules, as intrinsic reducing and capping agents, thereby avoiding hazardous reagents and significantly lowering the ecological footprint of nanoparticle production [19]. In this study, the choice of purslane extract as a "bionanofactory" is in line with this approach: microbial enzymes, peptides, and metabolites simultaneously drive metal-ion reduction and surface capping, yielding AgNPs with improved colloidal stability, narrower size distributions, and biologically active surface coronas [20]. Such biomolecular coatings have been shown to enhance antimicrobial and anticancer performance while dampening offtarget toxicity, largely by improving hemocompatibility and reducing nonspecific damage to normal mammalian cells. This safety dimension is particularly critical when AgNPs are envisioned for longterm chemoprevention or as adjuvants alongside cytotoxic cancer drugs [21].

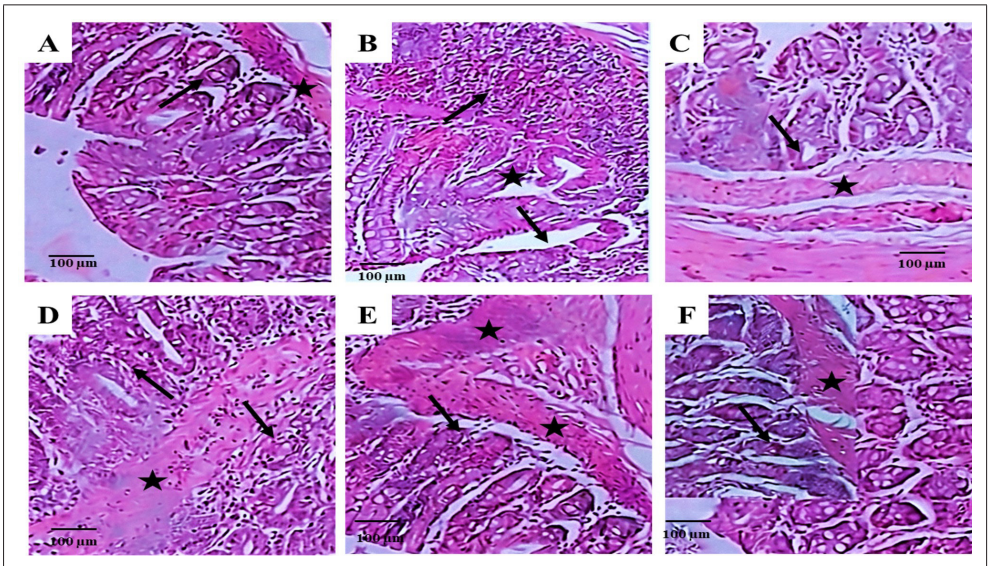

Fig 5. Histological assessment of rat colon tissue following MNU induction and AgNPs treatments. Photomicrographs (A-F) show H&E-stained sections of rat colon (magnification X400). Pointers indicate notable pathological features. **(A)** Control Group: Exhibiting normal tissue architecture with well-organized crypts and intact mucosal layers. **(B)** MNU-Treated Rats (Untreated): Showing significant disruption of crypt architecture, loss of goblet cells, and signs of inflammatory cell infiltration. **(C)** MNU + Chemical AgNPs (320 mg/kg): Demonstrating moderate restoration of tissue structure with a visible increase in goblet cells compared to the untreated MNU group. **(D)** MNU + Green AgNPs (320 mg/kg): Revealing substantial tissue repair with near-normal crypt morphology and abundant regenerated goblet cells. **(E)** MNU + Chemical AgNPs (Preventative): Displaying significant protection against MNU-induced damage, with tissue architecture resembling the control group. **(F)** MNU + Green AgNPs (Preventative): Exhibiting excellent preventative effects, maintaining healthy tissue structure and abundant goblet cells, similar to the control

Multiple comparative studies indicate that greensynthesized AgNPs exhibit stronger antioxidant activity than chemically synthesized AgNPs at comparable doses, and this aligns with the current findings. In a direct comparison using *Mussaenda frondosa* extract vs sodium citrate, green AgNPs showed "remarkable antioxidant activity" in the DPPH assay, clearly surpassing chemically synthesized AgNPs and being highlighted as preferable for biomedical use [22]. A second comparative study using *Cassia fistula* also reported higher antioxidant activity for green AgNPs (84.48% vs 75.87% for chemical AgNPs) and a lower IC_{50} for the green formulation, indicating more efficient radical scavenging at lower concentrations [23]. Mechanistically, this superiority is attributed to phytochemical capping layers (polyphenols, flavonoids, tannins, alkaloids) on green AgNPs, which provide additional redoxactive sites and stabilize surface electrons, enhancing radical scavenging compared with citratecapped or chemically reduced AgNPs that lack these bioactive shells [24].

Green-synthesized AgNPs, which show larger ZOIs and ~2-fold lower MICs than chemical AgNPs, are strongly supported by comparable studies. In this regard, Barabadi et al.[25] prepared plant-mediated AgNPs from *Zataria multiflora* and directly compared them to commercial AgNPs against *S. aureus*. Green AgNPs were roughly twice as potent, with an MIC of 4 µg/mL versus 8 µg/mL for commercial particles, and also displayed superior biofilm inhibition, especially at sub-MIC levels. This mirrors the two-fold MIC reduction and enhanced ZOIs observed in our data, particularly for *S. aureus*.

Several comparative or review studies conclude that green AgNPs generally outperform chemically synthesized AgNPs at the same or lower doses. A recent systematic review of green-synthesized, bio-capped AgNPs against multidrug-resistant bacteria reports MICs as low as 2.5 µg/mL, ZOIs up to 25 mm, and emphasizes that capping by plant/bacterial metabolites synergistically enhances antibacterial activity compared with "bare" or simply polymer-stabilized chemical AgNPs [26]. They achieve this primarily by utilizing metal nanoparticle mechanisms, such as cell membrane disruption and reactive oxygen species (ROS) generation, to effectively bypass traditional bacterial resistance pathways in a head-to-head test of green vs chemically produced AgNPs against *Salmonella typhi*, *Bacillus cereus*, and *Pseudomonas aeruginosa*, and likewise reported consistently higher antimicrobial efficacy for green particles [27-29].

More mechanistic comparisons support our interpretation that particle size, surface chemistry, and phytochemical capping explain the superior activity. A focused comparison on *S. aureus* found that greensynthesized AgNPs from Cassia seed or green tea had MICs of 5-25 µg/mL, significantly lower than citrate or $NaBH_4$ reduced AgNPs of similar size; antibacterial potency correlated inversely with size but remained higher for green AgNPs even when size was controlled [30].

The ranking of susceptibility in the study, with *S. aureus* among the most sensitive strains and some Gram-positive and Gram-negative species more tolerant, is consistent with the variable MIC ranges reported for green AgNPs. Sahu et al.[31] found that green AgNPs synthesized using citrus extract had substantially lower MICs than chemically synthesized AgNPs against both *S. aureus* and *E. coli* (~46-50 vs 77-87 µg/mL), again paralleling our ~2fold MIC advantage.

Green AgNPs show dosedependent, significantly superior antimicrobial activity compared with chemically synthesized AgNPs with roughly twofold lower MICs and larger ZOIs across diverse pathogens is in strong agreement with the broader literature, which attributes this to smaller particle size, higher surface reactivity, and synergistic phytochemical capping [26].

Green-synthesized silver nanoparticles (AgNPs) using purslane extract, which show markedly greater cytotoxicity and apoptosis in HCT116 cells than chemically synthesized AgNPs, are highly consistent with broader findings on green AgNPs in colon cancer models. Multiple studies report low micromolar IC_{50} values for plant-mediated AgNPs against HCT116 and other colorectal lines, often markedly lower than either the corresponding plant extract or a simple silver salt, reflecting synergistic effects between the metal core and the phytochemical capping layer [32]. For example, Marine algal AgNPs from *Chaetomorpha linum* and *Ulva lactuca* showed clear dosedependent cytotoxicity toward HCT116, with selective toxicity over normal colon epithelial cells and mechanistic signatures similar to our work: upregulation of proapoptotic Bax, p53, caspase3/9, and Bid, and downregulation of antiapoptotic Bcl2/Bclxl, indicating mitochondrial (intrinsic) apoptosis as the dominant pathway [33].

The marked shift in the Bax/Bcl-2 ratio and robust caspase-3 activation observed with purslane AgNPs parallel these reports. Green-synthesized *Moringa oleifera* and *Adansonia digitata* AgNPs also showed pronounced, dose-dependent killing of HCT-116 and other colon lines and modulation of key survival pathways (Wnt/β-catenin components CTNNB1, APC, LRP5/6), consistent with profound interference in proliferative signaling [34]. A recent review on green AgNPs in colon cancer highlights that, compared with chemically synthesized particles, green AgNPs generally achieve greater reductions in cell viability at lower doses, with better selectivity toward tumor over normal cells, largely via ROS-mediated mitochondrial apoptosis and p53-linked pathways [35].

Although explicit headtohead comparisons with a chemically

synthesized AgNPs control are rare, greensynthesized AgNPs frequently outperform metal salt, plant extract alone, or polymercapped AgNPs at equivalent or lower concentrations, and induce higher caspase activity and more extensive apoptosis [36]. The approximately 2fold lower IC_{50} of purslaneAgNPs compared with chemical AgNPs and the stronger activation of caspase3 and Bax, with greater Bcl2 suppression and higher apoptotic fractions, therefore fits well into a broader pattern where plantcapped AgNPs show enhanced potency and efficacy in colorectal cancer models, likely due to smaller size, improved stability, and cooperative effects of codelivered phytochemicals.

The present findings concern an MNU induced colorectal cancer model treated with green versus chemical AgNPs, focusing on growth performance/feed efficiency *(Table 4)* and tumor burden/multiplicity and histopathology *(Table 5)*. No prior work was found using exactly the same model and formulations, but several lines of evidence from other species and tumor types are relevant.

The marked reductions in tumor incidence, size, multiplicity, and dysplasia score with green AgNPs *(Table 5)* align with general oncologic observations that smaller, fewer, and lowergrade tumors are associated with better outcomes. In intrahepatic cholangiocarcinoma, tumor multiplicity is an independent adverse prognostic factor; patients with multiple tumors have survival similar to those with more advanced stage disease, leading authors to call for multiplicity to be explicitly weighted in staging systems [37]. For hepatocellular carcinoma, tumor size strongly predicts microscopic vascular invasion and high histologic grade, with lesions >5 cm having substantially higher rates of occult vascular invasion and poor differentiation than smaller tumors [38]. Analogous relationships between size and aggressive histology are seen in welldifferentiated thyroid cancer, where larger tumors show worse survival, particularly when combined with other highrisk features [39].

Histopathologic scoring systems in other tumor types (adipose and phyllodes tumors) similarly demonstrate that increasing grades of atypia, mitotic activity, and necrosis correlate with more aggressive biological behavior and worse prognosis [40]. Within this context, the shift from multiple, larger tumors with moderate dysplasia in MNU-only or chemically treated rats to fewer, smaller lesions with largely mild dysplasia under green AgNPs treatment, as shown in *Table 6*, is consistent with a genuine reduction in malignant potential rather than merely a cytostatic delay. This robust tumor suppression is strongly linked to the high concentration of plant polyphenols capping the green AgNPs, which have been independently shown to effectively manage and prevent colorectal cancer in rodent models [41].

Green AgNPs effectively mitigate MNU-induced oxidative damage in colon tissue and outperform chemically synthesized AgNPs, yielding near-complete redox and tumor protection. This aligns with extensive evidence that green AgNPs exert anticancer effects via redox modulation and apoptosis. Naringenin-capped AgNPs, are highly cytotoxic to HCT116 cells, increasing ROS/MDA, impairing ATP, triggering p53-mediated apoptosis and cell-cycle arrest, with transcriptomic enrichment of oxidation-reduction pathways [42]. Nostocsynthesized AgNPs against HCT116 and other cancer lines via oxidative stress and p53/caspase3 activation, and a range of plantmediated AgNPs are summarized in recent mechanistic and review articles [43]. A focused review on greensynthesized AgNPs for colon cancer further concludes that these particles typically induce ROS and mitochondrial dysfunction in tumor cells while showing improved biocompatibility and selective cytotoxicity relative to chemical AgNPs [35]. Collectively, these sources support the idea that green AgNPs can both protect normal tissue and attack malignant cells through contextdependent redox modulation.

The bidirectional redox behavior observed here, antioxidant in normal colon while antitumor in cancer, is also mirrored in other *in vivo* models. Chlorogenic acid–BSA AgNPs in lymphoma-bearing mice enhanced host antioxidant defenses (↑GSH, SOD, CAT, GPx; ↓MDA) while reducing tumor burden, similar to the normalization of TAC and enzyme activities observed with higher doses of green AgNPs in the current colon model [44]. In contrast, Nostoc-synthesized AgNPs selectively increased oxidative stress within tumor cells and activated p53 and caspase-3, yet spared systemic parameters, suggesting that green AgNPs can drive tumors toward lethal oxidative imbalance while maintaining host redox homeostasis [45]. Toxicological work in healthy rats shows that coating chemistry is critical: ethylene glycol AgNPs increased TAC and CAT and lowered TBARS, whereas PVP-coated AgNPs decreased GSH and TAC and increased protein carbonyls, demonstrating that surface functionalization dictates whether AgNPs shift the organism toward an antioxidant or pro-oxidant state [46]. This is consistent with broader reviews documenting that plantderived capping layers rich in polyphenols and flavonoids confer more favorable redox and safety profiles than many chemically coated formulations [8].

The present study introduces several novel elements. Most colondirected AgNPs research has been *in vitro* (HCT116, DLD1, SW480) with a focus on ROSmediated cytotoxicity and apoptosis, often without parallel evaluation of effects on normal tissue [43]. *In vivo* studies demonstrating enhancement of systemic antioxidant capacity and tumor suppression exist but typically do not directly compare

green and chemically synthesized AgNPs or quantify detailed redox-tumor correlations in a colonspecific carcinogenesis model [14]. By directly contrasting green and chemical AgNPs at matched doses, the current work extends coatingdependent redox phenomena described in toxicology models [46] into a colon carcinogen setting. The quantitative linkage between oxidative markers (MDA, TAC) and tumor size, multiplicity, body weight, and mortality also extends beyond the more inferential associations reported earlier [14]. Finally, the demonstration that prophylactic green AgNPs can almost completely prevent carcinogen-induced oxidative stress and colon tumor formation, whereas therapeutic dosing only partially reverses established lesions, addresses an early-versus-lateintervention question that has rarely been explored in AgNPs colon cancer research.

The chemopreventive and therapeutic effects of green AgNPs on MNU-induced colorectal carcinogenesis align with numerous studies on plant-mediated AgNPs in colon cancer. Multiple reports show green AgNPs exert potent, selective cytotoxicity against colorectal cancer cell lines (HCT116, HT29, Caco-2, etc.) while sparing normal cells, mirroring the tumor suppression and safety observed in our colon histology [36]. For example, pectinstabilized AgNPs showed strong cytotoxicity toward several human colorectal lines with minimal toxicity to HUVECs [47], consistent with our study.

The *in vivo* superiority of green over chemical AgNPs parallels other models, with lower toxicity. Croton tiglium AgNPs in AOM-induced colon cancer improved oxidative/inflammatory markers and histopathology, supporting a generalizable chemopreventive/therapeutic role [48].

This study confirms that purslane-derived green AgNPs are safe, eco-friendly, and potent with dual antimicrobial and anticancer applications. The sustainable synthesis avoids toxic agents and yields favorable physicochemical properties. These findings support green AgNPs as chemopreventive/adjunctive agents for colon cancer and as antimicrobials against multidrug-resistant pathogens, underscoring the value of biologically driven nanofabrication.

Declarations

Availability of Data and Materials: The datasets and analyzed during the current study available from the corresponding author (ASA) on reasonable request.

Ethical Statement: The animal study has been reviewed and approved by ZU-IACUC committee. was performed in accordance with the guidelines of the Egyptian Research Ethics Committee and the guidelines specified in the Guide for the Care and Use of Laboratory Animals (2023). Ethical code number ZU-IACUC/2/F/313/2023.

Funding Support: This research was funded by Princess Nourah bint Abdulrahman University Researchers Supporting Project number (PNURSP2026R461), Princess Nourah bint Abdulrahman University, Riyadh, Saudi Arabia Deanship of Research and Graduate Studies at King Khalid University for funding work through the Large Research Project under grant number RGP.2/586/46.

Acknowledgment: The authors gratefully acknowledge Princess Nourah bint Abdulrahman University Researchers Supporting Project number (PNURSP2026R461), Princess Nourah bint Abdulrahman University, Riyadh, Saudi Arabia. The authors extend their appreciation to the Deanship of Research and Graduate Studies at King Khalid University for funding work through the Large Research Project under grant number RGP.2/586/46.

Conflict of Interest: The authors declare that they have no conflicts of interest. All authors have given their consent that this work is valid and represent their views of the study and have given their consent for this work to be published.

Declaration of Generative Artificial Intelligence (AI): The authors declare that the article, tables and figures were not written/created by AI and AI-assisted Technologies.

Author Contributions: Conceptualization, ASA, SSM, AMA, KMA, and KAM, formal analysis, MAA, AOS, AMA, MOA, and SAA, investigation, ASA, SSM, AMA, KMA, and KAM, data curation, MAA, AOS, AMA, MOA, SMAB, and MAA, writing original draft preparation, ASA, SSM, AMA, KMA, and KAM, writing final manuscript and editing, MAA, AOS, AMA, MOA, SMAB, and MAA, visualization and methodology, ASA, SSM, AMA, KMA, KAM, MAA, AOS, AMA, MOA, SMAB, and MAA. All authors have read and agreed to the published version of the manuscript.

References

1. **Dawadi S, Katuwal S, Gupta A, Lamichhane U, Thapa R, Jaisi S, Lamichhane G, Bhattarai D, Parajuli N:** Current research on silver nanoparticles: Synthesis, characterization, and applications. *J Nanomater,* 2021:6687290, 2021. DOI: 10.1155/2021/6687290
2. **Duman H, Eker F, Akdaşçi E, Witkowska A, Bechelany M, Karav S:** Silver nanoparticles: A comprehensive review of synthesis methods and chemical and physical properties. *Nanomaterials,* 14 (18):1527, 2024. DOI: 10.3390/Nano14181527
3. **Bamal D, Singh A, Chaudhary G, Kumar M, Singh M, Rani N, Mundlia P, Sehrawat A:** Silver nanoparticles biosynthesis, characterization, antimicrobial activities, applications, cytotoxicity and safety issues: An updated review. *Nanomaterials,* 11 (8):2086, 2021. DOI: 10.3390/nano11082086
4. **Abuzeid H, Julien C, Zhu L, Hashem A:** Green synthesis of nanoparticles and their energy storage, environmental, and biomedical applications. *Crystals,* 13 (11):1576, 2023. DOI: 10.3390/cryst13111576
5. **Hamouda R, Hussein M, Abo-Elmagd R, Bawazir S:** Synthesis and biological characterization of silver nanoparticles derived from the cyanobacterium *Oscillatoria limnetica*. *Sci Rep,* 9:13071, 2019. DOI: 10.1038/s41598-019-49444-y
6. **Sadan M, Almundarij R, Haridy M, EL-Khodery S, Elzarei MF, Abo-Aziza FAM, Ibrahim ZH, Abdellatif AAH:** Can Silver nanoparticles stabilized by Shilajit *(Asphaltum punjabianum)* accelerate tibial bone defects repair in rabbits: A preliminary study. *Int J Vet Sci,* 14 (3): 512-519, 2025. DOI: 10.47278/journal.ijvs/2024.276
7. **AlGheffari HK, Aljahdali SM, Albalawi M, Obidan A, Binothman N, Aljadani M, Aldawood N, Alahmady NF, Alqahtani SS, Alkahtani AM, Allohibi A, Abu Al-Khair W, Wahdan KM, Bouqellah NA:** Mycogenic zinc nanoparticles with antimicrobial, antioxidant, antiviral, anticancer, and anti-alzheimer activities mitigate the aluminium toxicity in mice: Effects on liver, kidney, and brain health and growth performance. *Pak Vet J,* 44 (3): 763-775, 2024. DOI: 10.29261/pakvetj/2024.252

8. **Sati A, Ranade T, Mali S, Yasin HKA, Pratap A:** Silver nanoparticles (AgNPs): Comprehensive insights into bio/synthesis, key influencing factors, multifaceted applications, and toxicity- A 2024 update. *ACS Omega,* 10 (8): 7549-7582, 2025. DOI: 10.1021/acsomega.4c11045

9. **Alsamhary K:** Eco-friendly synthesis of silver nanoparticles by *Bacillus subtilis* and their antibacterial activity. *Saudi J Biol Sci,* 27 (8): 2185-2191, 2020. DOI: 10.1016/j.sjbs.2020.04.026

10. **Yu X, Li J, Mu DS, Zhang H, Liu Q, Chen G:** Green synthesis and characterizations of silver nanoparticles with enhanced antibacterial properties by secondary metabolites of *Bacillus subtilis* (SDUM301120). *Green Chem Lett Rev,* 14, 190-203, 2021. DOI: 10.1080/17518253.2021.1894244

11. **Xu J, Yıldıztekin M, Han D, Keskin C, Baran A, Baran MF, Eftekhari A, Ava CA, Kandemir Sİ, Cebe DB, Dağ B, Beilerli A, Khalilov R:** Biosynthesis, characterization, and investigation of antimicrobial and cytotoxic activities of silver nanoparticles using *Solanum tuberosum* peel aqueous extract. *Heliyon,* 9 (8):e19061, 2023. DOI: 10.1016/j.heliyon.2023.e19061

12. **Solís-Sandí I, Cordero-Fuentes S, Pereira-Reyes R, Vega-Baudrit JR, Batista-Menezes D, Montes de Oca-Vásquez G:** Optimization of the biosynthesis of silver nanoparticles using bacterial extracts and their antimicrobial potential. *Biotechnol Rep,* 40:e00816 2023. DOI: 10.1016/j.btre.2023.e00816

13. **Ali E, Abu-Hussien SH, Hesham E, Ahmed S, Mostafa H, Gamal A, El-Sayed SM, Hemdan B, Bakry A, Ebeed NM, Elhariry H, Galal A, Abd-Elhalim BT:** Compatibility and antimicrobial activity of silver nanoparticles synthesized using *Lycopersicon esculentum* peels. *AMB Express,* 14 (1):120, 2024. DOI: 10.1186/s13568-024-01774-5

14. **Wypij M, Jędrzejewski T, Trzcińska-Wencel J, Ostrowski M, Rai M, Golińska P:** Green synthesized silver nanoparticles: Antibacterial and anticancer activities, biocompatibility, and analyses of surface-attached proteins. *Front Microbiol,* 12:632505, 2021. DOI: 10.3389/fmicb.2021.632505

15. **Abada E, Habib F, Mashraqi A, Modafer Y, Alsolami W, Ismail K, Alamri A, Mashlawi A, Shater AR:** Eco-friendly synthesis and characterization of *Senna italica*-derived silver nanoparticles with broad-spectrum antimicrobial activity. *Int J Microbiol,* 2025:2072594, 2025, DOI: 10.1155/ijm/2072594

16. **Afrin S, Giampieri F, Forbes-Hernández TY, Gasparrini M, Amici A, Cianciosi D, Quiles JL, Battino M:** Manuka honey synergistically enhances the chemopreventive effect of 5-fluorouracil on human colon cancer cells by inducing oxidative stress and apoptosis, altering metabolic phenotypes and suppressing metastasis ability. *Free Radic Biol Med,* 126, 41-54, 2018. DOI: 10.1016/j.freeradbiomed.2018.07.014

17. **Poimenova I, Sozarukova M, Ratova DM, Nikitina V, Khabibullin V, Mikheev I, Proskurnina E, Proskurnin M:** Analytical methods for assessing thiol antioxidants in biological fluids: A review. *Molecules,* 29 (18):4433, 2024, DOI: 10.3390/molecules29184433

18. **Harshavardhini R, Dayanand G, Bheeshma B, Kumar OS:** A spectrum of colonic lesions in a study done at a tertiary care hospital, telangana. *Int J Multidiscip Res,* 8 (2): 1-19, 2024. DOI: 10.36948/ijfmr.2024.v06i05.28336

19. **Zehra SH, Ramzan K, Viškelis J, Viškelis P, Balčiūnaitienė A:** Advancements in green synthesis of silver-based nanoparticles: Antimicrobial and antifungal properties in various films. *Nanomaterials,* 15 (4):252, 2025, DOI: 10.3390/nano15040252

20. **Rónavári A, Igaz N, Adamecz D, Szerencsés B, Molnár C, Kónya Z, Pfeiffer I, Kiricsi M:** Green silver and gold nanoparticles: Biological synthesis approaches and potentials for biomedical applications. *Molecules,* 26 (4):844, 2021, DOI: 10.3390/molecules26040844

21. **Arshad F, Naikoo G, Hassan I, Chava S, El-Tanani M, Aljabali A, Tambuwala M:** Bioinspired and green synthesis of silver nanoparticles for medical applications: A green perspective. *Appl Biochem Biotechnol,* 196, 3636-3669, 2023, DOI: 10.1007/s12010-023-04719-z

22. **Sreelekha E, George B, Shyam A, Sajina N, Mathew B:** A comparative study on the synthesis, characterization, and antioxidant activity of green and chemically synthesized silver nanoparticles. *BioNanoSci,* 11, 489-496, 2021. DOI: 10.1007/s12668-021-00824-7

23. **Arland SE, Kumar J:** Green and chemical syntheses of silver nanoparticles: Comparative and comprehensive study on characterization, therapeutic potential, and cytotoxicity. *Eur J Med Chem Rep,* 11:100168, 2024. DOI: 10.1016/j.ejmcr.2024.100168

24. **Sarwer Q, Amjad M, Mehmood A, Binish Z, Mustafa G, Farooq A, Qaseem M, Abasi F, De La Lastra JP:** Green synthesis and characterization of silver nanoparticles using *Myrsine africana* leaf extract for their antibacterial, antioxidant and phytotoxic activities. *Molecules,* 27 (21):7612, 2022. DOI: 10.3390/molecules27217612

25. **Barabadi H, Mojab F, Vahidi H, Marashi B, Talank N, Hosseini O, Saravanan M:** Green synthesis, characterization, antibacterial and biofilm inhibitory activity of silver nanoparticles compared to commercial silver nanoparticles. *Inorg Chem Commun,* 129:108647, 2021. DOI: 10.1016/j.inoche.2021.108647

26. **Girma A, Alamnie G, Bekele T, Mebratie G, Mekuye B, Abera B, Workineh D, Tabor A, Jufar D:** Green-synthesised silver nanoparticles: Antibacterial activity and alternative mechanisms of action to combat multidrug-resistant bacterial pathogens: A systematic literature review. *Green Chem Lett Rev,* 17:108647, 2024, DOI: 10.1080/17518253.2024.2412601

27. **Hannan A, Du XX, Maqbool B, Khan A:** Nanoparticles as potent allies in combating antibiotic resistance: A promising frontier in antimicrobial therapy. *Pak Vet J,* 44 (4): 957-967, 2024. DOI: 10.29261/pakvetj/2024.227

28. **Batool S, Hashim M, Naseem F, Razzaq MF, Fakhar M, Khalid RUB, Ejaz H, Minal Z, Asad A, Khan AMA, Shakir MZ:** Mechanism and application of metal nanoparticles as antimicrobial agents. *Continental Vet J,* 5 (1): 93-102, 2025. DOI: 10.71081/cvj/2025.041

29. **Chahar V, Sharma B, Shukla G, Srivastava A, Bhatnagar A:** Study of antimicrobial activity of silver nanoparticles synthesized using green and chemical approach. *Colloids Surf A: Physicochem Eng Asp,* 554, 149-155, 2018, DOI: 10.1016/j.colsurfa.2018.06.012

30. **Secario MK, Truong T, Chen CC, Lai J, Lue S:** Exploring antibacterial effectiveness: A comparative analysis of green and chemical synthesis of silver nanoparticles against *Staphylococcus aureus. J Taiwan Inst Chem Eng,* 165:105750, 2024. DOI: 10.1016/j.jtice.2024.105750

31. **Sahu SK, Sahoo P, Dash S, Mishra SR, Behera PC:** Antimicrobial activity of silver nanoparticles against common bovine mastitis pathogens: A comparative analysis. *Curr Microbiol,* 82 (3):121, 2025. DOI: 10.1007/s00284-025-04101-8

32. **Zhai Y, Wang B, Han W, Yu B, Ci J, An F:** Green synthesis of AgNPs using plant extract and investigation of its anti-human colorectal cancer application. *Open Chem,* 21 (1):174, 2023. DOI: 10.1515/chem-2023-0174

33. **Acharya D, Satapathy S, Yadav K, Somu P, Mishra G:** Systemic evaluation of mechanism of cytotoxicity in human colon cancer HCT-116 cells of silver nanoparticles synthesized using marine algae *Ulva lactuca* extract. *J Inorg Organomet Polym Mater,* 32, 596-605, 2021. DOI: 10.1007/s10904-021-02133-8

34. **Khajeh H, Fazeli-Nasab B, Pourshahdad A, Mirzaei AR, Ghorbanpour M:** Green-synthesized silver nanoparticles induced apoptotic cell death in $CACO_2$ cancer cells by activating MLH1 gene expression. *Sci Rep,* 14:29601, 2024. DOI: 10.1038/s41598-024-80809-0

35. **Dohare S, Khandal J, Dongsar TS, Gupta G, Sahebkar A, Abourehab M, Kesharwani P:** Green-synthesized silver nanoparticles: A sustainable nanoplatform for targeted colon cancer therapy. *Int J Pharm,* 683:126015, 2025. DOI: 10.1016/j.ijpharm.2025.126015

36. **Bidian C, Filip GA, David L, Moldovan B, Olteanu D, Clichici S, Olănescu-Vaida-Voevod MC, Leostean C, Macavei S, Muntean DM, Cenariu M, Albu A, Baldea I:** Green synthesized gold and silver nanoparticles increased oxidative stress and induced cell death in colorectal adenocarcinoma cells. *Nanomaterials,* 13 (7):1251, 2023. DOI: 10.3390/nano13071251

37. **Yoon SJ, Park S, Kim H, Shin SH, Heo JS, Rhu J, Choi GS, Kim JM, Joh JW, Han IW:** The oncologic implications of tumor multiplicity

in intrahepatic cholangiocarcinoma: Its prognostic value might be underestimated. *Cancer Res Treat,* 55, 948-955, 2023. DOI: 10.4143/crt.2023.290

38. **Pawlik TM, Delman KA, Vauthey JN, Nagorney DM, Ng IO, Ikai I, Yamaoka Y, Belghiti J, Lauwers GY, Poon RT, Abdalla EK:** Tumor size predicts vascular invasion and histologic grade: Implications for selection of surgical treatment for hepatocellular carcinoma. *Liver Transplantation,* 11 (9): 1086-1092, 2005. DOI: 10.1002/lt.20472
39. **Ginzberg SP, Sharpe J, Passman JE, Amjad W, Wirtalla CJ, Soegaard Ballester JM, Finn CB, Mandel SJ, Kelz RR, Wachtel H:** Revisiting the relationship between tumor size and risk in well-differentiated thyroid cancer. *Thyroid,* 34 (8): 980-989, 2024. DOI: 10.1089/thy.2023.0327
40. **Deacu M, Bosoteanu M, Enciu M, Cozaru GC, Cojocaru O, Baltatescu GI, Nicolau AA, Orasanu CI, Caraban BM, Voda RI:** The predictive role of the histopathological scoring system in adipose tumors-lipoma, atypical lipomatous tumor, and liposarcoma. *Diagnostics,* 13 (24):3606, 2023. DOI: 10.3390/diagnostics13243606
41. **Gurunathan S, Qasim M, Park C, Yoo H, Kim JH, Hong K:** Cytotoxic potential and molecular pathway analysis of silver nanoparticles in human colon cancer cells HCT116. *Int J Mol Sci,* 19 (8):2269, 2018. DOI: 10.3390/ijms19082269
42. **Liu D, Huang L, Zhou Q, Meng Y:** Colorectal cancer management and prevention using plant polyphenols in the rodent models. *Pak Vet J,* 44 (3): 571-580, 2024. DOI: 10.29261/pakvetj/2024.231
43. **Khan MS, Alomari A, Tabrez S, Hassan I, Wahab R, Bhat SA, Alafaleq NO, Altwaijry N, Shaik GM, Zaidi SK, Nouh W, Alokail MS, Ismael MA:** Anticancer potential of biogenic silver nanoparticles: A mechanistic study. *Pharmaceutics,* 13 (5):707, 2021. DOI: 10.3390/pharmaceutics13050707
44. **Roy T, Dey S,K Pradhan A, Chaudhuri AD, Dolai M, Mandal SM, Choudhury SM:** Facile and green fabrication of highly competent surface-modified chlorogenic acid silver nanoparticles: Characterization and antioxidant and cancer chemopreventive potential. *ACS Omega,* 7, 48018-48033, 2022. DOI: 10.1021/acsomega.2c05989
45. **Hamida RS, Albasher G, Bin-Meferij MM:** Oxidative stress and apoptotic responses elicited by nostoc-synthesized silver nanoparticles against different cancer cell lines. *Cancers,* 12 (8):2099, 2020. DOI: 10.3390/cancers12082099
46. **Docea AO, Calina D, Buga AM, Zlatian O, Paoliello MMB, Mogosanu GD, Streba CT, Popescu EL, Stoica AE, Bîrcă AC, Vasile BŞ, Grumezescu AM, Mogoanta L:** The effect of silver nanoparticles on antioxidant/pro-oxidant balance in a murine model. *Int J Mol Sci,* 21 (4):1233, 2020. DOI: 10.3390/ijms21041233
47. **Wang D, Geng W, Li Q, Li G, Zhang D, Zhang H:** Ultrasonic green synthesis of silver nanoparticles mediated by pectin: Characterization and evaluation of the cytotoxicity, antioxidant, and colorectal carcinoma properties. *Arabian J Chem,* 15:103500, 2021, DOI: 10.1016/j.arabjc.2021.103500
48. **Aboulthana W, Ibrahim N, Osman NM, Seif M, Hassan A, Youssef AM, El-Feky AM, Madboli A:** Evaluation of the biological efficiency of silver nanoparticles biosynthesized using *Croton tiglium* L. seeds extract against azoxymethane induced colon cancer in rats. *Asian Pac J Cancer Prev,* 21, 1369-1389, 2020. DOI: 10.31557/apjcp.2020.21.5.1369

Kafkas Universitesi Veteriner Fakultesi Dergisi
Journal Home-Page: http://vetdergikafkas.org
E-ISSN: 1309-2251

Kafkas Univ Vet Fak Derg
32 (4): 585-595, 2026
DOI: 10.9775/kvfd.2026.37003

RESEARCH ARTICLE

The Toxic Effects of Combined Exposure to Copper Sulfate and Polystyrene Microplastics on Sperm Quality and Testicular Tissues in Male Mice

Sheng KANG [1,2 (‡)], Mi CHEN [1,2 (‡)], Yaao PAN [1,2], Bingxin LV [1,2], Zhenyu CHANG [1,2 (*)]

[‡] *These authors contributed equally to this work*

[1] Xizang Agriculture and Animal Husbandry University, College of Animal Science, Linzhi 860000, Xizang, P. R. CHINA

[2] Key Laboratory for Prevention and Control of Hydatid Disease in Xizang (Co-constructed by Ministry and Province), Ministry of Agriculture and Rural Affairs,College of Animal Science, Xizang Agricultural and Animal Husbandry University, Linzhi 860000, Xizang, P. R. CHINA

(*) Corresponding author:
Zhenyu Chang
Phone: +86-17689548312
E-mail: changzhenyu@xza.edu.cn

How to cite this article?

Kang S, Chen M, Pan Y, Lv B, Chang Z: The Toxic Effects of Combined Exposure to Copper Sulfate and Polystyrene Microplastics on Sperm Quality and Testicular Tissues in Male Mice. *Kafkas Univ Vet Fak Derg*, 32 (4): 585-595, 2026.
DOI: 10.9775/kvfd.2026.37003

Article ID: KVFD-2026-37003
Received: 04.05.2026
Accepted: 23.07.2026
Published Online: 27.07.2026

Abstract

Both copper sulfate ($CuSO_4$) and polystyrene microplastics (PS-MPs) exhibit toxic effects on the male reproductive system. Notably, PS-MPs can adsorb copper ions, making their combined pollution-induced reproductive toxicity and underlying mechanisms urgent to clarify. This study aimed to investigate the toxic effects of $CuSO_4$ and PS-MPs co-exposure on sperm quality and testicular tissue in male mice, and to determine potential synergism, thereby providing a basis for assessing reproductive health risks. Male mice were randomly divided into control, $CuSO_4$, PS-MPs, and combined exposure groups, with continuous intragastric administration for 30 days. Sperm parameters, testicular histopathology, cell apoptosis, and apoptosis-related protein expressions [Bcl-2-associated X protein (Bax), B-cell lymphoma-2 (Bcl-2), cysteinyl aspartate specific proteinase-3 (Caspase-3), tumor protein p53 (p53)] were detected. Results showed that combined exposure most significantly inhibited body weight gain ($P<0.05$). Compared with single exposure, the combined group exhibited more severe sperm quality deterioration, severe testicular histopathological lesions, and a significant increase in Terminal deoxynucleotidyl transferase dUTP nick end labeling (TUNEL)-positive cells ($P<0.05$ or $P<0.01$). Western blot analysis confirmed upregulated expressions of Bax, Caspase-3, and p53, and downregulated Bcl-2 in the combined group, indicating activation of the apoptotic pathway. In conclusion, $CuSO_4$ and PS-MPs have aggravated toxic effects on the male reproductive system, and the mechanism involves the activation of apoptotic signaling.

Keywords: Combined exposure, $CuSO_4$, Male reproductive toxicity, PS-MPs, Sperm quality

INTRODUCTION

The rapid pace of industrialization and urbanization has led to the coexistence of various pollutants in the environment. Copper sulphate ($CuSO_4$) is a chemical commonly used in electroplating, pesticides and aquaculture; the copper pollution in water bodies caused by the discharge of wastewater containing this substance cannot be overlooked [1,2]. Meanwhile, polystyrene microplastics (PS-MPs) are one of the most frequently detected types of microplastics in the environment [3], and they can coexist with $CuSO_4$ in the environment [4]. Recent studies have shown that the combined exposure of PS-MPs and heavy metals such as cadmium can synergistically damage male reproductive functions through the ferroptosis pathway [5], suggesting that the combined pollution of microplastics and metal ions may have similar synergistic toxicity mechanisms. However, the toxic effects of $CuSO_4$ combined with PS-MPs on the male reproductive system, as well as the underlying molecular mechanisms, remain largely unexplored, representing a critical scientific gap in the field of environmental reproductive toxicology.

Previous studies have demonstrated that excessive exposure to $CuSO_4$ has significant toxicity to the male reproductive system [6,7]. The main target organs of excessive copper are the testes, especially the spermatogenic tubules and supporting cells, followed by the interstitial tissue. Notably, most existing studies have focused on copper-induced damage to spermatogenic tubules, while research on the effects of $CuSO_4$ exposure on testicular interstitial tissue remains scarce. Specifically, copper exposure first

leads to damage of the spermatogenic epithelium, causing disruption of the structure of the spermatogenic tubules, with the main characteristics being the detachment, disorder, and even vacuolation of spermatogenic epithelial cells [7,8]. The mechanism involves the accumulation of copper ions in the testicular tissue: excessive copper triggers oxidative stress and damages mitochondrial function, ultimately leading to apoptosis of reproductive cells [1]; at the same time, it can interfere with the function of the hypothalamus-pituitary-gonadal axis, inhibit the ERK signaling pathway, and reduce the levels of gonadotropin-releasing hormone, follicle-stimulating hormone, and luteinizing hormone, ultimately resulting in spermogenesis disorders and decreased fertility [9]. Particularly importantly, recent studies suggest that copper nanoparticles can also directly damage the interstitial tissue, inducing Leydig cell apoptosis and steroidogenesis disorders through activating the ERK1/2 signaling pathway [10]; this is different from the mechanism of $CuSO_4$ inhibiting the ERK pathway. However, whether traditional $CuSO_4$ exposure can directly damage interstitial tissue, and if so, how this damage interacts with spermatogenic tubule injury, remains unclear and requires further investigation.

PS-MPs are formed by the long-term weathering and mechanical fragmentation of polystyrene in the environment, with most of them having a diameter of less than 5 mm [3]. Due to their small particle size and large specific surface area, PS-MPs can adsorb and carry other pollutants for migration, and enter the animal body through ingestion or respiration [11,12]. After reaching the testes, PS-MPs can penetrate the blood-testis barrier and directly act on the epithelial cells of the spermatogenic tubules [11,12]. The disruption of the structure of the spermatogenic tubules leads to the inhibition of spermatogenic cell proliferation, resulting in a decrease in sperm concentration and motility, and an increase in the rate of sperm abnormalities. Deng et al. [13] confirmed that PS-MPs can damage the reproductive performance of male mice and disrupt the lipid homeostasis of the offspring, suggesting their transgenerational toxicity risk; Hou et al.[14] reported that continuous intragastric administration of 5 μm PS-MPs (5 mg/d) significantly reduced the testosterone level in mice. These studies indicate that PS-MPs can interfere with testosterone secretion [15,16], but compared to heavy metals, the damage effect of PS-MPs exposed alone is relatively mild, mainly showing chronic and progressive damage characteristics [17]. Heavy metals such as copper can cause significant oxidative stress and cell apoptosis within a short period of time [1,2]. However, the reproductive toxicity of PS-MPs often only becomes apparent after long-term low-dose exposure, through the continuous activation of the p38 MAPK signaling pathway [18], the upregulation of the Bax/Caspase-3 apoptotic cascade reaction, and the progressive disruption of the blood-testis barrier integrity [12,19], resulting in reproductive system damage. It is particularly important to note that there are differences in reproductive toxicity among different particle sizes of PS-MPs (0.1 μm vs 1 μm). The toxicity of small particle sizes is more significant when combined with cadmium exposure [20]. Additionally, the surface of PS-MPs can adsorb copper ions in the environment, altering the bioavailability and toxicity effects of copper [4,21]. This carrier effect may enhance the combined toxicity risk of the two [22]. Further research has found that the combined exposure of PS-MPs and arsenic has been proven to cause transgenerational reproductive toxicity [23], confirming that the combined exposure of microplastics and metal pollutants has a synergistic reproductive risk and cross-generational health hazards.

Given the combined exposure risk of $CuSO_4$ and PS-MPs and the carrier effect of PS-MPs, the synergistic toxicity of both on the male reproductive system and its mechanism need to be clarified. Therefore, in this study, male mice were used as the subjects, and models of $CuSO_4$ and PS-MPs exposure alone and in combination were established. The indicators such as sperm concentration, motility, and deformity rate were detected, and the pathological changes of testicular tissues were observed. The expressions of apoptosis-related proteins such as Bax, Bcl-2, Caspase-3, and p53 were analyzed to explore the toxic effects and synergistic effects of combined exposure, providing experimental basis for the reproductive health risk assessment of environmental complex pollutants.

Material and Methods

Ethical Approval

All experimental procedures conformed to the ethical standards for laboratory animals, and the animal experimental protocol was reviewed and approved by the Animal Ethics Committee of South China Agricultural University with the ethics approval number 2025F386. During the feeding process, care was taken to handle the mice gently to reduce their stress response.

Experimental Animals and Conditions

Twenty-four 6-week-old male C57BL/6J mice (weighing 20-22 g) were selected (purchased from Guangdong Zhiyuan Biomedical Technology Co., Ltd.). The experimental diet and bedding materials for the mice were also purchased simultaneously. Before the start of the experiment, the mouse cages were thoroughly cleaned and disinfected. All the experimental animals were housed in the Experimental Center of the Animal Hospital of South China Agricultural University. The

environmental conditions were strictly controlled at a temperature of 22°C-24°C, a relative humidity of 50±10%, and a 12-h light/dark cycle. The mice had free access to food and water. The body weight, food intake, and water intake of each group of mice were weighed and recorded before each intragastric administration. Fresh mouse food and water were changed daily, and the bedding material was replaced every 3 days. After 1 week of adaptive feeding, the mice were randomly divided into 4 groups (n=6) according to their body weight: the control group (Ctrl), the copper sulfate group (Cu), the polystyrene microplastic group (Ps), and the combined exposure group (Cu+Ps). The names of each group corresponded to the treatment methods the mice received. The Ctrl group did not undergo any special treatment and was given 0.1 mL of deionized water by intragastric administration. The Cu group was given 0.1 mL of $CuSO_4$ solution, the Ps group was given 0.1 mL of PS-MPs solution, and the Cu+Ps group was given 0.1 mL of $CuSO_4$ solution + 0.1 mL of PS-MPs solution. The treatment was continued for 30 days, and then the mice were sacrificed by cervical dislocation and tissue samples were collected.

Instruments and Reagents

The main experimental instruments used in this study are: Vortex TM-1F Vortex Mixer (WIGGENHAUSER, Germany), DM1000 Optical Microscope (Leica, Germany), KZ Tissue Grinder (Wuhan Sevier Biotechnology Co., Ltd.), TGL-16B Benchtop Centrifuge (Shanghai Anting Scientific Instrument Factory), ME204 Electronic Balance (Mettler Toledo), 5804R Refrigerated Centrifuge (Eppendorf, Germany), Nanodrop 2000 Micro-Volume UV-Vis Spectrophotometer (ThermoFisher Scientific, USA), HI1220 Slide Holder (Leica, Germany), DHG-9123A Forced Air Drying Oven (Shanghai Yiheng Technology Co., Ltd.), SLK-O3000-S Shaker (Sorvall, USA), ELx808 Microplate Reader (BIOTECK, USA), PB-10 pH Meter (Sartorius, Germany), Unique-R10 Ultrapure Water System (Wuxi Xinyi Science Instrument Co., Ltd.), UVPChemStudio515 Multi-Mode Imager (Jena Analytics Co., Ltd.), DW-86L626 -80□ Ultra-Low Temperature Freezer (Haier Home Appliance Co., Ltd.), IMS Automatic Snowflake Ice Maker (Shanghai Xueshuo Ke Electrical Appliance Co., Ltd.), RH Basic2 Heating Magnetic Stirrer (IKA, Germany), EPS600 Electrophoresis System (Shanghai Tianeng Co., Ltd.), BG-Power600 SDS-PAGE Protein Electrophoresis Apparatus (Shanghai Tianeng Technology Co., Ltd.), DMi8 Inverted Fluorescence Microscope (Leica, Germany), RM2235 Rotary Microtome (Leica, Germany).

The main reagents and consumables are as follows: 2.5% (w/v) Microplastic Monodisperse Suspension (Cat. SEQ01-00250, Tianjin Saierqun Technology Co., Ltd.), Hematoxylin-Eosin Staining Solution (Cat. G1005-500ML, Wuhan Sevier Biotechnology Co., Ltd.), Copper Sulfate (500 g, Tianjin Zhiyuan Chemical Reagent Co., Ltd.), Paraformaldehyde (Cat. EKKS1699, Shanghai Ika Biotechnology Co., Ltd.), Ethanol (500 mL, Guangzhou Chemical Reagent Factory), PBS Buffer (Cat. G0002-2L, Wuhan Sevier Biotechnology Co., Ltd.), PMSF (Cat. ST505, Wuhan Sevier Biotechnology Co., Ltd.), RIPA Lysis Buffer (Cat. P0013B, Shanghai Beyotime Biotechnology Co., Ltd.), Universal Antibody Diluent (Cat. WB500D, Shanghai Xinseme Biotechnology Co., Ltd.), SDS-PAGE Gel Preparation Kit (Cat. E304-01, Nanjing Novizan Biotechnology Co., Ltd.), PVDF Membrane (Cat. ISEQ15150, Sigma, USA), BCA Protein Concentration Assay Kit (Cat. E112-01, Shanghai Xinseme Biotechnology Co., Ltd.), Tris (Cat. T8060, Shanghai Solabao Technology Co., Ltd.), SDS (Cat. 227, Biosharp, USA), Chemiluminescent Substrate (Cat. P2100, Shanghai Xinseme Biotechnology Co., Ltd.), Protein Marker (Cat. RM19001, Beijing Kangwei Century Biotechnology Co., Ltd.), Primary Antibodies (Bcl-2, Cat. A19693; Bax, Cat. A19684; p53, Cat. A19585; Caspase-3, Cat. A19664, all from Wuhan Abiotech Biotechnology Co., Ltd.; GAPDH, Cat. A19056, from Beijing Boacon Biotechnology Co., Ltd.), Secondary Antibodies (Goat Anti-Mouse IgG, Cat. CW0102S; Goat Anti-Rabbit IgG, Cat. CW0103S, both from Beijing Kangwei Century Biotechnology Co., Ltd.).

The concentration settings of $CuSO_4$ and microplastic gavage solutions in this study were supported by published oral toxicological models of male mice [24-26]. The reagents used in this paper are prepared as follows: $CuSO_4$ solution: Weigh 1.4 g of anhydrous $CuSO_4$ precisely according to the experimental requirements and add it to 70 mL of deionized water. Finally, prepare a working solution of $CuSO_4$ with a concentration of 20 mg/mL and store it for later use [24]. Microplastic solution: Precisely measure 8.4 mL of the single-dispersed suspension of microplastics (2.5%, w/v) and add it to 26.6 mL of deionized water. Finally, prepare a microplastic mixture solution with a concentration of 6 mg/mL and store it for later use [25]. The grouping scheme of single exposure and combined co-exposure was designed with reference to Chang et al.[26]. Polyformaldehyde fixative solution (4%): Dissolve 40 g of polyformaldehyde in 800 mL of PBS, heat it and add NaOH to fully dissolve it. Let it cool naturally and then adjust the pH to 7.2-7.4 with 1 mol/L HCl. Finally, make up to 1000 mL with PBS. Transfer solution: Weigh 3.03 g of Tris and 14.41 g of glycine, mix them thoroughly with 800 mL of ddH_2O, and then add 200 mL of methanol to fully dissolve them. TBST working solution (1x): Mix 50 mL of TBST (10x) with 450 mL of deionized water thoroughly, prepare TBST (1x), store it at 4□ for later use. Blocking solution: Weigh 6 g of skimmed milk powder, add it to 120 mL of TBST (1×), and mix thoroughly to fully dissolve it.

General Physiological Indicators

The body weight, food intake and water intake of each mouse were measured and recorded before each gavage.

The average body weight of the mice in this group = total weight of all mice in the group/number of mice in the group

The average daily water intake of the mice in this group = total daily water intake of all mice in the group / number of mice in the group

Sample Collection

After continuous intragastric administration for 30 days, all the experimental mice were sacrificed by cervical dislocation. Then, the bilateral testicles and epididymis of the mice were removed, weighed precisely, and used to calculate the organ coefficient. One testicle from each mouse was taken out, rinsed with normal saline to remove surface impurities, and then one testis was fixed in 4% formaldehyde for subsequent histopathological examination and Terminal deoxynucleotidyl transferase dUTP nick end labeling (TUNEL) staining, while the other was rapidly preserved in liquid nitrogen for subsequent Western blot analysis.

Sperm Count, Motility, and Abnormality Rate

After the animals are sacrificed, the epididymis is quickly collected and the surrounding tissues are removed. It is slowly placed into 1 mL of physiological saline at 37□, sterilized under high pressure, and then cut into pieces using an ophthalmic scalpel to fully disperse the sperm at the tail end of the epididymis in the physiological saline. The sperm count is determined using a sperm counting plate under an optical microscope. The number of sperm within the grid is counted using a cell counting plate to determine the sperm count. The proportion of live sperm to the total sperm count is defined as sperm motility, and the proportion of abnormal sperm to the total sperm count is defined as sperm abnormality rate. Then, according to the manufacturer's instructions, the slides are stained with sperm staining solution. Each sample is observed three times. To reduce subjective bias, the relevant observations and counts are completed by personnel who are not aware of the experimental grouping.

Testicular Index

After the 30-day trial period ended, the body weight of the mice was measured. Then, the mice were dislocated and processed, and their testicles were immediately removed, with the surrounding fat and connective tissues being removed and weighed. The ratio of testicle weight to mouse weight (testicle coefficient) was expressed as (testicle weight/mouse weight) x 100%.

Observation of Testicular Histopathology

The fixed testicles were cut into small blocks measuring 5 mm x 5 mm x 3 mm, which were then subjected to stepwise ethanol dehydration, xylene clearing and paraffin infiltration before being embedded to produce paraffin blocks. Using a microtome, the paraffin block was sectioned into a series of 3-5 μm thick sections. The sections were mounted onto slides and heat-set at 60°C for 2-4 h to fix them. Following dewaxing in xylene and a gradient of ethanol, the sections were rinsed twice with distilled water; hematoxylin-eosin (HE) staining was then performed, involving sequential treatment with hematoxylin solution for 5-10 min, followed by rinsing with water, differentiation with hydrochloric acid-alcohol for 30 sec to 1 min, re-staining with ammonia solution, and staining with eosin solution for 1-3 min. Following staining, the sections were rapidly dehydrated using a gradient of ethanol and cleared with xylene, before being mounted with neutral resin. Upon completion of mounting, the sections were examined under a microscope and photographed.

TUNEL Staining

After paraffin sections have been deparaffinised using an environmentally friendly deparaffinising solution, they are sequentially rehydrated using a gradient of anhydrous ethanol, rinsed with distilled water, and a hydrophobic ring is drawn around the specimen using an immunohistochemistry waterproof pen. Proteinase K working solution (1:9) is then added, and the sections are incubated at 37°C for 20 min; Membrane lysis was performed as required (20 min at room temperature), followed by three 5-min washes in PBS and a 10-min incubation in equilibrated buffer at room temperature; Incubate with TUNEL reaction mixture (TdT enzyme: dUTP: buffer = 2:5:50) at 37°C in the dark for 1 h; wash with PBS, counterstain with DAPI for 10 min, mount with anti-fade mounting medium, observe under a fluorescence microscope to capture images, and analyse positive expression using ImageJ software.

Extraction of Total Protein and Western Blotting

Remove testicular tissue from the -80°C freezer, cut 0.2-0.3 g into an Eppendorf tube, add 250 μL of RIPA lysis buffer containing protease inhibitors, homogenise on an ice bath, and centrifuge at 4°C and 12.000 rpm for 10 min; collect the supernatant. Determine protein concentration using the BCA method: Dispense 25 μL of sample into a 96-well plate, add 200 μL of BCA working solution, incubate at 37°C for 30 min, and measure absorbance at 562 nm.

Western blotting: Prepare a 12% SDS-PAGE gel; load biological replicate samples from six individual mice

per group (n = 6), with each sample run once without technical replication (4 μL marker + 10 μL sample); run on a 80 V focusing gel for 30 min, followed by a 120 V separating gel for 60 min; after methanol-activating the PVDF membrane, transfer at 150 mA for 90 min; Block with 5% skimmed milk powder at room temperature for 1 h, wash three times with TBST for 10 min each; incubate with primary antibody at 4°C for 16 h, wash three times with TBST for 10 min each; incubate with the appropriate secondary antibody at room temperature for 1 h, wash three times with TBST for 5 min each; develop with developing solution, expose on an imaging system, and normalize band grayscale values to the corresponding internal reference (β-actin) prior to analyse grayscale values using ImageJ.

Statistical Analysis

All the data were sorted by Microsoft Office 2024 software and analyzed statistically using GraphPad Prism 9.5.0 software. The number of repetitions for each group of experiments was ≥3. The data were expressed as the mean ± standard deviation. When comparing between two groups, Student's t test or Mann–Whitney non-parametric test was used according to the type of data distribution to determine whether the differences between the groups were statistically significant. In multi-group comparisons, one-way ANOVA was used for continuous variables and chi-square test for categorical variables. Pairwise comparisons between groups were conducted based on Bonferroni method. When $P<0.05$, it was considered statistically significant.

Results

Changes in Mouse Body Weight, Feed Intake, and Water Intake

To evaluate the effects of $CuSO_4$, PS-MPs, and combined exposure on the general growth status of mice, the body weight changes of each group of mice were continuously recorded during the 30-day intragastric administration period, and the feed intake and water intake were statistically analyzed. The results are shown in *Fig. 1-A*. Compared with the control group, the inhibition of weight gain in the combined exposure group was the most significant, and the weight of the $CuSO_4$ group and the microplastics group also showed a certain downward trend. *Fig. 1-B, C* show that there were no statistically significant differences in feed intake and water intake among the groups ($P>0.05$

Analysis of Changes in Sperm Quantity, Vitality, Abnormality Rate and Testis Index

As shown in *Fig. 2-A*, compared with the control group, the sperm quantity in the combined exposure group significantly decreased ($P<0.01$), and the $CuSO_4$ group and the microplastic group also showed a decreasing trend; *Fig. 2-B*, the sperm vitality in the combined exposure group significantly decreased ($P<0.01$), and the $CuSO_4$ group was also lower than the control group ($P<0.05$); *Fig. 2-C*, the sperm abnormality rate in the combined exposure group significantly increased ($P<0.05$). *Fig. 2-D*, there was no statistically significant difference in the testis coefficient among the groups ($P>0.05$).

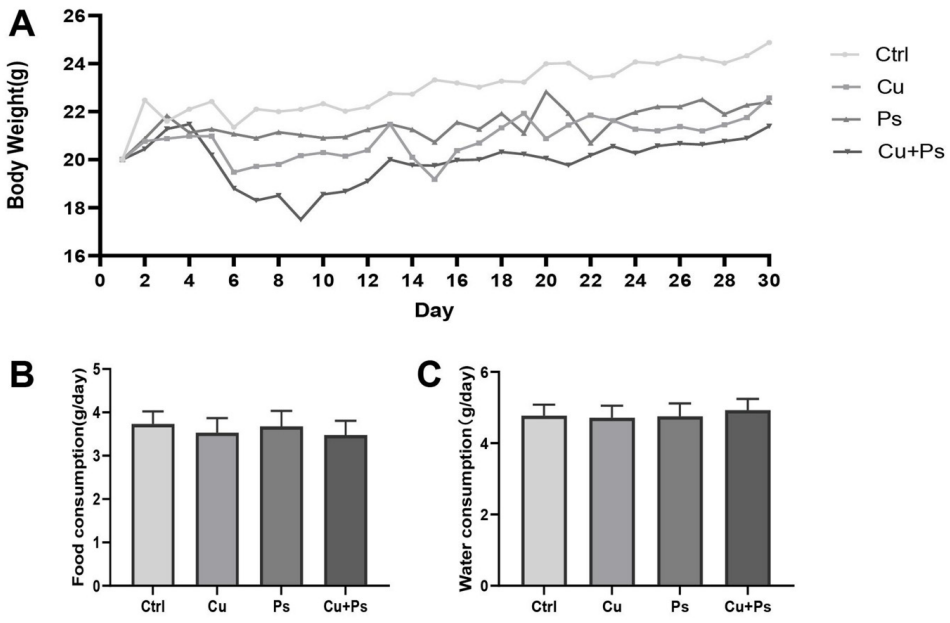

Fig 1. Changes in body weight, feed intake, and water intake of mice in each treatment group. **(A)** Body weight; **(B)** Feed intake; **(C)** Water intake. All data are presented as mean ± standard deviation (SD), n = 6 per group

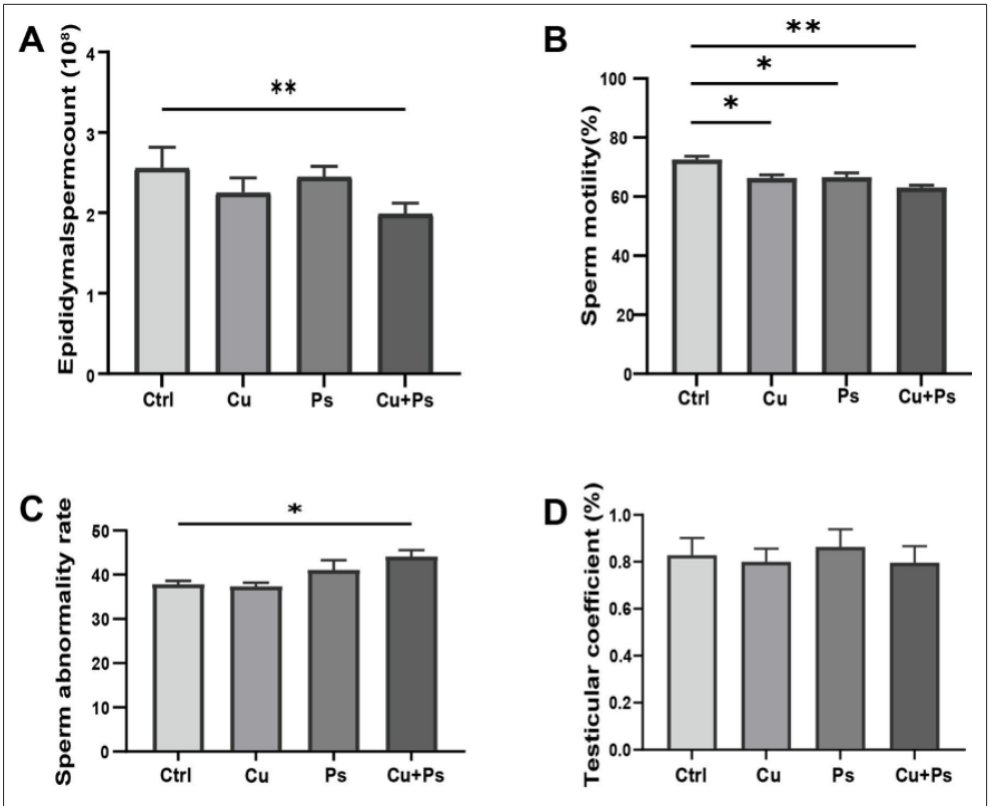

Fig 2. Sperm quality and testicular coefficient of male mice in each treatment group. (A) Seminal fluid sperm count (×108); (B) sperm motility (%); (C) sperm abnormality rate (%); (D) testicular coefficient (%). All data are presented as mean ± SD, n = 6 per group. Asterisks indicate significant differences: *P<0.05, **P<0.01

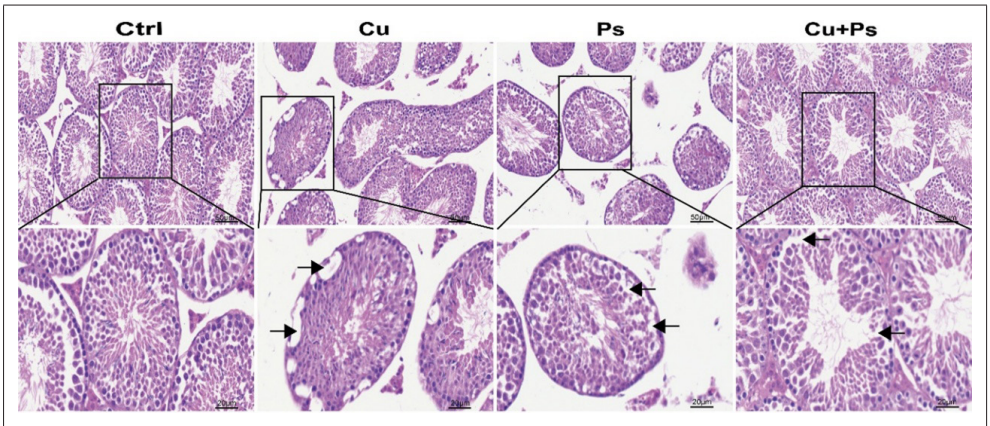

Fig 3. Morphology of mouse testicular tissue. Control group (Ctrl); copper sulfate group (Cu); polystyrene microplastics group (PS); combined exposure group (Cu + PS). Representative hematoxylin-eosin (HE) staining sections of testicular tissue. The upper row has a scale bar of 50 μm, and the lower row has a scale bar of 20 μm. Black arrows indicate typical pathological changes in testicular tissue, including vacuolation of seminiferous tubules, loose tubular wall structure, increased cell detachment, and reduced cellular components in the lumen

Pathological Observation of Testicular Tissue

H&E staining was used to observe the pathological changes of testicular tissue in each group of mice. The results are shown in *Fig. 3*. The testicular tissue structure of the control group was intact, with regular arrangement of seminiferous tubules, clear basement membrane, and distinct layers of spermatogenic epithelium. Both the $CuSO_4$ group and the microplastic group showed varying degrees of tissue damage, mainly manifested as atrophy of seminiferous tubules, disordered arrangement, shedding and vacuolation of spermatogenic epithelial cells, etc. Among them, the $CuSO_4$ group showed more obvious damage. Compared with the single exposure group, the testicular tissue damage in the combined exposure group

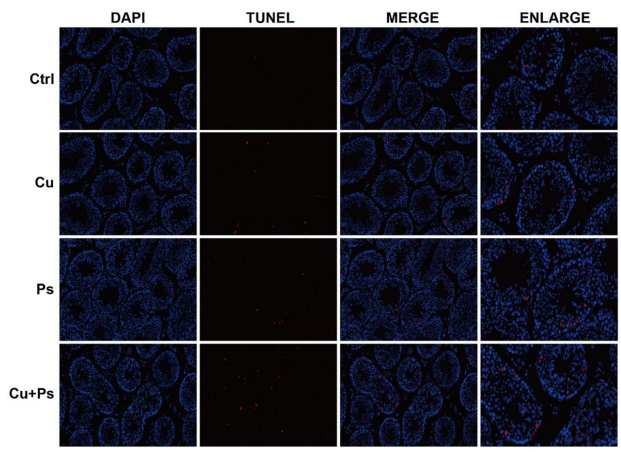

Fig 4. Results of Terminal deoxynucleotidyl transferase dUTP nick end labeling (TUNEL) fluorescence staining of testicular tissues in each treatment group. Cell nuclei stained with 4′,6-diamidino-2-phenylindole (DAPI) appear blue under ultraviolet excitation, while positive apoptotic cells are red

was the most severe, manifested as significant atrophy of seminiferous tubules, disordered structure, damage to the continuity of spermatogenic epithelium, and layer separation.

TUNEL Staining Results

TUNEL staining was used to detect the apoptosis of testicular cells in each group of mice. The results are shown in *Fig. 4*. In the control group (Ctrl), only a few red fluorescent positive cells were observed; in the $CuSO_4$ group, the microplastic group, and the combined exposure group, red fluorescent positive signals were visible, among which the positive signal in the combined exposure group was the most obvious.

Expression of Testicular Apoptosis Proteins

As shown in *Fig. 5-A*, the relative expression level of Bax protein in the testicular tissue of the combined exposure group was higher than that of the control group, and the difference was statistically significant (P<0.05). As shown in *Fig. 5-B*, compared with the control group, the relative expression level of Bcl-2 protein in the testicular tissue of the combined exposure group significantly decreased (P<0.01); although there was no significant difference between the copper group and the microplastic group (P>0.05), both showed a downward trend. As shown in *Fig. 5-C*, compared with the control group, the relative expression level of Caspase-3 protein in the testicular tissue of the combined exposure group significantly increased (P<0.05). As shown in *Fig. 5-D*, compared with the control group, the relative expression level of p53 protein in the testicular tissue of the combined exposure group significantly increased (P<0.05).

Discussion

This study established a gastric gavage exposure model to evaluate the effects of $CuSO_4$ and PS-MPs, either alone or in combination, on the reproductive system of male mice. The focus was on analyzing changes in sperm quality, pathological damage to testicular tissue, and the expression of apoptosis-related molecules. After 30 days of exposure, all the mice in each treatment group showed varying degrees of body weight reduction. Among them, the combined exposure group showed the most significant growth inhibition, followed by the $CuSO_4$ group and the microplastic group; however, there were no significant differences in food intake and water intake among the

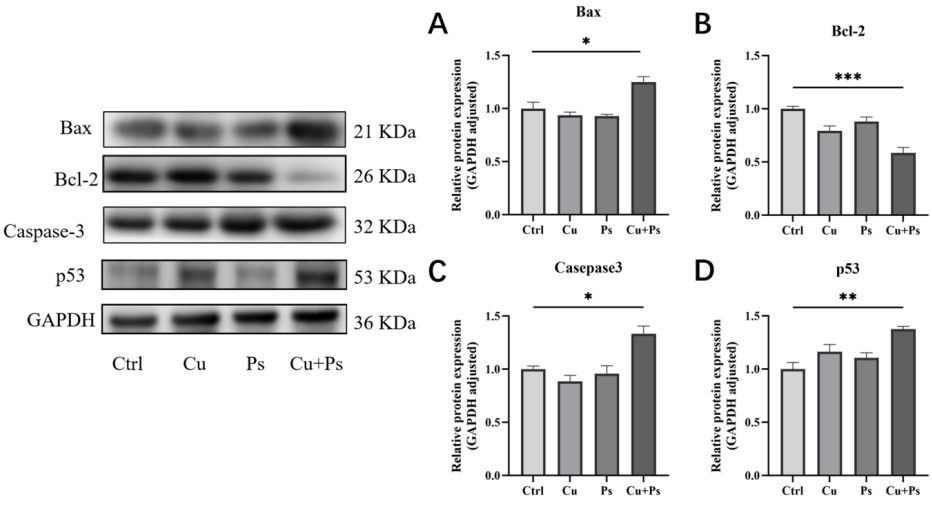

Fig 5. Expression of apoptosis-related proteins. (A) Relative expression level of Bcl-2-associated X protein (Bax); (B) Relative expression level of B-cell lymphoma-2 protein (Bcl-2); (C) Relative expression level of cysteinyl aspartate specific proteinase-3 (Caspase-3); (D) Relative expression level of tumor protein p53 (p53). All data are presented as mean ± SD, n = 6 per group. Significant differences are indicated by the symbols within the figure: *P<0.05, **P<0.01, ***P<0.001

groups. Notably, no significant inter-group differences were detected in food or water consumption, suggesting that the observed weight suppression was attributable to toxicant-induced metabolic perturbations rather than reduced caloric intake. Weight changes are often used as an indicator to reflect the overall health status of the body, so this study used it as a reference indicator for evaluating systemic toxic effects and conducted a comprehensive analysis in combination with subsequent histological and molecular detection results.

The evaluation results of sperm quality showed that both $CuSO_4$ and microplastics alone could have adverse effects on the reproductive function of male mice. Moreover, the combined exposure had a more significant impact. Compared with the control group, the combined exposure group exhibited more pronounced reductions in sperm count, decreased sperm motility, and increased sperm deformity rate, indicating a stronger interference with the process of sperm generation and maturation under the condition of combined exposure. Previous studies have shown that copper exposure can cause damage to the ultrastructure of the testis and epididymis, reduce sperm count, and accompany the occurrence of various forms of cell death [27]. While copper primarily disrupts mitochondrial electron transport and metal ion homeostasis through redox cycling, microplastics may exert toxicity via physical particle irritation, inflammatory cytokine induction, and gut-liver-testis axis perturbation. These distinct yet potentially convergent mechanisms may account for the aggravated reproductive impairment observed under co-exposure conditions, although whether this constitutes additive potentiation or true synergism remains to be statistically validated. In the cadmium testicular toxicity study by Wang et al.[28], it was also confirmed that heavy metals can cause disordered arrangement of spermatogenic cells and decline in sperm quality by inducing the accumulation of ROS, which is similar to the copper toxicity effect observed in this study. Furthermore, in the study by Elsayed et al.[29] on the reproductive toxicity of acrylamide, changes in functional indicators (sperm quality, sex hormone levels) occurred earlier than changes in testicular weight, confirming that the damage caused by environmental pollutants to the reproductive system often follows the temporal sequence of "function before structure". In the study by Ullah et al.[30] on calcium nanoparticles, it was also confirmed that particulate pollutants can induce sperm arrest and reduction of spermatogenic cells through oxidative damage, which is consistent with the reproductive damage characteristics observed in this study of PS-MPs. Although there was no significant difference in testicular index among the various treatment groups in this study, functional indicators such as sperm quantity, vitality, and deformity rate have changed significantly, indicating that at the doses and periods examined in this study, the exposure effect may initially manifest as damage to the spermatogenic process and sperm maturation quality rather than a synchronous change in testicular weight. The phenomenon of functional changes preceding structural changes is not uncommon in reproductive toxicology research. In conclusion, in subsequent studies, one can examine the effects of higher doses or longer exposure times on testicular weight, as well as assess whether there is a dose-effect relationship.

The mild dilation of the seminiferous tubule's lumen, reduced number of spermatogenic cells, and widened interstitial tissue are common pathological changes in this organ of mice after exposure to copper and microplastics [31]. In this experiment, the reproductive tissues of mice were observed through H&E staining, and it was found that the structure of the organ in the control group was intact, the seminiferous tubules were arranged neatly, and the layers of spermatogenic cells were distinct, reflecting the normal spermatogenic process. However, both the $CuSO_4$ group and the microplastic group showed varying degrees of tissue damage, such as atrophy of the seminiferous tubules, vacuolation, and shedding of spermatogenic cells. In contrast, the combined exposure group showed more obvious tissue lesions, in addition to the above changes, there were also disordered structures of the spermatogenic epithelium and local disruption of continuity, indicating that the spermatogenic function was significantly affected. Previous studies have shown that copper ions can promote the production of reactive oxygen species (ROS) and induce mitochondrial damage, thereby causing degenerative changes in reproductive tissues. While microplastics, as exogenous particles, can induce inflammatory responses and exacerbate oxidative stress levels [17]. Abduallah et al.[32] further demonstrated that metallic nanocomposites induce testicular oxidative stress, spermatogenic tubule degeneration, and epithelial detachment, suggesting that particulate pollutants may converge on oxidative stress pathways to damage testicular tissue. Additionally, Ijaz et al.[33] documented Caspase-3 activation and seminiferous tubule disruption following acrylamide exposure, while stigmasterol-mediated alleviation of PS-MP nephrotoxicity implicated the NF-κB inflammatory pathway and Bax/Caspase-3 apoptotic cascade in microplastic-induced tissue injury. Collectively, these reports suggest that under co-exposure conditions, $CuSO_4$ and PS-MPs may amplify testicular damage through the convergence of oxidative stress and inflammatory signaling pathways, rather than through isolated, independent toxic actions.

Apoptosis is one of the important pathological processes caused by environmental exposure leading to damage to

the reproductive system. Spermatogenic cells are more sensitive to oxidative stress, inflammatory responses, and barrier damage, so the level of apoptosis is often used as an indicator to evaluate reproductive toxicity [19]. The TUNEL staining results of this study showed that positive apoptotic signals appeared in the $CuSO_4$ group, microplastic group, and combined exposure group. Among them, the positive cell number in the combined exposure group was the most obvious, reflecting that the programmed cell death level of spermatogenic cells further increased under the condition of combined exposure. Further protein expression detection results showed that compared with the control group, the pro-apoptotic related proteins Bax, Caspase-3, and p53 in the combined exposure group were significantly upregulated, while the anti-apoptotic protein Bcl-2 expression decreased, indicating that the cell death-related signals in the testicular tissue were further activated. These expression patterns are consistent with the canonical intrinsic apoptotic pathway: p53 activation transcriptionally induces Bax, which oligomerizes on the mitochondrial outer membrane to form pores, triggering cytochrome c release and subsequent Caspase-3 activation, while Bcl-2 downregulation alleviates its inhibitory constraint on mitochondrial permeabilization. Studies on the toxicity of environmental toxins to the testis have also observed similar molecular expression patterns: oxidative stress activates the p53 pathway, which then upregulates pro-apoptotic proteins and inhibits the anti-apoptotic protein Bcl-2, ultimately leading to the activation of effect caspase and causing spermatogenic cell apoptosis [34]. Previous studies have shown that microplastics can promote the death of reproductive cells by inducing oxidative stress and lipid peroxidation [35], and copper homeostasis disorder may also be involved in the process of spermogenesis cell death [36]. Mechanically, oxidative stress can upregulate Bax and inhibit Bcl-2 through the p53-mediated pathway, thereby causing a decrease in mitochondrial membrane potential and the release of cytochrome C, activating the Caspase cascade reaction, and ultimately leading to reproductive cell apoptosis and testicular tissue damage [37,38]. Given the central role of oxidative stress in the reproductive toxicity of copper and microplastics, the study by El-Sayed et al.[39] on the alleviation of thiamethoxam toxicity by vitamin C suggests that antioxidant intervention may provide a potential strategy for reducing the reproductive damage caused by such environmental pollutants.

Several methodological and interpretive limitations of this study should be acknowledged. First, the sample size (n = 6 per group) is relatively modest, which may have limited the statistical power to detect subtle inter-group differences and increases the risk of type II errors. Second, although oxidative stress was repeatedly invoked as the putative underlying mechanism, the absence of direct oxidative stress biomarkers (e.g., MDA, SOD, CAT, GPx, and GSH) precludes definitive mechanistic conclusions and represents a significant gap that future studies should address. Third, no formal interaction analysis -such as two-way ANOVA interaction terms or combination index calculations- was conducted to statistically discriminate between additive, synergistic, or antagonistic effects. Therefore, descriptions implying synergistic interaction should be interpreted cautiously, and the observed exacerbation may reflect additive toxicity rather than true synergism. Fourth, the 30-day exposure duration may be insufficient to capture delayed or chronic reproductive sequelae, and the lack of a dose-response assessment limits the environmental relevance and extrapolation of these findings.

In conclusion, this study demonstrates that individual exposure to $CuSO_4$ or PS-MPs induces spermatogenic cell apoptosis and compromises sperm quality, whereas combined exposure exacerbates these adverse outcomes. The co-exposure-mediated enhancement of apoptotic responses is associated with activation of the p53-Bax/Bcl-2-Caspase-3 signaling axis, indicative of mitochondrial-dependent apoptotic pathway engagement. These findings provide experimental evidence that complex environmental pollutant mixtures pose enhanced risks to male reproductive health through the convergent activation of pro-apoptotic signaling cascades. Future investigations should incorporate larger cohorts, comprehensive oxidative stress profiling, formal interaction analyses, and extended exposure durations to substantiate the mechanisms underlying $CuSO_4$ and PS-MP co-toxicity and to inform the development of targeted antioxidant intervention strategies.

Declarations

Availability of Data and Materials: Data and materials are available from the corresponding author (ZC) upon reasonable request.

Acknowledgements: The authors thank the supporting laboratory and the reviewers and editors.

Funding Support: This work was supported by the Tibet Autonomous Region Natural Science Foundation (XZ202401ZR0003) and the Nyingchi Science and Technology Special Project (XDHZ-2025-07).

Conflict of interest: The authors declare that they have no competing interests.

Declaration of Generative Artificial Intelligence (AI): Generative AI was used only for text polishing; authors take full responsibility for the work.

Author Contributions: Conceptualization, C.Z.; methodology, C.Z., K.S.; validation, K.S., C.M., P.Y.; formal analysis, K.S., C.M., L.B.; writing - original draft preparation, K.S., C.M.; writing - review and editing, K.S., C.M.; supervision, C.Z.

References

1. **Kang Z, Qiao N, Liu G, Chen H, Tang Z, Li Y:** Copper-induced apoptosis and autophagy through oxidative stress-mediated mitochondrial dysfunction in male germ cells. *Toxicol In Vitro,* 61:104639, 2019. DOI: 10.1016/j.tiv.2019.104639
2. **Sarawi WS, Alhusaini AM, Fadda LM, Alomar HA, Albaker AB, Alghibiwi HK, Aljrboa AS, Alotaibi AM, Hasan IH, Mahmoud AM:** Nano-curcumin prevents copper reproductive toxicity by attenuating oxidative stress and inflammation and improving Nrf2/HO-1 signaling and pituitary-gonadal axis in male rats. *Toxics,* 10 (7):356, 2022. DOI: 10.3390/toxics10070356
3. **Li Y, Tao L, Wang Q, Wang F, Li G, Song M:** Potential health impact of microplastics: A review of environmental distribution, human exposure, and toxic effects. *Environ Health,* 1 (4): 249-257, 2023. DOI: 10.1021/envhealth.3c00052
4. **Qiao R, Lu K, Deng Y, Ren H, Zhang Y:** Combined effects of polystyrene microplastics and natural organic matter on the accumulation and toxicity of copper in zebrafish. *Sci Total Environ,* 682, 128-137, 2019. DOI: 10.1016/j.scitotenv.2019.05.163
5. **Lan Y, Hu L, Feng X, Wang M, Yuan H, Xu H:** Synergistic effect of PS-MPs and Cd on male reproductive toxicity: Ferroptosis via Keap1-Nrf2 pathway. *J Hazard Mater,* 461:132584, 2024. DOI: 10.1016/j.jhazmat.2023.132584
6. **Sakhaee E, Emadi L, Abshenas J, Kheirandish R, Azari O, Amiri E:** Evaluation of epididymal sperm quality following experimentally induced copper poisoning in male rats. *Andrologia,* 44, 110-116, 2012. DOI: 10.1111/j.1439-0272.2010.01147.x
7. **Chen H, Kang Z, Qiao N, Liu G, Huang K, Wang X, Pang C, Zeng Q, Tang Z, Li Y:** Chronic copper exposure induces hypospermatogenesis in mice by increasing apoptosis without affecting testosterone secretion. *Biol Trace Elem Res,* 195 (2): 472-480, 2020. DOI: 10.1007/s12011-019-01852-x
8. **Li X, Ru S, Tian H, Zhang S, Lin Z, Gao M, Wang J:** Combined exposure to environmentally relevant copper and 2,2'-dithiobis-pyridine induces significant reproductive toxicity in male guppy *(Poecilia reticulata). Sci Total Environ,* 797:149131, 2021. DOI: 10.1016/j.scitotenv.2021.149131
9. **Wang T, Wu L, Chen Q, Chen K, Tan F, Liu J, Liu X, Han H:** Copper deposition in Wilson's disease causes male fertility decline by impairing reproductive hormone release through inducing apoptosis and inhibiting ERK signal in hypothalamic-pituitary of mice. *Front Endocrinol,* 13, 961748, 2022. DOI: 10.3389/fendo.2022.961748
10. **Zheng X, Chen J, Kang L, Wei Y, Wu Y, Hong Y, Wang X, Li D, Shen L, Long C, Wei G, Wu S:** Prepubertal exposure to copper oxide nanoparticles induces Leydig cell injury with steroidogenesis disorders in mouse testes. *Biochem Biophys Res Commun,* 654, 62-72, 2023. DOI: 10.1016/j.bbrc.2023.02.067
11. **Wei Y, Zhou Y, Long C, Wu H, Hong Y, Fu Y, Wang J, Wu Y, Shen L, Wei G:** Polystyrene microplastics disrupt the blood-testis barrier integrity through ROS-mediated imbalance of mTORC1 and mTORC2. *Environ Pollut,* 289:117904, 2021. DOI: 10.1016/j.envpol.2021.117904
12. **Jin H, Ma T, Sha X, Liu Z, Zhou Y, Meng X, Chen Y, Han X, Ding J:** Polystyrene microplastics induced male reproductive toxicity in mice. *J Hazard Mater,* 401:123430, 2021. DOI: 10.1016/j.jhazmat.2020.123430
13. **Deng Y, Chen H, Huang Y, Wang Q, Chen W, Chen D:** Polystyrene microplastics affect the reproductive performance of male mice and lipid homeostasis in their offspring. *Environ Sci Technol Lett,* 9 (9): 752-757, 2022. DOI: 10.1021/acs.estlett.2c00262
14. **Hou B, Wang F, Liu T, Wang Z: Reproductive toxicity of polystyrene microplastics:** *In vivo* experimental study on testicular toxicity in mice. *J Hazard Mater,* 405:124028, 2021. DOI: 10.1016/j.jhazmat.2020.124028
15. **D'Angelo S, Meccariello R: Microplastics:** A threat for male fertility. *Int J Environ Res Public Health,* 18 (5):2392, 2021. DOI: 10.3390/ijerph18052392
16. **Jin H, Yan M, Pan C, Liu Z, Sha X, Jiang C, Li L, Pan M, Li D, Han X:** Chronic exposure to polystyrene microplastics induced male reproductive toxicity and decreased testosterone levels via the LH-mediated LHR/cAMP/PKA/StAR pathway. *Part Fibre Toxicol,* 19 (1):13, 2022. DOI: 10.1186/s12989-022-00453-2
17. **Wu D, Zhang M, Bao TT, Lan H:** Long-term exposure to polystyrene microplastics triggers premature testicular aging. *Part Fibre Toxicol,* 20 (1):35, 2023. DOI: 10.1186/s12989-023-00546-6
18. **Xie X, Deng T, Duan J, Xie J, Yuan J, Chen M:** Exposure to polystyrene microplastics causes reproductive toxicity through oxidative stress and activation of the p38 MAPK signaling pathway. *Ecotoxicol Environ Saf,* 190:110133, 2020. DOI: 10.1016/j.ecoenv.2019.110133
19. **Li S, Wang Q, Yu H, Yang L, Sun Y, Xu N, Wang N, Lei Z, Hou J, Jin Y, Zhang H, Li L, Xu F, Zhang L:** Polystyrene microplastics induce blood-testis barrier disruption regulated by the MAPK-Nrf2 signaling pathway in rats. *Environ Sci Pollut Res,* 28 (35): 47921-47931, 2021. DOI: 10.1007/s11356-021-13911-9
20. **Zhang Q, Xia W, Zhou X, Yang C, Lu Z, Wu S, Lu X, Yang J, Jin C:** PS-MPs or their co-exposure with cadmium impair male reproductive function through the miR-199a-5p/HIF-1α-mediated ferroptosis pathway. *Environ Pollut,* 339:122723, 2023. DOI: 10.1016/j.envpol.2023.122723
21. **Santos D, Cabecinha E, Luzio A, Bellas J, Monteiro SM:** Long-term effects of individual and combined exposure to microplastics and copper in zebrafish hypothalamic-pituitary-gonadal axis - A multi-biomarker evaluation. *J Environ Manage,* 378:124770, 2025. DOI: 10.1016/j.jenvman.2025.124770
22. **Cao Y, Zhao M, Ma X, Song Y, Zuo S, Li H, Deng W:** A critical review on the interactions of microplastics with heavy metals: Mechanism and their combined effect on organisms and humans. *Sci Total Environ,* 788:147620, 2021. DOI: 10.1016/j.scitotenv.2021.147620
23. **Luo Y, Zhang Z, Li X, Zhuang Z, Li Y, Wang X, Liao C, Chen L, Luo Q, Chen X:** Reproductive toxicity and transgenerational effects of co-exposure to polystyrene microplastics and arsenic in zebrafish. *Comp Biochem Physiol C Toxicol Pharmacol,* 290:110134, 2025. DOI: 10.1016/j.cbpc.2025.110134
24. **Li Y, Wang H, Zhang Y:** Copper sulfate oral gavage induces testicular oxidative damage and spermatogenesis dysfunction in adult male mice. *J Trace Elem Med Biol,* 72:126985, 2022. DOI: 10.1016/j.jtemb.2022.126985
25. **Chen X, Xu L, Chen Q:** Polystyrene micro- and nanoparticles exposure induced anxiety-like behaviors, gut microbiota dysbiosis and metabolism disorder in adult mice. *Ecotoxicol Environ Saf,* 259:115000, 2023. DOI: 10.1016/j.ecoenv.2023.115000
26. **Lv BX, Zhang H, Zhang ZQ, Pan YA, Kang S, Chen M, Li XY, Ataya FS, Luo RB, Chang ZY:** Combined exposure to copper sulfate and polystyrene microplastics alters intestinal microbiota structure and induces barrier damage in male mice. *Pak Vet J,* 46 (5): 1264-1275, 2026. DOI: 10.29261/pakvetj/2026.113
27. **Zhao D, Wu L, Fang X, Wang L, Liu Q, Jiang P, Ji Z, Zhang N, Yin M, Han H:** Copper exposure induces inflammation and PANoptosis through the TLR4/NF-κB signaling pathway, leading to testicular damage and impaired spermatogenesis in Wilson disease. *Chem Biol Interact,* 396:111060, 2024. DOI: 10.1016/j.cbi.2024.111060
28. **Wang J, Zhu H, Zhang C, Wang H, Yang Z:** Protective effects of baicalein against cadmium-induced oxidative stress in rat testes. *Pak Vet J,* 39 (2): 216-220, 2019. DOI: 10.29261/pakvetj/2019.025
29. **Elsayed A, Aboubakr M, Hassan FW, Zakaria M, Abdelhiee EY, Soliman A:** Testicular injury of acrylamide in rats and potential protection of coenzyme Q10 and rosuvastatin. *Pak Vet J,* 44 (2): 344-351, 2024. DOI: 10.29261/pakvetj/2024.146
30. **Ullah A, Al-Saeed FA, Abduallah AM, Ahmed AE, Shahzad A, Amjad N, Al-Ghanim KA, Atique U:** Calcium nanoparticles induce oxidative stress in erythrocytes, neurotoxicity and testicular toxicity in albino rats *(Rattus norvegicus). Pak Vet J,* 43 (2): 241-247, 2023. DOI: 10.29261/pakvetj/2023.036
31. **Fang Q, Wang C, Xiong Y:** Polystyrene microplastics induce male reproductive toxicity in mice by activating spermatogonium mitochondrial oxidative stress and apoptosis. *Chem Biol Interact,*

396:111043, 2024. DOI: 10.1016/j.cbi.2024.111043

32. **Abduallah AM, Aslam Z, Aldawood N, Sindi RA, Mahmood Y, Mustafa G, Ahmed AE:** Investigation of toxic effects of vanadium, magnesium and nickel nanocomposite on erythrocytes and reproductive organ of male albino rats. *Pak Vet J,* 45 (1): 328-335, 2025. DOI: 10.29261/pakvetj/2025.125
33. **Ijaz MU, Nadeem A, Hayat MF, Ehsan N, Al-Ghanim KA, Atique U:** Evaluation of possible ameliorative role of robinetin to counteract polystyrene microplastics instigated renal toxicity in rats. *Pak Vet J,* 44 (2): 400-404, 2024. DOI: 10.29261/pakvetj/2024.164
34. **Banerjee B, Chakraborty S, Ghosh D, Raha S, Sen PC, Jana K:** Benzo(a)pyrene induced p53 mediated male germ cell apoptosis: Synergistic protective effects of curcumin and resveratrol. *Front Pharmacol,* 7, 245-255, 2016. DOI: 10.3389/fphar.2016.00245
35. **Ijaz MU, Shahzadi S, Samad A, Ehsan N, Ahmed H, Tahir A, Rehman H, Anwar H:** Dose-dependent effect of polystyrene microplastics on the testicular tissues of the male Sprague Dawley rats. *Dose Response,* 19 (2):15593258211019882, 2021. DOI: 10.1177/15593258211019882
36. **Zhang JY, Yu XJ, Li JJ, Xiao Y, Li GS, Yang F, Dong L:** Cuproptosis mediates copper-induced testicular spermatogenic cell death. *Asian J Androl,* 26 (3): 295-301, 2024. DOI: 10.4103/aja202383
37. **Li Y, Chen H, Liao J, Chen K, Javed MT, Qiao N, Zeng Q, Liu B, Yi J, Tang Z, Li Y:** Long-term copper exposure promotes apoptosis and autophagy by inducing oxidative stress in pig testis. *Environ Sci Pollut Res,* 28 (39): 55140-55153, 2021. DOI: 10.1007/s11356-021-14853-y
38. **Liu Y, Li X, Xiong Y:** Chronic polystyrene microplastic exposure reduces testosterone levels in mice through mitochondrial oxidative stress and BAX/BCL2-mediated apoptosis. *Toxics,* 12 (8):561, 2024. DOI: 10.3390/toxics12080561
39. **El-Sheikh ESA, Hamed IA, Alduwish MA, Momenah MA, Melebary SJ, Alsolmy SA, Alghamdi MS, Alharbi AA, Sherif RM, Shalaby AA:** The ameliorative effect of vitamin C against sub-chronic thiamethoxam toxicity in male rats. *Pak Vet J,* 44 (3): 803-811, 2024. DOI: 10.29261/pakvetj/2024.206

Kafkas Universitesi Veteriner Fakultesi Dergisi
Journal Home-Page: http://vetdergikafkas.org
E-ISSN: 1309-2251

Kafkas Univ Vet Fak Derg
32 (4): 597-606, 2026
DOI: 10.9775/kvfd.2026.37010

Research Article

Evaluation of Serum MMP-9, IL-8, and Novel Inflammatory Indices (SIRI, AISI, SII) as Prognostic Markers in Feline Infectious Peritonitis with and without Seizure

Zeynep Nurselin KOT [1], Umit OZCAN [1 (*)], Samil Bugra KOSE [1], Tunahan KURT [1], Zulal Feyza EKER [1]

[1] Ondokuz Mayıs University, Faculty of Veterinary Medicine, Internal Medicine Department, TR-55200 Samsun - TÜRKİYE

(*) **Corresponding author:**
Umit Ozcan
Phone: +90 362 312 1919-1545
Cellular phone: +90 539 546 99 88
E-mail: umit.ozcan@omu.edu.tr

How to cite this article?

Kot ZN, Ozcan U, Kose SB, Kurt T, Eker ZF: Evaluation of Serum MMP-9, IL-8, and Novel Inflammatory Indices (SIRI, AISI, SII) as Prognostic Markers in Feline Infectious Peritonitis with and without Seizure. *Kafkas Univ Vet Fak Derg*, 32 (4): 597-606, 2026.
DOI: 10.9775/kvfd.2026.37010

Article ID: KVFD-2026-37010
Received: 25.03.2026
Accepted: 26.06.2026
Published Online: 03.07.2026

Abstract

This study aimed to evaluate serum matrix metalloproteinase-9 (MMP-9), interleukin-8 (IL-8), and hematology-derived inflammatory indices as potential prognostic markers in cats with FIP, with particular emphasis on seizure activity. Forty-eight client-owned cats diagnosed with FIP and 14 healthy control cats were included. Cats with FIP were categorized into three groups: effusive FIP (EFIP, n=11), non-effusive FIP (NFIP, n=30), and non-effusive FIP with seizures (NFIP-S, n=7). Hematological parameters were analyzed to calculate inflammatory indices including dLNR, SIRI, AISI, SII, NLR, and related ratios. Serum MMP-9 and IL-8 concentrations were measured using ELISA. Serum MMP-9 concentrations were significantly higher in cats with NFIP-S group compared with other groups ($P<0.05$). IL-8 levels were higher in the seizure group but did not differ significantly between groups. Hematology-derived inflammatory indices were significantly elevated in EFIP and NFIP groups compared with controls ($P<0.05$), whereas NFIP-S group showed values comparable to controls. MMP-9 levels were positively correlated with IL-8 (Spearman's $\rho=0.44$, $P=0.001$). MMP-9 levels were significantly associated with seizure occurrence (OR=1.13, $P=0.016$). Survival analysis demonstrated significantly shorter survival in the NFIP-S group ($P=0.042$). Elevated serum MMP-9 in cats with non-effusive FIP and seizures suggests a potential role of MMP-9 mediated blood-brain barrier disruption and neuroinflammation in seizure pathogenesis. MMP-9 may serve as a useful biomarker for neurological involvement and prognosis in FIP.

Keywords: Feline infectious peritonitis, MMP-9, IL-8, Seizure, Neuroinflammation, Blood-brain barrier

Introduction

Feline infectious peritonitis (FIP), caused by a mutated form of feline coronavirus (FCoV), is a viral disease characterized by immune-mediated vasculitis and granulomatous inflammation in its pathogenesis. FIP presents with a wide spectrum of clinical manifestations, including abdominal signs such as ascites, neurological signs such as seizures, and ocular findings such as corneal edema, and is classified into two clinical forms: effusive and non-effusive [1]. In classical models explaining the development of these clinical forms, a strong humoral (antibody) response combined with an insufficient or impaired cellular immune response leads to immune complex-mediated vasculitis and the accumulation of protein-rich serous effusions, resulting in the effusive form of the disease. In contrast, when a partially effective cellular immune response is present, widespread effusion does not occur; instead, pyogranulomatous or granulomatous lesions develop in various organs, representing the non-effusive form. These two forms should be considered as part of a disease continuum, as the pathology in an individual cat may include both effusion and granulomatous lesions [2,3].

Matrix metalloproteinase-9 (MMP-9) is a zinc-dependent endopeptidase and a member of the matrix metalloproteinase family, produced by macrophages, neutrophils, endothelial cells, and astrocytes. In FIP, intense monocyte/macrophage activation leads to increased MMP-9 activity, which degrades type IV collagen in the vascular basement membrane, thereby disrupting vascular integrity and contributing to the development of vasculitis [4,5]. In humans and laboratory animals, increased expression and activation of MMP-9 have been shown to disrupt blood-brain barrier integrity, leading to blood-brain

barrier dysfunction and contributing to the development of seizures [6,7]. Interleukin-8 (IL-8), a member of the CXC chemokine family primarily produced by monocytes and macrophages, is a proinflammatory cytokine that plays a key role in the recruitment and activation of neutrophils at sites of inflammation, and its levels have been reported to vary during the progression and remission phases of FIP alongside other proinflammatory mediators such as TNF-α, IL-1β, and IL-6 [8,9].

Because multiple inflammatory pathways are involved in the pathophysiology of FIP, the severity and duration of the disease may vary depending on the host immune response and the pathogenicity of the virus. Following the therapeutic success of nucleoside analogues in the treatment of FIP, increasing attention has been directed toward identifying factors that may help predict treatment response and prognosis [10,11]. In human medicine, several hematology-derived inflammatory markers, including the neutrophil-to-lymphocyte ratio (NLR), lymphocyte-to-monocyte ratio (LMR), platelet-to-lymphocyte ratio (PLR), and systemic immune-inflammation index (SII), have been identified as predictive indicators in severe inflammatory diseases such as COVID-19 and have also been investigated in cats with FIP [12]. However, the levels of several other hematology derived inflammatory parameters-including the derived neutrophil-to-lymphocyte ratio (dNLR), the systemic inflammation response index (SIRI), an indicator of systemic inflammation and immune activation, the aggregate index of systemic inflammation (AISI), a composite inflammation score derived from multiple hematological parameters, the platelet-to-neutrophil ratio (PNR), the neutrophil-to-monocyte ratio (NMR), and mean corpuscular volume (MCV) -have not been fully evaluated across different clinical forms of FIP.

Seizures represent one of the neurological manifestations that may develop in cats with non-effusive FIP. These seizures may persist despite antiviral treatment and may require antiepileptic therapy [13]. In some cases, persistent seizure activity may even lead to euthanasia decisions [14,15]. Previous studies have suggested that the occurrence of seizures in FIP indicates widespread systemic inflammation and structural brain damage and may therefore serve as an unfavorable prognostic indicator [14,16]. This study aimed to evaluate serum MMP-9 and IL-8 concentrations and to investigate their associations with hematology-derived inflammatory indices in cats with FIP-associated seizure activity.

Material and Methods

Ethical Statement

This study was approved by the Local Ethics Committee for Animal Experiments at Ondokuz Mayıs University on June 30, 2025, under decision number 2025/38.

Animals and Study Desing

A total of 48 cats that fulfilled the diagnostic criteria for FIP, as described by Thayer et al. [1], were included in the study. The diagnosis of FIP was based on the presence of typical clinicopathological findings. These included history of anorexia and weight loss; clinical signs including uveitis and persistent fever; ultrasonographic evidence of effusion and enlargement of abdominal lymph nodes; hematological abnormalities such as anemia; and biochemical alterations including hypoalbuminemia, hyperglobulinemia, and an albumin-to-globulin ratio below 0.4. In effusive cases, the characteristics of the effusion, a positive Rivalta test, and a high macrophage cell density in the effusion were used as key diagnostic criteria. The presence of FCoV RNA was confirmed using quantitative RT-PCR performed on whole blood samples at a commercial diagnostic laboratory according to previously described protocols [17].

Based on the clinical classification, 11 cats with effusive FIP were assigned to the EFIP group. Among cats with non-effusive FIP, 30 cats without seizure activity were assigned to the NFIP group, whereas 7 cats with seizure activity were assigned to the NFIP-S group. Seizure activity was defined as episodic focal or generalized motor events characterized by tonic, tonic-clonic, or myoclonic activity. The presence of seizures was confirmed either during clinical examination or by review of owner-provided video recordings. In addition, 14 clinically healthy cats presented for routine check-up examinations and showing no abnormalities on clinical, hematological, or biochemical evaluation were included as the healthy control (HC) group.

Blood samples were collected from the vena cephalica antebrachii of each cat. Samples for hematological analysis were obtained into EDTA-containing tubes, while samples for serum biochemistry and MMP-9 and IL-8 measurements were collected into plain tubes. Serum samples were stored at −80°C until the analysis of MMP-9 and IL-8 concentrations. Following blood sample collection, all cats received antiviral therapy with the adenosine nucleoside analogue molnupiravir at a dosage of 18 mg/kg orally twice daily (PO BID) for 60 days [14,18]. The survival status of the cats, including death, was monitored during follow-up examinations up to day 60.

Hematological Analyses and Hematology-Derived Inflammatory Indices

Blood samples collected for hematological analysis were analyzed using a Mindray BC-60R Vet Hematology

Analyzer (Mindray, China). Based on the absolute hematological parameters obtained from the complete blood count, several hematology-derived inflammatory indices were calculated, including the derived neutrophil-to-lymphocyte ratio (dNLR; N/(WBC-N)), systemic inflammation response index (SIRI; (N×M)/L), aggregate index of systemic inflammation (AISI; (N×M×P)/L), systemic immune-inflammation index (SII; (N×P)/L), neutrophil-to-lymphocyte ratio (NLR; N/L), neutrophil-to-monocyte ratio (NMR; N/M), lymphocyte-to-monocyte ratio (LMR; L/M), platelet-to-lymphocyte ratio (PLR; P/L), platelet-to-neutrophil ratio (PNR; P/N), and platelet-to-monocyte ratio (PMR; P/M).

Serum Biochemical Analyses

Serum total protein and albumin concentrations were measured as part of routine baseline laboratory analyses. Globulin concentration was calculated by subtracting albumin from total protein, and the albumin-to-globulin (A/G) ratio was subsequently determined. Serum biochemical analyses were performed using an automated analyzer (DRI-CHEM NX600; Fujifilm, South Korea).

Measurement of MMP-9 and IL-8

Serum MMP-9 and IL-8 concentrations were determined using species-specific quantitative sandwich enzyme-linked immunosorbent assay (ELISA) kits according to the manufacturer's instructions (Cat IL-8 ELISA Kit, Cat. No: E0052Cat, Lot No: 202509003; Cat MMP-9 ELISA Kit, Cat. No: E0082Cat, Lot No: 202503007; Bioassay Technology Laboratory, China).

Briefly, microplate wells precoated with specific antibodies against feline MMP-9 or IL-8 were incubated with standards and serum samples. After incubation, unbound components were removed by washing, and a biotin-labeled detection antibody was added to each well. Following further incubation and washing steps, horseradish peroxidase (HRP)-conjugated streptavidin was added to form an antibody-antigen-antibody complex. Subsequently, tetramethylbenzidine (TMB) substrate solution was added to produce a color reaction proportional to the concentration of the analyte. The reaction was terminated with stop solution, and optical density (OD) was measured at 450 nm using a microplate reader. Concentrations of MMP-9 and IL-8 were calculated from standard curves generated using known concentrations of the respective standards.

Statistical Analysis

Statistical analyses were performed using IBM SPSS Statistics version 21.0 (IBM Corp., Chicago, IL, USA). The normality of data distribution was assessed using the Shapiro-Wilk and Kolmogorov-Smirnov tests. For parameters showing normal distribution (neutrophil, monocyte, lymphocyte, NMR, MPV, PNR, PMR, total protein, and albumin), intergroup comparisons were performed using one-way analysis of variance (ANOVA), followed by Tukey's post hoc test for multiple comparisons. For parameters that did not follow a normal distribution, comparisons among groups were conducted using the Kruskal-Wallis test, followed by Dunn's post hoc test with Bonferroni correction.

The relationship between MMP-9 and IL-8 levels was evaluated using Spearman's rank correlation analysis. Kaplan-Meier survival analysis was used to estimate survival functions of the groups. Time-to-event was defined as the time from baseline to death, with event status coded as 0 = alive and 1 = death. Differences between survival curves were assessed using the log-rank test. The predictive performance of inflammatory parameters for survival was evaluated using receiver operating characteristic (ROC) curve analysis. The area under the curve (AUC) and its 95% confidence interval (CI) were calculated to determine the discriminatory ability of the parameters. The optimal cut-off value was determined using the Youden index (J = sensitivity + specificity − 1). Cox proportional hazards regression analysis was performed to evaluate the association between MCV and mortality. The association between seizure occurrence and MMP-9 levels was assessed using binary logistic regression analysis.

Descriptive statistics were presented as mean ± standard deviation (SD) for normally distributed variables and median (minimum-maximum) for non-normally distributed variables. A P-value <0.05 was considered statistically significant.

Results

Demographic Characteristics

The breed distribution of the cats included in the study showed that the HC group consisted of Domestic Shorthair (n=6), Scottish Fold (n=2), British Shorthair (n=3), Siamese (n=2), and Angora (n=1) cats. All cats in the NFIP-S group (n=7) were Domestic Shorthair. The NFIP group consisted predominantly of Domestic Shorthair cats (n=28), with one British Shorthair and one Scottish Fold. In the EFIP group, nine cats were Domestic Shorthair and two were British Shorthair.

Baseline demographic characteristics and mean survival times are summarized in *Table 1*, with no statistically significant differences observed among the groups. Seizure semiology in the NFIP-S group revealed generalized tonic-clonic seizures in five cats and focal seizures in two cats.

Hematological Parameters

Neutrophil and monocyte counts were significantly higher,

Table 1. *Demographic characteristics and mean survival time of the groups*

Group		HC	NFIP	NFIP-S	EFIP	P-value
Mean Survival Time (days)		- (not applicable)	22.14±25.86 7 (7-60)[a]	48.56±21.18 60 (3-60)[b]	40.63±23.80 60 (2-60)[ab]	
Age (months)		40.21±25.32	23.71±15.33	27.93±15.72	35.54±22.84	0.17
Sex	Male	10	5	13	7	0.23
	Female	4	2	17	4	

Values are expressed as mean ± standard deviation (median, min-max); [ab] *Different superscript letters indicate significant differences between groups (P<0.05); HC: healthy control; NE: non-effusive FIP; NES: non-effusive FIP with seizures; E: effusive FIP*

while lymphocyte counts were significantly lower in the NFIP and EFIP groups compared with the HC group (P<0.05). In contrast, cats in the NFIP-S group showed intermediate values for neutrophils, lymphocytes, and monocytes, which were higher than those of the HC group but lower than those of the NFIP and EFIP groups, without reaching statistical significance. A significant increase in WBC count was observed only in the EFIP group compared with the HC group (P<0.05).

In Group EFIP, the neutrophil-to-lymphocyte ratio (NLR) and neutrophil-to-monocyte ratio (NMR) were 8.38 (1.97-63.20) and 26.14±26.48 (16.54, 8.49-93.52), respectively, and only the values in Group EFIP were significantly higher than those of the HC group (P<0.05). The LMR and PNR values were lower in all three FIP groups compared with the HC group; however, no significant differences were observed among the FIP groups (P>0.05).

Mean corpuscular volume (MCV) values were higher in the NFIP-S group than in the other groups; however, this difference was statistically significant only when compared with the HC group. Conversely, mean corpuscular hemoglobin concentration (MCHC) was significantly lower in the NFIP-S group compared with all other groups.

Inflammatory Indices

Systemic inflammatory indices, including dNLR, SII, and AISI, were significantly elevated in both the EFIP and NFIP groups compared with the HC group (P<0.05), indicating a more pronounced systemic inflammatory response in cats with effusive and non-effusive FIP.

In Group NFIP-S, the median dNLR and SII levels were higher than those in the HC group and lower than those in the other FIP groups; however, the differences were not statistically significant. Although SIRI values were higher in all groups compared with the HC value of 0.20 (0.08-1.14), statistical significance was observed only in Group EFIP, where the median value was 7.00 (0.50-41.08). Similarly, AISI values were significantly higher in Groups NFIP and EFIP compared with the HC group (P<0.05). Hematological parameters and hematology-derived inflammatory indices are presented in *Table 2*.

Biochemical and Cytokine Findings

Intergroup comparison of total protein levels showed that the TP concentration in Group NFIP was 9.72±1.97 mg/dL, while the value in Group NFIP-S was 8.74±1.60 mg/dL. The mean TP level in Group NFIP was significantly higher than those of the other groups except for Group NFIP-S. Albumin levels were significantly lower in Groups EFIP and NFIP compared with the HC group *Table 3*.

Correlation Analysis

The mean serum MMP-9 concentration in Group NFIP-S was 19.32±8.91 ng/mL, which was significantly higher than those of Groups HC, EFIP, and NFIP *(Table 3, Fig. 1)*. Although the mean IL-8 concentration in Group NFIP-S (1.75±2.61 pg/mL) was higher than those observed in the other groups (HC: 0.46±0.92 pg/mL; NE: 0.98±1.53 pg/mL; E: 0.20±0.69 pg/mL), no statistically significant differences were detected among the groups *(Table 3, Fig. 2)*.

A moderate positive correlation was observed between IL-8 and MMP-9 concentrations (Spearman's rho= 0.44, P=0.001) *(Fig. 3)*.

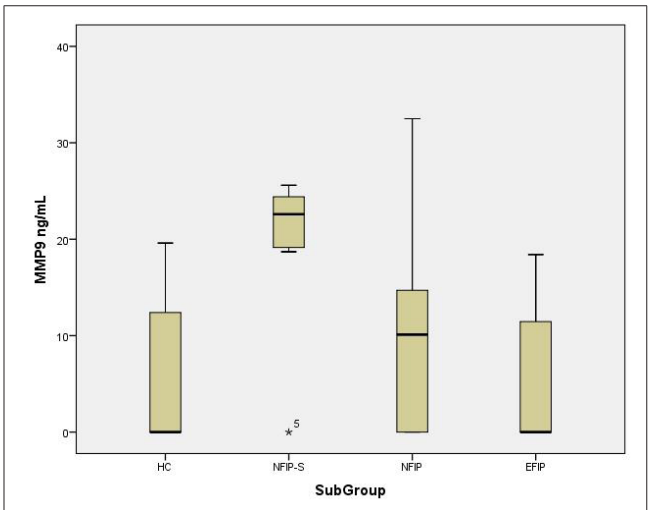

Fig 1. Distribution of serum MMP-9 concentrations among the study groups. Box plots represent the median and interquartile range, while whiskers indicate the minimum and maximum values. Circles and asterisks represent outliers. Serum MMP-9 concentrations were significantly higher in the NFIP-S group compared with the HC, NFIP, and EFIP groups (P<0.05)

Table 2. *Comparison of hematological parameters and derived inflammatory indices among groups*

Group Parameter	HC	NFIP-S	NFIP	EFIP
dNLR	0.99±0.68[a] 0.68 (0.32-2.52)	3.85±3.68[ab] 1.739 (0.22-9.10)	4.13±3.05[b] 3.83 (0.96-16.10)	6.96±5.52[b] 5.61 (1.50-20.19)
SIRI	0.35±0.30[a] (0.20, 0.08-1.14)	5.89±6.59[ab] (1.08, 0.20-14.03)	7.16±9.07[b] (4.16, 0.26-40.84)	13.40±14.09[b] (8.97, 1.00-41.08)
AISI	70.64±78.73[a] 59.19 (2.45-314.04)	1240.87±1628.53[ab] 249.07(25.30-4405.44)	1937.03±2222.86[b] 1237.75 (36.67-8092.78)	2087.05±2175.76[b] 1303.54 (291.41-6326.32)
SII	243.55±180.03[a] 212.74 (5.57-592.53)	1676.46±1967.78[ab] 436.96 (31.62-5244.57)	2343.91±2146.60[b] 1655.80 (174.64-11086.00)	3503.34±3445.88[b] 1676.09 (555.71-9732.80)
WBC (×10³/µL)	7.79±2.52[a] 7.85 (2.80-11.58)	12.54±5.76[ab] 10.16 (7.60-22.43)	12.67±6.09[ab] 11.16 (4.60-26.22)	15.45±7.20[b] 13.71 (6.31-27.34)
NEU (×10³/µL)	3.44±1.70[a] 2.99 (1.48-7.26)	8.69±5.98[ab] 7.66 (1.40-20.21)	9.51±4.59[b] 9.19 (2.75-22.92)	12.15±6.73[b] 9.73 (4.33-21.79)
LYM (×10³/µL)	3.66±1.93[a] 3.42 (0.96-6.52)	2.99±2.37[ab] 3.54 (0.37-6.33)	1.73±1.40[b] 1.45 (0.38-7.12)	1.57±1.05[b] 1.85 (0.10-2.98)
MON (×10³/µL)	0.30±0.15[a] 0.23 (0.12-0.53)	0.64±0.22[ab] 0.57 (0.29-0.94)	0.76±0.51[b] 0.64 (0.06-2.22)	0.73±0.62[b] 0.54 (0.15-2.24)
NLR	1.33±0.99[a] 0.79 (0.38-3.39)	8.24±8.75 [ab] 1.90 (0.25-20.70)	8.45±7.22[ab] 6.93 (1.30-28.34)	16.95±19.35[b] 8.38 (0.10-63.20)
NMR	12.13±6.40[a] 11.30 (5.04-31.00)	14.37±7.96[ab] 15.01 (1.75-24.05)	20.02±33.19[ab] 13.21 (5.18-192.20)	26.14±26.48[b] 16.54 (8.49-93.52)
LMR	13.40±5.88[a] 13.70 (4.61-21.43)	5.58±4.88[b] 6.21 (0.55-12.27)	3.79±5.32[b] 2.26 (0.39-26.47)	2.48±1.96[b] 2.09 (0.15-4.94)
PLT (×10³/µL)	235.21±129.12[a] 235.00 (3.00-452.00)	191.85±68.46[a] 155.00 (122.00-314.00)	301.83±158.90[a] 238.00 (88.00-736.00)	240.36±158.44[a] 168.00 (42.00-578.00)
MPV (fL)	12.10±1.08[a] 11.80 (10.60-14.00)	13.05±2.09[a] 12.70 (9.20-15.60)	12.31±1.34[a] 12.15 (9.90-15.30)	11.45±0.55[a] 11.60 (10.50-12.20)
PLR	78.20±55.03[a] 72.59 (1.40-192.70)	162.65±156.38[a] 71.75 (22.59-408.10)	242.83±206.50[a] 185.70 (45.12-1150.00)	387.15±494.83[a] 179.06 (25.50-1540.00)
PNR	85.29±50.60[a] 94.88 (0.75-152.70)	85.29±50.60[b] 94.88 (0.75-152.70)	37.63±23.27[b] 32.27 (8.55-105.10)	24.54±19.31[b] 24.36 (2.07-66.74)
PMR	960.33±559.56[a] 858.00 (6.81-1766.66)	338.36±178.35[a] 296.07 (152.50-665.51)	772.12±1488.41[a] 391.47 (108.88-8352.94)	497.43±464.59[a] 334.04 (32.55-1494.73)
MCV (fL)	37.59±5.11[a] 39.15 (26.50-45.30)	43.95±4.85[b] 42.10 (37.30-50.70)	38.70±4.93[ab] 38.00 (29.50-49.30)	38.64±4.17[ab] 39.30 (32.30-45.30)
MCHC (g/dL)	381.28±34.48[a] 365.50 (344.00-455.00)	284.02±111.03[b] 322.00 (35.20-347.00)	350.63±18.87[a] 353.00 (298.00-412.00)	350.72±18.37[a] 349.00 (325.00-381.00)

Values are expressed as mean ± standard deviation (median, min-max); [ab] Different superscript letters indicate significant differences between groups (P<0.05); dNLR: derived neutrophil-to-lymphocyte ratio; SIRI: the systemic inflammation response index; AISI: aggregate index of systemic inflammation; SII: systemic immune-inflammation index; WBC: White blood cell; LYM: Lymphocytes; MON: Monocytes NLR: neutrophil-to-lymphocyte ratio; NMR: Neutrophil-to-monocyte ratio; LMR: lymphocyte-to-monocyte ratio; PLT: Platelets; MPV: Mean platelet volume; PLR: platelet-to-lymphocyte ratio; PNR: platelet-to-neutrophil ratio; PMR: Platelet-to-monocyte ratio; MCV: mean corpuscular volume; MCHC: Mean corpuscular volume concentration; HC: healthy control; NE: non-effusive FIP; NES: non-effusive FIP with seizures; E: effusive FIP

Survival and Prognostic Analyses

During the 60-day follow-up period, death was recorded in five cats in the NFIP-S group, nine cats in the NFIP group, and six cats in the EFIP group. A significant difference in survival times among the three groups during the 60-day treatment period was observed according to the Kaplan-Meier analysis (log-rank test, χ^2=6.34, df=2, P=0.042). The mean survival time was 22.14 days (95% CI: 4.40-39.88) in the NFIP-S group, 48.56 days (95% CI: 41.11-56.02) in the NFIP group, and 40.63 days (95% CI: 27.22-54.04) in the EFIP group. Cats in the NFIP-S group exhibited significantly shorter survival times compared with the other groups.

The predictive ability of MCV for survival was evaluated using ROC curve analysis. The area under the curve (AUC) was 0.696 (95% CI: 0.546-0.845), indicating a statistically significant discriminatory ability (P=0.022) *(Fig. 4)*. At a cut-off value of 39.05 fL, MCV predicted survival with 80% sensitivity and 61% specificity. Cox regression analysis demonstrated a significant positive association between

Table 3. *Comparison of biochemical parameters and cytokine levels among the study groups*

Group Parameter	HC	NFIP-S	NFIP	EFIP
TP mg/dL	7.52±0.59[a] 7.59 (6.20-8.19)	8.74±1.60[ab] 9.30 (6.40-10.40)	9.72±1.97[b] 9.27 (7.00-15.84)	7.47±2.29[a] 6.97 (4.39-11.00)
ALB mg/dL	3.40±0.47[a] 3.00 (2.40-3.70)	3.01±0.47[ab] 3.00 (2.40-3.70)	2.80±0.47[b] 2.80 (1.90-3.90)	2.48±0.46[b] 2.70 (1.90-3.20)
AGR	1.19±1.45[a] 0.81 (0.53-6.00)	0.59±0.31[ab] 0.53 (0.31-1.27)	0.44±0.17[b] 0.43 (0.16-1.02)	0.55±0.17[ab] 0.61 (0.30-0.76)
MMP-9 ng/mL	6.67±8.38[a] 0 (0-19.6)	19.32±8.91[b] 22.60 (0-25.60)	9.00±10.08[a] 10.10 (0-32.50)	7.60±7.52[a] 10.40 (0-18.40)
IL-8 pg/mL	0.46±0.92[a] 0 (0-2.40)	1.75±2.61[a] 0 (0-6.90)	0.98±1.53[a] 0 (0-4.70)	0.20±0.69[a] 0 (0-2.30)

Values are expressed as mean ± standard deviation (median, min-max); [ab] Different superscript letters indicate significant differences between groups (P<0.05); TP: Total Protein; ALB: Albumin; AGR: Albumin to Globulin Ratio; MMP-9: Matrix Metalloproteinase-9; IL-8: Interleukin 9; HC: healthy control; NE: non-effusive FIP; NES: non-effusive FIP with seizures; E: effusive FIP

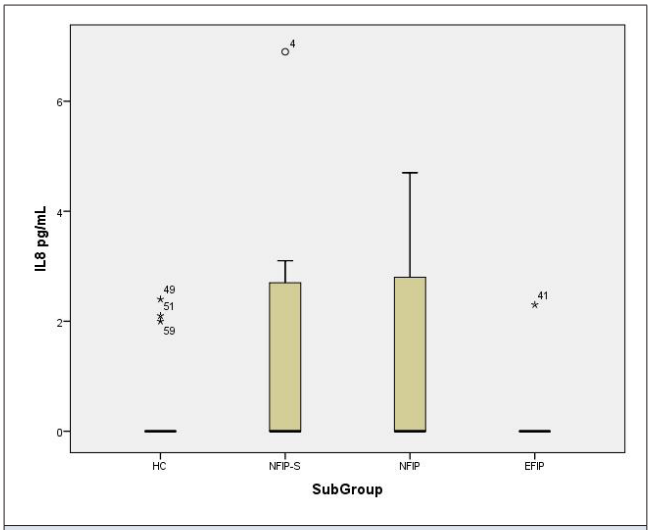

Fig 2. Distribution of serum IL-8 concentrations among the study groups. Box plots represent the median and interquartile range, while whiskers indicate the minimum and maximum values. Circles and asterisks represent outliers. No statistically significant differences were observed among the groups (P>0.05)

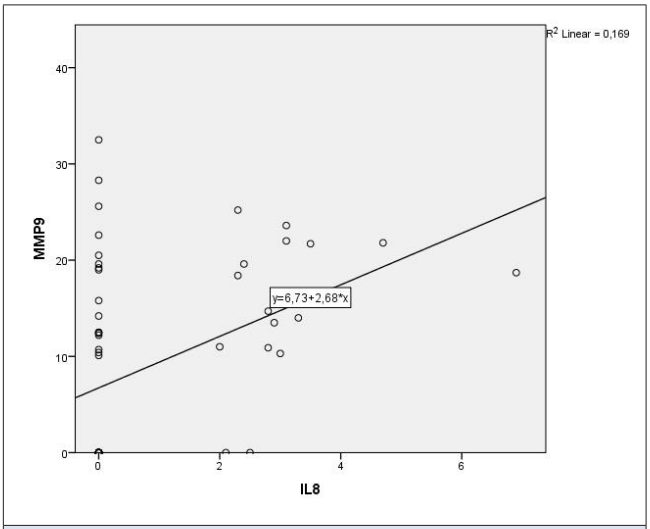

Fig 3. Correlation between serum IL-8 and MMP-9 concentrations in cats included in the study. Scatter plot showing the relationship between IL-8 and MMP-9 levels. The solid line represents the linear regression model (y = −6.73 + 2.68x). A moderate positive correlation was observed between IL-8 and MMP-9 concentrations (Spearman's rho = 0.44, P=0.001).

MCV levels and mortality. Each one-unit increase in MCV was associated with a 10.6% increase in the risk of death (HR = 1.106, 95% CI: 1.003-1.219, P=0.043).

The relationship between seizure occurrence and MMP-9 levels was evaluated using binary logistic regression analysis. An increase in MMP-9 levels was found to significantly increase the likelihood of seizure occurrence (OR = 1.13, 95% CI: 1.023-1.252, P=0.016). The Hosmer-Lemeshow test indicated a good model fit (P=0.53) *(Fig. 5)*.

Discussion

The most important finding of this study was the markedly elevated MMP-9 levels observed in cats with non-effusive FIP presenting with seizures compared with healthy cats and the other groups (non-effusive and effusive FIP).

Feline infectious peritonitis is an immune-mediated disease triggered by feline coronavirus infection. The development of the effusive (wet) or non-effusive (dry) form of the disease is thought to depend on the complex interaction between the replication rate of the virus in monocytes and the host immune response. The pathogenesis of effusive FIP is associated with a severely impaired cellular immune response in affected cats [1]. Infected macrophages release large amounts of vascular endothelial growth factor (VEGF), which markedly increases vascular permeability and leads to the accumulation of protein-rich effusions within body cavities [19].

The non-effusive form occurs in situations where the host is able to mount a partial cellular immune response [4]. In this case, the virus cannot be completely eliminated, but its dissemination is partially controlled. As a result,

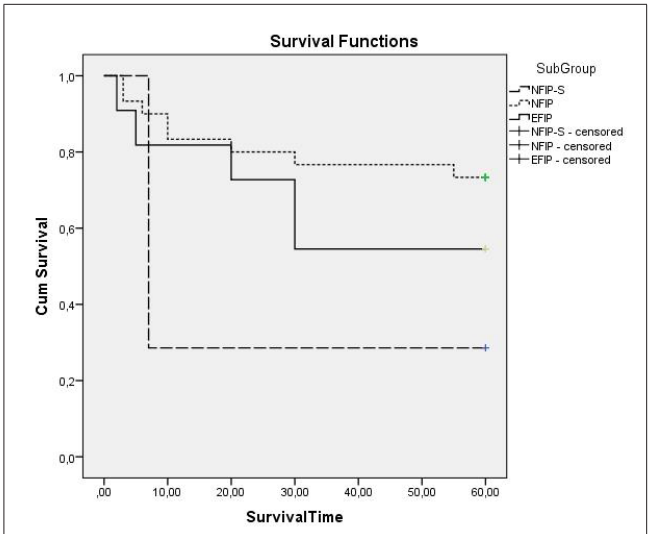

Fig 4. Kaplan-Meier survival curves of cats with different forms of FIP. Kaplan-Meier analysis illustrating the cumulative survival probabilities of cats with non-effusive FIP with seizures (NFIP-S), non-effusive FIP (NFIP), and effusive FIP (EFIP) during the 60-day follow-up period. Cross symbols indicate censored observations

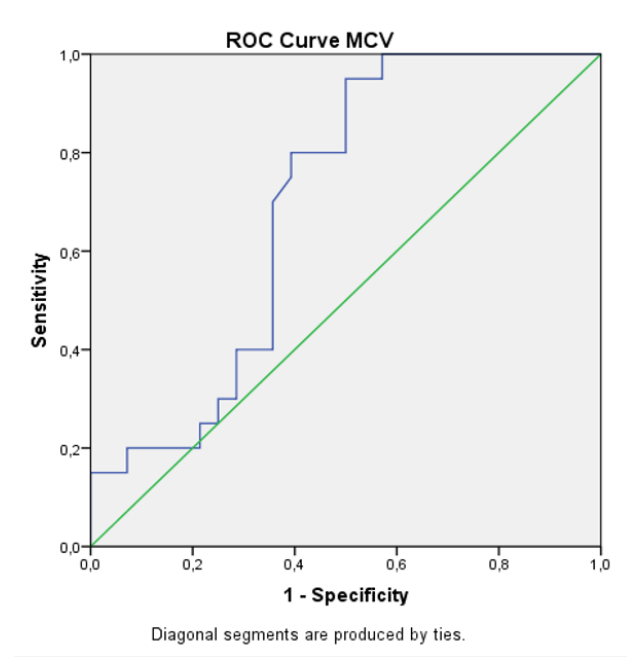

Fig 5. Receiver operating characteristic (ROC) curve analysis of MCV for predicting survival in cats with FIP

pyogranulomatous lesions composed of macrophage and B-cell accumulations develop in various organs, including the kidneys, liver, eyes, and brain [4,5].

Excessive activation of infected monocytes/macrophages, which plays a central role in the pathogenesis of the disease, leads to the release of matrix metalloproteinase-9 (MMP-9). This enzyme degrades type IV collagen in the vascular basement membrane, resulting in increased vascular permeability and the development of effusions in different body compartments in cats [19]. In addition, experimental animal studies have demonstrated that elevated MMP-9 levels are closely associated with epileptogenesis and contribute to neuronal damage and neuroinflammation. Increased MMP-9 protein expression and activity have been shown to induce blood-brain barrier disruption during glutamate-mediated epileptic seizures in humans and rats [6,20]. In the present study, the markedly higher MMP-9 levels observed in the NFIP-S group, particularly compared with the EFIP group, support the hypothesis that FIP may induce seizures in cats through a more specific pathophysiological mechanism.

Furthermore, the observation that the inflammatory indices SII, AISI, SIRI, and dNLR were markedly elevated in the effusive and non-effusive FIP groups but remained comparable to control levels in cats with seizures suggests that seizure development and mortality may not primarily result from a systemic cytokine storm [21]. Instead, these findings support the presence of a more localized inflammatory process involving the central nervous system and blood-brain barrier disruption. Evaluation of albumin, globulin, and AGR values also showed that the NFIP-S group did not differ significantly from the healthy control group, whereas significant alterations were observed in the effusive and non-effusive FIP groups. Although the relatively short survival time of cats with seizures may have limited the progression of systemic inflammatory responses, the markedly elevated MMP-9 levels ($P<0.001$), together with a trend toward increased IL-8 concentrations ($P=0.058$), suggest that localized inflammatory mechanisms may contribute to seizure development. IL-8 signaling has been reported to play an important role in neutrophil activation and degranulation during inflammatory responses, and cats with FIP have been shown to exhibit higher IL-8 levels compared with healthy controls [9]. Increased MMP-9 activity has also been demonstrated to contribute to epileptogenesis through extracellular matrix degradation and blood–brain barrier disruption [6,7]. In the present study, the positive correlation between IL-8 and MMP-9 further supports the involvement of neutrophil-mediated inflammatory pathways in the pathophysiology of seizure development. Taken together, these findings suggest that seizures in cats with non-effusive FIP may be associated with MMP-9-mediated extracellular matrix degradation and neutrophil-driven blood-brain barrier damage, indicating that seizure development in FIP may involve secondary neuroinflammatory mechanisms in addition to viral replication. These findings collectively support the hypothesis that neuroinflammatory mechanisms involving MMP-9 and neutrophil activation may contribute to seizure development in cats with FIP.

Biochemical findings also partially support the pathophysiological differences observed in the NFIP-S group. In FIP, the most frequently reported hematological and biochemical alterations include typical changes reflecting the systemic inflammatory nature of the disease, such as non-regenerative anemia, lymphopenia, neutrophilia, and hyperglobulinemia [5,22]. In particular, an albumin-to-globulin ratio (AGR) below 0.4 is considered one of the most important biochemical parameters that increases the suspicion of FIP [1,23]. While decreased albumin levels in the NFIP and EFIP groups compared with the healthy control group are consistent with systemic inflammation and protein loss, the observation that albumin, total protein, and AGR values in the NFIP-S group were closer to those of the healthy control group suggests that the systemic biochemical profile in FIP cases presenting with seizures may not fully conform to the typical biochemical pattern observed in FIP.

The aggregate index of systemic inflammation (AISI) has been considered one of the most reliable indices for predicting systemic inflammation during the COVID-19 pandemic in human medicine [24]. The systemic inflammation response index (SIRI), which incorporates monocyte counts in its formula, may be particularly relevant for monitoring the systemic manifestations of FIP, given the central role of monocytes in the pathophysiology of the disease. Hematology-derived inflammatory indices such as NLR, LMR, PLR, PNR, and SII have been reported to show significant alterations in cats suspected of having FIP compared with healthy cats, and they are considered sensitive indicators for detecting systemic inflammation even in cases without marked leukocytosis [12,25]. Similarly, the mean platelet volume-to-platelet ratio (MPV/PLT) has been reported to be elevated in FIP-suspected cases due to inflammatory activity, whereas the platelet-to-lymphocyte ratio did not show a statistically significant difference for disease discrimination [25]. These findings are consistent with the results observed in the NFIP and EFIP groups in the present study. The use of these indices provides a cost-effective approach that adds depth to routine hemogram data for evaluating the severity of cytokine-driven inflammation and monocyte/neutrophil activation, which play critical roles in the pathogenesis of FIP [9,24,26,27].

In FIP, lesions affecting the brain and meninges may develop, resulting in various neurological manifestations. These clinical signs may include ataxia, anisocoria, postural abnormalities, behavioral changes, and seizures [1]. Kunzel et al.[28] reported that FIP was diagnosed in 48% of cats with meningoencephalitis. Rissi [29], reported that seizures were present in 5 of 26 cats (19%) diagnosed with FIP, noting that neurological signs occurred more frequently in the non-effusive form and that, in some cases, seizures may represent the only clinical manifestation of the disease. In another study, seizures were observed in 14 of 55 cats (25%) diagnosed with FIP, and a positive association was identified between forebrain inflammation and enlargement and the occurrence of seizures. Accordingly, the presence of seizures in FIP indicates extensive brain damage and may therefore be considered an unfavorable prognostic sign [30]. It has also been reported that cats with epilepsy associated with structural brain lesions have shorter survival times compared with cats with epilepsy without detectable brain lesions [27]. Furthermore, Rissi [29] demonstrated that among five cats presenting with seizures, three had hydrocephalus and one had ventricular fibrin accumulation. In light of these findings, the significantly shorter survival observed in the NFIP-S group compared with the NFIP and EFIP groups in the Kaplan-Meier analysis is consistent with previous reports identifying seizures as an unfavorable prognostic indicator in FIP.

In the present study, the finding that MCV demonstrated a significant discriminatory ability for predicting survival, and that each unit increase in MCV was associated with an increased risk of mortality, suggests that MCV may represent not only a hematological parameter but also a potential biomarker reflecting disease severity. Mean corpuscular volume (MCV) is a parameter routinely included in complete blood count analysis and is commonly used in the classification of anemia. Previous studies in humans have demonstrated an association between increased MCV values and malignant conditions [31]. Moreover, several studies have reported that elevated MCV values are associated with poorer prognosis in chronic diseases, findings that are consistent with the results of the present study [32]. Therefore, MCV may contribute to clinical evaluation as a potential prognostic biomarker in cats with FIP, particularly in the presence of neurological involvement. However, further prospective and multivariable studies are required to clarify the underlying causal mechanisms of this association.

Increased MMP-9 activity may contribute to inflammation of the blood-brain barrier, which can subsequently lead to neurological manifestations. Neurological conditions such as uncontrolled seizures, structural brain abnormalities, and inflammatory brain diseases have been shown to influence survival rates in humans, dogs, and cats. In particular, uncontrolled seizures have been reported to increase mortality in humans and dogs [33] as well as in cats [27]. In cases where seizures cannot be adequately controlled, euthanasia decisions are frequently made [14,15], and seizures have therefore been recognized as an unfavorable prognostic indicator [30]. Furthermore, studies investigating epileptic cats with structural brain lesions have highlighted the involvement of different clinicopathological pathways in seizure development,

which may provide alternative perspectives for disease management, including potential therapeutic approaches targeting MMP-9 activity. Notably, the present study demonstrated that each unit increase in MMP-9 concentration was associated with a 13% increase in the likelihood of seizure occurrence. Therefore, therapeutic strategies combining antiepileptic treatment with approaches targeting MMP-9 activity may represent a potential area for future investigation in cats presenting with seizures.

This study has several limitations. The relatively small number of cats in the NFIP-S group represents an important limitation. Nevertheless, the finding that MMP-9 levels differed significantly between groups supports the robustness of the observed association. Another limitation is the absence of advanced neurological imaging (MRI) and cerebrospinal fluid (CSF) analysis for the characterization of intracranial pathologies. However, the inclusion of cases based on standardized diagnostic criteria and consistent clinical evaluation procedures partially mitigates this limitation.

In conclusion, the marked increase in serum MMP-9 levels observed in cats with non-effusive FIP presenting with seizures suggests that MMP-9-mediated blood-brain barrier disruption and neuroinflammation may contribute to both seizure development and poorer prognosis in these cases. Interestingly, the absence of marked increases in hematology-derived systemic inflammatory indices in the seizure group, despite significantly elevated MMP-9 levels, supports the hypothesis that seizures in FIP may reflect a distinct neuro-immunopathological phenotype characterized by localized rather than generalized inflammation. Collectively, these findings suggest that MMP-9 may represent not only a prognostic biomarker of neurological involvement and poor outcome, but also a potential therapeutic target in the neuroinflammatory manifestations of the disease.

Declarations

Availability of Data and Materials: The data sets generated and/or analyzed during the current study are available from the corresponding author (UO) upon reasonable request.

Acknowledgements: The authors thank Merve Gizem Sezener Kabay for her assistance with laboratory work and for her support in performing the ELISA analyses.

Funding Support: No funding was received for this study.

Ethical Statement: This study was approved by the Local Ethics Committee for Animal Experiments at Ondokuz Mayıs University on June 30, 2025, under decision number 2025/38.

Competing Interests: The authors declared that there is no conflict of interest.

Declaration of Generative Artificial Intelligence (AI): The authors declare that the article, tables and figures were not written/created by AI and AI-assisted Technologies.

Author Contributions: Methodology, study design and writing - original draft: ZNK; Conceptualization, methodology, data analysis, interpretation, funding acquisition and writing - review and editing: UO; Methodology and sample collection: SBK; Field examinations and sample collection: YTK; Field examinations and sample collection: ZFE. All authors read and approved the final manuscript.

References

1. **Thayer V, Gogolski S, Felten S, Hartmann K, Kennedy M, Olah GA:** 2022 AAFP/EveryCat Feline Infectious Peritonitis Diagnosis Guidelines. *J Feline Med Surg,* 24 (9): 905-933, 2022. DOI: 10.1177/1098612X221118761
2. **Pedersen NC:** An update on feline infectious peritonitis: Virology and immunopathogenesis. *Vet J,* 201 (2): 123-132, 2014. DOI: 10.1016/j.tvjl.2014.04.017
3. **Özaydın İ, Erkılıç EE:** Clinical approach and treatment strategies for abdominal compartment syndrome in cats and dogs: A review. *Pak Vet J,* 44 (4): 968-977, 2024. DOI: 10.29261/pakvetj/2024.261
4. **Kipar A, Meli ML:** Feline infectious peritonitis: Still an enigma? *Vet Pathol,* 51 (2): 505-526, 2014. DOI: 10.1177/0300985814522077
5. **Addie DD, Silveira C, Aston C, Brauckmann P, Covell-Ritchie J, Felstead C, Fosbery M, Gibbins C, Macaulay K, McMurrough J, Pattison E, Robertson E:** Alpha-1 acid glycoprotein reduction differentiated recovery from remission in a small cohort of cats treated for feline ınfectious peritonitis. *Viruses,* 14 (4):744, 2022. DOI: 10.3390/v14040744
6. **Rempe RG, Hartz AMS, Soldner ELB, Sokola BS, Alluri SR, Abner EL, Kryscio RJ, Pekcec A, Schlichtiger J, Bauer B:** Matrix metalloproteinase-mediated blood-brain barrier dysfunction in epilepsy. *J Neurosci,* 38 (18): 4301-4315, 2018. DOI: 10.1523/JNEUROSCI.2751-17.2018
7. **Pijet B, Kostrzewska-Ksiezyk A, Pijet-Kucicka M, Kaczmarek L:** Matrix metalloproteinase-9 contributes to epilepsy development after ıschemic stroke in mice. *Int J Mol Sci,* 25 (2):896, 2024. DOI: 10.3390/ijms25020896
8. **Remick DG:** Interleukin-8. *Crit Care Med,* 33 (12): S466-S467, 2005. DOI: 10.1097/01.ccm.0000186783.34908.18
9. **Lee JY, Cho HR, Oh HG, Hwang JH:** Comparative transcriptome analysis of PBMCs in cats diagnosed with and recovered from FIPV. *Lab Anim Res,* 41 (1):18, 2025. DOI: 10.1186/s42826-025-00247-5
10. **Gulersoy E, Ok M, Uney K, Durgut MK, Parlak TM, Ekici YE:** Intestinal injury and vasculitis biomarkers in cats with feline enteric coronavirus and effusive feline infectious peritonitis. *Vet Med Sci,* 9 (6): 2420-2429, 2023. DOI: 10.1002/vms3.1299
11. **Anwer AZ, Abdulkader MS, Massieh ESA:** Outcomes of treatment of cats with effusive feline infectious peritonitis using parenterally administered remdesivir with two different maintenance dose concentrations. *Kafkas Univ Vet Fak Derg,* 31 (2): 259-266, 2025. DOI: 10.9775/kvfd.2024.33487
12. **Trsar L, Strljic M, Svete AN, Koprivec S, Tozon N, Zel MK, Pavlin D:** Evaluation of selected inflammatory markers in cats with feline infectious peritonitis before and after therapy. *BMC Vet Res,* 21 (1):330, 2025. DOI: 10.1186/s12917-025-04731-x
13. **Sase O, Iwami T, Sasaki T, Sano T:** GS-441524 and molnupiravir are similarly effective for the treatment of cats with feline infectious peritonitis. *Front Vet Sci,* 11:1422408, 2024. DOI: 10.3389/fvets.2024.1422408
14. **Reagan KL, Brostoff T, Pires J, Rose A, Castillo D, Murphy BG:** Open label clinical trial of orally administered molnupiravir as a first-line treatment for naturally occurring effusive feline infectious peritonitis. *J Vet Intern Med,* 38 (6): 3087-3094, 2024. DOI: 10.1111/jvim.17187

15. **Roy M, Jacque N, Novicoff W, Li E, Negash R, Evans SJM:** Unlicensed molnupiravir is an effective rescue treatment following failure of unlicensed GS-441524-like therapy for cats with suspected feline ınfectious peritonitis. *Pathogens,* 11 (10):1209, 2022. DOI: 10.3390/pathogens11101209
16. **Bastan İ, İrdem Dİ, Kartal YK, Ergin SH, Tunç AS:** Oxidative stress in neurological feline infectious peritonitis: Cerebrospinal fluid 8-hydroxy-2. *Kafkas Univ Vet Fak Derg,* 31 (4): 547-556, 2025. DOI: 10.9775/kvfd.2025.34251
17. **Murphy BG, Castillo D, Neely NE, Kol A, Brostoff T, Grant CK, Reagan KL:** Serologic, virologic and pathologic features of cats with naturally occurring feline ınfectious peritonitis enrolled in antiviral clinical trials. *Viruses,* 16 (3):462, 2024. DOI: 10.3390/v16030462
18. **Sase O:** Molnupiravir treatment of 18 cats with feline infectious peritonitis: A case series. *J Vet Intern Med,* 37 (5): 1876-1880, 2023. DOI: 10.1111/jvim.16832
19. **Kipar A, May H, Menger S, Weber M, Leukert W, Reinacher M:** Morphologic features and development of granulomatous vasculitis in feline infectious peritonitis. *Vet Pathol,* 42 (3): 321-330, 2005. DOI: 10.1354/vp.42-3-321
20. **Wang Q, Lin Z, Yao C, Liu J, Chen J, Diao L:** Meta-analysis of MMP-9 levels in the serum of patients with epilepsy. *Front Neurosci,* 18:1296876, 2024. DOI: 10.3389/fnins.2024.1296876
21. **Çenesiz S:** The role of oxidant and antioxidant parameters in the infectious diseases: A systematic literature review. *Kafkas Univ Vet Fak Derg,* 26 (6): 849-858, 2020. DOI: 10.9775/kvfd.2020.24618
22. **Moyadee W, Sunpongsri S, Choowongkomon K, Roytrakul S, Rattanasrisomporn A, Tansakul N, Rattanasrisomporn J:** Feline infectious peritonitis: A comprehensive evaluation of clinical manifestations, laboratory diagnosis, and therapeutic approaches. *J Adv Vet Anim Res,* 11 (1): 19-26, 2024. DOI: 10.5455/javar.2024.k742
23. **Ergin I, Sainkaplan S, Sayim AA, Senel OO:** Suspicion of feline infectious peritonitis in cats with uveitis: Diagnostic value of coronavirus antibodies and blood parameters. *Kafkas Univ Vet Fak Derg,* 30 (6): 769-777, 2024. DOI: 10.9775/kvfd.2024.32144
24. **Zinellu A, Paliogiannis P, Mangoni AA:** Aggregate index of systemic inflammation (AISI), disease severity, and mortality in COVID-19: A systematic review and meta-analysis. *J Clin Med,* 12 (14):4584, 2023. DOI: 10.3390/jcm12144584
25. **Kopilović A, Gvozdić D, Radaković M, Spariosu K, Andrić N, Francuski Andrić J:** Selected hematology ratios in cats with non-septic effusions highly suspected of feline infectious peritonitis. *Vet Glas,* 77 (2): 164-175, 2023. DOI: 10.2298/VETGL230710008K
26. **Yanar KE:** Evaluation of haematological ındices in relation to the severity of the disease in cats with feline ınfectious peritonitis. *F U Saglik Bil Vet Derg,* 38 (2): 142-146, 2024.
27. **Prompinichpong K, Suwanna N, Hunprasit V, Thongbai A, Theerapan W, Thengchaisri N, Sattasathuchana P:** Survival outcomes and predictive factors of mortality in feline epilepsy: A comprehensive retrospective study. *Animals (Basel),* 15 (11):1504, 2025. DOI: 10.3390/ani15111504
28. **Kunzel F, Rebel-Bauder B, Kassl C, Leschnik M, Url A:** Meningoencephalitis in cats in Austria: A study of infectious causes, including Encephalitozoon cuniculi. *J Feline Med Surg,* 19 (2): 171-176, 2017. DOI: 10.1177/1098612X15621352
29. **Rissi DR:** A retrospective study of the neuropathology and diagnosis of naturally occurring feline infectious peritonitis. *J Vet Diagn Invest,* 30 (3): 392-399, 2018. DOI: 10.1177/1040638718755833
30. **Timmann D, Cizinauskas S, Tomek A, Doherr M, Vandevelde M, Jaggy A:** Retrospective analysis of seizures associated with feline infectious peritonitis in cats. *J Feline Med Surg,* 10 (1): 9-15, 2008. DOI: 10.1016/j.jfms.2007.06.004
31. **Yoon HJ, Kim K, Nam YS, Yun JM, Park M:** Mean corpuscular volume levels and all-cause and liver cancer mortality. *Clin Chem Lab Med,* 54 (7): 1247-1257, 2016. DOI: 10.1515/cclm-2015-0786
32. **Hsieh YP, Chang CC, Kor CT, Yang Y, Wen YK, Chiu PF:** Mean corpuscular volume and mortality in patients with CKD. *Clin J Am Soc Nephrol,* 12 (2): 237-244, 2017. DOI: 10.2215/CJN.00970116
33. **Hamamoto Y, Hasegawa D, Mizoguchi S, Yu Y, Wada M, Kuwabara T, Fujiwara-Igarashi A, Fujita M:** Retrospective epidemiological study of canine epilepsy in Japan using the International Veterinary Epilepsy Task Force classification 2015 (2003-2013): Etiological distribution, risk factors, survival time, and lifespan. *BMC Vet Res,* 12 (1): 248, 2016. DOI: 10.1186/s12917-016-0877-3

Kafkas Universitesi Veteriner Fakultesi Dergisi
Journal Home-Page: http://vetdergikafkas.org
E-ISSN: 1309-2251

Kafkas Univ Vet Fak Derg
32 (4): 607-616, 2026
DOI: 10.9775/kvfd.2026.37051

Research Article

Molecular Identification, Typing, and Virulence Gene Profiling of *Salmonella* Isolates Recovered from Cattle and Buffaloes in Egypt

Amany Dieb BAHR [1] (*), Hend Mohsen AUDA [1], Yousef Adel SOLIMAN [2], Michael Rasmy FAKHRY [2], Maha Abo El-naga GAMAL [2], Mohamed Gomaa SEADAWY [3], Eman Mohamed Samy ELNAGAR [4], Emil Saad ABDEL MASSIEH [1]

[1] Department of Medicine and Infectious Diseases, Faculty of Veterinary Medicine, Cairo University, 12211, Giza, EGYPT
[2] Biotechnology Department, Central Laboratory for Evaluation of Veterinary Biologics, Agriculture Research Center (ARC), EGYPT
[3] Biodefense Center for Infectious and Emerging Diseases, Ministry of Defence (MOD), EGYPT
[4] Department of Genetic Engineering, Veterinary Serum and Vaccine Research Institute (VSVRI), Agriculture Research Center (ARC), EGYPT

Abstract

Salmonella is a major cause of diarrhea in cattle and buffaloes. This study aimed to isolate and biochemically identify *Salmonella* species from faeces of cattle and buffaloes, confirm and type isolated *Salmonella* species molecularly, determine *Salmonella* infection-associated risk factors, and detect selected virulence genes. A total of 123 fecal samples were collected from cattle and buffaloes from different Egyptian governorates. All samples were processed using standard culture methods, followed by biochemical identification using conventional methods and the VITEK-2 System, with confirmation by qPCR. Conventional PCR was also used for *Salmonella* serovar identification and detection of the virulence genes *spvB, spvC, spvR,* and *pefA*. Bacteriological examinations revealed 13 *Salmonella* isolates (10.57%); however, the VITEK-2 identification system detected only 12. The qPCR confirmed that 13 were positive for *Salmonella*. Conventional PCR demonstrated that all 13 *Salmonella* isolates were of the Typhimurium serovar. Salmonella isolation was significantly higher in diarrheic animals and in animals younger than 3 months (P<0.05), while species, sex, season, and geographic location had no significant effect (P>0.05). Out of 13 S. Typhimurium isolates, 8 isolates tested positive for *spvC*, 7 for both *spvB* and *pefA*, and 5 for *spvR*, suggesting their limited role in the pathogenesis of diarrhea. This study concluded that qPCR showed higher detection performance for *Salmonella* isolates than the VITEK-2 system.

Keywords: Cattle and buffaloes, Molecular typing, qPCR, *Salmonella*, Virulence genes, VITEK-2

(*) **Corresponding author:**
Amany Dieb Bahr
Phone: +20-2-24708544
Cellular Phone number: +20 01220419334
E-mail: amanyd@cu.edu.eg

How to cite this article?

Bahr AD, Auda HM, Soliman YA, Fakhry MR, Gamal MAE, Seadawy MG, Elnagar EMS, Abdel Massieh ES: Molecular Identification, Typing, and Virulence Gene Profiling of *Salmonella* Isolates Recovered from Cattle and Buffaloes in Egypt. *Kafkas Univ Vet Fak Derg*, 32 (4): 607-616, 2026.
DOI: 10.9775/kvfd.2026.37051

Article ID: KVFD-2026-37051
Received: 11.05.2026
Accepted: 27.07.2026
Published Online: 28.07.2026

Introduction

Salmonella are asporogenic, non-capsulated, rod-shaped bacteria measuring approximately 2.0-5.0 µm in length and 0.7-1.5 µm in width. They are Gram-negative bacteria belonging to the family *Enterobacteriaceae* [1]. *Salmonella* is widely distributed among animals, humans, and the environment, enabling transmission and cross-contamination [2]. It exhibits enormous species variety, with more than 2.600 identified serovars [3]. *Salmonella enterica* is a major pathogen that impacts cattle and buffalo-rearing systems globally [4,5], with *Salmonella enterica* serovar Typhimurium being the most recognized *Salmonella* serovar in African food animals and meat products [6].

Salmonella is an infectious, contagious bacterium that causes a range of clinical problems in cattle and buffaloes, including enteritis, septicemia, pneumonia, and reproductive disorders, all of which are potential manifestations of *Salmonella* infection in cattle and buffaloes [4,7,8]. Animals, frequently being asymptomatic carriers of infections, excrete them with feces, thus distributing them to the environment [9].

Enteric disease can affect cattle of all ages, from neonates to adults [10]. Among the causative agents, *Salmonella* is a major pathogen responsible for diarrhea in both cattle and buffaloes, particularly in young calves [4,7]. Notably, the prevalence of *Salmonella* shedding decreases with

increasing age in calves [11]. *Salmonella enterica* serovar Typhimurium is associated with severe diarrheal disease, often characterized by fibrinous enteritis as a prominent postmortem finding, and contributes to substantial economic losses worldwide [4,7].

The isolation of the organism from tissues obtained aseptically during necropsy or from faeces, rectal swabs, or environmental samples, food products, and feedstuffs is the basis for diagnosis [12].

PCR-based technology can be employed for the rapid and precise detection of *Salmonella* [13]. The invasion *(invA)* gene is a virulence gene related to host recognition/invasion [5] and is also a common molecular target for *Salmonella*-specific detection methods, and the U.S. Food and Drug Administration Bacteriological Analytical Manual recommends it for PCR confirmation of *Salmonella* isolates [3].

Real-time quantitative polymerase chain reaction (qPCR), a molecular approach, has become a highly effective diagnostic alternative for the rapid and specific identification of several pathogens, including *Salmonella*. qPCR is a simple, fast (detection in less than 24 h), sensitive, specific, and repeatable technique [14].

Salmonella colonizes its hosts by invading, adhering to, and evading the host's intestinal defensive mechanisms, such as gastric acid, using different virulence markers and determinants, including flagella, capsule, plasmids, adhesion systems, and secretion systems [12]. *Salmonella's* pathogenicity is complicated, due to the presence of multiple virulence genes housed in *Salmonella* pathogenicity islands (SPIs), plasmids, and other gene cassettes. The high frequency of virulence genes in *Salmonella* indicates that the bacteria have a high potential for pathogenicity [15]. Mobile elements, such as plasmids, play an important role in the rapid evolution of *Salmonella* in adaptability to environmental challenges, allowing the survival and extensive distribution of diverse *Salmonella* serovars [16].

The *Salmonella* plasmid virulence *(spv)* region is the *Salmonella* virulence plasmids' signature locus. It contains the *spvR* gene, which encodes a LysR-like transcriptional regulator that positively regulates both the independent transcription of its own gene as well as the *spvABCD* operon. The *spvB, spvC,* and *spvD* proteins enter host cells via a type-three secretion system (T3SS) encoded by the *Salmonella* pathogenicity island-2 [17]. It has been established that *SpvB* inhibits actin polymerization by ADP-ribosylation of actin monomers, a well-recognized process during host intracellular infection [17], while *spvC* possesses phosphothreonine lyase activity and has been identified as a suppressor of MAP kinase signaling [18]. In *Salmonella* Typhimurium, the production of surface filamentous structures is determined by plasmid-encoded fimbriae locus *(pef)* genes carried on a multicopy plasmid. *Pef* promotes adherence to the small intestine [19].

In Egypt, cattle and buffaloes represent the primary sources of red meat and milk for human consumption [20,21]. Studies investigating *Salmonella* infection in Egyptian livestock, particularly buffaloes, remain limited, especially regarding its types, associated risk factors, and virulence determinants.

This study aimed to isolate and biochemically identify *Salmonella* species using conventional methods and the advanced VITEK-2 technique from the faeces of cattle and buffaloes from different locations in Egypt. Confirmation of isolated *Salmonella* species using the real-time PCR technique, and subsequent typing of confirmed *Salmonella* species using the conventional PCR technique. Assessment of *Salmonella* infection-associated risk factors. Detection of different virulence factors *(spvR, spvB, spvC,* and *pefA)* using the conventional PCR technique.

Material and Methods

Ethical Approval

The Institutional Animal Care and Use Committee of the Faculty of Veterinary Medicine, Cairo University (Vet. CU. IACUC), with code number (Vet CU301220251286) approved all the methods of animal handling and sampling included in this study.

Animal Sampling and Data Collection

A total of 123 individual fecal samples were collected from cattle and buffalo herds across five Egyptian governorates. The sampled animals included 66 animals showing diarrhea and 57 apparently healthy animals that had been in contact with diarrheic cases. Fecal samples were obtained directly from the rectum using sterile gloves and aseptically transferred into labeled, sterile, screw-capped containers. Following collection, samples were transported to the laboratory in an icebox and stored at 4°C until processing within 24 h [22].

The collected data from the sampled animals were classified according to their health status (diarrheic and apparently healthy), location (Faiyum, Alexandria, Behera, Menoufia, and Giza), age (<3 months, 3-6 months, and >6 months), sex (female and male), and season (Summer-Spring and Autumn-Winter).

Isolation and Identification of *Salmonella*

Isolation was carried out in accordance with the previously described protocol [23]. The specimens were pre-enriched in buffered peptone water (BPW, Oxoid, UK) and incubated at 37±1°C for 18±2 h. A 0.1 mL aliquot of the pre-enrichment broth was transferred to 10 mL of Rappaport-Vassiliadis (RV, HiMedia, India) broth

and incubated at 41±1°C for 24±3 h. After incubation, a loopful of culture was streaked over the surface of xylose-lysine-deoxycholate (XLD, HiMedia, India) and hektoen enteric agar (HE, HiMedia, India) media, which were then incubated at 37°C for 24 h. The XLD and HE plates were examined for the presence of *Salmonella* colonies. The production of red colonies with black centers and black colonies was inspected on XLD and HE plates, respectively.

Presumptive colonies were selected based on their cultural and morphological characteristics in Gram-stained films and then processed for biochemical analysis, which included oxidase, catalase, urease, citrate utilization, indole, triple sugar iron (TSI), and lysine iron agar tests. A single pure colony from each isolate was subcultured on nutrient semisolid agar at 37±1°C for 24 h and preserved for further molecular analysis.

Biochemical Identification Using the VITEK-2 System

All suspected colonies were biochemically tested using the VITEK-2 system (bioMérieux, France) and the VITEK-2 Gram-negative identification cards, following the manufacturer's instructions. Briefly, three to five fresh colonies from each isolate were transferred into tubes containing 3 mL of the suspension buffer provided with the VITEK-2 cards. The OD was adjusted to ~0.8 and used to load the identification cards into the vacuum chambers. The cards were then placed in the automated laser detection chambers and left to complete the identification process and create the log file [24].

Molecular Identification and Typing of Isolated *Salmonella*

DNA Extraction: A single colony grown on XLD agar plates was picked up, inoculated into brain heart infusion (BHI, HiMedia, India) broth, and incubated overnight at 37°C with shaking. The culture was then centrifuged, and DNA was extracted from cell pellets using the EasyPure® Bacteria Genomic DNA Kit (TransGen Biotech Co., LTD, China), following the manufacturer's instructions.

DNA Quantitation: The DNA concentration was determined using the Qubit 2.0 Fluorometer and the dsDNA BR test kit (Thermo Fisher Scientific, USA), following the manufacturer's instructions. Briefly, 1 µL of DNA was mixed with 199 µL of the DNA dilution buffer and incubated for 3 min at room temp. The mixture's absorbance was measured, and the results were plotted against a standard curve created using the kit's standard DNA concentration.

Real-Time PCR for Detection of *Salmonella* spp.

InvA primers (F:5'-ACAGTGCTCGTTTACGACCTGAAT-3', R:5'-AGACGGCTGGTACTGATTATAAT-3') and TaqMan probe (5'-Fam-CGA-CCC-CAT-AAACACCAATATCGCC-BHQ1b-3') sequences were purchased from Metabion company (Germany). The primers were analyzed using fast PCR v6 [25] to amplify 243 bp of *Salmonella* spp. *invA* gene. They were blasted against the nucleotide database of the NCBI website to ensure identity among published BLAST sequences for the target gene and the absence of significant similarity with other microorganism sequences. The probe was labeled with a fluorescent reporter dye, 6-carboxyfluorescein (FAM), on the 5' end and with Black Hole Quencher R (BHQ) at the 3' end of the probe.

The qPCR was run in a Taqman mastermix containing 10 µL of EasyScript qPCR Master Mix (Agilent Technologies, USA), 250 nM of each *invA* primer, 100 nM of *invA* probe, and 2 µL of purified DNA in a final volume of 20 µL using nuclease-free water. The qPCR experiments were performed using the AriaMx real-time PCR thermocycler equipment. The optimal qPCR efficacy was achieved using a cycling profile including a denaturation at 95°C for 30 s, followed by 40 cycles of 95°C/20sec, 60°C/20sec and 72°C/30 sec. Each qPCR had one positive control (*S. enterica* DNA) and a no-template control (master mix and sterile water) [26].

Molecular Typing of *Salmonella* Serovars Using Conventional PCR

Each serovar-specific PCR assay included a positive control consisting of DNA from the corresponding target serovar and a no-template negative control. The primer sets used were selected from previously validated studies demonstrating specificity for their respective target serovars. Uniplex PCR was used for the detection of the *MDH* (malic acid dehydrogenase) gene of serovar Typhimurium [27]. Multiplex PCR was applied using three pairs of oligonucleotide primers *(tcpS*, *lygD*, and *flhBinner*) for the detection of *S.* Enteritidis and *S.* Dublin [28] *(Table 1)*.

Molecular Detection of Virulence Factors' Genes

Plasmid Extraction Using a Miniprep Purification Kit: A single colony grown on XLD agar plates was picked up, inoculated into BHI broth, and incubated overnight at 37°C with shaking, then cooled down and centrifuged at 4000 rpm/10 min at 4°C; plasmids were recovered using the miniprep purification kit (EasyPure® Plasmid MiniPrep Kit, TransGen Biotech Co., LTD, China) following the manufacturer's instructions.

Amplification of the Virulence Factors' Genes: The purified plasmids from various colonies were tested for the presence of several genes known to be responsible for virulence *(pefA, spvB, spvC,* and *spvR)* using different sets of primers using conventional PCR. The primer sets and thermal cycling conditions of different virulence genes are presented in *Table 2*.

The reaction mixture was prepared in 25 µL. It consisted

Table 1. *Primers used for the identification of S. Typhimurium, S. Enteritidis, and S. Dublin*				
Target Gene	**Primer Sequence (5' - 3')**	**Annealing Temperature (°C)**	**Amplicon Size (bp)**	**References**
MDH	F: TGCCAACGGAAGTTGAAGTG R: CGCATTCCACCACGCCCTTC	55	261	[27]
tcpS	F: ATGTCTATAAGCACCACAATG R: TCATTTCAATAATGATTCAAGC	55	882	[28]
lygD	F: CATTCTGACCTTTAAGCCGGTCAATGAG R: CCAAAAAGCGAGACCTCAAACTTACTCAG	55	339	[28]
flhBinner	F: GCGGACGTCATTGTCACTAACCCGACG R: TCTAAAGTGGGAACCCGATGTTCAGCG	55	155	[28]
MDH gene for detection of S. Typhimurium, tcpS, lygD, and flhBinner for detection of S. Enteritidis, and tcpS and flhBinner for detection of S. Dublin				

of: 12.5 µL of 2X PCR Master Mix (TransGen Biotech Co., LTD, China), 1 µL of each forward and reverse primer (20 pmol) (Metabion, Germany), 4.5 µL of PCR-grade water, and 6 µL of purified plasmids. DNAse-free RNAse-free water was used as a negative control.

Visualization of the PCR Products

Ten microliters of each PCR product were electrophoresed in 1.5% agarose gel containing 0.5 µg/mL ethidium bromide (Sigma, Germany) in 1× TBE buffer against a 100 bp DNA ladder (Qiagen, USA). The gel was then visualized and photographed with a gel documentation system (Alpha Inno tech, Biometra, USA).

Statistical Analysis

Fisher's exact test and the chi-square test were used to assess associations between the studied variables and *Salmonella* isolation rates. Statistical significance was defined as a P-value <0.05. Odds ratios (ORs) with 95% confidence intervals (CIs) were calculated for each variable, with baseline categories specified in *Table 3*. All statistical analyses were performed using SPSS software, version 24 (IBM Corp., Armonk, NY, USA).

Results

Cultural, Morphological, and Conventional Biochemical Identification of *Salmonella*

Out of 123 cultured fecal samples, 13 showed colonies with morphological characteristics consistent with *Salmonella* on XLD and HE media *(Fig. 1)*. The thin smears prepared from the colony for Gram staining revealed Gram-negative, pink-coloured, small rod-shaped organisms, single, paired, or arranged in short chains on microscopic examination. Thirteen *Salmonella* isolates on TSI slants showed fermentation of glucose and H2S formation, but none of the isolates fermented either lactose or sucrose. They are catalase positive, oxidase negative, indole negative, and they reproduce in citrated media (Simmon), and they do not digest urea. In Lysine-Iron Agar medium, they are purple colored "alkaline reactions".

Biochemical Identification Using the VITEK-2 System

The suspected isolates were biochemically confirmed as *Salmonella enterica* at the species level using the VITEK-2 system. Of these, twelve isolates were successfully identified, whereas one isolate could not be identified.

Real-Time PCR for Detection of *Salmonella* spp.

All thirteen suspected isolates obtained from the bacteriological examination gave positive results for the *invA* gene in real-time PCR. *Fig. 2* shows the amplification of *invA* gene in 10 *Salmonella* isolates.

Molecular Typing of *Salmonella* Serovars Using Conventional PCR

PCR amplified 261 bp DNA fragments from the *MDH* gene in all isolates, which indicates that all isolates belong to the Typhimurium serovar, with negative results obtained in other *Salmonella* serovars based on the PCR protocol and primer sets used in this study.

Table 2. *The primer sets and thermal cycling conditions of different virulence genes*				
Gene	**Primer Sequence (5'- 3')**	**Annealing Temperature (°C)**	**Amplicon Size (bp)**	**Reference**
spvB	F: CTATCAGCCCCGCACGGAGAGCAGTTTTTA R: GGAGGAGGCGGTGGCGGTGGCATCATA	66.5	717	[29]
spvC	F: ACT CCT TGC ACA ACC AAA TGC GGA R: TGT CTT CTG CAT TTC GCC ACC	58	467	[16]
spvR	F: CAG GTT CCT TCA GTA TCG CA R: TTT GGC CGG AAA TGG TCA GT	57	310	[30]
pefA	F: GCGCCGCTCAGCCGAACCAG R: GCAGCAGAAGCCCAGGAAACAGTG	66.5	157	[29]

Table 3. Salmonella isolation rate, odds ratio (OR), and P-value regarding different variables

Variable	Categories	Total Examined Animals	Number and Percentage of Positive Animals	OR (95%CI)	P-value[a]
Healthy status	Diarrheic	66	11(16.7%)	5.5 (1.16-25.97)	P=0.02
	Apparently Healthy	57	2 (3.5%)	1.0 (baseline group)	
Animal species	Cattle	62	8 (12.9%)	1.66 (0.51-5.39)	P=0. 56
	Buffaloes	61	5 (8.2%)	1.0 (baseline group)	
Age	<3 months	48	9 (18.8%)	8.77 (2.63-26.31)	P=0.046
	3-6 months	36	3 (8.3%)	3.45 (1.036-10.36)	
	>6 months	39	1 (2.6%)	1.0 (baseline group)	
Season	Summer-Spring	63	9 (14.3%)	2.33 (0.68-8.03)	P=0.242
	Autumn- Winter	60	4 (6.7%)	1.0 (baseline group)	
Sex	Female	70	8 (11.4%)	1.24 (0.38-4.03)	P=0.776
	Male	53	5 (9.4%)	1.0 (baseline group)	
Location	Faiyum	25	6 (24%)	12 (1.35-106.9)	P=0.08
	Alexandria	18	2 (11.1%)	4.75 (0.4-56.18)	
	Behera	24	3 (12.5%)	5.43 (0.53-55.52)	
	Menoufia	17	1 (5.9%)	2.37 (0.140-40.35)	
	Giza	39	1 (2.6%)	1.0 (baseline group)	

Salmonella-Associated Risk Factors Analysis

The overall *Salmonella* isolation rate from the collected fecal samples was 10.57% (13/123). Isolation was significantly higher in diarrheic animals (16.7%) than in apparently healthy animals (3.5%), with a significant association between diarrheal status and *Salmonella* isolation (P=0.02). The odds of diarrhea among *Salmonella*-positive animals were 5.5 times higher than those among *Salmonella*-negative animals. Regarding other risk factors, age had a significant effect on the *Salmonella* isolation rate (P=0.046), with animals younger than 3 months showing the highest susceptibility (OR=8.77). In contrast, no significant associations were observed between *Salmonella* isolation and other variables, including animal species, season, sex, or location (P>0.05) *(Table 3)*.

Molecular Detection of Virulence Genes in *Salmonella* Isolates Using Conventional PCR

PefA, *spvB*, *spvC*, and *spvR* were successfully amplified. Of 13 *S.* Typhimurium isolates, 8 isolates (61.5%) were positive for *spvC*, 7 (53.8%) were positive for both *spvB* and *pefA*, and 5 (38.5%) for *spvR*. Six isolates from cattle and 3 isolates from buffaloes were tested positive for different virulence genes, while 4 isolates (2 from cattle, 2

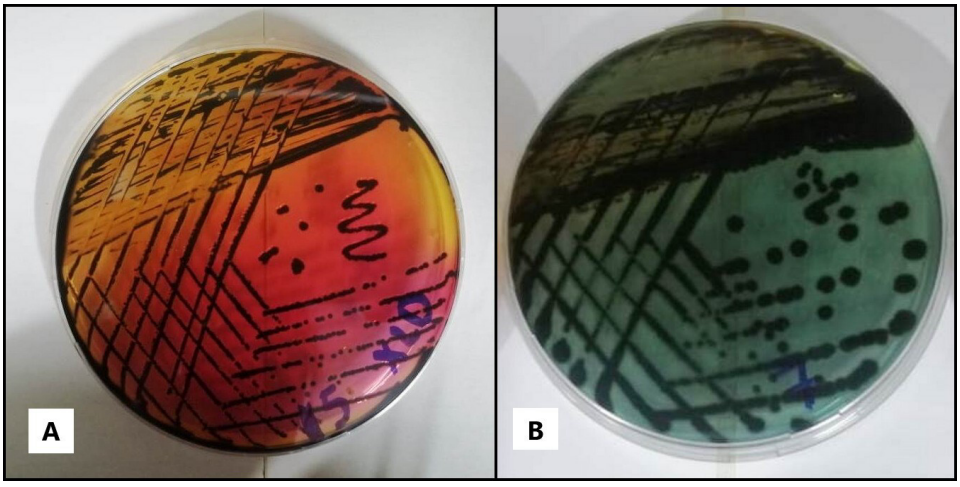

Fig 1. Typical colonies of *Salmonella* grown on selective media: **(A)** On XLD agar, colonies exhibit a black centre with a lightly transparent reddish zone, **(B)** On HE agar, colonies appear as transparent green or blue-green with black centres, sometimes presenting as almost completely black colonies

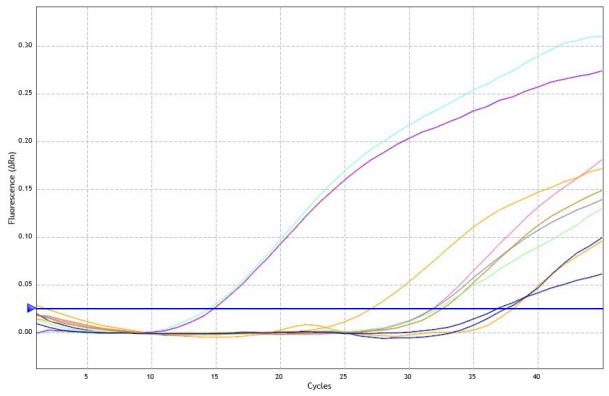

Fig 2. Shows the amplification plot of the amplified invA gene of 10 *Salmonella* isolates, which gave positive Ct after cycle 15 in 2 isolates, and the remaining 8 isolates gave positive after 25 cycles

Isolate Number	Animal species	Diarrheic	*PefA*	*SpvR*	*SpvB*	*SpvC*
1	Buffalo	✓	✓	✓	×	✓
2	Cattle	✓	✓	✓	✓	✓
3	Cattle	✓	✓	✓	✓	✓
4	Cattle	✓	✓	×	×	×
5	Cattle	✓	×	×	✓	✓
6	Cattle	✓	✓	×	✓	✓
7	Buffalo	✓	✓	×	✓	✓
8	Cattle	✓	✓	✓	✓	✓
9	Buffalo	✓	×	✓	✓	✓
10	Cattle	✓	×	×	×	×
11	Cattle	✓	×	×	×	×
12	Buffalo	×	×	×	×	×
13	Buffalo	×	×	×	×	×

Fig 3. Distribution of virulence genes among S. Typhimurium isolates recovered from Cattle and Buffaloes. (✓) indicates presence of the gene, while (×) indicates absence

from buffaloes) were negative for the four virulence genes, as shown in *Fig. 3*.

Discussion

Salmonella-induced diarrhea is a major cause of neonatal calf morbidity and mortality in several countries of the world, including Egypt, leading to significant economic losses for the beef and dairy industries [31].

In the present study, a total of 123 fecal samples were collected from cattle and buffaloes from different governorates in Egypt. Bacteriological examinations revealed 13 *Salmonella* isolates; however, the VITEK identification system detected only 12. The qPCR was used for confirmation of the results, which detected that 13 isolates (10.57%) were positive for *Salmonella*. There was an excellent correlation between the culture and PCR methods, and the PCR method did not report any false-negative results. Gebeyehu et al.[32] isolated *Salmonella* from 10.42% of the total samples, which corresponds to our findings. *Salmonella* incidence ranges from 1% as reported by Abd El-Tawab et al.[33] to 43.53% as reported by Moussa et al.[34]. These variations may be explained by differences in study location, climate, management practices, production categories used (dairy, beef, mixed), sample sources (slaughterhouse, farms, marketplace), sample type, species, age, and study protocol [35-37].

The detection of *Salmonella* by PCR results in a faster method than standard culture methods [38]. A real-time PCR *Salmonella* screening method detects *S. enterica* accurately and efficiently. It saves time, producing results in 18 to 24 h, making it an ideal method of diagnosis [39], whereas O'Hara and Miller [40] reported that the VITEK-2 system demonstrated an accuracy of 93.0% for the identification of enteric bacterial strains, as it misidentified 3 out of 15 *Salmonella* spp. Also, Simgamsetty et al.[24] detected that the VITEK-2 Compact system identified various Gram-negative bacterial strains with a level of 95-99% probability.

Following confirmation of the isolates as *Salmonella enterica*, molecular typing was performed using serovar-specific PCR assays targeting characteristic genetic markers to identify *S.* Typhimurium, *S.* Enteritidis, and *S.* Dublin. This approach was selected because PCR-based serovar identification provides rapid, sensitive, and reliable discrimination of the most epidemiologically and clinically significant *Salmonella* serovars while avoiding the technical limitations and high cost associated with conventional Kauffmann-White serotyping [28,41]. All of the *Salmonella* found in this investigation are serovar Typhimurium, which is still the most predominant serovar causing enteritis in cattle and buffalo calves, as noted in previous studies [4,34,37]. When digestive disease or diarrhea is the reason for consultation or the primary clinical symptom displayed by calves, *S.* Typhimurium is the most likely serotype involved, particularly in younger calves. Possibly, the adaptations of the neonate digestive tract, as well as the action of this serotype, favor this presentation [5].

This study assessed the impact of some risk factors, including sex, age, season, geographical location, health status, and species, on *Salmonella* detection.

This study found a statistically significant difference in the total prevalence of *Salmonella* between age groups (P=0.046), aligning with the findings of Yirsa and Tigistu [42]. The highest isolation rate was observed in animals under 3 months of age. Some precipitating factors, such as transportation, concomitant disease, or acute food deprivation, may cause disease in young animals more frequently than in adults [43].

The observed decline in fecal shedding of *Salmonella* spp. with increasing calf age suggests that younger calves are

more susceptible to intestinal colonization and subsequent bacterial shedding. This age-related pattern is biologically plausible and may reflect the progressive maturation of the immune system together with gastrointestinal development. As calves mature, rumen function becomes established, the intestinal microbiota becomes more diverse and stable, abomasal pH decreases, and the resident enteric microflora becomes more effective at limiting *Salmonella* colonization than the immature neonatal microbiota [44]. These physiological and microbial changes likely contribute to the lower prevalence of fecal shedding observed in older calves.

The prevalence was significantly higher in diarrheic animals than in apparently healthy animals, which is consistent with a previous study [22]. There are two isolates from apparently healthy animals, implying that these animals may act as a potential source of *Salmonella* infection to humans and other animals through contact. In this regard, it is worth noting that the ability of carrier animals to contaminate the environment by shedding *Salmonella* increases when animals are exposed to stressors such as transportation or holding before slaughter, or late pregnancy [43].

Although *Salmonella* frequency was numerically higher in the summer and spring, this difference was not statistically significant, indicating that season alone may not be a strong determinant of fecal shedding in this population - a pattern consistent with findings by Huston et al.[45]. This lack of a clear seasonal effect is plausibly explained by stress-related factors such as transportation, weaning, overcrowding, and concurrent disease, all of which are known to promote *Salmonella* shedding independently of season [45]. Because these stressors can occur at any time of year, they may sustain a baseline level of infection that masks or overrides any true seasonal signal. Climatic factors likely reinforce this pattern in the present setting: in tropical and subtropical regions, temperature and humidity remain within ranges favorable for *Salmonella* survival throughout the year, so the organism's environmental persistence is unlikely to fluctuate sharply with season [46]. Taken together, these factors suggest that management-related stressors and a consistently permissive climate, rather than seasonality itself, are the more relevant drivers of *Salmonella* shedding in this context.

However, the isolation rate was higher in cattle (12.9%) than in buffaloes (8.2%). No statistically significant difference was detected between the two species. Consistent with our findings, other studies [36,47] reported similar or non-significant differences in isolation rates between cattle and buffaloes. In contrast, Borriello et al.[4] demonstrated a higher susceptibility of buffaloes to salmonellosis compared to cattle. The authors attributed this increased susceptibility to differences in husbandry practices, particularly the relatively lower standards of hygiene commonly associated with buffalo rearing systems. Such conditions may facilitate the persistence and transmission of gastroenteric pathogens, thereby increasing the risk of infection in buffalo populations.

In this study, no statistically significant association was found between *Salmonella* isolation rates and geographic location. This finding is consistent with a previous study [48], which also reported that location has no significant effect on *Salmonella* detection. The lack of association in the present study may be attributed to the uneven distribution of sample sizes across the investigated localities. However, the relatively higher isolation rate observed in Faiyum governorate could be explained by the predominant use of recycled water for animal husbandry, which is more susceptible to contamination and may create favorable conditions for bacterial growth and persistence [49,50].

In this investigation, the higher prevalence of *Salmonella* isolates was observed in female cattle and buffaloes (11.4%) than in males (9.4%), although the association between sexes was not statistically significant (P>0.05). Matchawe et al.[48], Hailu and Kebede [51] also found no statistically significant difference in *Salmonella* detection between the sexes in cattle and sheep, respectively. This finding may be attributed to the fact that both males and females are generally exposed to similar environmental and management conditions, including shared housing, feed, and water supplies, which are the main routes of transmission. Although sex-related hormonal differences can influence immunological responses, they appear to have a minor impact when compared to stronger risk factors, including age, hygiene, stocking density, and stress. As a result, the role of sex as a determinant of *Salmonella* infection is probably obscured by these more influential factors, resulting in the lack of a significant association [48].

The virulence of *Salmonella* is linked to a combination of chromosomal and plasmid factors [52,53]. In this investigation, all isolates carried the *invA* gene, which was expected since *invA* is an invasion gene conserved among *Salmonella* serotypes.

PCR amplification of virulence genes *pefA, spvB, spvC,* and *spvR* was performed using plasmid DNA because these virulence genes are encoded on the *Salmonella* virulence plasmid. Accordingly, plasmid DNA was considered an appropriate template for the specific detection of these plasmid-associated virulence genes [54,55].

The results revealed that different virulence genes were found in the *Salmonella* isolates under investigation. Additionally, the study's findings support the idea that there is genetic differentiation between isolates of the same serotype in the distribution of virulent genes, as in

a previous study [56], since both *spvB* and *pefA* genes were detected in 53.8% of the isolates, *spvC* was detected in 61.5% of the isolates, while the *spvR* gene was detected in 38.5% of the isolates. Chuanchuen et al.[57] found the virulence plasmid-associated genes *spvC* and *pefA* in only two (1.3%) and one (0.6%) *Salmonella* isolates obtained from dairy cows, respectively. Also, Dahshan et al.[52] found that out of 17 *S.* Typhimurium isolates, 14 isolates were positive for the *spvC* gene, and 13 were positive for the *pefA* gene. Amini et al.[58] detected *spvB* and *spvC* genes in 100% (15/15) of *S.* Typhimurium from bovines. Sudrik et al.[59] found *spvR* in 26.31% of *Salmonella* isolated from cattle farms.

The *pefA* gene was associated with the Typhimurium serotype; the association between the Typhimurium serotype and the *pefA* gene may explain the high frequency of diarrhea in the presence of this serotype, as this gene allows bacterial adhesion to intestinal epithelial cells [5].

However, variations in the detection of *Salmonella* virulence genes, particularly *spvB*, *spvC*, and *spvR*, have been reported across different studies. Experimental and epidemiological evidence from both animals and humans suggests that these genes are not essential for the development of gastroenteritis or diarrhea caused by various *Salmonella* serovars, including *Salmonella enterica* serovar Typhimurium. Instead, their role appears to be more critical in cases of extraintestinal infections [18,60]. Nevertheless, some studies indicate that *Salmonella* isolates harboring virulence plasmids may be associated with more severe forms of diarrhea [60].

In conclusion, *Salmonella* is prevalent in cattle and buffaloes in Egypt. Quantitative PCR (qPCR) demonstrates higher detection performance for *Salmonella* isolates than the VITEK-2 system in the present study. *Salmonella enterica* serovar Typhimurium was identified as the only detected serovar based on the PCR protocol and primer sets used in this study. The isolation rate is significantly higher in diarrheic animals compared to apparently healthy ones. Age is significantly associated with *Salmonella* isolation, with animals younger than 3 months being the most susceptible, whereas species, sex, season, and geographic location show no significant effect. Plasmid-associated virulence genes *(spvB, spvC, spvR,* and *pefA)* are detected at varying frequencies among the isolates, suggesting a limited role in the pathogenesis of diarrhea.

Declarations

Availability of Data and Materials: Data and materials are available from the corresponding author (ADB) upon reasonable request.

Acknowledgements: None.

Funding Support: This work was supported by the "Science, Technology & Innovation Funding Authority (STDF)" under the One Health grant (Project ID 49155).

Ethical Approval: The Institutional Animal Care and Use Committee of the Faculty of Veterinary Medicine, Cairo University (Vet. CU. IACUC), with code number (Vet CU301220251286) approved all the methods of animal handling and sampling included in this study.

Competing Interests: The authors declared that there is no conflict of interest.

Declaration of Generative Artificial Intelligence (AI): The authors declare that the article and/or tables and figures were not written/created by AI and AI-assisted technologies.

Authors' Contributions: AD: Conceptualization, Data curation, Methodology, Formal analysis, Funding acquisition, Investigation, Writing - original draft, Writing - reviewing and editing. HM: Methodology, Investigation, Validation, Writing - review and editing. YA: Conceptualization, Methodology. MR: Methodology, Investigation, Writing - review and editing. MAN: Methodology, Writing - review and editing. MG: Methodology. EM: Writing - review and editing. ES: Conceptualization, Data curation, Methodology, Formal analysis, Investigation, Writing - original draft, Writing - review and editing.

References

1. **Özkalp B:** Isolation and Identification of *Salmonellas* from Different Samples, **In,** Mahmoud BSM (Ed): *Salmonella* - A Dangerous Foodborne Pathogen, 123-156. InTech, 2012.
2. **Kebede A, Kemal J, Alemayehu H, Mariam SH:** Isolation, identification, and antibiotic susceptibility testing of *Salmonella* from slaughtered bovines and ovines in Addis Ababa Abattoir Enterprise, Ethiopia: A cross-sectional study. *Int J Bacteriol,* 2016:3714785, 2016. DOI: 10.1155/2016/3714785
3. **Buehler AJ, Wiedmann M, Kassaify Z, Cheng RA:** Evaluation of *invA* diversity among *Salmonella* species suggests why some commercially available rapid detection kits may fail to detect multiple *Salmonella* subspecies and species. *J Food Prot,* 82 (4): 710-717, 2019. DOI: 10.4315/0362-028X.JFP-18-525
4. **Borriello G, Lucibelli MG, Pesciaroli M, Carullo MR, Graziani C, Ammendola S, Battistoni A, Ercolini D, Pasquali P, Galiero G:** Diversity of *Salmonella spp.* serovars isolated from the intestines of water buffalo calves with gastroenteritis. *BMC Vet Res,* 25 (8):201, 2012. DOI: 10.1186/1746-6148-8-201
5. **Casaux ML, Neto WS, Schild CO, Costa RA, MacíasRioseco M, Cafarena RD, Silveira CS, Aráoz V, Díaz BD, Giannitti F, Fraga M:** Epidemiological and clinicopathological findings in 15 fatal outbreaks of salmonellosis in dairy calves and virulence genes in the causative *Salmonella enterica* Typhimurium and Dublin strains. *Braz J Microbiol,* 54, 475-490, 2023. DOI: 10.1007/s42770-022-00898-9
6. **Thomas KM, De Glanville WA, Barker GC, Benschop J, Buza JJ, Cleaveland S, Davis MA, French NP, Mmbaga BT, Prinsen G, Swai ES, Zadoks RN, Crump JA:** Prevalence of *Campylobacter* and *Salmonella* in African food animals and meat: A systematic review and meta-analysis. *Int J Food Microbiol,* 315:108382, 2020. DOI: 10.1016/j.ijfoodmicro.2019.108382
7. **Casaux ML, Caffarena RD, Schild CO, Giannitti F, Riet-Correa F, Fraga M:** Antibiotic resistance in *Salmonella enterica* isolated from dairy calves in Uruguay. *Braz J Microbiol,* 50, 1139-1144, 2019. DOI: 10.1007/s42770-019-00151-w
8. **Fonseca M, Heider LC, Stryhn H, McClure JT, Léger D, Rizzo D, Dufour S, Roy J-P, Kelton DF, Renaud DL, Barkema HW, Sanchez J:** Frequency of isolation and phenotypic antimicrobial resistance of fecal *Salmonella enterica* recovered from dairy cattle in Canada. *J Dairy Sci,*

107, 2357-2373, 2024. DOI: 10.3168/jds.2023-23937

9. **Chlebicz A, ´Slizewska K:** Campylobacteriosis, Salmonellosis, Yersiniosis, and Listeriosis as Zoonotic Foodborne Diseases: A review. *Int J Environ Res Public Health,* 15:863, 2018. DOI: 10.3390/ijerph15050863

10. **Holschbach CL, Peek SF:** *Salmonella* in dairy cattle. *Vet Clin Food Anim,* 34, 133-154, 2018. DOI: 10.1016/j.cvfa.2017.10.005

11. **Berge ACB, Moore DA, Sischo WM:** Prevalence and antimicrobial resistance patterns of *Salmonella enterica* in preweaned calves from dairies and calf ranches. *Am J Vet Res,* 67 (9): 1580-1588, 2006. DOI: 10.2460/ajvr.67.9.1580

12. **Adem J, Ame MM, Ali A, Mokeria E:** Review of the zoonotic importance of salmonellosis and associated risk factors. *Vet Med Open J,* 7 (2): 62-69, 2022.

13. **Sallam KI, Mohammed MA, Hassan MA, Tamura T:** Prevalence, molecular identification and antimicrobial resistance profile of *Salmonella* serovars isolated from retail beef products in Mansoura, Egypt. *Food Control,* 38, 209-214, 2014. DOI: 10.1016/j.foodcont.2013.10.027

14. **Rodríguez-Lázaro D, Hernández M:** Next-day *Salmonella* spp. detection method based on real-time PCR for foods. **In,** Schatten H (Ed): *Salmonella*: Methods and Protocols, Methods in Molecular Biology. 3rd ed., 2182: 1-6, Springer Nature, Columbia, MO, USA, 2021.

15. **Pavon RDN, Mendoza PDG, Flores CAR, Calayag AMB, Rivera WL:** Genotypic virulence profiles and associations in *Salmonella* isolated from meat samples in wet markets and abattoirs of Metro Manila, Philippines. *BMC Microbiol,* 22:292, 2022. DOI: 10.1186/s12866-022-02697-6

16. **Huehn S, La Ragione RM, Anjum M, Saunders M, Woodward MJ, Bunge C, Helmuth R, Hauser E, Guerra B, Beutlich J, Brisabois A, Peters T, Svensson L, Madajczak G, Litrup E, Imre A, Herrera-Leon S, Mevius D, Newell DG, Malorny B:** Virulotyping and antimicrobial resistance typing of *Salmonella enterica* serovars relevant to human health in Europe. *Foodborne Pathog Dis,* 7 (5): 523-535, 2010. DOI: 10.1089/fpd.2009.0447

17. **Silva C, Puente JL, Calva E:** *Salmonella* virulence plasmid: Pathogenesis and ecology. *Pathog Dis,* 75:ftx070, 2017. DOI: 10.1093/femspd/ftx070

18. **Guiney DG, Fierer J:** The role of the *spv* genes in *Salmonella* pathogenesis. *Front Microbiol,* 2:129, 2011. DOI: 10.3389/fmicb.2011.00129

19. **Singh Y, Saxena A, Kumar R, Saxena MK:** Virulence System of *Salmonella* with Special Reference to *Salmonella enterica.* **In,** Mascellino MT (Ed): *Salmonella* - A Re-emerging Pathogen. 41-53, 2018.

20. **Abd-Elghany SM, Fathy TM, Zakaria AI, Imre K, Morar A, Herman V, Pașcalău R, Șmuleac L, Morar D, Imre M, Sallam KI:** Prevalence of multidrug-resistant *Salmonella enterica* Serovars in buffalo meat in Egypt. *Foods,* 11:2924, 2022. DOI: 10.3390/foods11182924

21. **Ismail HM, Khalil M, Attalla NR:** Assessment of dairy farms and milk collection centers in El-Gharbia Governorate as a model of the Egyptian Delta (Case study). *Egypt J Anim Prod,* 62 (2): 103-111, 2025. DOI: 10.21608/ejap.2025.361054.1104

22. **Khan MNK, Das MR, Sabur MA, Rahman MM, Uddin MB, Cho HS, Hossain MM:** Isolation, identification, molecular detection and sensitivity to antibiotics of *Salmonella* from cattle faeces. *Bulg J Vet Med,* 24 (1): 57-66, 2021. DOI: 10.15547/bjvm.2019-0061

23. **International Organization for Standardization (ISO 6579):** Microbiology of food and animal feeding stuffs - Horizontal method for the detection of *Salmonella* spp. 511-525, Geneva, Switzerland, 2002.

24. **Simgamsetty S, Yarlagadda P, Yenigalla BM, Myneni RB:** Ease with VITEK 2 systems, biomerieux in identification of non-lactose fermenting bacteria including their antibiotic drug susceptibility: our experience. *Int J Res Med Sci,* 4 (3): 813-817, 2016. DOI: 10.18203/2320-6012.ijrms20160524

25. **Kalendar R, Antonius K, Smýkal P, Schulman AH:** iPBS: A universal method for DNA fingerprinting and retrotransposon isolation. *Theor Appl Genet,* 121, 1419-1430, 2010. DOI: 10.1007/s00122-010-1398-2

26. **Siala M, Barbana A, Smaoui S, Hachicha S, Marouane C, Kammoun S, Gdoura R, Messadi-Akrout F:** Screening and detecting *Salmonella* in different food matrices in southern tunisia using a combined enrichment/real-time PCR method: Correlation with conventional culture method. *Front Microbiol,* 8:2416, 2017. DOI: 10.3389/fmicb.2017.02416

27. **Amavisit P, Boonyawiwat W, Bangtrakulnont A:** Characterization of *Salmonella enterica* serovar Typhimurium and monophasic *Salmonella* serovar 1,4,[5],12:i:- Isolates in Thailand. *J Clin Microbiol,* 43 (6): 2736-2740, 2005. DOI: 10.1128/jcm.43.6.2736-2740.2005

28. **Xiong D, Song L, Tao J, Zheng H, Zhou Z, Geng S, Pan Z, Jiao X:** An efficient multiplex PCR-based assay as a novel tool for accurate inter-serovar discrimination of *Salmonella* Enteritidis, *S.* Pullorum/Gallinarum and *S.* Dublin. *Front Microbiol,* 8:420, 2017. DOI: 10.3389/fmicb.2017.00420

29. **Tarabees R, Elsayed MSA, Shawish R, Basiouni S, Shehata AA:** Isolation and characterization of *Salmonella* Enteritidis and *Salmonella* Typhimurium from chicken meat in Egypt. *J Infect Dev Ctries,* 11 (4): 314-319, 2017. DOI: 10.3855/jidc.8043

30. **Pasmans F, Van Immerseel F, Heyndrickx M, Martel A, Godard C, Wildemauwe C, Ducatelle R, Haesebrouck F:** Host adaptation of pigeon isolates of *Salmonella enterica* subsp. enterica serovar Typhimurium variant copenhagen phage type 99 is associated with enhanced macrophage cytotoxicity. *Infect Immun,* 71 (10): 6068-6074, 2003. DOI: 10.1128/IAI.71.10.6068-6074.2003

31. **Nabih AM, Arafa MM:** Application of some *Lactobacillus* strains product for control of *Salmonella* Typhimurium infection in diarrhoeic neonatal calves. *Assiut Vet Med J,* 58 (133): 184-196, 2012. DOI: 10.21608/avmj.2012.172825

32. **Gebeyehu A, Taye M, Abebe R:** Isolation, molecular detection and antimicrobial susceptibility profile of *Salmonella* from raw cow milk collected from dairy farms and households in southern Ethiopia. *BMC Microbiol,* 22:84, 2022. DOI: 10.1186/s12866-022-02504-2

33. **Abd El-Tawab AA, Hofy FI, Mohamed SR, Salim RA:** Bacteriological and molecular studies on some bacterial agents from neonatal calf diarrhea. *Benha Vet Med J,* 33 (2): 465-475, 2017. DOI: 10.21608/BVMJ.2017.30596

34. **Moussa IM, Ashgan MH, Mohamed MS, Mohamed KHF, Al-Doss AA:** Rapid detection of *Salmonella* species in newborne calves by polymerase chain reaction. *Int J Genet Mol Biol,* 2 (4): 62-66, 2010.

35. **Gutema FD, Agga GE, Abdi RD, De Zutter L, Duchateau L, Gabriël S:** Prevalence and serotype diversity of *Salmonella* in apparently healthy cattle: Systematic review and meta-analysis of published studies, 2000-2017. *Front Vet Sci,* 6:102, 2019. DOI: 10.3389/fvets.2019.00102

36. **Ahmed LM, Sayed ASM, Abd ElKader HA, Abu Faddan NH, Al Hosary AAT:** Phylogenetic analysis of *Salmonella* species isolated from cows, buffaloes, and humans based on *gyrB* gene sequences. *Trop Anim Health Prod,* 52, 1487-1492, 2020. DOI: 10.1007/s11250-019-02155-y

37. **Ibrahim HS, Abdelhamed GS, Elgohary AH, Fathi M:** Relationship between virulence and antibiotic resistant genes in some Gram negative bacteria causing diarrhea in calves. *J Adv Vet Res,* 15 (1): 6-12, 2025.

38. **Stone GG, Oberst RD, Hays MP, McVey S, Chengappa MM:** Detection of *Salmonella* serovars from clinical samples by enrichment broth cultivation-PCR procedure. *J Clin Microbiol,* 32 (7): 1742-1749, 1994. DOI: 10.1128/JCM.32.7.1742-1749.1994

39. **Salman HA, Abdulmohsen AM, Falih MN, Romi ZM:** Detection of multidrug-resistant *Salmonella enterica* subsp. enterica serovar Typhi isolated from Iraqi subjects. *Vet World,* 14 (7): 1922-1928, 2021. DOI: 10.14202/vetworld.2021.1922-1928

40. **O'Hara CM, Miller JM:** Evaluation of the Vitek 2 ID-GNB assay for identification of members of the family *Enterobacteriaceae* and other nonenteric gram-negative bacilli and comparison with the Vitek GNI card. *J Clin Microbiol,* 41 (5): 2096-2101, 2003. DOI: 10.1128/JCM.41.5.2096-2101.2003

41. **Yoshida C, Gurnik S, Ahmad A, Blimkie T, Murphy SA, Kropinski AM, Nash JHE:** Evaluation of molecular methods for identification of *Salmonella* serovars. *J Clin Microbiol,* 54, 1992-1998, 2016. DOI:

10.1128/JCM.00262-16

42. **Yirsa T, Tigistu A:** Occurrence, risk factors, and antibiotic resistance patterns of *Salmonella* isolates obtained from dairy farms in Gondar Town, Northwest Ethiopia. *BioMed Res Int,* 2025:7778947, 2025. DOI: 10.1155/bmri/7778947
43. **Kassa T, Sebhat B, Kassaye D:** Isolation of nontyphoidal *Salmonella* in cattle, sheep and goats among three different agroecologies of Eastern Hararghe, Ethiopia. *Int J Microbiol Res,* 8 (1): 9-18, 2017.
44. **Constable PD:** Treatment of calf diarrhea: antimicrobial and ancillary treatments. *Vet Clin North Am Food Anim Pract,* 25, 101-120, 2009. DOI: 10.1016/j.cvfa.2008.10.012
45. **Huston CL, Wittum TE, Love BC, Keen JE:** Prevalence of fecal shedding of *Salmonella* spp in dairy herds. *J Am Vet Med Assoc,* 220 (5): 645-649, 2002. DOI: 10.2460/javma.2002.220.645
46. **Winfield MD, Groisman EA:** Role of nonhost environments in the lifestyles of *Salmonella* and *Escherichia coli*. *Appl Environ Microbiol,* 69 (7): 3687-3694, 2003. DOI: 10.1128/AEM.69.7.3687-3694.2003
47. **Sychanh T, Chaunchom S, Pulsrikarn C, Pornreongwong S, Chaichana P, Boonmar S:** *Salmonella* prevalence in slaughtered buffaloes and cattle in Champasak Province, Lao People's Democratic Republic. *Agric Nat Resour,* 47 (4): 561-570, 2013.
48. **Matchawe C, Godwe C, Mbah CE, Ndakoh TB, Gondam MFK, Essomba HA, Ahmadou F, Baomog MA, Wangue M, Loul S, Ngond´e MC, Nsawir BJ, Ndip LM, Galeotti M, Piasentier E:** Impacts of zootechnical factors on *Salmonella* contamination in swab samples using real-time PCR at the Yaounde slaughterhouse. *Sci Afr,* 31:e03183, 2026. DOI: 10.1016/j.sciaf.2026.e03183
49. **Ofori LA, Fosu D, Ofori S, Akenten CW, Flieger A, Simon S, Jaeger A, Lamshöft M, May J, ObiriDanso K, Phillips R, Chercos DH, Paintsil EK, Dekker D:** *Salmonella enterica* in farm environments in the Ashanti Region of Ghana. *BMC Microbiol,* 23:370, 2023. DOI: 10.1186/s12866-023-03121-3
50. **Kotb S, Cheng L, Amin M, Elzoghby MM, Nasr A:** Strategic water resource management: Pump stations in Fayoum City, Egypt. *Front Water,* 6:1386303, 2024. DOI: 10.3389/frwa.2024.1386303
51. **Hailu T, Kebede B:** Isolation of non-typhoidal *Salmonella* from sheep faeces in Eastern Hararghe, Ethiopia. *Appl Microb Open Access,* 2 (3):1000120, 2016. DOI: 10.4172/2471-9315.1000120
52. **Dahshan H, Shahada F, Chuma T, Moriki H, Okamoto K:** Genetic analysis of multidrug-resistant *Salmonella enterica* serovars Stanley and Typhimurium from cattle. *Vet Microbiol,* 145, 76-83, 2010. DOI: 10.1016/j.vetmic.2010.02.035
53. **Li Q, Cheng W, Zhang D, Yu T, Yin Y, Ju H, Ding S:** Rapid and sensitive strategy for *Salmonella* detection using an *InvA* genebased electrochemical DNA sensor. *Int J Electrochem Sci,* 7 (1): 844-856, 2012. DOI: 10.1016/S1452-3981(23)13380-3
54. **Rotger R, Casadesús J:** The virulence plasmids of *Salmonella*. *Int Microbiol,* 2 (3): 177-184, 1999.
55. **Rychlik I, Gregorova D, Hradecka H:** Distribution and function of plasmids in *Salmonella enterica*. *Vet Microbiol,* 112, 1-10, 2006. DOI: 10.1016/j.vetmic.2005.10.030
56. **Nikiema MEM, Kakoungazoa S, Ky/Ba A, Sylla A, Bako E, Addablah AYA, Ouoba JB, Sampo E, Gnada K, Zongo O, Traoré KA, Sanou A, Bonkoungou IJO, Ouédraogo R, Barro N, Sangaré L:** Characterization of virulence factors of *Salmonella* isolated from human stools and street food in urban areas of Burkina Faso. *BMC Microbiol,* 21:338, 2021. DOI: 10.1186/s12866-021-02398-6
57. **Chuanchuen R, Ajariyakhajorn K, Koowatananukul C, Wannaprasat W, Khemtong S, Samngamnim S:** Antimicrobial resistance and virulence genes in *Salmonella enterica* isolates from dairy cows. *Foodborne Pathog Dis,* 7 (1): 63-69, 2010. DOI: 10.1089/fpd.2009.0341
58. **Amini K, Nazari Z, Mokhtari A:** Molecular detection of *invA* and *spv* virulence genes in *Salmonella* typhimurium isolated from human and animals in Iran. *Sci J Microbiol,* 4 (7): 49-57, 2015.
59. **Sudrik S, Kolhe R, Bhong C, Shende T, Jadhav S, Mhase P, Waskar V, Hinge G, Gadhave S:** Detection of virulent and ESBL-resistant *Salmonella* species from cattle and associated farm environment. *Indian J Anim Sci,* 94 (10): 831-836, 2024. DOI: 10.56093/ijans.v94i10.141354
60. **Fierer J, Okamoto S, Banerjee A, Guiney DG:** Diarrhea and colitis in mice require the *Salmonella* pathogenicity island 2-encoded secretion function but not *SifA* or *Spv* effectors. *Infect Immun,* 80 (10): 3360-3370, 2012. DOI: 10.1128/IAI.00404-12

Kafkas Universitesi Veteriner Fakultesi Dergisi
Journal Home-Page: http://vetdergikafkas.org
E-ISSN: 1309-2251

Kafkas Univ Vet Fak Derg
Volume: 32, Issue: 4, Year: 2026

ETHICAL PRINCIPLES AND PUBLICATION POLICY

Kafkas Universitesi Veteriner Fakultesi Dergisi follows and implements internationally accepted ethical standards to provide the necessary support to original scientific ideas and to publish high quality, reliable scientific articles in this direction. The journal's publication policy and ethical principles include the ethical standards of conduct that should be followed by author(s), journal editor(s), associate editors, subject editors, reviewers, and publishers who are the participants of this action.

The ethical statement of Kafkas Universitesi Veteriner Fakultesi Dergisi is based on the principles indicated in the "COPE Code of Conduct and Best Practice Guidelines for Journal Editors" (http://publicationethics.org/files/Code_of_conduct_for_journal_editors_Mar11.pdf) and "COPE Best Practice Guidelines for Journal Editors" (http://publicationethics.org/files/u2/Best_Practice.pdf).

GENERAL ETHICAL PRINCIPLES

• Objectivity and Independence

Editor-in-chief, editors, associate editors, and referees conduct the evaluation process of the manuscript sent to the journal objectively and in coordination within the framework of ethical principles. Editorial decisions are independent, and internal or external factors cannot influence these decisions. In accordance with the principle of impartiality, academics working in our institution are not deemed eligible to work as a section editor in Kafkas Universitesi Veteriner Fakultesi Dergisi, in order not to be effective in the evaluation of articles due to conflict of interest.

• Privacy

The content of the articles and the personal information of the authors such as name, e-mail address, and telephone numbers that are sent to Kafkas Universitesi Veteriner Fakultesi Dergisi are used only for the scientific purposes of the journal and not for other purposes, and cannot be shared with third parties. Article evaluation processes are also carried out confidentially.

• Authorship and Authors Rights

The authors of the manuscripts sent to Kafkas Universitesi Veteriner Fakultesi Dergisi must have contributed significantly to the design, execution or interpretation of the study. For example, in view of the research and publication ethics as well as authors rights, it is not acceptable to include those as authors who do not actively contribute to the research but just only help in writing or data collection processes, which may not require any scientific knowledge. All the authors in a publication should be in agreement of the names and the orders of the authors in the manuscript.

The competence of the authors to the subject of the study is evaluated by the editor within the framework of deontological rules and the professional fields of each author.

The corresponding author of the article should declare the contributions of the authors to the work under the title of "Author contributions". The corresponding author is primarily responsible for the problems that may arise in this regard.

In multidisciplinary studies, 2 authors who are from different disciplines can be "equivalent first name authors" and up to most 3 authors who are also from different disciplines can be "equivalent second name authors".

• Generative Artificial Intelligence (AI)

This declaration outlines the acceptable uses of generative AI technology in writing or editing manuscripts submitted to Kafkas Universitesi Veteriner Fakultesi Dergisi. During the writing process, AI and AI-assisted technologies are prohibited from writing or creating the article, tables, or figures. Authors should use AI and AI-assisted technologies solely to enhance the readability and language of the article. Authors should carefully review and edit the result of assisted parts of the manuscript by AI in term of reliability of the applying technologies.

When using generative AI and AI-assisted technologies in scientific writing, authors must declare this by including a statement in the cover letter when the article is first submitted. Once the article is accepted for publication, this statement should be included in the declarations section of the manuscript's final part.

If anything other than the declared conditions is detected, the articles in the evaluation stage will be rejected, and if it is detected in the published articles, the article will be retracted.

• Originality of Research Findings

The authors should declare that the article they presented contained the original research results, that the study data were analyzed correctly, and that they were prepared for publication using adequate and appropriate references, in the "cover letter" section of the on-line system at the submission stage. Using expressions such as "it is the first study done", "there has been no previous study on this subject" and "there is a limited number of studies" to add originality and importance to the article is not acceptable and may cause prevention of the scientific evaluation of the article by the editor.

• Similarity

Articles submitted to the journal are subjected to similarity analysis using appropriate software (iThenticate by CrossCheck) at the beginning and at every required stage. If unethical similarities are detected regardless of the rate of similarity, this situation is reported to the authors and corrections are requested or articles containing excessive similarities are rejected at the first evaluation stage without being evaluated.

• Plagiarism/Self-Plagiarism, Duplicate Publication

Kafkas Universitesi Veteriner Fakültesi Dergisi applies publication ethics and verifies the originality of content submitted before publication and checks all submitted manuscripts for plagiarism/self-plagiarism, similarity and duplication. All submitted manuscripts are meticilously screened by a similarity detection software (iThenticate by CrossCheck). Papers previously presented at scientific meetings and published only as an "abstract" should be indicated in the Title Page file as stated in the "Guidance for Authors". Authors do not have the right to use entire paragraphs from their previous publications into a new submission. These actions are also considered as a plagiarism. In any case, the manuscript should be original in terms of scientific contents and writing. In the event of alleged or suspected research misconduct, the Editorial Board will follow and act in accordance with "COPE Guidelines".

• Multi-part Publication (Piecemeal Publication)

Some authors may tend to divide study data into two or more articles and publish the results in different journals also having different authors names and orders. In principal, Kafkas Universitesi Veteriner Fakultesi Dergisi is against multi-part publication. When necessary, the ethical committee approval information of the study, project information, congress presentations, etc. are checked and such situations that will create an ethical problem are identified and reported to the authors.

Authors may think that their work should be published in multi parts that complement each other. For this, each part of the article should be titled "Part-I", "Part-II" and submitted to the journal "simultaneously". This issue can be evaluated by the editor-in-chief/subject editors/referees who may suggest that the article can be published in parts or as a whole. In addition, rejection of a submission presented in parts means that all parts will be rejected.

• Animal Rights and Ethics

The authors are responsible for conducting experimental and clinical studies on animal experiments within the framework of existing international legislation on animal rights. Authors must also obtain permission from the Animal Experiment Ethics Committees and provide relevant information in the Material and Method section to experiment with animals. In clinical studies, as well as the approval of the ethics committee, an "informed consent form" should be obtained from the animal owners and the information related to it should be declared in the Material and Method section. Declaration of "informed consent form" is sufficient for the articles in the "Case report" and "Letter to the Editor" category.

Ethics committee permission taken for a study can only be used in one article. It is unacceptable to use the same ethics committee approval number in articles with different names and contents. The editor/subject editors can request from the corresponding author, if necessary, to send a copy of the ethics committee approval form to the journal (electronically or by post).

In cases of violation ethical rules, the article is not taken into consideration or if it is in the evaluation stage, the procedure is terminated and the article is rejected.

• Conflicts of Interest/Competing Interests

The editor-in-chief pays attention to whether there is a conflict of interest or union of interest between editors, reviewers and author (s) for an objective and unbiased evaluation of the article. In addition, the authors should disclose any financial interests or links or any conditions that may raise the bias issue in research and article under the above heading.

• Copyright

The authors must fill in the "Copyright Agreement Form" and sign it with a wet signature. Authors who submit articles from abroad should scan the signed form and send it to the editor via the system or by e-mail. Original forms that are wet signed for articles sent domestically should be submitted to the journal via mail or cargo. The works of the authors who do not submit the Copyright Agreement Form on time are not published.

• Withdrawal of a Submission

In case of if the authors detect a significant error or deficiency in their article under review or if this error is reported to them by the editor/subject editor/referees they can contact immediately to the editor-in-chief and ask the request to withdraw the article by stating the reason. The decision on this issue is up to the editorial board.

• Erratum

After an article has been published, the corresponding author may request the editor to publish "erratum" for any errors or inaccuracies noticed by the authors, editors or readers. In collaboration with the authors, the editor prepares and publishes the Erratum article in the first upcoming issue. These articles, like other publications, should contain the publication tag and DOI number.

• Retraction

If any ethical problem is detected about the article that cannot be compensated and cannot be eliminated with erratum after the article is published, the editor-in-chief and associate editors prepare a justification about the article and apply the retraction procedure to the article. The text file on the web page of a retracted article is blocked and the reason for retraction is added to the system as a file, ensuring that it is constantly in the archive.

• Advertising

Kafkas Universitesi Veteriner Fakultesi Dergisi do not accept advertising and sponsorships that are believed to create a potential conflict of interest. If the article sent to Kafkas Universitesi Veteriner Fakultesi Dergisi is for the promotion of a commercial product and/or the work carried out is directly supported by a company, it is rejected without consideration.

OPEN ACCESS STATEMENT

Kafkas Universitesi Veteriner Fakultesi Dergisi
Journal Home-Page: http://vetdergikafkas.org
E-ISSN: 1309-2251

Kafkas Univ Vet Fak Derg
Volume: 32, Issue: 4, Year: 2026

ARTICLE EVALUATION AND PUBLICATION PROCESS

• Initial Evaluation Process

Articles submitted to Kafkas Universitesi Veteriner Fakultesi Dergisi are primarily evaluated by the editors and associate editors. At this stage, articles not having suitable scope and aims, with low original research value, containing scientific and ethically important errors, having low potential to contribute to science and the journal, and having poor language and narration are rejected by the editor without peer-review process. Initial evaluation process takes up to most 2 weeks.

• Preliminary Evaluation Process

Articles that are deemed appropriate for editorial evaluation are sent to the subject editor related to the category of articles to be examined in terms of scientific competence and to the statistics editor for evaluation in terms of statistical methods. The suject editors examine the article in all aspects and report their decisions (rejection, revision or peer-review) to the chief editor. This stage takes about 1 month.

• Peer-review Process

Double-blind peer-review is applied to the articles that have completed preliminary evaluation process. Suggestions of subject editors are primarily considered in referee assignment. In addition, reviews can be requested from the referees registered in the journal's referee pool. At least 2 referees are assigned for peer-review. Opinion of more referees can be required depending on the evaluation process. At this stage, referees send their decision (reject, revision or accept) about the article to the editor-in-chief. If the rejection decision given by a referee reflects sufficient examination and evidence-based negativities or ethical problems about the scientific content and accuracy of the article, this decision is checked by the editor-in-chief and associate editors and submitted to the authors regardless of the other referees' decisions. The time given to referees to evaluate an article is ~4 weeks.

• Publication Process of an Article

Total evaluation period of an article, which is completed in the peer-review phase after completing the initial and preliminary evaluation process, takes 4-6 months. The articles that have completed the subject editorial and peer-review evaluation stages and accepted by the editorial are sent to the corresponding author for final checks and necessary final additions. After the acceptance, the article designed in the publication format of the journal is given an DOI number and published immediately on the Article in Press page. When it is time to publish the periodic edition of the journal, a selection is made from the articles kept on the Article in Press page, taking into account the submission date. The time it takes for the article to be published by taking the page number is 6-12 months.

NO PUBLICATION FEE

Processing and publication are free of charge with the journal. There is no article processing charges, submission fees or any other fees for any submitted or accepted articles.

RESPONSIBILITIES OF THE PUBLISHER, EDITORS AND ASSOCIATE EDITORS

The publisher (Dean of the Faculty of Veterinary Medicine of Kafkas University) contributes to the execution of the journal's routine processes such as printing, archiving, and mailing, in line with requests from the editor.

The publisher undertakes to carry out an independent and fair decision-making mechanism for its editors and assistants in the article evaluation process and decisions.

The publisher undertakes to carry out an independent and fair decision-making mechanism for its editors and associate editors in the article evaluation process and decisions.

Editor-in-chief/editors/associate editors of Kafkas Universitesi Veteriner Fakultesi Dergisi evaluate the articles submitted to the journal regardless of their race, gender, religious belief, ethnicity, citizenship or political views. In addition, it undertakes not to give any information about the article except for the authors, subject editors and referees.

Kafkas Universitesi Veteriner Fakultesi Dergisi follows internationally accepted principles and criteria and takes the necessary decisions to apply in the journal.

Editor-in-chief/editors/associate editors conduct the evaluation and decision process in the journal in coordination within the principles of confidentiality and have independent decision-making authority and responsibility without being affected by any internal or external factors.

Editor-in-chief/editors/associate editors make and implement all kinds of planning for the development of the journal and its international recognition. They also follow national and international meetings or events on the development of journals and article evaluation, and ensures that the journal is represented on these platforms.

The editor-in-chief/editors/associate editors make every effort to ensure that the journal's subject editors and referee pool have international qualifications. Likewise, it makes the necessary attempts to strengthen the author's profile.

Editor-in-chief/editors/associate editors make plans to improve the quality of the articles published in the journal and carry out the necessary process.

Editor-in-chief/editors/associate editors regularly conduct and control the initial evaluation, preliminary evaluation, peer review and acceptance-rejection decisions of articles submitted to the journal. While carrying out these procedures, features such as the suitability of the study for the aims and scope of the journal, its originality, the up-to-date and reliability of the scientific methods used, and the potential it will contribute to the development of the journal as well as its benefit to science/practice are taken into consideration.

Editor-in-chief/editors/associate editors systematically review, inspect and make decisions about the articles submitted to the journal in terms of features such as author rights, conflict of interest, observance and protection of animal rights, and compliance with research and publication ethics.

The editor-in-chief conducts the evaluation/revision process between the authors and subject editors and referees, and ensures that it is completed within the prescribed time.

Kafkas Universitesi Veteriner Fakultesi Dergisi
Journal Home-Page: http://vetdergikafkas.org
E-ISSN: 1309-2251

Kafkas Univ Vet Fak Derg
Volume: 32, Issue: 4, Year: 2026

ARCHIVE POLICY

The editorial office of the Kafkas Üniversitesi Veteriner Fakültesi Dergisi and the publisher (Dean's Office of the Faculty of Veterinary Medicine, Kafkas University) keep all the articles (electronic and printed) published in the journal in their archives. All articles and their attachment files sent to the journal are kept securely in the archive. In light of the technological developments, the editorial office of the Kafkas Üniversitesi Veteriner Fakültesi Dergisi regularly performs electronic processes for the development and updating of materials in digital environment and presents them to its readers on condition of keeping in safe the original documents and information regarding the articles.

Even if the journal ceases to be published for any reason, the publisher (Dean's Office of the Faculty of Veterinary Medicine, Kafkas University) will continue to protect the journal content in the long term and provide convenient access to users. Electronic services of Kafkas University Information Technologies Department will be used for the journal to maintain this responsibility.

RESPONSIBILITIES OF SUBJECT EDITORS

Subject editors do reviews and evaluations in accordance with the main publication goals and policies of the journal and in line with the criteria that will contribute to the development of the journal.

Author information is kept confidential in articles sent to the subject editor for preliminary evaluation by the editor.

Subject editors thoroughly examine the sections of the introduction, materials and methods, results, discussion and conclusion, in terms of journal publication policies, scope, originality and research ethics. Subject editor submits its decision (rejection, revision or peer-review) after evaluation to the chief editor in a reasoned report.

Subject editor may request additional information and documents related to the study from the authors, when necessary.

In multidisciplinary studies, the article can be submitted for the evaluation of multiple subject editors.

RESPONSIBILITIES OF REFEREES

Double-blinded peer-review procedure is applied in Kafkas Universitesi Veteriner Fakultesi Dergisi in order to evaluate the articles submitted to the journal in accordance with the principle of impartiality and in objective criteria; that is, referees and writers do not know about each other.

The referees submit their opinions and reports to the editor-in-chief to ensure the control and suitability of a submitted article, its scientific content, scientific consistency and compliance with the principles of the journal. When a referee makes a decision "reject" about an article, he/she prepares the reasons for the decision in accordance with the scientific norms and presents it to the editor.

The referee(s) also gives the authors the opportunity to improve the content of the article. Accordingly, the revisions requested from the authors should be of a quality that explains/questions specific issues rather than general statements.

Referees appointed for the evaluation of the articles agree that the articles are confidential documents and will not share any information about these documents with third parties, except for the editors participating in the evaluation.

Referees should place their criticism on scientific infrastructure and write their explanations based on scientific evidence. All comments made by the referees to improve the articles should be clear and direct, and should be written away from disturbing the feelings of the author. Insulting and derogatory statements should be avoided.

If a referee has an interest relationship with the author(s) on one or more issues, he/she must report the situation to the editor and ask his/her to withdraw from the referee position. The same is also applicable when the authors illegally obtain information about the referees of the article and try to influence them.

The editor-in-chief can share the comments and reports from the referees with the editors/associate editors and the relevant subject editor, as necessary, to ensure that the decision on the article is optimal. If necessary, the editor may share the critical decision and its grounds that a referee has sent about the article with the other referee(s) and present them to their attention.

Referee(s) may request revision many times for the article they evaluated.

The content of the referee reports is checked and evaluated by editor-in-chief/editors/associate editors. The final decision belongs to the editorial.

RESPONSIBILITIES OF AUTHOR(S)

It is not tolerable for the author (s) to send an article, which has been already sent to another journal, to Kafkas Universitesi Veteriner Fakultesi Dergisi within the scope of "which accepts" or "which publishes first" approach. If this is detected, the article is rejected at any stage of the evaluation. As a possible result of these actions, in the process following the previous acceptance of the article sent to another journal, the withdrawal request with this excuse that the authors submit for this article, the evaluation process of which is going on in our journal, is evaluated by the editors and associate editors of the journal and disciplinary action on the grounds of ethical violations about those responsible is started. This unethical action is also informed to the journal editor (if known) who accepted the article.

It is essential that the articles to be sent to Kafkas Universitesi Veteriner Fakultesi Dergisi include studies that have up-to-date, original and important clinical/practical results and prepared in accordance with the journal's writing rules.

Authors should choose the references they use during the writing of the article in accordance with the ethical principles and cite them according to the rules.

The authors are obliged to revise the article in line with the issues conveyed to them during the initial evaluation, preliminary evaluation and peer-review phases of the article and to explain the changes they made/did not make sequentially in the "response to editor" and "response to reviewer comments" sections.

If information, documents or data regarding to the study are requested during the evaluation process, the corresponding author is obliged to submit them to the editorial.

Authors should know and take into account the issues listed in the "General Ethical Principles" section regarding scientific research and authors.

The authors do not have the right to simultaneously submit multiple articles to Kafkas Universitesi Veteriner Fakultesi Dergisi. It is more appropriate to submit them with acceptable time intervals for the journal's policy.

Kafkas Universitesi Veterinar Fakultesi Dergisi
Journal Home-Page: http://vetdergikafkas.org
E-ISSN: 1309-2251

Kafkas Univ Vet Fak Derg
Volume: 32, Issue: 4, Year: 2026

INSTRUCTION FOR AUTHORS

1- Kafkas Universitesi Veteriner Fakultesi Dergisi (abbreviated title: Kafkas Univ Vet Fak Derg), published bi-monthly (E-ISSN: 1309-2251). We follow a double-blind peer-review process, and therefore the authors should remove their name and any acknowledgment from the manuscript before submission. Author names, affiliations, present/permanent address etc. should be given on the title page only.

The journal publishes full-length research papers, short communications, preliminary scientific reports, case reports, observations, letters to the editor, and reviews. The scope of the journal includes all aspects of veterinary medicine and animal science.

Kafkas Universitesi Veteriner Fakultesi Dergisi is an Open Access journal, which means that all content is freely available without charge to the user or his/her institution. Users are allowed to read, download, copy, distribute, print, search, or link to the full texts of the articles, or use them for any other lawful purpose, without asking prior permission from the publisher or the author. This is in accordance with the BOAI definition of Open Access.

2- The official language of our journal is English.

3- The manuscripts submitted for publication should be prepared in the format of Times New Roman style, font size 12, A4 paper size, 1.5 line spacing, and 2.5 cm margins of all edges. The legend or caption of all illustrations such as figure and table and their appropriate position should be indicated in the text. Refer to tables and figures in the main text by their numbers. Also figure legends explanations should be given at the end of the text.

The figures should be at least 300 dpi resolution.

The manuscript and other files (figure etc.) should be submitted by using online manuscript submission system at the address of http://vetdergi.kafkas.edu.tr/

During the submission process, the authors should upload the figures of the manuscript to the online manuscript submission system. If the manuscript is accepted for publication, the Copyright Agreement Form signed by all the authors should be sent to the editorial office.

4- The authors should indicate the name of the institute approves the necessary ethical commission report and the serial number of the approval in the material and methods section. If necessary, the editorial board may also request the official document of the ethical commission report. In case reports, a sentence stating that "informed consent" was received from the owner should be added to the main document. If an ethical problem is detected (not reporting project information, lack of ethical committee information, conflict of interest, etc.), the editorial board may reject the manuscript at any stage of the evaluation process.

5- Authors should know and take into account the "Generative Artificial Intelligence (AI)" and other matters listed in the **"Ethical Principles and Publication Policy"** section regarding scientific research and authors.

6- Types of Manuscripts

Original (full-length) manuscripts are original and proper scientific papers based on sufficient scientific investigations, observations and experiments.

Manuscripts consist of the title, abstract and keywords, introduction, material and methods, results, discussion, and references and it should not exceed 12 pages including text. The number of references should not exceed 50. The page limit does not include tables and illustrations. Abstract should contain 200±20 words.

Short communication manuscripts contain recent information and findings in the related topics; however, they are written with insufficient length to be a full-length original article. They should be prepared in the format of full-length original article but the abstract should not exceed 100 words, the reference numbers should not exceed 15 and the length of the text should be no longer than 6 pages in total. The page limit does not include tables and illustrations. Additionally, they should not contain more than 4 figures or tables.

Preliminary scientific reports are a short description of partially completed original research findings at an interpretable level. These should be prepared in the format of full-length original articles. The length of the text should be no longer than 4 pages in total.

Case reports describe rare significant findings encountered in the application, clinic, and laboratory of related fields. The title and abstract of these articles should be written in the format of full-length original articles (but the abstract should not exceed 100 words) and the remaining sections should be followed by the Introduction, Case History, Discussion and References. The reference numbers should not exceed 15 and the length of the text should be no longer than 4 pages in total. The page limit does not include tables and illustrations.

Letters to the editor are short and picture-documented presentations of subjects with scientific or practical benefits or interesting cases. The length of the text should be no longer than 3 pages in total. The page limit includes tables and illustrations.

Reviews are original manuscripts that gather the literature on the current and significant subject along with the commentary and findings of the author on a particular subject (It is essential that the author/s have international scientific publications on this subject). The title and summary of this manuscript should be prepared as described for the full-length original articles and the remaining sections should be followed by introduction, text (with appropriate titles), conclusion, and references.

"Invited review" articles requested from authors who have experience and recognition in international publishing in a particular field are primarily published in our journal.

Review articles submitted to our journal must be prepared in accordance with any of the three categories listed below.

Narrative reviews describe current published information on a scientific topic. However, it does not include a specific methodological process.

Systematic reviews include the search for original studies published in that field on a specific topic, the evaluation of validity, synthesis and interpretation within a systematic methodology.

Meta-analysis is a method of evaluating the results of many studies on a subject with the methods defined in this category and statistical analysis of the obtained findings.

7- The necessary descriptive information (thesis, projects, financial supports, etc.) scripted as an italic font style should be explained below the manuscript title after placing a superscript mark at the end of the title.

8- At least 30% of the references of any submitted manuscript (for all article categories) should include references published in the last five years.

References should be listed with numerical order as they appear in the text and the reference number should be indicated inside the parentheses at the cited text place. References should have the order of surnames and initial letters of the authors, title of the article, title of the journal (original abbreviated title), volume and issue numbers, page numbers and the year of publication and the text formatting should be performed as shown in the example below.

Example: Yang L, Liu B, Yan X, Zhang L, Gao F, Liu Z: Expression of ISG15 in bone marrow during early pregnancy in ewes. *Kafkas Univ Vet Fak Derg*, 23 (5): 767-772, 2017. DOI: 10.9775/kvfd.2017.17726

If the reference is a book, it should follow surnames and initial letters of the authors, title of the book, edition number, page numbers, name and location of publisher and year of publication. If a chapter in a book with an editor and several authors is used, names of chapter authors, name of chapter, editors, name of the book, edition number, page numbers, name and location of publisher and year of publication and the formatting should be performed as shown in the example below.

Example: Mcllwraith CW: Disease of joints, tendons, ligaments, and related structures. **In,** Stashak TS (Ed): Adam's Lameness in Horses. 4th ed., 339-447, Lea and Febiger, Philadelphia, 1988.

DOI number should be added to the end of the reference.

In the references can be reached online only, the web address and connection date should be added at the end of the reference information. The generally accepted scientific writing instructions must comply with the other references. Abbreviations, such as "et al" and "and friends" should not be used in the list of the references.

Follow the link below for EndNote Style of Kafkas Universitesi Veteriner Fakultesi Dergisi;
https://researchsoftware.com/downloads/journal-faculty-veterinary-medicine-kafkas-university

9- Latin expression such as species names of bacteria, virus, parasite, and fungus and anatomical terms should be written in italic character, keeping their original forms.

10- The editorial board has the right to perform necessary modifications and a reduction in the manuscript submitted for publication and to express recommendations to the authors. The manuscripts sent to authors for correction should be returned to the editorial office within a month. After pre-evaluation and agreement of the submitted manuscripts by the editorial board, the article can only be published after the approval of the field editor and referee/s specialized in the particular field.

11- All responsibilities from published articles merely belong to the authors. According to the ethical policy of our journal, plagiarism/self-plagiarism will not be tolerated. All manuscripts received are checking by plagiarism checker software, which compares the content of the manuscript with a broad database of academic publications.

12- The editorship may request the language editing of the manuscript submitted to the journal. If the article is accepted, it will not be published without language editing. Before publication, a declaration and/or certificate stating that proofreading is done by a registered company will be requested from the corresponding author.

13- No fee is charged at any stage in Kafkas Üniversitesi Veteriner Fakültesi Dergisi (No APC/APF)

SUBMISSION CHECKLIST

Please use below list to carry out a final check of your submission before you send it to the journal for review. Ensure that the following items are present in your submission:

- Cover Letter

• Importance and acceptability of the submitted work for the journal have been discussed (Please avoid repeating information that is already present in the abstract and introduction).

• Other information has been added that should be known by the editorial board (e.g.; the manuscript or any part of it has not been published previously or is not under consideration for publication elsewhere.

- Title Page

• Title, Running Title (should be a brief version of the title of your paper, no exceed 50 characters)

• The author's name, institutional affiliation, Open Researcher and Contributor ID (ORCID)

• Congress-symposium, project, thesis etc. information of the manuscript (if any)

• Corresponding author's address, phone, fax, and e-mail information

- Manuscript

• Title, abstract, keywords and main text

• All figures (include relevant captions)

• All tables (including titles, description, footnotes)

• Ensure all figure and table citations in the text match the files provided

- Declarations

• Availability of Data and Materials

• Acknowledgements

• Funding Support

• Competing Interests

• Generative Artificial Intelligence (AI)

• Authors' Contributions

Further Considerations

• Journal policies detailed in this guide have been reviewed

• The manuscript has been "spell checked" and "grammar checked"

• Relevant declarations of interest have been made

• Statement of Author Contributions added to the text

• Acknowledgment and conflicts of interest statement provided